Arthritis & Rheumatology

An Official Journal of the American College of Rheumatology
www.arthritisrheum.org and wileyonlinelibrary.com

GENERAL INFORMATION

TO SUBSCRIBE

Institutions and Non-Members

Email: wileyonlinelibrary.com
Phone: (201) 748-6645
Write: Wiley Periodicals LLC
Attn: Journals Admin Dept
UK
111 River Street
Hoboken, NJ 07030

Volumes 75, 2023:
Institutional Print Only: **Arthritis & Rheumatology and Arthritis Care & Research:** $2,708 in US, Canada, and Mexico; $2,708 outside North America
Institutional Online Only: $2,595 in US, Canada, Mexico, and outside North America
Institutional Print and Online Only: $2,915 in US, Canada, and Mexico; $2,915 outside North America

For submission instructions, subscription, and all other information visit: wileyonlinelibrary.com.

Arthritis & Rheumatology accepts articles for Open Access publication. Please visit https://authorservices.wiley.com/author-resources/Journal-Authors/open-access/hybrid-open-access.html for further information about OnlineOpen.

Wiley's Corporate Citizenship initiative seeks to address the environmental, social, economic, and ethical challenges faced in our business and which are important to our diverse stakeholder groups. Since launching the initiative, we have focused on sharing our content with those in need, enhancing community philanthropy, reducing our carbon impact, creating global guidelines and best practices for paper use, establishing a vendor code of ethics, and engaging our colleagues and other stakeholders in our efforts.
Follow our progress at www.wiley.com/go/citizenship.

Access to this journal is available free online within institutions in the developing world through the HINARI initiative with the WHO. For information, visit www.healthinternetwork.org.

Disclaimer

The Publisher, the American College of Rheumatology, and Editors cannot be held responsible for errors or any consequences arising from the use of information contained in this journal; the views and opinions expressed do not necessarily reflect those of the Publisher, the American College of Rheumatology or Editors, neither does the publication of advertisements constitute any endorsement by the Publisher, the American College of Rheumatology or Editors of the products advertised.

Members:

American College of Rheumatology/Association of Rheumatology Professionals

For membership rates, journal subscription information, and change of address, please write:
American College of Rheumatology
2200 Lake Boulevard
Atlanta, GA 30319-5312
(404) 633-3777

ADVERTISING SALES AND COMMERCIAL REPRINTS

Sales: Kathleen Malseed, National Account Manager
E-mail: kmalseed@pminy.com
Phone: (215) 852-9824
Pharmaceutical Media, Inc.
30 East 33rd Street, New York, NY 10016

Production: Patti McCormack
E-mail: pmccormack@pminy.com
Phone: (212) 904-0376
Pharmaceutical Media, Inc.
30 East 33rd Street, New York, NY 10016

Publisher: Arthritis & Rheumatology is published by Wiley Periodicals LLC, 101 Station Landing, Suite 300, Medford, MA 02155
Production Editor: Ramona Talantor, artprod@wiley.com

ARTHRITIS & RHEUMATOLOGY (Print ISSN 2326-5191; Online ISSN 2326-5205 at Wiley Online Library, wileyonlinelibrary.com) is published monthly on behalf of the American College of Rheumatology by Wiley Periodicals LLC, a Wiley Company, 111 River Street, Hoboken, NJ 07030-5774. Periodicals postage paid at Hoboken, NJ and additional offices. POSTMASTER: Send all address changes to Arthritis & Rheumatology, Wiley Periodicals LLC, c/o The Sheridan Press, PO Box 465, Hanover, PA 17331. **Send subscription inquiries care of** Wiley Periodicals LLC, Attn: Journals Admin Dept UK, 111 River Street, Hoboken, NJ 07030, (201) 748-6645 (nonmember subscribers only; American College of Rheumatology/Association of Rheumatology Health Professionals members should contact the American College of Rheumatology). **Subscription Price:** (Volumes 75, 2023: Arthritis & Rheumatology and Arthritis Care & Research) Print only: $2,708.00 in U.S., Canada and Mexico, $2,708.00 rest of world. For all other prices please consult the journal's website at wileyonlinelibrary.com. All subscriptions containing a print element, shipped outside U.S., will be sent by air. Payment must be made in U.S. dollars drawn on U.S. bank. Prices are exclusive of tax. Asia-Pacific GST, Canadian GST and European VAT will be applied at the appropriate rates. For more information on current tax rates, please go to www.wileyonlinelibrary.com/tax-vat. The price includes online access to the current and all online backfiles for previous 5 years, where available. For other pricing options including access information and terms and conditions, please visit https://onlinelibrary.wiley.com/library-info/products/price-lists. Terms of use can be found here: https://onlinelibrary.wiley.com/terms-and-conditions. **Delivery Terms and Legal Title:** Where the subscription price includes print issues and delivery is to the recipient's address, delivery terms are **Delivered at Place (DAP);** the recipient is responsible for paying any import duty or taxes. Title to all issues transfers Free of Board (FOB) our shipping point, freight prepaid. **Claims for Missing or Damaged Print Issues:** Our policy is to replace missing or damaged copies within our reasonable discretion, subject to print issue availability, and subject to the following terms: Title to all issues transfers Freight on Board ("FOB") to the address specified in the order; (1) Freight costs are prepaid by Wiley; and (2) Claims for missing or damaged copies must be submitted by the Customer or Subscription Agent within the claims window, as noted below. **Claims window – General:** Claims for missing print issues must be sent to cs-agency@wiley.com (and the Subscription Agent or Customer may be referred to a society) within three months of whichever of these dates is the most recent: date of subscription payment; or date of issue publication. **Claims window – India:** Both Subscription Agents and Customers in India have 48 hours after receipt of goods to confirm that all content listed on the packing label has been received. In the event of any discrepancy, SPUR Infosolutions, Wiley's delivery partner in India, needs to be notified within forty-eight (48) hours using this email address: support@spurinfo.com. All claims will be checked against SPUR Infosolutions delivery records before the claim is accepted. The above terms for Wiley's claims policy otherwise apply. **Journal Customer Services:** For ordering information, claims and any enquiry concerning your journal subscription please go to https://wolsupport.wiley.com/s/contactsupport?tabset-a7d10=2 or contact your nearest office. **Americas:** Email: cs-journals@wiley.com; Tel: +1 877 762 2974. **Europe, Middle East and Africa:** Email: cs-journals@wiley.com; Tel: +44 (0) 1865 778315; 0800 1800 536 (Germany). **Germany, Austria, Switzerland, Luxembourg, Liechtenstein:** cs-germany@wiley.com; Tel: 0800 1800 536 (Germany). **Asia Pacific:** Email: cs-journals@wiley.com; Tel: +65 3165 0890. **Japan:** For Japanese speaking support, Email: cs-japan@wiley.com. **Visit our Online Customer Help** at https://wolsupport.wiley.com/s/contactsupport?tabset-a7d10=2. **Back Issues:** Single issues from current and prior year volumes are available at the current single issue price from csjournals@wiley.com. Earlier issues may be obtained from Periodicals Service Company, 351 Fairview Avenue-Ste 300, Hudson, NY 12534, USA. Tel: + 1 518 822-9300, Fax: +1 518 822-9305, Email: psc@periodicals.com. Printed in the USA by The Sheridan Group.

Arthritis & Rheumatology

An Official Journal of the American College of Rheumatology
www.arthritisrheum.org and wileyonlinelibrary.com

Cover design: Todd Machen

♾This journal is printed on acid-free paper.

Arthritis & Rheumatology

An Official Journal of the American College of Rheumatology
www.arthritisrheum.org and wileyonlinelibrary.com

VOLUME 75 • January 2023 • NO. 1

In This Issue A11

Journal Club A12

Clinical Connections A13

COVID-19

American College of Rheumatology Guidance for COVID-19 Vaccination in Patients With Rheumatic and Musculoskeletal Diseases: Version 5
Jeffrey R. Curtis, Sindhu R. Johnson, Donald D. Anthony, Reuben J. Arasaratnam, Lindsey R. Baden, Anne R. Bass, Cassandra Calabrese, Ellen M. Gravallese, Rafael Harpaz, Andrew Kroger, Rebecca E. Sadun, Amy S. Turner, Eleanor Anderson Williams, and Ted R. Mikuls E1

Special Articles

Notes from the Field: The Climate Emergency and the Health of Our Patients: The Role of the Rheumatologist
Paul F. Dellaripa, Thomas Bush, Frederick W. Miller, and Candace H. Feldman 1

Review: Management of Orofacial Manifestations of Juvenile Idiopathic Arthritis: Interdisciplinary Consensus-Based Recommendations
Peter Stoustrup, Cory M. Resnick, Shelly Abramowicz, Thomas K. Pedersen, Ambra Michelotti, Annelise Küseler, Bernd Koos, Carlalberta Verna, Ellen B. Nordal, Eric J. Granquist, Josefine Mareile Halbig, Kasper D. Kristensen, Leonard B. Kaban, Linda Z. Arvidsson, Lynn Spiegel, Matthew L. Stoll, Melissa A. Lerman, Mia Glerup, Patrizia Defabianis, Paula Frid, Per Alstergren, Randy Q. Cron, Sarah Ringold, Sven Erik Nørholt, Timo Peltomaki, Tore A. Larheim, Troels Herlin, Zachary S. Peacock, Christian J. Kellenberger, and Marinka Twilt, On behalf of the Temporomandibular Joint Juvenile Arthritis Working Group 4

Special: American College of Rheumatology/EULAR Remission Criteria for Rheumatoid Arthritis: 2022 Revision
Paul Studenic, Daniel Aletaha, Maarten de Wit, Tanja A. Stamm, Farideh Alasti, Diane Lacaille, Josef S. Smolen, and David T. Felson 15

Editorial: Should Low Serum Urate Be Exonerated? Untangling the Influence of Sarcopenia in Observational Studies
Kanon Jatuworapruk and Nicola Dalbeth 23

Special: Winner of the 2022 American College of Rheumatology Annual Image Competition
American College of Rheumatology Image Library Subcommittee and Image Library Diversity Taskforce of the American College of Rheumatology Committee on Education 26

Osteoarthritis

Peripheral Blood DNA Methylation–Based Machine Learning Models for Prediction of Knee Osteoarthritis Progression: Biologic Specimens and Data From the Osteoarthritis Initiative and Johnston County Osteoarthritis Project
Christopher M. Dunn, Cassandra Sturdy, Cassandra Velasco, Leoni Schlupp, Emmaline Prinz, Vladislav Izda, Liubov Arbeeva, Yvonne M. Golightly, Amanda E. Nelson, and Matlock A. Jeffries 28

Spondyloarthritis

Both Disease Activity and HLA–B27 Status Are Associated With Gut Microbiome Dysbiosis in Spondyloarthritis Patients
Magali Berland, Victoria Meslier, Samar Berreira Ibraim, Emmanuelle Le Chatelier, Nicolas Pons, Nicolas Maziers, Florence Thirion, Franck Gauthier, Florian Plaza Oñate, Jean-Pierre Furet, Ariane Leboime, Roula Said-Nahal, Florence Levenez, Nathalie Galleron, Benoît Quinquis, Philippe Langella, Stanislav Dusko Ehrlich, and Maxime Breban 41

Psoriatic Arthritis

Dysregulation of Bile Acids, Lipids, and Nucleotides in Psoriatic Arthritis Revealed by Unbiased Profiling of Serum Metabolites
Ananta Paine, Paul S. Brookes, Soumyaroop Bhattacharya, Dongmei Li, Maria De La Luz Garcia-Hernandez, Francisco Tausk, and Christopher Ritchlin 53

Vasculitis

Brief Report: Phosphatidylinositol 3-Kinase δ Deficiency Protects From Antimyeloperoxidase Vasculitis
Fernanda Flórez-Barrós, Simon Freeley, El Li Tham, and Michael G. Robson 64

Regulation of NETosis and Inflammation by Cyclophilin D in Myeloperoxidase-Positive Antineutrophil Cytoplasmic Antibody–Associated Vasculitis
Takashi Kudo, Daigo Nakazawa, Kanako Watanabe-Kusunoki, Masatoshi Kanda, Satoka Shiratori-Aso, Nobuya Abe, Saori Nishio, Jun-ichiro Koga, Sari Iwasaki, Takahiro Tsuji, Yuichiro Fukasawa, Miwako Yamasaki, Masahiko Watanabe, Sakiko Masuda, Utano Tomaru, Masaaki Murakami, Yasuaki Aratani, Akihiro Ishizu, and Tatsuya Atsumi 71

Syk Activation in Circulating and Tissue Innate Immune Cells in Antineutrophil Cytoplasmic Antibody–Associated Vasculitis
Maria Prendecki, Kavita Gulati, Noelle Pisacano, Damilola Pinheiro, Tejal Bhatt, Marie-Anne Mawhin, Frederic Toulza, Esteban S. Masuda, Andrew Cowburn, Katharine M. Lodge, Frederick W. K. Tam, Candice Roufosse, Charles D. Pusey, and Stephen P. McAdoo 84

Association of ^{18}F-Fluorodeoxyglucose–Positron Emission Tomography Activity With Angiographic Progression of Disease in Large Vessel Vasculitis
Kaitlin A. Quinn, Mark A. Ahlman, Hugh D. Alessi, Michael P. LaValley, Tuhina Neogi, Jamie Marko, Elaine Novakovich, and Peter C. Grayson 98

Systemic Sclerosis

Alterations of the Primary Cilia Gene *SPAG17* and *SOX9* Locus Noncoding RNAs Identified by RNA-Sequencing Analysis in Patients With Systemic Sclerosis
Elisha D. O. Roberson, Mary Carns, Li Cao, Kathleen Aren, Isaac A. Goldberg, David J. Morales-Heil, Benjamin D. Korman, John P. Atkinson, and John Varga 108

Clinical Images

Clinical Images: Chronic, Refractory Childhood-Onset Cutaneous Lupus Erythematosus of the Face Responsive to Lenalidomide
Matthew A. Sherman, Hemalatha Srinivasalu, A. Yasmine Kirkorian, and Michael A. Cardis 120

Clinical Images: Nivolumab-Induced Tracheobronchial Chondritis in a Patient with Hypopharyngeal Cancer
Kazu Hamada-Ode, Yoshinori Taniguchi, Marina Osaki, Rika Yoshimatsu, and Noriko Nitta 121

Gout

Gout and Excess Risk of Severe SARS–CoV-2 Infection Among Vaccinated Individuals: A General Population Study
Dongxing Xie, Hyon K. Choi, Nicola Dalbeth, Zachary S. Wallace, Jeffrey A. Sparks, Na Lu, Chao Zeng, Xiaoxiao Li, Jie Wei, Guanghua Lei, and Yuqing Zhang 122

Associations Between Low Serum Urate, Body Composition, and Mortality
Joshua F. Baker, David R. Weber, Tuhina Neogi, Michael D. George, Jin Long, Lindsay N. Helget, Bryant R. England, and Ted R. Mikuls 133

Letters

No Differences in Myocardial Perfusion Between Treatment-Naive, Early Rheumatoid Arthritis Patients and Healthy Controls
John D. Biglands, Bara Erhayiem, Graham Fent, John P. Greenwood, Raluca B. Dumitru, Jacqueline Andrews, Paul Emery, Maya H. Buch, and Sven Plein 141

Itaconate for Lupus Remission: The Next Therapeutic Frontier? Comment on the Article by Blanco et al
Qi Huang and Wang-Dong Xu 143

Reply
Luz P. Blanco and Mariana J. Kaplan 143

Cover image: The figure on the cover (from Prendecki et al, pages 84-97) shows immunohistochemical staining of cutaneous tissue from a patient with ANCA-associated vasculitis. Infiltrating leukocytes at an area of capillaritis stained positive for SYK (brown) and CD15 (blue).

In this Issue

Highlights from this issue of *A&R* | By Lara C. Pullen, PhD

Use of Peripheral Blood DNA Methylation to Predict Knee OA Progression

Although past studies have used radiographic features to predict knee osteoarthritis (OA) progression, relatively little has been published regarding peripheral blood epigenomic or transcriptomic biomarkers in human OA. In this issue, Dunn et al (p. 28) report the results of their investigation on whether it is possible to use a baseline blood sample from a single time point to identify peripheral blood–based epigenetic biomarkers that could be used to differentiate future rapid radiographic and/or pain OA progressors from nonprogressors. The researchers found that a single baseline blood sample could predict future radiographic and/or pain progression, results suggesting that pain and structural progression share similar, early systemic immune epigenotypes.

p. 28

The investigators had previously published the results of a pilot study modeling peripheral blood DNA methylation data as a predictor of radiographic progression. They advanced this work in the current study by dividing the genome-wide buffy coat DNA methylation patterns of 554 individuals from the Osteoarthritis Biomarkers Consortium (OBC) into model development and validation sets. Parsimonious models identified 13 CpG sites, 12 of which are within known genes or regulatory elements, but only 2 of which have previous links to OA. The authors acknowledge in their discussion that since the study is correlative, these sites may or may not be directly related to OA pathophysiology.

The researchers found that while predictions based on clinical characteristics alone were not accurate, predictions of pain and radiographic progression within the OBC cohort were highly accurate. That said, they were surprised to note that they were not able to discriminate pain-only from radiographic-only progression. They also acknowledge that they have not yet examined the predictive capability of baseline blood epigenetic patterns for other radiographic end points, beyond joint space narrowing. The authors suggest that further studies focus on evaluating the pathophysiologic consequences of differential DNA methylation and peripheral blood cell epigenotypes in individuals with knee OA.

Syk Activation in Innate Immune Cells Points to Treatment Option for Vasculitis

In this issue, Prendecki et al (p. 84) report findings indicating that Syk plays a critical role in myeloperoxidase (MPO)–antineutrophil cytoplasm antibody (ANCA) IgG–induced myeloid cell responses. Although B cell maturation, survival, and activation are Syk-dependent, the researchers focused their study on Syk expression and activation in innate immune cells. The researchers thus examined circulating neutrophils and monocytes from patients with acute ANCA-associated vasculitis (AAV) that had been isolated prior to immunosuppression.

p. 84

The investigators began by isolating myeloid cells from healthy controls and AAV patients. They used flow cytometry to analyze intracellular phosphoproteins and found that, in the circulating innate immune cells of patients with active untreated AAV, the activation of Syk via up-regulation of Syk phosphorylation correlated with measures of disease activity. They then performed transcriptional analysis on granulocytes and monocytes activated in vitro by stimulation with MPO-ANCA IgG and identified up-regulation of several pathways likely to contribute to disease pathogenesis in AAV.

The researchers concluded their study by demonstrating that Syk is expressed and phosphorylated in the tissue of organs affected by vasculitis. The authors note that Syk inhibition may be a potential therapeutic option for AAV and point to their previous studies that demonstrated, in preclinical models, that fostamatinib is an effective treatment for pulmonary and renal disease. They suggest, therefore, that Syk inhibition with fostamatinib should be prioritized for future clinical studies in vasculitis.

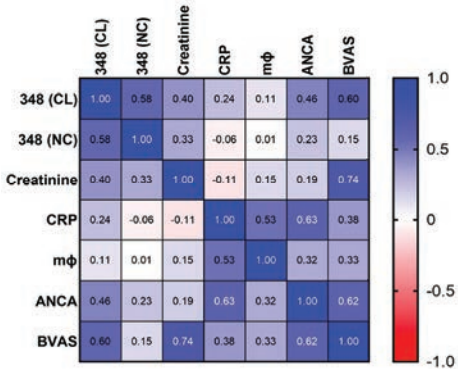

Figure 1. Correlation matrix of P-Syk levels at Y^{348} and clinical parameters in patients with active ANCA-associated vasculitis.

RNA-Seq Analysis in Systemic Sclerosis

Rheumatologists describe systemic sclerosis (SSc) as a complex and progressive inflammatory and fibrotic disease. In this issue, Roberson et al (p. 108) report results of their network analysis, using skin fibrosis and lung function parameters, of peripheral blood mononuclear cells (PBMCs) and skin transcriptomes from individuals with SSc. Their investigation revealed noncoding RNAs and the cilia component *SPAG17* as novel factors potentially implicated in the pathogenesis of SSc.

p. 108

The researchers identified type I interferon (IFN) signaling, with enrichment for targets of IFN regulatory factors (IRFs) IRF-5 and IRF-9, as the predominant signaling in PBMCs. When they analyzed skin samples from SSc patients, they again found the type I IFN signature, but in the skin the signature was coupled with the presence of B cells and additional signals for increased extracellular matrix (ECM) genes, as well as enrichment for pathways related to classical (antibody-mediated) complement activation. The team also found a marked decrease in the expression of *SPAG17* in SSc skin and decreased expression of *LGR5*.

The investigators then used weighted gene coexpression network analysis of SSc PBMCs and skin to identify genes that correlated with the modified Rodnan skin thickness score (MRSS), diffusing capacity for carbon monoxide, and forced vital capacity. In the case of PBMCs, the type I IFN signatures negatively correlated with the DL_{CO}, whereas in SSc skin, ECM gene expression positively correlated with MRSS. When the investigators performed network analysis of SSc skin genes that correlated with clinical features, they found that the noncoding RNAs *SOX9-AS1* and *ROCR*, both near the SOX9 locus, were highly connected, "hub-like" genes in the network. Their network analysis of PBMCs and skin transcriptomes with skin fibrosis and lung function parameters thus demonstrates that both tissues are informative for different traits.

Journal Club

A monthly feature designed to facilitate discussion on research methods in rheumatology.

Association of FDG-PET Activity With Angiographic Progression of Disease in Large Vessel Vasculitis

Quinn et al, *Arthritis Rheumatol.* 2023;75:98–107

Multimodal imaging is increasingly incorporated into clinical practice for patients with large vessel vasculitis (LVV). In recent recommendations, both the American College of Rheumatology and the European Alliance of Associations for Rheumatology support the use of noninvasive angiography and ^{18}F-fluorodeoxyglucose–positron emission tomography (FDG-PET) to diagnose giant cell arteritis (GCA) and Takayasu arteritis (TAK), the 2 major forms of LVV. Whether FDG-PET can be useful in monitoring disease activity or identifying vascular territories at risk for progressive damage is not known. Both angiographic progression of disease and FDG-PET activity within large arteries have been reported during periods of apparent clinical remission in patients with LVV. There is, however, minimal prospective data about the longitudinal relationship between findings on FDG-PET and noninvasive angiography.

Quinn et al designed a prospective, longitudinal study to determine whether FDG-PET activity is associated with future angiographic progression of disease in patients with LVV. In this study, 1,091 arterial territories from 38 patients with TAK and 32 patients with GCA were evaluated. All patients underwent FDG-PET imaging and noninvasive angiography at the baseline study visit with repeat angiography ≥6 months later. Over 1.6 years of median follow-up, change in arterial damage was observed in 30 territories. New arterial lesions developed in only 8 vascular territories, exclusively in 5 patients with TAK. FDG-PET activity in an arterial territory at baseline was associated with change in that arterial territory on follow-up angiography, with a positive predictive value of 8% and a negative predictive value of 99%. In a within-person, arterial territory–matched approach, an arterial territory with baseline FDG-PET activity had 20-times increased odds for angiographic progression of disease over follow-up compared to the matched arterial territory without PET activity. Concomitant findings on angiography, namely increased wall thickening and vascular edema, were useful to predict which territories with FDG-PET activity were most likely to develop angiographic progression of disease.

Questions

1. **What are the current recommendations regarding use of imaging in LVV, and how should these data potentially inform future recommendations in TAK and GCA?**
2. **What are the advantages and potential disadvantages of conditional logistic regression as it was used in this study?**
3. **What are some potential confounders and forms of bias that might affect the association between FDG-PET activity and angiographic change in this cohort?**
4. **How does the low prevalence of angiographic change observed affect the performance characteristics (i.e., positive and negative predictive value) of FDG-PET to predict angiographic change?**

Clinical Connections

Disease Activity, HLA–B27 Status Associate With Gut Microbiome Dysbiosis in SpA

Berland et al, *Arthritis Rheumatol.* 2023;75:41–52

CORRESPONDENCE
Maxine Breban, MD, PhD: maxime.breban@aphp.fr

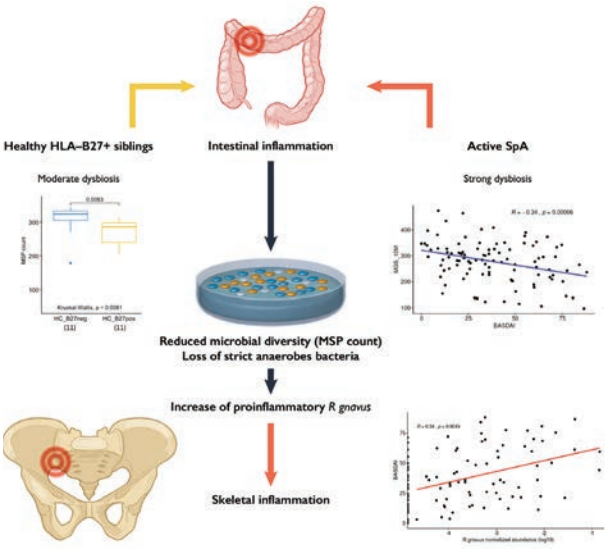

KEY POINTS

- Gut dysbiosis in SpA is proportional to disease activity.
- It is characterized by a reduction of bacterial diversity, a decreased abundance of Clostridiales, and an increased abundance of few potentially pathogenic species, including *R gnavus*.
- In healthy siblings of SpA patients, HLA–B27 is associated with dysbiosis that may reflect subclinical gut inflammation and pave the way to full-blown SpA.

SUMMARY

Spondyloarthritis (SpA) is frequently associated with intestinal inflammation. One of the mechanisms underlying such association could reside in altered gut microbiota composition, i.e., dysbiosis, that is well known in the context of inflammatory bowel disease (IBD) and has been previously reported in SpA.

Using shotgun sequencing of fecal samples, Berland et al compared the microbiota composition between SpA patients and healthy controls, including siblings of patients genotyped for HLA–B27, the strongest genetic factor predisposing one to SpA. They observed dysbiosis, consisting of a reduced microbial diversity in SpA in correlation with disease activity and their HLA–B27–positive healthy siblings, albeit less pronounced than in SpA patients with active disease. In SpA, the largest changes in bacterial species consisted of a reduced abundance of strict anaerobes belonging mostly to the Clostridiales order. In contrast, the abundance of only few species was increased. The most significant increase concerned *Ruminococcus gnavus*, known as relatively aerotolerant and increased in IBD. Its greatest abundance was observed in SpA patients with history of IBD but correlated positively with SpA not IBD activity. Interestingly, some strains of *R gnavus* bear potentially harmful properties, including degradation of the protective mucus layer of the colon, potentially weakening the gut barrier. Thus, an outburst of *R gnavus* could provide a causal link between IBD and SpA.

In addition, the presence of some dysbiosis in HLA–B27–positive healthy siblings of SpA patients may reflect some minor degree of inflammation due to the carriage of this allele and suggests a mechanism by which it could pave the way for the development of SpA.

PI3Kδ Deficiency Protects From Antimyeloperoxidase Vasculitis

Flórez-Barrós et al, *Arthritis Rheumatol.* 2023;75:64–70

CORRESPONDENCE
Michael G. Robson, PhD, MBBS: michael.robson@kcl.ac.uk

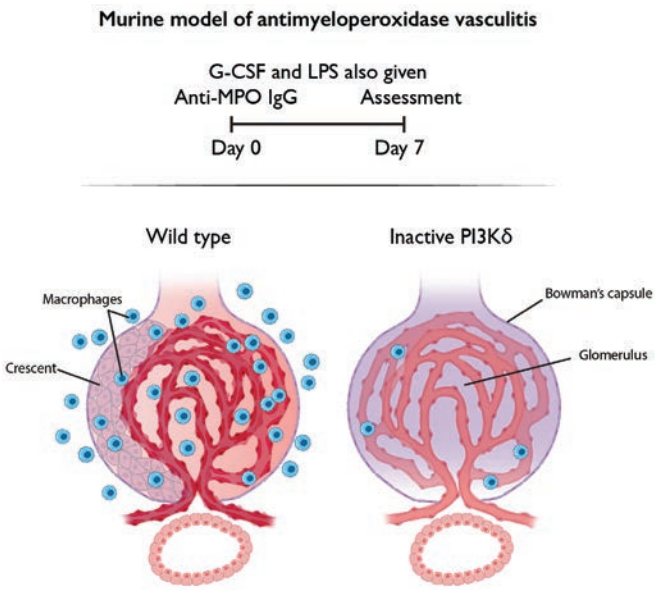

Fewer glomerular and periglomerular macrophages in mice with inactive PI3Kδ
Also fewer glomerular crescents with severe but not mild disease

KEY POINTS

- Mice with an PI3Kδ are protected from disease in a murine model of anti-MPO vasculitis.
- Monocytes from mice with an inactive PI3Kδ had a defect in recruitment to the kidney.
- PI3K inhibitors are a potential treatment for AAV.

SUMMARY

Antineutrophil cytoplasmic antibody–associated vasculitis (AAV) is a severe disease that can cause life-threatening pulmonary hemorrhage and severe glomerulonephritis. It is characterized by antibodies to myeloperoxidase (MPO) and proteinase 3, which are expressed by neutrophils and monocytes. The pathogenicity of anti-MPO antibodies was demonstrated in a murine model 20 years ago. Current treatments cause significant morbidity and there is a particular need for treatments that will reduce inflammation and replace glucocorticoids. A major advance was recently made with successful results in clinical trials for the C5a receptor antagonist avacopan. It is noteworthy that work identifying the C5a receptor as a therapeutic target began in a murine model.

The phosphoinositide 3-kinases (PI3Ks) are heterodimers composed of a catalytic subunit (p110α, p110β p110γ, or p110δ) combined with a regulatory subunit. In a previous study using a murine model of AAV, mice deficient in p110γ were protected from disease, and pharmacologic inhibition of p110γ was effective. Here, Flórez-Barrós et al assess PI3Kδ as a therapeutic target in AAV. Activated PI3Kδ syndrome in humans is caused by mutations that increase activity leading lymphoproliferation and infections. Given the dominance of effects of p110δ on lymphoid cells, modulation of disease induced by passive transfer of anti-MPO antibody was unexpected. However, mice with an inactive form of p110δ were protected. The model has limitations as granulocyte colony-stimulating factor (G-CSF) and lipopolysaccharide (LPS) were needed to induce robust disease. Further experiments showed that monocytes from these mice had a defect in recruitment to the kidney. The findings suggest that drugs inhibiting p110δ may have potential in the treatment of AAV. Many PI3K inhibitors are in clinical trials or are under development for hematologic malignancies, and these may also have a potential benefit in the treatment of AAV.

Arthritis & Rheumatology
Vol. 75, No. 1, January 2023, pp E1–E16
DOI 10.1002/art.42372

American College of Rheumatology
Empowering Rheumatology Professionals

SPECIAL

American College of Rheumatology Guidance for COVID-19 Vaccination in Patients With Rheumatic and Musculoskeletal Diseases: Version 5

Jeffrey R. Curtis,[1] Sindhu R. Johnson,[2] Donald D. Anthony,[3] Reuben J. Arasaratnam,[4] Lindsey R. Baden,[5] Anne R. Bass,[6] Cassandra Calabrese,[7] Ellen M. Gravallese,[5] Rafael Harpaz,[8] Andrew Kroger,[9] Rebecca E. Sadun,[10] Amy S. Turner,[11] Eleanor Anderson Williams,[12] and Ted R. Mikuls[13]

Due to the rapidly expanding information and evolving evidence related to COVID-19, which may lead to modification of some guidance statements over time, it is anticipated that updated versions of this article will be published, with the version number included in the title. Readers should ensure that they are consulting the most current version.

However, because of publication timelines, there may be more updated recommendations online at the ACR website that are pending journal peer review and full manuscript publication. Readers should check the ACR website at https://www.rheumatology.org/Practice-Quality/Clinical-Support/COVID-19-Guidance to confirm the ACR's most recent recommendations. The online version of the tables as they were originally published, as well as a summary of revisions over time and their location, are included in Supplementary Tables 2–6.

Guidance developed and/or endorsed by the American College of Rheumatology (ACR) is intended to inform particular patterns of practice and not to dictate the care of a particular patient. The ACR considers adherence to this guidance to be voluntary, with the ultimate determination regarding its application to be made by the physician in light of each patient's individual circumstances. Guidance statements are intended to promote beneficial or desirable outcomes but cannot guarantee any specific outcome. Guidance developed or endorsed by the ACR is subject to periodic revision as warranted by the evolution of medical knowledge, technology, and practice.

The American College of Rheumatology is an independent, professional, medical and scientific society which does not guarantee, warrant, or endorse any commercial product or service.

Objective. To provide guidance to rheumatology providers on the use of COVID-19 vaccines for patients with rheumatic and musculoskeletal diseases (RMDs).

Methods. A task force was assembled that included 9 rheumatologists/immunologists, 2 infectious diseases specialists, and 2 public health physicians. After agreeing on scoping questions, an evidence report was created that summarized the published literature and publicly available data regarding COVID-19 vaccine efficacy and safety, as well as literature for other vaccines in RMD patients. Task force members rated their agreement with draft consensus statements on a 9-point numerical scoring system, using a modified Delphi process and the RAND/University of California Los Angeles Appropriateness Method, with refinement and iteration over 2 sessions. Consensus was determined based on the distribution of ratings.

Results. Despite a paucity of direct evidence, statements were developed by the task force and agreed upon with consensus to provide guidance for use of the COVID-19 vaccines, including supplemental/booster dosing, in RMD patients and to offer recommendations regarding the use and timing of immunomodulatory therapies around the time of vaccination.

Conclusion. These guidance statements are intended to provide direction to rheumatology health care providers on how to best use COVID-19 vaccines and to facilitate implementation of vaccination strategies for RMD patients.

INTRODUCTION

The pandemic caused by SARS–CoV-2 has caused untold disruption to nearly all aspects of human health globally. The substantial morbidity and excess mortality attributed to COVID-19 has had a major impact on health and the delivery of health care. Given the role that rheumatology providers have in serving patients with rheumatic and musculoskeletal diseases (RMDs) (1), particularly those with autoimmune and inflammatory rheumatic diseases (AIIRDs), there is an urgent need to optimize strategies to curb the incidence of COVID-19. In addition to preventive measures such as physical distancing, mask-wearing, handwashing, shelter-in-place orders, quarantining, and isolation, available COVID-19 vaccines provide a powerful tool to mitigate the burgeoning growth of adverse outcomes resulting from COVID-19.

Given the leadership role of the American College of Rheumatology (ACR) in facilitating dissemination of high-quality evidence and promoting best practices for the care of RMD patients, the ACR periodically convenes task forces charged with developing methodologically rigorous clinical practice guidelines and guidance documents. Previous ACR guidelines developed for the management of rheumatoid arthritis (RA) and psoriatic arthritis (PsA) have included some information regarding optimal use of vaccines for patients with those conditions. However, because the immunologic principles related to the use of vaccines and the impact of vaccine-preventable illnesses on patients cross a broad range of RMDs, the ACR altered its approach in 2020 and convened a new guideline development group to focus exclusively on vaccination. This cross-cutting team was charged with developing encompassing vaccination considerations for all disease and treatment-related areas within rheumatology, rather than embedding them into narrower, disease-specific clinical practice guidelines.

The development process of ACR guidelines follows a rigorous and formal methodology, is based on a reproducible and transparent systematic literature review, incorporates panelist expertise from rheumatology health care professionals and input from related medical experts in other disciplines (e.g., infectious disease, epidemiology), includes direct participation by patients that reflects their values and preferences, and is typically conducted over an extended time frame (e.g., 1 year or longer). In contrast, the ACR develops "guidance" documents when the components needed to develop a formal guideline are not present, e.g., if the need to provide guidance is more urgent than a longer guideline timeline would allow, there is not enough peer-reviewed evidence available to conduct a formal literature review, or when there is very limited expertise and experience, particularly on the part of patients, to help inform the development of recommendations. In these situations, an expert task force is formed to provide the best guidance possible based on the limited information available. The ACR expects that guidance documents will need to be updated with some frequency as new data become available and greater experience is acquired.

Responding to the need to provide timely guidance to practicing clinicians, the ACR COVID-19 Vaccine Guidance Task Force was created as a branch of the ACR Vaccine Guideline effort, to summarize the available evidence for newly available COVID-19 vaccines and to make timely clinical recommendations to rheumatology providers for their optimal use. It relied on a limited evidence base derived from clinical trials evaluating the COVID-19 vaccines in non-RMD populations and also included indirect evidence regarding the immunogenicity, clinical effectiveness, and safety of other vaccines administered to RMD patients receiving various immunomodulatory therapies. Armed with this information, task force members were asked to extrapolate across diseases and integrate relevant basic science and immunologic principles to inform the use of the COVID-19

The findings and conclusions in this report are those of the authors and do not necessarily represent the views of the Centers for Disease Control and Prevention/the Agency for Toxic Substances and Disease Registry.

Supported by the American College of Rheumatology. The effort of some individual authors was supported in part by the NIH (National Institute of Arthritis and Musculoskeletal and Skin Diseases grant P30-AR072583).

[1]Jeffrey R. Curtis, MD, MS, MPH: University of Alabama at Birmingham; [2]Sindhu R. Johnson, MD, PhD: Toronto Western Hospital, Mount Sinai Hospital, and University of Toronto, Toronto, Ontario, Canada; [3]Donald D. Anthony, MD, PhD: Louis Stokes Cleveland VA Medical Center, MetroHealth Medical Center, and Case Western Reserve University, Cleveland, Ohio; [4]Reuben J. Arasaratnam, MD: VA North Texas Health Care System and University of Texas Southwestern Medical Center, Dallas; [5]Lindsey R. Baden, MD, MSc, Ellen M. Gravallese, MD: Brigham and Women's Hospital, Boston, Massachusetts; [6]Anne R. Bass, MD: Hospital for Special Surgery and Weill Cornell Medicine, New York, New York; [7]Cassandra Calabrese, DO: Cleveland Clinic, Cleveland, Ohio; [8]Rafael Harpaz, MD: Harpaz Herman Consultants, Atlanta, Georgia; [9]Andrew Kroger, MD, MPH: CDC, Atlanta, Georgia; [10]Rebecca E. Sadun, MD, PhD: Duke University, Durham, North Carolina; [11]Amy S. Turner: American College of Rheumatology, Atlanta, Georgia; [12]Eleanor Anderson Williams, MD: The Permanente Medical Group, Union City, California; [13]Ted R. Mikuls, MD, MSPH: University of Nebraska Medical Center and VA Nebraska–Western Iowa Health Care System, Omaha.

Dr. Curtis has received consulting fees, speaking fees, and/or honoraria from AbbVie, Bristol Myers Squibb, GlaxoSmithKline, Eli Lilly, and Novartis (less than $10,000 each) and from Amgen, Janssen, Pfizer, Myriad, and Sanofi (more than $10,000 each) and research grants from Genentech, Gilead, AbbVie, Bristol Myers Squibb, GlaxoSmithKline, Eli Lilly, Amgen, Janssen, Pfizer, Myriad, and Sanofi. Dr. Johnson has received consulting fees, speaking fees, and/or honoraria from Ikarai and Boehringer Ingelheim (less than $10,000 each) and research grants from Bayer, Boehringer Ingelheim, Corbus, and GlaxoSmithKline. Dr. Baden has received salary support form the *New England Journal of Medicine* (less than $10,000). Dr. Calabrese has received consulting fees, speaking fees, and/or honoriaria from AbbVie and Sanofi Genzyme (less than $10,000 each). Dr. Gravallese has received salary support from the *New England Journal of Medicine* (more than $10,000). Dr. Mikuls has received consulting fees, speaking fees, and/or honoraria from Sanofi, Horizon, Pfizer, and Gilead (less than $10,000 each) and research support from Bristol Myers Squibb and Horizon. No other disclosures relevant to this article were reported.

Address correspondence via email to Jeffrey R. Curtis, MD, MS, MPH, at jrcurtis@uabmc.edu.

Submitted for publication September 6, 2022; accepted in revised form September 22, 2022.

vaccines available in the US and apply them to the care of RMD patients.

METHODS

Convening the ACR COVID-19 Vaccine Guidance Task Force and defining the scope of the clinical guidance. In October 2020, the ACR began assembling the ACR COVID-19 Vaccination Guidance Task Force. Invitations were made following a general solicitation sent to the broad ACR membership seeking interested volunteers. The task force consisted of 13 members from North America and included 9 rheumatologists, 2 infectious diseases specialists, and 2 public health experts. Rheumatology task force members were chosen to represent various areas of specialty expertise within the field and to achieve diversity in geographic region, career stage, practice setting, sex, and race/ethnicity, while also ensuring that the majority of task force members had no conflicts of interest. The task force defined the intended scope of the guidance based on input from individual members, and external input was obtained informally from various stakeholders. The process was informed by the previously published ACR Guidance for the Management of Rheumatic Disease in Adult Patients During the COVID-19 Pandemic (2). The scope of this guidance includes clinically relevant questions that were intended to inform rheumatology patient care related to COVID-19 vaccination and treatment considerations around the time of vaccination. The scoping questions were agreed upon by all panel members at an initial teleconference conducted on January 21, 2022.

Developing the evidence summary. The task force was divided into teams that worked in parallel, each charged with summarizing the published literature and other available evidence spanning 4 topics: 1) the efficacy, immunogenicity, and safety data derived from clinical trials of late-stage (i.e., phase III) COVID-19 vaccines ongoing within the US or COVID-19 vaccines already available under the US Food and Drug Administration (FDA) Emergency Use Authorization (EUA) act; 2) the epidemiology of COVID-19 risk and outcomes in RMD patients; 3) the attenuation of immunogenicity to other vaccines (e.g., influenza, pneumococcal) associated with certain immunomodulatory therapies; and 4) the safety profile (e.g., disease flare, new-onset autoimmune conditions) of non–COVID-19 vaccines in RMD populations. The scoping questions were grouped into these domains and distributed to the teams, which were tasked with gathering and summarizing evidence that addressed the questions within their assigned domains.

The task force agreed that the intended audience for the guidance was rheumatology health care providers managing their individual patients, but they felt that some attention should be directed to a societal perspective, when relevant. The task force took the perspective of developing guidance for people living in the US, particularly in view of the fact that the review of COVID-19 vaccine clinical trials was US-focused. Recognizing that RMD patients exhibit high variability with respect to their underlying health conditions, disease severity, treatments, and degree of multimorbidity, these considerations were noted as important facets of individualizing care. Therefore, this guidance was not intended to supersede the judgment of rheumatology care providers nor override the values and perspectives of their patients. Foundational principles, guiding assumptions, and acknowledged limitations were discussed and agreed upon throughout the process (Table 1) and are discussed in this document where most relevant.

Table 1. Foundational principles, assumptions, and considerations for the guidance statements*

ACR guidance statements are not intended to supersede the judgment of rheumatology care providers nor override the values and perspectives of their patients. Guidance was, in some cases, based on weak and/or indirect evidence and required substantial extrapolation by an expert task force. All statements, therefore, should be considered conditional or provisional. The ACR is committed to updating this guidance document as new evidence emerges.
The rheumatology community lacks important knowledge on how to best maximize vaccine-related benefits. RMD patients exhibit high variability with respect to their underlying health condition, disease severity, treatments, degree of multimorbidity, and relationship with their specialist provider. These considerations must be considered when individualizing care.
There is limited direct evidence about mRNA COVID-19 vaccine safety and efficacy in RMD patients. There is no reason to expect vaccine harms will trump expected COVID-19 vaccine benefits in RMD patients.
Evidence about the mRNA COVID-19 vaccine suggests that the benefits outweigh the risks in RMD patients.
The risk of deferring vaccination and thus failing to mitigate COVID-19 risk should be weighed against a possible blunted response to the vaccine if given under suboptimal circumstances. As a practical matter, this tension must be resolved in the context of imperfect prediction as to whether those circumstances may be transient as well as a paucity of scientific evidence.
Both individual and societal considerations should be considered in issuing vaccine guidance and making policy decisions. Given that context, simplicity should be the touchstone: to avoid confusion, improve implementation, and maintain scientific credibility.
Any vaccination strategy is a reasonable starting point, and decisions about implementation details reflect tradeoffs in the allocation of scarce vaccine resources.

* ACR = American College of Rheumatology; RMD = rheumatic and musculoskeletal disease.

Development of the evidence review summary document. Given the accelerated time frame for guidance development, a nonsystematic evidence review was completed and included serial PubMed searches supplemented by postings from the Centers for Disease Control and Prevention (CDC); briefings and other documents available from the FDA, such as dossiers submitted by vaccine manufacturers and transcripts of data presented at the FDA's Vaccines and Related Biological Products Advisory Committee meetings (3,4); and other electronic media

sources. References and original articles related to vaccination were culled from the systematic literature reviews developed for ACR guidelines for the management of RA in 2012, 2015, and 2021 (5–7), PsA in 2018 (8), and vaccination guidelines for RMD patients published by EULAR in 2019 (9–11). Articles were dated 1994 through January 2021 (English language, domestic and international).

The scoping questions and the relevant evidence reviews contributed by team members were collated into a single evidence summary document, which was disseminated by email to the entire task force for review 2 days prior to initial ratings. Following the development of the evidence summary, regular PubMed searches were undertaken, and new evidence was shared with the task force prior to follow-up webinars. As limited direct evidence was anticipated to be immediately available for use of the COVID-19 vaccine in RMD patients, no formal assessment of evidence quality (e.g., using Grading of Recommendations Assessment, Development and Evaluation methodology [12]) was attempted, and all evidence was assumed to be indirect. For this reason, all guidance statements should be considered as provisional, or "conditional," until further evidence becomes available.

Initial ratings. The standard guideline development processes currently used by the ACR (13) were deemed to be too time-intensive to be feasible, given the immediate need for the guidance document. Therefore, following distribution of the evidence review document, the scoping questions were transformed into proposed positive statements for which task force members were asked to rate their initial agreement or disagreement. These statements were grouped into 4 broad categories: 1) general medical considerations that provided foundational information for the guidance document; 2) specific recommendations related to COVID-19 vaccination in RMD patients; 3) treatment-specific considerations regarding the timing of COVID-19 vaccination; and 4) the timing of RMD treatments in relation to vaccine administration.

A modified Delphi approach conducted as part of the RAND/University of California at Los Angeles Appropriateness Method (14) was used for guidance development. This method has been used for some past ACR guidelines and the more recent ACR COVID-19 guidance (15); it has been shown to be reproducible and to have content, construct, and predictive validity. Using this method, an initial round of rating was conducted anonymously by email. Task force members were asked to rate their level of agreement, and all votes were weighted equally. Voting was completed using a numerical rating scale of 1–9 for all items. Ratings of 9 corresponded to "complete agreement," 5 to "uncertain," and 1 to "complete disagreement." Median ratings for each statement falling into intervals of 1–3, 4–6, and 7–9 were interpreted as disagreement, uncertainty, and agreement, respectively. Agreement with each of the proposed guidance statements submitted by individual panel members was tabulated for the entire panel and used to classify consensus. Consensus was deemed "strong" when all 13 panel members' ratings fell within a single tertile (e.g., 7–9, indicative of agreement); all other combinations where consensus was achieved were considered to reflect "moderate" consensus. A lack of consensus was identified when the median rating fell into the uncertain range (4–6 interval), or more than one-quarter of the ratings fell into the opposite extreme tertile from the median (e.g., ≥4 panelists rated 1–3 [disagree] when the overall median rating was in the 7–9 [agree] range) (14).

Review and iteration for the ratings of the proposed guidance statements by the task force. Results from the first round of rating were reviewed and discussed in a task force webinar on January 15, 2021. Discussion was focused on statements for which there was no consensus. Individuals were given the opportunity to comment on all items presented in the initial rating process. Informed by voting results and the group discussion, the task force members refined the wording of several of the rated statements.

Revised statements were sent back to task force members and agreement was again assessed by email, using the same scoring approach described above. Results from the second round of voting were presented to the task force via webinar on January 22, 2021, and minor text revisions were made iteratively in real time until consensus was achieved. A draft manuscript was developed describing the results of the rating process, and all coauthors were given an opportunity to provide direct edits to the document. The ACR Guidance Subcommittee and ACR Quality of Care Committee were given the document in order to provide feedback. It was subsequently sent to the ACR Board of Directors, which approved these recommendations on February 8, 2021. Public vetting of the guidance document was held via an electronic and widely publicized "town hall" held on February 16, 2021 that was open to ACR members and the public, with questions solicited in advance and during the town hall webinar. Finally, given the multitude of uncertainties and evidence gaps considered by the task force, the panel proposed a research agenda of high-impact topics that would advance the science and inform the optimal use of COVID-19 vaccines in RMD patients treated with immunomodulatory therapies. After publication, an ACR project librarian will refresh the specified literature search on a regular basis and submit new articles to the task force for review, and this document will be updated through a similar process as new evidence emerges.

RESULTS

Of the guidance statements considered across the 2 rounds of ratings, the majority were rated with a median score of 7, 8, or 9 (i.e., agreement), and 3 of them were not agreed upon. Among the statements achieving agreement, consensus was strong for 16 and moderate for the remainder. One guidance statement

Table 2. General considerations related to COVID-19 vaccination in patients with RMD*

Statement domain	Guidance statement	Level of task force consensus
Clinical practice	The rheumatology health care provider is responsible for engaging the RMD patient in a discussion to assess COVID-19 vaccination status.	Strong
Clinical practice	The rheumatology health care provider is responsible for engaging the RMD patient in a shared decision-making process to discuss receiving the COVID-19 vaccine.	Moderate
Epidemiology	AIIRD patients are at higher risk for incident viral infections compared to the general population.	Moderate
Epidemiology	After considering the influence of age and sex, AIIRD patients are at higher risk for COVID-19 hospitalization compared to the general population.	Moderate
Epidemiology	Acknowledging heterogeneity due to disease- and treatment-related factors, AIIRD patients have worse outcomes associated with COVID-19 compared to the general population of similar age and sex.	Moderate
Epidemiology	Across AIIRD conditions, and within any specific disease, there is substantial variability in disease- and treatment-related risk factors for COVID-19 that may put some patients at higher risk than others.†	Moderate
Public health	Based on increased risk for COVID-19, AIIRD patients should be prioritized for vaccination before the nonprioritized general population of similar age and sex.	Moderate
Vaccine safety	There are no known additional contraindications to COVID-19 vaccination for AIIRD patients.	Moderate
Vaccine effectiveness	The expected response to COVID-19 vaccination for many AIIRD patients receiving systemic immunomodulatory therapies is blunted in its magnitude and duration compared to the general population.	Moderate
Disease-related	As a general principle, vaccination should optimally occur in the setting of well-controlled AIIRD.	Moderate
Disease-related	A potential risk exists for AIIRD flare or disease worsening following COVID-19 vaccination.	Moderate
Vaccine safety	The benefit of COVID-19 vaccination for RMD patients outweighs the potential risk for new-onset autoimmunity.	Moderate

* RMD = rheumatic and musculoskeletal disease.
† For examples of these autoimmune and inflammatory rheumatic disease (AIIRD) conditions, see Supplementary Table 1, on the *Arthritis & Rheumatology* website at http://onlinelibrary.wiley.com/doi/10.1002/art.42372.

related to COVID-19 vaccination in children was rated with a median value of 5 (uncertain) by the task force, in part reflecting the desire to obtain more feedback from pediatric rheumatology providers. Additional input was therefore sought from the ACR Pediatric Rheumatology Clinical Guidance Task Force. This task force had acknowledged ongoing clinical trials of COVID-19 vaccines in children and evolving FDA EUAs for the COVID-19 vaccine in children as young as 6 months of age, although it recognized that ≥1 COVID-19 vaccine clinical trial has enrolled patients as young as age 5 years (ClinicalTrials.gov identifiers: NCT04649151 and NCT04368728) (16–19). Now trials have enrolled patients as young as 6 months of age. On this basis, our task force and the Pediatric Task Force have consistently recommended to await appropriate evidence from clinical trials regarding the safety and effectiveness of COVID-19 vaccination in children and align our guidance with FDA EUAs. The FDA now has authorized Pfizer-BioNTech and Moderna vaccines for children as young as 6 months of age based on trial evidence to support EUAs in children. The second statement for which the task force was unable to reach consensus relates to vaccination in the context of ongoing treatment with high-dose glucocorticoids, discussed in detail below.

General considerations related to vaccination against COVID-19 in patients with RMDs. Twelve guidance statements related to general considerations of COVID-19 vaccination in RMD patients achieved consensus (Table 2). Statements were descriptively categorized into ≥1 domain to facilitate ease of reference. The panel concurred that rheumatology health care providers were responsible for engaging RMD patients in discussions to assess whether they had been vaccinated against COVID-19 and to document related details (e.g., which vaccine had been administered, timing of vaccination, whether the series and all recommended booster doses had been completed). For those not vaccinated, and similar to other vaccination guidelines for immunocompromised patients such as those from the Infectious Diseases Society of America (20,21), it was thought that the rheumatology provider should share responsibility with the patients' primary care provider (when available) to ensure appropriate vaccinations are administered. Rheumatology providers should also engage patients in a shared decision-making process to discuss the following: their attitudes, intent, and concerns related to vaccination; local incidence of COVID-19; individual circumstances (e.g., disease activity, medications, comorbidities) that may affect risk; ability to adhere to nonpharmacologic public health interventions; and vaccine efficacy and potential safety concerns (e.g., local or systemic reactogenicity, potential for disease worsening or flare).

The epidemiology of viral infection risk in RMD patients, and specifically, the risk for infection due to SARS–CoV-2, was then discussed. For this topic, the task force elected to narrow the scope of the patient population under consideration and define a presumably higher-risk subgroup of patients with RMDs. Some RMD conditions would include those managed by rheumatology

providers but not generally associated with high levels of systemic inflammation (e.g., osteoarthritis, fibromyalgia, osteoporosis) and for which conventional, biologic, or targeted synthetic disease-modifying antirheumatic drugs (DMARDs) or other therapies with immunosuppressive effects are typically not indicated. The patient population was thus restricted to those with AIIRDs (see Supplementary Table 1 for definitions, available on the *Arthritis & Rheumatology* website at http://onlinelibrary.wiley.com/doi/10.1002/art.42372). Among these individuals, the risk for incident viral infections (e.g., herpes zoster) was rated as being higher than for the general population (22–24). There was also agreement that AIIRD patients are likely to be at increased risk for hospitalized SARS–CoV-2 infection (25–29) and that age, race/ethnicity (especially for underrepresented minorities), and sex were important risk factors that needed to be considered (30–32) in evaluating risk at the individual patient level.

Multimorbidity was felt to likewise play an important role in the risk for developing severe COVID-19. While some population-based epidemiologic studies of COVID-19 incidence and outcomes in AIIRD patients have controlled for general multimorbidity or specific comorbidities (25,26,34), the panel recognized that some comorbidities that increase infection risk were shared risk factors for development of AIIRDs (e.g., smoking and related pulmonary conditions associated with incident RA). These may represent direct manifestations such as interstitial lung disease associated with some AIIRDs, or they could be downstream sequelae causally related to the underlying inflammatory processes of AIIRDs or their treatment (e.g., premature and advanced atherosclerotic vascular disease in systemic lupus erythematosus (SLE) patients; obesity, diabetes, and features of the metabolic syndrome in PsA patients or those receiving long-term glucocorticoids). For that reason, adjustment for these comorbidities might be inappropriate and would underestimate the risk of COVID-19 infection in patients with AIIRDs. Therefore, age- and sex-adjusted risk estimates were preferred by some task force members when comparing risk and outcomes of COVID-19 in AIIRD patients to the general population.

The few large population-based studies of COVID-19 incidence and outcomes in AIIRD patients had minimal demographic diversity, and therefore race/ethnicity could not be easily evaluated as an independent risk factor. Finally, the panel acknowledged challenges in being able to disentangle the independent role of the disease activity and severity of various AIIRDs from the medications used to treat them (e.g., higher-dose glucocorticoids [35]), so-called confounding by severity, as risk factors for worse COVID-19 outcomes.

Despite these important methodologic caveats and acknowledged limitations in the evidence base, AIIRD patients were rated as having worse outcomes (e.g., need for intensive care unit [ICU] treatment, mechanical ventilation, persistent infection, death) following COVID-19 compared to patients of similar age and sex without such conditions (25–29,36). In terms of the policy implications of this reasoning, the task force agreed that when the vaccine supply is constrained, as it was early in the pandemic, AIIRD patients should be prioritized to be allocated to receive vaccination before the nonprioritized general population of similar age and sex (37). The panel recognized important heterogeneity across AIIRD conditions, such that (for example) an RA patient with quiescent disease treated only with hydroxychloroquine likely has a lower risk for COVID-19 and adverse outcomes compared to a patient with very active vasculitis treated with intravenous (IV) cyclophosphamide or rituximab (RTX) and high-dose glucocorticoids (33), although the protection conferred by COVID-19 vaccination may also differ greatly.

Turning attention to vaccination of individual patients, the task force felt that there were no additional known contraindications to receipt of the COVID-19 vaccine other than known allergies to vaccine components as stipulated by guidance from the CDC (38) and thrombosis with thrombocytopenia following a previous dose of the Janssen COVID-19 vaccine (or other vaccines not currently authorized that are based on adenovirus vectors, e.g., AstraZeneca COVID-19 vaccine). Extrapolating evidence derived from studies of other vaccines, the expected response to vaccination in many AIIRD patients receiving certain systemic immunomodulatory therapies was deemed likely to be blunted, albeit with uncertain diminution in either the magnitude or duration of response compared to the general population (38,39). The task force acknowledged a paucity of direct evidence supporting this assertion and placed great importance on prioritizing this topic as part of a future research agenda. The timing of vaccination was considered more ideal in the setting of well-controlled disease, yet the task force noted that patients and their providers should not be dissuaded from vaccination under less-than-ideal conditions, with additional timing considerations as discussed below.

Based on data derived from the published literature, a potential risk for a flare of the patient's underlying AIIRD following vaccination was acknowledged. For example, based on randomized controlled trial data (40), the frequency of flare was higher in RA patients randomized to have methotrexate (MTX) withheld at the time of influenza vaccination compared to those randomized to continue (10.6% versus 5.1%, respectively), with flare defined as an increase in the Disease Activity Score in 28 joints (DAS28) of >1.2, or >0.6 if the baseline DAS28 was ≥3.2 (41). A subsequent pooled analysis that included that trial and another showed that while the mean change in DAS28 did not differ between groups, the adjusted flare rate in the 2-week withhold group (MTX withhold) was 2.90-fold higher (95% confidence interval 0.96–4.56; $P = 0.063$) compared to the group that continued MTX (MTX continue), with a difference in proportions experiencing flare of 10.8% (MTX withhold group) versus 5.8% (MTX continue group) (40,42–44). This risk of flare or disease worsening was catalogued as an important topic slated for the future research agenda. Finally, although some new-onset AIIRDs (e.g., RA, vasculitis) or

Table 3. Recommendations for primary and supplemental dosing of the COVID-19 vaccine in RMD patients*

Statement domain	Guidance statement	Level of task force consensus
Clinical practice	RMD and AIIRD patients should receive COVID-19 vaccination, consistent with the age restriction of the EUA and/or FDA approval.†	Strong
Clinical practice	RMD patients without an AIIRD who are receiving immunomodulatory therapy should be vaccinated in a similar manner as described in this guidance as AIIRD patients receiving those same treatments.	Moderate
Vaccine effectiveness/ safety	For AIIRD patients who are not yet vaccinated, either of the mRNA vaccines is recommended over the Johnson & Johnson vaccine. There is no recommendation for one mRNA vaccine over another.†	Moderate
Vaccine effectiveness	For a multidose primary vaccine, AIIRD patients should receive the second dose of the same vaccine, even if there are nonserious adverse events associated with receipt of the first dose, consistent with timing described in CDC guidelines (32).	Strong
Clinical practice	**RMD and AIIRD patients who completed the primary COVID vaccine series of 3 doses and are expected to have mounted an inadequate vaccine response should receive supplemental doses (e.g., ≥2 additional boosters, for a total of 5 doses) as recommended by the CDC for immunocompromised individuals.‡**	**Strong**
Clinical practice	For patients who previously completed the mRNA COVID-19 vaccine series an mRNA vaccine supplemental dose of either type (Pfizer or Moderna) is preferred.	Moderate
Clinical practice	**Primary vaccination, supplemental dosing, and booster doses should be given regardless of whether patients have experienced natural COVID-19 infection.**	**Strong**
Clinical practice	Health care providers should not routinely order any laboratory testing (e.g., antibody tests for IgM and/or IgG to spike or nucleocapsid proteins) to assess immunity to COVID-19 postvaccination, nor to assess the need for vaccination in an as-yet-unvaccinated person.§	Strong
Public health	Following COVID-19 vaccination, RMD patients should continue to follow all public health guidelines regarding physical distancing and other preventive measures.¶	Strong
Clinical practice	**For high-risk AIIRD patients, pre-exposure prophylaxis monoclonal antibody treatment is recommended when available, if licensed or approved under FDA EUA.#**	**Moderate**
Clinical practice/public health	Household members and other frequent close contacts of AIIRD patients should undergo COVID-19 vaccination when available to them to facilitate a "cocooning effect" that may help protect the AIIRD patient.	Moderate
Vaccine effectiveness/ disease-related	While vaccination would ideally occur in the setting of well-controlled AIIRD, except for AIIRD patients with life-threatening disease (e.g., in the ICU for any reason), COVID-19 vaccination should occur as soon as possible for those for whom it is being recommended, irrespective of disease activity and severity.	Strong

* Boldface text indicates updates that were added to the version 5 summary document in early 2022. RMD = rheumatic and musculoskeletal disease; EUA = Emergency Use Authorization; AAIRD = autoimmune and inflammatory rheumatic disease; ICU = intensive care unit.
† Age ≥6 months as of June 19, 2022.
‡ **The timing of booster shot intervals is somewhat vaccine-dependent. For both the Moderna and Pfizer mRNA vaccines, a booster shot is recommended ≥3–4 months after completion of the 3-dose primary vaccine series. The recommended interval for those having received the Johnson & Johnson vaccine is ≥2 months (ref. 47).**
§ Given uncertainties in the interpretation of laboratory testing following vaccination as it would impact clinical decision-making, the panel reaffirmed this statement in Version 4 of this guidance document.
¶ The task force discussed the possibility of recommending additional and more sustained public health measures for patients with AIIRD. After deliberation, they did not elect to exceed current public health authority guidance given uncertainties about the clinical effectiveness of vaccination in such patients. The appropriateness for continued preventive measures (e.g., masking, physical distancing) should be discussed with patients as their rheumatology providers deem appropriate.
# **High risk is defined as moderately to severely compromised immune systems in individuals who may not mount an adequate immune response to COVID-19 vaccination. Note that the US Food and Drug Administration (FDA) authorization and Centers for Disease Control and Prevention (CDC) recommendations will be influenced based upon the dominant variants of SARS–CoV-2 circulating in the US (http://www.fda.gov/news-events/press-announcements/coronavirus-covid-19-update-fda-limits-use-certain-monoclonal-antibodies-treat-covid-19-due-omicron). At the time of this update, neither bamlanivimab and etesevimab (administered together) nor casirivimab and imdevimab are licensed or available under FDA EUA given their lack of activity against the omicron variant, the dominant strain circulating in the US. See Supplementary Table 5 for further details (on the *Arthritis & Rheumatology* website at http://onlinelibrary.wiley.com/doi/10.1002/art.42372).**

flares of preexisting AIIRDs have been reported after COVID-19 in published case reports (45,46), the expected benefit of vaccination for AIIRD patients was thought to outweigh any theoretical risk for the development of new-onset autoimmune conditions or other potentially immune-mediated manifestations or abnormalities (e.g., Bell's palsy, Guillain-Barré syndrome, anti-RNA antibodies in SLE patients, immune thrombocytopenic purpura) following vaccination.

Indications for vaccination and timing considerations. As summarized in Table 3, and consistent with guidance from the CDC for the general US population and for immunocompromised individuals (47), the panel recommended that RMD and AIIRD patients be offered and receive vaccination against SARS–CoV-2. Discussion was held regarding the age cutoff for vaccination, and the panel agreed that guidance should be made consistent with the EUA of available vaccines (i.e., age ≥6 months as of June 19, 2022).

Recommendations on which patients should be vaccinated were extended to patients with RMDs who did not have conditions typically considered to be AIIRDs but for which immunomodulatory or DMARD therapies might be used off-label. For example, patients with erosive osteoarthritis might receive MTX, or gout patients treated with pegloticase might be concomitantly treated with MTX to reduce pegloticase immunogenicity. These circumstances, in which MTX or another immunomodulatory therapy is being used for a non-AIIRD condition, would be treated synonymously with the guidance for MTX offered in this document. However, within the category of patients with AIIRDs and/or those receiving immunomodulatory therapies, substantial heterogeneity of disease- and treatment-related risk factors was noted. Some AIIRD patients were expected to be at higher risk for infection and morbidity than others, and thus the impetus for COVID-19 vaccination might be stronger for some individual patients or patient groups (e.g., patients with SLE receiving cytotoxic therapy and higher-dose glucocorticoids, or patients receiving RTX therapy), although the vaccine might be less effective in these same individuals.

Extensive discussion was held regarding whether consideration for a particular vaccine or vaccine platform (e.g., messenger RNA [mRNA] versus adenoviral vector) might be preferred in general, or for select patients, based on potential differences in effectiveness or safety. Based on the task force members' ratings and the vaccine options in the US, the expert panel reached consensus on the guidance that RMD patients undergoing vaccination are recommended to receive whichever SARS–CoV-2 mRNA vaccine is available to them. Either of the mRNA vaccines is recommended over the single-dose Johnson & Johnson vaccine. The task force noted that none of the other SARS–CoV-2 vaccine candidates in development would be classified as a canonical live virus vaccine, including the adenoviral vector–based vaccines which are replication deficient (48). Thus, the usual prohibitions against the use of live virus vaccines in immunosuppressed patients do not apply. The conclusions in this report predated the EUA for the Novavax COVID-19 vaccine in the US.

Following receipt of the first dose in a vaccine series, patients were recommended to receive the second dose of the same type of vaccine, assuming no contraindication to the second dose per CDC guidance (e.g., a severe allergic reaction, or an immediate allergic reaction of any severity to the vaccine or any of its components, including polyethylene glycol) (37,49). Persons who develop SARS–CoV-2 infection between the first and second dose of a 2-dose vaccine series should delay the second dose until they have recovered from the acute illness (if symptomatic) and discontinued isolation, and then they should receive the second dose without delay (37,49). Consistent with CDC guidance (50), SARS–CoV-2–infected patients who received monoclonal antibodies or convalescent plasma as part of treatment for COVID-19 are no longer recommended to defer vaccination following receipt of antibody products (anti–SARS–CoV-2 monoclonal antibodies or convalescent plasma). Also consistent with CDC guidance (49), providers may co-administer other vaccines at the same time as COVID-19 vaccines, and without regard to the timing of other vaccines.

According to CDC guidelines, for patients who previously completed the 2-dose mRNA series or received the 1-dose Johnson & Johnson COVID-19 vaccine, a supplemental COVID-19 vaccine dose is recommended ≥28 days after the completion of the vaccine series so as to complete the recommended 3-dose primary vaccine series. This guidance applies to AIIRD patients receiving any immunosuppressive or immunomodulatory therapy other than hydroxychloroquine monotherapy. In making this statement, the task force recognized the high potential for confusion related to nomenclature between an additional primary dose and a booster dose. A "third dose" is the term that had typically been used to refer to an additional primary dose of a vaccine given to patients who previously completed the primary vaccine series (i.e., the 2-dose mRNA vaccine series) and who may have mounted a suboptimal response due to immunosuppressive medications or an immunocompromised medical condition (49–55). In contrast, a "booster dose" refers to an additional dose given to patients who are expected to have mounted an adequate response but in whom the response may have waned over time (49,55–61). AIIRD patients are now recommended to receive a total of 5 vaccine doses, consistent with CDC guidance (47–49). The timing of booster doses may be as early as 3–4 months for mRNA vaccines, following the CDC guidance for moderately to severely immunocompromised patients (50). At this time, AIIRD patients being "up-to-date" in relation to vaccination means they have received all 3 doses of the primary series plus 2 boosters. Future FDA and CDC guidance may recommend subsequent booster doses beyond the fifth dose, based upon evolving science as to the duration of protection conferred by booster doses and in light of the dominant circulating strains of SARS–CoV-2 present in the community.

The task force reviewed the evidence for homologous versus heterologous (i.e., "mix and match") supplemental/booster dosing (62–69). After consideration, and similar to the preference for an mRNA vaccine for primary vaccination, patients who previously completed the mRNA COVID-19 vaccine series or 1-dose Johnson & Johnson COVID-19 vaccine are recommended to receive an mRNA vaccine supplemental/booster dose, either Pfizer or Moderna (70–72).

AIIRD patients at high risk for poor outcomes related to COVID-19 were recommended to receive monoclonal antibody therapy with casirivimab and imdevimab (Regeneron) if available, either as prevention (i.e., post-exposure prophylaxis for asymptomatic, recently exposed patients) or as treatment for newly symptomatic patients (see Supplementary Table 3, http://onlinelibrary.wiley.com/doi/10.1002/art.42372). Other therapies are now available for outpatient treatment of high-risk patients with symptomatic infection, and these should be strongly

considered in AIIRD patients, most of whom qualify as high-risk and are therefore likely to benefit from antiviral therapy. Household members and other frequent close contacts of AIIRD patients were recommended to undergo COVID-19 vaccination when available, in order to facilitate a "cocooning effect" that may help protect at-risk AIIRD patients. However, the priority for vaccination for these close contacts does not need to be elevated at this time, since there is adequate vaccine supply.

A series of statements were rated by the panel with respect to the general timing of COVID-19 vaccination in relation to AIIRD disease activity, again acknowledging a dearth of direct evidence. Except for those with severe and life-threatening illness (e.g., a hospitalized patient receiving treatment in the ICU for any condition), vaccination was recommended irrespective of disease activity and severity. Even for ICU-treated patients for whom vaccination was recommended to be deferred for a short time, the task force felt that when the patient was well enough to be discharged from the hospital, vaccination would likely be appropriate. For AIIRD patients in other settings, including those with either active but non–life-threatening disease, and certainly for patients with stable and/or low disease activity, vaccination was recommended. Multisystem inflammatory syndrome in children (MIS-C) and multisystem inflammatory syndrome in adults (MIS-A) are hyperinflammatory conditions that occur several weeks following COVID-19 and can lead to hospitalization, organ failure, and death. It is clear that COVID-19 immunization is protective against MIS-C and MIS-A, with very few MIS cases occurring in breakthrough infections (73). There has been historical concern regarding whether it is safe to vaccinate patients with a history of MIS. A recent case series supports safety of post–MIS-C vaccination (74), and current CDC guidance encourages post–MIS-C vaccination once patients are >90 days out from infection, have recovered from active infection, and have regained normal cardiac function (75). Finally, patients naive to or not currently receiving immunomodulatory therapies were recommended to receive their first dose of vaccine without delay. Additional considerations for medication timing are subsequently discussed.

Treatment-specific timing of primary vaccination. There was recognition that the ability to carefully time COVID-19 vaccination is sometimes limited in a real-world setting, and the overarching view was that COVID-19 vaccination should be given rather than not given if timing in relation to immunomodulatory drugs is not under the provider's or patient's control.

Strong consensus was achieved regarding the statement to not delay COVID-19 vaccination for patients receiving hydroxychloroquine, sulfasalazine, leflunomide, apremilast, or IV immunoglobulin (10,76). A similar recommendation with moderate consensus was achieved for most of the remaining immunomodulatory therapies considered (77–88).

One exception was RTX (10,11,89–93), for which the panel recommended to schedule vaccination such that the vaccine series would be initiated ~4 weeks prior to the next scheduled RTX dose. For example, a patient receiving RTX as a 2-dose cycle (spaced 2 weeks apart), with cycles repeating every 6 months, would be recommended to initiate vaccination ~5 months after the start of the prior RTX cycle. RTX dosing could then be resumed 2–4 weeks after the second COVID-19 vaccination, as discussed in the next section. Those receiving RTX cycles at 4-month intervals would initiate vaccination 3 months after the prior RTX cycle. In order to follow this recommendation, the task force invoked the assumption that a patient's COVID-19 risk was low or able to be mitigated by preventive health measures. The rationale for this recommendation comes from a study demonstrating minimal response to influenza vaccination in 11 patients vaccinated 4–8 weeks after RTX treatment, with modestly restored responses in patients vaccinated 6–10 months after their last RTX dose (94), as well as data demonstrating that B cell–depleting therapy greatly attenuates the response to COVID-19 vaccination (95).

As the second statement for which consensus was not achieved, the panel was uncertain about whether to delay vaccination if an AIIRD patient was receiving glucocorticoids at a prednisone-equivalent dose of ≥20 mg per day. Controversy stemmed as to whether vaccine response might be blunted in this circumstance, which may relate to the glucocorticoids themselves or to the presumably high disease activity and severity (96,97). Other factors discussed included the disease being treated and the medical management considerations if the patient were to manifest systemic reactogenicity (e.g., persistent high fever). Concern regarding an attenuated response to the vaccine in this circumstance would be partially mitigated if there was a possibility to later order serologies or other laboratory tests, and clinicians were able to assess vaccine-induced immunity and administer a booster or revaccinate if needed. However, such laboratory-based correlates of protection are not currently available.

Use and timing of immunomodulatory therapies in relation to COVID-19 vaccination administration. The task force continued to update its literature review through October 2021 and selectively beyond that cutoff date based on content importance, including published information regarding the immunogenicity and safety of primary vaccination in RMD patients (70,71,98) and the literature on supplemental/booster vaccine dosing in non-RMD patients (99,100). Considering the goal to align guidance for recommendations related to primary vaccination, additional primary vaccination, and booster dosing to facilitate ease of implementation, the task force harmonized their recommendations for the use and timing of immunomodulatory therapies related to all vaccine administrations. Updated recommendations are shown in Table 4.

Based on some evidence that immunosuppressive therapies may attenuate vaccine response (70,101–103), for abatacept, belimumab, and most conventional (e.g., mycophenolate mofetil,

Table 4. Guidance related to the use and timing of immunomodulatory therapies in relation to COVID-19 vaccination administration in RMD patients*

Medication(s)	Timing considerations for immunomodulatory therapy and vaccination	Level of task force consensus
Abatacept (IV)	Time vaccination to occur 1 week prior to the next dose of abatacept (IV).	Moderate
Abatacept (SC)	Withhold for 1–2 weeks (as disease activity allows) after each COVID-19 vaccine dose.	Moderate
Acetaminophen, NSAIDs	Assuming that disease is stable, withhold for 24 hours prior to vaccination. No restrictions on use post vaccination to once symptoms develop.	Moderate
Belimumab (SC)	Withhold for 1–2 weeks (as disease activity allows) after each COVID-19 vaccine dose.	Moderate
TNFi, IL-6R, IL-1R, IL-17, IL-12/23, IL-23, and other cytokine inhibitors†	The task force failed to reach consensus on whether or not to temporarily interrupt these following each COVID-19 vaccine dose, including both primary vaccination and supplemental/booster dosing.	Moderate
Cyclophosphamide (IV)	Time cyclophosphamide administration so that it will occur ~1 week after each vaccine dose, when feasible.	Moderate
HcQ, **IVIG**	No modifications to either immunomodulatory therapy or vaccination timing.	Strong (HcQ), **Moderate (IVIG)**
Rituximab or other anti-CD20 B cell–depleting agents	Discuss the optimal timing of dosing and vaccination with rheumatology provider before proceeding.‡	Moderate
All other conventional and targeted immunomodulatory or immunosuppressive medications (e.g., JAK inhibitors, MMF) except for those listed above§	Withhold for 1–2 weeks (as disease activity allows) after each COVID-19 vaccine dose.	Moderate

* This guidance applies to both primary vaccination and supplemental/booster dosing. Boldface text indicates updates that were added to the version 5 summary document early in 2022. For details on the history of updates to these guidance statements, see Supplementary Table 6, on the *Arthritis & Rheumatology* website at http://onlinelibrary.wiley.com/doi/10.1002/art.42372. RMD = rheumatic and musculoskeletal disease; IV = intravenous; SC = subcutaneous; NSAIDs = nonsteroidal antiinflammatory drugs; TNFi = tumor necrosis factor inhibitor; HcQ = hydroxychloroquine; IVIG = intravenous immunoglobulin.
† Examples of cytokine and kinase inhibitors include the following: for interleukin-6 receptor (IL-6R), sarilumab and tocilizumab; for IL-1 receptor antagonist (IL-1Ra), anakinra and canakinumab; for IL-17, ixekizumab and secukinumab; for IL-12/IL-23, ustekinumab; for IL-23, guselkumab and rizankizumab; for JAK inhibitors, tofacitinib, and upadacitinib.
‡ Some practitioners measure CD19 B cells as a tool with which to time the booster and subsequent rituximab dosing. For those who elect to dose without such information, or for whom such measurement is not available or feasible, a supplemental vaccine dose 2–4 weeks should be provided before next anticipated rituximab dose (e.g., at month 5.0 or 5.5 in patients being administered rituximab every 6 months).
§ Includes apremilast, azathioprine, calcineurin inhibitors, cyclophosphamide (oral), intravenous immunoglobulin (IVIG), leflunomide, methotrexate, JAK inhibitors (tofacitinib, upadacitinib), mycophenolate mofetil (MMF), and sulfasalazine.

MTX [104], azathioprine) and targeted (e.g., JAK inhibitor) immunomodulatory therapies, the task force recommended to withhold these for 1–2 weeks after each COVID-19 vaccine dose, assuming disease activity allows. For biologics that inhibit certain cytokines (e.g., tumor necrosis factor, interleukin-6 receptor [IL-6R], IL-1R, IL-17, IL-12/23, IL-23), the task force failed to reach consensus on whether or not to temporarily interrupt these following each COVID-19 vaccine dose. Some panel members felt that withholding treatment for 1–2 weeks was unnecessary, had minimal effect on vaccine response (70,105), and could put the patient at greater increased risk for disease to worsen. In contrast, other task force members felt that even limited evidence suggesting the possibility that these therapies could attenuate vaccine response should result in a recommendation of a temporary interruption of therapy (106,107). For that reason, no consensus was reached, and decision-making was deferred to the discretion of individual providers and patients.

Hydroxychloroquine was a notable exception, as the task force recommended that this therapy not be interrupted. Given the complexities of RTX dosing for RA, vasculitis, and other potential off-label uses (e.g., SLE), as well as the substantial literature suggesting that vaccine response is attenuated by B cell–depleting therapies (70,101,108,109), the task force recommended that patients discuss the optimal timing of RTX and other B cell–depleting therapies and vaccination timing with their rheumatology provider before proceeding. While some clinicians measure CD19 B cells and use the information to time the vaccine booster and subsequent RTX dosing, this option may not be available in community practice settings. For those who elect to dose B cell–depleting therapies without such information, or for whom such measurement is not available or feasible, additional doses of the vaccine were recommended 2–4 weeks before the next anticipated dose (e.g., at month 5.0 or 5.5 for patients on an recurring 6-month RTX dosing schedule).

Finally, based on the literature suggesting that acetaminophen and/or nonsteroidal antiinflammatory drugs may somewhat impair vaccine response (110), the task force recommended withholding these for 24 hours prior to vaccination, assuming that

Table 5. Research agenda for future COVID-19 vaccine studies in RMD patients proposed by the task force*

Conduct clinical efficacy and laboratory-based immunogenicity studies in RMD patients following vaccination, especially for AIIRD patients receiving certain immunomodulatory therapies (e.g., methotrexate, abatacept, JAK inhibitors, rituximab, mycophenolate, GCs).
Optimize response to primary vaccination and supplemental/booster dose by considering timing related to intentional short-term cessation of certain immunomodulatory therapies (e.g., methotrexate, subcutaneous abatacept, JAK inhibitors, mycophenolate) to optimize vaccine response.
Evaluate risk of disease flare, disease worsening, and systemic reactogenicity following COVID-19 vaccination in RMD patients, by disease and in relation to background immunomodulatory therapies.
Directly compare vaccines and vaccine platforms for the above efficacy, immunogenicity, and safety outcomes: notable given the potential for some COVID-19 vaccines to achieve the minimum threshold for the FDA's EUA yet have seemingly lower vaccine efficacy based on large clinical trials in non-RMD patients.
Conduct long-term follow-up for durability and magnitude of vaccine protection in relation to various immunomodulatory medications, and as new SARS–CoV-2 strains emerge.
Assess benefits and timing of additional COVID-19 vaccine administration (i.e., booster doses).
Generate real-world evidence (e.g., large pragmatic trial or observational studies) embedded in routine clinical practice to study the above topics, especially to promote large-scale safety surveillance.
Establish a biorepository with associated clinical data infrastructure to facilitate future COVID-19 (and possibly other) vaccine-related research in RMD patients, considering the future potential to identify laboratory-based correlates of protection relevant for individual patients.
Identify laboratory-based serologic testing to identify patients with a suboptimal response to COVID-19 vaccination who might be candidates for additional booster doses or need to repeat the vaccination series.
Evaluate the impact of coadministration of the COVID-19 vaccine given concurrently with other, non–live-virus vaccines (e.g., shingles, influenza, pneumococcal) on vaccine immunogenicity and tolerability.
Optimize approaches to address vaccine hesitancy for high-risk RMD patients who are reticent or unwilling to undergo vaccination, with particular attention to vulnerable populations (e.g., underrepresented racial/ethnic groups).
Identify COVID-19 vaccine–induced immune parameters (immunogen-specific neutralizing antibody levels, total immunogen-specific antibody levels or isotypes, T cell immunity, innate immunity) or host determinants that are predictive of successful host response to vaccine, as reflected by protection from infection or mitigation of morbidity during subsequent infection.
Conduct large epidemiology studies of COVID-19 outcomes (e.g., using large administrative databases of health plans, electronic health record data [e.g., the ACR RISE registry], or other data sources or methods) and examine the role of AIIRD disease features, treatments, and vaccination. While risk factors for incident disease may be shaped by confounding and unmeasured variability in exposure, examining outcomes conditioning on incident COVID-19 diagnosis may be more fruitful.

* RMD = rheumatic and musculoskeletal disease; AIIRD = autoimmune and inflammatory rheumatic disease; GCs = glucocorticoids; FDA = US Food and Drug Administration; EUA = Emergency Use Authorization; ACR = American College of Rheumatology; RISE = Rheumatology Informatics System for Effectiveness.

disease is stable. There was no prohibition against their use in patients who experience local or systematic symptoms postvaccination (49).

As an outgrowth of the evidence report, the task force assembled a research agenda where evidence was lacking (Table 5). Given that there was little direct evidence in any RMD population, the topics were broad and spanned domains related to clinical effectiveness, safety, flare, reactogenicity, study design, immunogenicity, and laboratory-based correlates of protection. With the relatively small size of the task force, no attempt was made to prioritize these topics given the expectation that they would evolve over time and as new science in non-RMD populations was forthcoming.

DISCUSSION

This ACR guidance encompasses the optimal use of COVID-19 vaccines, including supplemental/booster dosing, for patients with rheumatic and musculoskeletal diseases. It is intended to aid in the care of individual patients but not to supplant personalized care or constrain shared decision-making with patients. The mRNA vaccine platform is novel, and considerations for vaccines developed on this platform may differ from those relevant to other vaccines. The guidance regarding the use and timing of immunomodulatory medications was often based on extrapolation of the available evidence of their immunologic effects as they relate to other vaccines and vaccine platforms. As such, all of these recommendations are considered conditional. Finally, the task force advised health care providers to avoid being overly dogmatic in following these recommendations. The attempt to optimize vaccine response in relation to the use and timing of immunosuppressive medications should not compromise a willing patient's ability to undergo vaccination in a timely manner and risk a missed vaccination opportunity.

As an overarching principle, the sparsity of information regarding COVID-19 vaccination in RMD patients yielded a need for extrapolation based on the literature published for other vaccines. The evidence base was, therefore, of low or very low quality and suffered from indirectness (12) in almost all respects. The guidance provided herein represents a balance between evidence regarding efficacy, effectiveness, safety, feasibility (e.g., withholding a therapy with a long half-life or extended recirculation like leflunomide may be unrealistic), expected vaccine availability, and tradeoffs in resource utilization. For example, vigorous debate was held about whether it was preferable to vaccinate a high-risk patient in a suboptimal circumstance (e.g., active disease, receiving high-dose glucocorticoids, receiving cytotoxic therapy), under the assumption that the vaccine would confer at least some protection to a patient at high risk for a poor outcome if they contract COVID-19. Or rather, might it be preferable to wait until a more optimal circumstance presented itself? However, given the uncertainty in most medical settings to predict the future course of a patient's AIIRD

or the need for additional immunomodulatory treatments, a more salutary setting to optimize vaccine response might never materialize. Thus, the task force typically favored proceeding more immediately with vaccination.

The strengths of this effort are notable given the need presented by the availability of new COVID-19 vaccines and critical questions about how to best use those vaccines for RMD patients. The task force generated an evidence summary over a very compressed time frame and leveraged a well-established consensus methodology process used previously by the ACR. Of high importance, the task force's composition included experts in rheumatology, infectious disease, and public health, representing a plurality of different stakeholder perspectives.

Regarding important limitations, our ability to generalize from the literature for other vaccines and vaccine platforms in RMD patients to the novel COVID-19 vaccines now available in the US is limited. Vaccination against SARS–CoV-2 raises different issues than those for other vaccine-preventable illnesses, given the potential for ongoing public health measures to partially mitigate exposure. This guidance therefore must be interpreted by clinicians and patients in light of underlying principles rather than considering them either prescriptive or proscriptive. For example, an AIIRD patient with minimal public contact who is able to strongly adhere to all preventive health measures might choose to withhold RMD treatments or briefly defer vaccination in accordance with this guidance, whereas this same decision may not be possible for a patient employed in a high-risk setting (e.g., front-line health care, or long-term care facility). From a vaccine policy and recommendation context, the task force prioritized simplicity, noting that this guidance would be expected to apply to the care of most RMD patients in most settings.

Finally, the procedures used to develop this guidance did not follow the rigorous methodology routinely used by the ACR when formal clinical practice guidelines are created, although they were adherent to the ACR standardized operating procedures for guidance documents (13). This was an expected limitation given the accelerated time frame desired by the ACR to issue practical and timely recommendations both to its membership and to the rheumatology community. Once the urgency of the pandemic has passed, the work of this task force will eventually be folded back under the aegis of the broader ACR vaccine guideline development group, charged with covering this and all other vaccines in the context of RMDs, and the more typical guideline development process favored by the ACR will be applied. Additional and important input from other stakeholders, including patients and patient advocates, will also be sought, as the ACR has done for past clinical practice guidelines (6). At present, and given the continued evolution in the literature for immunosuppressed individuals with respect to SARS–CoV-2 vaccination, embedding COVID vaccination guidelines into the more traditional ACR guideline process is not expected until 2024 or beyond.

Note that these revisions predated the EUA for the Novavax COVID-19 vaccine in the US and the availability of the monkeypox vaccine. As new safety and efficacy evidence becomes available for COVID-19 vaccines in patients with RMDs and AIIRDs, the ACR's guidance document will continue to be updated and expanded, consistent with the notion of a "living document." The need for future updates will be routinely assessed by the ACR, this task force, and the larger ACR guideline development group; they will do this by considering publications and evidence generated by the literature and public health agencies. The ACR is committed to maintaining this process throughout the pandemic to facilitate evidence-based practice and promote optimal outcomes for all patients with RMDs and AIIRDs with respect to mitigating COVID-19 risk.

ACKNOWLEDGMENTS

The task force would like to thank Regina Parker (ACR) for her role in coordinating the activities of the Task Force.

AUTHOR CONTRIBUTIONS

All authors were involved in drafting the article or revising it critically for important intellectual content, and all authors approved the final version to be published. Dr. Curtis had full access to all of the data in the study and takes responsibility for the integrity of the data and the accuracy of the data analysis.

Study conception and design. Curtis, Johnson, Anthony, Arasaratnam, Baden, Bass, Calabrese, Gravallese, Harpaz, Kroger, Sadun, Turner, Williams, Mikuls.

Acquisition of data. Curtis, Johnson, Anthony, Arasaratnam, Baden, Bass, Calabrese, Gravallese, Harpaz, Kroger, Sadun, Turner, Williams, Mikuls.

Analysis and interpretation of data. Curtis, Johnson, Anthony, Arasaratnam, Baden, Bass, Calabrese, Gravallese, Harpaz, Kroger, Sadun, Turner, Williams, Mikuls.

REFERENCES

1. Van der Heijde D, Daikh DI, Betteridge N, Burmester GR, Hassett AL, Matteson EL, et al. Common language description of the term rheumatic and musculoskeletal diseases (RMDs) for use in communication with the lay public, healthcare providers, and other stakeholders endorsed by the European League Against Rheumatism (EULAR) and the American College of Rheumatology (ACR). Arthritis Rheumatol 2018;70:826–31.
2. Mikuls TR, Johnson SR, Fraenkel L, Arasaratnam RJ, Baden LR, Bermas BL, et al. American College of Rheumatology guidance for the management of rheumatic disease in adult patients during the COVID-19 pandemic: version 3. Arthritis Rheumatol 2021;73:e1–12.
3. US Food and Drug Administration. Vaccines and Related Biological Products Advisory Committee meeting: FDA briefing document Pfizer-BioNTech COVID-19 vaccine. December 2020. URL: https://www.fda.gov/media/144245/download.
4. US Food and Drug Administration. Vaccines and Related Biological Products Advisory Committee meeting: FDA briefing document Moderna COVID-19 vaccine. December 2020. URL: https://www.fda.gov/media/144434/download.
5. Singh JA, Furst DE, Bharat A, Curtis JR, Kavanaugh AF, Kremer JM, et al. 2012 update of the 2008 American College of Rheumatology

recommendations for the use of disease-modifying antirheumatic drugs and biologic agents in the treatment of rheumatoid arthritis. Arthritis Care Res (Hoboken) 2012;64:625–39.

6. Singh JA, Saag KG, Bridges SL Jr, Akl EA, Bannuru RR, Sullivan MC, et al. 2015 American College of Rheumatology guideline for the treatment of rheumatoid arthritis. Arthritis Rheumatol 2016; 68:1–26.
7. Fraenkel L, Bathon JM, England BR, St. Clair EW, Arayssi T, Carandang K, et al. 2021 American College of Rheumatology guideline for the treatment of rheumatoid arthritis. Arthritis Rheumatol 2021;73:1108–23.
8. Singh JA, Guyatt G, Ogdie A, Gladman DD, Deal C, Deodhar A, et al. 2018 American College of Rheumatology/National Psoriasis Foundation guideline for the treatment of psoriatic arthritis. Arthritis Rheumatol 2019;71:5–32.
9. Furer V, Rondaan C, Heijstek MW, Agmon-Levin N, van Assen S, Bijl M, et al. 2019 update of EULAR recommendations for vaccination in adult patients with autoimmune inflammatory rheumatic diseases. Ann Rheum Dis 2020;79:39–52.
10. Rondaan C, Furer V, Heijstek MW, Agmon-Levin N, Bijl M, Breedveld FC, et al. Efficacy, immunogenicity and safety of vaccination in adult patients with autoimmune inflammatory rheumatic diseases: a systematic literature review for the 2019 update of EULAR recommendations. RMD Open 2019;5:e001035.
11. Van Assen S, Agmon-Levin N, Elkayam O, Cervera R, Doran MF, Dougados M, et al. EULAR recommendations for vaccination in adult patients with autoimmune inflammatory rheumatic diseases. Ann Rheum Dis 2011;70:414–22.
12. Guyatt GH, Oxman AD, Kunz R, Woodcock J, Brozek J, Helfand M, et al. GRADE guidelines: 8. Rating the quality of evidence–indirectness. J Clin Epidemiol 2011;64:1303–10.
13. American College of Rheumatology. American College of Rheumatology Guidance Subcommittee and Endorsement of Guidance Documents, 2020. URL: https://www.rheumatology.org/Portals/0/Files/ACR-Guidance-Subcommittee-Processes-Framework.pdf.
14. Fitch K, Bernstein SJ, Aguilar MD, Burnand B, LaCalle JR, Lazaro P, et al. The RAND/UCLA appropriateness method user's manual. Santa Monica (CA): RAND; 2001.
15. American College of Rheumatology. COVID-19 guidance. URL: https://www.rheumatology.org/Practice-Quality/Clinical-Support/COVID-19-Guidance.
16. Moderna TX, sponsor. A study to evaluate the safety, reactogenicity, and effectiveness of mRNA-1273 vaccine in adolescents 12 to <18 years old to prevent COVID-19 (TeenCove). ClinicalTrials.gov identifier: NCT04649151.
17. BioNTech SE and Pfizer, sponsors. Study to describe the safety, tolerability, immunogenicity, and efficacy of RNA vaccine candidates against COVID-19 in healthy individuals. ClinicalTrials.gov identifier: NCT04368728.
18. Centers for Disease Control and Prevention. Pfizer-BioNTech COVID-19 vaccine (5 through 11 years of age). February 2022. https://www.cdc.gov/vaccines/covid-19/info-by-product/pfizer/pfizer-bioNTech-children-adolescents.html.
19. Walter E, Talaat K, Sabharwal C, Gurtman A, Lockhart S, Paulsen G, et al. Evaluation of the BNT162b2 COVID-19 vaccine in children 5 to 11 years of age. N Engl J Med 2022;386:35–46.
20. Rubin LG, Levin MJ, Ljungman P, Davies EG, Avery R, Tomblyn M, et al. 2013 IDSA clinical practice guideline for vaccination of the immunocompromised host. Clin Infect Dis 2014;58:e44–100.
21. Rubin LG, Levin MJ, Ljungman P, Davies EG, Avery R, Tomblyn M, et al. 2013 IDSA clinical practice guideline for vaccination of the immunocompromised host. Clin Infect Dis 2014;58:309–18.
22. Blumentals WA, Arreglado A, Napalkov P, Toovey S. Rheumatoid arthritis and the incidence of influenza and influenza-related complications: a retrospective cohort study. BMC Musculoskelet Disord 2012;13:158.
23. Van Assen S, Elkayam O, Agmon-Levin N, Cervera R, Doran MF, Dougados M, et al. Vaccination in adult patients with auto-immune inflammatory rheumatic diseases: a systematic literature review for the European League Against Rheumatism evidence-based recommendations for vaccination in adult patients with auto-immune inflammatory rheumatic diseases [review]. Autoimmun Rev 2011; 10:341–52.
24. Yun H, Yang S, Chen L, Xie F, Winthrop K, Baddley JW, et al. Risk of herpes zoster in autoimmune and inflammatory diseases: implications for vaccination. Arthritis Rheumatol 2016;68:2328–37.
25. Cordtz R, Lindhardsen J, Soussi BG, Vela J, Uhrenholt L, Westermann R, et al. Incidence and severeness of COVID-19 hospitalisation in patients with inflammatory rheumatic disease: a nationwide cohort study from Denmark. Rheumatology (Oxford) 2020 doi: https://doi.org/10.1093/rheumatology/keaa897. E-pub ahead of print.
26. Williamson EJ, Walker AJ, Bhaskaran K, Bacon S, Bates C, Morton CE, et al. Factors associated with COVID-19-related death using OpenSAFELY. Nature 2020;584:430–6.
27. D'silva KM, Jorge A, Cohen A, McCormick N, Zhang Y, Wallace ZS, et al. COVID-19 outcomes in patients with systemic autoimmune rheumatic diseases compared to the general population: a US multicenter, comparative cohort study. Arthritis Rheumatol 2021;73: 914–20.
28. Topless R, Phipps-Green A, Leask M, Dalbeth N, Stamp LK, Robinson P, et al. Gout, rheumatoid arthritis and the risk of death from COVID-19: an analysis of the UK Biobank. ACR Open Rheumatol 2021;3:333–40.
29. Eder L, Croxford R, Drucker A, Mendel A, Kuriya B, Touma Z, et al. COVID-19 hospitalizations, ICU admission, and death among patients with immune mediated inflammatory diseases (IMID) - a population based study [abstract]. Ann Rheum Dis 2021;80 Suppl 1:173.
30. Zhou F, Yu T, Du R, Fan G, Liu Y, Liu Z, et al. Clinical course and risk factors for mortality of adult inpatients with COVID-19 in Wuhan, China: a retrospective cohort study. Lancet 2020;395:1054–62.
31. Wu C, Chen X, Cai Y, Xia J, Zhou X, Xu S, et al. Risk factors associated with acute respiratory distress syndrome and death in patients with coronavirus disease 2019 pneumonia in Wuhan, China. JAMA Intern Med 2020;180:934–43.
32. Gianfrancesco MA, Leykina LA, Izadi Z, Taylor T, Sparks JA, Harrison C, et al. Association of race and ethnicity with COVID-19 outcomes in rheumatic disease: data from the COVID-19 Global Rheumatology Alliance physician registry. Arthritis Rheumatol 2021; 73:374–80.
33. Strangfeld A, Schäfer M, Gianfrancesco MA, Lawson-Tovey S, Liew JW, Ljung L, et al. Factors associated with COVID-19-related death in people with rheumatic diseases: results from the COVID-19 Global Rheumatology Alliance physician-reported registry. Ann Rheum Dis 2021;80:930–42.
34. Gianfrancesco M, Hyrich KL, Al-Adely S, Carmona L, Danila MI, Gossec L, et al. Characteristics associated with hospitalisation for COVID-19 in people with rheumatic disease: data from the COVID-19 Global Rheumatology Alliance physician-reported registry. Ann Rheum Dis 2020;79:859–66.
35. Ungaro RC, Agrawal M, Park S, Hirten R, Colombel JF, Twyman K, et al. Autoimmune and chronic inflammatory disease patients with COVID-19. ACR Open Rheumatol 2021;3:111–5.
36. Choi B, Choudhary MC, Regan J, Sparks JA, Padera RF, Qiu X, et al. Persistence and evolution of SARS-CoV-2 in an immunocompromised host [letter]. N Engl J Med 2020;383:2291–3.

37. Centers for Disease Control and Prevention. Vaccine recommendations and guidelines of the ACIP: COVID-19 vaccine recommendations. March 2021. URL: https://www.cdc.gov/vaccines/hcp/acip-recs/vacc-specific/covid-19.html.
38. Centers for Disease Control and Prevention. Vaccines and immunizations: Interim considerations—preparing for the potential management of anaphylaxis after COVID-19. vaccination. March 2021. URL: https://www.cdc.gov/vaccines/covid-19/clinical-considerations/managing-anaphylaxis.html?CDC_AA_refVal=https%3A%2F%2Fwww.cdc.gov%2Fvaccines%2Fcovid-19%2Finfo-by-product%2Fpfizer%2Fanaphylaxis-management.html.
39. Yun H, Xie F, Baddley JW, Winthrop K, Saag KG, Curtis JR. Long-term effectiveness of herpes zoster vaccine among patients with autoimmune and inflammatory diseases. J Rheumatol 2017;44:1083–7.
40. Park JK, Lee YJ, Shin K, Ha YJ, Lee EY, Song YW, et al. Impact of temporary methotrexate discontinuation for 2 weeks on immunogenicity of seasonal influenza vaccination in patients with rheumatoid arthritis: a randomised clinical trial. Ann Rheum Dis 2018;77:898–904.
41. Van der Maas A, Lie E, Christensen R, Choy E, de Man YA, van Riel P, et al. Construct and criterion validity of several proposed DAS28-based rheumatoid arthritis flare criteria: an OMERACT cohort validation study. Ann Rheum Dis 2013;72:1800–5.
42. Park JK, Kim MJ, Choi Y, Winthrop K, Song YW, Lee EB. Effect of short-term methotrexate discontinuation on rheumatoid arthritis disease activity: post-hoc analysis of two randomized trials. Clin Rheumatol 2020;39:375–9.
43. Park JK, Choi Y, Winthrop KL, Song YW, Lee EB. Optimal time between the last methotrexate administration and seasonal influenza vaccination in rheumatoid arthritis: post hoc analysis of a randomised clinical trial [letter]. Ann Rheum Dis 2019;78:1283–4.
44. Park JK, Lee MA, Lee EY, Song YW, Choi Y, Winthrop KL, et al. Effect of methotrexate discontinuation on efficacy of seasonal influenza vaccination in patients with rheumatoid arthritis: a randomised clinical trial. Ann Rheum Dis 2017;76:1559–65.
45. Oda R, Inagaki T, Ishikane M, Hotta M, Shimomura A, Sato M, et al. Case of adult large vessel vasculitis after SARS-CoV-2 infection [letter]. Ann Rheum Dis 2020 doi: https://doi.org/10.1136/annrheumdis-2020-218440. E-pub ahead of print.
46. Perrot L, Hemon M, Busnel JM, Muis-Pistor O, Picard C, Zandotti C, et al. First flare of ACPA-positive rheumatoid arthritis after SARS-CoV-2 infection. Lancet Rheumatol 2021;3:e6–8.
47. Centers for Disease Control and Prevention. COVID-19 vaccines for people who are moderately or severely immunocompromised. September 2022. URL: https://www.cdc.gov/coronavirus/2019-ncov/vaccines/recommendations/immuno.html.
48. Baden LR, Walsh SR, Seaman MS, Tucker RP, Krause KH, Patel A, et al. First-in-human evaluation of the safety and immunogenicity of a recombinant adenovirus serotype 26 HIV-1 Env vaccine (IPCAVD 001). J Infect Dis 2013;207:240–7.
49. Centers for Disease Control and Prevention. Vaccines and immunizations: interim clinical considerations for use of COVID-19 vaccines currently authorized in the United States. July 16, 2021. URL: https://www.cdc.gov/vaccines/covid-19/info-by-product/clinical-considerations.html.
50. Centers for Disease Control and Prevention. Stay up to date with COVID-19 Vaccines including boosters. September 2022. URL: https://www.cdc.gov/coronavirus/2019-ncov/vaccines/booster-shot.html.
51. Khan N, Mahmud N. Effectiveness of SARS-CoV-2 vaccination in a Veterans Affairs cohort of patients with inflammatory bowel disease with diverse exposure to immunosuppressive medications. Gastroenterology 2021;161:827–36.
52. Boyarsky BJ, Werbel WA, Avery RK, Tobian AAR, Massie AB, Segev DL, et al. Antibody response to 2-dose SARS-CoV-2 mRNA vaccine series in solid organ transplant recipients. JAMA 2021;325:2204–6.
53. Boyarsky BJ, Ruddy JA, Connolly CM, Ou MT, Werbel WA, Garonzik-Wang JM, et al. Antibody response to a single dose of SARS-CoV-2 mRNA vaccine in patients with rheumatic and musculoskeletal diseases. Ann Rheum Dis 2021 doi: 10.1136/annrheumdis-2021-220289. E-pub of print.
54. Hall VG, Ferreira VH, Ku T, Ierullo M, Majchrzak-Kita B, Chaparro C, et al. Randomized trial of a third dose of mRNA-1273 vaccine in transplant recipients. N Engl J Med 2021;385:1244–6.
55. Centers for Disease Control and Prevention. Science brief: COVID-19 vaccines and vaccination 2021. September 2021. URL: https://www.cdc.gov/coronavirus/2019-ncov/science/science-briefs/fully-vaccinated-people.html.
56. Pegu A, O'Connell SE, Schmidt SD, O'Dell S, Talana CA, Lai L, et al. Durability of mRNA-1273 vaccine-induced antibodies against SARS–CoV-2 variants. Science 2021;373:1372–7.
57. Wu K, Choi A, Koch M, LingZhi M, Hill A, Nunna N, et al. Preliminary analysis of safety and immunogenicity of a SARS–CoV-2 variant vaccine booster [preprint]. medRxiv 2021.
58. Tenforde MW, Self WH, Naioti EA, Ginde AA, Douin DJ, Olson SM, et al. Sustained effectiveness of Pfizer-BioNTech and Moderna vaccines against COVID-19 associated hospitalizations among adults - United States, March-July 2021. MMWR Morb Mortal Wkly Rep 2021;70:1156–62.
59. Mizrahi B, Lotan R, Kalkstein N, Peretz A, Perez G, Ben-Tov A, et al. Correlation of SARS-CoV-2-breakthrough infections to time-from-vaccine. Nat Commun 2021;12:6379.
60. Thompson MG, Burgess JL, Naleway AL, Tyner H, Yoon SK, Meece J, et al. Prevention and attenuation of Covid-19 with the BNT162b2 and mRNA-1273 vaccines. N Engl J Med 2021;385:320–9.
61. Kustin T, Harel N, Finkel U, Perchik S, Harari S, Tahor M, et al. Evidence for increased breakthrough rates of SARS-CoV-2 variants of concern in BNT162b2-mRNA-vaccinated individuals. Nature Med 2021;27:1379–84.
62. Atmar RL, Lyke KE, Deming ME, Jackson LA, Branche AR, El Sahly HM, et al. Heterologous SARS-CoV-2 booster vaccinations - preliminary report [preprint]. medRxiv 2021.
63. Behrens GM, Cossmann A, Stankov MV, Nehlmeier I, Kempf A, Hoffmann M, et al. SARS-CoV-2 delta variant neutralisation after heterologous ChAdOx1-S/BNT162b2 vaccination. Lancet 2021;398:1041–2.
64. Borobia AM, Carcas AJ, Pérez-Olmeda M, Castaño L, Bertran MJ, García-Pérez J, et al. Immunogenicity and reactogenicity of BNT162b2 booster in ChAdOx1-S-primed participants (Com-VacS): a multicentre, open-label, randomised, controlled, phase 2 trial. Lancet 2021;398:121–30.
65. Normark J, Vikström L, Gwon YD, Persson IL, Edin A, Björsell T, et al. Heterologous ChAdOx1 nCoV-19 and mRNA-1273 vaccination. N Engl J Med 2021;385:1049–51.
66. Rose R, Neumann F, Grobe N, Lorentz T, Fickenscher HK, A. Heterologous immunisation with vector vaccine as prime followed by mRNA vaccine as boost leads to humoral immune response against SARS-CoV-2, which is comparable to that according to a homologous mRNA vaccination scheme [preprint]. medRxiv 2021.
67. Groß R, Zanoni M, Seidel A, Conzelmann, C., Gilg A, Krnavek D, Erdemci-Evin S, et al. Heterologous ChAdOx1 nCoV-19 and BNT162b2 prime-boost vaccination elicits potent neutralizing antibody responses and T cell reactivity against prevalent SARS–CoV-2 variants. EBioMedicine 2022;75:103761.

68. Schmidt T, Klemis V, Schub D, Mihm J, Hielscher F, Marx S, et al. Immunogenicity and reactogenicity of heterologous ChAdOx1 nCoV-19/mRNA vaccination. Nat Med 2021;27:1530–5.
69. Barros-Martins J, Hammerschmidt SI, Cossmann A, Odak I, Stankov MV, Morillas Ramos G, et al. Immune responses against SARS-CoV-2 variants after heterologous and homologous ChAdOx1 nCoV-19/BNT162b2 vaccination. Nat Med 2021;27:1525–9.
70. Furer V, Eviatar T, Zisman D, Peleg H, Paran D, Levartovsky D, et al. Immunogenicity and safety of the BNT162b2 mRNA COVID-19 vaccine in adult patients with autoimmune inflammatory rheumatic diseases and in the general population: a multicentre study. Ann Rheum Dis 2021;80:1330–8.
71. Felten R, Kawka L, Dubois M, Ugarte-Gil MF, Fuentes-Silva Y, Piga M, et al. Tolerance of COVID-19 vaccination in patients with systemic lupus erythematosus: the international VACOLUP study. Lancet Rheumatol 2021;3:e613–5.
72. Papagoras C, Fragoulis GE, Zioga N, Simopoulou T, Deftereou K, Kalavri E, et al. Better outcomes of COVID-19 in vaccinated compared to unvaccinated patients with systemic rheumatic diseases. Ann Rheum Dis 2021 doi:10.1136/annrheumdis-2021-221539. E-pub ahead of print.
73. Centers for Disease Control and Prevention. Effectiveness of BNT162b2 (Pfizer-BioNTech) mRNA vaccination against multisystem inflammatory syndrome in children among persons aged 12–18 years — United States, July. December 2021. URL: https://www.cdc.gov/mmwr/volumes/71/wr/mm7102e1.htm.
74. Wisniewski M, Chun A, Volpi S, Muscal E, Sexson Tejtel SK, Munoz F, Vogel TP. Outcomes after SARS-CoV-2 vaccination among children with a history of multisystem inflammatory syndrome. JAMA Netw Open 2022;5:e224750.
75. Centers for Disease Control and Prevention. Interim clinical considerations for use of COVID-19 vaccines currently approved or authorized in the United States. September 2022. URL: https://www.cdc.gov/vaccines/covid-19/clinical-considerations/interim-considerations-us.html#covid19-vaccination-misc-mis.
76. Elkayam O, Amir S, Mendelson E, Schwaber M, Grotto I, Wollman J, et al. Efficacy and safety of vaccination against pandemic 2009 influenza A (H1N1) virus among patients with rheumatic diseases. Arthritis Care Res (Hoboken) 2011;63:1062–7.
77. Battafarano DF, Battafarano NJ, Larsen L, Dyer PD, Older SA, Muehlbauer S, et al. Antigen-specific antibody responses in lupus patients following immunization. Arthritis Rheum 1998;41:1828–34.
78. Mok CC, Ho LY, Fong LS, To CH. Immunogenicity and safety of a quadrivalent human papillomavirus vaccine in patients with systemic lupus erythematosus: a case–control study. Ann Rheum Dis 2013;72:659–64.
79. Bingham CO III, Rizzo W, Kivitz A, Hassanali A, Upmanyu R, Klearman M. Humoral immune response to vaccines in patients with rheumatoid arthritis treated with tocilizumab: results of a randomised controlled trial (VISARA). Ann Rheum Dis 2015;74:818–22.
80. Mori S, Ueki Y, Akeda Y, Hirakata N, Oribe M, Shiohira Y, et al. Pneumococcal polysaccharide vaccination in rheumatoid arthritis patients receiving tocilizumab therapy. Ann Rheum Dis 2013;72:1362–6.
81. Mori S, Ueki Y, Hirakata N, Oribe M, Hidaka T, Oishi K. Impact of tocilizumab therapy on antibody response to influenza vaccine in patients with rheumatoid arthritis. Ann Rheum Dis 2012;71:2006–10.
82. Sahin U, Muik A, Derhovanessian E, Vogler I, Kranz LM, Vormehr M, et al. COVID-19 vaccine BNT162b1 elicits human antibody and TH1 T cell responses. Nature 2020;586:594–9.
83. Tsuru T, Terao K, Murakami M, Matsutani T, Suzaki M, Amamoto T, et al. Immune response to influenza vaccine and pneumococcal polysaccharide vaccine under IL-6 signal inhibition therapy with tocilizumab. Mod Rheumatol 2014;24:511–6.
84. Migita K, Akeda Y, Akazawa M, Tohma S, Hirano F, Ideguchi H, et al. Pneumococcal polysaccharide vaccination in rheumatoid arthritis patients receiving tacrolimus. Arthritis Res Ther 2015;17:149.
85. Doornekamp L, Goetgebuer RL, Schmitz KS, Goeijenbier M, van der Woude CJ, Fouchier R, et al. High immunogenicity to influenza vaccination in Crohn's disease patients treated with ustekinumab. Vaccines (Basel) 2020;8:455.
86. Furer V, Rondaan C, Heijstek M, van Assen S, Bijl M, Agmon-Levin N, et al. Incidence and prevalence of vaccine preventable infections in adult patients with autoimmune inflammatory rheumatic diseases (AIIRD): a systemic literature review informing the 2019 update of the EULAR recommendations for vaccination in adult patients with AIIRD. RMD Open 2019;5:e001041.
87. Furer V, Zisman D, Kaufman I, Arad U, Berman M, Sarbagil-Maman H, et al. Immunogenicity and safety of vaccination against seasonal influenza vaccine in patients with psoriatic arthritis treated with secukinumab. Vaccine 2020;38:847–51.
88. Richi P, Martín MD, de Ory F, Gutiérrez-Larraya R, Casas I, Jiménez-Díaz AM, et al. Secukinumab does not impair the immunogenic response to the influenza vaccine in patients. RMD Open 2019;5:e001018.
89. Bar-Or A, Calkwood JC, Chognot C, Evershed J, Fox EJ, Herman A, et al. Effect of ocrelizumab on vaccine responses in patients with multiple sclerosis: the VELOCE study. Neurology 2020;95:e1999–2008.
90. Nazi I, Kelton JG, Larche M, Snider DP, Heddle NM, Crowther MA, et al. The effect of rituximab on vaccine responses in patients with immune thrombocytopenia. Blood 2013;122:1946–53.
91. Houot R, Levy R, Cartron G, Armand P. Could anti-CD20 therapy jeopardise the efficacy of a SARS-CoV-2 vaccine? Eur J Cancer 2020;136:4–6.
92. Baker D, Roberts CA, Pryce G, Kang AS, Marta M, Reyes S, et al. COVID-19 vaccine-readiness for anti-CD20-depleting therapy in autoimmune diseases [review]. Clin Exp Immunol 2020;202:149–61.
93. Hua C, Barnetche T, Combe B, Morel J. Effect of methotrexate, anti–tumor necrosis factor α, and rituximab on the immune response to influenza and pneumococcal vaccines in patients with rheumatoid arthritis: a systematic review and meta-analysis. Arthritis Care Res (Hoboken) 2014;66:1016–26.
94. Van Assen S, Holvast A, Benne CA, Posthumus MD, van Leeuwen MA, Voskuyl AE, et al. Humoral responses after influenza vaccination are severely reduced in patients with rheumatoid arthritis treated with rituximab. Arthritis Rheum 2010;62:75–81.
95. Paley MA, Deepak P, Kim W, Yang M, Carividi A, Demissie EG, et al. Immunosuppression attenuates antibody and neutralization titers in patients with chronic inflammatory disease following SARS-CoV-2 vaccination [abstract]. Arthritis Rheumatol 2021;73 Suppl:S945–7.
96. Aikawa NE, Campos LM, Silva CA, Carvalho JF, Saad CG, Trudes G, et al. Glucocorticoid: major factor for reduced immunogenicity of 2009 influenza A (H1N1) vaccine in patients with juvenile autoimmune rheumatic disease. J Rheumatol 2012;39:167–73.
97. Kim EY, Lim JE, Jung JY, Son JY, Lee KJ, Yoon YW, et al. Performance of the tuberculin skin test and interferon-γ release assay for detection of tuberculosis infection in immunocompromised patients in a BCG-vaccinated population. BMC Infect Dis 2009;9:207.
98. Li X, Tong X, Yeung WWY, Kuan P, Yum SHH, Chui CSL, et al. Two-dose COVID-19 vaccination and possible arthritis flare among patients with rheumatoid arthritis in Hong Kong. Ann Rheum Dis 2021 doi: 10.1136/annrheumdis-2021-221571. E-pub ahead of print.
99. Levin EG, Lustig Y, Cohen C, Fluss R, Indenbaum V, Amit S, et al. Waning immune humoral response to BNT162b2 Covid-19 vaccine over 6 months. N Engl J Med 2021;385:e84.

100. Bar-On YM, Goldberg Y, Mandel M, Bodenheimer O, Freedman L, Kalkstein N, et al. Protection of BNT162b2 vaccine booster against Covid-19 in Israel. N Engl J Med 2021;385:1393–1400.
101. Deepak P, Kim W, Paley MA, Yang M, Carvidi AB, Demissie EG, et al. Effect of immunosuppression on the immunogenicity of mRNA vaccines to SARS-CoV-2: a prospective cohort study. Ann Intern Med 2021;174:1572–85.
102. Prendecki M, Clarke C, Edwards H, McIntyre S, Mortimer P, Gleeson S, et al. Humoral and T-cell responses to SARS-CoV-2 vaccination in patients receiving immunosuppression. Ann Rheum Dis 2021;80: 1322–9.
103. Kearns P, Siebert S, Willicombe M, Gaskell C, Kirkham A, Pirrie S, et al. Examining the immunological effects of COVID-19 vaccination in patients with conditions potentially leading to diminished immune response capacity – The OCTAVE Trial [preprint]. SSRN 2021.
104. Abhishek A, Boyton RJ, Peckham N, McKnight Á, Coates LC, Bluett J, Barber V, Cureton L, et al. VROOM study investigators. Effect of a 2-week interruption in methotrexate treatment versus continued treatment on COVID-19 booster vaccine immunity in adults with inflammatory conditions (VROOM study): a randomised, open label, superiority trial. Lancet Respir Med 2022;10:840–50.
105. Venerito V, Stefanizzi P, Fornaro M, Cacciapaglia F, Tafuri S, Perniola S, et al. Immunogenicity of BNT162b2 mRNA SARS-CoV-2 vaccine in patients with psoriatic arthritis on TNF inhibitors. RMD Open 2022; 8:e001847.
106. Connolly CM, Chiang TP, Boyarsky BJ, Ruddy JA, Teles M, Alejo JL, et al. Temporary hold of mycophenolate augments humoral response to SARS-CoV-2 vaccination in patients with rheumatic and musculoskeletal diseases: a case series. Ann Rheum Dis 2022;81:293–5.
107. Park JK, Lee YJ, Shin K, Ha YJ, Lee EY, Song YW, et al. Impact of temporary methotrexate discontinuation for 2 weeks on immunogenicity of seasonal influenza vaccination in patients with rheumatoid arthritis: a randomised clinical trial. Ann Rheum Dis 2018;77:898–904.
108. Moor MB, Suter-Riniker F, Horn MP, Aeberli D, Amsler J, Möller B, et al. Humoral and cellular responses to mRNA vaccines against SARS-CoV-2 in patients with a history of CD20 B-cell-depleting therapy (RituxiVac): an investigator-initiated, single-centre, open-label study. The Lancet Rheumatol 2021;3:e789–97.
109. Felten R, Gallais F, Schleiss C, Chatelus E, Javier RM, Pijnenburg L, et al. Cellular and humoral immunity after the third dose of SARS-CoV-2 vaccine in patients treated with rituximab. Lancet Rheumatol 2022;4:e13–6.
110. Saleh E, Moody MA, Walter EB. Effect of antipyretic analgesics on immune responses to vaccination. Hum Vaccin Immunother 2016; 12:2391–2402.

Arthritis & Rheumatology
Vol. 75, No. 1, January 2023, pp 1–3
DOI 10.1002/art.42279

American College of Rheumatology
Empowering Rheumatology Professionals

NOTES FROM THE FIELD

The Climate Emergency and the Health of Our Patients: The Role of the Rheumatologist

Paul F. Dellaripa,[1] Thomas Bush,[2] Frederick W. Miller,[3] and Candace H. Feldman[1]

The climate crisis represents an emerging threat to the health of humanity and to the health of our planet. Since the start of the Industrial Era, the average global air temperature has risen by ~1°C, due mainly to human-caused emissions of greenhouse gases related to the use of fossil fuels. The link between warming temperatures and greenhouse gas production was first described in 1896 and was confirmed by the measurement of rising atmospheric CO_2 in the late 1950s (1). Despite years of accumulating scientific evidence and the stated objectives of the United Nations Framework Convention on Climate Change, a concerted global effort to slow and decrease greenhouse gas production has lagged (2). We are now faced with the consequences of this inaction, such that the climate crisis has now become a climate emergency (2,3). Rising temperatures have led to more extreme weather events and negative health impacts, which include more frequent and severe heat waves, more wildfires with greater particulate matter (PM) exposure, prolonged allergies and asthma symptoms due to longer pollen seasons, a greater range and impact of vector-borne and other infectious diseases, and warmer oceans and rising sea levels leading to more severe storms (2,4). These changes, along with worsening droughts and flooding, can lead to food insecurity, population displacement, increased psychological stress and mental health disorders, and civil unrest.

As health care professionals and as rheumatologists, specifically, we must understand that the emerging effects of this climate emergency represent a public health crisis that will affect the health of our patients. Thus, we must prepare ourselves and our patients with rheumatic disease to adapt to our changing environment. As concerned physicians and researchers, we believe that all rheumatologists, with the support of the American College of Rheumatology (ACR), must confront the reality of the climate emergency and act on behalf of our patients' health and well-being now and for the future.

How can the climate emergency affect the health of our patients?

The effects of the climate emergency on patients with rheumatic disease have not yet been rigorously investigated. Data from other disciplines of medicine such as allergy medicine, pulmonary medicine, nephrology, and cardiovascular medicine clearly show the significant impact of climate-related factors on disease exacerbation (4). Similar mechanisms of disease exacerbation for these conditions likely apply to individuals with rheumatic diseases. For example, excessive heat exposure represents an important risk for morbidity and mortality, especially in urban environments in what are called heat islands. Many of our patients with systemic lupus erythematous, rheumatoid arthritis, or vasculitis have systemic manifestations that include renal, pulmonary, and cardiovascular complications that may be exacerbated with heat exposure. Greater pollution exposure and more frequent coexistent allergic disorders due to longer pollen seasons increase our patients' risk for respiratory complications, especially in those with lung disorders related to their rheumatic disease (5). Our patients who are exposed to more expansive and severe wildfires may be at risk for exposure to PM2.5 (particles ≤2.5 μm in diameter), which can worsen morbidity in those with underlying respiratory and cardiac diseases that are common in patients with rheumatic disease.

Of particular concern are patients from groups that have been historically, economically, and socially marginalized, and specifically, patients with rheumatic disease from racial and ethnic minority groups whom we know fare worse with their disease.

The content of this article is solely the responsibility of the authors and does not necessarily represent the official view of the sources providing funding support to the authors.

Supported in part by the Intramural Research Program of the NIH, National Institute of Environmental Health Sciences.

[1]Paul F. Dellaripa, MD, Candace H. Feldman, MD, MPH, ScD: Brigham and Women's Hospital and Harvard Medical School, Boston, Massachusetts; [2]Thomas Bush, MD: Santa Clara Valley Medical Center, San Jose, California; [3]Frederick W. Miller, MD, PhD, MACR: National Institute of Environmental Health Sciences, Research Triangle Park, North Carolina.

Author disclosures are available at https://onlinelibrary.wiley.com/action/downloadSupplement?doi=10.1002%2Fart.42279&file=art42279-sup-0001-Disclosureform.pdf.

Address correspondence via email to Paul F. Dellaripa, MD, at pdellaripa@bwh.harvard.edu.

Submitted for publication March 4, 2022; accepted in revised form June 10, 2022.

Thus, the effects of the climate emergency could become a force multiplier of morbidity among vulnerable groups with rheumatic diseases (6,7). It is imperative that we better understand which patients and communities are at highest risk for exposure to climate-related effects so that adaptive strategies can be tailored to these specific populations to prevent further health disparities.

What is the role of the rheumatologist and the ACR?

Educate physicians and patients. There had been no known efforts made to educate our rheumatology workforce on this critical topic until the 2021 ACR Convergence conference, which had an educational session and a newly formed study group focusing on climate and health, which were attended by over 200 participants. The discussion indicated that there was significant interest among rheumatology health professionals to better understand the health effects of the climate emergency and to discuss what research questions should be considered moving forward. Numerous medical societies have already undertaken this effort, and there are now widely available resources through organizations such as the American College of Physicians and the Medical Society Consortium on Climate that offer patient and physician education. These issues should be integrated into our present ACR educational infrastructure, both online and in our ongoing in-person, virtual, and hybrid conferences (7,8).

Engage in research on the effects of climate and the environment on the immune system and on rheumatic disease. Very little research is available that directly and comprehensively links environmental exposures, pollution, stress, and other emerging climate threats with specific rheumatic diseases and adverse effects on the immune system. A higher incidence of rheumatic disease was found among individuals with high dust cloud exposure at the site of the September 11 attacks on the World Trade Center, raising the possibility that exposure to and inhalation of PM may play a role in autoimmunity (9). Populations exposed to industrial pollution, which include historically marginalized populations, and those exposed to repeated smoke and PM caused by wildfires represent potential areas of epidemiologic study to assess the possible links between environmental exposures related to the climate emergency and the development of autoimmunity. There are substantial data that suggest a relationship between air pollution (PM exposure) and risk of systemic lupus erythematosus and increased disease activity (10,11). Inhalation has been postulated as a potential mechanism for the development of autoimmunity, and a recent analysis of a large cohort of patients with rheumatoid arthritis suggested a relationship between recent PM exposure and the development of rheumatoid arthritis flares and elevated C-reactive protein (12).

It is plausible that perturbations in our environment related to climate may lead to alterations of our immune system that may predispose us to the development of autoimmune diseases, increase the likelihood of flares of disease, and alter responses to therapy. Understanding the potential mechanisms of how these environmental exposures can cause such changes in the immune system will be challenging but may provide novel insights into mechanisms of diseases that we still struggle to understand (13). The ACR, the Rheumatology Research Foundation, the National Institutes of Health, and other rheumatic disease–related foundations should encourage collaboration among investigators that leads to large-scale research efforts to better understand these mechanisms and develop strategies to mitigate the effects of the climate emergency on our patients (14). A forthcoming white paper commissioned by the ACR will delve deeper into the current state of the literature and examine specific associations between environmental factors and rheumatic conditions.

Encourage sustainability in health care. Health care accounts for 8–10% of greenhouse gas emissions in the US, and efforts to limit energy expenditure and waste have become a priority in many health care systems (2). These efforts apply to all health care activities, including inpatient, outpatient, and research laboratory settings. We call upon rheumatologists and the ACR, alongside all medical professionals, to promote sustainability in their own settings and work toward cutting waste and lowering our institutional energy and carbon expenditure. Such efforts may also offer cost savings as an additional benefit (8). For example, Health Care Without Harm is an organization that offers practical guidance and resources to help reduce the environmental burden of health care delivery.

Advocate for strategies that adapt to and mitigate effects of the climate emergency. It is critical that rheumatologists advocate on a local, national, or global level to support public health policies that foster adaptative strategies to extreme weather events. Examples include targeted communication, education and emergency planning for patients living in urban heat islands, and providing additional resources like access to cooling centers. Advocacy for mitigative strategies to speed our transition from carbon energy sources toward renewable energy will be critical to limit the damage to our environment and the risks incurred to our patients.

Although addressing the climate emergency represents a daunting task, there is hope moving forward. Renewable energy is quickly becoming more affordable and widely available, and fossil fuel investments are losing value, making it easier to decarbonize our environment and limit the rise in global temperature, which we need to accomplish within the next decade based on goals set by the Paris Agreement and the Glasgow Climate Change Conference. With each challenge we face in the climate emergency, there are known solutions or resources that we can use right now in cost-effective ways, and more will emerge going forward (15). Not engaging on this critical issue and standing with our colleagues

across other fields of medicine would be a great disservice to our patients with rheumatic conditions whom we know will be affected. Just as we faced the challenge of the COVID-19 pandemic, we will now need to adapt again and bring our skills and resources to act, this time through the lens of the climate emergency, for the sake of our patients and for the sake of our planet.

ACKNOWLEDGMENTS

We thank Dr. Aubrey Miller and Dr. Ejaz Shamim for their expert comments.

AUTHOR CONTRIBUTIONS

Dr. Dellaripa drafted the article, and Drs. Bush, Miller, and Feldman revised it critically for important intellectual content. All authors approved the final version to be published.

REFERENCES

1. Keeling CD. The concentration and isotopic abundances of carbon dioxide in the atmosphere. Tellus 1960;12:200–3.
2. Solomon CG, LaRocque RC. Climate change - a health emergency. N Engl J Med 2019; 380:209–11.
3. The climate emergency: a last chance to act? Lancet 2021;398:1541.
4. Rocque RJ, Beaudoin C, Ndjaboue R, et al. Health effects of climate change: an overview of systematic reviews. BMJ Open 2021;11: e046333.
5. Pacheco SE, Guidos-Fogelbach G, Annesi-Maesano I, et al. Climate change and global issues in allergy and immunology. J Allergy Clin Immunol 2021;148:1366–77.
6. US Environmental Protection Agency. Climate change and social vulnerability in the United States: a focus on six impacts. 2021. URL: https://www.epa.gov/cira/social-vulnerability-report.
7. Bush, T. Potential adverse health consequences of climate change related to rheumatic diseases [review]. J Clim Chang Health 2021;3: 100029.
8. American College of Physicians. Toolkit: climate change and health. 2022. URL: https://www.acponline.org/advocacy/advocacy-in-action/climate-change-toolkit.
9. Miller-Archie SA, Izmirly PM, Berman JR, et al. Systemic autoimmune disease among adults exposed to the September 11, 2001 terrorist attack. Arthritis Rheumatol 2020;72:849–59.
10. Stojan G, Kvit A, Curriero FC, et al. A spaciotemporal analysis of organ-specific lupus flares in relation to atmospheric variables and fine particulate matter pollution. Arthritis Rheumatol 2020;72:1134–42.
11. Bernatsky S, Fournier M, Pineau CA, et al. Associations between ambient fine particulate levels and disease activity in patients with systemic lupus erythematosus (SLE). Environ Health Perspect 2011;119: 45–9.
12. Adami G, Viapiana O, Rossini M, et al. Association between environmental air pollution and rheumatoid arthritis flares. Rheumatology (Oxford) 2021;60:4591–7.
13. Bauer RN, Diaz-Sanchez D, Jaspers I. Effects of air pollutants on innate immunity: the role of Toll-like receptors and nucleotide-binding oligomerization domain-like receptors. J Allergy Clin Immunol 2012; 129:14–24.
14. National Institutes of Health. Climate change and health initiative. URL: https://www.nih.gov/climateandhealth.
15. Markandya A, Sampedro, J, Smith, SJ, et al. Health co-benefits from air pollution and mitigation costs of the Paris Agreement: a modelling study. Lancet Planet Health 2018;2:e126–33.

Arthritis & Rheumatology
Vol. 75, No. 1, January 2023, pp 4–14
DOI 10.1002/art.42338

American College of Rheumatology
Empowering Rheumatology Professionals

REVIEW

Management of Orofacial Manifestations of Juvenile Idiopathic Arthritis: Interdisciplinary Consensus-Based Recommendations

Peter Stoustrup,[1] Cory M. Resnick,[2] Shelly Abramowicz,[3] Thomas K. Pedersen,[4] Ambra Michelotti,[5] Annelise Küseler,[4] Bernd Koos,[6] Carlalberta Verna,[7] Ellen B. Nordal,[8] Eric J. Granquist,[9] Josefine Mareile Halbig,[10] Kasper D. Kristensen,[1] Leonard B. Kaban,[11] Linda Z. Arvidsson,[12] Lynn Spiegel,[13] Matthew L. Stoll,[14] Melissa A. Lerman,[15] Mia Glerup,[16] Patrizia Defabianis,[17] Paula Frid,[18] Per Alstergren,[19] Randy Q. Cron,[14] Sarah Ringold,[20] Sven Erik Nørholt,[4] Timo Peltomaki,[21] Tore A. Larheim,[12] Troels Herlin,[16] Zachary S. Peacock,[11] Christian J. Kellenberger,[22] and Marinka Twilt,[23] on behalf of the Temporomandibular Joint Juvenile Arthritis Working Group

Involvement of the temporomandibular joint (TMJ) is common in juvenile idiopathic arthritis (JIA). TMJ arthritis can lead to orofacial symptoms, orofacial dysfunction, and dentofacial deformity with negative impact on quality of life. Management involves interdisciplinary collaboration. No current recommendations exist to guide clinical management. We undertook this study to develop consensus-based interdisciplinary recommendations for management of orofacial manifestations of JIA, and to create a future research agenda related to management of TMJ arthritis in children with JIA. Recommendations were developed using online surveying of relevant stakeholders, systematic literature review, evidence-informed generation of recommendations during 2 consensus meetings, and Delphi study iterations involving external experts. The process included disciplines involved in the care of orofacial manifestations of JIA: pediatric rheumatology, radiology, orthodontics, oral and maxillofacial surgery, orofacial pain specialists, and pediatric dentistry. Recommendations were accepted if agreement was >80% during a final Delphi study. Three overarching management principles and 12 recommendations for interdisciplinary management of orofacial manifestations of JIA were outlined. The 12 recommendations pertained to diagnosis (n = 4), treatment of TMJ arthritis (active TMJ inflammation) (n = 2), treatment of TMJ dysfunction and symptoms (n = 3), treatment of arthritis-related dentofacial deformity (n = 2), and other aspects related to JIA (n = 1). Additionally, a future interdisciplinary research agenda was developed. These are the first interdisciplinary recommendations to guide clinical management of TMJ JIA. The 3 overarching principles and 12 recommendations fill an important gap in current clinical practice. They emphasize the importance of an interdisciplinary approach to diagnosis and management of orofacial manifestations of JIA.

INTRODUCTION

Temporomandibular joint (TMJ) arthritis is a frequent manifestation of juvenile idiopathic arthritis (JIA). TMJ arthritis often occurs early in the JIA disease course, and the inflammatory process and related orofacial signs and symptoms can persist into adulthood (1–7). Occasionally, TMJ arthritis is the only manifestation of JIA (8). Early TMJ arthritis may be asymptomatic, but many patients experience orofacial symptoms, orofacial dysfunction, and a decrease in quality of life as the disease progresses

[1]Peter Stoustrup, DDS, PhD, Kasper D. Kristensen, DDS, PhD: Section of Orthodontics, Aarhus University, Aarhus, Denmark; [2]Cory M. Resnick, DMD, MD: Department of Plastic and Oral Surgery, Boston Children's Hospital, Boston, Massachusetts; [3]Shelly Abramowicz, DMD, MPH: Division of Oral and Maxillofacial Surgery, Departments of Surgery and Pediatrics, Emory University School of Medicine, Atlanta, Georgia; [4]Thomas K. Pedersen, DDS, PhD, Annelise Küseler, DDS, PhD, Sven Erik Nørholt, DDS, PhD: Section of Orthodontics and Department of Oral and Maxillofacial Surgery, Aarhus University Hospital, Aarhus, Denmark; [5]Ambra Michelotti, BSc, DDS: University of Naples Federico II, Naples, Italy; [6]Bernd Koos, DMD: Department of Orthodontics, University Hospital Tübingen, Tübingen, Germany; [7]Carlalberta Verna, DDS, PhD: Department of Pediatric Oral Health and Orthodontics, UZB University Center for Dentistry Basel, University of Basel, Basel, Switzerland; [8]Ellen B. Nordal, MD, PhD: Department of Pediatrics, University Hospital of North Norway and the Pediatric Research Group, Department of Clinical Medicine, UiT The Arctic University of Norway, Tromsø, Norway; [9]Eric J. Granquist, MD, DMD: Department of Oral and Maxillofacial Surgery, School of Dental Medicine, University of Pennsylvania, Philadelphia; [10]Josefine Mareile Halbig, DDS, Dr. med dent: The Public Dental Health Competence Centre of North Norway, and the Department of Clinical Medicine, Faculty of Health Sciences, UiT The Arctic University of Norway, Tromsø, Norway; [11]Leonard B. Kaban, DMD, MD, FACS, Zachary S. Peacock, DMD, MD: Massachusetts

(1–3,5,6,9–12). In skeletally immature patients, TMJ arthritis can interfere with facial growth and development, resulting in dentofacial deformity (13,14).

Management of the orofacial manifestations of TMJ arthritis requires an interdisciplinary care team which includes pediatric rheumatology, oral and maxillofacial surgery, orthodontics, radiology, pediatric dentistry, specialists in orofacial pain and jaw function, and others. In 2019, consensus-based terminology specific to JIA-associated TMJ arthritis was introduced (15). Standardization of terminology provides a platform for communication among the many healthcare providers involved in the integrative care of this condition, facilitates research, and may improve outcomes.

Management of TMJ arthritis varies widely in different regions and healthcare systems (16,17); interdisciplinary consensus-based recommendations to guide clinical decision-making and standardize care are necessary. The objectives of this project were to develop interdisciplinary recommendations for management of orofacial manifestations of JIA and to create a future research agenda related to TMJ arthritis management in JIA.

MATERIALS AND METHODS

This study was conducted by a steering committee consisting of members of the Temporomandibular Joint Juvenile Arthritis Working Group (TMJaw), an international, interdisciplinary research network dedicated to the study of TMJ involvement in JIA. All task force members are experts in JIA-associated TMJ arthritis within their respective professional fields. This study adheres to the consensus-based terminology for JIA-associated TMJ arthritis (15) (Table 1). Methodologic details are displayed in Figure 1.

Prior to the first working group meeting, the steering committee distributed an online survey to TMJaw members using the Mentimeter survey system (Stockholm, Sweden) to determine the disciplines involved in the integrated care of orofacial manifestations of JIA within their healthcare systems. The core team (PS and MT) developed 4 standardized questions based on the online survey, and systematic reviews were performed to develop evidence-based tables according to the modified Grading of Recommendations Assessment, Development and Evaluation (GRADE) method. An international TMJaw task force assembled in Rostock, Germany in March 2017 (17 participants representing 10 countries in Europe and North America), including representatives from each discipline represented in the initial survey. During the initial meeting, the project was outlined (Figure 1). Target populations for future recommendations were defined as 1) healthcare professionals involved in the integrative care of TMJ arthritis and related manifestations and 2) public health authorities and policy makers. Working groups of 3 to 5 members were formed, representing pediatric rheumatology, radiology, orthodontics, maxillofacial surgery, and pediatric dentistry. Working groups were provided with the 4 standardized questions and the literature search and asked to answer the predefined research questions (Table 2), and to recommend principles to guide clinical decision-making and grade the evidence level for those principles.

The results of the working group were combined to guide the proposal of preliminary recommendations for diagnosis and management of TMJ arthritis. Three overarching consensus-based

Table 1. Standardized, consensus-based terminology for juvenile idiopathic arthritis (JIA)–associated temporomandibular joint (TMJ) arthritis*

Terminology	Consensus-based definition
TMJ arthritis	Active inflammation in the TMJ
TMJ involvement	Abnormalities presumed to be the result of TMJ arthritis
TMJ arthritis management	Diagnosis, treatment, and monitoring of TMJ arthritis and involvement
Dentofacial deformity	Abnormality in the growth, development, structure, and/or alignment of the facial bones and dentition
TMJ deformity	Abnormality in the growth, development, or structure of the osseous and/or soft tissue components of the TMJ
TMJ dysfunction	Physician-reported functional examination abnormalities related to TMJ arthritis or involvement
TMJ symptoms	Patient or parent-reported conditions related to TMJ arthritis or involvement

* The consensus-based definitions are derived from ref. 15 (Stoustrup et al).

General Hospital, Harvard School of Dental Medicine, Boston, Massachusetts; [12]Linda Z. Arvidsson, DDS, PhD, Tore A. Larheim, DDS, PhD: Department of Maxillofacial Radiology, Institute of Clinical Dentistry, University of Oslo, Oslo, Norway; [13]Lynn Spiegel, MD, FRCPC: The Hospital for Sick Children, University of Toronto, Toronto, Ontario, Canada; [14]Matthew L. Stoll, MD, PhD, MSCS, Randy Q. Cron, MD, PhD: University of Alabama at Birmingham; [15]Melissa A. Lerman, MD, PhD, MSCE: Children's Hospital of Philadelphia and University of Pennsylvania Perelman School of Medicine, Philadelphia, Pennsylvania; [16]Mia Glerup, MD, PhD, Troels Herlin, MD, DMSc: Department of Pediatrics and Adolescent Medicine, Aarhus University Hospital, Aarhus, Denmark; [17]Patrizia Defabianis, MD, DDS: Section of Paediatric Dentistry, Dental School, University of Turin, Turin, Italy; [18]Paula Frid, DDS, PhD: Department of Otorhinolaryngology, Division of Oral and Maxillofacial Surgery, University Hospital of North Norway, Public Dental Service Competence Centre of North Norway, and Department of Clinical Dentistry, UiT The Arctic University of Norway, Tromsø, Norway; [19]Per Alstergren, DDS, PhD: Faculty of Odontology, Orofacial Pain Unit, Malmö University, Malmö, Sweden; [20]Sarah Ringold, MD, MS: Seattle Children's Hospital, Seattle, Washington; [21]Timo Peltomaki, DDS, PhD: Faculty of Medicine and Health Technology, and Department of Ear and Oral Diseases, Tampere University, Tampere, Finland, and Institute of Dentistry, Faculty of Health Sciences, University of Eastern Finland and Department of Oral and Maxillofacial Diseases, Kuopio University Hospital, Kuopio, Finland; [22]Christian J. Kellenberger, MD: Department of Diagnostic Imaging, University Children's Hospital Zürich, Zürich, Switzerland; [23]Marinka Twilt, MD, MScE, PhD: Alberta Children's Hospital and University of Calgary, Calgary, Alberta, Canada.

Author disclosures are available at https://onlinelibrary.wiley.com/action/downloadSupplement?doi=10.1002%2Fart.42338&file=art42338-sup-0001-Disclosureform.pdf.

Address correspondence via email to Peter Stoustrup, DDS, PhD, at pstoustrup@dent.au.dk.

Submitted for publication December 21, 2021; accepted in revised form August 19, 2022.

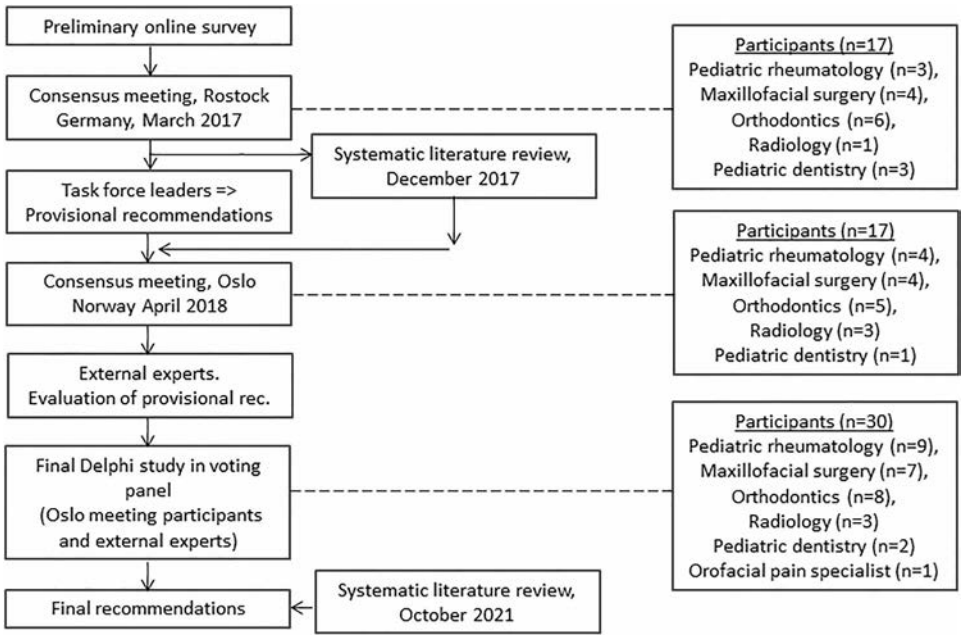

Figure 1. Outline of the consensus process for the development of interdisciplinary recommendations for the management of temporomandibular joint arthritis in children with juvenile idiopathic arthritis.

principles were created. Additionally, specific preliminary recommendations were formulated for each of 5 relevant domains, including domains for diagnosis (domain I; n = 4), treatment of TMJ arthritis (domain II; n = 2), treatment of TMJ dysfunction and symptoms related to JIA (domain III; n = 3), treatment of arthritis-related dentofacial deformity (domain IV; n = 2), and other orofacial aspects related to JIA (domain V; n = 1).

The preliminary recommendations were discussed at a subsequent task force meeting in Oslo, Norway in April 2018. The task force consisted of 17 participants representing 5 specialties (Figure 1). Subsequently, the overarching principles and provisional recommendations were refined using a task force–driven consensus process involving nominal group techniques and 2 Delphi iterations.

Table 2. Tasks relevant to the management of temporomandibular joint (TMJ) arthritis in patients with juvenile idiopathic arthritis (JIA) addressed by the working groups after the 2017 Rostock meeting*

	Working group tasks
1	Define orofacial diagnostic/treatment strategies relevant for the management of JIA in the TMJ and the related conditions
2	Define indications for these management strategies (imaging, radiologic, clinical indications)
3	Define contraindications for these management strategies (imaging, radiologic, clinical indications)
4	Define, if relevant, specifications on how to conduct these management strategies

* Working groups were provided with these 4 predefined standardized research questions and a literature search and tasked with providing principles to guide clinical decision-making and grade the evidence level for each principle.

Following the Oslo meeting, external experts (n = 13) who were previously not involved in the process were invited to assess the content validity of the provisional recommendations. These experts were identified based on internationally recognized clinical expertise and general contribution to research and publications related to TMJ arthritis in JIA. The external experts were asked to comment on the provisional recommendations and suggest improvements. Feedback from this exercise was incorporated into the next round of recommendations.

As a final step, the participants from the Oslo meeting (n = 17) and the external experts (n = 13) formed a voting panel which completed 3 online Delphi iterations and agreed upon a final set of recommendations. Characteristics of the voting panel are in Figure 1. The members of the voting panel assessed the perceived strength of each recommendation (SoR) based on a visual analog scale (VAS) scale (0 = no SoR, 10 = great SoR). Recommendations receiving agreement from ≥80% of the voting panel members were accepted. The level of evidence (LoE) of each recommendation was assessed using the Oxford Centre for Evidence-Based Medicine (OCEBM) level of evidence table (18).

All members of the voting panel were invited to formulate items for a future research agenda. During the Delphi iterations, the level of importance of each proposed research item was assessed using a 0–10-point VAS (0 = not important, 10 = extremely important). Only items receiving a mean level of importance VAS score of ≥7 were included on the future research agenda.

An updated systematic literature review was conducted in October 2021 to determine if any new literature was identified supporting or contradicting each of the specific management

recommendations. The new literature identified did not lead to any changes in the recommendations.

RESULTS

This process generated 3 overarching principles and 12 recommendations pertaining to the 5 following domains: domain I (diagnosis); domain II (treatment of TMJ arthritis, defined as active TMJ inflammation); domain III (treatment of TMJ dysfunction and symptoms); domain IV (treatment of arthritis-related dentofacial deformity); and domain V (other related aspects) (Table 3). A full reference list for articles supporting the generation of each of the 12 recommendations is available in the Supplementary Material on the *Arthritis & Rheumatology* website at http://onlinelibrary.wiley.com/doi/10.1002/art.42338.

Level of evidence

The LoEs provided in the available literature with regard to support of these principles and recommendations varied, falling at either steps 2, 3, or 4 on the OCEBM level of evidence table (ranging from step 1 [highest LoE] to step 5 [lowest LoE]) (18); in general, the LoEs were low. Hence, this proposal should be regarded as conditional where the voting panel finds that the desirable effects outweigh the undesirable effects, but the members of the panel appreciate that uncertainties exist related to resources, settings, and costs (19,20).

Overarching principles

The 3 overarching principles represent a contemporary view on the management of TMJ arthritis and the related orofacial manifestations of JIA. These principles serve as a framework for the specific recommendations that follow.

Overarching principle A. TMJ arthritis is a common finding in patients with JIA and standardized evaluation is recommended. No population-based studies exist on this matter. Estimates from non–population-based studies (n > 100 participants) indicate that a substantial proportion of subjects with JIA have TMJ inflammation (termed "TMJ arthritis"), with prevalence ranging between 34% and 43% (1–3). The voting panels acknowledge that this estimate is subject to uncertainty due to methodologic differences, such as differences in patient populations. Other studies have reported >50% prevalence of TMJ arthritis in patients with JIA. However, these estimates mostly originated from studies with smaller sample sizes that included patients from the pre–biologic era, studies characterized by unspecified diagnostic MRI criteria, and studies in which patients with clinical and/or radiologic signs of previous TMJ arthritis (termed "TMJ involvement") are also included in the estimates (21).

Overarching principle B. Goals of management are to 1) provide timely diagnosis of TMJ arthritis and TMJ involvement, 2) reduce TMJ inflammation, 3) reduce TMJ arthritis–related symptoms and dysfunction, 4) normalize dentofacial development, and 5) address dentofacial deformities. Timely diagnosis and resolution of TMJ inflammation are pivotal management objectives. Additionally, orofacial symptoms and dysfunction and dentofacial deformity that results from prior TMJ arthritis can persist and progress even after active arthritis has been managed. These sequelae have a significant negative impact on health-related quality of life, and as such they must be equally included in management principles (9–11).

Overarching principle C. Optimal management of TMJ arthritis requires an interdisciplinary approach and longitudinal evaluation of patients from childhood into adulthood, regardless of their current TMJ disease activity. Interdisciplinary management is important for optimal patient outcomes, though it is recognized that the availability and expertise of providers and the accessibility of resources (e.g., government programs, health insurance) may vary by region and healthcare setting. The voting panel stresses the importance of implementing orofacial health evaluations in general JIA health assessments and the management of JIA.

Specific recommendations

Diagnosis and monitoring. Timely diagnosis is a critical first step in the management of TMJ arthritis and the related orofacial manifestations. Monitoring orofacial health in patients with TMJ involvement requires a standardized approach. No method of assessment can stand alone. Optimal TMJ monitoring should involve multiple modalities of assessment, including different aspects of patient history and clinical examination, patient-reported outcomes, and imaging and radiology (15). Recommendations 1–4 (see below) refer to the diagnosis of TMJ arthritis and longitudinal monitoring of orofacial health.

Recommendation 1. Contrast-enhanced magnetic resonance imaging (MRI) is currently the best method to detect active TMJ arthritis (LoE 2, mean ± SD SoR 8.4 ± 2.1). This recommendation specifies "active" TMJ inflammation to differentiate from TMJ involvement without active inflammation (Table 1) (15). The use of JIA-specific TMJ MRI protocols and scoring systems is recommended (22–25). It is recognized that the interpretation of MRI findings has an element of subjectivity and is influenced by the technique and equipment used for image capture, as well as by the expertise of the reader. Additional standardization of both image acquisition and interpretation is needed. It is stressed that the presence of a small amount of TMJ fluid and/or minor contrast enhancement may be considered a normal variation in a healthy TMJ, rather than a sign of active TMJ arthritis (26–28).

Table 3. Recommendations for the management of temporomandibular joint (TMJ) arthritis and the related orofacial manifestations of juvenile idiopathic arthritis (JIA)

Recommendations	Level of evidence*	SoR†	Agreement
Overarching principles			
TMJ arthritis is a common finding in patients with JIA and standardized evaluation is recommended.	–	–	100%
Goals of management are to 1) provide timely diagnosis of TMJ arthritis and TMJ involvement, 2) reduce TMJ inflammation, 3) reduce TMJ arthritis–related symptoms and dysfunction, 4) normalize dentofacial development, and 5) address dentofacial deformities.	–	–	100%
Optimal TMJ arthritis management requires an interdisciplinary approach and longitudinal evaluation into adulthood regardless of the current TMJ disease activity.	–	–	100%
Diagnosis			
Contrast-enhanced MRI is currently the best method to detect active TMJ arthritis.	2	8.4 ± 2.1	94%
Patient (or proxy) history should be used to assess TMJ involvement. While often absent, orofacial symptoms should be regularly reassessed. A standardized approach is recommended.	3	8.8 ± 2.2	100%
Clinical examination should be used to diagnose TMJ arthritis–related dysfunction; a standardized approach is recommended to monitor changes over time.	3	8.5 ± 2.7	100%
All patients should be evaluated for dentofacial deformity; a standardized approach is recommended to monitor changes over time.	3	8.9 ± 2	100%
Treatment of TMJ arthritis (active TMJ inflammation)			
Optimal systemic treatment should be considered for active TMJ arthritis in patients with JIA.	4	7.9 ± 2.4	90%
Skeletally immature patients: Intraarticular glucocorticoid injection is not recommended as first-line management of TMJ arthritis in skeletally immature patients. Intraarticular glucocorticoids may be used cautiously in patients with refractory TMJ arthritis and orofacial symptoms. Repeated glucocorticoid injection is not recommended.	2	8.3 ± 2.5	97%
Skeletally mature patients: Intraarticular glucocorticoid injection may be indicated in skeletally mature patients with active TMJ arthritis and orofacial symptoms.	4	7.7 ± 2.4	87%
Treatment of TMJ dysfunction and symptoms			
Occlusal splints and/or physical therapy may be beneficial in patients with orofacial symptoms and/or TMJ dysfunction.	4	8.3 ± 2.2	100%
Intraarticular glucocorticoid injection may be indicated in arthritis-induced refractory and symptomatic TMJ dysfunction, but is not recommended for first-line management in skeletally immature patients (see recommendation 6).	2	7.4 ± 2.7	87%
Intraarticular lavage (without steroid) may be beneficial for TMJ arthritis–related symptoms and dysfunction. Lavage without steroid can be used in both growing and skeletally mature patients. No additional effect of lavage with steroid injection has been reported.	4	6.5 ± 2.6	90%
Treatment of arthritis-related dentofacial deformity			
Dentofacial orthopedics and orthodontics may improve facial development, occlusion, and function in skeletally immature patients.	4	8.1 ± 2.5	100%
Skeletal surgery may be indicated in skeletally immature and skeletally mature patients with dentofacial deformities and quiescent/controlled TMJ arthritis.	4	8.1 ± 2.4	97%
Other			
Screening and monitoring of the oral cavity with a focus on dental decay, gingivitis, and ulcerations are recommended.	3	6.5 ± 3.4	84%

* Level of evidence according to criteria from the Oxford Center of Evidence Based Medicine (1 = highest evidence level, 5 = lowest evidence level). MRI = magnetic resonance imaging.
† Mean ± SD strength of recommendation (SoR) is based on a visual analog scale of 0–10, with 0 being no SoR and 10 being great SoR.

Ultrasonography is operator-dependent and appears to have limited sensitivity to detect TMJ inflammation in patients with JIA (29–32). Future research is needed to elucidate the role of ultrasonography in the diagnosis and monitoring of JIA and TMJ arthritis.

This recommendation is consistent with the 2019 interdisciplinary consensus-based recommendation on the method of assessment of TMJ arthritis (15,33). The voting panel acknowledges that accurate patient history (recommendation 2) and clinical orofacial examination (recommendation 3) may often precede imaging in the diagnostic sequence for TMJ arthritis.

Recommendation 2. Patient (or proxy) history should be used to assess involvement of the TMJ in JIA. While often absent, orofacial symptoms should be regularly reassessed. A standardized approach is recommended (LoE 3, mean ± SD SoR 8.8 ± 2.2). JIA-specific tools such as the Childhood Health Assessment Questionnaire, the Juvenile Arthritis Disease Activity Score, and the Juvenile Arthritis Multidimensional Assessment Report are popular tools used for general disease assessment (34–36). However, because these tools provide limited or no assessment of the orofacial manifestations of JIA, TMJ and orofacial conditions may be overlooked.

Recommendation 3. Clinical examination should be used to diagnose TMJ arthritis–related dysfunction; a standardized approach is recommended to monitor changes over time (LoE 3, mean ± SD SoR 8.5 ± 2.7). Orofacial examination aids timely diagnosis and facilitates longitudinal monitoring of patients

with existing TMJ involvement. While the use of orofacial examination alone for the diagnosis of TMJ involvement in JIA is limited, examination remains an important form of screening to inform the need for further diagnostic evaluation and serves as a low-cost method for serial follow-up. Additionally, orofacial examination improves the assessment of response to therapy and the evaluation of treatment options (33). A standardized orofacial examination approach that complies with consensus-based standards is recommended (33). A consensus-based JIA-specific orofacial examination protocol was recently published (37).

Recommendation 4. All patients should be evaluated for dentofacial deformity; a standardized approach for evaluation is recommended to monitor changes in facial morphology over time (LoE 3, mean ± SD SoR 8.9 ± 2.0). Dentofacial deformity is a common complication of JIA. This occurs most frequently in patients who experience TMJ arthritis/involvement prior to reaching skeletal maturity (6,38,39). Assessment of facial morphology can be conducted during a clinical examination or by 3-dimensional imaging and a conventional radiologic examination (15), in accordance with consensus-based standards (33,37). Progressive deviation in the mandibular morphology and facial profiles (e.g., mandibular asymmetry/retrognathia) of patients with JIA should prompt further radiographic examination and/or referral.

No protocol exists to guide decision-making regarding the indications, timing, and frequency of TMJ imaging. Currently, radiologic evaluation of TMJ and facial morphology are variable and provider-dependent. Assessment of TMJ and dentofacial deformities should adhere to consensus-based standards (22,40).

Treatment of TMJ arthritis (active TMJ inflammation). Recommendations 5 and 6 (see below) refer to the management of TMJ inflammation (termed "TMJ arthritis") (Table 1). Resolution of TMJ arthritis is considered a key component to optimal TMJ arthritis management.

Recommendation 5. The optimal systemic treatment should be considered for active TMJ arthritis in patients with JIA (LoE 4, mean ± SD SoR 7.9 ± 2.4). Longitudinal observational studies have reported a beneficial effect of systemic immunosuppressive therapy on TMJ arthritis, mandibular growth, and the progression of TMJ deformity (41,42). The term "optimal" in this recommendation reflects the fact that the current level of evidence is insufficient to direct the administration of specific modalities. Empiric, early, and aggressive systemic treatment of TMJ arthritis is recommended, as this may reduce TMJ arthritis–related sequelae. Hence, TMJ disease status should be considered when determining the optimal systemic medical therapy to be used to treat all manifestations of JIA.

Recommendation 6a for skeletally immature patients. Intraarticular glucocorticoid injection is not recommended as the first-line treatment for the management of TMJ arthritis in skeletally immature patients. Intraarticular glucocorticoids may be used cautiously in patients with refractory TMJ arthritis and orofacial symptoms. Repeated glucocorticoid injection is not recommended (LoE 2, mean ± SD SoR 8.3 ± 2.5).

Recommendation 6b for skeletally mature patients. Intraarticular glucocorticoid injection may be indicated in skeletally mature patients with active TMJ arthritis and orofacial symptoms (LoE 4, mean ± SD SoR 7.7 ± 2.4). Controversy prevails over the use of intraarticular glucocorticoid injections for the treatment of TMJ arthritis in growing patients (43). Longitudinal observational studies have demonstrated an antiinflammatory effect of intraarticular glucocorticoid injections in JIA patients with TMJ arthritis (44,45). However, outcomes are variable and the effect is considered to be temporary and not curative (44–48). The voting panel stresses the importance of reducing inflammatory activity in the TMJ as early as possible to prevent signs and symptoms of TMJ arthritis, cartilage and bone tissue destruction, and growth inhibition. However, the side effects of TMJ intraarticular glucocorticoid injections are not yet fully understood. Recent research has suggested that the risks of the suppression of mandibular growth and/or the development of intraarticular calcifications may outweigh the antiinflammatory benefits of TMJ intraarticular glucocorticoid injection, particularly in skeletally immature patients (44–46,49). A precautionary approach to the use of TMJ intraarticular glucocorticoid injection in skeletally immature patients is therefore recommended.

In skeletally mature patients, TMJ intraarticular glucocorticoid injections have been reported to have beneficial antiinflammatory effects without significant side effects (50). However, as in skeletally immature patients, the effects were temporary and not curative. The risk of side effects associated with TMJ intraarticular glucocorticoid injections in skeletally mature patients requires further investigation. At this point, TMJ intraarticular glucocorticoid injections may be used in skeletally mature patients with signs of TMJ arthritis on MRI and orofacial symptoms who have had an inadequate response to other treatment modalities (44,50).

Treatment of TMJ symptoms and dysfunction. The relationship between the presence and severity of TMJ arthritis and the development of orofacial signs and symptoms is unclear (33,51), because many patients with TMJ inflammation will not manifest orofacial symptoms. Conversely, orofacial signs/symptoms can progress in well-treated patients without MRI evidence of TMJ inflammation (33,51). A potential mechanistic model is that the sequelae of previous TMJ arthritis (e.g., TMJ deformity) may cause mechanical overloading of the TMJ during function. In turn, mechanical dysfunction can lead to orofacial signs and symptoms despite the absence of TMJ inflammation (52). The mechanism for the relationship between arthritis and symptoms requires further study. Given the dissociation between arthritic activity and orofacial signs and symptoms, it is

essential to monitor and address TMJ-related dysfunction and symptoms regardless of TMJ inflammatory status.

Recommendation 7. Occlusal splints and/or physical therapy may be beneficial in patients with orofacial symptoms and/or TMJ dysfunction (LoE 4, mean ± SD SoR 8.3 ± 2.2). Data from longitudinal observational case series have documented significant improvement in JIA-related orofacial dysfunction and symptoms after treatment with oral splints, although the complete resolution of pain is rare (53–55). The design of the oral splint varied between studies (e.g., activators and flat stabilizing splints). Regardless of splint design, this treatment modality is considered reversible, safe, and of low cost in most healthcare settings (55). Oral splints also play a role in the treatment of dentofacial deformity (see recommendation 10).

No data exist regarding the effect of physiotherapy on JIA-related orofacial signs and symptoms. Physiotherapy and jaw exercises are evidence-based treatments for related conditions such as other temporomandibular dysfunctions, and can reasonably be extrapolated to patients with JIA-related orofacial symptoms (56). The recommendation for the use of orofacial physiotherapy for JIA is solely based on empirical evidence and mechanism-based reasoning (LoE 5). This is a subject of further study. In summary, splint therapy and physiotherapy are considered safe and reversible modalities for the management of orofacial signs and symptoms in JIA patients, and are therefore recommended despite a low level of evidence.

Recommendation 8. Intraarticular glucocorticoid injection may be indicated in arthritis-induced refractory and symptomatic TMJ dysfunction, but is not recommended as first-line management in skeletally immature patients (LoE 2, mean ± SD SoR 7.4 ± 2.7). Recommendation 8 relates to the role of TMJ intraarticular glucocorticoid injections in the management of TMJ symptoms and dysfunction in patients with refractory (active) TMJ arthritis, as opposed to recommendations 6a and b which relate to the management of TMJ inflammation. Longitudinal observational studies have demonstrated pain relief and improvement in TMJ function after intraarticular glucocorticoid injection to the TMJ (44,45). Likewise, intraarticular glucocorticoid injection has been shown to decrease short-term TMJ inflammation based on MRI (44,45). However, as discussed earlier, the effects and the duration of the benefits of intraarticular glucocorticoid injections on the signs and symptoms of TMJ dysfunction are highly variable and temporary (44–48). The risk of side effects has been discussed above (see recommendations 6a and b).

Despite controversy regarding the use of TMJ intraarticular glucocorticoid injections, they are still indicated in specific circumstances (e.g., arthritis-induced refractory and symptomatic TMJ dysfunction). The use of this treatment modality calls for special attention to the risks and benefits of the technique and to the level of skeletal maturity of the patient. Further study may help to clarify the role of this technique.

Recommendation 9. Intraarticular lavage (without steroids) may be beneficial for TMJ arthritis–related symptoms and dysfunction. Lavage without steroids can be used in both growing and skeletally mature patients. No additional effect of lavage with steroid injection has been reported (LoE 4, mean ± SD SoR 6.5 ± 2.6). In 2 prospective longitudinal case series, the effect of TMJ lavage (with or without steroid treatment) was studied in patients with MRI-verified TMJ arthritis (44,57). Temporary pain relief and improvement in TMJ function have been demonstrated, though outcomes are highly variable and benefits may be time-limited. Complete resolution of orofacial signs and symptoms following this treatment is rare. The available literature indicates that there are limited benefits when steroids are added to the lavage procedure, and the addition of steroids is not routinely recommended (see recommendations 6 and 8). No severe side effects have been reported with TMJ lavage without steroid in JIA patients.

The limited evidence for this recommendation is acknowledged, and more evidence is needed to differentiate between the efficacy of the procedure compared to the placebo effect resulting from an operative intervention. This recommendation is made to provide clinicians with an option for the management of orofacial pain and dysfunction that has an improved safety profile in comparison to TMJ intraarticular glucocorticoid injection. Further studies are needed to determine the role of TMJ lavage in the management of JIA-related TMJ arthritis.

Treatment of dentofacial deformity. TMJ arthritis impacts mandibular growth and development (38–40,58). The severity of dentofacial deformity depends on the timing of the onset of TMJ arthritis in relation to growth trajectory and laterality (unilateral/bilateral). JIA-induced dentofacial deformities can occur early in the disease course (6). As for orofacial signs and symptoms, the relationship between the severity of TMJ arthritis and the severity of dentofacial deformity is indirect and incompletely understood (6,59). The severity of dentofacial deformity and the degree of skeletal maturity is a major factor in decision-making with regard to disease management (38,39,58,60,61).

Recommendation 10. Dentofacial orthopedics and orthodontics may improve facial development, occlusion, and function in skeletally immature patients (LoE 4, mean ± SD SoR 8.1 ± 2.5). Observational studies have documented the benefits of dentofacial orthopedic appliances (oral splints) for the management of minor-to-moderate dentofacial deformities resulting from JIA (61–65). These splints are used in growing patients with the aim of supporting normal mandibular growth and occlusal development (52). Clinical evidence suggests that the optimal effect of this modality is achieved by initiating treatment early in the development of dentofacial deformity (65). Splints are used in conjunction with antiinflammatory therapies for active TMJ arthritis.

The use of oral splints may normalize minor-to-moderate dentofacial deformities and may have a preventative effect against

the worsening of the deformity. This approach is therefore recommended for interceptive treatment of early dentofacial deformities in JIA (60–62,64,65). However, the availability of this treatment varies by region and healthcare setting. Other barriers exist and have been discussed elsewhere (52).

Little is known about the effects of orthodontic treatment with fixed orthodontic appliances (braces) in patients with JIA (61,64,66). However, orthodontic treatment is mainly considered as a modality to establish dental occlusion after the use of orthopedic appliances or in conjunction with surgical correction. Fixed appliance orthodontic treatment may also be used to correct minor malocclusions separately from orthopedic or surgical treatment. This is a subject for further recommendations from the TMJaw group.

Recommendation 11. Skeletal surgery may be indicated in skeletally immature and skeletally mature patients with dentofacial deformities and quiescent/controlled TMJ arthritis (LoE 4, mean ± SD SoR 8.1 ± 2.4). Surgical procedures aim to correct dentofacial deformities related to TMJ arthritis/involvement. The available surgical modalities have been systematically reviewed by Frid et al (67). There are 3 general surgical approaches, as follows: 1) mandibular distraction osteogenesis, 2) orthognathic surgery with TMJ preservation, and 3) TMJ reconstruction with autologous or alloplastic implants. A combination of these surgical modalities may be used. The current scientific evidence is scarce, and the choice of surgical approach varies widely. The selection of the surgical method used for the management of dentofacial deformity resulting from TMJ arthritis is influenced by the skeletal maturity of the patient, the level of TMJ inflammatory activity, the stability of the TMJ and dentofacial deformity, and the preference and experience of the surgeon (67). Resnick et al recently presented a consensus-based algorithm for the management of dentofacial deformity resulting from JIA (60). The algorithm proposes a conceptual framework for an interdisciplinary approach involving the use of dentofacial orthopedic appliances and surgical management.

Other recommendation 12. Screening and monitoring of the oral cavity with a focus on dental decay, gingivitis, and ulcerations are recommended (LoE 3, mean ± SD SoR 6.5 ± 3.4). Recommendation 12 is directed toward the oral consequences of JIA and is not specifically for patients with TMJ arthritis/involvement. The impact of JIA on oral health was recently systematically reviewed by Skeie et al (68). The relationship between JIA and oral health conditions is not completely understood. However, there is evidence that periodontal disease (e.g., gingival inflammation, periodontitis) is more prevalent in patients with JIA compared to healthy controls (68–70). An association between JIA and dental caries has not been established (68). Little is known about the relationship between periodontal conditions and JIA (68,69). Cross-talk between the oral microbiota and the immune response has been suggested in the setting of rheumatoid arthritis, and periodontal pathogens have been considered a trigger of the autoimmune reaction in patients with rheumatoid arthritis (71,72). The influence of the oral microbiota in the setting of JIA has only just begun to be investigated (73). Further investigation is needed before a bidirectional relationship between periodontal conditions and JIA can be established.

Table 4. Proposal for a future research agenda on TMJ arthritis in patients with JIA*

Future research agenda	Level of importance
Etiology and diagnosis of TMJ arthritis	
Identification of biomarkers for TMJ disease progression and treatment response	8.7
Effect of inflammation on facial growth	8.6
Differentiating JIA-induced TMJ arthritis from idiopathic condylar resorption	7.9
Clinical diagnosis of TMJ arthritis	7.6
TMJ imaging	
Standardization of MRI assessment	9.4
Develop noninvasive diagnostic imaging techniques for young/noncooperative children	7.9
Systemic treatment of TMJ arthritis	
Prospective evaluation of systemic therapy on TMJ arthritis: methotrexate versus biologics as first-line therapy	8.2
Orthopedic/orthodontic treatment of dentofacial deformity	
Effect of different types of orthopedic appliances (oral splints) for treatment of dentofacial deformity	8.3
Determine optimal developmental stage for initiation of orthopedic/orthodontic treatment with oral splints.	7.7
Surgical treatment of dentofacial deformity	
Prospective evaluation of surgical treatment modalities for arthritis-related dentofacial deformity	7.8
Intraarticular treatment of TMJ arthritis	
Impact of intraarticular steroid on condylar growth	7.9
Study the effects of intraarticular administration drug therapy	7.7
Controlled randomized trial of intraarticular lavage and steroids versus intraarticular lavage alone versus control	7.6
Guidelines and protocols	
Develop an interdisciplinary management algorithm for TMJ arthritis management	8.2
Develop recommendations for monitoring orofacial health in JIA	8.2
Tutorial instruction video for standardized orofacial examination	7.4
Develop orofacial examination protocol for small children (2–5 years old) with JIA	7.4
Patient-reported outcome	
Study quality of life of patients and families with JIA and TMJ arthritis	8.4
Study the burden of care for patients with TMJ arthritis/TMJ involvement/dentofacial deformity	8

* Levels of importance were assessed using a 10-point visual analog scale, with 0 being not important and 10 being extremely important. See Table 3 for definitions.

Future research agenda. A comprehensive research agenda was developed to provide a framework for future interdisciplinary research efforts. The full list of agenda items is provided in Table 4.

DISCUSSION

These are the first interdisciplinary recommendations for the management of JIA-related TMJ arthritis and the associated orofacial manifestations. Despite a lack of high-level evidence, we created the 3 overarching principles and 12 recommendations outlined above to try to address the clinical questions clinicians are struggling with when treating patients with JIA-associated TMJ arthritis. This article is considered to be a working document, with plans for revision as new evidence emerges. The 2021 American College of Rheumatology (ACR) guideline for the treatment of JIA was recently published and included therapeutic approaches for TMJ arthritis (74). Both the 2021 ACR guideline and the recommendations in this review caution against the use of intraarticular glucocorticoid injections in skeletally immature patients and the use of biologic DMARDs in patients who have had an insufficient response to synthetic DMARDs. In addition to the 2021 ACR treatment guideline, our recommendations include evidence not only for therapeutic approaches, but also for orthopedic devices, orthodontic devices, and surgical interventions for the management of JIA-associated TMJ arthritis and the related manifestations.

Due to the low quality of available evidence, all recommendations are considered to be conditional to denote the uncertainty regarding the balance of benefits and harms (75). The proposed research agenda constitutes a framework for future interdisciplinary research efforts to improve the evidence of care. It is presented in the form of specific research questions to make the future research relevant and directly applicable to clinical practice. Future research should also focus on the burden of care and consider the cost-effectiveness of the proposed diagnostic and treatment modalities. The proposed areas of study are suggestions and are not intended to exclude other research questions.

Optimal management of TMJ arthritis and the associated manifestations requires an interdisciplinary approach and should be recognized as an integrated part of contemporary JIA disease control. Management strategies should be individualized according to the specific JIA-related orofacial manifestations of each patient. The voting panel highlights the importance of shared decision-making involving patients, parents, and clinicians in defining targets of treatment and approaches to management. We acknowledge that management may vary by region and healthcare system. The voting panel hopes that the current recommendations help to facilitate a process for specialties to collaborate on local and national strategies for the management of TMJ arthritis and related orofacial manifestations. Furthermore, we hope that the current recommendations will increase attention to this common manifestation of JIA disease (1,2,5,6).

AUTHOR CONTRIBUTIONS

All authors were involved in drafting the article or revising it critically for important intellectual content, and all authors approved the final version to be published. Drs. Stoustrup and Twilt had full access to all of the data in the study and take responsibility for the integrity of the data and the accuracy of the data analysis.

Study conception and design. Stoustrup, Resnick, Abramowicz, Pedersen, Twilt.

Acquisition of data. Stoustrup, Resnick, Abramowicz, Pedersen, Michelotti, Küseler, Koos, Verna, Nordal, Granquist, Halbig, Kristensen, Kaban, Arvidsson, Spiegel, Stoll, Lerman, Glerup, Defabianis, Frid, Alstergren, Cron, Ringold, Nørholt, Peltomaki, Larheim, Herlin, Peacock, Kellenberger, Twilt.

Analysis and interpretation of data. Stoustrup, Resnick, Abramowicz, Pedersen, Michelotti, Küseler, Koos, Verna, Nordal, Granquist, Halbig, Kristensen, Kaban, Arvidsson, Spiegel, Stoll, Lerman, Glerup, Defabianis, Frid, Alstergren, Cron, Ringold, Nørholt, Peltomaki, Larheim, Herlin, Peacock, Kellenberger, Twilt.

REFERENCES

1. Cannizzaro E, Schroeder S, Müller LM, et al. Temporomandibular joint involvement in children with juvenile idiopathic arthritis. J Rheumatol 2011;38:510–5.
2. Stoll ML, Sharpe T, Beukelman T, et al. Risk factors for temporomandibular joint arthritis in children with juvenile idiopathic arthritis. J Rheumatol 2012;39:1880–7.
3. Von Schuckmann L, Klotsche J, Suling A, et al. Temporomandibular joint involvement in patients with juvenile idiopathic arthritis: a retrospective chart review. Scand J Rheumatol 2020;49:271–80.
4. Arvidsson LZ, Smith HJ, Flato B, et al. Temporomandibular joint findings in adults with long-standing juvenile idiopathic arthritis: CT and MR imaging assessment. Radiology 2010;256:191–200.
5. Glerup M, Stoustrup P, Matzen LH, et al. Longterm outcomes of temporomandibular joints in juvenile idiopathic arthritis: 17 years of followup of a Nordic juvenile idiopathic arthritis cohort. J Rheumatol 2020;47:730–8.
6. Stoustrup P, Glerup M, Bilgrau AE, et al. Cumulative incidence of orofacial manifestations in early juvenile idiopathic arthritis: a regional, three-year cohort study. Arthritis Care Res (Hoboken) 2020;72:907–16.
7. Weiss PF, Arabshahi B, Johnson A, et al. High prevalence of temporomandibular joint arthritis at disease onset in children with juvenile idiopathic arthritis, as detected by magnetic resonance imaging but not by ultrasound. Arthritis Rheum 2008;58:1189–96.
8. Hugle B, Spiegel L, Hotte J, et al. Isolated arthritis of the temporomandibular joint as the initial manifestation of juvenile idiopathic arthritis. J Rheumatol 2017;44:1632–5.
9. Frid P, Nordal E, Bovis F, et al. Temporomandibular joint involvement in association with quality of life, disability, and high disease activity in juvenile idiopathic arthritis. Arthritis Care Res (Hoboken) 2017;69:677–86.
10. Rahimi H, Twilt M, Herlin T, et al. Orofacial symptoms and oral health-related quality of life in juvenile idiopathic arthritis: a two-year prospective observational study. Pediatr Rheumatol Online J 2018;16:47.
11. Carlsson AD, Wahlund K, Kindgren E, et al. Orofacial pain in juvenile idiopathic arthritis is associated with stress as well as psychosocial and functional limitations. Pediatr Rheumatol Online J 2019;17:83.
12. Fischer J, Skeie MS, Rosendahl K, et al. Prevalence of temporomandibular disorder in children and adolescents with juvenile idiopathic arthritis: a Norwegian cross-sectional multicentre study. BMC Oral Health 2020;20:282.

13. Stoustrup P, Traberg MS, Matzen LH, et al. Initial radiological signs of dentofacial deformity in juvenile idiopathic arthritis. Sci Rep 2021;11: 13142.
14. Von Bremen J, Ruf S. Juvenile idiopathic arthritis-and now?: a systematic literature review of changes in craniofacial morphology. J Orofac Orthop 2012;73:265–76.
15. Stoustrup P, Resnick CM, Pedersen TK, et al. Standardizing terminology and assessment for orofacial conditions in juvenile idiopathic arthritis: international, multidisciplinary consensus-based recommendations. J Rheumatol 2019;46:518–22.
16. Foeldvari I, Tzaribachev N, Cron RQ. Results of a multinational survey regarding the diagnosis and treatment of temporomandibular joint involvement in juvenile idiopathic arthritis. Pediatr Rheumatol Online J 2014;25;12:6.
17. Kinard BE, Abramowicz S. Juvenile idiopathic arthritis practice patterns among oral and maxillofacial surgeons. J Oral Maxillofac Surg 2017;75:2333.e1–8.
18. Howick J, Chalmers I, Glasziou P, et al. OCEBM Levels of Evidence Working Group. "The Oxford 2011 Levels of Evidence." Oxford Centre for Evidence-Based Medicine. URL: https://www.cebm.ox.ac.uk/resources/levels-of-evidence/ocebm-levels-of-evidence.
19. Andrews J, Guyatt G, Oxman AD, et al. GRADE guidelines: 14. Going from evidence to recommendations: the significance and presentation of recommendations. J Clin Epidemiol 2013;66:719–25.
20. Andrews JC, Schünemann HJ, Oxman AD, et al. GRADE guidelines: 15. Going from evidence to recommendation-determinants of a recommendation's direction and strength. J Clin Epidemiol 2013;66: 726–35.
21. Larheim TA, Doria AS, Kirkhus E, et al. TMJ imaging in JIA patients—An overview. Semin Orthod 2015;21:102–10.
22. Kellenberger CJ, Junhasavasdikul T, Tolend M, et al. Temporomandibular joint atlas for detection and grading of juvenile idiopathic arthritis involvement by magnetic resonance imaging. Pediatr Radiol 2018; 48:411–26.
23. Tolend M, Junhasavasdikul T, Cron RQ, et al. Discrete choice experiment on a magnetic resonance imaging scoring system for temporomandibular joints in juvenile idiopathic arthritis. Arthritis Care Res (Hoboken) 2021;74:308–16.
24. Tolend MA, Twilt M, Cron RQ, et al. Toward establishing a standardized magnetic resonance imaging scoring system for temporomandibular joints in juvenile idiopathic arthritis. Arthritis Care Res (Hoboken) 2018;70:758–67.
25. Tolend M, Doria AS, Meyers AB, et al. Assessing the reliability of the OMERACT juvenile idiopathic arthritis magnetic resonance scoring system for temporomandibular joints (JAMRIS-TMJ). J Clin Med 2021;10:4047.
26. Angenete OW, Augdal TA, Jellestad S, et al. Normal magnetic resonance appearances of the temporomandibular joints in children and young adults aged 2-18 years. Pediatr Radiol 2018;48:341–9.
27. Kottke R, Saurenmann RK, Schneider MM, et al. Contrast-enhanced MRI of the temporomandibular joint: findings in children without juvenile idiopathic arthritis. Acta Radiol 2015;56:1145–52.
28. Stoll ML, Guleria S, Mannion ML, et al. Defining the normal appearance of the temporomandibular joints by magnetic resonance imaging with contrast: a comparative study of children with and without juvenile idiopathic arthritis. Pediatr Rheumatol Online J 2018;16:8.
29. Hechler BL, Phero JA, Van Mater H, et al. Ultrasound versus magnetic resonance imaging of the temporomandibular joint in juvenile idiopathic arthritis: a systematic review. Int J Oral Maxillofac Surg 2018; 47:83–9.
30. Muller L, Kellenberger CJ, Cannizzaro E, et al. Early diagnosis of temporomandibular joint involvement in juvenile idiopathic arthritis: a pilot study comparing clinical examination and ultrasound to magnetic resonance imaging. Rheumatology (Oxford) 2009;48:680–5.
31. Zwir LF, Terreri MT, do Amaral EC, et al. Is power Doppler ultrasound useful to evaluate temporomandibular joint inflammatory activity in juvenile idiopathic arthritis? Clin Rheumatol 2020;39:1237–40.
32. Kirkhus E, Gunderson RB, Smith HJ, et al. Temporomandibular joint involvement in childhood arthritis: comparison of ultrasonography-assessed capsular width and MRI-assessed synovitis. Dentomaxillofac Radiol 2016;45:20160195.
33. Stoustrup P, Twilt M, Spiegel L, et al. Clinical orofacial examination in juvenile idiopathic arthritis: International consensus-based recommendations for monitoring patients in clinical practice and research studies. J Rheumatol 2017;44:326–33.
34. Consolaro A, Ruperto N, Bazso A, et al. Development and validation of a composite disease activity score for juvenile idiopathic arthritis. Arthritis Rheum. 2009;61:658–66.
35. Filocamo G, Consolaro A, Schiappapietra B, et al. A new approach to clinical care of juvenile idiopathic arthritis: the Juvenile Arthritis Multidimensional Assessment Report. J Rheumatol 2011;38:938–53.
36. Ruperto N, Ravelli A, Pistorio A, et al. Cross-cultural adaptation and psychometric evaluation of the Childhood Health Assessment Questionnaire (CHAQ) and the Child Health Questionnaire (CHQ) in 32 countries. Review of the general methodology. Clin Exp Rheumatol 2001;19:S1–9.
37. Stoustrup P, Herlin T, Spiegel L, et al. Standardizing the clinical orofacial examination in juvenile idiopathic arthritis: an interdisciplinary, consensus-based, short screening protocol. J Rheumatol 2020;47: 1397–404.
38. Fjeld MG, Arvidsson LZ, Smith HJ, et al. Relationship between disease course in the temporomandibular joints and mandibular growth rotation in patients with juvenile idiopathic arthritis followed from childhood to adulthood. Pediatr Rheumatol Online J 2010 22;8:13.
39. Fjeld MG, Arvidsson LZ, Stabrun AE, et al. Average craniofacial development from 6 to 35 years of age in a mixed group of patients with juvenile idiopathic arthritis. Acta Odontol Scand 2009;67:153–60.
40. Stoustrup P, Iversen CK, Kristensen KD, et al. Assessment of dentofacial growth deviation in juvenile idiopathic arthritis: reliability and validity of three-dimensional morphometric measures. PloS One 2018;13:e0194177.
41. Bollhalder A, Patcas R, Eichenberger M, et al. Magnetic resonance imaging followup of temporomandibular joint inflammation, deformation, and mandibular growth in juvenile idiopathic arthritis patients receiving systemic treatment. J Rheumatol 2020;47:909–16.
42. Ince DO, Ince A, Moore TL. Effect of methotrexate on the temporomandibular joint and facial morphology in juvenile rheumatoid arthritis patients. Am J Orthod Dentofacial Orthop 2000;118:75–83.
43. Resnick CM, Pedersen TK, Abramowicz S, et al. Time to reconsider management of the temporomandibular joint in juvenile idiopathic arthritis. J Oral Maxillofac Surg 2018;76:1145–6.
44. Antonarakis GS, Blanc A, Courvoisier DS, et al. Effect of intra-articular corticosteroid injections on pain and mouth opening in juvenile idiopathic arthritis with temporomandibular involvement: a systematic review and meta-analysis. J Craniomaxillofac Surg 2020;48:772–8.
45. Stoustrup P, Kristensen KD, Verna C, et al. Intra-articular steroid injection for temporomandibular joint arthritis in juvenile idiopathic arthritis: a systematic review on efficacy and safety. Semin Arthritis Rheum 2013;43:63–70.
46. Lochbühler N, Saurenmann RK, Müller L, et al. Magnetic resonance imaging assessment of temporomandibular joint involvement and mandibular growth following corticosteroid injection in juvenile idiopathic arthritis. J Rheumatol 2015;42:1514–22.
47. Resnick CM, Vakilian PM, Kaban LB, et al. Quantifying the effect of temporomandibular joint intra-articular steroid injection on synovial

enhancement in juvenile idiopathic arthritis. J Oral Maxillofac Surg 2016;74:2363–9.

48. Stoustrup P, Kristensen KD, Küseler A, et al. Temporomandibular joint steroid injections in patients with juvenile idiopathic arthritis: an observational pilot study on the long-term effect on signs and symptoms. Pediatr Rheumatol Online J 2015;13:62.
49. Stoll ML, Amin D, Powell KK, et al. Risk factors for intraarticular heterotopic bone formation in the temporomandibular joint in juvenile idiopathic arthritis. J Rheumatol 2018;45:1301–7.
50. Frid P, Augdal TA, Larheim TA, et al. Efficacy and safety of intraarticular corticosteroid injections in adolescents with juvenile idiopathic arthritis in the temporomandibular joint: a Norwegian 2-year prospective multicenter pilot study. Pediatr Rheumatol Online J 2020;18:75.
51. Kristensen KD, Stoustrup P, Küseler A, et al. Clinical predictors of temporomandibular joint arthritis in juvenile idiopathic arthritis: a systematic literature review. Semin Arthritis Rheum 2016;45:717–32.
52. Stoustrup P, Pedersen TK, Nørholt SE, et al. Interdisciplinary management of dentofacial deformity in juvenile idiopathic arthritis. Oral Maxillofac Surg Clin North Am 2020;32:117–34.
53. Isola G, Ramaglia L, Cordasco G, et al. The effect of a functional appliance in the management of temporomandibular joint disorders in patients with juvenile idiopathic arthritis. Minerva Stomatol 2017;66: 1–8.
54. Portelli M, Matarese G, Militi A, et al. Temporomandibular joint involvement in a cohort of patients with Juvenile Idiopatic Arthritis and evaluation of the effect induced by functional orthodontic appliance: clinical and radiographic investigation. Eur J Paediatr Dent 2014;15:63–6.
55. Stoustrup P, Kristensen KD, Kuseler A, et al. Management of temporomandibular joint arthritis-related orofacial symptoms in juvenile idiopathic arthritis by the use of a stabilization splint. Scand J Rheumatol 2014;43:137–45.
56. Lindfors E, Arima T, Baad-Hansen L, et al. Jaw exercises in the treatment of temporomandibular disorders: an international modified delphi study. J Oral Facial Pain Headache 2019;33:389–98.
57. Olsen-Bergem H, Bjørnland T. A cohort study of patients with juvenile idiopathic arthritis and arthritis of the temporomandibular joint: outcome of arthrocentesis with and without the use of steroids. Int J Oral Maxillofac Surg 2014;43:990–5.
58. Arvidsson LZ, Fjeld MG, Smith HJ, et al. Craniofacial growth disturbance is related to temporomandibular joint abnormality in patients with juvenile idiopathic arthritis, but normal facial profile was also found at the 27-year follow-up. Scand J Rheumatol 2010;39:373–9.
59. Stoustrup PB, Ahlefeldt-Laurvig-Lehn N, Kristensen KD, et al. No association between types of unilateral mandibular condylar abnormalities and facial asymmetry in orthopedic-treated patients with juvenile idiopathic arthritis. Am J Orthod Dentofacial Orthop 2018;153: 214–23.
60. Resnick CM, Frid P, Norholt SE, et al. An algorithm for management of dentofacial deformity resulting from juvenile idiopathic arthritis: results of a multinational consensus conference. J Oral Maxillofac Surg. 2019;77:1152.e1–33.
61. Von Bremen J, Ruf S. Orthodontic and dentofacial orthopedic management of juvenile idiopathic arthritis: a systematic review of the literature. Orthod Craniofac Res 2011;14:107–15.
62. Farronato G, Carletti V, Maspero C, et al. Craniofacial growth in children affected by juvenile idiopathic arthritis involving the temporomandibular joint: functional therapy management. J Clin Pediatr Dent 2009;33:351–7.
63. Isola G, Ramaglia L, Cordasco G, et al. The effect of a functional appliance in the management of temporomandibular joint disorders in patients with juvenile idiopathic arthritis. Minerva Stomatol 2017;66: 1–8.
64. Kjellberg H, Kiliaridis S, Thilander B. Dentofacial growth in orthodontically treated and untreated children with juvenile chronic arthritis (JCA). A comparison with Angle Class II division 1 subjects. Eur J Orthod 1995;17:357–73.
65. Stoustrup P, Kuseler A, Kristensen KD, et al. Orthopaedic splint treatment can reduce mandibular asymmetry caused by unilateral temporomandibular involvement in juvenile idiopathic arthritis Eur J Orthod 2013;35:191–8.
66. Abate A, Cavagnetto D, Rusconi FM, et al. Safety and effects of the rapid maxillary expander on temporomandibular joint in subjects affected by juvenile idiopathic arthritis: a retrospective study. Children (Basel) 2021;8:33.
67. Frid P, Resnick C, Abramowicz S, et al. Surgical correction of dentofacial deformities in juvenile idiopathic arthritis: a systematic literature review. Int J Oral Maxillofac Surg 2019;48:1032–42.
68. Skeie MS, Gil EG, Cetrelli L, et al. Oral health in children and adolescents with juvenile idiopathic arthritis: a systematic review and meta-analysis. BMC Oral Health 2019;19:285.
69. Grevich S, Lee P, Leroux B, et al. Oral health and plaque microbial profile in juvenile idiopathic arthritis. Pediatr Rheumatol Online J 2019;17:81.
70. Merle CL, Hoffmann R, Schmickler J, et al. Comprehensive assessment of orofacial health and disease related parameters in adolescents with juvenile idiopathic arthritis: a cross-sectional study. J Clin Med 2020;9:513.
71. Hussain SB, Botelho J, Machado V, et al. Is there a bidirectional association between rheumatoid arthritis and periodontitis? A systematic review and meta-analysis. Semin Arthritis Rheum 2020;50:414–22.
72. Potempa J, Mydel P, Koziel J. The case for periodontitis in the pathogenesis of rheumatoid arthritis [review]. Nat Rev Rheumatol 2017;13: 606–20.
73. Frid P, Baraniya D, Halbig J, et al. Salivary oral microbiome of children with juvenile idiopathic arthritis: a Norwegian cross-sectional study. Front Cell Infect Microbiol 2020;10:602239.
74. Onel KB, Horton DB, Lovell DJ, et al. American College of Rheumatology Guideline for the treatment of juvenile idiopathic arthritis: therapeutic approaches for oligoarthritis, temporomandibular joint arthritis, and systemic juvenile idiopathic arthritis. Arthritis Rheumatol 2022;74:553–69.
75. World Health Organization. WHO handbook for guideline development, 2nd ed; 2014. URL: https://apps.who.int/iris/handle/10665/145714.

Arthritis & Rheumatology
Vol. 75, No. 1, January 2023, pp 15–22
DOI 10.1002/art.42347

AMERICAN COLLEGE of RHEUMATOLOGY
Empowering Rheumatology Professionals

SPECIAL

American College of Rheumatology/EULAR Remission Criteria for Rheumatoid Arthritis: 2022 Revision

Paul Studenic,[1] Daniel Aletaha,[2] Maarten de Wit,[3] Tanja A. Stamm,[4] Farideh Alasti,[2] Diane Lacaille,[5] Josef S. Smolen,[2] and David T. Felson[6]

This criteria set has been approved by the American College of Rheumatology (ACR) Board of Directors and the EULAR Executive Committee. This signifies that the criteria set has been quantitatively validated using patient data, and it has undergone validation based on an independent data set. All ACR/EULAR-approved criteria sets are expected to undergo intermittent updates.

The ACR is an independent, professional, medical and scientific society that does not guarantee, warrant, or endorse any commercial product or service.

Objective. In 2011, the American College of Rheumatology (ACR) and EULAR endorsed provisional criteria for remission in rheumatoid arthritis (RA), both Boolean- and index-based. Based on recent studies indicating that a higher threshold for the patient global assessment (PtGA) may improve agreement between the 2 sets of criteria, our goals were to externally validate a revision of the Boolean remission criteria using a higher PtGA threshold and to validate the provisionally endorsed index-based criteria.

Methods. We used data from 4 randomized trials comparing biologic disease-modifying antirheumatic drugs to methotrexate or placebo. We tested the higher proposed PtGA threshold of 2 cm (Boolean2.0) (range 0–10 cm) compared to the original threshold of 1 cm (Boolean1.0). We analyzed agreement between the Boolean- and index-based criteria (Simplified Disease Activity Index [SDAI] and Clinical Disease Activity Index [CDAI]) for remission and examined how well each remission definition predicted later good physical function (Health Assessment Questionnaire [HAQ] score ≤0.5) and radiographic nonprogression.

Results. Data from 2,048 trial participants, 1,101 with early RA and 947 with established RA, were included. The proportion of patients with disease in remission at 6 months after treatment initiation increased when using Boolean2.0 compared to Boolean1.0, from 14.8% to 20.6% in early RA and 4.2% to 6.0% in established RA. Agreement between Boolean2.0 and the SDAI or CDAI remission criteria was better than for Boolean1.0, particularly in early disease. Boolean2.0, SDAI, and CDAI remission criteria had similar positive likelihood ratios (LRs) to predict radiographic nonprogression and a HAQ score of ≤0.5 (positive LR 3.8–4.3). The omission of PtGA (BooleanX) worsened the prediction of good functional outcomes.

Conclusion. Using the Boolean 2.0 criteria classifies more patients as achieving remission and increases the agreement with index-based remission criteria without jeopardizing predictive value for radiographic or functional outcomes. This revised Boolean definition and the previously provisionally endorsed index-based criteria were endorsed by ACR and EULAR.

This article is published simultaneously in *Annals of the Rheumatic Diseases*.

[1]Paul Studenic, MD, PhD: Division of Rheumatology, Department of Medicine (Solna), Karolinska Institutet, Stockholm, Sweden, and Division of Rheumatology, Department of Internal Medicine 3, Medical University of Vienna, Vienna, Austria; [2]Daniel Aletaha, MD, MSc, Farideh Alasti, MSc, Josef S. Smolen, MD: Division of Rheumatology, Department of Internal Medicine 3, Medical University of Vienna, Vienna, Austria; [3]Maarten de Wit, PhD: EULAR Community of People with Arthritis/Rheumatism in Europe (PARE), Zürich, Switzerland; [4]Tanja A. Stamm, MSc, MBA, PhD:

INTRODUCTION

Disease activity in rheumatoid arthritis (RA) was initially defined by a number of core set variables, agreed upon by the American College of Rheumatology (ACR) and EULAR in the 1990s (1,2). These variables comprised tender joint count (TJC) and swollen joint count (SJC), patient assessment of global disease activity (PtGA) and of pain, evaluator/physician global assessment (EGA), a measure of function such as the Health Assessment Questionnaire (HAQ), and an acute-phase reactant such as C-reactive protein (CRP) level.

At the time of defining the core set variables, remission was more aspirational than a realistic goal (3). Today, however, remission can be obtained in a sizable portion of patients and is seen as a major therapeutic target (4–6). A clinical definition of remission for RA should reflect no or only minimal disease activity, and patients attaining this state should have a low risk of both structural progression and functional impairment (6).

ACR and EULAR endorsed provisional remission criteria over 10 years ago (7). Their publication served the purpose of providing a common definition for this prime treatment target (8). Two types of remission definitions were agreed upon by the ACR/EULAR committee after extensive data analyses and consensus-based deliberations. The Boolean definition required that, to attain remission, each of 4 core set variables (TJC, SJC, PtGA, CRP) must have a value of ≤1. (PtGA is scored on a 0–10-point or 0–10-cm scale, CRP in mg/dl.) The index-based definition used the remission cutoff point of the simplified disease activity index (SDAI) (9). The committee also endorsed remission criteria that did not include CRP level, namely a Boolean definition that comprised SJC, TJC, and PtGA and an index definition based on the remission threshold of the clinical disease activity index (CDAI) (10).

Since their publication, arguments have been made claiming that remission definitions may, on the one hand, be too stringent, with the risk of overtreatment if used as treatment targets, or, on the other hand, too lenient, proposing addition of imaging confirmation of remission. A particular matter of debate was the requirement of achieving a PtGA score of ≤1; the stringent threshold for the PtGA has been criticized, because some patients do not achieve it despite the absence of tender and swollen joints and an elevated CRP level (11). Moreover, the agreement between the Boolean and index definitions was only moderate, primarily due to the PtGA threshold (12). However, the PtGA is the core set measure most sensitive to change in RA trials (1,13–15), best differentiating between patients receiving active treatment and those receiving placebo. Thus, PtGA is an important measure of disease activity. Consequently, the PtGA was included in the ACR core set, composite activity scores, and remission definitions. However, PtGA may also be influenced by other factors related to RA. For example, patients with pain from irreversible joint damage may have elevations in PtGA even if their RA is in clinical remission (16,17).

To circumvent the strictness of the 1.0 rule for PtGA and to increase the agreement with SDAI-defined remission, a higher PtGA threshold has been proposed (18,19). Furthermore, since the index-based criteria can be used instead of Boolean criteria, both criteria should identify the same patients as having disease in remission. However, remission rates based on SDAI are higher than those using the Boolean criteria, because summing several components permits 1 component, such as the PtGA, to be slightly elevated if compensated by a lower score in others (20). A study evaluating alternative Boolean definitions of remission, with PtGA thresholds ranging 1.0–2.5, found that using a threshold of 2 cm (Boolean2.0) led to a higher agreement with the index-based definition without jeopardizing the strong association between remission and subsequent good functional and radiographic outcomes, a key criterion in the development of the provisional definition of remission (12). The purpose of the present study is to externally validate the performance characteristics of this revision of the Boolean criteria (12) and provide external validation of the provisionally endorsed SDAI and CDAI remission definitions. This provides the evidence base for ACR and EULAR to fully endorse the remission criteria, changing their status from the current "provisional" to a "definite" status.

PATIENTS AND METHODS

Patients. RA patient data were retrieved from 4 clinical trials testing the efficacy of biologic disease-modifying antirheumatic drugs (bDMARDs) against placebo or placebo with methotrexate (MTX), with an available observation period between 1 and 2 years. The GO-AFTER trial tested golimumab as an active compound, the FUNCTION and LITHE trials tested tocilizumab, and the SERENE trial tested rituximab. GO-AFTER evaluated patients who were insufficient responders to TNF inhibitors (TNFi), LITHE and SERENE included patients with an insufficient response to MTX, and FUNCTION included MTX-naive patients with early RA. Results and detailed patient characteristics of the individual trials have been previously reported (21–24). These trials included RA patients with varying disease durations and treatment

Institute for Outcomes Research, Center for Medical Statistics, Informatics, and Intelligent Systems, Medical University of Vienna, Vienna, Austria; [5]Diane Lacaille, MD, MHSc: Division of Rheumatology, Department of Medicine, University of British Columbia and Arthritis Research Canada, Vancouver, Canada; [6]David T. Felson, MD, MPH: Section of Rheumatology, Boston University School of Medicine, Boston, Massachusetts.

Author disclosures are available at https://onlinelibrary.wiley.com/action/downloadSupplement?doi=10.1002%2Fart.42347&file=art42347-sup-0001-Disclosureform.pdf.

Address correspondence via email to Paul Studenic, MD, PhD, at paul.studenic@meduniwien.ac.at.

Submitted for publication April 13, 2022; accepted in revised form September 2, 2022.

histories. In all 4 trials, the PtGA was evaluated using a 100-mm visual analog scale (VAS).

Definitions of remission and their modifications. The Boolean definition includes SJC, TJC, PtGA (cm), and CRP levels (mg/dl); for a patient to meet remission criteria, all component scores must be ≤1 (in the case of a 100-mm VAS, this translates to a score of ≤10). A version without CRP was also approved by the ACR/EULAR committee (3-variable Boolean [3vBoolean]). The SDAI-based definition of remission sums the scores for the components used in the Boolean definition in addition to EGA, and patients meet criteria if the score is ≤3.3. The CDAI-based remission definition consists of the same components, excluding CRP level, and remission is fulfilled at a score of ≤2.8 (7).

Similar to a previous study (12), we increased the threshold of the PtGA criterion by steps of 0.5 cm from 1 cm up to 2.5 cm, and labeled these as Boolean1.0, Boolean1.5, Boolean2.0, and Boolean2.5. The Boolean definition that does not include the PtGA criterion was labeled as BooleanX; in this definition, only CRP, TJC, and SJC needed a score of ≤1 to attain remission, regardless of PtGA value (25).

Statistical analysis. We performed descriptive analyses and tested the revised Boolean2.0 criteria against the provisional Boolean1.0 criteria for convergent and predictive validity. Finally, we investigated the impact of the exclusion of the PtGA from the definition of remission (BooleanX). Analyses were performed on 6-month and 12-month data using SPSS Statistics 25 and Stata version 15. An experienced patient research partner (MW) was involved throughout the study. He took part in all meetings, reviewed data at different time points, and provided written as well as oral feedback. His contribution focused on a critical review of the PtGA as part of the RA definition of remission.

Descriptive analysis. We analyzed how the rates of remission at 6 and 12 months after treatment initiation in the trials were affected by the different modifications described above. For the Boolean modifications, we also studied which components prevented achievement of full remission by identifying participants who fulfilled 3 of 4 required criteria but not all 4 of them (11).

Convergent validity. We tested the agreement of different Boolean criteria with the index-based remission definitions. We cross-tabulated remission fulfilment for Boolean remission versions with the SDAI and CDAI definitions and analyzed their agreement using McNemar's test for agreement with kappa statistics. In addition, the well-established concordance between SDAI- and CDAI-defined remission was tested to confirm the interchangeability of these definitions.

We examined the optimal PtGA threshold to achieve concordance with SDAI-defined remission by carrying out classification and regression trees (CART) analyses (R rpart package; https://cran.r-project.org/web/packages/rpart/index.html), in which, after assuming that CRP, TJC, and SJC were all in remission (BooleanX), we asked what threshold of PtGA would provide the best prediction of SDAI-defined remission.

Predictive validity. As a next step, we explored the impact of using the modified Boolean- and index-based remission definitions assessed at 6 months after treatment initiation on outcomes at 1 year. Differences in mean radiographic progression (based on the change in modified total Sharp and van der Heijde score [mTSS] between baseline and 1 year) and the proportions of patients without progression (change in score ≤0) and with good function at 1 year (HAQ ≤0.5) were assessed. Attaining an HAQ of ≤0.5 without radiographic progression at 1 year of treatment was defined as a good combined outcome, similar to the procedure used to develop the provisional ACR/EULAR remission definition (7). These analyses were repeated separately for early and late RA participants. Positive and negative likelihood ratios (LRs) were calculated separately for each remission definition to assess predictive validity for good functional and structural outcomes.

Impact of PtGA score and PtGA exclusion from the remission definition. In addition to the comparison of Boolean2.0 to Boolean 1.0, we analyzed the effect of excluding PtGA from remission criteria (BooleanX) in the context of each of the above analyses.

RESULTS

Patients, remission rates, and components limiting achievement of remission. Data from 2,048 clinical trial participants, 1,101 with early RA (mean ± SD disease duration 0.8 ± 0.5 years) and 947 with established RA (mean ± SD disease duration 7.1 ± 5.4 years), were included. As expected, using Boolean2.0 yielded higher remission rates compared to Boolean1.0 at 6 months: 20.6% (n = 227) compared to 14.8% (n = 163) in early RA; 6.0% (n = 57) versus 4.2% (n = 40) in established RA (Figure 1). These correspond to a relative increase in remission rates of 39% and 42%, in early and established RA, respectively. This trend was consistent at 1 year, although remission rates were generally higher (Supplementary Figure 1, on the *Arthritis & Rheumatology* website at https://onlinelibrary.wiley.com/doi/10.1002/art.42347). Omitting the PtGA criterion using the BooleanX definition further increased remission rates over Boolean2.0, in early RA (from 227 patients [20.6%] to 297 patients [27%]) and in established RA (from 57 patients [6%] to 95 patients [10%] patients at 6 months), with relative increases of 31% and 66%, respectively.

Within the total study population, 311 participants (15.2%) achieved "near misses" of Boolean remission, meaning that they fulfilled 3 of the 4 criteria. In 60% of these participants, this was due to not meeting the criterion of PtGA ≤1cm. By using Boolean2.0, this proportion was reduced to 47% of all near misses. Consequently, among all participants, 14% were classified as having Boolean2.0-defined remission, 5% missed achieving remission only because of the PtGA criterion, and 3% missed achieving

Figure 1. Rates of rheumatoid arthritis (RA) disease remission according to modified Boolean classifications, using a patient global assessment (PtGA) threshold of 1.0 ("Boolean"), 1.5, 2.0, 2.5, or omitting the PtGA completely (BooleanX), as well as according to the Simplified Disease Activity Index (SDAI), Clinical Disease Activity Index (CDAI), and Disease Activity Score in 28 joints (DAS28) definitions. Rates at 6 months after treatment initiation are shown for patients with early RA and those with established RA. Color figure can be viewed in the online issue, which is available at http://onlinelibrary.wiley.com/doi/10.1002/art.42347/abstract.

remission only because of the SJC criterion (Supplementary Figure 2, https://onlinelibrary.wiley.com/doi/10.1002/art.42347).

Convergent validity. Increasing the PtGA cutoff from 1.0 to 2.0 cm for participants with early RA yielded higher concordance rates between Boolean- and SDAI-defined criteria for remission. This led to more participants contemporaneously fulfilling the SDAI and respective Boolean remission definition (increase from 71% to 92% of participants when using Boolean1.0 versus Boolean2.0) (Table 1). Rates of concordantly classified participants with respect to remission increased from 93.4% to 95.9% at 6 months. A similar increase in concordantly classified participants was observed for the agreement between the corresponding Boolean and CDAI definitions (Supplementary Table 1, https://onlinelibrary.wiley.com/doi/10.1002/art.42347). In patients with established RA, the percentage classified as having disease in remission by Boolean and CDAI or SDAI definitions likewise increased from 74% to 94% for SDAI and from 70% to 83% for CDAI, when using Boolean1.0 versus Boolean 2.0; and from 78% to 96% when using 3vBoolean1.0 versus 3vBoolean2.0 to assess agreement with CDAI. The proportion of participants concordantly classified as having disease in remission remained similar in established RA.

Kappa analyses showed higher agreement between SDAI-defined remission and Boolean2.0-defined than with Boolean1.0-defined remission at 6 months (Figure 2). The 12-month data showed similar results and are depicted in Supplementary Figure 3 (https://onlinelibrary.wiley.com/doi/10.1002/art.42347). Kappa estimates and 95% confidence intervals (95% CIs) of agreement with SDAI- and CDAI-defined remission at 6 months increased when using Boolean2.0 compared to Boolean1.0 definitions (0.86 [95% CI 0.83–0.89] versus 0.77 [95% CI 0.74–0.82] for SDAI at 6 months, and 0.81 [95% CI 0.77–0.84] versus 0.76 [95% CI 0.72–0.81] for CDAI at 6 months) (kappa

Table 1. Agreement rates between different modified Boolean remission definitions and the SDAI remission definition in RA patients at 6 months*

	Boolean1.0, no. in remission/ total no. (%)	Boolean2.0, no. in remission/ total no. (%)	BooleanX, no. in remission/ total no. (%)
Early RA			
Patients with disease in SDAI-based remission among those fulfilling Boolean remission definition	153/163 (93.9)	199/227 (87.7)	206/297 (69.4)
Patients with disease in Boolean-based remission among those fulfilling SDAI remission definition	153/216 (70.8)	199/216 (92.1)	206/216 (95.4)
Total concordantly classified	1,028/1,101 (93.4)	1,056/1,101 (95.9)	1,000/1,101 (90.8)
Established RA			
Patients with disease in SDAI-based remission among those fulfilling Boolean remission definition	34/40 (85)	43/57 (75.4)	45/95 (47.4)
Patients with disease in Boolean-based remission among those fulfilling SDAI remission definition	34/46 (73.9)	43/46 (93.5)	45/46 (97.8)
Total concordantly classified	929/947 (98)	930/947 (98.2)	896/947 (94.6)

* RA = rheumatoid arthritis; SDAI = Simplified Disease Activity Index.

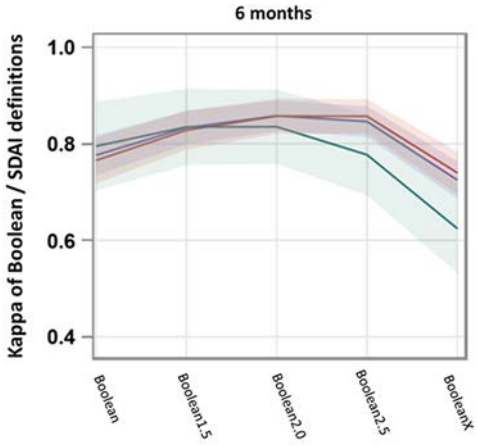

Kappa	All patients	Early RA	Established RA
Boolean	0.77 (0.74 – 0.82)	0.77 (0.72 – 0.81)	0.80 (0.70 – 0.89)
Boolean1.5	0.83 (0.79 – 0.87)	0.83 (0.79 – 0.87)	0.83 (0.76 – 0.91)
Boolean2.0	0.86 (0.83 – 0.89)	0.86 (0.82 – 0.89)	0.84 (0.75 – 0.91)
Boolean2.5	0.85 (0.81 – 0.87)	0.86 (0.82 - 0.89)	0.78 (0.70 – 0.90)
BooleanX	0.72 (0.69 - 0.76)	0.74 (0.69 – 0.78)	0.62 (0.53 – 0.72)

Figure 2. Kappa values and 95% confidence intervals (95% CIs) representing agreement between modified Boolean remission definitions and SDAI-defined remission, for patients with early RA (red line), those with established RA (green line), and all RA patients (blue line) at 6 months. Kappa estimates and 95% CIs are provided in the accompanying table. See Figure 1 for definitions. Color figure can be viewed in the online issue, which is available at http://onlinelibrary.wiley.com/doi/10.1002/art.42347/abstract.

curves for CDAI are shown in Supplementary Figure 4, https://onlinelibrary.wiley.com/doi/10.1002/art.42347).

A further increase in the PtGA threshold beyond 2 cm led to a decrease in concordance. Reduced concordance was particularly seen when omitting the PtGA (BooleanX) both in terms of percentage agreement and according to kappa estimates (Table 1 and Figure 2).

Additionally, CART analyses confirmed the percent agreement and kappa results: in participants with SJC, TJC, and CRP values of ≤1, and PtGA values of ≤2.3 cm at 6 months and ≤1.8 cm at 12 months showed the highest likelihood of concurrent SDAI-defined remission. The same analyses stratified by early or established RA yielded a PtGA threshold value of ≤2.3 cm in early RA and ≤1.4 cm in established RA at 6 months (≤1.5 cm in early RA and ≤1.9 cm in established RA at 12 months). Generally, all agreement estimates point to 2.0 cm as the optimal threshold.

Predictive validity. We studied rates of participants achieving a good functional outcome (HAQ ≤0.5) and no radiographic progression (ΔmTSS) at 1 year for participants classified by the different Boolean definitions at 6 months.

Similar results were found for Boolean2.0 and index-based definitions when predicting good functional outcome. HAQ scores at 12 months were as follows: mean ± SD 0.24 ± 0.40 for Boolean1.0, 0.31 ± 0.45 for Boolean2.0, 0.41 ± 0.53 for BooleanX, 0.27 ± 0.42 for SDAI, and 0.26 ± 0.42 for CDAI. Fewer participants scored an HAQ of ≤0.5 when the PtGA was omitted (70% in BooleanX versus 78% in Boolean2.0) (Table 2). Increasing the PtGA threshold for Boolean-based remission was associated with a linear increase in HAQ scores. While there was a drop in positive LR from 6.1 to 4.4 when using the Boolean2.0, this was similar to the positive LR predicting a good functional outcome for SDAI- and CDAI-based remission, which ranged from 4.3 to 4.9.

Table 2 outlines the similarity of LRs for predicting lack of radiographic progression during the first year when the different remission definitions were fulfilled at 6 months of treatment. The radiographic outcomes were similar regardless of the PtGA threshold or whether PtGA was included in the Boolean criteria, and scores were similar between different definitions (mean ± SD ΔmTSS 0.29 ± 2.08 for Boolean1.0, 0.25 ± 1.81 for Boolean2.0, 0.21 ± 1.9 for BooleanX, 0.27 ± 1.86 for SDAI, and 0.27 ± 1.9 for CDAI). This observation is consistent with

Table 2. Rates and LRs of RA patients achieving a good functional outcome (HAQ ≤0.5) and/or no radiographic progression (ΔmTSS) at 1 year, according to different remission criteria*

	HAQ ≤0.5				No increase in mTSS				Combined variables			
Criteria fulfilled	No	Yes	LR+ (range)	LR− (range)	No	Yes	LR+ (range)	LR− (range)	No	Yes	LR+ (range)	LR− (range)
Early RA												
Boolean1.0	43.3	85.9	6.19 (4.0–9.5)	0.78 (0.7–0.8)	65.6	78.5	1.76 (1.2–2.5)	0.92 (0.9–1.0)	31.7	67.5	3.54 (2.6–4.8)	0.79 (0.7–0.8)
Boolean2.0	41.5	80.6	4.23 (3.1–5.7)	0.72 (0.7–0.8)	64.4	79.3	1.85 (1.4–2.4)	0.87 (0.8–0.9)	29.6	65.2	3.19 (2.5–4.1)	0.72 (0.7–0.8)
BooleanX	40.5	74.1	2.76 (2.3–3.3)	0.58 (0.5–0.7)	63.1	79.5	1.86 (1.4–2.4)	0.82 (0.8–0.9)	28.4	60.3	2.59 (2.1–3.2)	0.67 (0.6–0.7)
SDAI	41.4	83.3	3.88 (3.1–4.9)	0.61 (0.5–0.7)	64.6	79.2	1.83 (1.2–2.5)	0.88 (0.8–0.9)	29.7	66.7	3.41 (2.6–4.4)	0.72 (0.7–0.8)
CDAI	41.6	83.7	4.25 (3.4–5.4)	0.60 (0.5–0.7)	64.8	78.9	1.81 (1.3–2.5)	0.89 (0.8–0.9)	29.9	67	3.46 (2.7–4.5)	0.73 (0.7–0.8)
Established RA												
Boolean1.0	29.2	72.5	5.86 (3.0–11.6)	0.92 (0.9–1.0)	32.6	37.5	1.23 (0.7–2.3)	0.99 (0.9–1.0)	12.1	22.5	2.02 (1.0–4.1)	0.96 (0.9–1.0)
Boolean2.0	28.7	68.4	4.19 (2.5–7.0)	0.85 (0.8–0.9)	32.4	40.4	1.38 (0.8–2.3)	0.98 (0.9–1.0)	11.8	24.6	2.27 (1.3–4.0)	0.93 (0.9–1.0)
BooleanX	28.1	57.9	2.42 (1.6–3.8)	0.86 (0.8–1.0)	31.3	46.3	1.76 (1.2–2.6)	0.93 (0.9–1.0)	11.6	21.1	1.86 (1.2–2.9)	0.91 (0.8–1.0)
SDAI	29	71.7	4.84 (2.7–8.5)	0.86 (0.8–0.9)	32.6	37	1.2 (0.7–2.1)	0.99 (0.9–1.0)	12	23.9	2.19 (1.1–4.2)	0.95 (0.9–1.0)
CDAI	28.7	76.1	4.84 (2.7–8.5)	0.86 (0.8–0.9)	32.6	37	1.2 (0.7–2.1)	0.99 (0.9–1.0)	11.8	28.3	2.74 (1.5–5.1)	0.93 (0.9–1.0)

* Positive likelihood ratios (LR+) and negative LRs (LR−) for reaching the respective outcome at 12 months if remission is achieved at 6 months are shown. RA = rheumatoid arthritis; HAQ = Health Assessment Questionnaire; ΔmTSS = change in modified Sharp/van der Heijde score; SDAI = Simplified Disease Activity Index; CDAI = Clinical Disease Activity Index.

previous findings that PtGA is not associated with radiographic progression (12,26). Using the different Boolean definitions as well as index-based definitions led to similar proportions of participants with disease in remission who had radiographic progression (defined as ΔmTSS>0) during the first year (29.6% for Boolean1.0, 28.5% for Boolean2.0, 28.6% for BooleanX, 28.2% for SDAI, and 28.6% for CDAI).

The proportion of participants achieving both good radiographic and functional outcomes were similar for all remission definitions, from 57% to 60% (58.6% for Boolean1.0, 57.3% for Boolean 2.0, 59.2% for SDAI, and 60.4% for CDAI), except for BooleanX (50.8%). Again, index-based remission definitions performed similarly to Boolean1.0 and Boolean2.0 definitions with respect to their predictive ability (positive LR between 3.8 and 4.3). This pattern could also be seen when analyzing data on early RA and established RA, separately (Table 2). However, good functional outcomes when using BooleanX were even less frequent in established RA compared to early RA (HAQ ≤0.5 in established RA was 57% compared to 74% in early RA). Of note, no differences in radiographic progression in patients with established RA were observed between the remission definitions fulfilled. Overall, more than two-thirds of patients with established RA showed radiographic progression throughout the first year.

DISCUSSION

This study provides evidence of external validation of the previously proposed modification of the Boolean ACR/EULAR remission criteria, to include a threshold of 2 cm rather than 1 cm for the PtGA criterion, and of the provisionally endorsed index-based remission definitions. The study was performed using independent clinical trial data sets not included in any of the previous studies (e.g., the data sets generating the provisional definition of remission and the recent analyses on raising the PtGA threshold [7,12] in which the revised threshold was derived). Our study assessed different aspects of validity for the revised definition of remission. The composition of this patient population was heterogenous in terms of disease duration and previous DMARD treatments, and our results are therefore applicable to a broad spectrum of patients with RA (21–24).

The remission validation outlined here builds on work done 10 years ago when the selection of components was undertaken by a large ACR/EULAR consortium (7). Due to criticism around the stringently low threshold of the PtGA component within the Boolean remission definition (11,25,27) and concerns that the 2 approaches (Boolean-based versus index-based) to remission were not concordant, alternative thresholds for the PtGA were explored using multiple clinical trial data sets (12). Our analyses support the notion of a slight increase of the PtGA threshold since it provides better agreement with the SDAI remission definition and higher rates of Boolean-defined remission, without jeopardizing the prediction of good long-term functional and radiographic outcomes.

Our results replicate previous findings that a Boolean definition using 2 cm as threshold for PtGA (Boolean2.0) yields better agreement with both index-based remission definitions than Boolean1.0 (12). Furthermore, patients who attain Boolean2.0, CDAI, and SDAI remission thresholds at 6 months have a higher likelihood of good functional and radiographic outcomes after 12 months of treatment than those attaining Boolean-based disease remission without PtGA (BooleanX). We have also shown the agreement between the 3-variable Boolean approach definition and the CDAI definition, which can be applied during a clinic visit, without knowledge of current acute-phase reactant levels.

The PtGA threshold within the remission criteria does not influence the prediction of radiographic nonprogression, as all tested definitions yielded the same positive LRs for nonprogression of ~1.7 and the same proportions of patients not progressing (~79%). This is consistent with findings from a recent meta-analyses including data from 11 clinical trials showing that people fulfilling the SJC, TJC, and CRP criteria but not the PtGA criterion demonstrate better radiographic outcomes than those not in any Boolean remission category (26). We note that successful management of RA is not only defined by the prevention of joint damage, but, ideally, attaining remission should also prevent residual symptoms that matter to patients, such as pain, fatigue, and anxiety.

The PtGA has not only been criticized for its stringent threshold in the remission definition. The Outcome Measures in Rheumatology (OMERACT) Working Group focusing on "Remission in RA: Patient Perspective" questioned whether the PtGA is the best instrument to reflect the perspective of patients in the current Boolean remission definition. They explored the effect of replacing PtGA with 3 patient-assessed domains identified by patients as most important: pain, fatigue, and independence. Their search for a better incorporation of the patient perspective has not yet resulted in a promising set of validated patient-reported outcome measures that can replace the PtGA. In their most recent working group report, they concluded that there is currently insufficient evidence to propose a change to the existing ACR/EULAR remission criteria (28). This report also discussed the concept of a "dual-target" approach, trying to decouple the assessment of disease activity from disease impact in defining remission (25,29). At this stage no data are available about the effectiveness and feasibility of such a dual-target approach.

Concerns have been expressed that the ACR/EULAR remission criteria allow few patients to achieve disease remission. Within our validation work, we additionally provide data on the shift in remission frequencies and the distribution of patients that miss Boolean-defined remission due to fulfilling only 3 of 4 criteria. By using a threshold of 2 cm rather than 1 cm in the revised Boolean definition, 40% more participants in our data sets achieved disease remission (14% instead of 10%). Importantly, when applying the Boolean2.0 definition, the SJC criterion threshold of 1 seems to be nearly as prominent in limiting participants

attaining full remission as the PtGA criterion (3% due to high SJC and 5% to high PtGA when fulfilling the other 3 criteria). The revised PtGA threshold of 2 cm has been proposed as 1 item in a set of 7 criteria that defined minimal disease activity of RA by OMERACT in 2005 (30). Notably, the definition of remission should remain strict and ensure beneficial long-term outcomes for patients with RA and prevent unnecessary treatment escalation at the same time. Furthermore, it appears that changes in the overall approach to treating RA before patients enter clinical trials or trends over time have led to much higher provisional ACR/EULAR remission rates in more recent clinical trials than in earlier ones, with recent rates reaching ~30% in early disease, 20% in patients with insufficient response to MTX, and 15–20% in patients with insufficient response to bDMARDs (31–35).

A preferable approach for more patients to achieve remission is to foster a collaborative relationship between patients and clinicians, to initiate treatment early, and to utilize a treat-to-target approach (8), rather than omitting potentially problematic items such as the PtGA (36,37). Studies have shown that a treat-to-target approach is not yet fully implemented in clinical practice; in one-third of instances where treatment was not increased, this was influenced by factors unrelated to RA and in another third it was the patient's preference to continue receiving the current treatment (38,39). All measurements and their interpretations need, in any case, to be complemented by the discussion between the patient and rheumatology clinician to reflect and decide on the appropriate steps in a shared decision (40,41).

Remission has become a key target for the management of patients with RA (42). The ACR/EULAR 2011 initiative on remission criteria was undertaken to harmonize the definition of the term "remission" and thus to facilitate the fair assessment and comparison of remission rates in clinical trials and clinical practice (e.g., for different health care settings or providers). It will be helpful to further study the performance of the revised criteria in trials using other antirheumatic drugs, such as JAK inhibitors, and in other countries and ethnic groups, since RA severity and the interpretation of the PtGA may vary across ethnicities. We validated the results of the performance of the Boolean2.0 and the provisionally endorsed index-based remission definitions. With the validation of the threshold of 2 cm for the PtGA, we propose that these revised ACR/EULAR remission criteria be adopted both for future clinical trials and as a target in clinical practice.

ACKNOWLEDGMENTS

We would like to thank the companies that kindly provided the patient-level data from their trials (Hoffmann-La Roche, Janssen Biotech).

AUTHOR CONTRIBUTIONS

All authors were involved in drafting the article or revising it critically for important intellectual content, and all authors approved the final version to be published. Dr. Studenic had full access to all of the data in the study and takes responsibility for the integrity of the data and the accuracy of the data analysis.

Study conception and design. Studenic, Aletaha, Lacaille, Smolen, Felson.

Acquisition of data. Studenic, Aletaha.

Analysis and interpretation of data. Studenic, Aletaha, de Wit, Stamm, Alasti, Lacaille.

REFERENCES

1. Felson DT, Anderson JJ, Boers M, et al. The American College of Rheumatology preliminary core set of disease activity measures for rheumatoid arthritis clinical trials. Arthritis Rheum 1993;36:729–40.
2. Scott D, van Riel P, van der Heijde D, et al. Assessing disease activity in rheumatoid arthritis: the EULAR handbook of standard methods. On behalf of the EULAR Standing Committee for International Clinical Studies Including Therapeutic Trials. Zürich: EULAR; 1993.
3. Emery P, Salmon M. Early rheumatoid arthritis: time to aim for remission? Ann Rheum Dis 1995;54:944–7.
4. Singh JA, Saag KG, Bridges SL Jr, et al. 2015 American College of Rheumatology guideline for the treatment of rheumatoid arthritis. Arthritis Rheumatol 2016;68:1–26.
5. Smolen JS, Landewé R, Bijlsma J, et al. EULAR recommendations for the management of rheumatoid arthritis with synthetic and biological disease-modifying antirheumatic drugs: 2016 update. Ann Rheum Dis 2017;76:960–977.
6. Smolen JS, Breedveld FC, Burmester GR, et al. Treating rheumatoid arthritis to target: 2014 update of the recommendations of an international task force. Ann Rheum Dis 2016;75:3–15.
7. Felson DT, Smolen JS, Wells G, et al. American College of Rheumatology/European League Against Rheumatism provisional definition of remission in rheumatoid arthritis for clinical trials. Arthritis Rheum 2011;63:573–86.
8. Smolen JS, Aletaha D, Bijlsma JW, et al. Treating rheumatoid arthritis to target: recommendations of an international task force. Ann Rheum Dis 2010;69:631–7.
9. Smolen JS, Breedveld FC, Schiff MH, et al. A Simplified Disease Activity Index for rheumatoid arthritis for use in clinical practice. Rheumatology (Oxford) 2003;42:244–57.
10. Aletaha D, Nell VP, Stamm T, Uffmann M, Pflugbeil S, Machold K, et al. Acute phase reactants add little to composite disease activity indices for rheumatoid arthritis: validation of a clinical activity score. Arthritis Res Ther 2005;7:R796–806.
11. Studenic P, Smolen JS, Aletaha D. Near misses of ACR/EULAR criteria for remission: effects of patient global assessment in Boolean and index-based definitions. Ann Rheum Dis 2012;71:1702–5.
12. Studenic P, Felson D, de Wit M, et al. Testing different thresholds for patient global assessment in defining remission for rheumatoid arthritis: are the current ACR/EULAR Boolean criteria optimal? Ann Rheum Dis 2020;79:445–52.
13. Bombardier C, Raboud J. A comparison of health-related quality-of-life measures for rheumatoid arthritis research. The Auranofin Cooperating Group. Control Clin Trials 1991;12 Suppl:243s–56s.
14. Gøtzsche PC. Sensitivity of effect variables in rheumatoid arthritis: a meta-analysis of 130 placebo controlled NSAID trials. J Clin Epidemiol 1990;43:1313–8.
15. Strand V, Kosinski M, Chen CI, et al. Sarilumab plus methotrexate improves patient-reported outcomes in patients with active rheumatoid arthritis and inadequate responses to methotrexate: results of a phase III trial. Arthritis Res Therapy 2016;18:198.

16. Aletaha D, Ward MM. Duration of rheumatoid arthritis influences the degree of functional improvement in clinical trials. Ann Rheum Dis 2006;65:227–33.
17. Aletaha D, Funovits J, Smolen JS. Physical disability in rheumatoid arthritis is associated with cartilage damage rather than bone destruction. Ann Rheum Dis 2011;70:733–9.
18. Studenic P, Radner H, Smolen JS, et al. Discrepancies between patients and physicians in their perceptions of rheumatoid arthritis disease activity. Arthritis Rheum 2012;64:2814–23.
19. Radner H, Yoshida K, Tedeschi S, et al. Different rating of global rheumatoid arthritis disease activity in rheumatoid arthritis patients with multiple morbidities. Arthritis Rheumatol 2017;69:720–7.
20. Mack ME, Hsia E, Aletaha D. Comparative assessment of the different American College of Rheumatology/European League Against Rheumatism Remission definitions for rheumatoid arthritis for their use as clinical trial end points. Arthritis Rheumatol 2017;69:518–28.
21. Smolen JS, Kay J, Doyle MK, et al. Golimumab in patients with active rheumatoid arthritis after treatment with tumour necrosis factor α inhibitors (GO-AFTER study): a multicentre, randomised, double-blind, placebo-controlled, phase III trial. Lancet 2009;374:210–21.
22. Burmester GR, Rigby WF, van Vollenhoven RF, et al. Tocilizumab combination therapy or monotherapy or methotrexate monotherapy in methotrexate-naive patients with early rheumatoid arthritis: 2-year clinical and radiographic results from the randomised, placebo-controlled FUNCTION trial. Ann Rheum Dis 2017;76:1279–84.
23. Fleischmann RM, Halland AM, Brzosko M, et al. Tocilizumab inhibits structural joint damage and improves physical function in patients with rheumatoid arthritis and inadequate responses to methotrexate: LITHE study 2-year results. J Rheumatol 2013;40:113–26.
24. Emery P, Deodhar A, Rigby WF, et al. Efficacy and safety of different doses and retreatment of rituximab: a randomised, placebo-controlled trial in patients who are biological naive with active rheumatoid arthritis and an inadequate response to methotrexate (Study Evaluating Rituximab's Efficacy in MTX iNadequate rEsponders (SERENE)). Ann Rheum Dis 2010;69:1629–35.
25. Ferreira RJ, Duarte C, Ndosi M, et al. Suppressing inflammation in rheumatoid arthritis: does patient global assessment blur the target? A practice-based call for a paradigm change. Arthritis Care Res (Hoboken) 2018;70:369–78.
26. Ferreira RJ, Welsing PM, Jacobs JW, et al. Revisiting the use of remission criteria for rheumatoid arthritis by excluding patient global assessment: an individual meta-analysis of 5792 patients. Ann Rheum Dis 2021;80:293–303.
27. Masri KR, Shaver TS, Shahouri SH, et al. Validity and reliability problems with patient global as a component of the ACR/EULAR remission criteria as used in clinical practice. J Rheumatol 2012;39:1139–45.
28. Jones B, Flurey CA, Proudman S, et al. Considerations and priorities for incorporating the patient perspective on remission in rheumatoid arthritis: an OMERACT 2020 special interest group report. Semin Arthritis Rheum 2021;51:1108–12.
29. Ferreira RJ, Landewé RB, da Silva JA. Definition of treatment targets in rheumatoid arthritis: is it time for reappraisal? [editorial]. J Rheumatol 2021;48:1763–6.
30. Wells GA, Boers M, Shea B, et al. Minimal disease activity for rheumatoid arthritis: a preliminary definition. J Rheumatol. 2005;32:2016–24.
31. Combe B, Kivitz A, Tanaka Y, et al. Filgotinib versus placebo or adalimumab in patients with rheumatoid arthritis and inadequate response to methotrexate: a phase III randomised clinical trial. Ann Rheum Dis 2021;80:848–58.
32. Westhovens R, Rigby WF, van der Heijde D, et al. Filgotinib in combination with methotrexate or as monotherapy versus methotrexate monotherapy in patients with active rheumatoid arthritis and limited or no prior exposure to methotrexate: the phase 3, randomised controlled FINCH 3 trial. Ann Rheum Dis 2021;80:727–38.
33. Rubbert-Roth A, Enejosa J, Pangan AL, et al. Trial of upadacitinib or abatacept in rheumatoid arthritis. N Engl J Med 2020;383:1511–21.
34. Van Vollenhoven R, Takeuchi T, Pangan AL, et al. Efficacy and safety of upadacitinib monotherapy in methotrexate-naive patients with moderately-to-severely active rheumatoid arthritis (SELECT-EARLY): a multicenter, multi-country, randomized, double-blind, active comparator–controlled trial. Arthritis Rheumatol 2020;72:1607–20.
35. Smolen JS, Pangan AL, Emery P, et al. Upadacitinib as monotherapy in patients with active rheumatoid arthritis and inadequate response to methotrexate (SELECT-MONOTHERAPY): a randomised, placebo-controlled, double-blind phase 3 study. Lancet 2019;393:2303–11.
36. Boers M. Patient global assessment to define remission in rheumatoid arthritis: quo vadis? [editorial] Ann Rheum Dis 2021;80:277–9.
37. Nikiphorou E, Santos EJ, Marques A, et al. 2021 EULAR recommendations for the implementation of self-management strategies in patients with inflammatory arthritis. Ann Rheum Dis 2021;80:1278–85.
38. Zak A, Corrigan C, Yu Z, et al. Barriers to treatment adjustment within a treat to target strategy in rheumatoid arthritis: a secondary analysis of the TRACTION trial. Rheumatology (Oxford) 2018;57:1933–7.
39. Yun H, Chen L, Xie F, et al. Do patients with moderate or high disease activity escalate rheumatoid arthritis therapy according to treat-to-target principles? Results from the Rheumatology Informatics System for Effectiveness Registry of the American College of Rheumatology. Arthritis Care Res 2020;72:166–75.
40. Smolen JS, Landewe RB, Bijlsma JW, et al. EULAR recommendations for the management of rheumatoid arthritis with synthetic and biological disease-modifying antirheumatic drugs: 2019 update. Ann Rheum Dis 2020;79:685–99.
41. Studenic P, Radner H. Back to basics: prioritizing communication as a key instrument in managing rheumatoid arthritis [editorial]. J Rheumatol 2022;49:123–5.
42. Fraenkel L, Bathon JM, England BR, et al. 2021 American College of Rheumatology guideline for the treatment of rheumatoid arthritis. Arthritis Rheumatol 2021;73:1108–23.

Arthritis & Rheumatology
Vol. 75, No. 1, January 2023, pp 23–25
DOI 10.1002/art.42322

American College of Rheumatology
Empowering Rheumatology Professionals

EDITORIAL

Should Low Serum Urate Be Exonerated? Untangling the Influence of Sarcopenia in Observational Studies

Kanon Jatuworapruk[1] and Nicola Dalbeth[2]

Low serum urate levels have been associated with a range of adverse health outcomes, most prominently all-cause mortality and progression of neurodegenerative diseases such as Parkinson's disease, Alzheimer's disease, and amyotrophic lateral sclerosis (1). The association between serum urate levels and all-cause mortality has been consistently described as U-shaped across different populations in observational studies (2). These associations led to the recommendation against lowering continuously the serum urate levels to below 3 mg/dl in the long term (that is, for several years) by the 2016 updated EULAR recommendation for the management of gout (3). Similarly, in their 2017 guideline for the management of gout, the British Society for Rheumatology recommended an initial target serum urate level of below 5 mg/dl, followed by a less stringent target of below 6 mg/dl after the patient has stabilized, due to the "possibility of adverse effects that may be associated with a very low [serum urate level]" (4). The antioxidant properties of urate, based largely on in vitro data, have been hypothesized as the main driver behind the link between low serum urate concentration and mortality.

Other evidence has contradicted the predominant narrative about the dangers of low serum urate, showing no increased mortality in people with hypouricemia (defined as a serum urate level below 2 mg/dl). In a 6-month clinical trial of pegloticase in patients with refractory gout, participants were randomly assigned to biweekly pegloticase, monthly pegloticase, or placebo (5). Responders in the biweekly pegloticase arm had a mean serum urate level below 2 mg/dl. No significant differences in rates of all-cause mortality and cardiovascular death among study arms were observed in the 6-month trial or in the subsequent 3-year open-label extension study (5,6).

Another study explored the in vivo oxidative effects of urate depletion by pegloticase in 26 patients with severe gout (7). Five rapid infusions of pegloticase at 3-week intervals resulted in mean serum urate concentrations below 1 mg/dl in all study participants. Oxidative stress was measured using plasma F_2-isoprostanes and protein carbonyls, products of arachidonic acid and protein oxidation. No correlation was shown between oxidative stress and serum urate depletion (7). The study provided in vivo evidence against the hypothesis that the association between low serum urate and mortality, if it exists, is mediated by dysregulated oxidative stress.

Another group of patients who are expected to be at exceptionally high risk for mortality are those with hereditary syndromes resulting in long-term hypouricemia (typically below 1 mg/dl), e.g., hereditary xanthinuria (underproduction of urate because of inherited xanthine oxidase deficiency) or familial renal hypouricemia (overexcretion of urate because of renal urate transporter variants). These syndromes are often associated with nephrolithiasis and exercise-induced acute kidney injury (in the case of familial renal hypouricemia) but not early death or neurodegenerative diseases (8).

One of the major influencers of serum urate levels is body composition, specifically fat mass and skeletal muscle mass. An association between serum urate levels and obesity, defined as excessive fat accumulation, is well established, with a study that used a Mendelian randomization approach showing that elevated serum urate levels are a consequence rather than a cause of adiposity (9). Recent data have shown that low urate levels are common in people with sarcopenia, defined as loss of skeletal muscle mass and function (10). Consequently, body composition (both muscle mass and fat mass) should ideally be accounted for when evaluating the effects of serum urate on any health outcomes.

In this issue of *Arthritis & Rheumatology*, Baker and colleagues (11) provide a more nuanced view on the association between low serum urate levels and mortality, demonstrating that this association can be better explained by sarcopenia. The investigators used whole-body dual-energy x-ray absorptiometry (DXA) data on participants from the National Health and Nutrition

[1]Kanon Jatuworapruk, MD, PhD: Faculty of Medicine, Thammasat University, Pathum Thani, Thailand; [2]Nicola Dalbeth, MD: Faculty of Medical and Health Sciences, University of Auckland, Auckland, New Zealand.

Author disclosures are available at https://onlinelibrary.wiley.com/action/downloadSupplement?doi=10.1002%2Fart.42322&file=art42322-sup-0001-Disclosureform.pdf.

Address correspondence via email to Nicola Dalbeth, MD, at n.dalbeth@auckland.ac.nz.

Submitted for publication June 27, 2021; accepted in revised form July 26, 2022.

Examination Survey, a nationally representative database, to explore the complex relationships between low serum urate levels, mortality, and sarcopenia. The investigators reported 3 major observations.

First, serum urate was significantly associated with sarcopenia outcomes, derived from recently validated measurements (appendicular lean mass index [ALMI] and ALMI relative to fat mass index [$ALMI_{FMI}$] Z scores). Second, low serum urate levels (below 2.5 mg/dl for women and below 3.5 mg/dl for men) were associated with all-cause mortality when adjusting for traditional body composition measurements (body mass index [BMI] and waist circumference). This particular observation echoed previous observational studies that linked serum urate to mortality (2). Third, the association between low serum urate levels and all-cause mortality disappeared when new body composition measurements (ALMI and $ALMI_{FMI}$ Z scores) were included in the regression models.

The observations from Baker et al suggest that the apparent link between low serum urate and mortality that was observed in other studies could have been explained by sarcopenia (a known risk factor for frailty and mortality), if measured accurately. Previous observational studies examining the link between low serum urate and mortality have included variables such as BMI and waist circumference (1,2). However, these traditional and easily measurable variables are limited by confounding relationships between muscle mass and fat mass (i.e., people with high muscle mass tend to have high fat mass), as well as the correlation between fat mass and serum urate (i.e., people with greater adipose tissue tend to have high serum urate). The DXA-derived ALMI, FMI, and $ALMI_{FMI}$ Z scores used in the study by Baker and colleagues allowed accurate estimation of muscle mass relative to fat mass (relative sarcopenia), thus overcoming this particular limitation (11).

The findings reported by Baker and colleagues also raise important questions about the widely published associations between low serum urate and progression of neurodegenerative diseases. Sarcopenia is commonly observed in people with dementia, brain atrophy, and neuropsychiatric symptoms. This condition occurs through a number of mechanisms, including reduced oral caloric intake, reduced physical activity, and other postulated factors such as vascular dysfunction, insulin resistance, and oxidative stress (12). Is it possible that the link between low serum urate levels and neurodegenerative diseases would be attenuated if accurate estimation of body composition was accounted for? We believe this could be the case, especially in light of the recent randomized controlled trial (RCT) that investigated the effects of urate-elevating inosine on Parkinson's disease progression (SURE-PD3) (13). This RCT found that increased serum urate levels did not significantly slow progression of Parkinson's disease, which is a strong rebuttal to the hypothesized causal relationship between low serum urate levels and progression of neurodegenerative diseases. Narratives surrounding the potential danger of low serum urate levels also exist for cardiovascular events, progression of chronic kidney disease, osteoporosis, and fracture risk (2,14). It

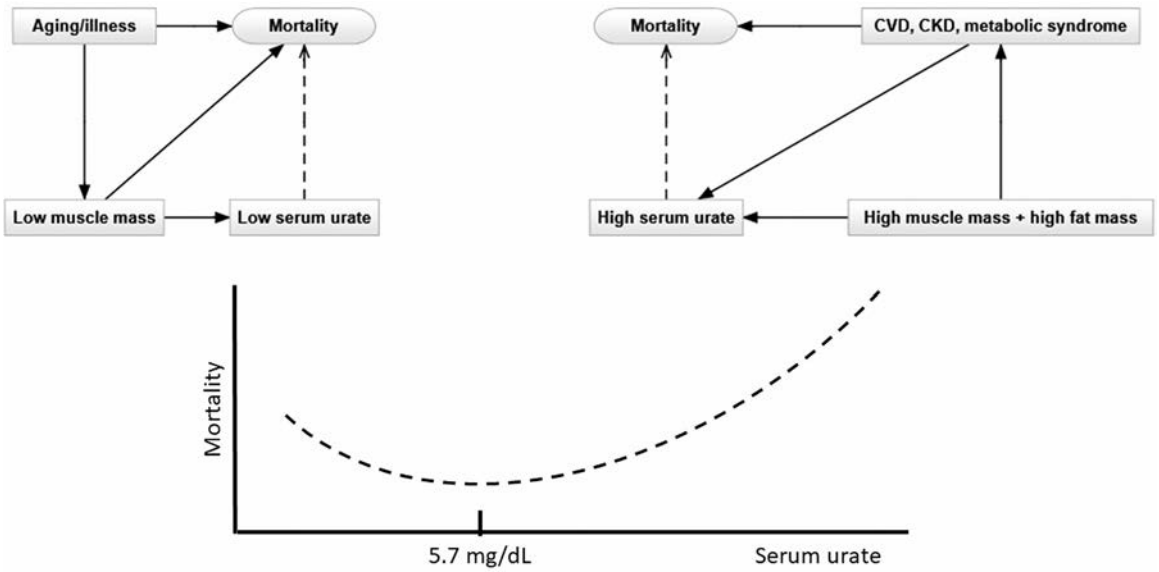

Figure 1. The hypothetical relationship between serum urate, body composition, and mortality. The U-shaped curve indicates the increased mortality observed in people with low serum urate or people with high serum urate concentrations. Each end of the curve is augmented with directed acyclic graphs (DAGs) illustrating the influence of body composition on both serum urate and mortality. The solid arrows indicate causal relationships, and the dashed arrows indicate noncausal relationships. The association between low serum urate and mortality is not causal but is instead mediated by low muscle mass (sarcopenia) and aging or chronic illness (left DAG). The association between high serum urate and mortality is also not causal but can be explained by high fat and muscle mass, as well as comorbid conditions, especially cardiovascular disease (CVD), chronic kidney disease (CKD), and metabolic syndrome (right DAG).

is worth noting that sarcopenia is common in most, if not all, of these conditions, and associations with low serum urate could be subjected to similar confounding.

What implications does this have for gout management guidelines that recommend against intensively lowering serum urate levels to below 3 mg/dl, citing concerns about safety from observational studies in the general populations? It is uncertain how low serum urate would contribute negatively to health outcomes of people with gout who have had long-term exposure to high serum urate levels. Furthermore, gout itself is associated with several comorbidities, including cardiovascular disease, obesity, and diabetes, all of which contribute to the risk of mortality. The study by Baker and colleagues nevertheless provides some reassurance that the apparent association between low serum urate levels and mortality in many observational studies is likely due to unmeasured confounding related to sarcopenia (11). However, it should be noted that achieving very low serum urate (below 3.3 mg/dl) with the currently available oral urate-lowering therapy is difficult, even in a clinical trial setting, with the high medication burden (15). Furthermore, targeting serum urate levels below 3.3 mg/dl when using oral urate-lowering therapy does not lead to better outcomes than a target of below 5 mg/dl in patients with erosive gout (15). Therefore, there is no clear benefit in gout management to reducing serum urate to a very low level when using currently available oral urate-lowering therapy. Maintaining a urate level below 6 mg/dl (or below 5 mg/dl in those with high monosodium urate crystal load) is safe and probably sufficient for most people with gout.

In conclusion, the study by Baker and colleagues showed that regression models examining associations between serum urate levels and health outcomes are only as good as the variables that we decide to include (or not include). Observational studies should carefully consider the confounding relationships between serum urate, body composition, and health outcomes (Figure 1). Distinguishing muscle mass from fat mass may be advisable for building robust predictive models involving serum urate because both sarcopenia and adiposity typically correlate with serum urate and with each other.

AUTHOR CONTRIBUTIONS

Dr. Jatuworapruk and Dr. Dalbeth drafted the article, revised it critically for important intellectual content, and approved the final version to be published.

REFERENCES

1. Perez-Gomez MV, Bartsch LA, Castillo-Rodriguez E, et al. Potential dangers of serum urate-lowering therapy. Am J Med 2019;132:457–67.
2. Crawley WT, Jungels CG, Stenmark KR, et al. U-shaped association of uric acid to overall-cause mortality and its impact on clinical management of hyperuricemia. Redox Biol 2022;51:102271.
3. Richette P, Doherty M, Pascual E, et al. 2016 updated EULAR evidence-based recommendations for the management of gout. Ann Rheum Dis 2017;76:29–42.
4. Hui M, Carr A, Cameron S, et al. The British Society for Rheumatology guideline for the management of gout. Rheumatology (Oxford) 2017;56:e1–20.
5. Sundy JS, Baraf HS, Yood RA, et al. Efficacy and tolerability of pegloticase for the treatment of chronic gout in patients refractory to conventional treatment: two randomized controlled trials. Jama 2011;306:711–20.
6. Becker MA, Baraf HS, Yood RA, et al. Long-term safety of pegloticase in chronic gout refractory to conventional treatment. Ann Rheum Dis 2013;72:1469–74.
7. Hershfield MS, Roberts LJ Jr, Ganson NJ, et al. Treating gout with pegloticase, a PEGylated urate oxidase, provides insight into the importance of uric acid as an antioxidant in vivo. Proc Natl Acad Sci U S A 2010;107:14351–6.
8. Dinour D, Gray NK, Campbell S, et al. Homozygous SLC2A9 mutations cause severe renal hypouricemia. J Am Soc Nephrol 2010;21:64–72.
9. Lyngdoh T, Vuistiner P, Marques-Vidal P, et al. Serum uric acid and adiposity: deciphering causality using a bidirectional Mendelian randomization approach. PLoS One 2012;7:e39321.
10. Nahas PC, Rossato LT, de Branco FM, et al. Serum uric acid is positively associated with muscle strength in older men and women: Findings from NHANES 1999–2002. Clin Nutr 2021;40:4386–93.
11. Baker JF, Weber DR, Neogi T, et al. Associations between low serum urate, body composition, and mortality. Arthritis Rheumatol. 2023. E-pub ahead of print. doi:10.1002/art.42301
12. Jo D, Yoon G, Kim OY, et al. A new paradigm in sarcopenia: Cognitive impairment caused by imbalanced myokine secretion and vascular dysfunction. Biomed Pharmacother 2022;147:112636.
13. Schwarzschild MA, Ascherio A, Casaceli C, et al. Effect of urate-elevating inosine on early Parkinson disease progression: the SURE-PD3 randomized clinical trial. JAMA 2021;326:926–39.
14. Veronese N, Carraro S, Bano G, et al. Hyperuricemia protects against low bone mineral density, osteoporosis and fractures: a systematic review and meta-analysis. Eur J Clin Invest 2016;46:920–30.
15. Dalbeth N, Doyle AJ, Billington K, et al. Intensive serum urate lowering with oral urate-lowering therapy for erosive gout: a randomized double-blind controlled trial. Arthritis Rheumatol 2022;74:1059–69.

American College of Rheumatology
Empowering Rheumatology Professionals

Arthritis & Rheumatology
Vol. 75, No. 1, January 2023, pp 26–27
DOI 10.1002/art.42367

SPECIAL

Winner of the 2022 American College of Rheumatology Annual Image Competition

American College of Rheumatology Image Library Subcommittee and Image Library Diversity Taskforce of the American College of Rheumatology Committee on Education

The mission of the American College of Rheumatology Image Library is to provide ACR members, as well as the entire medical community, access to a wide variety of clinical images to help educators effectively present the manifestations of rheumatic diseases. Additionally, the images have been widely used in peer-reviewed publications and textbooks. Since its inception, the ACR's Rheumatology Image Library has become the preeminent collection devoted to rheumatic diseases. The collection is a dynamic one, changing yearly because of submissions from the medical community. Additionally, many nonwinning images are introduced into the Image Library, enhancing the collection. Winners, as well as those images selected for inclusion in the

Figure 1. A 12-year-old girl with a diagnosis of Moebius syndrome was evaluated for a clinical presentation of progressive tongue hemi-atrophy that was reported to have been developing for 1 year, resulting in feeding and speech difficulties. Magnetic resonance imaging of the patient's brain (right) demonstrated evidence of tongue hemi-atrophy without involvement of the hypoglossal nerve. A tongue biopsy showed atrophy of the skeletal muscle, variably sized nerves, stromal calcification, mild hyperplasia of overlying mucosa, parakeratosis, and mild subepithelial inflammation (bottom left). Clinical evaluation revealed forehead and postauricular skin discolorations (top left panels). The patient was diagnosed as having Parry Romberg syndrome and en coup de sabre scleroderma. If the diagnosis is delayed, this rare complication of scleroderma can result in cosmetic disfigurement and functional impairments, including impairments with speech and eating.

Members of the Image Library Subcommittee: Lesley Saketkoo, MD: New Orleans, Louisiana (Chair); Senada Arabelovic, DO: Boston, Massachusetts; Sharon Banks, DO: Hershey, Pennsylvania; Elana Bernstein, MD: New York, New York; Michael Jennings, BS, RT, CBDT: New Lebanon, Pennsylvania; Konstantinos Loupasakis, MD: New York, New York; Abhishek Nandan, MD: Williamsburg, Virginia; Rochella Ostrowski, MD, MS: Maywood, Illinois; Anjani Pillarisetty, MD, and Virginia Steen, MD: Washington, DC.

Members of the Image Library Diversity Taskforce of the American College of Rheumatology Committee on Education: Noelle Rolle, FACR, MBBS: Augusta, Georgia (Chair); Reem Alkilany, MD: Cleveland, Ohio; Senada Arabelovic, DO: Boston, Massachusetts; Ashira Blazer, MD: New York, New York; Sonam Kiwalkar, MD: Portland, Oregon; Ronald Laxer, MD: Toronto, Ontario, Canada; Mohammad Ursani, MD: Kingwood, Texas.

Submitted for publication September 12, 2022; accepted for publication September 12, 2022.

Image Library, are chosen based on image quality and educational value.

The ACR held its annual image competition in conjunction with ACR Convergence 2022, with the purpose of identifying images representing a diverse range of patients who displayed either characteristic or unusual manifestations of a rheumatic disease in one of the following categories: systemic sclerosis, localized scleroderma, or scleroderma mimics. For the 2022 competition, 46 entries were received, and the reviewers carefully evaluated each entry.

The 2022 grand prize winner was a series of images showing localized scleroderma in a 12-year-old girl (Figure 1). The winning submission, as well as other outstanding images, will be added to the Image Library.

The Rheumatology Image Library provides the medical community with 24/7 online access to the world's foremost collection of rheumatology images. It features contributions from all over the world and is an invaluable resource for countless physicians and other health care professionals, researchers, and journalists. Since the launch of the online edition of the Rheumatology Image Library in 2009, it has received more than 2.5 million unique visitors worldwide. To view the winning images and many others, visit the Rheumatology Image Library at http://images.rheumatology.org.

The ACR encourages the continued submission of images to its annual Image Competition. Submissions of high-quality images that illustrate rheumatic conditions or are relevant to the practice of rheumatology are welcomed. Visit https://www.rheumatology.org/Annual-Meeting/Program/Image-Competition for competition rules and entry/deadline dates. Details about the 2023 Image Competition will be available in spring 2023. If you have any questions regarding the Image Competition, please contact education@rheumatology.org.

American College of Rheumatology
Empowering Rheumatology Professionals

Arthritis & Rheumatology
Vol. 75, No. 1, January 2023, pp 28–40
DOI 10.1002/art.42316

Peripheral Blood DNA Methylation–Based Machine Learning Models for Prediction of Knee Osteoarthritis Progression: Biologic Specimens and Data From the Osteoarthritis Initiative and Johnston County Osteoarthritis Project

Christopher M. Dunn,[1] Cassandra Sturdy,[2] Cassandra Velasco,[1] Leoni Schlupp,[2] Emmaline Prinz,[2] Vladislav Izda,[3] Liubov Arbeeva,[4] Yvonne M. Golightly,[5] Amanda E. Nelson,[4] and Matlock A. Jeffries[1]

Objective. The lack of accurate biomarkers to predict knee osteoarthritis (OA) progression is a key unmet need in OA clinical research. The objective of this study was to develop baseline peripheral blood epigenetic biomarker models to predict knee OA progression.

Methods. Genome-wide buffy coat DNA methylation patterns from 554 individuals from the Osteoarthritis Biomarkers Consortium (OABC) were determined using Illumina Infinium MethylationEPIC 850K arrays. Data were divided into model development and validation sets, and machine learning models were trained to classify future OA progression by knee pain, radiographic imaging, knee pain plus radiographic imaging, and any progression (pain, radiographic, or both). Parsimonious models using the top 13 CpG sites most frequently selected during development were tested on independent samples from participants in the Johnston County Osteoarthritis (JoCo OA) Project (n = 128) and a previously published Osteoarthritis Initiative (OAI) data set (n = 55).

Results. Full models accurately classified future radiographic-only progression (mean ± SEM accuracy 87 ± 0.8%, area under the curve [AUC] 0.94 ± 0.004), pain-only progression (accuracy 89 ± 0.9%, AUC 0.97 ± 0.004), pain plus radiographic progression (accuracy 72 ± 0.7%, AUC 0.79 ± 0.006), and any progression (accuracy 78 ± 0.4%, AUC 0.86 ± 0.004). Pain-only and radiographic-only progressors were not distinguishable (mean ± SEM accuracy 58 ± 1%, AUC 0.62 ± 0.001). Parsimonious models showed similar performance and accurately classified future radiographic progressors in the OABC cohort and in both validation cohorts (mean ± SEM accuracy 80 ± 0.3%, AUC 0.88 ± 0.003 [using JoCo OA Project data], accuracy 80 ± 0.8%, AUC 0.89 ± 0.002 [using previous OAI data]).

Conclusion. Our data suggest that pain and structural progression share similar early systemic immune epigenotypes. Further studies should focus on evaluating the pathophysiologic consequences of differential DNA methylation and peripheral blood cell epigenotypes in individuals with knee OA.

INTRODUCTION

Osteoarthritis (OA) is the leading cause of chronic disability in the US and among the most rapidly rising disability-associated medical conditions worldwide (1,2). Despite its widespread prevalence, neither the US Food and Drug Administration nor the European Medicines Agency have yet approved any disease-modifying drug therapy for OA, although several agents are in late-stage clinical trials (3,4). One of the largest obstacles encountered in OA clinical trial design is the unpredictable nature

The content is solely the responsibility of the authors and does not necessarily represent the official views of the NIH nor the Department of Defense. This manuscript was prepared using an Osteoarthritis Initiative (OAI) public use data set and does not necessarily reflect the opinions or views of the OAI investigators, the NIH, or the private funding partners.

Supported by the NIH (grants K08-AR-070891, P20-GM-125528, R61-AR-078075, and R01AR076440), along with the Congressionally Directed Medical Research Program (grant PR191652). The OAI is a public-private partnership comprising 5 contracts (N01-AR-2-2258, N01-AR-2-2259, N01-AR-2-2260, N01-AR-2-2261, and N01-AR-2-2262) funded by the NIH and conducted by the OAI Study Investigators. Private funding partners include Merck Research Laboratories, Novartis Pharmaceuticals Corporation, GlaxoSmithKline, and Pfizer, Inc. Private sector funding for the OAI is managed by the Foundation for the National Institutes of Health.

The Johnston County Osteoarthritis Project is funded in part by the Association of Schools of Public Health (grants S043, S1734, S3486), Centers for Disease Control and Prevention (grants U01 DP003206 and U01 DP006266), and National Institutes of Health/National Institute of Arthritis and Musculoskeletal and Skin Diseases (grants P60AR30701, P60AR049465, P60AR064166, and P30AR072580).

[1]Christopher M. Dunn MS, Cassandra Velasco, BS, Matlock A. Jeffries, MD: Division of Rheumatology, Immunology, and Allergy, Department of Internal Medicine, University of Oklahoma Health Sciences Center, and Arthritis and Clinical Immunology Program, Oklahoma Medical Research Foundation,

of disease progression. Only a small minority of patients (~4–8%) will experience radiographic progression within 4 years (5,6), which is the median length of phase III clinical trials in the US (7). Therefore, including individuals who are likely to experience rapid radiographic and/or pain progression in OA clinical trial populations will be critical to accelerate OA drug development and advance personalized, precision-guided OA therapies.

Recent studies have sought to identify biomarkers for prediction of rapid OA progression. The largest of these, from the Foundation for the National Institutes of Health OA Biomarkers Consortium (OABC), performed an analysis of serum and urine protein and radiographic biomarkers using a nested case–control design in a subset of 600 patients from the (OAI) cohort (8–12). Using multivariable analysis, Kraus et al developed a model predictive of both pain and radiographic progression using baseline blood and serum markers with a receiver operating characteristic area under the curve (AUC) of 0.586 (8). Using a 24-month time-integrated concentration measure, based on the change in biomarker levels over 24 months to predict the subsequent 24 months, models improved to an AUC of 0.618 using 10-fold cross-validation (8). Other recent studies have also identified baseline radiographic characteristics that can predict future rapid radiographic progression, including periarticular bone area (10) and 24-month change in effusion- and Hoffa-synovitis, meniscal morphometry, and cartilage thickness and surface area (AUC 0.740) (11). Additionally, a multivariable modeling analysis from the OABC was performed in which combined radiographic and biochemical time-integrated concentration biomarkers yielded an AUC of 0.716–0.832 to predict future radiographic progression (13).

A drawback of these biochemical and radiographic biomarker approaches is their inherent variability; that is, the best predictive capability comes from models integrating biomarker change over time rather than baseline values. By contrast, epigenetic patterns are among the first biologic changes in disease pathogenesis, as an appropriately modified chromatin microenvironment is required prior to the expression of disease-associated gene transcripts. Additionally, epigenetic patterns are relatively stable over time (14), suggesting that baseline epigenetic assays from a single time point may reflect disease-associated changes earlier than traditional protein-based approaches.

Several studies, including our own, have demonstrated epigenetic changes in OA joint tissues (15–18). Furthermore, in 2019, we developed peripheral blood DNA methylation models to predict future radiographic progression in a small cohort of 116 participants from the OAI, which yielded a mean accuracy of 73% and an AUC of 0.81 for prediction of OA progression within 48 months based on evaluation of blood samples collected from a single time point at baseline (19).

In the present study, we sought to expand upon these data by developing and validating peripheral blood DNA methylation-based machine learning models to predict future radiographic and/or pain progression in the larger OABC cohort, allowing us to directly compare our outcomes with previous Foundation for the National Institutes of Health biomarker projects. Additionally, we sought to validate our results in two independent cohorts, the Johnston County Osteoarthritis (JoCo OA) Project and our previous OAI epigenetic biomarker data.

PATIENTS AND METHODS

Study design. Samples for initial model development were obtained from the OABC (20), a subset of the OAI, including pain-only, radiographic-only, and pain plus radiographic progressors, with matched nonprogressor controls. Although the OABC has a total of 600 patients, samples from 46 patients were removed from our final analysis due to low DNA concentration or low-quality DNA methylation data. Our final model development cohort included 554 individuals representing 91 pain-only progressors, 81 radiographic-only progressors, 193 pain plus radiographic progressors, and 189 nonprogressor controls.

The validation cohorts were 77 future radiographic-only progressors and 51 nonprogressors from the JoCo OA Project and 27 future radiographic-only progressors and 28 nonprogressors from our previous OAI study (19). There were no patient or control overlaps between the OABC model development cohort and the OAI validation cohort. Details of both studies have been previously published (8,20,21). All JoCo OA Project and OAI participants provided written informed consent, and the studies were approved by the Committee on Human Research of the Institutional Review Board for the University of California San Francisco and the University of North Carolina at Chapel Hill, respectively. The institutional review boards of the University of Oklahoma Health Sciences Center and Oklahoma Medical Research Foundation also reviewed and approved the present study.

Patient characteristics. OAI patients' baseline and yearly follow-up knee radiographs and baseline buffy coat DNA were available. Kellgren/Lawrence (K/L) grades of radiographic OA severity, and quantitative tibiofemoral joint space width (JSW)

Oklahoma City; [2]Cassandra Sturdy, BS, Leoni Schlupp, BS, Emmaline Prinz, BS: Arthritis and Clinical Immunology Program, Oklahoma Medical Research Foundation, Oklahoma City; [3]Vladislav Izda, BS: Icahn School of Medicine at Mount Sinai, New York, New York; [4]Liubov Arbeeva, MS, Amanda E. Nelson, MD, MSCR: Thurston Arthritis Research Center, University of North Carolina at Chapel Hill; [5]Yvonne M. Golightly, PT, PhD: College of Allied Health Professions, University of Nebraska Medical Center, Omaha.

Author disclosures are available at https://onlinelibrary.wiley.com/action/downloadSupplement?doi=10.1002%2Fart.42316&file=art42316-sup-0001-Disclosureform.pdf.

Address correspondence via email to Matlock A. Jeffries, MD, at matlock-jeffries@omrf.org.

Submitted for publication May 9, 2022; accepted in revised form July 20, 2022.

(22) were assessed by a central reading site using nonfluoroscopic fixed-flexion knee radiographs with a SynaFlexer positioning frame (Synarc). All buffy coat samples from the OABC and OAI patients were derived from their baseline visit blood sample.

JoCo OA Project samples were obtained from patients in whom radiographic progression occurred at the baseline and later time points (e.g., progression from baseline to a second visit, second to a third visit, or third to a fourth visit). In each case, buffy coat samples were obtained from the patient's visit immediately prior to radiographic progression, equating to a mean ± SD of 5.6 ± 1.1 years prior to progression. In the JoCo OA Project, fixed-flexion knee radiographs with a SynaFlexer positioning frame were graded using K/L grades.

All participants in all cohorts had a baseline K/L grade of 2–3 in at least 1 knee without a history of previous total knee joint replacement. Demographic variables including age, sex, body mass index, baseline K/L grade, baseline JSW, baseline Western Ontario and McMaster Universities Osteoarthritis Index (WOMAC) pain subscale, nonsteroidal antiinflammatory drug use, opiate pain medication use, and White, Black, Asian American, and Hispanic race were obtained and compared among progressor groups.

DNA extraction. DNA used in this study was derived from buffy coat cells. In the OABC model development and OAI validation samples, DNA was previously extracted by OAI personnel, stored within the OAI biobank, and shipped to our laboratory for further analysis. In the JoCo OA Project cohort, buffy coat samples were shipped to our laboratory and DNA was extracted using a DNEasy kit (Qiagen). In all cases, 500 ng of DNA was treated with sodium bisulfite using an EZ DNA Methylation kit (Zymo) and loaded onto Infinium MethylationEPIC 850K arrays (Illumina). Arrays were imaged by the Clinical Genomics Center at the Oklahoma Medical Research Foundation.

OA progression definitions. In the OABC model development cohort, the definitions of radiographic and pain progression were the same as a previous biochemical biomarker study in these same patients (8). Radiographic progressors were defined as having a longitudinal loss in the minimum JSW of at least 0.7 mm from baseline to 48-month follow-up in 1 index knee. In each participant, the contralateral (nonindex) knee had less or no progression over the follow-up period. Participants with a tibial plateau rim distance of 6.5 mm at baseline, or with a change in the rim distance of >2.0 mm between baseline and follow-up were excluded due to inappropriate or unreliable radiographic positioning. Nonprogressors were defined as those with ≤0.5 mm of JSW loss from baseline to 48-month follow-up in both knees. Pain progressors were defined by an increase of ≥9 points at 2 or more time points on the WOMAC pain subscale (normalized to a 0–100 scale) from the 24-month to 60-month pain assessment.

In the JoCo OA Project validation cohort, radiographic progression was defined as an increase of ≥1 K/L grade in the index knee between 2 visits. Nonprogressors had no evidence for progression at any study time point. In the OAI validation cohort, radiographic progression was defined similar to the OABC, except that 0.7 mm of JSW loss had to occur within the first 24 months and remain narrowed at the 48-month follow-up visit (19).

Data preprocessing. Statistical analysis was performed using R version 4.0.2. Raw data files were loaded and processed using the ChAMP package version 3.14. After loading raw array data, CpG site methylation data were converted to beta value methylation estimates representing the ratio of methylated to unmethylated probe intensities at a given CpG site. Beta values ranged from 0 (unmethylated) to 1 (fully methylated). Normalization was then performed on beta values using the champ.norm function with default options using a beta-mixture quantile normalization procedure. From an initial set of 865,918 probes, the following were excluded: 1) probes with detected *P* values ≥0.01, 2) probes targeting non-CpG sites, 3) probes located on sex chromosomes, and 4) probes with known single-nucleotide polymorphisms within 5 bp of the 3′ end of the CpG probe with minor allele frequency ≥1% (23) (n = 158,841), leaving 707,077 CpG probes available for further analysis. Data were batch corrected for methylation plate and array.

Mixed peripheral blood DNA methylation analyses can be confounded by changes in cellular composition among study groups, as immune cell subsets have distinct epigenetic signatures (24). Therefore, to exclude composition as a confounder in our modeling, we estimated cell composition using the estimateCellCounts function of the minfi package (25) version 3.15.

Models were generated both with and without correction of cell composition using surrogate variable analysis (26) with the sva package version 3.28.0. This method has been previously shown to robustly correct for cell count variation and other batch effects in large-scale epigenomic studies (26–28). Models demonstrated no differences after surrogate variable analysis adjustment, suggesting no significant skewing of our findings by differences in cellular composition (Supplementary Table 4, https://onlinelibrary.wiley.com/doi/art.42316).

Model development. Data were first split into 70% development and 30% lockbox validation subsets and modeling performed on the development set (Figure 1). We first tested 3 methods for model development and feature selection. Elastic net regularized, generalized logistic models were developed using the glmnet package version 2.0-16 with feature selection. Models were tuned using 10-fold internal cross-validation. Further cross-validation was performed by looping random data splitting and model development for a total of 40 cycles. Models were then

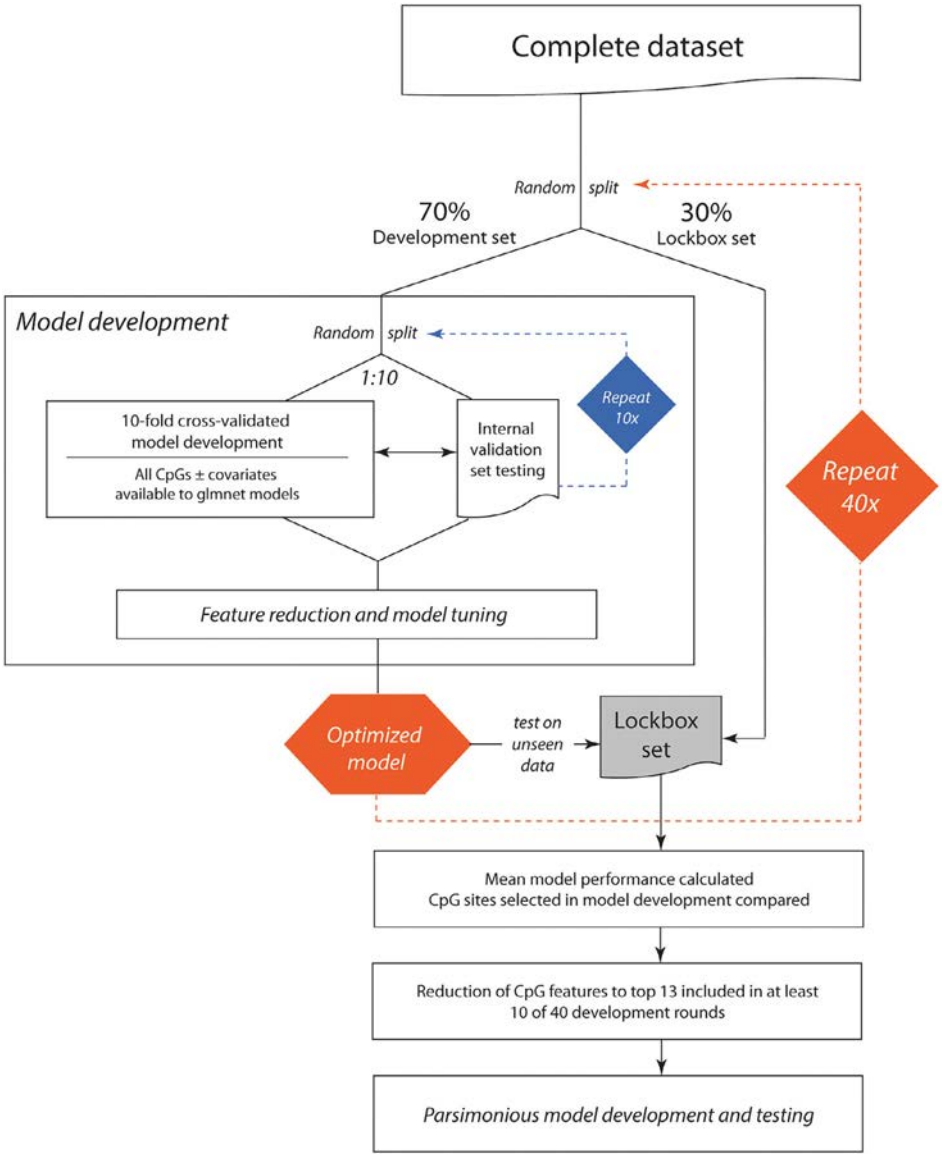

Figure 1. Diagram of workflow to develop machine learning models to predict future osteoarthritis progression.

applied to the lockbox set, and performance characteristics, including receiver operating characteristic AUC, diagnostic odds ratio, accuracy, sensitivity, specificity, and F1 score (the weighted average of precision and recall) were recorded. DNA methylation sites (features) selected for inclusion in each model were recorded and compared.

For feature reduction and parsimonious model development, we used the glmnet package with an elastic net approach, which combines ridge regression and least absolute shrinkage and selection operator regression to perform both feature selection and regularization. The resulting models included only the CpG sites important to discrimination of progressors versus nonprogressors, removing unnecessary features (see Supplementary Table 5 available on the *Arthritis & Rheumatology* website at https://onlinelibrary.wiley.com/doi/art.42316). The performance characteristics of development models (based on training rather than test data) are presented in Supplementary Table 6, https://onlinelibrary.wiley.com/doi/art.42316. Models developed to discriminate any progressors (pain-only, radiographic-only, and pain plus radiographic) versus nonprogressors using the entire DNA methylation data set selected a mean ± SEM of 14 ± 2 CpG sites (features) during development, with 13 CpG features being chosen in at least 10 of 40 development rounds. Accordingly, we then reduced our data set to include only these 13 features and derived new parsimonious models. Surprisingly, we were also able to derive parsimonious models for the remaining comparisons (pain-only, radiographic-only, and pain plus radiographic progressors versus nonprogressors) based on these same 13 CpG sites. Parsimonious models developed based on the most frequently selected CpGs in each comparison were not

Table 1. Characteristics of patients in the model development and validation cohorts in DNA methylation data–based models assessing OA progression versus nonprogression*

		OA progressors		
	Nonprogressors	Radiographic only	Pain only	Radiographic + pain
Model development cohort (FNIH OABC)†				
Age, mean ± SD years	61 ± 9	63 ± 8	59 ± 9‡	62 ± 9
Sex, % female	64	44§	63	56
BMI, mean ± SD kg/m^2	31 ± 5	31 ± 5	31 ± 5	31 ± 5
Baseline K/L grade, mean ± SD	1.8 ± 0.9	2.0 ± 0.9	1.9 ± 0.9	2.2 ± 0.9¶
Baseline JSW, mean ± SD mm	4.0 ± 1.3	4.0 ± 1.3	3.9 ± 1.4	3.9 ± 1.4
Baseline WOMAC pain subscale, mean ± SD score	12.0 ± 16.0	14.0 ± 19.2	14.0 ± 17.6	13.3 ± 16.7
NSAID use, %	16	23	22	35#
Pain medication use, %	13	10	12	10
Race/ethnicity, %				
Black	21	10**	30	17
Asian American	2	0	0	1
Hispanic	0	1	0	2
White	79	79	70	80
Validation cohort (JoCo OA Project)††				
Age, mean ± SD years	66 ± 9	64 ± 8	–	–
Sex, % female	73	80	–	–
BMI, mean ± SD kg/m^2	34 ± 8	36 ± 8	–	–
Baseline K/L grade, mean ± SD	2.5 ± 0.5	2.3 ± 0.5‡‡	–	–
Baseline WOMAC pain subscale, mean ± SD score	33 ± 20	30 ± 20	–	–
NSAID use, %	19	32	–	–
Pain medication use, %	12	4	–	–
Race/ethnicity, %				
Black	27	47§§	–	–
White	73	53¶¶	–	–
Time between blood sample visit and progression visit, mean ± SD years	NA	5.6 ± 1.1	–	–
Validation cohort (OAI) ##				
Age, mean ± SD years	60 ± 8	60 ± 8	–	–
Sex, % female	50	52	–	–
BMI, mean ± SD kg/m^2	30 ± 4	31 ± 5	–	–
Baseline K/L grade, mean ± SD	2.3 ± 0.7	1.9 ± 0.7	–	–
Baseline JSW, mean ± SD mm	4.0 ± 1.3	4.2 ± 1.2	–	–
Baseline WOMAC pain subscale, mean ± SD score	17.0 ± 5.3	21.0 ± 4.6***	–	–
NSAID use, %	7	22	–	–
Pain medication use, %	7	30†††	–	–
Race/ethnicity, %				
Black	11	11	–	–
White	89	89	–	–

* OA = osteoarthritis; BMI = body mass index; K/L = Kellgren/Lawrence; JSW = joint space width; WOMAC = Western Ontario and McMaster Universities Osteoarthritis Index; NSAID = nonsteroidal antiinflammatory drug; NA = not applicable.
† The model development Foundation for the National Institutes of Health Osteoarthritis Biomarkers Consortium (FNIH OABC) cohort had a total of 554 patients, among which 189 were nonprogressors, 81 were radiographic-only progressors, 91 were pain-only progressors, and 193 were pain plus radiographic progressors.
‡ In the OABC cohort, pain-only progressors versus nonprogressors had a significant difference in age, $P = 0.02$ versus nonprogressors.
§ In the OABC cohort, radiographic-only progressors versus nonprogressors had a significant difference in sex, $P = 0.003$ versus nonprogressors.
¶ In the OABC cohort, pain plus radiographic progressors versus nonprogressors had a significant difference in baseline K/L grade, $P < 0.0001$ versus nonprogressors.
# In the OABC cohort, pain plus radiographic progressors versus nonprogressors had a significant difference in NSAID use, $P = 0.02$ versus nonprogressors.
** In the OABC cohort, radiographic-only progressors versus nonprogressors had a significant difference in Black race, $P = 0.04$ versus nonprogressors.
†† The Johnston County Osteoarthritis (JoCo OA) Project validation cohort had a total of 128 patients, among which 51 were nonprogressors and 77 were radiographic-only progressors.
‡‡ In the JoCo OA Project validation cohort, radiographic-only progressors versus nonprogressors had a significant difference in baseline K/L grade, $P = 0.03$ versus nonprogressors.
§§ In the JoCo OA Project validation cohort, radiographic-only progressors versus nonprogressors had a significant difference in Black race, $P = 0.03$ versus nonprogressors.
¶¶ In the JoCo OA Project validation cohort, radiographic-only progressors versus nonprogressors had a significant difference in White race, $P = 0.03$ versus nonprogressors.
The Osteoarthritis Initiative (OAI) validation cohort had a total of 55 patients, among which 28 were nonprogressors and 27 were radiographic-only progressors.
*** In the OAI validation cohort, radiographic-only progressors versus nonprogressors had a significant difference in baseline WOMAC pain scores, $P = 0.004$ versus nonprogressors.
††† In the OAI validation cohort, radiographic-only progressors versus nonprogressors had a significant difference in pain medication use, $P = 0.04$ versus nonprogressors.

Table 2. Performance characteristics of models developed from the OABC model development cohort*

Model, comparison	Accuracy, mean ± SEM %	ROC AUC, mean ± SEM	Sensitivity, mean ± SEM %	Specificity, mean ± SEM %	Diagnostic OR, mean ± SEM	F1 score, mean ± SEM	CpG sites, mean ± SEM number
OABC model development cohort, full model†							
Radiographic-only progressor vs. nonprogressor	87 ± 0.8	0.94 ± 0.004	0.88 ± 0.01	0.88 ± 0.01	83 ± 12	0.78 ± 0.01	17 ± 2
Pain-only progressor vs. nonprogressor	89 ± 0.9	0.97 ± 0.004	0.92 ± 0.01	0.89 ± 0.01	120 ± 20	0.83 ± 0.02	13 ± 2
Pain + radiographic progressor vs. nonprogressor	72 ± 0.7	0.79 ± 0.006	0.70 ± 0.01	0.74 ± 0.01	7.4 ± 0.4	0.74 ± 0.01	7 ± 2
Any progressor vs. nonprogressor	78 ± 0.4	0.86 ± 0.004	0.78 ± 0.004	0.78 ± 0.01	15 ± 1.0	0.85 ± 0.003	14 ± 2
Radiographic-only progressor vs. pain-only progressor	58 ± 1	0.62 ± 0.01	0.54 ± 0.02	0.60 ± 0.01	2.2 ± 0.2	0.51 ± 0.02	14 ± 3
Pain + radiographic progressor vs. radiographic-only progressor	76 ± 0.6	0.82 ± 0.007	0.78 ± 0.06	0.72 ± 0.03	12 ± 1.3	0.86 ± 0.003	10 ± 2
Pain + radiographic progressor vs. pain-only progressor	71 ± 0.6	0.79 ± 0.007	0.74 ± 0.006	0.76 ± 0.03	7.8 ± 0.7	0.84 ± 0.003	5 ± 1
OABC model development cohort, parsimonious model‡							
Radiographic-only progressor vs. nonprogressor	89 ± 0.5	0.94 ± 0.003	0.83 ± 0.01	0.91 ± 0.004	77 ± 11	0.81 ± 0.01	NA
Pain-only progressor vs. nonprogressor	90 ± 0.7	0.95 ± 0.004	0.88 ± 0.01	0.92 ± 0.01	125 ± 21	0.86 ± 0.01	NA
Pain + radiographic progressor vs. nonprogressor	76 ± 0.6	0.85 ± 0.006	0.75 ± 0.01	0.78 ± 0.01	12 ± 0.8	0.77 ± 0.01	NA
Any progressor vs. nonprogressor	82 ± 0.3	0.89 ± 0.003	0.84 ± 0.004	0.78 ± 0.008	20 ± 1.0	0.87 ± 0.002	NA
OABC-developed parsimonious model applied to JoCo OA Project cohort							
Radiographic-only progressor vs. nonprogressor	80 ± 0.3	0.88 ± 0.003	0.78 ± 0.004	0.88 ± 0.004	28 ± 1	0.86 ± 0.002	NA
OABC-developed parsimonious model applied to previous OAI data set							
Radiographic-only progressor vs. nonprogressor	80 ± 0.8	0.89 ± 0.002	0.80 ± 0.008	0.82 ± 0.01	20 ± 1.4	0.80 ± 0.005	NA

* OABC = Osteoarthritis Biomarkers Consortium; ROC = receiver operating characteristic; AUC = area under the curve; OR = odds ratio; NA = not applicable; JoCo OA Project = Johnston County Osteoarthritis Project; OAI = Osteoarthritis Initiative.
† In the OABC cohort full model, 707,077 CpGs were available for modeling.
‡ In the OABC cohort parsimonious model, 13 CpGs were used for modeling.

superior to this core list of 13 CpGs. These newly derived parsimonious models were then tested on JoCo OA Project and OAI validation cohort data sets and performance tabulated.

RESULTS

Poor performance of models developed using only patient characteristics or cellular composition. Demographic and baseline clinical characteristics were generally well matched among various groups in the model development and validation cohorts (Table 1). Models developed using only baseline radiographic and pain data, age, sex, race/ethnicity, body mass index, and medication use performed poorly (accuracy 62–69%, AUC 0.54–0.68) (see Supplementary Table 4 available on the *Arthritis & Rheumatology* website at https://onlinelibrary.wiley.com/doi/art.42316). DNA methylation data from mixed buffy coat samples may be skewed by variations in cellular composition between groups. As direct measures of cellular composition were not collected in any of the cohorts studied, we estimated these values computationally (24). In the OABC model development cohort, proportions of B cells were lower in radiographic-only progressors versus nonprogressors (mean ± SD 4.7 ± 2.6% versus 6.0 ± 3.3% [$P = 0.002$]) (see Supplementary Table 1, available on the *Arthritis & Rheumatology* website at https://onlinelibrary.wiley.com/doi/art.42316). There were no differences in estimated cell composition in either validation cohort (Supplementary Tables 2 and 3, https://onlinelibrary.wiley.com/doi/art.42316).

Similar to demographic and clinical characteristics, models developed using cell composition data alone were unable to differentiate groups (Supplementary Table 4, https://onlinelibrary.wiley.com/doi/art.42316), suggesting no significant skewing of results owing to buffy coat composition heterogeneity. Methylation-based models developed after adjusting for demographic, clinical (including baseline pain and radiographic data and medication use), and cell composition data performed identically to models without covariate adjustment.

Robust discrimination of future pain and radiographic progressors from nonprogressors from models developed using baseline peripheral blood DNA methylation data. We generated logistic regression models based on peripheral blood DNA methylation data and assessed these models' ability to discriminate various progressor groups from nonprogressors. Radiographic-only progressor versus nonprogressor models performed robustly (mean ± SEM accuracy 87 ± 0.8%, AUC 0.94 ± 0.004 [when tested on unseen lockbox data], number of CpG sites [features] 17 ± 2) (Table 2, Figure 2A). Pain-only progressor versus nonprogressor models also performed well (mean ± SEM accuracy 89 ± 0.9%, AUC 0.97 ± 0.004, CpG sites 13 ± 2). Pain plus radiographic progressor versus nonprogressor models did not perform as well (mean ± SEM accuracy 72 ± 0.7%, AUC 0.79 ± 0.006, CpG sites 7 ± 2). Models discriminating any progressor (pain, radiographic, or both) from nonprogressors performed moderately (mean ± SEM accuracy 78 ± 0.4%, AUC 0.86 ± 0.004, CpG sites 14 ± 2). These full models based on peripheral blood DNA methylation data were not able to distinguish pain-only progressors from radiographic-only progressors (mean ± SEM accuracy 58 ± 1%, AUC 0.62 ± 0.001); however, pain plus radiographic progressors were readily distinguishable from radiographic-only progressors (mean ± SEM accuracy 76 ± 0.6%, AUC 0.82 ± 0.007) and pain-only progressors (mean ± SEM accuracy 71 ± 0.6%, AUC 0.79 ± 0.007).

We then added baseline demographic and clinical data to the full DNA methylation–based model data set, including age, sex, body mass index, baseline JSW, baseline pain (WOMAC pain subscale) scores, nonsteroidal antiinflammatory drug use, pain medication use, and estimated buffy coat cell composition and redeveloped multivariable models. None of these additional factors were identified by the glmnet package as significant predictive factors for inclusion in models, indicating that DNA methylation data are stronger predictors of OA outcomes than baseline demographic and clinical data. Intriguingly, including baseline serum and urine protein biomarker data from previous biochemical biomarker studies on these same patients (8,13) also did not change modeling outcomes (data not shown). In a previous study, we noted improved performance in models when DNA methylation data were log transformed to M values compared to untransformed beta values (19). However, in the present study we found no such differences when comparing accuracy of pain, radiographic, or pain plus radiographic progressor models versus nonprogressor models ($P = 0.16$ for transformed M values versus untransformed beta values; trend towards lower error rate in beta value–based models); therefore, beta value–based models were used for all analyses.

Similar discriminatory ability of parsimonious models as models trained on the entire methylation data set. Next, we reduced our training data set to the top 13 CpG sites most frequently included during initial model development (i.e., in ≥10 of 40 development rounds) in models of any progressors (pain, radiographic, and pain plus radiographic progressors) (see Supplementary Table 5 available on the *Arthritis & Rheumatology* website at https://onlinelibrary.wiley.com/doi/art.42316). We then rederived parsimonious models for pain-only progressors, radiographic-only progressors, and pain plus radiographic progressors using this reduced data set (Tables 2–3, Figure 2B). These parsimonious models demonstrated modest improvements in predictive capability compared to full models; the mean ± SEM accuracy of parsimonious models for distinguishing progressors was as follows: any progressors (82 ± 0.3%), pain-only progressors (90 ± 0.7%),

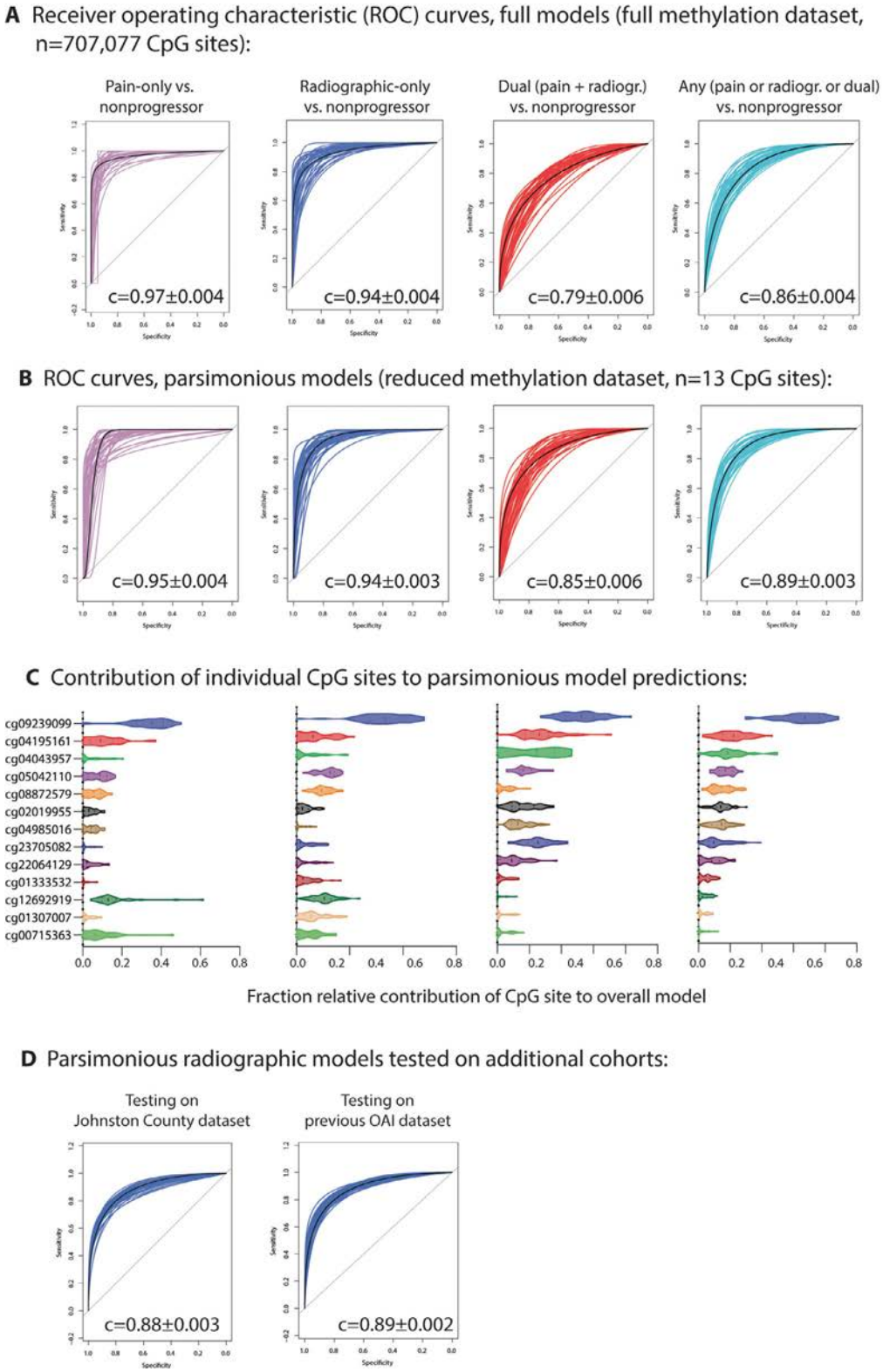

Figure 2. Performance of peripheral blood DNA methylation machine learning models to predict future knee osteoarthritis progression. **A**, Receiver operating characteristic (ROC) curves and mean ± SEM areas under the curve (AUCs) for progressors versus nonprogressors comparisons using the full models. **B**, ROC curves and mean ± SEM AUCs for progressors versus nonprogressors comparisons using parsimonious models following reduction in data set to 13 CpG sites most frequently selected during full model development. **C**, Relative contribution of individual CpG sites (features) to model predictions in 40 rounds of parsimonious model development. **D**, ROC curves and mean ± SEM AUCs for parsimonious models tested on independent data sets including the Johnston County Osteoarthritis Project cohort and a previously published Osteoarthritis Initiative (OAI) buffy coat DNA methylation data set.

Table 3. The 13 CpG sites (features) used to derive the reduced parsimonious models

CpG site	Chromosome	Gene symbol	CpG location	CpG island	Relative contribution to progressor model*			
					Pain-only progressor model	Radiographic-only progressor model	Pain plus radiographic progressor model	Any progressor model
cg09239099	12	*ERC1*	TSS200	Island	0.34 ± 0.02	0.32 ± 0.02	0.26 ± 0.01	0.33 ± 0.01
cg04195161	17	*ARHGAP23*	1stExon	S_Shelf	0.11 ± 0.01	0.07 ± 0.01	0.14 ± 0.01	0.11 ± 0.008
cg04043957	11	*TNNI2*	TSS1500	–	0.03 ± 0.009	0.04 ± 0.01	0.11 ± 0.01	0.10 ± 0.009
cg05042110	8	*PKIA*	5′UTR	–	0.08 ± 0.008	0.12 ± 0.006	0.09 ± 0.005	0.08 ± 0.004
cg08872579	1	*TTC22*	Body	N_Shore	0.06 ± 0.007	0.10 ± 0.005	0.02 ± 0.004	0.07 ± 0.005
cg02019955	9	–	–	–	0.04 ± 0.005	0.03 ± 0.004	0.08 ± 0.007	0.07 ± 0.005
cg04985016	2	*TRIP12*	5′UTR	–	0.04 ± 0.005	0.01 ± 0.003	0.07 ± 0.005	0.07 ± 0.005
cg23705082	22	*TBC1D22A*	Body	–	0.01 ± 0.003	0.03 ± 0.006	0.13 ± 0.007	0.06 ± 0.007
cg22064129	18	*SLC14A2*	TSS1500	–	0.03 ± 0.006	0.03 ± 0.006	0.05 ± 0.007	0.04 ± 0.006
cg01333532	16	*PHLPP2*	TSS1500	–	0.01 ± 0.003	0.04 ± 0.006	0.02 ± 0.004	0.02 ± 0.003
cg12692919	8	*TSNARE1*	Body	N_Shore	0.16 ± 0.02	0.10 ± 0.007	0.01 ± 0.002	0.02 ± 0.003
cg01307007	19	*FZR1*	TSS1500	–	0.02 ± 0.004	0.06 ± 0.008	0.01 ± 0.003	0.01 ± 0.003
cg00715363	17	*MIR548W*	Body	–	0.08 ± 0.01	0.05 ± 0.007	0.02 ± 0.004	0.01 ± 0.002

* Values are the mean ± SEM weight.

radiographic-only progressors (89 ± 0.5%), and pain plus radiographic progressors (76 ± 0.6%).

Accurate classification of future radiographic progressors when parsimonious models validated in JoCo OA Project and previous OAI data set cohorts. Finally, we sought to validate the parsimonious models on 2 independent data sets. First, we applied these models to buffy coat DNA methylation data from the JoCo OA Project cohort. Of note, both the definition of radiographic progression (increase of ≥1 grade on the K/L radiographic knee OA severity score at follow-up) and time to progression (mean 5.6 years) were different in the JoCo OA Project cohort compared with the model development cohort. We then also validated these parsimonious models by applying to our previously published OAI methylation data set (19).

For the present analysis, we restricted our previous data set to those samples run on Infinium MethylationEPIC 850K arrays, as the previous generation 450K arrays did not include the necessary 13 CpG sites. Like the JoCo OA Project cohort, the OAI cohort had slightly different progressor definitions compared to our model development samples (JSW loss required at 24 months and maintained at 48 months) (Table 1, Figures 2A–C, Figure 3). Models demonstrated similar performance at distinguishing radiographic-only progressors from nonprogressors when tested on both validation cohorts (mean ± SEM accuracy 80 ± 0.3%, AUC 0.88 ± 0.003, using JoCo OA Project cohort data; mean ± SEM accuracy 80 ± 0.8%, AUC 0.89 ± 0.002 using data from the previous OAI cohort data set) (Figure 2D).

DISCUSSION

The aim of this study was to evaluate whether peripheral blood–based epigenetic biomarkers could be used to differentiate future rapid radiographic and/or pain OA progressors from nonprogressors using a baseline blood sample from a single time point. To do this, we first determined genome-wide DNA methylation patterns using Infinium MethylationEPIC 850K arrays in 554 patients from the OABC cohort of the OAI, consisting of patients who experienced radiographic and/or pain progression within 48 months of baseline blood sample and matched nonprogressor controls. We then applied machine learning techniques to develop models to differentiate pain-only progressors, radiographic-only progressors, pain plus radiographic progressors, and any (pain, radiographic, and pain plus radiographic) progressors from nonprogressors. We used a generalized logistic modeling approach with feature reduction which allowed us to determine the subset of DNA methylation sites most predictive of progression status. All models were trained on a 70% development data split and tested on a 30% validation data split, and random development/validation data splits followed by model development were performed in a looped fashion over the course of 40 development cycles (Figure 1). Then, we re-derived models based on a reduced data set incorporating only the 13 CpG methylation sites most frequently selected during initial development. These parsimonious models were then tested on 2 validation cohorts: the JoCo OA Project and a previously generated methylation data set from the OAI.

Predictions based on clinical characteristics alone were not accurate. Including additional baseline serum and urine biomarker data from the OABC study to our models did not improve discrimination capability. We found parsimonious models to be roughly equivalent to the full models in predicting pain and/or radiographic progression within OABC data. Furthermore, the radiographic-only progressor prediction subset of these parsimonious models remained accurate when applied to the independent JoCo OA Project and OAI validation cohorts, despite differences in both OA progression definition and time to progression.

Prediction of pain and radiographic progression within the OABC cohort was highly accurate, although surprisingly, we were not able to discriminate pain-only from radiographic-only

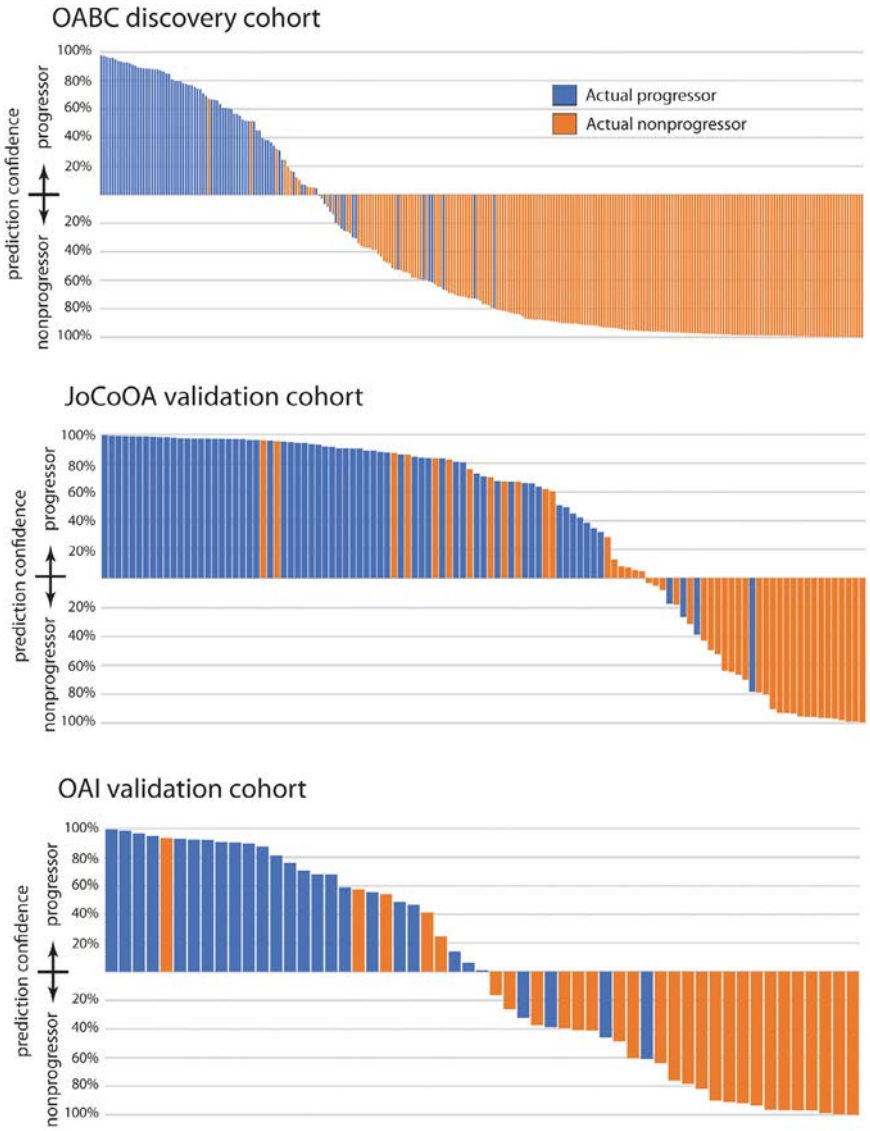

Figure 3. Plot of prediction confidence in radiographic-only progressor versus nonprogressor parsimonious models for all model development cohort and validation cohort samples (mean of 40 rounds of model development or validation). The vertical axis represents the model's confidence for prediction of osteoarthritis progression, and the horizontal axis represents individual patients (actual radiographic progressors [**blue bars**] and actual nonprogressors [**orange bars**]). OABC = Osteoarthritis Biomarkers Consortium; JoCo OA = Johnston County Osteoarthritis Project; OAI = Osteoarthritis Initiative.

progression. This is a curious finding. It may be artifactual, or it may reflect an underlying inflammatory process shared among early OA pain and radiographic progressors in the OABC cohort itself, although we encountered a similar inability to distinguish pain-only progressors versus radiographic-only progressors within the JoCo OA Project cohort (data not shown because only a small number of patients met these criteria [14 pain-only progressors and 45 radiographic-only progressors]).

Also curious is our finding that pain plus radiographic progressors were less accurately distinguished from nonprogressors than single-domain progressors (pain-only or radiographic-only progressors). As above, this may be artifactual and related to our particular data set or might suggest that pain plus radiographic progressors represent an independent OA phenotype/epigenotype when compared to pain-only or radiographic-only progressors. This is supported by the lack of overlap in CpG sites selected for modeling of pain plus radiographic progressors compared to single-domain progressors. This intriguing finding should be confirmed in additional cohorts of pain plus radiographic OA progressors.

This study builds on our previous pilot data modeling peripheral blood DNA methylation data as a predictor of radiographic progression (19) while adding several important additional features. First, we evaluated significantly more patients, including

different OA phenotypes, using a newer and more complete DNA methylation array (Infinium MethylationEPIC 850K). Additionally, the development cohort of our current study was performed on the same patients as the phase I Foundation for the National Institutes of Health OABC analyses, meaning that we can directly compare our findings to those previously published for both biochemical (8) and radiographic (9,10,29) models. Our models compare favorably to previously published OA predictive models. In the same cohort of patients, the OABC developed models to differentiate future pain plus radiographic progressors from pain-only progressors, radiographic-only progressors, and nonprogressors (8). Models based on baseline proteomics data performed relatively poorly with an AUC of 0.586, whereas time-integrated concentration models comparing the change in biomarkers over 12 or 24 months (compared to baseline) to predict disease status at 48 months were better, reaching an AUC of 0.669 without cross-validation and an AUC of 0.618 with cross-validation. No confirmation of these models in an independent cohort was performed.

Progression prediction using radiographic features has also been performed within this same cohort. In 2015, Eckstein et al determined that central medial femorotibial compartment thickness loss determined by magnetic resonance imaging between baseline and 12- or 24-month follow-up was predictive of future progression with an odds ratio of 4 (9). Similarly, in 2016 Hunter et al demonstrated that 24-month changes in periarticular bone area and shape were associated with both pain and radiographic progression at 48 months with odds ratios in the ~1.25 to 2.62 range for each 1 SD increase in bone area or shape (10). A separate multivariable radiographic model including cartilage thickness, surface area, effusion-synovitis, Hoffa-synovitis, and meniscal morphology change over 24 months to predict pain plus radiographic progression reached an AUC of 0.740 within the OABC cohort (11). A 2021 study by Hunter et al combined time-integrated concentration biochemical and radiographic biomarkers from the OABC to develop models to predict pain plus radiographic progressors versus controls (AUC 0.680–0.724) and radiographic-only progressors (AUC 0.716–0.832), although similar to previous studies, time-integrated concentration biomarker change over 24 months was used to predict outcomes at 48 months (13). Using a multivariate approach to OABC data, a 2019 study implemented a distance-weighted discrimination linear machine learning analysis and showed that progressor status was more strongly related to baseline magnetic resonance imaging features than with demographic/clinical variables or with baseline biochemical biomarkers (30).

Relatively little has been published regarding peripheral blood epigenomic or transcriptomic biomarkers in human OA. A 2018 analysis of publicly available blood gene expression profiles from a small set of OA patients and controls identified a 23-gene set with a reported accuracy of 0.971 to distinguish OA patients from controls, although no confirmation was performed (31). A study by Attur et al developed a multivariate model including a 3-gene inflammatory gene expression panel from mixed peripheral blood samples and radiographic data to predict radiographic OA progression within 24 months, yielding an AUC of 0.75 with an odds ratio of 19.10 (32). This study included only data from a single baseline time point, and the authors confirmed their findings in 2 independent cohorts, although the models were not able to predict pain outcomes.

Of the 13 CpG sites included in our parsimonious models, 12 are within known genes or regulatory elements, but only 2 of these have previous links to OA. *ERC1* is an antiapoptotic gene found down-regulated in OA fibroblast-like synoviocytes (33). *TRIP12* is an E3 ubiquitin ligase that complexes with tankyrase in chondrocytes; tankyrase inhibitors reduce surgically induced OA in mice (34). These findings are not surprising; given the lack of previous epigenetic analyses of circulating immune cells in OA patients, we would expect that the majority of epigenetic dysregulation within immune cells or cell subsets would be distinct from patterns seen within joint tissues. Considering our findings, future pathogenesis-focused OA studies should specifically evaluate immune cell epigenetic dysregulation. These should focus on individual immune cell subsets, as relatively little pathogenic information can be gleaned from the biomarker-focused mixed buffy coat methylation data we have generated in the present study.

Our study has several strengths. Most importantly, we found superior predictive capability for future radiographic and/or pain progression from a single baseline blood sample. This predictive capability appears to be valid as early as 2 years (OAI validation cohort) and as late as 5 years (JoCo OA Project validation cohort). The fact that predicted cell counts and baseline demographic information did not alter model performance broadens applicability, as does the fact that DNA processed by independent institutions demonstrated similar performance. Also striking was the clear distinguishability of pain-only and radiographic-only progressors from pain plus radiographic progressors, who were more difficult to distinguish from nonprogressor controls, suggesting a distinct epigenetic endophenotype in pain plus radiographic progressors that should be further evaluated in future studies. The parsimonious models we developed retained high levels of accuracy, including in validation cohorts, when data were reduced to a relatively small number (13 CpG features). This suggests that our findings may be translatable to inexpensive, sequencing-based assays with higher throughput, rather than requiring genome-wide DNA methylation arrays.

Our analysis has several limitations. Our development and validation cohorts were not ideally matched; specifically, follow-up periods and radiographic measurements differed between the 3 cohorts. Although this mismatch reduces the ability for us to fine-tune our development models, it may also be considered a strength, as accurate predictions were still able to be made despite these differences.

We have not yet examined the predictive capability of baseline blood epigenetic patterns for other radiographic endpoints beyond joint space narrowing; future analyses should focus on radiographic markers previously identified as strongly predictive of progression, including synovitis (11). Furthermore, our study focused exclusively on knee OA outcomes, despite the likelihood that a number of our samples included individuals with additional joint involvement (e.g., hand, hip), which may also be amenable to a systemic immune epigenetic modeling approach (35). This is a limitation shared by most of the OA systemic biomarker studies published to date and should be further evaluated in future studies designed to investigate potential epigenetic biomarkers of OA in multiple joints.

A major limitation of our study (as in any biomarker study) is that our findings are correlative rather than reflective of underlying disease mechanisms. Therefore, the CpG methylation sites we identified as strongly predictive of OA progression may or may not be directly related to OA pathophysiology, and caution must be taken when interpreting these findings.

In summary, our study offers compelling evidence that peripheral blood epigenetic-based models may be used as baseline predictive biomarkers for future rapid progression in symptomatic knee OA patients. We have identified a small subset of CpG sites that appear to be highly correlated with pain and radiographic progression, although we were unable to differentiate between them. The AUC we describe for radiographic progression, confirmed in 2 independent validation sets, is the highest yet published for a baseline biomarker and is similar to the best models produced by multivariate time-integrated concentration biochemical and radiographic biomarkers from the OABC.

Our results should be applied to other large OA data sets to confirm validity. Additional work should be done to translate our findings into an inexpensive and high-throughput clinical assay. Future studies should also evaluate the pathophysiologic implications, if any, of epigenetic changes in individual immune cell subsets in OA patients. Nonetheless, our results offer hope for an easily accessible, blood sample–based, single-timepoint biomarker to include patients likely to experience rapid progression in OA clinical trials, thereby accelerating drug and precision-guided therapy development for adults with knee OA.

AUTHOR CONTRIBUTIONS

All authors were involved in drafting the article or revising it critically for important intellectual content, and all authors approved the final version to be published. Dr. Jeffries had full access to all of the data in the study and takes responsibility for the integrity of the data and the accuracy of the data analysis.

Study conception and design. Dunn, Arbeeva, Golightly, Nelson, Jeffries.

Acquisition of data. Sturdy, Velasco, Schlupp, Prinz, Izda, Jeffries.

Analysis and interpretation of data. Dunn, Arbeeva, Golightly, Nelson, Jeffries.

REFERENCES

1. Vos T, Flaxman AD, Naghavi M, et al. Years lived with disability (YLDs) for 1160 sequelae of 289 diseases and injuries 1990-2010: a systematic analysis for the Global Burden of Disease Study 2010 [published correction appears in Lancet 2013;381:628]. Lancet 2012;380:2163–96.
2. Centers for Disease Control and Prevention (CDC). Prevalence of doctor-diagnosed arthritis and arthritis-attributable activity limitation—United States, 2010-2012. MMWR Morb Mortal Wkly Rep 2013;62:869–73.
3. Eckstein F, Hochberg MC, Guehring H, et al. Long-term structural and symptomatic effects of intra-articular sprifermin in patients with knee osteoarthritis: 5-year results from the FORWARD study. Ann Rheum Dis 2021;80:1062–9.
4. Yazici Y, McAlindon T, Gibofsky A, et al. Results from a 52 week randomised, double-blind, placebo-controlled, phase 2 study of a novel, wnt pathway inhibitor (SM04690) for knee osteoarthritis treatment [abstract]. Ann Rheum Dis 2018;77:1146–7.
5. Driban JB, Harkey MS, Barbe MF, et al. Risk factors and the natural history of accelerated knee osteoarthritis: a narrative review [review]. BMC Musculoskelet Disord 2020;21:332.
6. Collins JE, Neogi T, Losina E. Trajectories of structural disease progression in knee osteoarthritis. Arthritis Care Res (Hoboken) 2021;73:1354–62.
7. Wong CH, Siah KW, Lo AW. Estimation of clinical trial success rates and related parameters [published correction appears in Biostatistics 2019;20:366]. Biostatistics 2019;20:273–86.
8. Kraus VB, Collins JE, Hargrove D, et al. Predictive validity of biochemical biomarkers in knee osteoarthritis: data from the FNIH OA Biomarkers Consortium. Ann Rheum Dis 2016;76:186–95.
9. Eckstein F, Collins JE, Nevitt MC, et al. Cartilage thickness change as an imaging biomarker of knee osteoarthritis progression: data from the Foundation for the National Institutes of Health Osteoarthritis Biomarkers Consortium. Arthritis Rheumatol 2015;67:3184–9.
10. Hunter D, Nevitt M, Lynch J, et al. Longitudinal validation of periarticular bone area and 3D shape as biomarkers for knee OA progression? Data from the FNIH OA Biomarkers Consortium. Ann Rheum Dis 2016;75:1607–14.
11. Collins JE, Losina E, Nevitt MC, et al. Semiquantitative imaging biomarkers of knee osteoarthritis progression: data from the Foundation for the National Institutes of Health Osteoarthritis Biomarkers Consortium. Arthritis Rheumatol 2016;68:2422–31.
12. Kraus VB, Collins JE, Charles HC, et al. Predictive validity of radiographic trabecular bone texture in knee osteoarthritis: the Osteoarthritis Research Society International/Foundation for the National Institutes of Health Osteoarthritis Biomarkers Consortium. Arthritis Rheumatol 2018;70:80–7.
13. Hunter DJ, Deveza LA, Collins JE, et al. Multivariable modeling of biomarker data from the phase I Foundation for the National Institutes of Health Osteoarthritis Biomarkers Consortium. Arthritis Care Res (Hoboken) 2022;74:1142–53.
14. Handy DE, Castro R, Loscalzo J. Epigenetic modifications: basic mechanisms and role in cardiovascular disease [review]. Circulation 2011;123:2145–56.
15. Jeffries MA, Donica M, Baker LW. Genome-wide DNA methylation study identifies significant epigenomic changes in osteoarthritic subchondral bone and similarity to overlying cartilage. Arthritis Rheumatol 2016;68:1403–14.
16. Rushton MD, Reynard LN, Barter MJ, et al. Characterization of the cartilage DNA methylome in knee and hip osteoarthritis. Arthritis Rheumatol 2014;66:2450–60.
17. Den Hollander W, Ramos YF, Bos SD, et al. Knee and hip articular cartilage have distinct epigenomic landscapes: implications for future

cartilage regeneration approaches. Ann Rheum Dis 2014;73: 2208–12.

18. Fernández-Tajes J, Soto-Hermida A, Vázquez-Mosquera ME, et al. Genome-wide DNA methylation analysis of articular chondrocytes reveals a cluster of osteoarthritic patients. Ann Rheum Dis 2014;73: 668–77.
19. Dunn CM, Nevitt MC, Lynch JA, et al. A pilot study of peripheral blood DNA methylation models as predictors of knee osteoarthritis radiographic progression: data from the Osteoarthritis Initiative (OAI). Sci Rep 2019;9:16880.
20. Hunter DJ, Nevitt M, Losina E, et al. Biomarkers for osteoarthritis: current position and steps towards further validation. Best Pract Res Clin Rheumatol 2014;28:61–71.
21. Jordan JM, Helmick CG, Renner JB, et al. Prevalence of knee symptoms and radiographic and symptomatic knee osteoarthritis in African Americans and Caucasians: the Johnston County Osteoarthritis Project. J Rheumatol 2007;34:172–80.
22. Wirth W, Duryea J, Hellio Le Graverand MP, et al. Direct comparison of fixed flexion, radiography and MRI in knee osteoarthritis: responsiveness data from the Osteoarthritis Initiative. Osteoarthritis Cartilage 2013;21:117–25.
23. Zhou W, Laird PW, Shen H. Comprehensive characterization, annotation and innovative use of Infinium DNA methylation BeadChip probes. Nucleic Acids Res 2017;45:e22.
24. Houseman EA, Accomando WP, Koestler DC, et al. DNA methylation arrays as surrogate measures of cell mixture distribution. BMC Bioinformatics 2012;13:86.
25. Aryee MJ, Jaffe AE, Corrada-Bravo H, et al. Minfi: a flexible and comprehensive Bioconductor package for the analysis of Infinium DNA methylation microarrays. Bioinformatics 2014;30:1363–9.
26. Parker HS, Corrada Bravo H, Leek JT. Removing batch effects for prediction problems with frozen surrogate variable analysis. PeerJ 2014;2:e561.
27. Kaushal A, Zhang H, Karmaus WJ, et al. Comparison of different cell type correction methods for genome-scale epigenetics studies. BMC Bioinformatics 2017;18:216.
28. McGregor K, Bernatsky S, Colmegna I, et al. An evaluation of methods correcting for cell type heterogeneity in DNA methylation studies. Genome Biol 2016;17:84.
29. Ruhdorfer A, Haniel F, Petersohn T, et al. Between-group differences in infra-patellar fat pad size and signal in symptomatic and radiographic progression of knee osteoarthritis vs non-progressive controls and healthy knees—data from the FNIH Biomarkers Consortium Study and the Osteoarthritis Initiative. Osteoarthritis Cartilage 2017;25:1114–21.
30. Nelson AE, Fang F, Arbeeva L, et al. A machine learning approach to knee osteoarthritis phenotyping: data from the FNIH Biomarkers Consortium. Osteoarthritis Cartilage 2019;27:994–1001.
31. Li J, Lan CN, Kong Y, et al. Identification and analysis of blood gene expression signature for osteoarthritis with advanced feature selection methods. Front Genet 2018;9:246.
32. Attur M, Krasnokutsky S, Zhou H, et al. The combination of an inflammatory peripheral blood gene expression and imaging biomarkers enhance prediction of radiographic progression in knee osteoarthritis. Arthritis Res Ther 2020;22:208.
33. Sun Y, Mauerhan DR, Firestein GS, et al. Telomerase transduced osteoarthritis fibroblast-like synoviocytes display a distinct gene expression profile. J Rheumatol 2009;36:141–55.
34. Kim S, Han S, Kim Y, et al. Tankyrase inhibition preserves osteoarthritic cartilage by coordinating cartilage matrix anabolism via effects on SOX9 PARylation. Nat Commun 2019;10:4898.
35. Gullo TR, Golightly YM, Cleveland RJ, et al. Defining multiple joint osteoarthritis, its frequency and impact in a community-based cohort. Semin Arthritis Rheum 2019;48:950–7.

Arthritis & Rheumatology
Vol. 75, No. 1, January 2023, pp 41–52
DOI 10.1002/art.42289

American College of Rheumatology
Empowering Rheumatology Professionals

Both Disease Activity and HLA–B27 Status Are Associated With Gut Microbiome Dysbiosis in Spondyloarthritis Patients

Magali Berland,[1] Victoria Meslier,[1] Samar Berreira Ibraim,[1] Emmanuelle Le Chatelier,[1] Nicolas Pons,[1] Nicolas Maziers,[1] Florence Thirion,[1] Franck Gauthier,[1] Florian Plaza Oñate,[1] Jean-Pierre Furet,[2] Ariane Leboime,[3] Roula Said-Nahal,[3] Florence Levenez,[1] Nathalie Galleron,[1] Benoît Quinquis,[1] Philippe Langella,[2] Stanislav Dusko Ehrlich,[4] and Maxime Breban[5]

Objective. Gut microbiome dysbiosis has previously been reported in spondyloarthritis (SpA) patients and could be critically involved in the pathogenesis of this disorder. The objectives of this study were to further characterize the microbiota structure in SpA patients and to investigate the relationship between dysbiosis and disease activity in light of the putative influence of the genetic background.

Methods. Shotgun sequencing was performed on fecal DNA isolated from stool samples from 2 groups of adult volunteers: SpA patients (n = 102) and healthy controls (n = 63). A subset of the healthy controls comprised the age-matched siblings of patients whose HLA–B27 status was known. Changes in gut microbiota composition were assessed based on species diversity, enterotypes, and taxonomic and functional differences.

Results. Dysbiosis was confirmed in SpA patients as compared to healthy controls. The restriction of microbiota diversity was detected in patients with the most active disease, and the abundance of several bacterial species was correlated with Bath Ankylosing Spondylitis Disease Activity Index score. Among healthy controls, significant differences in microbiota composition were also detected between the HLA–B27–positive and the HLA–B27–negative siblings of SpA patients. We highlighted a decreased abundance of several species of bacteria in SpA patients, especially those bacteria belonging to the Clostridiales order. Among the few species of bacteria showing increased abundance, *Ruminococcus gnavus* was one of the top differentiating species.

Conclusion. These findings reveal that genetic background and level of disease activity are likely to influence the composition of the gut microbiota of patients with SpA. It may be appropriate for further research on chronic arthritis to focus on these key parameters.

INTRODUCTION

Spondyloarthritis (SpA) is a group of inflammatory rheumatic disorders with a population prevalence ranging between 0.2% and 1.6% (1). During the disease course, osteoarticular inflammation predominantly affects the axial skeleton (i.e., the sacroiliac, spinal, and thoracic joints), but may also involve the peripheral joints and entheses. Moreover, patients with SpA frequently experience extraarticular manifestations, including anterior uveitis, psoriasis, and inflammatory bowel diseases (IBDs) such as Crohn's disease or ulcerative colitis (2).

This multifaceted disease is thought to result from complex interactions between the genetic background and environmental

Supported by the GEnétique, Microbiote, Inflammation, et Spondylarthrite Ankylosante (GEMISA) grant from the French National Agency for Research (ANR-Blanc 2011-2015), the MetaGenoPolis (grant ANR-11-DPBS-0001), Assistance-Hôpitaux de Paris (grant CRC-2010), and la Fondation Arthritis Recherche & Développement.

Drs. Berland, Meslier, and Berreira Ibraim contributed equally to this work.

[1]Magali Berland, PhD, Victoria Meslier, PhD, Samar Berreira Ibraim, MSc, Emmanuelle Le Chatelier, PhD, Nicolas Pons, PhD, Nicolas Maziers, MD, PhD, Florence Thirion, MSc, Franck Gauthier, MSc, Florian Plaza Oñate, PhD, Florence Levenez, MSc, Nathalie Galleron, BSc, Benoît Quinquis, BSc: Université Paris-Saclay and MetaGenoPolis, INRAE, Jouy-en-Josas, France; [2]Jean-Pierre Furet, BSc, Philippe Langella, PhD: AgroParisTech, Université Paris-Saclay and the Micalis Institute, INRAE, Jouy-en-Josas, France, and Paris Center for Microbiome Medicine (PaCeMM) FHU, Paris, France; [3]Ariane Leboime, MD, Roula Said-Nahal, MD: Service de Rhumatologie, Hôpital Ambroise Paré, AP-HP, Boulogne, France; [4]Stanislav Dusko Ehrlich, PhD: Université Paris-Saclay, MetaGenoPolis, INRAE, Jouy-en-Josas, France, and the Department of Clinical and Movement Neurosciences, UCL Queen Square Institute of Neurology, University College London, London, UK, and Paris Center for Microbiome Medicine (PaCeMM) FHU, Paris, France; [5]Maxime Breban, MD, PhD: Service de Rhumatologie, Hôpital Ambroise Paré, AP-HP, Boulogne, France, Infection & Inflammation, UMR 1173, Inserm, Université de Versailles-Paris-Saclay, Montigny-le-Bretonneux, France, and Laboratoire d'Excellence Inflamex, Université Paris Descartes, Sorbonne Paris Cité, and Paris Center for Microbiome Medicine (PaCeMM) FHU, Paris, France.

Author disclosures are available at https://onlinelibrary.wiley.com/action/downloadSupplement?doi=10.1002%2Fart.42289&file=art42289-sup-0001-Disclosureform.pdf.

Address correspondence via email to Maxime Breban, MD, PhD, at maxime.breban@aphp.fr.

Submitted for publication October 28, 2021; accepted in revised form June 30, 2022.

factors. Several genetic polymorphisms have been shown to be associated with an increased risk of SpA (3). The genetic factor most strongly associated with the development of SpA, which was discovered nearly 50 years ago, is the presence of the major histocompatibility complex class I allele HLA–B27. More recently, genome-wide studies have demonstrated that other polymorphisms which predispose to SpA also predispose to IBD, reinforcing the possibility of shared mechanisms between both diseases (3). Of note, a large subset of responsible genes code for proteins involved in the immune response, and in particular for the interleukin-23/Th17 pathway of T cell differentiation, which is primarily implicated in the response against extracellular pathogens including bacteria and yeasts and/or in microbial sensing (2,3). Given that deregulated gut microbial composition, i.e., dysbiosis, is a hallmark of IBD (4,5), the foregoing observations lend support to the hypothesis that microbial dysbiosis could also contribute to the pathogenesis of SpA. Observations from animal models of SpA also support such a hypothesis (6). For example, dysbiosis is present in HLA–B27/human β_2-microglobulin–transgenic rats that develop both arthritis and IBD, but breeding under germ-free conditions has been shown to prevent the development of both joint and gut inflammation.

In several recent studies, the composition of the microbiota in gut mucosal biopsy samples or stool samples from SpA patients was investigated using high-throughput sequencing technologies. In most of these studies, including our own previous work, targeted amplicon sequencing of the 16S ribosomal RNA (16S rRNA) gene (6,7) was used, whereas a whole-metagenome shotgun sequencing approach was used on stool samples (8–10) in only 3 of these previous studies. As highlighted by the recent literature, shotgun sequencing is superior for all aspects of metagenomic analysis. Indeed, although the 16S rRNA gene is widely used for the taxonomic profiling of microbial communities, the methodology suffers from low taxonomic resolution and poor taxa quantification, which may lead to erroneous conclusions (11–13). Shotgun sequencing is a much preferred method to accurately detect and quantify microbial species, estimate species richness, and perform functional analysis up to the strain level (14–17). Whatever the methodology, dysbiosis was shown in all of the studies described, but there were differences in their specific findings. In a study by Costello et al and a study by Tito et al, increased taxa diversity was described in the mucosal-associated microbiota, although one limitation of those studies was the relatively few number of samples examined (9–27 patients versus 9–15 healthy controls) (18,19). In contrast, reduced diversity of the microbiota has been observed in studies of fecal samples from SpA and ankylosing spondylitis patients, which is a finding similar to those usually reported in the context of IBD (7,8,10). Despite the larger number of analyzed samples, results from the latter studies were quite divergent with respect to the contrasted bacterial genera/species between SpA patients and controls, with one of the major differences being the sequencing technology that was used.

In the present study, we sequenced DNA from the fecal samples of SpA patients and healthy controls (including a subset of HLA–B27–positive individuals and HLA–B27–negative individuals who were the spouses or siblings of SpA patients) using whole-metagenome shotgun sequencing. Our findings will help to refine the analysis of SpA dysbiosis.

PATIENTS AND METHODS

Participant recruitment and study design. This study was conducted according to the Declaration of Helsinki and the French legislation. Before study inclusion, each participant gave written informed consent for research use and publication of their data. Stool samples were collected from 197 volunteers, including 102 SpA patients fulfilling the Assessment of SpondyloArthritis international Society classification criteria for SpA (20) and 63 healthy controls. The healthy controls included 23 genetically independent controls and 40 controls who were recruited as siblings of SpA patients enrolled in the study (21 HLA–B27–positive and 19 HLA–B27–negative siblings) (Table 1). Of those, 82 samples from SpA patients and 62 samples from healthy controls had been included in our previous analysis of 16S rDNA targeted sequencing (7). Notably, the cohort comprised 11 sibling trios, each consisting of an HLA–B27–positive SpA patient matched with an HLA–B27–positive healthy control and an HLA–B27–negative healthy control.

Study samples were obtained from patients with established SpA who were seen in a tertiary care center (i.e., the Rheumatology clinic of the Ambroise Paré Hospital, Boulogne, France), or from SpA patients belonging to French families whose samples had been collected by Groupe Français d'Etude Génétique des Spondyloarthrites for genetic purposes as previously described (21,22). The healthy control group consisted of hospital staff members and the age-matched healthy spouses or siblings of SpA patients. Additional details on the methods used in this study are available on the *Arthritis & Rheumatology* website at http://onlinelibrary.wiley.com/doi/10.1002/art.42289.

All participants were required not to have received antibiotics during the preceding month, nor to have undergone gut preparation for colonoscopy during the preceding 6 months. Individuals affected by medical conditions other than the diseases under investigation, which we thought could potentially affect the results of the study, were excluded. Notably, this included other osteoarticular inflammatory disorders and/or autoimmune disorders, obesity, diabetes, cancer, and any chronic organ failure. Clinicobiologic data relevant to disease classification or disease activity evaluation (i.e., Bath Ankylosing Spondylitis Disease Activity Index [BASDAI]) and current treatments were collected.

Table 1. Characteristics of spondyloarthritis (SpA) patients and healthy controls included in this study on the microbiota structure of the gut in SpA patients and the relationship between dysbiosis and disease activity*

Characteristic	SpA patients (n = 102)	Healthy controls (n = 63)	P†
Age, mean ± SD years	50 ± 11.3	48.7 ± 11.7	0.8
Disease duration, mean ± SD years	25.1 ± 11.9	NA	
Sex ratio, % of men	49	39.7	0.3
HLA–B27 positivity‡	82.5	43.1	1.8^{-06}
BASDAI, mean ± SD score	3.78 ± 2.29	NA	
Axial/peripheral SpA	88.2/11.8	NA	
Radiographic sacroiliitis§	56	ND	
Extraarticular manifestations			
Uveitis	28.4	ND	–
Psoriasis	30.4	ND	–
Inflammatory bowel disease	12.7	0	0.03
Treatments of interest			
Any treatment	67.3	6.5	1^{-13}
NSAID	53.5	4.8	7.7^{-10}
Glucocorticoid	5.0	0	0.1
DMARD	4.0	0	0.2
Anti-TNF biotherapy	28.4	0	8.5^{-06}
Antacid	32.7	1.6	5.62^{-06}

* Except where indicated otherwise, values are the percent of participants. The registered manifestations correspond to those present at the time of examination or retrieved from medical history. The only disease-modifying antirheumatic drug (DMARD) received by patients in the study was sulfasalazine. The anti–tumor necrosis factor (anti-TNF) medications received by patients in the study included etanercept (n = 12 patients), infliximab (n = 11 patients), and adalimumab (n = 5 patients). BASDAI = Bath Ankylosing Spondylitis Disease Activity Index; NSAID = nonsteroidal antiinflammatory drug; NA = not applicable; ND = not determined.
† *P* values were determined by chi-square test, except for the variables of age, sex ratio, HLA–B27 status, and inflammatory bowel disease, which were determined by Wilcoxon's test. *P* values of ≤0.05 were considered significant.
‡ HLA–B27 status was determined in all SpA patients and in 51 of 63 healthy controls.
§ Radiographic sacroiliitis diagnoses fulfilling the modified New York criteria (50) were determined in 100 of 102 SpA patients.

Fecal DNA extraction, metagenomic sequencing, and mapping procedures. Details of the fecal DNA extraction procedure used in this study have been described previously (7). Whole-metagenome shotgun sequencing was performed using 5500 SOLiD Wildfire (Life Technologies) to generate single-end reads 35–50 bases long. Read quality control was performed with an in-house pipeline using a quality score cutoff of >20. In addition, reads aligned to the human genome (GRCh38.p13) or to the SOLiD adapter sequences were discarded. The resulting filtered, high-quality reads (mean ± SEM 47.8 ± 24.7 million reads per sample) were mapped onto the 10.4 million-gene reference catalog IGC2 (8) using the in-house Meteor software suite (software available upon request). Read alignments were performed in colorspace with Bowtie software version 1.2.3 in a 2-step procedure (using the options -f -C –integer-quals -v 2 -k 10000 –sam –sam-nohead –sam-nosq –no-unal and an identity threshold of 95% to account for gene variability). In the first step, unique mapped reads (reads mapped to a unique gene in the catalog) were attributed to their corresponding genes. In the second step, shared reads (reads that mapped with the same alignment identity to multiple genes in the catalog) were weighted according to the ratio of unique mapped counts. The subsequent steps to generate the gene abundance profiling table included first a rarefaction procedure, which involved drawing out 10 million mapped reads per sample without replacement (to account for difference in sequencing depth between samples), followed by the normalization of fragments per kilobase million (normalization by gene size and total number of mapped reads per sample, reported in relative frequency), which was completed using the MetaOMineR (momr) R package (23).

Metagenomic species pangenome (MSP) determination and assessment of the gut microbiome functional potential. Metagenomic species pangenomes (MSPs) were used to identify and quantify the microbial species associated with the IGC2 reference catalog (8). MSPs are clusters of coabundant genes (minimum size >100 genes) reconstructed from 1,601 metagenomes into 1,990 MSP species and used as proxies for microbial species (14,24). MSP abundances were estimated as the mean abundance of their 100 marker genes, as far as at least 20% of these genes are detected. An MSP abundance table was then normalized for each sample by dividing the abundance of the MSP by the sum of MSP abundances detected in the sample. MSP taxonomical annotation was processed as previously described (6). MSP species richness was determined by counting the number of MSPs detected in the corresponding sample.

Assessment of the gut microbiome functional potential. The metabolic potential of the intestinal microbiome

was assessed using an in-house pipeline. Genes of the 10.4 million-gene reference catalog were annotated using the KEGG version 8.9 database (25), the eggNOG database (26), and the TIGRFAMs database (27). Using DIAMOND (28), each gene from the IGC2 catalog was mapped onto KEGG orthologs from the KEGG database and was assigned to the best-ranked KEGG ortholog among hits with E-values of $<10^{-5}$ and a bit score of >60. The same procedure was used with eggNOG version 3.0. The gene catalog was searched against TIGRFAM version 15.0 profiles using HMMER version 3.2.1 (29). Next, KEGG modules, gut metabolic modules (30), and gut-brain modules (31) were reconstructed for each metagenomic species using their pathway structures (and potential alternative pathways), based on their detected annotated KEGG orthologs (or NOGs, or TIGRFAMs). Since MSPs are pangenomes, their genes are divided into "core" genes, which are present in all samples harboring the MSP, and "accessory" genes, which are specific to certain strains of the MSP and might be absent from a sample even if the MSP is detected. Functional modules were considered to be present in a given species if at least 90% of its components were present in the core genes of the corresponding MSP. Core modules were then considered to be present whenever the MSP was present in a given sample. Other modules (accessory modules) were identified sample-by-sample according to all of the MSP genes (core and accessory) in a given sample. Finally, we estimated the abundance of a module in a sample by summing the abundances of all MSPs found to carry this module in the sample.

Enterotype determination. Enterotyping was performed using the species abundance table for a Dirichlet Multinomial Mixtures approach (32) by means of the Dirichlet Multinomial R package version 1.24.1 (33). The optimal number of clusters was determined based on the stability of the clustering; enterotypes were considered stable if samples were affected into the same cluster in at least 15 out of 20 tests performed. Three enterotypes were obtained corresponding to Bacteroides, Firmicutes, and Prevotella.

Data analysis and statistical methods. Prior to the analyses, the normalized MSP abundance table was filtered out by using a 10% occurrence threshold across samples, which resulted in a total of 662 MSPs. The nonparametric Wilcoxon test was used to compare 2 conditions, and the Kruskal-Wallis test was used to compare more than 2 conditions. The Benjamini-Hochberg adjustment was used to control for the false discovery rate and provided q values that gave the expected proportion of false positives among all positive results. Unless stated otherwise, q values of ≤0.1 were considered significant, and q values between 0.1 and 0.3 were considered to show a tendency toward significance. All statistical analyses and visualizations were performed in R environment version 3.6.0 (https://www.r-project.org). Box plots and bar plots were computed using the ggpubr R package (34), and the metagenomic analyses were performed using the momr R package (23). Heatmaps were created with the ComplexHeatmap package (35). Observed richness, the Shannon diversity index, the inverse Simpson index, and the Fisher index were used for the α-diversity analysis and all were computed with the R package VEGAN (36). For the β-diversity analysis, Bray–Curtis distances were computed with the R package VEGAN (36), the principal coordinates analysis was computed with the R package ade4, and graphical displays were produced with the R package factoextra. To assess the differences in β-diversity, we performed permutational multivariate analysis of variance (PERMANOVA) using distance matrices with the function Adonis (n = 10,000 permutations).

Data availability. Metagenomic reads generated in this study are available on the INRAE data portal (dataset X9BHTZ), a public, open access repository, at https://doi.org/10.15454/X9BHTZ.

RESULTS

Alteration of the SpA gut microbiome in proportion to disease activity. We compared the composition of the gut microbiota between patients with SpA and healthy controls, taking into account clinical parameters which included disease activity index. MSP richness was not significantly different between SpA patients and healthy controls (P = 0.12 by nonparametric Wilcoxon test), although it was lower in SpA patients (Figure 1A). However, a significant negative correlation was observed between MSP richness and BASDAI score in SpA patients (Pearson's r = –0.34; $P = 6.6^{-4}$) (Figure 1D). By partitioning patients into tertiles based on their BASDAI score (BASDAI score ≤2.3 for mild SpA [n = 34], BASDAI score >2.3 and <4.8 for moderate SpA [n = 33], and BASDAI score ≥4.8 for severe SpA [n = 33]), we consistently found a progressive loss of richness concomitant with increasing disease activity (Figure 1B), which was strongly significant in patients with the most active SpA compared to healthy controls (for details on the characteristics of the SpA patients according to BASDAI score group, see Supplementary Information 1, available at http://onlinelibrary.wiley.com/doi/10.1002/art.42289). For further comparisons with other studies, we also performed the comparisons using the traditional BASDAI cutoff score of 4 (Supplementary Figures 2–4, http://onlinelibrary.wiley.com/doi/10.1002/art.42289), which led to similar results.

We also determined the gut microbiome enterotypes of the SpA patients and the healthy controls (Figure 1C). Three enterotypes were observed in both groups and were similarly dominated by the Firmicutes and Bacteroides. Interestingly, disease activity was associated with enterotype prevalence, and the most dramatic differences in enterotype prevalence occurred in the severe SpA patient group compared to healthy controls

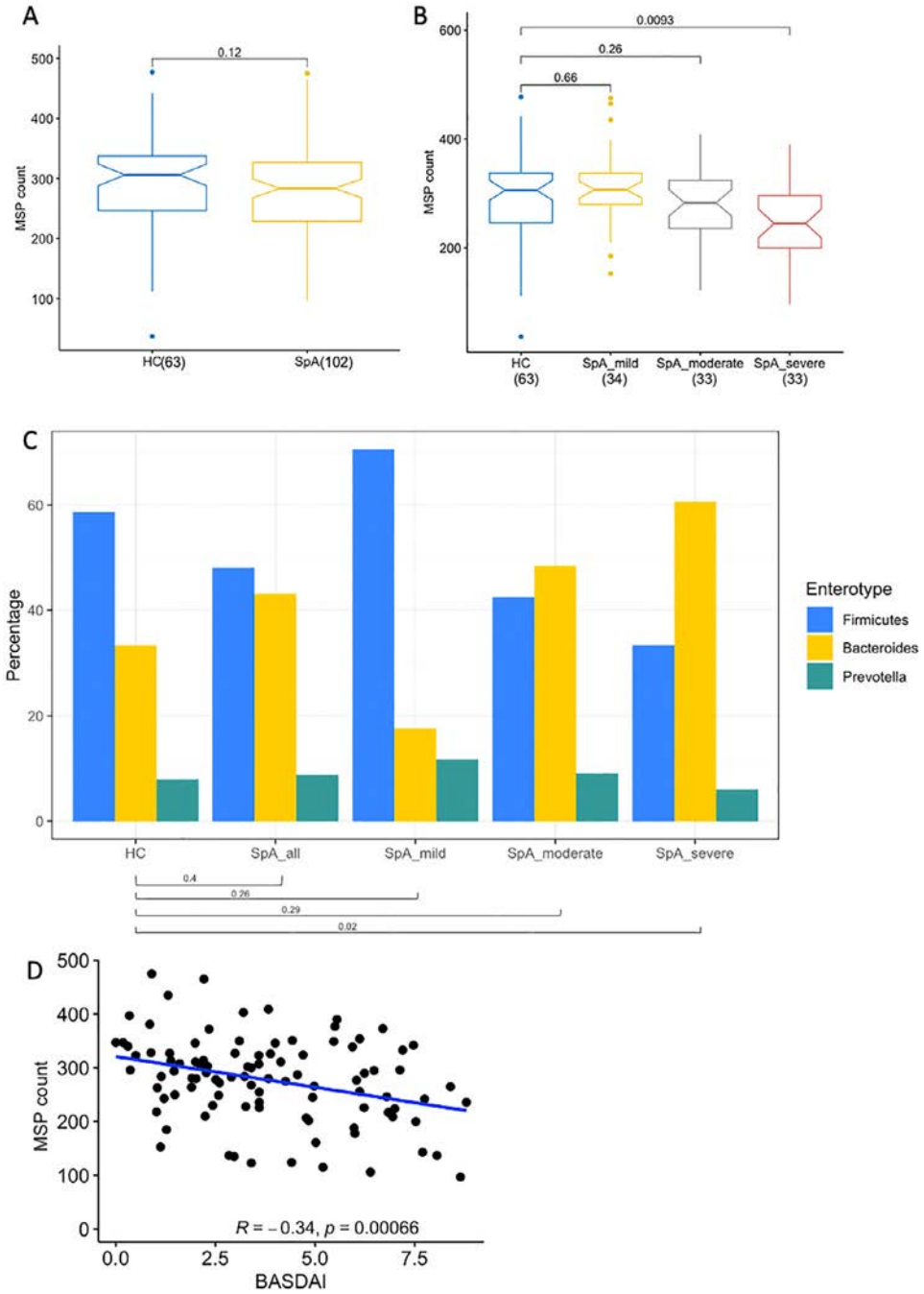

Figure 1. Gut microbiome dysbiosis in patients with spondyloarthritis (SpA) and the relation to disease activity. **A** and **B**, Metagenomic species pangenome (MSP) richness in healthy controls (HC) and SpA patients in total (**A**) and in SpA patients according to severity of disease based on the Bath Ankylosing Spondylitis Disease Activity Index (BASDAI) score tertile (**B**). Results are shown as box plots, in which lines inside the box represent the mean, boxes show the upper and lower interquartile range (IQR), and whiskers show 1.5 times the upper and lower IQRs. Circles indicate outliers. **C**, Distribution of the 3 main enterotypes among healthy controls and SpA patients, in total and according to BASDAI score tertiles. Values over horizontal lines in **A–C** indicate *P* values, determined by Wilcoxon's test in **A** and **B** and by chi-square test in **C** and **D**. **D**, Pearson's correlations between BASDAI score and MSP richness in SpA patients.

(*P* = 0.02 by chi-square test) (Figure 1C). Of note, compared to healthy controls, the Bacteroides enterotype was increased in patients with severe SpA and decreased in patients with mild SpA (adjusted *P* = 0.028 by chi-square test with post hoc correction).

Taxonomic analysis of the gut microbiome dysbiosis in SpA patients. Finer analysis was performed at the MSP level (i.e., species level), resulting in 16 differentially abundant MSPs between SpA patients and healthy controls (q ≤0.3) (Supplementary Table 1, http://onlinelibrary.wiley.com/doi/10.

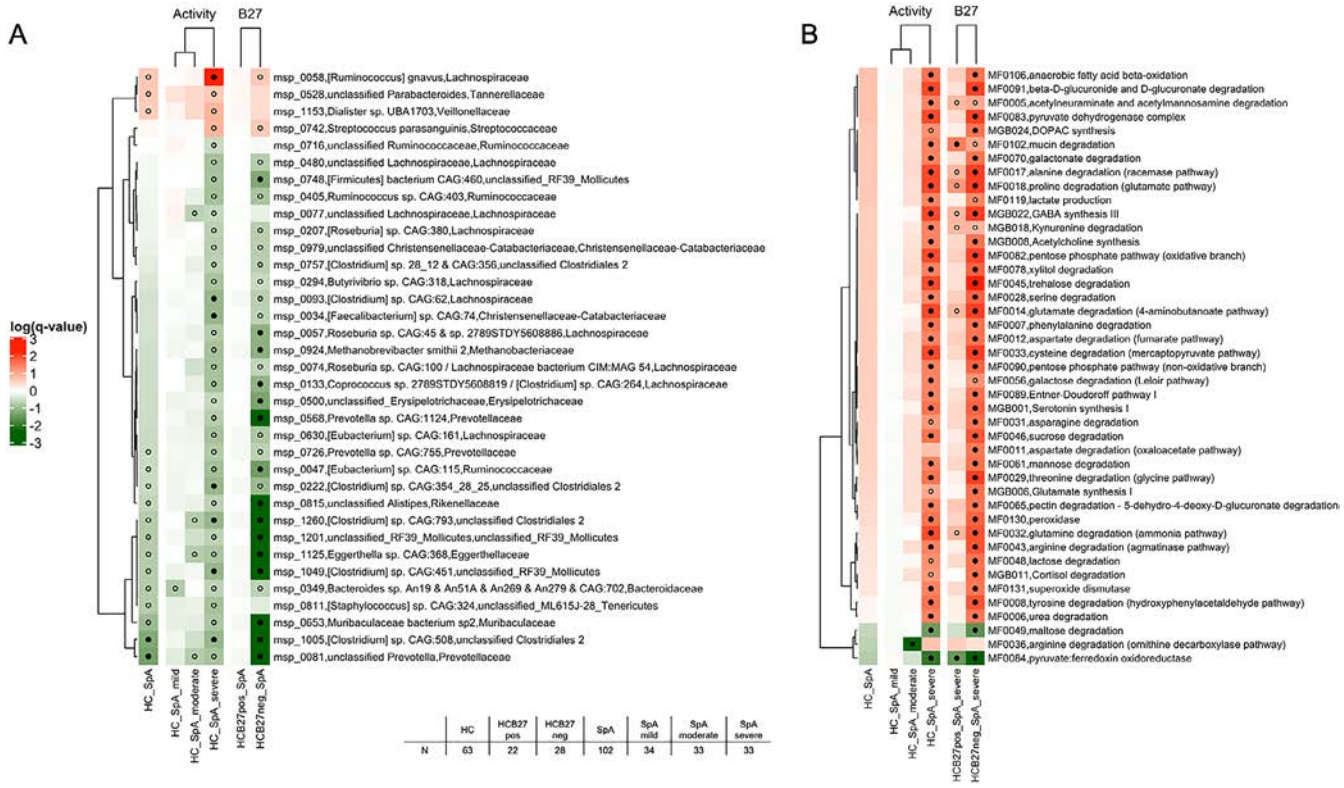

Figure 2. Summary heatmaps for comparisons of MSPs (**A**) and MSP functional modules (MF) (**B**) between SpA patients as a whole or by disease activity level and healthy controls according to HLA–B27 status. Wilcoxon's tests were performed for the following comparisons: healthy controls vs. all SpA; healthy controls vs. mild SpA; healthy controls vs. moderate SpA; healthy controls vs. severe SpA; HLA–B27–positive or negative healthy controls vs. all SpA; and HLA–B27–positive or negative healthy controls vs. severe SpA. All q-values were log-transformed, signed, and color coded according to their respective status: green = negative and enriched in the healthier condition; red = positive and enriched in the diseased condition. Those MSPs or MFs in which comparison resulted in a q-value of ≤0.3 are indicated with open circles; those in which comparison resulted in a q-value of ≤0.1 are indicated with solid circles. See Figure 1 for other definitions.

1002/art.42289). Most of these contrasted MSPs were found to be enriched in healthy controls (81%), and corresponded to species not yet isolated. The 3 MSPs highly enriched in SpA patients were *Ruminococcus gnavus*, unclassified *Dialister*, and *Parabacteroides* species (Figure 2A).

We observed that alterations in the gut microbiota composition at the species level increased in parallel with SpA activity index scores. We detected 182 differentially abundant MSPs between the BASDAI tertiles (q ≤0.3 by Kruskal-Wallis test) (Supplementary Table 2, http://onlinelibrary.wiley.com/doi/10.1002/art.42289), representing a variation of almost 30% of the SpA microbiome composition related to BASDAI stratification. Among these MSPs, 22% were found to be differentially abundant between the mild and moderate SpA groups, and 88% were found to be differentially abundant between the mild and severe SpA groups. These progressive changes were not related to clinical characteristics other than the BASDAI scores. A set of 30 MSPs was found to be consistently enriched in patients with moderately active SpA and patients with highly active SpA and all were correlated to BASDAI score (q ≤0.3 by Kruskal-Wallis test, Spearman's rho >0 for BASDAI score, and q ≤0.3 by Spearman's correlation test) (Supplementary Table 2).

Within the most contrasted MSP (q ≤0.1; Figure 3), most of the species enriched in the mild SpA group corresponded to unknown species from different Firmicutes families, whereas the 4 MSPs enriched in the severe SpA group were of the following known species: *Ruminococcus gnavus*, *Erysipelatoclostridium ramosum*, *Clostridium symbiosum*, and *Clostridium bolteae*. Comparisons of each SpA patient group with healthy controls reinforced the evidence of a progressive alteration of the SpA microbiome structure corresponding to increasing disease activity, by showing a much larger difference in MSPs between patients with highly active SpA and healthy controls than between patients with mild or moderate SpA and healthy controls (Figure 2A and Supplementary Table 3, http://onlinelibrary.wiley.com/doi/10.1002/art.42289). We also performed a β-diversity analysis, and the difference in species-level microbial composition between the mild, moderate, and severe SpA patient groups was nearly significant (P = 0.072 by PERMANOVA; R^2 = 0.025) (Supplementary Figure 1, http://onlinelibrary.wiley.com/doi/10.1002/art.42289).

Functional overview of the gut microbiome dysbiosis in SpA patients. Similar to what was observed at the

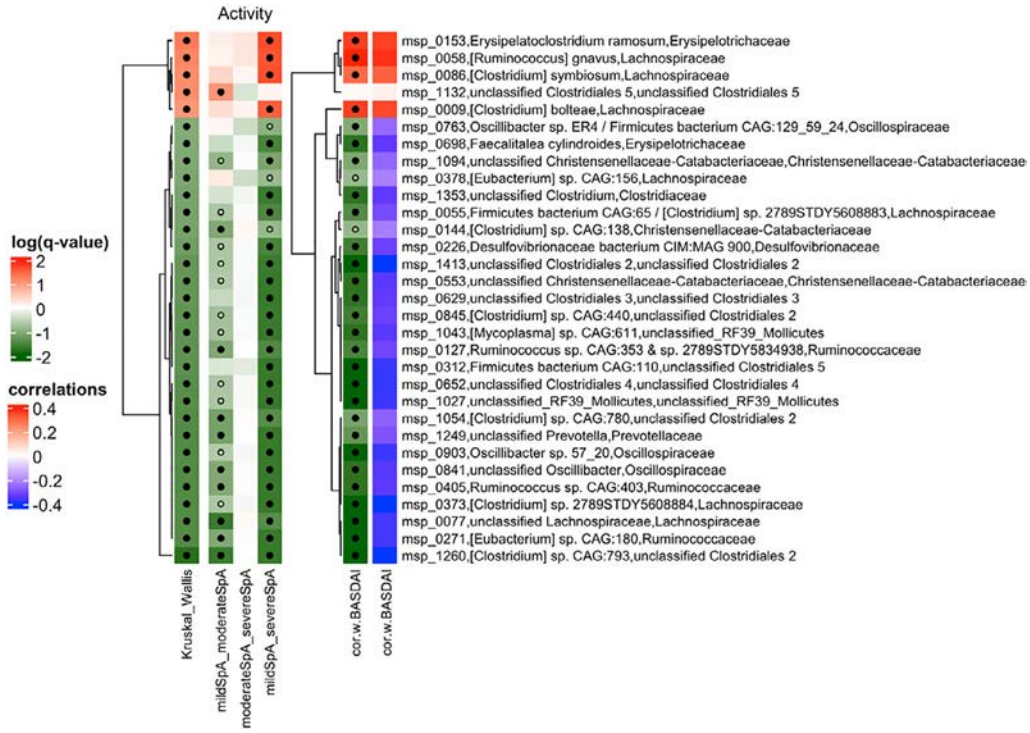

Figure 3. Summary heatmaps for comparisons of MSPs that were differentially abundant in at least 1 of the disease activity groups among SpA patients (q-values of ≤0.1 by Kruskal-Wallis test), and MSPs that showed a positive or negative correlation with the BASDAI score (by Pearson's correlation test). All log-transformed q-values and rho values were signed and color coded according to their respective status: green or blue = negative and enriched in the healthier condition; red = positive and enriched in the diseased condition. Solid dots indicate q-values of ≤0.1; open dots indicate q-values of ≤0.3. See Figure 1 for definitions.

species level, there was a progressive shift of contrasted microbial functional modules from mild to severe SpA (Figure 2B). There were no significant differences in microbial functions between patients with mildly active SpA and healthy controls. In patients with moderately active SpA, the module for arginine degradation via the ornithine decarboxylase pathway (MF0036) was depleted compared to healthy controls. Of note, 18 metabolic pathways differed between healthy controls and patients with severely active SpA (q ≤0.1). Among these, 17 metabolic pathways were enriched in patients with highly active SpA. In particular, pathways related to the following 8 functions involved in amino acid degradation were enriched: alanine, proline, glutamate, phenylalanine, cysteine, threonine, glutamine, and tyrosine degradation. Interestingly, 2 metabolic pathways involved in energy metabolism were conversely contrasted between patients with highly active SpA and healthy controls. The pathway for pyruvate synthesis with the ferredoxin oxidoreductase enzyme was enriched in healthy controls, whereas the pyruvate dehydrogenase complex module was increased in patients with SpA. The degradation of several glycans constituents of mucin 2, including sialic acid (*N*-acetylneuraminate) and its *N*-acetylmannosamine precursor, *N*-acetylglucosamine as well as fucose, was increased in patients with highly active SpA (q ≤0.3) (Supplementary Table 4, http://onlinelibrary.wiley.com/doi/10.1002/art.42289).

Influence of HLA–B27 status. We further investigated the potential influence of HLA–B27 status on the microbiome structure by comparing SpA patients and healthy controls stratified based on their HLA–B27 status. Interestingly, MSP richness was significantly decreased in SpA patients compared to HLA–B27–negative healthy controls (n = 28), whereas there was no significant difference between SpA patients and HLA–B27–positive healthy controls (n = 22) (Figure 4A). Moreover, a comparison of the microbiome compositions at the species level between SpA patients and healthy controls stratified by HLA–B27 status revealed several contrasting MSPs that were not detected in the whole-group comparisons (Figure 2A). Strikingly, the composition of the gut microbiome of SpA patients was found to be more divergent from that of HLA–B27–negative healthy controls than from that of HLA–B27–positive healthy controls (Figure 2 and Supplementary Table 5, http://onlinelibrary.wiley.com/doi/10.1002/art.42289), suggesting early microbiome alterations in HLA–B27–positive individuals who had not developed any SpA symptoms. Similar results were found when analyzing the samples of the 11 sibling trios. The HLA–B27–negative healthy controls had a significantly greater MSP richness than both their HLA–B27–positive healthy siblings and their siblings with SpA (Figure 4B).

We also performed a β-diversity analysis, and the differences in MSP composition between patients with SpA

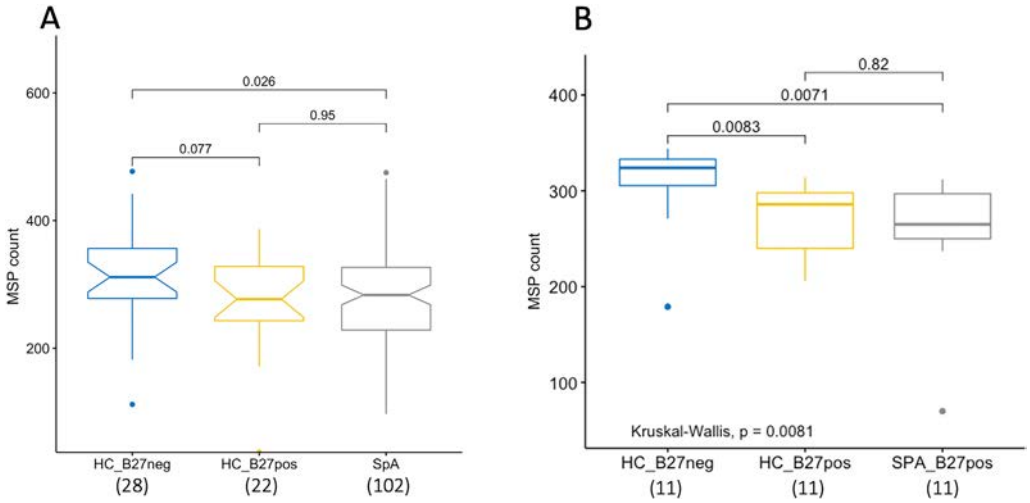

Figure 4. Impact of the HLA–B27 allele on gut microbiome dysbiosis. MSP counts in HLA–B27–negative (neg) healthy controls, HLA–B27–positive (pos) healthy controls, and SpA patients (**A**) and in the subcohort of family trios comprising healthy control siblings (HLA–B27–negative and HLA–B27–positive) of the HLA–B27–positive SpA patients (**B**). Results are shown as box plots, in which lines inside the box represent the mean, each box shows the upper and lower IQR, and whiskers show 1.5 times the upper and lower IQRs. Circles indicate outliers. *P* values shown over the horizontal lines were determined by Wilcoxon's test. See Figure 1 for other definitions. Color figure can be viewed in the online issue, which is available at http://onlinelibrary.wiley.com/doi/10.1002/art.42289/abstract.

and HLA–B27–positive and HLA–B27–negative healthy controls were nearly significant (P = 0.0625 by PERMANOVA; R^2 = 0.017) (Supplementary Figure 1, http://onlinelibrary.wiley.com/doi/10.1002/art.42289). This was not the case for the sibling trios (P = 0.39; data not shown), which was probably due to the smaller size of the groups.

The metabolic functions of patients with severe SpA were also more highly divergent from the metabolic functions of the HLA–B27–negative healthy controls than from the HLA–B27–positive healthy controls (Figure 2B). Similar but more striking contrasts in metabolic pathways (i.e., more statistically significant differences) were seen in comparing patients with severe SpA to HLA–B27–negative healthy controls than in comparing severe SpA patients to the healthy control group as a whole. Of note, several suggestive modules with a q value of ≤0.3 in comparison with the HLA–B27–positive healthy controls reached a q value of ≤0.1 in comparison with the HLA–B27–negative healthy controls, including those modules involved in the degradation of several amino acids (aspartate, serine, asparagine, arginine [Figure 2B]).

Impact of treatments on gut microbiota in patients with SpA. We investigated whether our observations of changes in the microbiota could be confounded by the effects of various drugs taken by the individuals participating in the study. The vast majority of healthy controls did not take any medication (n = 58 patients [94%]), whereas 4 individuals were taking nonsteroidal antiinflammatory drugs (NSAIDs) (n = 3) or antacids (n = 1) and information was missing for 1 individual. For the SpA patients, 32% did not take any medication, 18% received only NSAIDs, 8% received treatment with only biologic agents, 1% received only glucocorticoids, and 1% received only antacids. The other SpA patients (40%) received treatment with a combination of drugs.

There was no significant difference in MSP richness between SpA patients who did not receive treatment and healthy controls (n = 280 MSPs and n = 293 MSPs, respectively; P = 0.296 by nonparametric Wilcoxon test). This is consistent with the fact that the mean BASDAI score of SpA patients who did not receive treatment was lower than the BASDAI score of SpA patients receiving at least 1 drug (3.2 versus 4.0; P = 0.0498 by nonparametric Wilcoxon test).

Similar to what we observed previously, the gap between healthy controls and SpA patients not receiving treatment was wider when considering only patients with highly active disease (n = 10 patients with severe SpA, n = 253 MSPs; P = 0.086 by nonparametric Wilcoxon test) or when compared to HLA–B27–negative healthy controls (n = 28 healthy controls, n = 313 MSPs; P = 0.037 by nonparametric Wilcoxon test). There was no significantly contrasted MSP between these groups, probably because of their small size. A negative correlation between BASDAI score and MSP richness was observed (Spearman's rho = –0.32; P = 0.007) for patients receiving treatment with at least 1 drug, and this negative correlation remained significant for patients not receiving treatment (Spearman's rho = –0.35; P = 0.049). Overall, these results suggest that the SpA microbiome signature exists independently of the treatment patients receive.

To strengthen our conclusion, we performed a β-diversity analysis (based on the Bray-Curtis distance) that did not show any significant differences between SpA patients receiving no treatment compared to SpA patients receiving treatment with at least 1 drug (P = 0.781 by PERMANOVA) (Supplementary

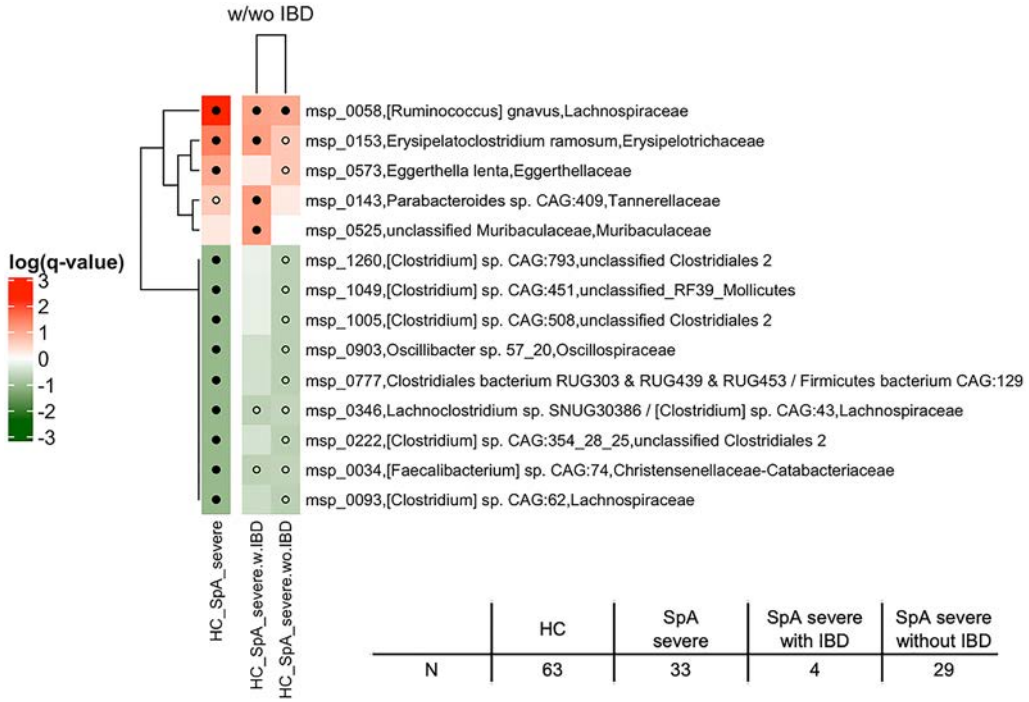

Figure 5. Gut microbiome dysbiosis in severe SpA patients with inflammatory bowel disease (w. IBD) compared to severe SpA patients without IBD (wo. IBD) and compared to healthy controls. Summary heatmaps show the MSPs ordered by q-value (determined by Wilcoxon's test) resulting from comparative analysis of the groups. All q-values of ≤0.1 in at least 1 of the comparisons are indicated (solid circles). Open circles indicate q-values of ≤0.3 All q-values were log-transformed, signed, and color coded according to their respective status: green = negative and enriched in the healthier condition; red = positive and enriched in the diseased condition. See Figure 1 for other definitions.

Figure 1, http://onlinelibrary.wiley.com/doi/10.1002/art.42289). Regarding antacid usage, the β-diversity analysis showed a weak but not statistically significant difference between the microbiota of patients taking antacids compared to others (P = 0.082). There was no such trend for patients receiving treatment with biologic agents (P = 0.996).

Association of extraarticular manifestations of disease with SpA microbiome structure. We evaluated the potential impact of extraarticular SpA manifestations on the microbiome structure by comparing patients with and without histories of uveitis, psoriasis, or IBD. A history of uveitis and psoriasis did not significantly affect the abundance of any MSPs (q > 0.97), nor did it affect global MSP richness (Supplementary Information 2, http://onlinelibrary.wiley.com/doi/10.1002/art.42289). In contrast, we found 25 differentially abundant MSPs (q ≤0.1) (Supplementary Table 6, http://onlinelibrary.wiley.com/doi/10.1002/art.42289) between SpA patients with and without a history of IBD, despite the low number of SpA patients with IBD. Members of the Ruminococcaceae family (such as *Faecalibacterium prausnitzii* and *Ruthenibacterium lactatiformans*) were decreased in SpA patients with IBD. In contrast, *R gnavus* was enriched with a moderate level of significance (q = 0.17). Figure 5 shows the discriminant MSPs between healthy controls and patients with severe SpA with or without IBD, showing that a history of IBD did not seem to significantly impact the SpA-associated variations in microbiota.

DISCUSSION

Using targeted sequencing of fecal samples, we previously reported gut dysbiosis in SpA patients which was characterized by decreased microbial diversity and increased levels of the *R gnavus* species correlated to disease activity in a subset of patients with a history of IBD (7). One limitation of this sequencing approach is that it rarely allows taxonomic characterization at the species level. Here, using a more thorough DNA shotgun sequencing method that allows precise detection and quantification of microbial species, we could refine SpA-associated fecal dysbiosis. This resulted in 2 new major findings. First, the extent of dysbiosis appeared to correlate strikingly with disease activity. Second, the HLA–B27 genotype, which strongly predisposes to SpA, was associated with significant dysbiosis in the healthy siblings of SpA patients, so that inclusion of this group of healthy controls in the primary whole analysis resulted in somewhat blunted differences between SpA patients and healthy controls.

Dysbiosis was first characterized by a reduction of microbial diversity, a consistent finding across several microbiota studies

in SpA and other inflammatory disorders that appeared here to predominate in the most active SpA cases (7,8,10,37,38). Moreover, the proportion of patients whose enterotype was dominated by the *Bacteroides* genus was increased among those with the most active disease, a finding consistent with this enterotype being associated with low-diversity microbiota (15). At the taxonomic level, the most striking changes also concerned patients with the most active disease and consisted predominantly of a decreased abundance of several species, the most numerous and significant belonging to the Clostridiales order.

In contrast, fewer species were found to be increased in SpA patients compared to controls, among which *R gnavus* was one of the top differentiating species, a finding consistent with our previous 16S rRNA study (7). Here, we showed that the abundance of *R gnavus* was positively correlated with disease activity in the SpA patient group as a whole, even if its abundance appeared to be greater in those with a history of IBD. Moreover, increased levels of *R gnavus* remained significantly associated with SpA in the comparison restricted to HLA–B27–negative participants, showing that it was associated with disease independently of HLA–B27 status. This highlights the potential role of *R gnavus* in the pathogenesis of SpA, which is known to produce proinflammatory metabolites and which has also been associated with IBD and lupus activity (39–41). *R gnavus* has the faculty to initiate the degradation of mucin 2 by removing sialic acid, a function that may weaken the mucus barrier (42). This is consistent with increased mucus degradation modules in the setting of active SpA.

The abundance of 6 other species was positively associated with SpA ($q < 0.3$) and/or positively correlated with BASDAI scores in our study ($q < 0.1$). Two of these species, *C bolteae* and *C symbiosum*, were found to be positively associated with ankylosing spondylitis in a previous shotgun sequencing study, in the whole SpA group (*C bolteae*) or in untreated patients compared to anti–tumor necrosis factor (TNF)–treated patients and healthy controls (*C symbiosum*), suggesting that the latter species was preferentially increased in the patients with the most active disease (9). In that same study, an unclassified *Eggerthella* (a genus that contains only a few species and has been associated with other inflammatory disorders including IBD and rheumatoid arthritis [43]) was increased in SpA patients. This observation could be consistent with an increase of *E lenta* in the patients with the most severe disease in our present study. An increase in *Dialister* species is also consistent with the reportedly increased abundance of the *Dialister* genus in the inflamed gut mucosa–associated microbiota, in correlation with disease activity in another study (19). It is noteworthy that the 4 species that were positively correlated with BASDAI scores in our study (i.e., *R gnavus*, *C bolteae*, *C symbiosum*, and *E ramosum*) have been associated with low-richness microbiota and autoimmune diseases (15,44). It must be mentioned that *Clostridium bolteae* has been recently reclassified as *Enterocloster bolteae* (45). Altogether, the most striking changes associated with SpA activity may reflect a shift of the gut lumen to a more oxidative milieu in the context of inflammation, conferring a survival advantage to bacteria such as the *Bacteroides* or *R gnavus* over strict anaerobes Clostridiales (46,47). This is consistent with increased aerobic pyruvate synthesis via pyruvate dehydrogenase in the setting of SpA and the opposite change for the anaerobic ferredoxin oxidoreductase module. It is noteworthy that several of the microbiota functional changes associated with severe SpA could have detrimental consequences on the host, such as the degradation of an array of amino acids, including the 2 essential amino acids phenylalanine and threonine.

Similar to SpA patients, the HLA–B27 genotype was associated with reduced microbiota diversity in healthy controls. This was particularly significant in the analysis restricted to paired trios, in which SpA patients were matched with an HLA–B27–negative and an HLA–B27–positive sibling. Since reduced diversity likely reflects some degree of inflammation, this indicated that HLA–B27 itself might pave the way for dysbiosis, even in asymptomatic healthy controls. Consistent with this interpretation, dysbiosis was more pronounced in SpA patients with active disease than in HLA–B27–positive healthy controls. However, the observation that HLA–B27–positive healthy controls had a microbial diversity profile that was in close proximity to that of SpA patients may explain why we could not find evidence of significant taxonomic differences between these groups. A previous study demonstrated that the composition of microbiota was influenced by the carriage of the HLA–B27 allele in healthy individuals but did not indicate whether this corresponded to dysbiosis (48).

SpA patients have long been divided into subgroups based on clinical findings that mostly include histories of extraarticular manifestations. This was the reason for separately analyzing patients who had a history of psoriasis, uveitis, or IBD. The former 2 groups did not differ, whereas the third group (even if IBD was inactive in a majority of the patients at the time of sampling [8 of 13 patients]) exhibited striking differences as compared to patients without these manifestations. A majority of the bacteria species were enriched in SpA patients who had a history of IBD, whereas fewer species were decreased, including *Faecalibacterium prausnitzii*, an antiinflammatory bacteria that is known to be negatively associated with IBD (49). Interestingly, despite a noticeable impact on microbiota structure, among the species that were significantly different between patients with and those without IBD, only *R gnavus* was found to be associated with disease activity, reinforcing the hypothesis that this species could provide a link between IBD and SpA.

The analysis of a possible confounder (especially medication) is always an interesting point as it may impact the gut microbiota composition. In our analysis, we did not observe a strong effect of the medication on the dysbiosis (Supplementary Figure 1, http://onlinelibrary.wiley.com/doi/10.1002/art.42289), but that

does not mean that the medication taken by the patients had no effect at all. We just may not have enough data to explore this question thoroughly. In summary, our findings in patients with SpA reveal that both genetic background and level of disease activity are likely to account for dysbiotic gut microbiota composition. Further elucidating the causal relationship between dysbiotic microbiota and SpA development may allow us to propose new therapeutic strategies.

ACKNOWLEDGMENT

We gratefully acknowledge the kind contribution of Mrs. Nabila Yasmine Domingo-Saidji from the Clinical Research Unit of Paris Ile-de-France Ouest (URCPO), who supervised the administrative paperwork and helped us to manage ethical issues related to the study.

AUTHOR CONTRIBUTIONS

All authors were involved in drafting the article or revising it critically for important intellectual content, and all authors approved the final version to be published. Dr. Breban had full access to all of the data in the study and takes responsibility for the integrity of the data and the accuracy of the data analysis.

Study conception and design. Furet, Langella, Ehrlich, Breban.
Acquisition of data. Leboime, Said-Nahal, Levenez, Galleron, Quinquis.
Analysis and interpretation of data. Berland, Meslier, Berreira Ibraim, Le Chatelier, Pons, Maziers, Thirion, Gauthier, Oñate, Ehrlich, Breban.

REFERENCES

1. Stolwijk C, van Onna M, Boonen A, et al. Global prevalence of spondyloarthritis: a systematic review and meta-regression analysis. Arthritis Care Res (Hoboken) 2016;68:1320–31.
2. Taurog JD, Chhabra A, Colbert RA. Ankylosing spondylitis and axial spondyloarthritis [review]. N Engl J Med 2016;374:2563–74.
3. Costantino F, Breban M, Garchon HJ. Genetics and functional genomics of spondyloarthritis. Front Immunol 2018;9:2933.
4. Qin J, Li R, Raes J, et al. A human gut microbial gene catalogue established by metagenomic sequencing. Nature 2010;464:59–65.
5. Huttenhower C, Kostic AD, Xavier RJ. Inflammatory bowel disease as a model for translating the microbiome. Immunity 2014;40:843–54.
6. Breban M, Beaufrère M, Glatigny S. The microbiome in spondyloarthritis. Best Prac Res Clin Rheumatol 2019;33:101495.
7. Breban M, Tap J, Leboime A, et al. Faecal microbiota study reveals specific dysbiosis in spondyloarthritis. Ann Rheum Dis 2017;76:1614–22.
8. Wen C, Zheng Z, Shao T, et al. Quantitative metagenomics reveals unique gut microbiome biomarkers in ankylosing spondylitis. Genome Biol 2017;18:142–13.
9. Yin J, Sternes PR, Wang M, et al. Shotgun metagenomics reveals an enrichment of potentially cross-reactive bacterial epitopes in ankylosing spondylitis patients, as well as the effects of TNFi therapy upon microbiome composition. Ann Rheum Dis 2020;79:132–40.
10. Zhou C, Zhao H, Xiao XY, et al. Metagenomic profiling of the pro-inflammatory gut microbiota in ankylosing spondylitis. J Autoimmun 2020;107:102360.
11. Větrovský T, Baldrian P. The variability of the 16S rRNA gene in bacterial genomes and its consequences for bacterial community analyses. PLoS ONE 2013;8:e57923.
12. Tremblay J, Singh K, Fern A, et al. Primer and platform effects on 16S rRNA tag sequencing. Front Microbio 2015;6:771.
13. Khachatryan L, de Leeuw RH, Kraakman ME, et al. Taxonomic classification and abundance estimation using 16S and WGS-A comparison using controlled reference samples. Forensic Sci Int Genet 2020;46:102257.
14. Plaza Onate F, Le Chatelier E, Almeida M, et al. MSPminer: abundance-based reconstitution of microbial pan-genomes from shotgun metagenomic data. Bioinformatics 2019;35:1544–52.
15. Le Chatelier E, Nielsen T, Qin J, et al. Richness of human gut microbiome correlates with metabolic markers. Nature 2013;500:541–6.
16. Brumfield KD, Huq A, Colwell RR, et al. Microbial resolution of whole genome shotgun and 16S amplicon metagenomic sequencing using publicly available NEON data. PLoS ONE 2020;15:e0228899.
17. Durazzi F, Sala C, Castellani G, et al. Comparison between 16S rRNA and shotgun sequencing data for the taxonomic characterization of the gut microbiota. Sci Rep 2021;11:3030–10.
18. Costello ME, Ciccia F, Willner D, et al. Intestinal dysbiosis in ankylosing spondylitis. Arthritis Rheumatol 2015;67:686–91.
19. Tito RY, Cypers H, Joossens M, et al. Dialister as a microbial marker of disease activity in spondyloarthritis. Arthritis Rheumatol 2017;69:114–21.
20. Rudwaleit M, van der Heijde D, Landewé R, et al. The Assessment of SpondyloArthritis International Society classification criteria for peripheral spondyloarthritis and for spondyloarthritis in general. Ann Rheum Dis 2011;70:25–31.
21. Said-Nahal R, Miceli-Richard C, Berthelot JM, et al, on behalf of the Groupe Français d'Etude Génétique des Spondylarthropathies. The familial form of spondylarthropathy: a clinical study of 115 multiplex families. Arthritis Rheum 2000;43:1356–65.
22. Said-Nahal R, Miceli-Richard C, D'Agostino MA, et al. Phenotypic diversity is not determined by independent genetic factors in familial spondylarthropathy. Arthritis Rheum 2001;45:478–84.
23. momr: Mining Metaomics Data (MetaOMineR).: Artistic–2.0. URL: https://CRAN.R-project.org/package=momr.
24. Nielsen HB, Almeida M, Juncker AS, et al. Identification and assembly of genomes and genetic elements in complex metagenomic samples without using reference genomes. Nat Biotechnol 2014;32:822–8.
25. Kanehisa M, Goto S. KEGG: kyoto encyclopedia of genes and genomes. Nucleic Acids Research 2000;28:27–30.
26. Huerta-Cepas J, Szklarczyk D, Forslund K, et al. eggNOG 4.5: a hierarchical orthology framework with improved functional annotations for eukaryotic, prokaryotic and viral sequences. Nucleic Acids Res 2016;44:D286–293.
27. Haft DH, Loftus BJ, Richardson DL, et al. TIGRFAMs: a protein family resource for the functional identification of proteins. Nucleic Acids Res 2001;29:41–3.
28. Buchfink B, Xie C, Huson DH. Fast and sensitive protein alignment using DIAMOND. Nat Methods 2014;12:59–60.
29. Eddy S, the HMMER development team. HMMER user's guide: biological sequence analysis using profile hidden markov models; 2020. URL: http://eddylab.org/software/hmmer/Userguide.pdf.
30. Vieira-Silva S, Falony G, Darzi Y, et al. Species-function relationships shape ecological properties of the human gut microbiome. Nat Microbiol 2016;1:16088–8.
31. Valles-Colomer M, Falony G, Darzi Y, et al. The neuroactive potential of the human gut microbiota in quality of life and depression. Nat Microbiol 2019;4:623–32.
32. Holmes I, Harris K, Quince C. Dirichlet multinomial mixtures: generative models for microbial metagenomics. PLoS ONE 2012;7:e30126.
33. version MMRP, 2019. DirichletMultinomial: Dirichlet-multinomial mixture model machine learning for microbiome data.

34. Kassambara A, Kassambara MA. Package "ggpubr." 2020.
35. Gu Z, Eils R, Schlesner M. Complex heatmaps reveal patterns and correlations in multidimensional genomic data. Bioinformatics 2016; 32:2847–9.
36. Dixon P. VEGAN, a package of R functions for community ecology. J Veg Sci 2003;14:927–30.
37. Scher JU, Ubeda C, Artacho A, et al. Decreased bacterial diversity characterizes the altered gut microbiota in patients with psoriatic arthritis, resembling dysbiosis in inflammatory bowel disease. Arthritis Rheumatol 2015;67:128–39.
38. Morgan XC, Tickle TL, Sokol H, et al. Dysfunction of the intestinal microbiome in inflammatory bowel disease and treatment. Genome Biol 2012;13:R79–18.
39. Henke MT, Kenny DJ, Cassilly CD, et al. Ruminococcus gnavus, a member of the human gut microbiome associated with Crohn's disease, produces an inflammatory polysaccharide. Proc Natl Acad Sci U S A 2019;116:12672–7.
40. Azzouz D, Omarbekova A, Heguy A, et al. Lupus nephritis is linked to disease-activity associated expansions and immunity to a gut commensal. Ann Rheum Dis 2019;78:947–56.
41. Hall AB, Yassour M, Sauk J, et al. A novel Ruminococcus gnavus clade enriched in inflammatory bowel disease patients. Genome Med 2017;9:103–12.
42. Crost EH, Tailford LE, Monestier M, et al. The mucin-degradation strategy of Ruminococcus gnavus: the importance of intramolecular trans-sialidases. Gut Microbes 2016;7:302–12.
43. Forbes JD, Chen CY, Knox NC, et al. A comparative study of the gut microbiota in immune-mediated inflammatory diseases-does a common dysbiosis exist? Microbiome 2018;6:221–15.
44. Plichta DR, Somani J, Pichaud M, et al. Congruent microbiome signatures in fibrosis-prone autoimmune diseases: IgG4-related disease and systemic sclerosis. Genome Med 2021;13:35–14.
45. Haas KN, Blanchard JL. Reclassification of the Clostridium clostridioforme and Clostridium sphenoides clades as Enterocloster gen. nov. and Lacrimispora gen. nov., including reclassification of 15 taxa. Int J Syst Evol Microbiol 2020;70:23–34.
46. Rigottier-Gois L. Dysbiosis in inflammatory bowel diseases: the oxygen hypothesis. ISME J 2013;7:1256–61.
47. Breban M, Beaufrère M, Glatigny S. Intestinal dysbiosis in spondyloarthritis: chicken or egg? Curr Opin Rheumatol 2021;33:341–7.
48. Asquith M, Sternes PR, Costello ME, et al. HLA alleles associated with risk of ankylosing spondylitis and rheumatoid arthritis influence the gut microbiome. Arthritis Rheumatol 2019;71:1642–50.
49. Sokol H, Pigneur B, Watterlot L, et al. Faecalibacterium prausnitzii is an anti-inflammatory commensal bacterium identified by gut microbiota analysis of Crohn disease patients. Proc Natl Acad Sci U S A 2008;105:16731–6.
50. Van der Linden S, Valkenburg HA, Cats A. Evaluation of diagnostic criteria for ankylosing spondylitis: a proposal for modification of the New York criteria. Arthritis Rheum 1984;27:361–8.

Arthritis & Rheumatology
Vol. 75, No. 1, January 2023, pp 53–63
DOI 10.1002/art.42288

American College of Rheumatology
Empowering Rheumatology Professionals

Dysregulation of Bile Acids, Lipids, and Nucleotides in Psoriatic Arthritis Revealed by Unbiased Profiling of Serum Metabolites

Ananta Paine,[1] Paul S. Brookes,[2] Soumyaroop Bhattacharya,[3] Dongmei Li,[4] Maria De La Luz Garcia-Hernandez,[1] Francisco Tausk,[1] and Christopher Ritchlin[1]

Objective. The transition from psoriasis to psoriatic arthritis (PsA) occurs in 20–30% of patients; however, the mechanisms underlying the emergence of musculoskeletal disease are not well understood. Metabolic disease is prevalent in psoriasis patients, but whether metabolic factors, other than obesity, increase arthritis risk in psoriasis patients is not known. This study was undertaken to investigate the link between metabolic changes and disease progression in psoriasis patients.

Methods. To characterize the metabolic alterations during the progression of arthritis in psoriasis patients, we analyzed cross-sectional healthy controls and PsA samples and longitudinal psoriasis serum samples, before and after PsA onset. Nontargeted metabolomic profiling was performed using liquid chromatography mass spectrometry.

Results. We identified several serum metabolites that differed between PsA patients, psoriasis patients, and healthy controls. Differentially abundant bile acids, purines, pyrimidines, glutathione, lipids, and amino acid metabolites were noted in these 3 groups. We also noted differences between psoriasis patients who progressed and those who did not progress to PsA. Bile acid and butyrate levels were depressed in those who progressed to PsA compared to those who did not, and the level of inflammatory lipid mediators increased following PsA diagnosis. In particular, the combination of leukotriene B4 and glycoursodeoxycholic acid sulfate were sensitive and specific predictors of PsA progression.

Conclusion. We observed notable differences in bile acid, purine, lipid, and amino acid–derived metabolites, among the healthy controls, psoriasis patients, and PsA patients and identified changes during the transition from psoriasis to PsA. The decreased bile acid and butyrate levels and elevated guanine levels in psoriasis patients at risk for PsA were particularly striking and may reflect gut microbial dysbiosis and dysregulated hepatic metabolism, leading to altered proliferation of immune cells and enhanced cytokine expression.

INTRODUCTION

Psoriatic arthritis (PsA) is closely associated with psoriasis, and 20–30% of patients with psoriasis develop PsA (1). Arthritis onset in psoriasis patients is often characterized by development of fatigue and arthralgia, while other patients develop rapid onset of joint pain and swelling (2). Several studies indicate that aberrant inflammatory pathways are triggered long before symptom onset, and the wide spectrum of presenting symptoms often results in delayed diagnosis, thereby increasing the likelihood of long-term musculoskeletal damage and permanent disability (3). Therefore, early identification of psoriasis patients at increased risk for PsA holds potential to facilitate prompt therapeutic intervention and improve outcomes. Unfortunately, established serum diagnostic biomarkers of PsA and arthritis risk in psoriasis patients are not available.

Supported by the National Psoriasis Foundation (PsA Biomarker Grant), AbbVie and UCB Pharmaceuticals through support of the International Psoriatic Arthritis Research Team (IPART) Registry, University of Rochester (Department of Medicine Pilot Grant, and Health Sciences Center for Computational Innovation Pilot Grant), and the NIH (grants R01-HL-071158 and R01-AR-069000).

[1]Ananta Paine, PhD, Maria De La Luz Garcia-Hernandez, PhD, Francisco Tausk, MD, Christopher Ritchlin, MD, MPH: Division of Allergy, Immunology and Rheumatology, Center for Musculoskeletal Research, School of Medicine and Dentistry, University of Rochester, Rochester, New York; [2]Paul S. Brookes, PhD: Department of Anesthesiology, University of Rochester Medical Center, Rochester, New York; [3]Soumyaroop Bhattacharya, MS, MEd: Division of Neonatology, Department of Pediatrics, University of Rochester, Rochester, New York; [4]Dongmei Li, PhD: Department of Clinical and Translational Research, University of Rochester Medical Center, Rochester, New York.

Author disclosures are available at https://onlinelibrary.wiley.com/action/downloadSupplement?doi=10.1002%2Fart.42288&file=art42288-sup-0001-Disclosureform.pdf.

Address correspondence via email to Ananta Paine, PhD, at anantapaine.urmc@gmail.com.

Submitted for publication February 16, 2022; accepted in revised form June 30, 2022.

One of the most striking relationships in psoriatic disorders is the strong association between obesity and the development of PsA (4). Furthermore, key metabolic diseases are often present in established PsA patients including type 2 diabetes mellitus (5), metabolic syndrome (6), and fatty liver (7). Moreover, PsA patients are at an increased risk of developing cardiovascular disease compared to controls (8). These epidemiologic associations raise the possibility of an interaction between metabolic and inflammatory pathways that favor the transition to PsA and propel synovial inflammation, enthesitis, and joint damage. This potential metabolic inflammation link (9) may provide opportunities to identify diagnostic and PsA transition biomarkers.

Several studies have examined serum and plasma metabolites in psoriasis patients, PsA patients, and healthy controls (10–14). Comparison of psoriasis and PsA serum or plasma metabolites have revealed differences between psoriasis and PsA patients (10–15). The majority of these prior studies were cross-sectional, and a significant proportion of patients were treated with systemic therapies (including biologics) before metabolomic profiling. Importantly, systemic treatments such as anti–tumor necrosis factor (anti-TNF) agents significantly alter patient metabolic profiles (16) and may obscure interpretation of metabolomic shifts that take place before or after disease onset. To investigate the link between metabolic changes and disease progression in psoriasis patients, we monitored a longitudinal cohort of psoriasis patients who were naive to biologic treatment, collected serial serum samples, and evaluated molecular differences in psoriasis patients who progressed (PsP) and those who did not progress (PsNP) to PsA and who were not receiving systemic therapies. To reveal metabolomic changes, we performed nontargeted metabolomic profiling of the collected serum samples using liquid chromatography mass spectrometry (LC-MS).

PATIENTS AND METHODS

Study design and patient cohort. This study was performed at the University of Rochester Medical Center and conducted in compliance with principles of the Declaration of Helsinki. The study protocol was approved by the Institutional Review Board of the University of Rochester. Serum samples were collected from psoriasis and PsA patients, along with healthy controls, who were recruited from the dermatology and rheumatology clinics of the University of Rochester Medical Center and provided consent. Patients were enrolled in the International Psoriatic Arthritis Research Team (IPART) Registry, a longitudinal cohort of psoriasis and PsA patients. The diagnosis of psoriasis was confirmed by a dermatologist (FT), and the diagnosis of PsA by a rheumatologist (CR) was based on the Classification Criteria for Psoriatic Arthritis (CASPAR) Study Group criteria (17). Psoriasis and PsA patients receiving systemic agents, including disease-modifying antirheumatic drugs or biologic agents, were excluded. PsA patients were enrolled in the IPART Registry before starting systemic therapies and served as cross-sectional controls. Psoriasis patients who were not receiving systemic therapy were also enrolled in the registry and were followed longitudinally for development of PsA based on the CASPAR criteria.

Patients in the IPART Registry were contacted by a coordinator every 6 months and completed a questionnaire. If they developed new musculoskeletal pain, they were evaluated by a rheumatologist for development of PsA (CASPAR criteria). They were also instructed to contact coordinators if they developed new joint symptoms. Patients who developed PsA had serum samples collected prior to initiation of systemic therapy which were stored in a freezer at –80° C for subsequent analysis. The average patient follow-up duration was 4.5 years.

Serum metabolomic analysis. Serum samples were collected, centrifuged at 1,700*g* for 10 minutes, and immediately stored at –80° C. To identify critical metabolic differences between psoriasis patients and PsA patients, we performed nontargeted global metabolic profiling of serum samples collected from a subset of PsNP patients (n = 21) and total PsA (PsA-T) patients (n = 34) in our biorepository and compared them to serum metabolites from healthy subjects (n = 16). Frozen serum sample aliquots were shipped on dry ice for metabolomic profiling at a facility of Metabolon, Inc. Thereby, samples were analyzed using reverse-phase and hydrophilic interaction liquid chromatography coupled to Q-Exactive mass spectrometry with the collected serum samples (18).

Statistical analysis. Statistical analysis was used to identify significantly altered metabolites within the cohorts. The raw metabolomic profiling data without further normalization was obtained from Metabolon, Inc. Subsequently, appropriate statistical analysis was performed with the metabolomics data after performing cumulative sum scaling normalization. The abundance of specific metabolites present in the serum samples was compared between groups based on the likelihood ratio test and considered statistically significant at a false discovery rate (FDR)–corrected *P* value of less than 0.05, referred to as differentially abundant metabolites. In-depth analysis was performed to compare 2 groups (e.g., psoriasis patients versus PsA patients) or to compare multiple groups (e.g., healthy controls versus psoriasis patients versus PsA patients), as specified. Data were evaluated for normal distribution on a per-metabolite basis within each sample group using a Jarque Bera test for skewness and kurtosis. Of 846 metabolites, the number normally distributed within each sample group was as follows: 514 for healthy controls, 440 for PsNP patients, 458 for PsA patients, 572 for PsP patients before the development of PsA (PsP-B), and 608 for PsP patients after the development of PsA (PsP-A). Overall, 61.3% of the data were normally distributed. Thus, nonparametric testing (Mann-Whitney U test) was performed to determine significance in comparisons

between groups. Cluster analysis was based on Ward's method to create heatmaps (19).

Multivariate analysis was performed using a combination of principal component analysis and orthogonal partial least-squares discriminant analysis (PLS-DA) (20) using MetaboAnalyst (19). Sparse PLS-DA was conducted following logarithmic transformation (base 10) and pareto scaling and considering all 846 variables per component. Odds ratios (ORs) and 95% confidence intervals (95% CIs) were calculated.

RESULTS

We recruited 71 subjects for this pilot study. Thirty-four psoriasis patients were recruited and followed longitudinally for the development of arthritis. Twenty-one psoriasis patients were nonprogressors and did not transition to PsA (PsNP), while 13 patients developed PsA (PsP) during a 4-year time period. We examined and collected sera from those who progressed before (PsP-B) and after the development of PsA (PsP-A). We enrolled 21 PsA patients and 16 healthy subjects as cross-sectional controls. The PsA-T group comprised the cross-sectional PsA group and the PsP-A group. PsP-A patients met the CASPAR criteria for PsA, and the metabolomic profiles of patients in the PsA and PsP-A groups demonstrated overlapping characteristics, so they were analyzed together (Supplementary Figure 1, available on the *Arthritis & Rheumatology* website at https://onlinelibrary.wiley.com/doi/10.1002/art.42288). Analysis of the serum samples using LC-MS enabled the quantification of 846 metabolites with adequate coverage. A schematic of the patient cohorts is depicted in Figure 1A, and Figure 1B demonstrates patient demographics and phenotypic features. The patients had a wide range of baseline Psoriasis Area and Severity Index scores (mean 9.8 [range 0.6–40.6]), and the 21 PsA patients had polyarthritis at baseline. A wide range of disease duration of PsA was observed in the cross-sectional PsA group and varied from <1 year to 26 years, with a median of 3 years.

The characteristics of the cross-sectional PsA patient group and the longitudinally followed psoriasis patient groups were consistent between the groups. Group-level comparisons were performed to identify differentially abundant metabolites between PsA and psoriasis patients and between PsP and PsNP patients (Supplementary Table 1, https://onlinelibrary.wiley.com/doi/10.1002/art.42288), over a period of 4 years. Statistical analysis using sparse PLS-DA (20) identified metabolites associated with diverse metabolic pathways that differed between PsNP

A

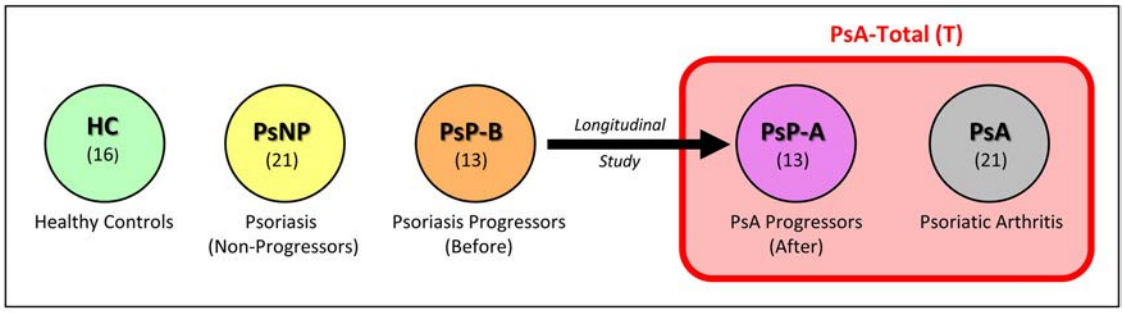

B

Subject cohorts	**HC** (n=16)	**PsNP** (n=21) (longitudinally followed)	**PsP** (n=13) (longitudinally followed)	**PsA** (n = 21) (Cross sectional)
Age (median, range in years)	46 (32 – 57)	56 (27 - 85)	56 (36 - 76)	42 (19 - 67)
Female (%)	55%	42%	36%	35%
BMI (median, range)	26.9 (18.0 - 46.8)	27.4 (20.4 – 42.8)	29.7 (25.6 -56.1)	29.6 (22.7 – 53.9)
Median duration of Ps (range in years)	-	20 (3 – 54)	25 (4 - 56)	13 (2 – 42)
Smoker (%)	Smoker =10%, Nonsmoker = 80% Former = 10%	Smoker = 21%, Nonsmoker = 21% Former = 58%	Smoker = 21%, Nonsmoker = 50% Former = 29%	Smoker = 33%, Nonsmoker = 45% Former = 22%
Diabetes (%)	0%	9.5%	7.7%	14.3%

Figure 1. Characteristics of the study cohorts. **A**, Schematic view of the subject cohorts. **B**, Clinical and demographic data on the study participants. BMI = body mass index; Ps = psoriasis.

and PsA-T groups or between PsP and PsNP groups. We also focused on identifying the major metabolic changes observed during disease progression to PsA.

Metabolic differences between controls, psoriasis patients, and PsA patients. Serum metabolites were compared in 34 PsA-T patients, 21 psoriasis patients, and 16 healthy controls. We identified distinct differences between the 3 groups (Figure 2A). The statistical analysis and subsequent visualization of the metabolomics data in the volcano plot revealed significant differences in metabolite levels between PsNP and PsA-T patients (Figure 2B). Most notably, the abundance of metabolites related to lipid and bile acid metabolism was altered in the sera of PsA-T patients compared to PsNP patients. Specifically, a higher level of 12-hydroxyheptadecatrenoic acid (12-HHTrE) in PsA-T patients (>2-fold) was observed compared to PsNP patients and healthy controls ($P < 0.0001$). In addition, decreased levels of bile acids were observed in sera from PsA-T patients compared to PsNP patients. Among these, levels of 3 secondary bile acids, glycoursodeoxycholic acid sulfate, glycodeoxycholate 3-sulfate, and deoxycholic acid 12-sulfate, significantly differed between these 2 groups (all >50% lower in PsA-T compared to

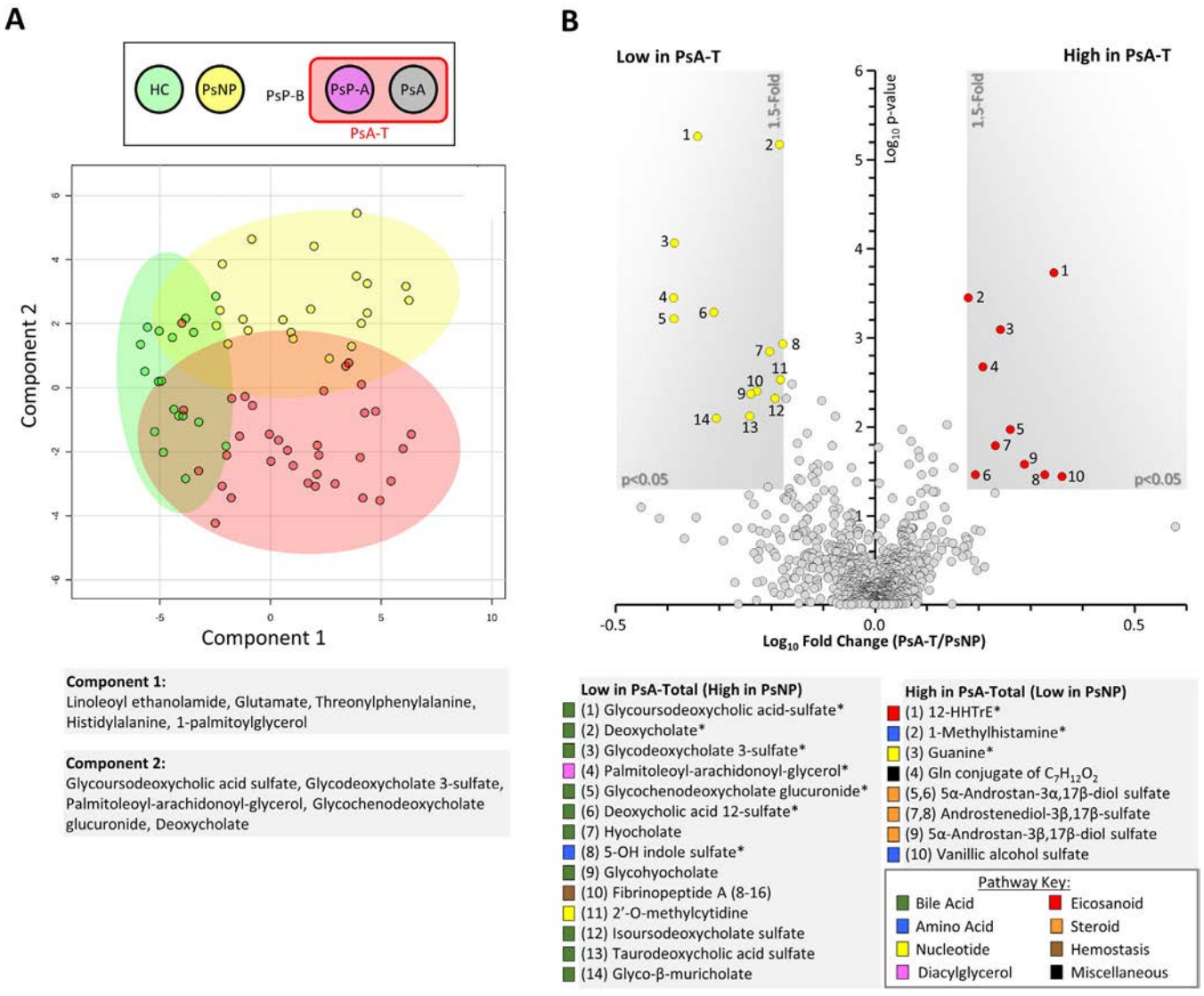

Figure 2. Metabolomic differences between healthy controls (HC), psoriasis (Ps) patients, and psoriatic arthritis (PsA) patients. **A**, Sparse partial least-squares discriminant analysis (PLS-DA) between healthy controls, psoriasis patients who did not progress to PsA (PsNP), and total PsA patients (PsA-T). Sparse PLS-DA plot from MetaboAnalyst 5 software is shown, with shaded areas representing 95% confidence intervals for each group. The top 5 loadings for each principal component are shown. **B**, Volcano plot comparison between PsA-T and PsNP groups. Metabolites achieving both statistical significance ($P < 0.05$) and >1.5-fold difference between groups are shown inside the shaded gray areas and identified with numbers. Relevant pathways for individual metabolites are color-coded. Data show the mean from 21 PsNP patients and 34 PsA-T patients. * = $P < 0.05$ after false discovery rate correction (Storey q value <0.05). PsP-B = psoriasis progressors before PsA development; PsP-A = psoriasis progressors after PsA development; 12-HHTrE = 12-hydroxyheptadecatrenoic acid. Color figure can be viewed in the online issue, which is available at http://onlinelibrary.wiley.com/doi/10.1002/art.42288/abstract.

PsNP; $P < 0.001$) (Figure 2B). Analysis also revealed higher levels (30–70% increase) of metabolites related to nucleic acid (purine) metabolism, including guanine, in PsA-T compared to PsNP samples ($P < 0.01$).

Metabolic differences between PsNP and PsP. To identify metabolic differences between PsP and PsNP, we analyzed serum samples from 13 PsP-B patients and 21 PsNP patients. Sparse PLS-DA revealed significant changes along the component 2 axis for PsP relative to PsNP (Figure 3), whereas within the PsP group, differences were primarily observed along the component 1 axis. We noted a shift in metabolite profiles in the transition to PsA. Further analysis revealed that 6 key metabolites related to bile acid metabolism were significantly lower in PsP-B compared to PsNP patients ($P < 0.01$) (Figure 4A). Among these metabolites, the secondary bile acid deoxycholate, glycoursodeoxycholic acid sulfate, and deoxycholic acid 12-sulfate, were most differentially abundant (>50% lower in PsP-B; $P < 0.001$). The heat map in Figure 4B shows differences in metabolite levels, which are consistent within the individual patient cohorts.

Multiple logistic regression analysis revealed that both leukotriene B4 and glycoursodeoxycholic acid sulfate on a logarithmic scale were significant predictors for progression to PsA. Higher levels of leukotriene B4 and glycoursodeoxycholic acid sulfate significantly decreased the odds of progressing to PsA. For every 1-unit increase in leukotriene B4 levels on a logarithmic scale, the odds of progressing to PsA decreased 47% (adjusted OR 0.53 [95% CI 0.30–0.96]). Similarly, for every 1-unit increase in glycoursodeoxycholic acid sulfate on a logarithmic scale, the odds of progressing to PsA decreased 95% (adjusted OR 0.05 [95% CI 0.01–0.49]). The receiver operating characteristic curve (Figure 4C) demonstrated both high sensitivity and high specificity for the 2 biomarkers in predicting progression to PsA, with an area under the curve (AUC) of 0.9462 (Figure 4C).

The level of bile acids differed significantly between PsNP and PsP-B patients (Figure 5A). In addition, levels of bile acids were lower in PsA-T compared to PsNP patients. The synthesis of primary bile acids takes place in the liver, and secondary bile acid production results from metabolism of primary bile acid metabolites by the gut microbiota as shown in Figure 5B.

Metabolic shifts in patients who progressed to PsA. To identify the major metabolic changes during the transition from psoriasis to PsA, we compared longitudinal serum samples collected before and after the onset of arthritis in 13 PsP patients. Levels of multiple purines and lipid and amino acid metabolites changed during the transition to PsA (Figures 6A and B). Levels of cysteinyl-glycine, guanine, and linoleoyl-linoleoyl glycerol significantly decreased (>50%; $P < 0.001$) after the onset of PsA (Figures 6A and B). Linoleoyl glycerol is an endocannabinoid that is transformed by neutrophils and eosinophils to novel lipoxygenase metabolites (21), and cysteinyl-glycine is a dipeptide intermediate in glutathione metabolism (22). In contrast, multiple inflammatory

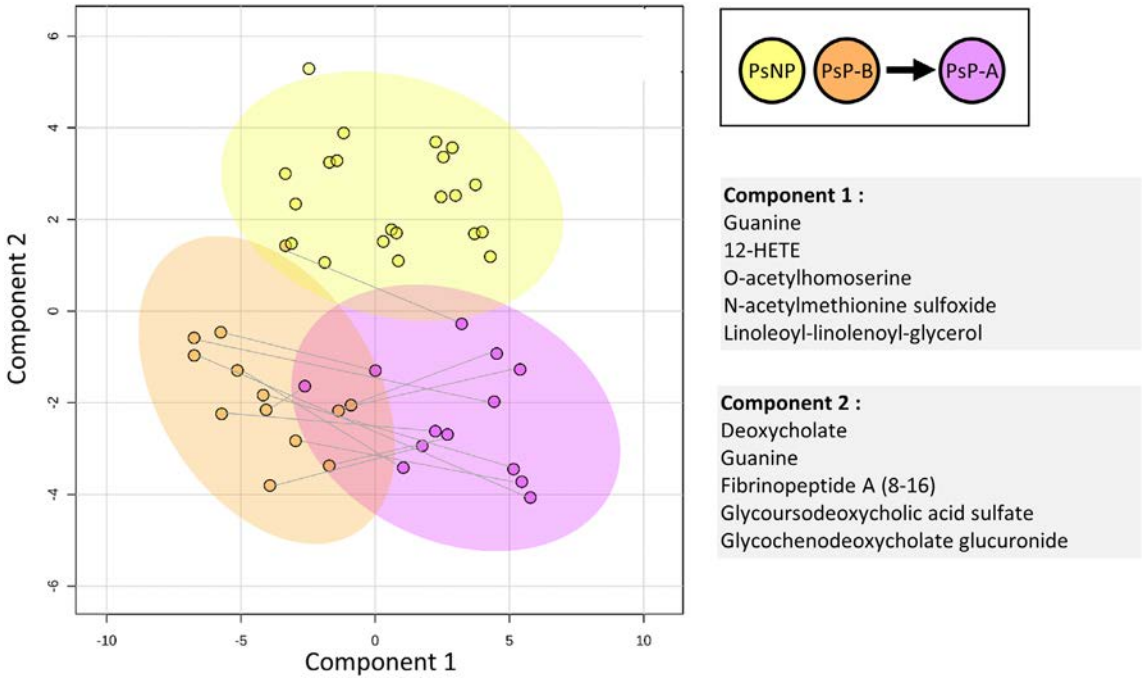

Figure 3. Metabolomic differences between PsA nonprogressors and progressors. Sparse PLS-DA between PsNP, PsP-B, and PsP-A patients. Sparse PLS-DA plot from MetaboAnalyst 5 software is shown, with shaded areas representing 95% confidence intervals for each group. The top 5 loadings for each principal component are shown. 12-HETE = 12-hydroxyeicosatetraenoic acid (see Figure 2 for other definitions). Color figure can be viewed in the online issue, which is available at http://onlinelibrary.wiley.com/doi/10.1002/art.42288/abstract.

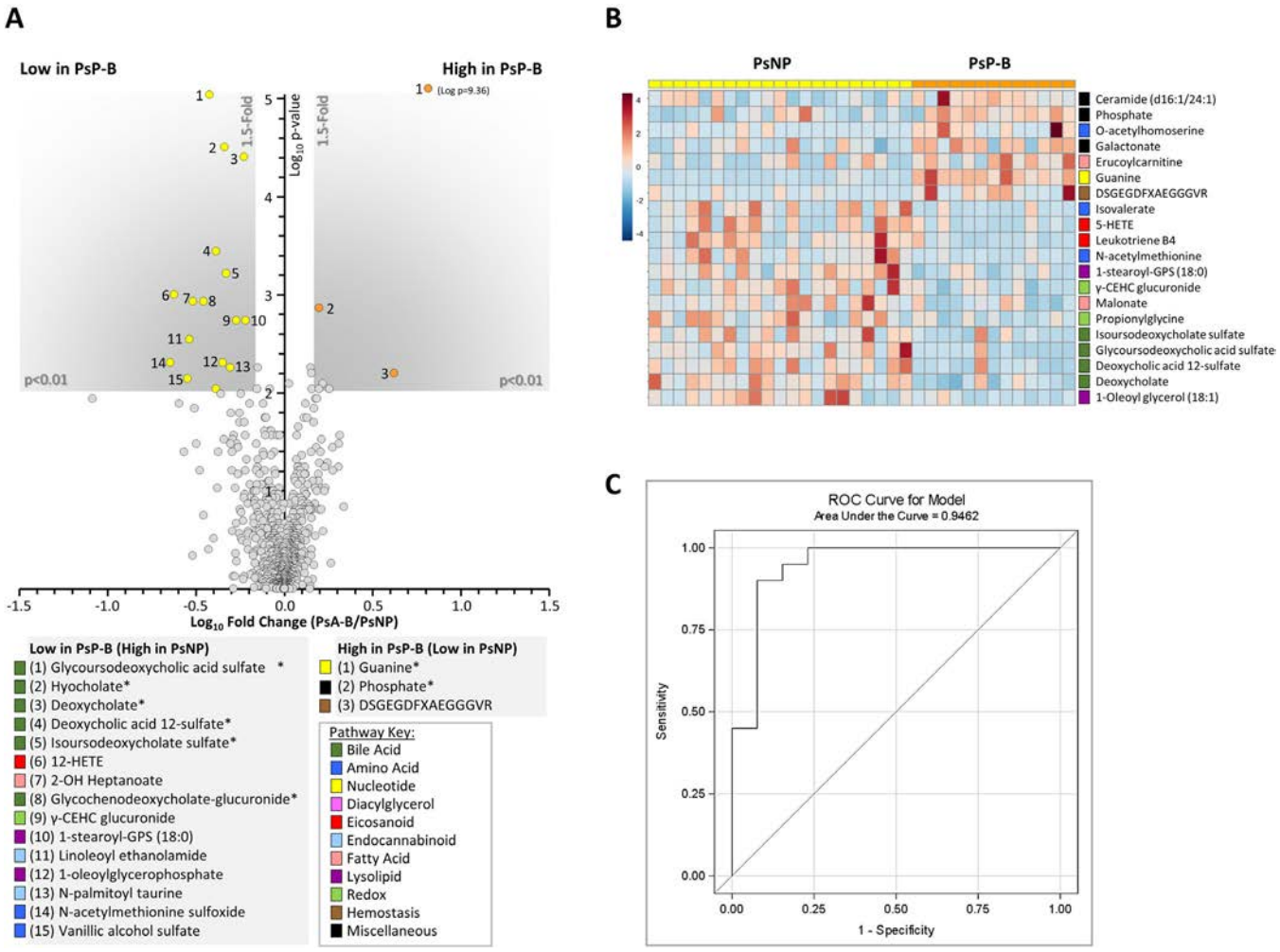

Figure 4. Metabolomic differences between PsNP and PsP. **A**, Volcano plot comparing metabolites between PsNP and PsP-B groups. Metabolites achieving both statistical significance ($P < 0.01$) and >1.5-fold difference between groups are shown inside the shaded gray areas and identified with numbers. The relevant pathways for individual metabolites are color-coded. * = $P < 0.05$ after false discovery rate correction (Storey q value <0.05). **B**, Cluster heatmap (MetaboAnalyst 5, Euclidean/Ward algorithm) showing the top 20 altered metabolites by *t*-test. Relevant pathways for individual metabolites are color-coded. **C**, Receiver operating characteristic (ROC) curve for the multiple logistic regression model. 12-HETE = 12-hydroxyeicosatetraenoic acid (see Figure 2 for other definitions). Color figure can be viewed in the online issue, which is available at http://onlinelibrary.wiley.com/doi/10.1002/art.42288/abstract.

lipid metabolites (4-hydroxydocosahexaenoic acid [4-HDoHE], 12-hydroxyeicosatetraenoic acid [12-HETE], 12-HHTrE) were elevated (>2-fold; $P < 0.01$) in the PsP-A patients. In addition, significant increases in several metabolites related to glutathione metabolism were noted after PsA progression, including 5-oxoproline, which exhibited a >2-fold increase ($P < 0.001$). Notably, although guanine was elevated prior to PsA progression, the level decreased following PsA onset (Figure 6C). In contrast, guanine levels were comparable between the PsNP patients and healthy controls (Supplementary Figure 2A, https://onlinelibrary.wiley.com/doi/10.1002/art.42288).

The low level of bile acids in the PsP-B patients remained low following development of PsA. The level of butyrate, a key short-chain fatty acid (SCFA) produced during gut flora-mediated fermentation of dietary fibers, was significantly lower in PsP-B patients compared to PsNP patients but increased following the development of PsA ($P < 0.05$) (Figure 6D). Levels of butyrate were higher in PsNP patients compared to the healthy controls and significantly higher compared to the PsP-B group (Supplementary Figure 2B). These data suggest that elevated butyrate in the PsNP group lessen the probability of developing arthritis, but further studies are required to support this impression. These findings highlight significant metabolic shifts in the transition to PsA characterized by depressed levels of dipeptides, guanine, bile acids, and butyrate, as well as increased levels of inflammatory lipid metabolites and glutathione metabolites following arthritis onset.

DISCUSSION

The circulating metabolome provides a continuous record of the production and consumption of metabolites and reflects the

A

BIOCHEMICAL	SUB PATHWAY	PsP-B/PsNP		PsA-T/PsNP	
		Fold	p-val	Fold	p-val
Glyco-beta-muricholate	Primary Bile Acid Metabolism	0.41	0.009	0.49	0.008
Glycochenodeoxycholate glucuronide		0.35	0.001*	0.41	> 0.001*
Deoxycholic acid 12-sulfate	Secondary Bile Acid Metabolism	0.41	0.002*	0.49	> 0.001*
Glycodeoxycholate 3-sulfate		0.56	> 0.001	0.41	> 0.001*
Deoxycholate		0.59	> 0.001*	0.66	0.008*
Hyocholate		0.46	0.006*	0.63	> 0.002
Glycoursodeoxycholic acid sulfate		0.38	> 0.001*	0.46	> 0.001*
Isoursodeoxycholate sulfate		0.47	0.009*	0.64	0.005

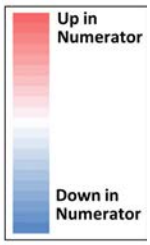

B

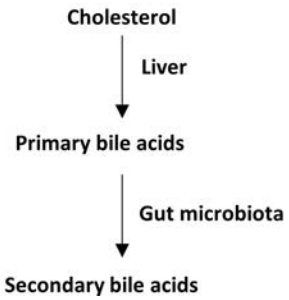

Figure 5. Bile acid levels differ significantly between PsNP and PsP patients. **A**, Differential abundance of primary and secondary bile acids in samples collected from psoriasis and PsA patients. Serum samples were analyzed with an unbiased approach and detected primary and secondary bile acid levels were compared between progressors (PsP; n = 13) and nonprogressors (PsNP; n = 21). Samples collected before or after the onset of arthritis from 13 PsP patients were compared with 21 PsNP patients. Differentially abundant primary and secondary bile acids achieving statistical significance ($P < 0.05$) are shown. * = $P < 0.05$ after false discovery rate correction (Storey q value <0.05). **B**, Schematic diagram depicting synthesis of primary and secondary bile acids from cholesterol in the liver and microbial metabolism in the gut. See Figure 2 for definitions. Color figure can be viewed in the online issue, which is available at http://onlinelibrary.wiley.com/doi/10.1002/art.42288/abstract.

combined input from environmental exposures and the gut microbiota (23,24). Moreover, metabolite analysis reveals pathways and mechanisms downstream of proteomics and genomics (24). We identified key metabolites that differ in abundance between psoriasis patients, PsA patients, and controls. We observed a metabolomic shift in bile acids and butyrate in psoriasis patients who progressed to PsA compared to those who did not progress. These findings provide insights into novel pathways linked to microbial dysbiosis and dysregulated hepatic metabolism, with potential to alter the immune response and promote joint inflammation.

Serum primary and secondary bile metabolites were significantly lower in PsP patients compared to PsNP patients and remained depressed following the onset of arthritis. Primary bile acids (cholic and deoxycholic acid) are synthesized in the liver from cholesterol, conjugated to glycine or taurine, and secreted in the duodenum (25). The majority of bile acids (95%) are reabsorbed in the ileum and undergo enterohepatic circulation and re-enter the liver via the portal vein (26,27). The remaining 5% of bile acids reach the colon and are deconjugated and metabolized to secondary bile acids by the resident microbiota. Bile acids are required for the emulsification of lipids, glucose metabolism, host defense, and immune homeostasis (28).

Bile acids regulate immunologic responses by multiple mechanisms. Both primary and secondary bile acids activate nuclear and plasma membrane receptors including farnesoid X receptor (FXR) and G protein–coupled bile acid receptor-1 (TGR5) expressed on macrophages, dendritic cells, and natural killer T cells (29). Engagement of these receptors by bile acids promote an antiinflammatory response through the suppression of tumor necrosis factor (TNF), interleukin-6 (IL-6), and IL-8 and by inhibition of the NF-κB transcription factor (30). Secondary bile acids suppress Th17 cell differentiation by direct suppression of RAR-related orphan receptor γt (RORγt) and enhance the differentiation of CD4+ lymphocytes to FoxP3+ Treg cells (31,32). Bile acids also modulate the gut microbiome structure by controlling bacterial overgrowth and protecting the epithelial barrier via FXR signaling (33). Thus, bile acids maintain immune homeostasis through regulation of the microbial environment, inhibition of innate immune signaling, and suppression of Th17 differentiation.

Decreased serum bile acid levels are associated with several immune-mediated inflammatory diseases, including multiple sclerosis (23), inflammatory bowel disease (34), and psoriasis (35). We did not observe a significant difference in bile acid levels between psoriasis patients and healthy controls; however, primary and secondary bile acids were reported to be lower in

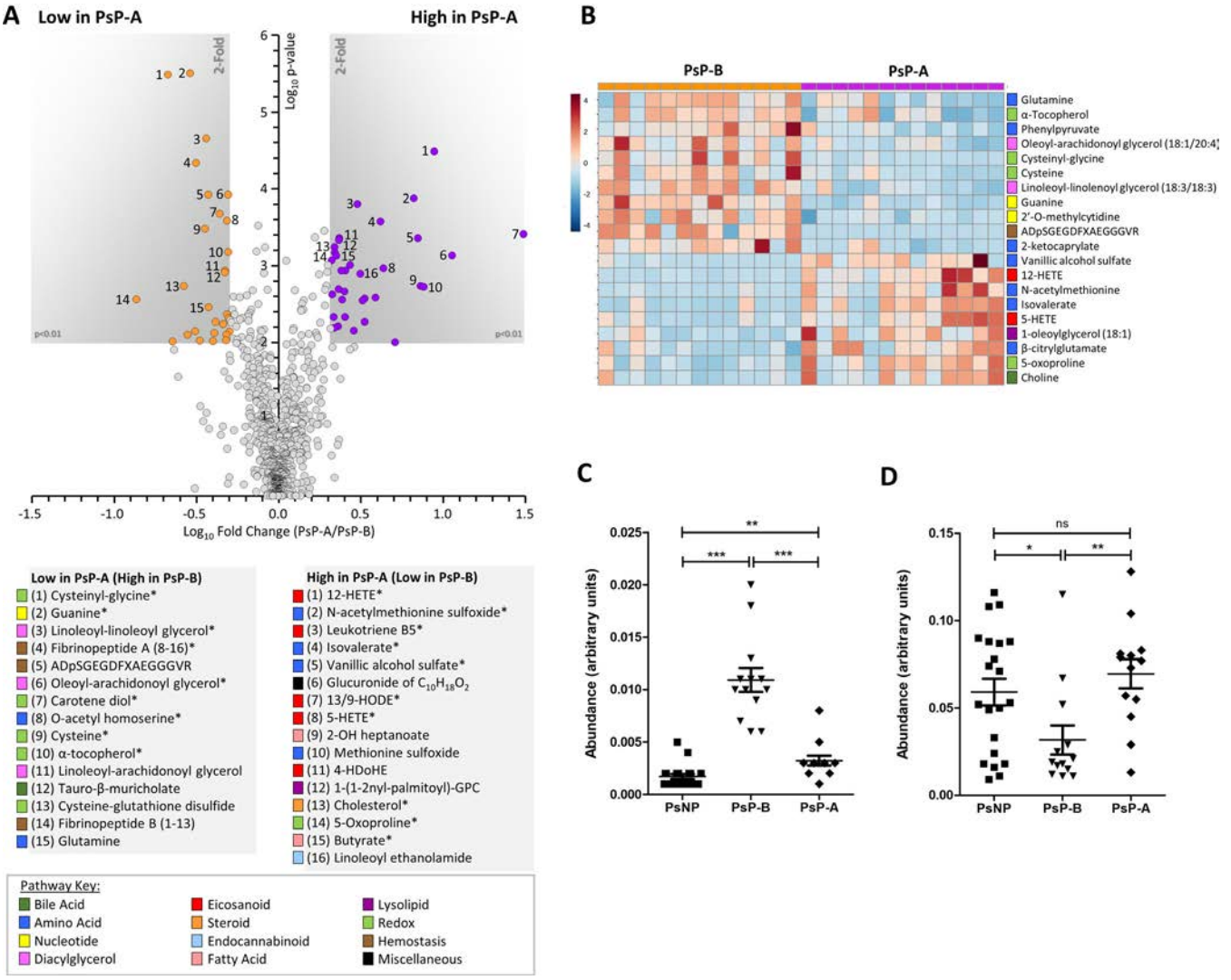

Figure 6. Metabolomic differences during longitudinal progression from Ps to PsA. **A**, Volcano plot comparing metabolites between PsP-B and PsP-A patients. Metabolites achieving both statistical significance ($P < 0.01$) and >1.5-fold difference between groups are shown inside the shaded gray areas and identified with numbers. The relevant pathways for individual metabolites are color-coded. Data show the mean from 13 subjects. * = $P < 0.01$ after false discovery rate correction (Storey q value <0.05). **B**, Cluster heatmap (MetaboAnalyst 5, Euclidean/Ward algorithm) showing top 20 altered metabolites by *t*-test. Relevant pathways for individual metabolites are color-coded. **C** and **D**, Levels of serum guanine (**C**) and butyrate (**D**) were compared between samples from 13 PsP patients and 21 PsNP patients, and normalized data are presented as a dot plot. Bars show the mean ± SEM. * = $P < 0.01$; ** = $P < 0.001$; *** = $P < 0.0001$. 12-HETE = 12-hydroxyeicosatetraenoic acid; 4-HDOHE = 4-hydroxydocosahexaenoic acid (see Figure 2 for other definitions). Color figure can be viewed in the online issue, which is available at http://onlinelibrary.wiley.com/doi/10.1002/art.42288/abstract.

psoriasis patients, although levels in those who went on to develop PsA were not examined (35,36). Based on the observation that rheumatoid arthritis (RA) improved in patients with jaundice (37), RA patients were treated with a short course of intravenous bile acids and experienced significant short-term improvement in arthritis, but treatment was complicated by development of phlebitis (38). In a subsequent study, expression of the TGR5 bile acid receptor was significantly lower in RA peripheral blood mononuclear cells compared to healthy controls, and levels correlated inversely with the Disease Activity Score in 28 joints outcome measure (30). In preclinical models, therapy with a secondary bile acid, lithocholic acid, significantly lessened joint inflammation in the collagen-induced arthritis (CIA) model (30), and bile acid treatment suppressed development of psoriasis lesions in the IL-23 minicircle model via inhibition of RORγt and CCL20 expression (39). Thus, accumulating evidence supports a role for disrupted bile acid metabolism in the development of systemic inflammation observed in RA, psoriasis, and a number of other immune-mediated disorders.

The low serum butyrate levels noted in the PsP-B cohort provide an additional link to dysbiosis in arthritis pathogenesis. Butyrate is an SCFA and the product of gut microbial metabolism

that maintains an intact intestinal barrier, inhibits NF-κB–mediated cytokine release and decreases bacterial translocation (40). Moreover, butyrate treatment of mice prior to the onset of CIA improved intestinal barrier function and significantly decreased the severity of inflammatory arthritis (41). Elevated serum levels of butyrate were associated with nonprogression to arthritis in individuals at increased risk (anti–citrullinated protein antibody–positive with musculoskeletal pain) to develop RA (42). Therefore, similar to findings in RA, lower levels of serum butyrate noted in the PsP patients may contribute to increased arthritis risk in this population. Interestingly, butyrate levels were lower in the PsP-B patients but increased after the onset of PsA. The mechanisms underlying this increase are unknown but may represent a homeostatic response to the onset of systemic inflammation following arthritis onset.

Depressed levels of bile acids, particularly primary bile acids may be due to impaired endogenous production of cholesterol, the key precursor. Nonalcoholic fatty liver disease is prevalent in PsA (43), yet levels of primary and secondary bile acids are elevated in this disorder (44). Moreover, none of the 13 patients who developed PsA had a history of fatty liver, metabolic syndrome, or elevated liver function tests prior to arthritis onset. Interactions between cholesterol pathways and immune function are well established, and inflammation, via Toll-like receptor activation, can inhibit cholesterol synthesis (45,46). Thus, cholesterol biosynthetic pathways can modulate immune function and inflammation can interfere with cholesterol synthesis. Collectively, the lower levels of butyrate and multiple secondary bile acid metabolites in PsP compared to PsNP support the contribution of gut microbiota and related metabolites to arthritis onset. Further studies are required, however, to determine whether the reduced levels of bile acids are also related to altered hepatic synthesis and whether the dysregulation of bile acid and butyrate have a correlative or causative role in the transition to PsA.

Elevated levels of inflammatory and antiinflammatory lipid metabolites were observed in PsP-A patients, including the docosanoid 4-HDoHE and multiple eicosanoids including 5-HETE, 12-HETE, and 12-HHTrE. It is important to note that Coras et al performed in-depth lipid profiling and reported elevated levels of many pro- and antiinflammatory eicosanoids in PsA, and elevated levels of some eicosanoids correlated with disease severity (10,15). Although our metabolomics platform was not directed toward in-depth profiling of lipids, our findings from untargeted analysis nevertheless are consistent with their results (10,15). The increase of proinflammatory lipid metabolites such as leukotriene B4 and leukotriene B5 are indicative of systematic inflammation in PsA patients, while elevated levels of antiinflammatory eicosanoids such as 5-HETE and 12-HETE likely result from inflammation-triggered responses to minimize tissue damage.

We observed differences in metabolites related to nucleotide metabolism between psoriasis and PsA patients. The elevated guanine level in Ps patients at risk for PsA was particularly striking and may reflect altered immune cell proliferation (47) and enhanced cytokine release (48). During the transition from psoriasis to PsA, we observed a changing pattern of purine and pyrimidine metabolites over time. In particular, guanine levels significantly decreased after the onset of arthritis. This paradoxical observation (increased guanine levels before PsA onset but decreased levels after PsA onset) requires further investigation. Published reports of serum or plasma metabolites in psoriasis and PsA showed that despite the apparent overlap in the disease pathology, several metabolic features differ between psoriasis patients and PsA patients (11,13,15). In particular, distinct differences in the abundance of key metabolites related to lipid and amino acid metabolism between psoriasis patients and PsA patients were identified (11,13,15). However, in these studies, a significant number of PsA patients received systemic treatment before sample collections. Systemic therapies alter metabolic profiles in psoriasis patients, as demonstrated by a recent study (16).

To our knowledge, our study is the first comprehensive analysis of longitudinal serum metabolites in patients before and after the onset of PsA who were not receiving systemic therapies. Despite the advantages of this approach, only 13 patients developed PsA over the course of the study. We are aware that our observations can potentially be confounded by a number of demographic and biologic factors. We matched our patients according to age and body mass index, but we were unable to adjust for other variables such as lipids, physical activity, and hormonal status, which may impact identified metabolites, due to the small sample size. Therefore, although our findings revealed distinctive metabolic alterations during disease progression to PsA, we do not know if these results are characteristic of a larger PsA population, a disease with considerable heterogeneity. The difficulties of recruiting and closely monitoring a large number of psoriasis patients for the development of PsA over months to years is a significant challenge that will have to be considered in future studies. Furthermore, it is unclear to what degree the changes we observed in the PsP cohort are unique to PsA, compared to other forms of inflammatory arthritis such as RA and axial spondyloarthritis (SpA).

The potential contribution of bile acids and butyrate to RA and other inflammatory disorders reviewed above, coupled with reports of altered inflammatory lipid signaling in both RA (49) and axial SpA (50), may limit the utility of such metabolites to serve as a unique PsA biomarker. Nonetheless, our multivariate logistic regression model that included known risk factors for development of PsA revealed that the inclusion of leukotriene B4 and glycoursodeoxycholic acid sulfate improved the sensitivity and specificity of the diagnosis of PsA transition, with an AUC of 0.94. These findings are very encouraging and point to the possibility of a diagnostic biomarker but require confirmation in a blinded cohort of psoriasis patients, along with patients at risk for RA and axial SpA.

In conclusion, nontargeted metabolomic analysis of a longitudinal psoriasis cohort and a cross-sectional group of PsA patients and healthy controls identified key metabolite differences in bile acid, lipid, and purine metabolism. Most notable were the bile acid and butyrate signatures in psoriasis patients who went on to develop PsA and the increased level of inflammatory lipid mediators in patients following the diagnosis of PsA. The implications of this study are that the transition from psoriasis to PsA may be influenced by liver dysfunction and the metabolites produced by commensal gut microbiota, thereby indicating the presence of a metabolic–inflammatory axis. Enhanced understanding of the differentially abundant serum metabolites may reveal pivotal disease mechanisms that underlie transition to PsA and biomarkers of arthritis risk in psoriasis patients.

ACKNOWLEDGMENTS

We thank Dustina Holt, Angela Kluzniak, Debbie Campbell, Amy Wielgosz, Amanda Howell, Marc Nuzzo, Samantha Moore, and Jennifer Albrecht for their technical assistance in patient selection, sample collection, biobanking of samples in our biorepository, sample retrieving, and blinding of samples for unbiased analysis of metabolites in this study. We also want to thank Drs. John Looney and Ben Korman for their informative suggestions.

AUTHOR CONTRIBUTIONS

All authors were involved in drafting the article or revising it critically for important intellectual content, and all authors approved the final version to be published. Dr. Paine had full access to all of the data in the study and takes responsibility for the integrity of the data and the accuracy of the data analysis.

Study conception and design. Paine, Ritchlin.

Acquisition of data. Paine, De La Luz Garcia-Hernandez, Tausk, Ritchlin.

Analysis and interpretation of data. Paine, Brookes, Bhattacharya, Li, De La Luz Garcia-Hernandez, Ritchlin.

REFERENCES

1. Ritchlin CT, Colbert RA, Gladman DD. Psoriatic Arthritis. N Engl J Med 2017;376:957–70.
2. Eder L, Polachek A, Rosen CF, et al. The development of psoriatic arthritis in patients with psoriasis is preceded by a period of nonspecific musculoskeletal symptoms: a prospective cohort study. Arthritis Rheumatol 2017;69:622–9.
3. Scher JU, Ogdie A, Merola JF, et al. Preventing psoriatic arthritis: focusing on patients with psoriasis at increased risk of transition [review]. Nat Rev Rheumatol 2019;15:153–66.
4. Kumthekar A, Ogdie A. Obesity and psoriatic arthritis: a narrative review. Rheumatol Ther 2020;7:447–56.
5. Eder L, Chandran V, Cook R, et al. The risk of developing diabetes mellitus in patients with psoriatic arthritis: a cohort study. J Rheumatol 2017;44:286–91.
6. Haroon M, Gallagher P, Heffernan E, et al. High prevalence of metabolic syndrome and of insulin resistance in psoriatic arthritis is associated with the severity of underlying disease. J Rheumatol 2014;41:1357–65.
7. Ortolan A, Lorenzin M, Tadiotto G, et al. Metabolic syndrome, nonalcoholic fatty liver disease and liver stiffness in psoriatic arthritis and psoriasis patients. Clin Rheumatol 2019;38:2843–50.
8. Gialouri CG, Fragoulis GE. Cardiovascular disease in Psoriatic arthritis: facts and unmet needs [editorial]. Rheumatology (Oxford) 2021;61:1305–6.
9. Hotamisligil GS. Inflammation, metaflammation and immunometabolic disorders. Nature 2017;542:177–85.
10. Coras R, Kavanaugh A, Kluzniak A, et al. Differences in oxylipin profile in psoriasis versus psoriatic arthritis. Arthritis Res Ther 2021;23:200.
11. Armstrong AW, Wu J, Johnson MA, et al. Metabolomics in psoriatic disease: pilot study reveals metabolite differences in psoriasis and psoriatic arthritis. F1000Res 2014;3:248.
12. Koussiouris J, Looby N, Anderson M, et al. Metabolomics studies in psoriatic disease: a review. Metabolites 2021;11:365.
13. Looby N, Roszkowska A, Reyes-Garces N, et al. Serum metabolic fingerprinting of psoriasis and psoriatic arthritis patients using solid-phase microextraction-liquid chromatography-high-resolution mass spectrometry. Metabolomics 2021;17:59.
14. Kishikawa T, Arase N, Tsuji S, et al. Large-scale plasma-metabolome analysis identifies potential biomarkers of psoriasis and its clinical subtypes. J Dermatol Sci 2021;102:78–84.
15. Coras R, Kavanaugh A, Boyd T, et al. Pro- and anti-inflammatory eicosanoids in psoriatic arthritis. Metabolomics 2019;15:65.
16. Kamleh MA, Snowden SG, Grapov D, et al. LC-MS metabolomics of psoriasis patients reveals disease severity-dependent increases in circulating amino acids that are ameliorated by anti-TNFα treatment. J Proteome Res 2015;14:557–66.
17. Taylor W, Gladman D, Helliwell P, et al. Classification criteria for psoriatic arthritis: development of new criteria from a large international study. Arthritis Rheum 2006;54:2665–73.
18. Sreekumar A, Poisson LM, Rajendiran TM, et al. Metabolomic profiles delineate potential role for sarcosine in prostate cancer progression. Nature 2009;457:910–4.
19. Chong J, Soufan O, Li C, et al. MetaboAnalyst 4.0: towards more transparent and integrative metabolomics analysis. Nucleic Acids Res 2018;46:W486–94.
20. Lee LC, Liong CY, Jemain AA. Partial least squares-discriminant analysis (PLS-DA) for classification of high-dimensional (HD) data: a review of contemporary practice strategies and knowledge gaps. Analyst 2018;143:3526–39.
21. Archambault AS, Tinto F, Dumais E, et al. Biosynthesis of the novel endogenous 15-lipoxygenase metabolites n-13-hydroxy-octodecadienoyl-ethanolamine and 13-hydroxy-octodecadienoyl-glycerol by human neutrophils and eosinophils. Cells 2021;10:2322.
22. Bachhawat AK, Yadav S. The glutathione cycle: glutathione metabolism beyond the γ-glutamyl cycle. IUBMB Life 2018;70:585–92.
23. Bhargava P, Smith MD, Mische L, et al. Bile acid metabolism is altered in multiple sclerosis and supplementation ameliorates neuroinflammation. J Clin Invest 2020;130:3467–82.
24. Wikoff WR, Anfora AT, Liu J, et al. Metabolomics analysis reveals large effects of gut microflora on mammalian blood metabolites. Proc Natl Acad Sci U S A 2009;106:3698–703.
25. Hang S, Paik D, Yao L, et al. Bile acid metabolites control TH17 and Treg cell differentiation. Nature 2019;576:143–8.
26. Hofmann AF, Hagey LR. Bile acids: chemistry, pathochemistry, biology, pathobiology, and therapeutics. Cell Mol Life Sci 2008;65:2461–83.
27. Fiorucci S, Carino A, Baldoni M, et al. Bile acid signaling in inflammatory bowel diseases. Dig Dis Sci 2021;66:674–93.
28. Perino A, Demagny H, Velazquez-Villegas L,et al. Molecular physiology of bile acid signaling in health, disease, and aging. Physiol Rev 2021;101:683–731.

29. Schaap FG, Trauner M, Jansen PL. Bile acid receptors as targets for drug development [review]. Nat Rev Gastroenterol Hepatol 2014;11: 55–67.
30. Li ZY, Zhou JJ, Luo CL, et al. Activation of TGR5 alleviates inflammation in rheumatoid arthritis peripheral blood mononuclear cells and in mice with collagen Ilinduced arthritis. Mol Med Rep 2019;20: 4540–50.
31. Campbell C, McKenney PT, Konstantinovsky D, et al. Bacterial metabolism of bile acids promotes generation of peripheral regulatory T cells. Nature 2020;581:475–9.
32. Li W, Hang S, Fang Y, et al. A bacterial bile acid metabolite modulates Treg activity through the nuclear hormone receptor NR4A1. Cell Host Microbe 2021;29:1366–77.
33. Long SL, Gahan CGM, Joyce SA. Interactions between gut bacteria and bile in health and disease. Mol Aspects Med 2017;56: 54–65.
34. Lloyd-Price J, Arze C, Ananthakrishnan AN, et al. Multi-omics of the gut microbial ecosystem in inflammatory bowel diseases. Nature 2019;569:655–62.
35. Sorokin AV, Domenichiello AF, Dey AK, et al. Bioactive lipid mediator profiles in human psoriasis skin and blood. J Invest Dermatol 2018; 138:1518–28.
36. Li L, Chuan-Jian L, Ling H, et al. Untargeted serum metabonomics study of psoriasis vulgaris based on ultra-performance liquid chromatography coupled to mass spectrometry. Oncotarget 2017;8: 95931–44.
37. Hench PS. Analgesia accompanying hepatitis and jaundice in cases of arthritis, fibrositis and siatic pain. JAMA 1933;101:1265–6.
38. Bruusgaard A, Andersen RB. Abnormal bile acid metabolism in rheumatoid arthritis. Preliminary communication. Dan Med Bull 1976;23: 95–8.
39. Shi Z, Wu X, Santos Rocha C, et al. Short-term western diet intake promotes IL-23-mediated skin and joint inflammation accompanied by changes to the gut microbiota in mice. J Invest Dermatol 2021; 141:1780–91.
40. Lewis K, Lutgendorff F, Phan V, et al. Enhanced translocation of bacteria across metabolically stressed epithelia is reduced by butyrate. Inflamm Bowel Dis 2010;16:1138–48.
41. Tajik N, Frech M, Schulz O, et al. Targeting zonulin and intestinal epithelial barrier function to prevent onset of arthritis. Nat Commun 2020;11:1995.
42. Martinsson K, Durholz K, Schett G, et al. Higher serum levels of short-chain fatty acids are associated with non-progression to arthritis in individuals at increased risk of RA. Ann Rheum Dis 2022;81:445–7.
43. Pakchotanon R, Ye JY, Cook RJ, et al. Liver abnormalities in patients with psoriatic arthritis. J Rheumatol 2020;47:847–53.
44. Gottlieb A, Canbay A. Why bile acids are so important in non-alcoholic fatty liver disease (NAFLD) progression [review]. Cells 2019;8:1358.
45. McGillicuddy FC, de la Llera Moya M, Hinkle CC, et al. Inflammation impairs reverse cholesterol transport in vivo. Circulation 2009;119: 1135-45.
46. Puleston DJ, Villa M, Pearce EL. Ancillary activity: beyond core metabolism in immune cells. Cell Metab 2017;26:131–41.
47. Rathbone MP, Middlemiss PJ, Gysbers JW, et al. Purine nucleosides and nucleotides stimulate proliferation of a wide range of cell types. In Vitro Cell Dev Biol 1992;28A:529–36.
48. Lee J, Chuang TH, Redecke V, et al. Molecular basis for the immunostimulatory activity of guanine nucleoside analogs: activation of Toll-like receptor 7. Proc Natl Acad Sci U S A 2003;100:6646–51.
49. Sano Y, Toyoshima S, Miki Y, et al. Activation of inflammation and resolution pathways of lipid mediators in synovial fluid from patients with severe rheumatoid arthritis compared with severe osteoarthritis. Asia Pac Allergy 2020;10:e21.
50. Ou J, Xiao M, Huang Y, et al. Serum metabolomics signatures associated with ankylosing spondylitis and TNF inhibitor therapy. Front Immunol 2021;12:630791.

Arthritis & Rheumatology
Vol. 75, No. 1, January 2023, pp 64–70
DOI 10.1002/art.42298

AMERICAN COLLEGE of RHEUMATOLOGY
Empowering Rheumatology Professionals

BRIEF REPORT

Phosphatidylinositol 3-Kinase δ Deficiency Protects From Antimyeloperoxidase Vasculitis

Fernanda Flórez-Barrós, Simon Freeley, El Li Tham, and Michael G. Robson

Objective. Antineutrophil cytoplasmic antibody–associated vasculitis (AAV) is a systemic autoimmune disease in which glomerulonephritis is an important manifestation. Antibodies against myeloperoxidase (MPO) or proteinase 3 are thought to be important in pathogenesis. Phosphoinositide 3-kinase δ (PI3Kδ) mediates a number of effects in lymphocytes, but its role in myeloid cell responses is less clear. Therefore, this study was undertaken to assess this in a preclinical model of glomerulonephritis induced by the transfer of antibodies to MPO.

Methods. D910A mice with inactive PI3Kδ were compared with wild-type controls. Disease protocols allowed for a comparison of experimental groups in the setting of both mild and more severe disease. Adoptive transfer experiments were performed, with flow cytometric analysis of digested kidneys taken at the end of the experiment.

Results. With mild disease, D910A mice had fewer glomerular macrophages, fewer glomerular neutrophils, and reduced albuminuria compared with wild-type controls. With more severe disease, they also had fewer glomerular crescents and lower serum creatinine levels, indicating protection from acute kidney injury. Adoptive transfer experiments showed a defect in the recruitment of D910A monocytes to the diseased kidney.

Conclusion. Mice with inactive PI3Kδ were protected from anti-MPO vasculitis. This is due to cell intrinsic defect in the recruitment of monocytes to the kidney. These findings suggest that PI3Kδ is a potential therapeutic target in AAV.

INTRODUCTION

Antineutrophil cytoplasmic antibody–associated vasculitis (AAV) is a systemic disease affecting the joints, lungs, kidneys, skin, and other tissues and occurs most often in older adults. It is characterized by autoantibodies against the neutrophil and monocyte expressed antigens myeloperoxidase (MPO) and proteinase 3, which are thought to be pathogenic. The class I phosphoinositide 3-kinase (PI3K) family mediate a wide range of cellular responses to cell surface receptors. The class IA PI3Ks are heterodimers composed of a catalytic subunit (p110α, p110β, or p110δ) combined with a p85 regulatory subunit. The class IB PI3Ks comprise the p110γ catalytic subunit combined with a p101 or p87/84 regulatory subunit. Mice deficient in p110γ were protected from disease in a mouse model of AAV, and a selective PI3Kγ inhibitor AS605240 also inhibited disease, with effects on neutrophil activation (1).

Activated PI3Kδ syndrome is caused by dominant mutations that increase activity of PI3Kδ. The clinical manifestations of respiratory tract infections, bronchiectasis, lymphadenopathy, and lymphoma are largely explained by activating effects on lymphocytes. Mice deficient in p110δ have impaired humoral immune responses (2), and there are direct effects on B and T cell receptor signaling (3). There are also effects on Th1, Th2, and Th17 T cell subsets (4). Catalytic subunit p110δ is important in autoimmunity, as evidenced by the reduction in autoantibodies to collagen with p110δ blockade (5). Furthermore, mice deficient in p110δ are protected from experimental allergic encephalomyelitis (6) and the development of a lupus-like disease in $Lyn^{-/-}$ mice (7).

Experiments using dual pharmacologic inhibition of p110γ and p110δ have been effective in preclinical models of rheumatoid arthritis and systemic lupus erythematosus (8). However, it is difficult to separate effects on autoimmunity from effects on downstream inflammation in these models. One study in a lupus

Supported by the Medical Research Council (grant MR/R004870/1), Kidney Research UK (grant RP1/2015), Guy's and St. Thomas' Charity (grant R121129), the NIHR Biomedical Research Centre based at Guy's and St. Thomas' NHS Foundation Trust and King's College London. The views expressed are those of the authors and not necessarily those of the NHS, the NIHR, or the Department of Health.

Fernanda Flórez-Barrós, PhD, Simon Freeley, PhD, El Li Tham, MSc, Michael G. Robson, PhD, MBBS: School of Immunology and Microbial Sciences, King's College London, Guy's Hospital, London, UK.

Author disclosures are available at https://onlinelibrary.wiley.com/action/downloadSupplement?doi=10.1002%2Fart.42298&file=art42298-sup-0001-Disclosureform.pdf.

Address correspondence via email to Michael Robson, PhD, MBBS, at michael.robson@kcl.ac.uk.

Submitted for publication December 23, 2021; accepted in revised form July 7, 2022.

nephritis model suggests specific effects of p110δ on renal monocyte/macrophage recruitment to the kidney (9). In the passive murine anti-MPO model, disease is induced by injection of anti-MPO antibody. In addition to providing confirmation of the pathogenicity of AAV, this model is ideal for the study of downstream inflammatory pathways. A limitation of the model is a lack of extrarenal manifestations. We have previously used this model to explore the role of granulocyte colony-stimulating factor (G-CSF) and complement (10,11), but the role of p110δ has not been explored in the context of AAV. We therefore decided to study the effect of p110δ inactivation in the passive murine anti-MPO model.

MATERIALS AND METHODS

Mice. D910A mice (2) backcrossed ≥10 generations to C57BL/6J and wild-type C57BL/6J control mice were bred at the Babraham Institute in Cambridge and transferred to King's College London for the experiment featured in Figure 1 and Supplementary Figure 1 (available on the *Arthritis & Rheumatology* website at https://onlinelibrary.wiley.com/doi/10.1002/art.42298). For the other experiments, D910A mice were obtained from University College London and bred at King's College London, with C57BL/6J control mice from Charles River (Margate, UK). C57BL/6 mice congenic for CD45.1 (B6.SJL-Ptprc^{a} Pepc^{b}/BoyJ) were obtained from The Jackson Laboratory and bred in-house. Female age-matched mice ages 8–12 weeks were used in all experiments. Cages were located together for all experiments, but strain identities were not concealed. Experiments were approved by the local Animal Welfare and Ethics Review Board (with lay representation) and the UK Home Office (project license P4D019509).

Induction of disease. Anti-MPO antibody was raised in MPO-deficient mice as described (10), and IgG was purified by protein G chromatography (HiTrap; GE Healthcare). In the experiment shown in Figure 1, pegylated G-CSF 30 μg (Neulasta; Amgen) was administered subcutaneously 8 and 4 days prior to disease induction, on the day of induction, and 4 days after induction. On day 0 (the day of disease induction), 2 mg/20 gm anti-MPO IgG raised in mice was given intravenously, and 10 μg lipopolysaccharide (*Escherichia coli* R515, ALX-581-007-L002; Enzo Life Sciences) was given intraperitoneally. Blood was taken from the saphenous vein on day −1. For the experiment in Figure 2, sheep were immunized with murine MPO (purified as previously described [10]) by IG Innovations (Ceredigion, Wales, UK).

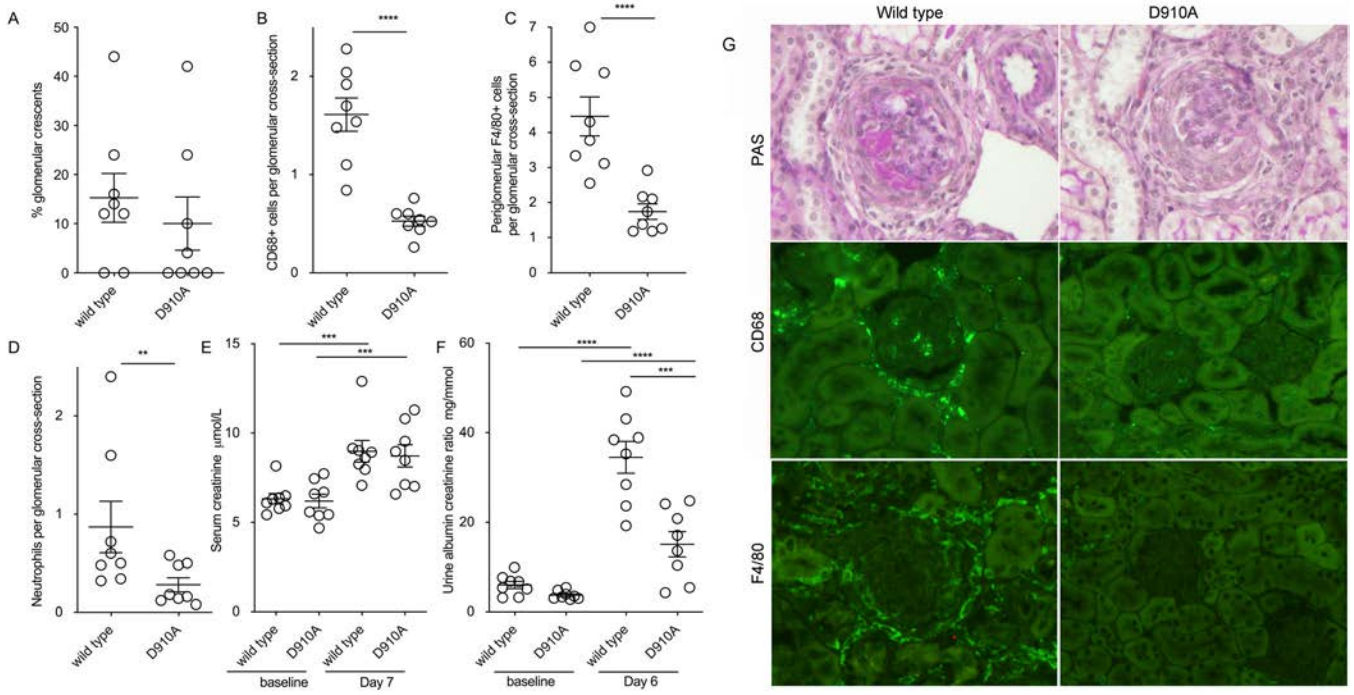

Figure 1. Antimyeloperoxidase (anti-MPO) vasculitis induced by mouse anti-MPO IgG in D910A and wild-type mice. **A–D**, Histologic parameters assessed included glomerular crescents (**A**), glomerular CD68+ macrophages (**B**), periglomerular F4/80+ macrophages (**C**), and glomerular neutrophils (**D**). **E** and **F**, Biochemical parameters included serum creatinine on day 7 (**E**) and albuminuria on day 6 (**F**). **G**, Representative images show periodic acid–Schiff (PAS)–stained sections and immunofluorescence staining for CD68 and F4/80 in wild-type and D910A mice with anti-MPO vasculitis. Original magnification ×400. In **A–F**, symbols represent individual mice (n = 8 per group). Bars show the mean ± SEM. In **E** and **F**, a 2-way analysis of variance with Šidák's multiple comparisons test was used to compare baseline data with day 6 or 7 data. Day 6 urine albumin:creatinine ratios and day 7 serum creatinine levels were compared using Student's *t*-test, as were baseline values. ** = $P < 0.01$; *** = $P < 0.001$; **** = $P < 0.0001$.

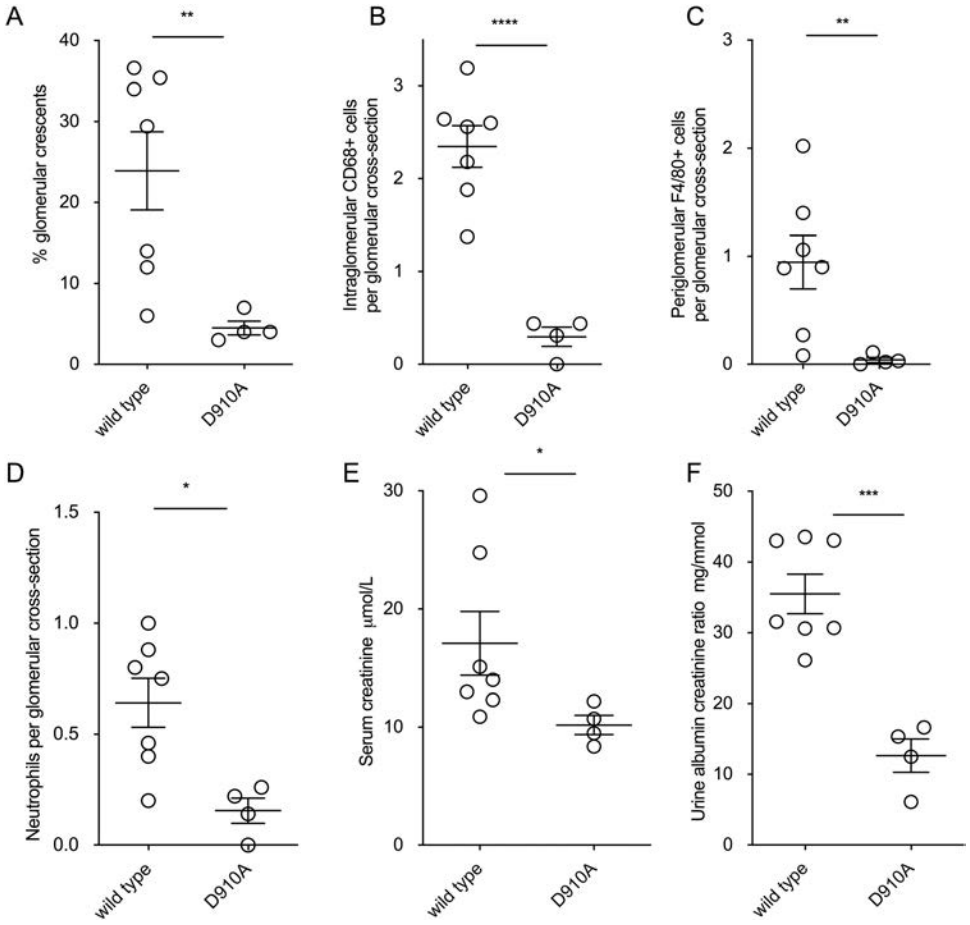

Figure 2. Antimyeloperoxidase (anti-MPO) vasculitis induced by sheep anti-MPO IgG in D910A and wild-type mice. **A–D**, Histologic parameters assessed included glomerular crescents (**A**), glomerular CD68+ macrophages (**B**), periglomerular F4/80+ macrophages (**C**), and glomerular neutrophils (**D**). **E** and **F**, Biochemical parameters included serum creatinine on day 7 (**E**) and albuminuria on day 6 (**F**). Symbols represent individual mice (n = 7 total, and 4 per group). Bars show the mean ± SEM. * = $P < 0.05$; ** = $P < 0.01$; *** = $P < 0.001$; **** = $P < 0.0001$.

Mice were injected intravenously with 200 µl/20 gm of heat inactivated serum on day 0. Mice were treated with 6 µg G-CSF (Neupogen; Amgen) subcutaneously daily from days −1 to 6. Lipopolysaccharide (*E coli* R515) was administered intraperitoneally at 10 µg/20 gm on days 0 and 3. Mice were euthanized on day 7. For the adoptive transfer experiments (Figure 3), mice were treated with 6 µg G-CSF subcutaneously daily from days −4 to 6. On day 0, 2 mg/20 gm anti-MPO IgG raised in mice was given. Lipopolysaccharide was given intraperitoneally at 10 µg/20 gm on days 0 and 3.

Assessment of disease. Spot urines for the albumin:creatinine ratio were obtained on day 6, and mice were euthanized on day 7, with blood collected from the axillary vessels under terminal anesthesia. Kidneys were fixed in Bouin's solution, and paraffin-embedded sections were stained with periodic acid–Schiff (PAS). A minimum of 100 glomeruli per animal were assessed to score the percentage of glomerular crescents and 50 glomeruli to obtain the number of neutrophils. Neutrophils were identified by their characteristic morphology on PAS sections. Periodate–lysine–paraformaldehyde–fixed tissue was used for immunofluorescence, with a minimum of 20 glomeruli per sample assessed in each case. Unlabeled primary antibodies were CD68 (clone FA11; Serotec), F4/80 (clone BM8; eBioscience), and C3 (clone RmC11H9; Cedar Lane). Detection was conducted with DyLight 488–conjugated mouse anti-rat IgG (Jackson ImmunoResearch). Direct immunofluorescence staining was performed with fluorescein isothiocyanate (FITC)–conjugated goat anti-mouse IgG (Fc-specific) and FITC-conjugated donkey anti-sheep IgG (both from Jackson ImmunoResearch). All slides were coded before scoring so the researcher performing the histologic assessment was unaware of sample identity.

Serum creatinine was measured using liquid chromatography with tandem mass spectrometry (Pediatric Clinical Chemistry Laboratory at Guy's and St. Thomas' NHS Foundation Trust), as was urine creatinine, for the data shown in Figure 2. For the data shown in Figure 1, urine creatinine was measured with a

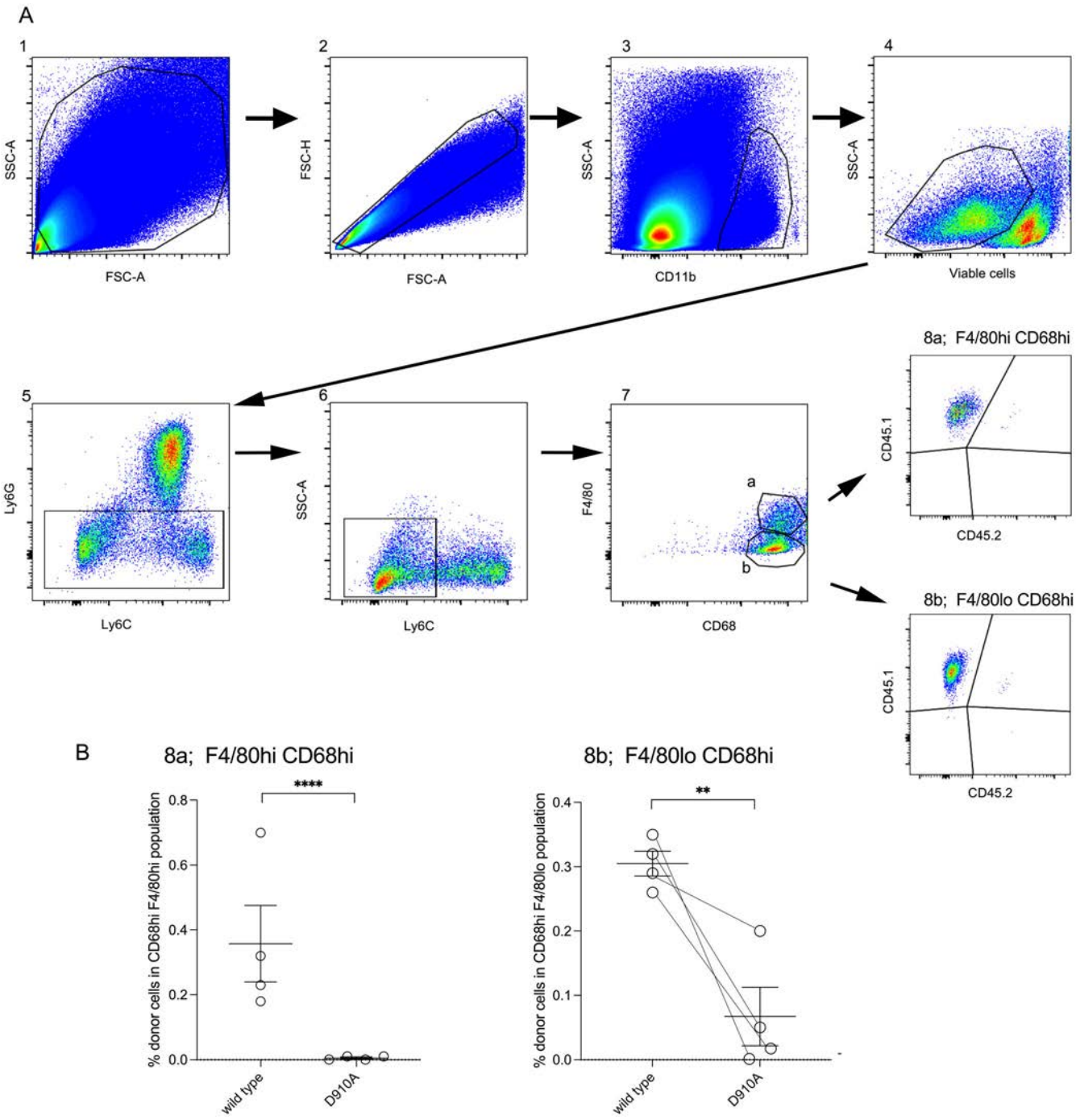

Figure 3. Recruitment of adoptively transferred bone marrow–derived monocytes from D910A and wild-type mice in antimyeloperoxidase vasculitis. **A**, The gating strategy for flow cytometric analysis of digested kidneys taken on day 7 is shown, with gates numbered in order. Wild-type recipient mice were CD45.2–CD45.1+, wild-type donor mice were CD45.2+CD45.1+, and D910A donor mice were CD45.2+CD45.1–. Each recipient mouse received monocytes from both wild-type and D910A donors. **B**, Data on $CD68^{high}$ $F4/80^{high}$ cells from gate 8a (left) and data on $CD68^{high}$ $F4/80^{low}$ cells from gate 8b (right) are shown, with lines joining symbols that represent data from the same animal (n = 4). Bars show the mean ± SEM. ** = $P < 0.01$; **** = $P < 0.0001$. Color figure can be viewed in the online issue, which is available at http://onlinelibrary.wiley.com/doi/10.1002/art.42298/abstract.

commercial creatinine assay using a plate reader and methodology based on instructions of the manufacturer (Diazyme), with a standard curve generated for all assays. Urine albumin was measured by enzyme-linked immunosorbent assay (ELISA) (Bethyl Laboratories). Monocyte chemotactic protein 1 (MCP-1) and CD163 were measured by ELISA (DuoSet) according to instructions of the manufacturer (Bio-Techne). For details on circulating leukocytes, please refer to the Supplementary Methods (available

on the *Arthritis & Rheumatology* website at https://onlinelibrary.wiley.com/doi/10.1002/art.42298).

Adoptive transfer experiments. Hind limbs were collected, bone marrow cells were extracted, and monocytes were isolated using a CD115 MicroBead kit (Miltenyi Biotec). Recipient mice were injected intravenously with 1×10^7 CD115+ cells from each of the donor strains on day 1 after disease induction. Mice were euthanized on day 7, and kidneys were collected for histology and kidney digestion.

Kidney digestion and flow cytometry. Kidney digestion is described in the Supplementary Methods (https://onlinelibrary.wiley.com/doi/10.1002/art.42298). Ten million cells from the kidney single-cell preparations were incubated with Fixable Viability Dye eFluor780 (ThermoFisher). Cells were blocked with 1 μg/ml Fc receptor block (anti-CD16/32 antibody; BD Biosciences) and stained with the following fluorochrome-conjugated antibodies for surface markers: CD11b (clone M1/70; BioLegend), CD45.1 (clone A20; Biolegend), CD45.2 (clone I04; ThermoFisher), Ly6G (clone IA8; BioLegend), Ly6C (AL-21; BD Biosciences), and F4/80 (clone BM8; eBioscience). Cells were permeabilized using a CytoFix/CytoPerm kit (BD Biosciences), blocked with anti-CD16/32 antibody (BD Biosciences), and incubated with anti-CD68 (clone FA/11; BD Biosciences). Samples were run on an LSRFortessa using FACSDiva software (BD Biosciences), and data were analyzed using FlowJo software.

Statistical analysis. GraphPad Prism version 9 was used for analyses. Student's unpaired *t*-test was used to compare 2 groups, unless another test is specified. Some data were logarithmically transformed before analysis.

RESULTS

Protection from anti-MPO vasculitis in D910A mice with mild disease. Anti-MPO vasculitis was induced in mice with inactive p110δ (D910A) and in wild-type mice. Immunofluorescence staining included both F4/80, a mature murine macrophage marker found in a predominantly periglomerular location (12), and CD68, which is found on all glomerular macrophages. Although there was no difference in glomerular crescents (Figure 1A), there were fewer glomerular CD68+ cells (Figure 1B), fewer periglomerular F4/80+ cells (Figure 1C), and fewer neutrophils (Figure 1D) in D910A mice. Serum creatinine was increased in both groups compared with baseline, but there was no difference between groups (Figure 1E). However, there was significantly less albuminuria in D910A mice compared with wild-type controls (Figure 1F). Figure 1G shows representative histologic sections and immunofluorescence staining for CD68 and F4/80.

No differences in circulating leukocytes. Peripheral blood leukocytes in D910A mice and wild-type mice were compared. There were no differences in total white cells, peripheral total blood monocytes, monocyte subsets, or neutrophils in untreated mice (Supplementary Figures 1A–E, https://onlinelibrary.wiley.com/doi/10.1002/art.42298). We also assessed neutrophil numbers on day –1, before disease induction and after G-CSF treatment for the experiment shown in Figure 1. No differences between wild-type and D910A mice were seen (Supplementary Figure 1F). These results show that the differences in glomerular macrophages and neutrophils did not simply reflect differences in circulating leukocytes.

Protection from acute kidney injury in D910A mice with more severe disease. Anti-MPO vasculitis was induced with sheep anti-MPO IgG to induce more severe disease, because we had not shown protection from acute kidney injury in our initial experiment. Using sheep IgG allowed for the injection of more IgG and led to more severe disease in wild-type mice. The use of sheep anti-MPO antibody did not result in glomerular deposition of sheep IgG (Supplementary Figure 2, https://onlinelibrary.wiley.com/doi/10.1002/art.42298). Weak staining for mouse IgG and C3 was seen in a mesangial pattern in mice with disease due to either mouse or sheep anti-MPO IgG, along with tubular C3 (Supplementary Figure 2). This pattern of IgG and C3 staining is also seen in untreated mice. Therefore, this remained a good model of anti-MPO vasculitis. Disease was less severe in D910A mice according to all experimental read outs. There were fewer glomerular crescents, fewer glomerular and periglomerular macrophages, fewer neutrophils, lower serum creatinine levels, and lower levels of albuminuria in D910A mice compared with wild-type mice (Figure 2). These results confirmed that D910A mice were protected and that this included protection from glomerular crescent formation and acute kidney injury.

Deficient recruitment of adoptively transferred bone marrow–derived monocytes from D910A mice in anti-MPO vasculitis. The most striking finding in the first experiment, with disease induced by murine anti-MPO IgG, was the lack of CD68+ and F4/80+ macrophages in and around glomeruli in D910A mice. This was observed despite the moderate disease severity. In view of their role in monocyte function, we measured MCP-1 and CD163 in serum from the experiment shown in Figure 2, and there were no significant differences (Supplementary Figure 3, https://onlinelibrary.wiley.com/doi/10.1002/art.42298). MCP-1 and CD163 were both undetectable in urine. Despite this, we decided to directly examine the recruitment of inflammatory monocytes in an adoptive transfer experiment. Each recipient mouse received bone marrow–derived monocytes from both wild-type and D910A donors on day 1 after disease induction and was euthanized on day 7.

This experimental design meant that in each recipient mouse with anti-MPO vasculitis, we could assess the relative recruitment to the kidney of adoptively transferred wild-type and D910A monocytes. Paired donor-derived cells from both strains experienced the same inflammatory environment and were extracted from the same kidney with a given disease severity. Significant disease was induced in all 4 mice with 9%, 20%, 28%, and 22% of glomerular cross sections having crescents on day 7, respectively. Figure 3A shows the gating strategy for flow cytometric analysis of digested kidneys taken on day 7. We identified populations of $CD68^{high}$ $F4/80^{low}$ and $CD68^{high}$ $F4/80^{high}$ cells corresponding to glomerular and periglomerular macrophages seen on immunofluorescence staining of tissue (Figure 1G). The data in Figure 3B show that there were significantly fewer $CD68^{high}$ $F4/80^{low}$ and $CD68^{high}$ $F4/80^{high}$ cells derived from transferred D910A monocytes than from wild-type monocytes. These data confirm that monocytes with an inactive p110δ have a reduced recruitment to the inflamed kidney in anti-MPO vasculitis.

DISCUSSION

We have demonstrated that mice with an inactive p110δ are protected from vasculitis induced by passive transfer of anti-MPO antibody. There was a striking reduction in renal macrophages and adoptive transfer experiments showed a defect in the recruitment of monocytes with an inactive p110δ to the kidney. Our results are consistent with previous data in a lupus model (9). In this study, there was a modest reduction in autoantibody levels with p110δ inhibition but a striking reduction in renal macrophages. The current data and findings from this previous study both suggest that p110δ is required for downstream inflammation in glomerulonephritis. In the previous report, in vitro data also suggested that p110δ was required for macrophage transmigration.

Previous in vitro data on human cells have shown a requirement for p110δ in monocyte adhesion and transmigration (13). Pharmacologic inhibition of p110δ decreased migration of both primary peripheral blood derived monocytes and THP-1 cells. Further experiments with THP-1 cells and a coronary artery endothelial cell layer showed that, in the absence of chemokines, PI3Kδ regulates the activation of β1 integrins mediating the binding of monocytes to vascular cell adhesion molecule 1, while in the presence of MCP-1, PI3Kδ regulates β2 integrin activation and adhesion to intracellular adhesion molecule 1. We have previously shown that anti-MPO IgG from patients affect macrophage development (14), and p110δ could play a role in mediating the response of monocytes to anti-MPO IgG. However, the previous in vitro data in both murine and human cells discussed above (9,13) suggest a more general effect on monocyte recruitment which could be relevant to other diseases. We have not identified the molecular mechanism by which p110δ enhances monocyte recruitment. An understanding of this will require further work beyond this brief report.

We focused on monocytes, and the most striking finding was a reduction in CD68+ and F4/80+ cells in the kidney in our initial experiments. However, we have not excluded a role for p110δ in neutrophils in addition to monocytes. A previous study using the murine anti-MPO model suggested that neutrophil depletion was protective (15). However, the depleting antibody used (NIMP-R14) would have also affected monocytes, so the relative importance of monocytes and neutrophils was not clear. We have shown that neutrophils are essential in the autologous nephrotoxic nephritis model of crescentic glomerulonephritis using mice with a genetic deficiency of neutrophils (16). Therefore, it seems likely that neutrophils are required in anti-MPO vasculitis.

The current study does not explore the effect of p110δ deficiency on autoimmunity to MPO, and one would predict that it will inhibit this in addition to the antiinflammatory effects we have demonstrated. PI3Kδ inhibitors are being studied with idelalisib (CAL-101), an older PI3Kδ inhibitor, which is approved for hematologic malignancy. However, adverse effects limit its potential as a therapy for AAV. Several PI3Kδ inhibitors are available that do not appear to have these side effects and could inhibit both autoimmunity and inflammation in AAV.

Therapies that target p110δ and p110γ are being developed for hematologic malignancies in addition to autoimmune disease. This is an advantage since safety data will accumulate at a faster rate because of this diverse clinical application. The major unmet need in AAV is for antiinflammatory therapies to reduce or eliminate the need for glucocorticoids. There has been progress in this respect, with positive results for the C5a receptor antagonist avacopan. However, additional treatments that target other pathways will be useful. The current study and previous work (1) suggest that p110δ and p110γ are both potential therapeutic targets. They may be more effective and serve as an alternative if avacopan is not tolerated or provide additional benefit when used in combination.

ACKNOWLEDGMENTS

We are grateful to Klaus Okkenhaug (University of Cambridge) and Bart Vanhaesebroeck (University College London) for providing the D910A mice.

AUTHOR CONTRIBUTIONS

All authors were involved in drafting the article or revising it critically for important intellectual content, and all authors approved the final version to be published. Dr. Robson had full access to all of the data in the study and takes responsibility for the integrity of the data and the accuracy of the data analysis.

Study conception and design. Robson.

Acquisition of data. Flórez-Barrós, Freeley, Tham.

Analysis and interpretation of data. Flórez-Barrós, Freeley, Tham, Robson.

REFERENCES

1. Schreiber A, Rolle S, Peripelittchenko L, et al. Phosphoinositol 3-kinase-γ mediates antineutrophil cytoplasmic autoantibody-induced glomerulonephritis. Kidney Int 2009;77:118–28.
2. Okkenhaug K, Bilancio A, Farjot G, et al. Impaired B and T cell antigen receptor signaling in p110δ PI 3-kinase mutant mice. Science 2002; 297:1031–4.
3. Ramadani F, Bolland DJ, Garcon F, et al. The PI3K isoforms p110α and p110δ are essential for pre-B cell receptor signaling and B cell development. Sci Signal 2012;3:ra60.
4. Soond, DR, Bjorgo E, Moltu K, et al. PI3K p110δ regulates T-cell cytokine production during primary and secondary immune responses in mice and humans. Blood 2010;115:2203–13.
5. Durand CA, Hartvigsen K, Fogelstrand L, et al. Phosphoinositide 3-kinase p110 δ regulates natural antibody production, marginal zone and B-1 B cell function, and autoantibody responses. J Immunol 2009;183:5673–84.
6. Haylock-Jacobs S, Comerford I, Bunting M, et al. PI3Kδ drives the pathogenesis of experimental autoimmune encephalomyelitis by inhibiting effector T cell apoptosis and promoting Th17 differentiation. J Autoimmun 2011;36:278–87.
7. Maxwell MJ, Tsantikos E, Kong AM, et al. Attenuation of phosphoinositide 3-kinase δ signaling restrains autoimmune disease. J Autoimmun 2012;38:381–91
8. Stark AK, Sriskantharajah S, Hessel EM, et al. PI3K inhibitors in inflammation, autoimmunity and cancer. Curr Opin Pharmacol 2015;23:82–91.
9. Suarez-Fueyo A, Rojas JM, Cariaga AE, et al. Inhibition of PI3Kδ reduces kidney infiltration by macrophages and ameliorates systemic lupus in the mouse. J Immunol 2014;193:544–54
10. Freeley SJ, Coughlan AM, Popat RJ, et al. Granulocyte colony stimulating factor exacerbates antineutrophil cytoplasmic antibody vasculitis. Ann Rheum Dis 2013;72:1053–8.
11. Freeley SJ, Popat RJ, Parmar K, et al. Experimentally-induced anti-myeloperoxidase vasculitis does not require properdin, MASP-2 or bone marrow-derived C5. J Pathol 2016;240:61–71.
12. Masaki T, Chow F, Nikolic-Paterson DJ, et al. Heterogeneity of antigen expression explains controversy over glomerular macrophage accumulation in mouse glomerulonephritis. Nephrol Dial Transplant 2003;18:178–81.
13. Ferreira AM, Isaacs H, Hayflick JS, et al. The p110δ isoform of PI3K differentially regulates β1 and β2 integrin-mediated monocyte adhesion and spreading and modulates diapedesis. Microcirculation 2006;13:439–56.
14. Popat RJ, Hakki S, Thakker A, et al. Anti-myeloperoxidase antibodies attenuate the monocyte response to LPS and shape macrophage development. JCI Insight 2017;2:e87379.
15. Xiao H, Heeringa P, Liu Z, et al. The role of neutrophils in the induction of glomerulonephritis by anti-myeloperoxidase antibodies. Am J Pathol 2005;167:39–45.
16. Tham EL, Freeley SJ, Bearder S, et al. VISTA deficiency protects from immune complex-mediated glomerulonephritis by inhibiting neutrophil activation. J Autoimmun 2020;113:102501.

Arthritis & Rheumatology
Vol. 75, No. 1, January 2023, pp 71–83
DOI 10.1002/art.42314

American College of Rheumatology
Empowering Rheumatology Professionals

Regulation of NETosis and Inflammation by Cyclophilin D in Myeloperoxidase-Positive Antineutrophil Cytoplasmic Antibody–Associated Vasculitis

Takashi Kudo,[1] Daigo Nakazawa,[1] Kanako Watanabe-Kusunoki,[1] Masatoshi Kanda,[2] Satoka Shiratori-Aso,[1] Nobuya Abe,[3] Saori Nishio,[1] Jun-ichiro Koga,[4] Sari Iwasaki,[5] Takahiro Tsuji,[5] Yuichiro Fukasawa,[5] Miwako Yamasaki,[6] Masahiko Watanabe,[6] Sakiko Masuda,[7] Utano Tomaru,[8] Masaaki Murakami,[9] Yasuaki Aratani,[10] Akihiro Ishizu,[7] and Tatsuya Atsumi[1]

Objective. Antineutrophil cytoplasmic antibody (ANCA)–associated vasculitis (AAV) is pathologically characterized by focal fibrinoid necrosis, in which ANCA-mediated neutrophil extracellular trap (NET) formation and subsequent endothelial cell necrosis occur. Cyclophilin D (CypD) plays an important role in mediation of cell necrosis and inflammation via the opening of mitochondrial permeability transition pores. This study was undertaken to examine the role of CypD in AAV pathogenesis.

Methods. We assessed the role and mechanism of CypD in ANCA-stimulated neutrophils in vitro by immunostaining and electron microscopy observation. We performed a comprehensive RNA-sequencing analysis on ANCA-treated murine neutrophils. To investigate the role of CypD in vivo, we assessed disease features in CypD-knockout mice and wild-type mice using 2 different murine AAV models: anti-myeloperoxidase IgG transfer–induced AAV and spontaneous AAV.

Results. In vitro experiments showed that pharmacologic and genetic inhibition of CypD suppressed ANCA-induced NET formation via the suppression of reactive oxygen species and cytochrome c release from the mitochondria. RNA-sequencing analyses in ANCA-treated murine neutrophils revealed the involvement of inflammatory responses, with CypD deficiency reducing ANCA-induced alterations in gene expression. Furthermore, analyses of upstream regulators revealed the relevance of intracellular calcium (CypD activator) and cyclosporin (CypD inhibitor) in ANCA stimulation, indicating that the CypD-dependent opening of mitochondrial permeability transition pores is associated with ANCA-induced neutrophil activation and NETosis. In both AAV mouse models, the genetic deletion of CypD ameliorated crescentic glomerulonephritis via the inhibition of CypD-dependent neutrophil and endothelial necrosis.

Conclusion. CypD targeting is a novel and specific therapeutic strategy for AAV via the resolution of necrotizing vasculitis.

INTRODUCTION

Antineutrophil cytoplasmic antibody (ANCA)–associated vasculitis (AAV) is a systemic autoimmune disease characterized by necrotizing vasculitis with pathogenic autoantibodies. In pathogenesis, excessive and dysregulated neutrophil extracellular traps (NETs) contribute to the development of AAV (1), and patients with AAV produce autoantibodies against components of NETs. NETs are formed in response to a diverse range of triggers and are believed to develop as a consequence of cell death or vital neutrophils (2). Patients with AAV typically produce autoantibodies against myeloperoxidase (MPO) or proteinase 3, and

Supported by a grant-in-aid from the Ministry of Education, Culture, Sports, Science, and Technology of Japan (grant JP 20K08581).

[1]Takashi Kudo, MD, PhD, Daigo Nakazawa, MD, PhD, Kanako Watanabe-Kusunoki, MD, PhD, Satoka Shiratori-Aso, MD, Saori Nishio, MD, PhD, Tatsuya Atsumi, MD, PhD: Department of Rheumatology, Endocrinology, and Nephrology, Faculty of Medicine and Graduate School of Medicine, Hokkaido University, Sapporo, Japan; [2]Masatoshi Kanda, MD, PhD: Department of Rheumatology and Clinical Immunology, Sapporo Medical University, Sapporo, Japan; [3]Nobuya Abe MD, PhD: Department of Rheumatology, Endocrinology, and Nephrology, Faculty of Medicine and Graduate School of Medicine, Hokkaido University, and Division of Molecular Psychoimmunology, Institute for Genetic Medicine, Graduate School of Medicine, Hokkaido University, Sapporo, Japan; [4]Jun-ichiro Koga, MD, PhD: Department of Cardiovascular Medicine, Kyushu University, Graduate School of Medical Sciences, Fukuoka, Japan; [5]Sari Iwasaki, MD, PhD, Takahiro Tsuji, MD, PhD, Yuichiro Fukasawa, MD, PhD: Department of Pathology, Sapporo City General Hospital, Sapporo, Japan; [6]Miwako Yamasaki, MD, PhD, Masahiko Watanabe, MD, PhD: Department of Anatomy, Hokkaido University Graduate School of Medicine, Sapporo, Japan; [7]Sakiko Masuda, PhD, Akihiro Ishizu, MD, PhD: Department

ANCAs activate neutrophils to form NETs, leading to further inflammation and endothelial injury (3). Furthermore, NETs play a role in the innate immune response and are involved in phagocytic uptake of microbes, including fungi (4), viruses (5), and parasites (6); however, targeted neutrophil therapy in patients with AAV remains elusive.

Because necrosis with NETs occurs in AAV, we focused on cyclophilin D (CypD) in ANCA-mediated NETs and endothelial injury. CypD is a mitochondrial matrix protein that controls metabolism and reactive oxygen species (ROS) production via the transient opening of mitochondrial permeability transition pores (mPTPs); however, dysregulation of mPTP opening results in necrosis via a loss of mitochondrial membrane potential with the release of mitochondrial ROS and cytochrome c into the cytoplasm (7–9). Furthermore, the inhibition of CypD in mice has been reported to protect organs from ischemia-reperfusion injury (10–16).

Herein, we investigated the involvement of CypD in the pathogenesis of AAV and its potential as a therapeutic target.

MATERIALS AND METHODS

Immunostaining of human renal tissue. Formalin-fixed, paraffin-embedded renal biopsy tissues from patients with AAV and minimal-change nephrotic syndrome were sliced into 4-μm sections and thereafter deparaffinized with lemosol. After antigen retrieval, we performed immunostaining using an anti–cytochrome c antibody (Abcam), TUNEL staining using a cell death detection kit according to the manufacturer's protocol, and DAPI staining to identify the nuclei in the tissues. We quantified the positive area as the mean luminance value of three 8-power fields in each sample using ImageJ software (National Institutes of Health). Characteristics of patients with AAV and minimal-change nephrotic syndrome are shown in Supplementary Table 1, available on the *Arthritis & Rheumatology* website at https://onlinelibrary.wiley.com/doi/10.1002/art.42314.

NET induction in human neutrophils. Neutrophils were isolated from healthy human donors by density centrifugation using PolymorphPrep (Axis-Shield). Neutrophils were suspended in RPMI 1640 (Merck) and seeded onto plates for incubation in a 5% carbon dioxide atmosphere at 37°C before stimulation. After pretreatment of neutrophils with cyclosporin A (CSA, 200 ng/ml; Merck) or phosphate buffered saline (PBS) for 30 minutes, followed by priming with human tumor necrosis factor (TNF) (5 ng/ml; Merck) for 15 minutes, we incubated the neutrophils for 4 hours with IgG (240 μg/ml) extracted from serum samples of healthy volunteers or patients with MPO-positive AAV (3 donors/group) (clinical characteristics of patients are shown in Supplementary Table 1, available at https://onlinelibrary.wiley.com/doi/10.1002/art.42314). Quantitative analysis was performed to evaluate serum isolated from each independent donor.

For assessment of NETs, we used immunofluorescence staining and flow cytometric (FCM) analysis using Sytox green (ThermoFisher Scientific). We performed immunostaining for cytochrome c and citrullinated histone H3 (CitH3) using an anti–cytochrome c antibody and anti-CitH3 antibody (Abcam), with incubation for 24 hours at 4°C after fixation with 4% paraformaldehyde. To evaluate the relationship between necrosis and NETs in crescentic glomerulonephritis, we performed immunostaining with hematoxylin and eosin (H&E), TUNEL, CD15 (Wako), CitH3, and peptidylarginine deiminase type 4 (PAD4) (Abcam) on serial kidney sections. We measured intracellular ROS and mitochondrial ROS with the ROS assay kit (Dojindo) and with MitoSox (Invitrogen), respectively, according to the manufacturers' instructions.

After specimens were washed, we allowed specimens to incubate with Alexa Fluor 488–conjugated goat anti-rabbit IgG (ThermoFisher Scientific) for 60 minutes at room temperature. We quantified the positive immunostained areas as the mean luminance value using ImageJ software. We performed these experiments using healthy human neutrophils isolated from 3 independent donors.

White blood cells in the peripheral blood. Total white blood cells in the peripheral blood of *CypD*$^{+/+}$ and *CypD*$^{-/-}$ mice (12–14-week-old mice) were counted after red blood cells were removed with lysis buffer. We determined the percentage of neutrophils as the number of neutrophils per 100 white blood cells using Giemsa-stained peripheral blood smears.

NET induction in murine neutrophils. C57BL/6J mice were procured from CLEA Japan, Inc. We isolated neutrophils from wild-type (WT) C57BL/6J or *CypD*$^{-/-}$ mice (10–14-week-old mice) using standard Dextran sulfate sedimentation followed by Ficoll-Hypaque density-gradient centrifugation (17). After neutrophils were primed with mouse TNF (5 ng/ml) for 15 minutes, we incubated the neutrophils for 4 hours with mouse IgG isotype control (20 μg/ml; R&D Systems) or anti–mouse MPO (anti-mMPO) monoclonal antibody (20 μg/ml; OriGene). We evaluated NETs with immunofluorescent staining with Sytox green and with electron microscopy as described below.

of Medical Laboratory Science, Faculty of Health Sciences, Hokkaido University, Sapporo, Japan; [8]Utano Tomaru, MD, PhD: Department of Pathology, Faculty of Medicine and Graduate School of Medicine, Hokkaido University, Sapporo, Japan; [9]Masaaki Murakami, VMD, PhD: Division of Molecular Psychoimmunology, Institute for Genetic Medicine, Graduate School of Medicine, Hokkaido University, Sapporo, Japan; [10]Yasuaki Aratani, PhD: Graduate School of Nanobioscience, Yokohama City University, Yokohama, Japan.

Author disclosures are available at https://onlinelibrary.wiley.com/action/downloadSupplement?doi=10.1002%2Fart.42314&file=art42314-sup-0001-Disclosureform.pdf.

Address correspondence via email to Daigo Nakazawa, MD, PhD, at daigo-na@med.hokudai.ac.jp.

Submitted for publication November 2, 2021; accepted in revised form July 20, 2022.

RNA-sequencing and data analysis. After murine neutrophils were primed with mouse TNF (5 ng/ml) for 15 minutes, the isolated neutrophils with 2 biologic replicates were incubated for 1.5 hours with or without anti-mMPO IgG (20 μg/ml) and stored at –80°C. A single batch of neutrophils was prepared from peripheral blood of 5 or 6 mice. RNA was isolated using the RNeasy Micro kit (Qiagen). We generated libraries using a Smart-seq v4 ultra low kit (Clontech-Takara Bio Inc) and a NEBNext Ultra RNA Library Prep kit for Illumina (E7530; New England Biolabs) according to the manufacturers' instructions. Libraries were sequenced on a NovaSeq 6000 system (Illumina) to obtain at least 25 million 150-bp paired-end reads. We removed low-quality raw sequencing reads and the adapter sequences using Trimmomatic version 0.38 (18). The trimmed reads were mapped to mm10 (Ensembl 87) using HISAT2 version 2.1.0 (19) and quantified using featureCounts version 1.6.3 (20). Differentially expressed genes (DEGs) were identified based on differences in expression levels ($\log_2$ fold change >1 and adjusted $P < 0.05$) between samples after we removed genes with zero read counts and non-protein–coding genes using DESeq2 version 1.24.0 (21). The Benjamini-Hochberg method was used to adjust the P value for multiple hypothesis testing. Gene ontology analysis was performed using the gprofiler2 R package (22). A heatmap of expression was made with Multiple Experiment Viewer version 4.9.0 software (23). We performed upstream pathway analysis of DEGs using Ingenuity Pathway Analysis version 51963813 (Qiagen; https://www.qiagenbioinformatics.com/products/ingenuity-pathway-analysis/). The data were deposited in the DNA Data Bank of Japan (DRA011272).

Endothelial cytotoxicity. A 1.0-μm 24-well culture insert (Corning) was precoated with type I collagen (Corning) as previously reported with some modifications (3). Human renal glomerular endothelial cells (HRGECs), purchased from ScienCell, were seeded at a density of 1.6×10^5/ml and cultured in HuMedia-EG2 (Kurabo). Human neutrophils were treated with control IgG or ANCA IgG (240 μg/ml) for 4 hours at 37°C, after which the supernatant was replaced with fresh medium. Bottom neutrophils or NETs were collected, and the supernatant was collected after centrifugation (1,200 revolutions per minute for 5 minutes). We pretreated HRGECs with CSA or PBS for 30 minutes and then allowed cells to incubate with neutrophil supernatants or ANCA-induced NETs (ANCA-NET supernatants) for 3 hours. After incubation, we evaluated endothelial injury by measuring the permeability of fluorescein isothiocyanate–conjugated bovine serum albumin (Merck) as previously described (24).

Animal models. Methods for animal models are described in the Supplementary Methods, available on the *Arthritis & Rheumatology* website at https://onlinelibrary.wiley.com/doi/10.1002/art.42314.

Identification of NETs morphology by electron microscopy. TNF-primed human and mouse neutrophils were treated with ANCAs and anti-mMPO IgG, respectively. Alternatively, human neutrophils were incubated with control IgG obtained from healthy donors or phorbol 12-myristate 13-acetate (PMA) (Merck). Incubated neutrophils were fixed with 2% glutaraldehyde and 2% paraformaldehyde, postfixed with 1% osmium tetroxide, dehydrated in ethanol, embedded in epoxy resin, and cut into ultrathin sections (80 nm) (15,25). Because NETs are fragile, each step was performed with minimal disturbance to the media. Unstimulated neutrophils were used as references.

Study approval. The animal experiments were approved by the Hokkaido University Animal Experiment Committee (approval number 2018-018). The experiments that used human materials were approved by the Sapporo City General Hospital Clinical Research Committee (approval number R02-059-726). Written informed consent was obtained from all patients and volunteers.

Statistical analysis. The normality of distribution for continuous variables was assessed using the Shapiro-Wilk's test. Descriptive statistics are presented as median and interquartile range for non-Gaussian distributions. For Gaussian distributions, results obtained from animal experiments and from in vitro experiments are presented as the mean ± SD and mean ± SEM, respectively. Differences between the 2 groups were compared using the Mann-Whitney U test for non-Gaussian distributions, Student's unpaired t-test for Gaussian distribution, and chi-square test for chi-square distribution. For parametric multiple comparisons, one-way analysis of variance with post hoc Tukey's test was used to compare differences between groups. Differences were considered significant at P values less than 0.05. We used JMP software (SAS Institute) for all statistical analyses. The survival rate shown by Kaplan-Meier survival curves and the statistical significance were determined with the Gehan-Breslow-Wilcoxon test using GraphPad Prism software.

RESULTS

Reduction of ANCA-induced NET formation in vitro by pharmacologic inhibition of CypD. We hypothesized that CypD mediates NET formation, which contributes to tissue necrosis in AAV. In our in vivo experiments to determine whether neutrophils form NETs via CypD by binding to ANCAs, ANCA IgG–treated neutrophils displayed NET formation with extracellular DNA, which was suppressed by CSA treatment (Figures 1A and 1B). In addition, FCM analysis showed that the Sytox green intensity in ANCA-induced NETs was decreased by CSA treatment (Figures 1C and 1D).

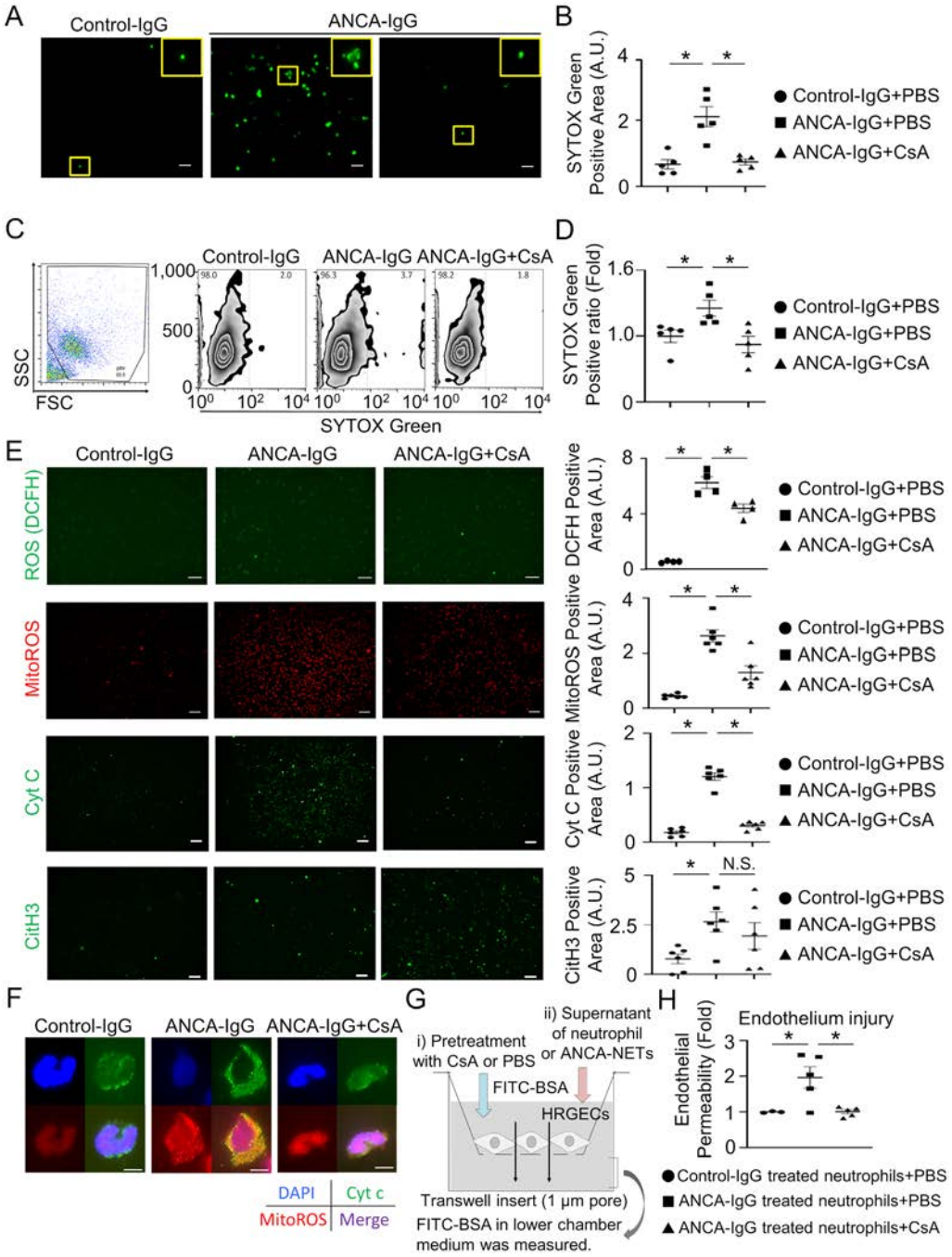

Figure 1. In vitro effects of antineutrophil cytoplasmic antibody (ANCA)–induced neutrophil extracellular trap (NET) formation in human neutrophils after treatment with the cyclophilin D (CypD) inhibitor cyclosporin A (CSA). **A** and **B**, Images (**A**) and quantification (**B**) of Sytox green immunostaining of peripheral blood neutrophils from healthy volunteers for assessment of NET formation. Cells were primed with tumor necrosis factor (5 ng/ml), pretreated with CSA (200 ng/ml) or control phosphate buffered saline (PBS), and stimulated with ANCA IgG from patients with ANCA-associated necrotizing vasculitis or control IgG from healthy donors (240 μg/ml). Boxed areas display magnified views of Sytox green–positive cells. Bars = 50 μm. **C** and **D**, Flow cytometry analyses of cell death in the same groups as in **A**, using contour plots of Sytox green immunostaining (**C**, right) in the gated fraction (**C**, left), and quantification of the results as the fold change in mean luminance values relative to controls (**D**). **E** and **F**, Images (**E**, left) and quantification (**E**, right) of immunofluorescence staining and colocalization of staining (nuclei counterstained with DAPI) (**F**) in neutrophils from the same groups as in **A**, showing release of mitochondrial reactive oxygen species (MitoROS), cytochrome c (Cyt c), and citrullinated histone H3 (citH3). Bars = 50 μm in **E** and 10 μm in **F**. **G** and **H**, Assessment of endothelial injury using fluorescein isothiocyanate (FITC)–conjugated bovine serum albumin (BSA) permeability assays of human renal glomerular endothelial cells (HRGECs). Cells were grown to confluence on culture inserts, pretreated with CSA or PBS (200 ng/ml), and coincubated with ANCA IgG (240 μg/ml). After 3 hours, medium was collected to evaluate FITC-BSA permeability (**G**), with quantification of the results as the fold change in permeability relative to controls (**H**). In **B**, **D**, **E**, and **H**, symbols represent individual samples; bars show the mean ± SEM. * = $P < 0.05$ by one-way analysis of variance with post hoc Tukey's test. A.U. = arbitrary units; FSC = forward scatter; SSC = side scatter; DCFH = 2',7'-dichlorofluorescein diacetate; N.S. = not significant. Color figure can be viewed in the online issue, which is available at http://onlinelibrary.wiley.com/doi/10.1002/art.42314/abstract.

Next, to verify whether CypD signaling during NETosis was induced by ANCAs, we evaluated the production of intracellular and mitochondrial ROS (mitoROS) and expression of cytochrome c and CitH3 in neutrophils. We found that the ANCA-induced NETs expressed high levels of intracellular ROS, mitoROS, cytochrome c, PAD4, and CitH3 and that CSA significantly reduced mitoROS and cytochrome c expression (Figure 1E and Supplementary Figures 1A and 1B available on the *Arthritis & Rheumatology* website at https://onlinelibrary.wiley.com/doi/10.1002/art.42314). However, only partial inhibition of intracellular ROS was shown. The intracellular ROS detects both cytoplasmic- and mitochondrial-derived ROS. These findings indicate that ANCA activates cytoplasmic ROS, which initiates mitoROS production via CypD signaling.

In contrast, CSA did not influence histone citrullination, which is regulated by PAD4 and initiates decondensation of chromatin. In addition, CSA inhibited NET release but did not affect the enhanced PAD4 expression. In neutrophils treated with ANCA IgG under a high-power field of view, we observed mitoROS and cytochrome c that extended into the perinuclear space and swollen nuclei; however, CSA treatment counteracted these dynamics (Figure 1F and Supplementary Figures 1A and 1B).

To investigate the morphologic changes, we used transmission electron microscopy to observe unstimulated, PMA-treated, control IgG–treated, and ANCA IgG–treated neutrophils (Supplementary Figure 1C). Similar to results shown in PMA-induced NETs (26,27), ANCA IgG–treated neutrophils exhibited indistinct organelles and decondensed chromatin with the loss of plasma membrane protrusions. When we consider the morphologic changes and the mitochondrial dynamics, the CypD signaling pathway might be involved in the formation of ANCA-induced NETs.

Attenuation of ANCA-mediated, NET-induced glomerular endothelial injury with CypD inhibitor. We examined the involvement of CypD-related necrosis in endothelial injury (28–31). We grew HRGECs in a monolayer and treated the cells with ANCA-NET supernatants in the presence of CSA or PBS in vitro (Figure 1G). The addition of ANCA-NET supernatants caused endothelial injury compared with results shown with addition of control supernatants, and CSA treatment protected the endothelium from NET toxicity (Figure 1H). These results indicate that endothelial injury in AAV is associated with CypD-related necrosis.

Vascular necrosis in patients with AAV. We explored whether CypD-related necrosis is involved in the pathophysiology of necrotizing glomerulonephritis in patients with AAV. In renal biopsy specimens, TUNEL-positive cells were detected in the glomeruli and tubulointerstitial spaces. At high magnification, some glomerular cells had TUNEL-positive swollen nuclei, indicating the development of necrosis (32). Furthermore, the expression of cytochrome c, released into the cytoplasm from the mitochondria during mPTP opening, was increased in the glomeruli. In contrast, renal specimens from patients with minimal-change nephrotic syndrome did not show positivity for TUNEL or cytochrome c (Supplementary Figure 2A, available on the *Arthritis & Rheumatology* website at https://onlinelibrary.wiley.com/doi/10.1002/art.42314). In our investigation of the relationship between necrosis and NETosis, in which we immunostained serial kidney sections with H&E and TUNEL to view NET formation, glomeruli with cellular crescents showed increased TUNEL staining and NET formation. However, fibrous crescent glomeruli showed weak TUNEL staining and NET positivity (Supplementary Figure 2B). These results imply that CypD-related NETosis may be involved in the pathogenesis of necrotizing vasculitis in AAV.

Role of CypD in anti-mMPO IgG–treated mouse neutrophils in vitro. Next, we investigated the effects of ANCA stimulation in neutrophils from WT C57BL/6 and CypD-deficient mice. Neutrophils derived from WT mice were primed with murine TNF and treated with murine control IgG or anti-mMPO monoclonal IgG. Sytox green–positive NETs were more abundant in anti-mMPO IgG–treated neutrophils than in control IgG–treated neutrophils (Supplementary Figures 3A and 3B, available on the *Arthritis & Rheumatology* website at https://onlinelibrary.wiley.com/doi/10.1002/art.42314). Anti-mMPO IgG–induced NETs were inhibited in *CypD*$^{-/-}$ mouse neutrophils (Figures 2A and 2B). With transmission electron microscopy, we observed that anti-mMPO IgG–treated WT mouse neutrophils were partially decondensed and had fragile chromatin, loss of the nuclear membrane, and a vulnerable plasma membrane; however, these findings were not observed in anti-mMPO IgG–treated *CypD*$^{-/-}$ neutrophils (Figure 2C).

To examine the mechanism of ANCA-induced NET formation, mouse neutrophils treated with anti-mMPO IgG were subjected to RNA sequencing. Analysis showed that 755 protein-coding genes were differentially regulated between unstimulated and anti-mMPO IgG–treated WT mouse neutrophils (cutoffs of adjusted $P < 0.05$ and $\log_2$ fold change >1). Among these protein-coding genes, 502 were transcriptionally repressed and 253 were up-regulated in anti-mMPO IgG–treated neutrophils versus results shown in unstimulated neutrophils (Supplementary Figure 3C and Supplementary Table 2, available on the *Arthritis & Rheumatology* website at https://onlinelibrary.wiley.com/doi/10.1002/art.42314).

Next, we compared anti-mMPO IgG–treated WT mouse neutrophils with anti-mMPO IgG–treated *CypD*$^{-/-}$ neutrophils. Among 818 genes differentially regulated between mMPO-IgG–treated WT and *CypD*$^{-/-}$ neutrophils, 660 genes were transcriptionally up-regulated and 158 were down-regulated in mMPO-IgG–treated *CypD*$^{-/-}$ neutrophils compared with that shown in mMPO-IgG–treated WT mouse neutrophils (Figure 2D and Supplementary Table 3, available on the *Arthritis &*

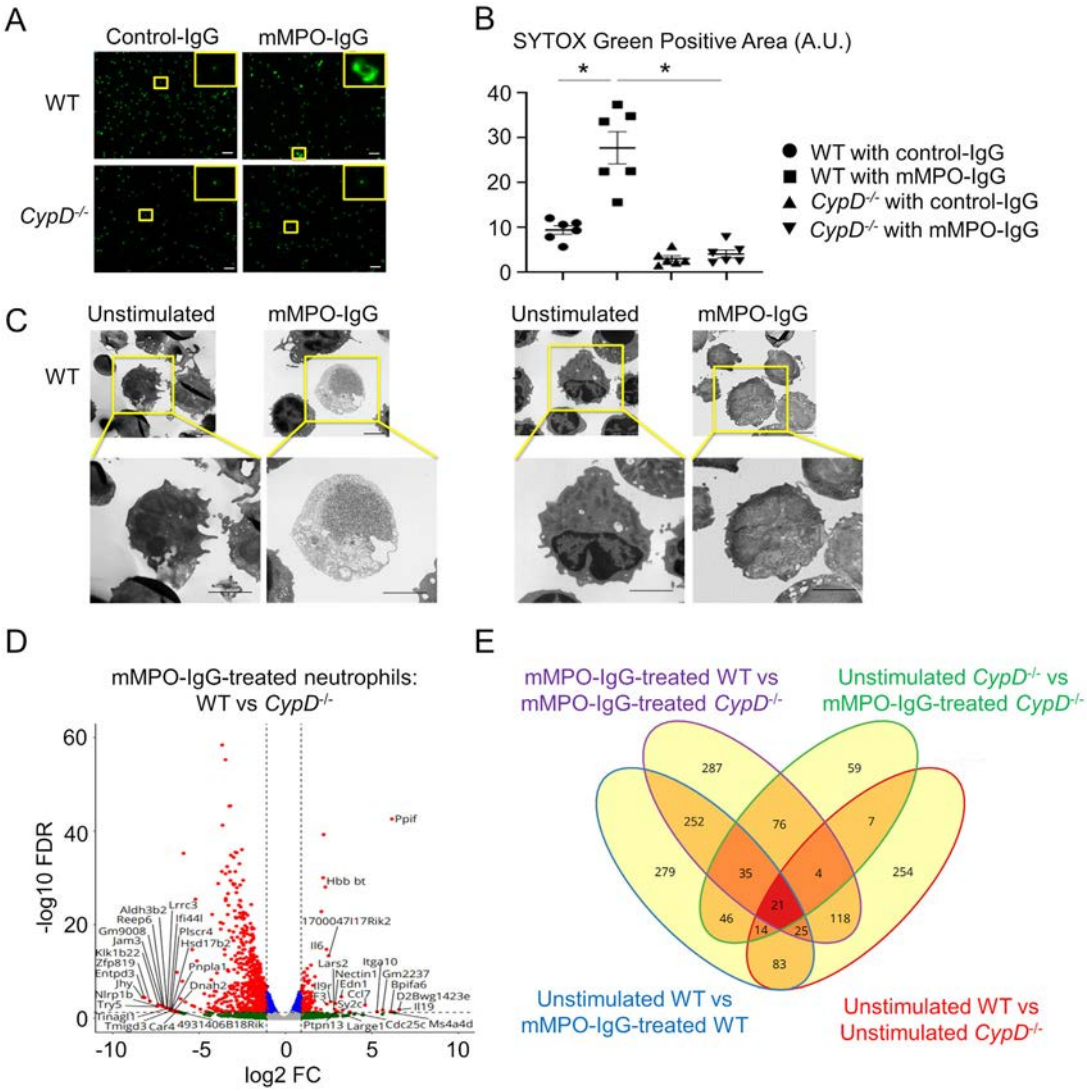

Figure 2. In vitro effects of ANCA-induced NET formation in mouse neutrophils by genetic ablation of CypD. **A** and **B**, Images (**A**) and quantification (**B**) of Sytox green immunofluorescence staining for NET formation in neutrophils isolated from *CypD*$^{-/-}$ mice or wild-type (WT) mice, after treatment with anti-mouse myeloperoxidase (anti-mMPO) IgG or control mouse IgG. In **A**, boxed areas display magnified areas of Sytox green–positive cells. Bars = 100 μm. In **B**, symbols represent individual samples; bars show the mean ± SEM on 2 low-power fields. * = $P < 0.05$ by one-way analysis of variance with post hoc Tukey's test. **C**, Transmission electron microscopy analyses of cell death in cultures of neutrophils from WT mice (left) or *CypD*$^{-/-}$ mice (right) left unstimulated or stimulated with anti-mMPO IgG. Boxed areas in top panels are shown at higher magnification than in the lower panels. Bars = 2 μm. **D**, Volcano plots of gene expression in neutrophils from WT mice versus neutrophils from *CypD*$^{-/-}$ mice after treatment with anti-mMPO IgG. Protein-coding genes that passed the thresholds for false discovery rate (FDR) and $\log_2$ fold change (FC) relative to values in WT mice (FDR < 0.05 and $\log_2$ FC > 1) were plotted in red; the top 20 genes by $\log_2$ FC are labeled. Dotted vertical lines indicate the threshold defining up-regulated or down-regulated genes. **E**, Venn diagram showing the number of protein-coding genes significantly up-regulated or down-regulated in neutrophils from WT mice or *CypD*$^{-/-}$ mice left unstimulated or stimulated with anti-mMPO IgG. See Figure 1 for other definitions. Color figure can be viewed in the online issue, which is available at http://onlinelibrary.wiley.com/doi/10.1002/art.42314/abstract.

Rheumatology website at https://onlinelibrary.wiley.com/doi/10.1002/art.42314). Only 5.1% of the down-regulated genes and 33.4% of the up-regulated genes overlapped between unstimulated WT and anti-mMPO IgG–treated *CypD*$^{-/-}$ mouse neutrophils compared with anti-mMPO IgG–treated WT mouse neutrophils (Figure 2E). Upstream analysis of differential gene expression using Ingenuity Pathway Analysis (based on a significance level of $\log_2$-adjusted $P < 0.05$ by Fisher's exact test) revealed DEGs to be significantly enriched in 223 canonical pathways in the mMPO IgG–treated WT mouse neutrophils (the top 20 enriched terms/pathways are shown in Supplementary Figure 3D).

Experiments using ANCA stimulation of mouse neutrophils revealed the relevance of immunologic responses, including high mobility group box chromosomal protein 1 (HMGB-1) signaling, the STAT3 pathway, and the production of ROS, which are involved in CypD-mediated mPTP opening and its related

necrosis. In neutrophils from mice with CypD deficiency compared with neutrophils from WT mice, ANCA stimulation mitigated these processes via the regulation of proinflammatory responses. Necrotic cells released HMGB-1 as a damage-associated molecular pattern. Importantly, in HMGB-1 signaling, proinflammatory DEGs, including *TNF, IL6, IL1A*, and *IFNG*, were found to be elevated in anti-mMPO IgG–treated WT mouse neutrophils, whereas disruption of CypD lowered the expression of these genes (Supplementary Figure 3E).

Because cytokines are known to affect the STAT3 pathway, controlling inflammation and mPTP opening (33), we examined the STAT3 pathway in WT mouse neutrophils and found DEGs of the cytokine-producing SH2 domain, which contains cytokine receptors, including interleukin-1 receptor type I (IL1RI) and interleukin-1α (IL1A), to be up-regulated by anti-mMPO IgG treatment; however, CypD deficiency ameliorated these activations (Supplementary Figure 3F). Inflammation and necrosis led to ROS production. The DEGs of S100A8 and SIRPA, which inhibit neutrophil oxidative metabolism (34) and NADPH oxidase (35), respectively, were down-regulated in anti-mMPO IgG–treated WT mouse neutrophils, whereas the deletion of CypD counteracted these suppressive effects (Supplementary Figure 3G).

Furthermore, in cultures of anti-mMPO IgG–treated WT mouse neutrophils stimulated with ANCA compared with anti-mMPO IgG–treated WT mouse neutrophils left unstimulated, upstream analysis revealed several mechanistic networks involved in NET formation, including intracellular calcium as an activator (Z score 2.842, $P = 9.55 \times 10^{-13}$) and CSA (CypD inhibitor) as a regulator (Z score 2.326, $P = 1.50 \times 10^{-12}$) (Supplementary Figure 3H). Intracellular calcium affected interleukin and ERK signaling as an activator (Supplementary Figure 3I), whereas CSA regulated Jnk and ERK1/2 signaling as a suppressor (Supplementary Figure 3J) during ANCA stimulation. These observations supported the notion that ANCA-treated neutrophil reactions were closely involved in CypD-mediated mPTP opening, which affected inflammation and necrosis in AAV.

Next, to elucidate the off-target effects of CypD on neutrophil physiology, the number of neutrophils and the MPO expression in *CypD*$^{-/-}$ mice were evaluated. In the cell count and FCM analysis, we found that CypD deficiency did not influence the number of white blood cells, including neutrophils, or the surface MPO expression (Supplementary Figures 4A–4C, available on the *Arthritis & Rheumatology* website at https://onlinelibrary.wiley.com/doi/10.1002/art.42314). Although anti-mMPO IgG–treated neutrophils showed massive NETs compared with control IgG–treated neutrophils, the difference in gene expression between the 2 groups was small (data shown in DNA Data Bank of Japan), indicating that ANCA-induced NETs would be driven by posttranslational modification rather than transcriptional gene expression.

CypD genetic ablation improved lung and kidney injury in the passive AAV mouse model. Because pharmacologic inhibition and genetic deficiency of CypD suppressed NET formation and endothelial injury in vitro, we next examined the role of CypD in 2 murine AAV models. First, we induced a passive anti-MPO IgG transfer (passive AAV) model in *CypD*$^{+/+}$ or *CypD*$^{-/-}$ mice. Passive AAV *CypD*$^{+/+}$ mice demonstrated renal dysfunction, hematuria, and histologic changes, including crescentic glomerulonephritis and pulmonary hemorrhage; however, injection of control serum in *CypD*$^{+/+}$ mice did not result in any remarkable findings. In *CypD*$^{-/-}$ mice, we observed recovery of these vasculitis-related features (Figures 3A–D). Albuminuria in the 2 groups (146 ± 55.2 mg/mg Cr in *CypD*$^{+/+}$ mice versus 152 ± 54.4 mg/mg Cr in *CypD*$^{-/-}$ mice, $P = 0.92$) did not differ significantly. Moreover, TUNEL staining revealed that necrosis in the kidneys and lungs of the *CypD*$^{-/-}$ mice was significantly reduced compared with that shown in the *CypD*$^{+/+}$ mice (Figures 3C and 3D). TUNEL-positive cells were identical to the lesions of glomerulonephritis identified by periodic acid–Schiff staining (Figure 3E). Cytochrome c in kidney tissues of passive AAV *CypD*$^{+/+}$ mice showed high expression, but this signal was reduced in CypD-deficient mice (Figure 3F).

Next, we investigated whether CypD deficiency altered NET formation in vivo. FCM analysis revealed that NETs in the peripheral blood of passive AAV *CypD*$^{+/+}$ mice were increased compared with that shown in the control IgG transfer *CypD*$^{+/+}$ mice (data not shown), with CypD deficiency reducing NETs in peripheral blood (Figures 4A and 4B). In contrast, the increased CitH3 and PAD4 expression levels, when colocalized with the neutrophil marker (Ly6b) in kidneys of passive AAV transfer mice, were not influenced by CypD deficiency, indicating that CypD controls NET formation without the inhibition of histone citrullination and PAD4 activation (Figures 4C and 4D). Accordingly, in the passive AAV model, CD31 expression was decreased in the glomeruli of *CypD*$^{+/+}$ mice but was observed to be retained at normal levels in the glomeruli of *CypD*$^{-/-}$ mice (Figures 4E and 4F), suggesting that CypD might be involved in the endothelial injury of AAV. Together, our data indicate that genetic ablation of CypD ameliorated autoimmune necrotizing vasculitis by suppressing CypD-mPTP–dependent NETosis and endothelial injury.

Protection of CypD-deficient mice from spontaneous development of vasculitis without suppression of ANCA production. Given the protective effects of CypD deficiency in the passive AAV model, we used spontaneous crescentic glomerulonephritis–forming/Kinjoh (SCG/Kj) mice, which develop systemic necrotizing vasculitis with ANCA production (36). In SCG/Kj mice with CypD deficiency, renal dysfunction, hematuria, and histologic damage in the glomeruli were ameliorated (Figures 5A–D). We detected TUNEL-positive cells in the glomeruli and lung capillaries; notably, some of these necrotic cells were MPO-positive neutrophils (Supplementary Figures 5A and 5B, available on the *Arthritis & Rheumatology* website at https://onlinelibrary.wiley.com/doi/10.1002/art.42314).

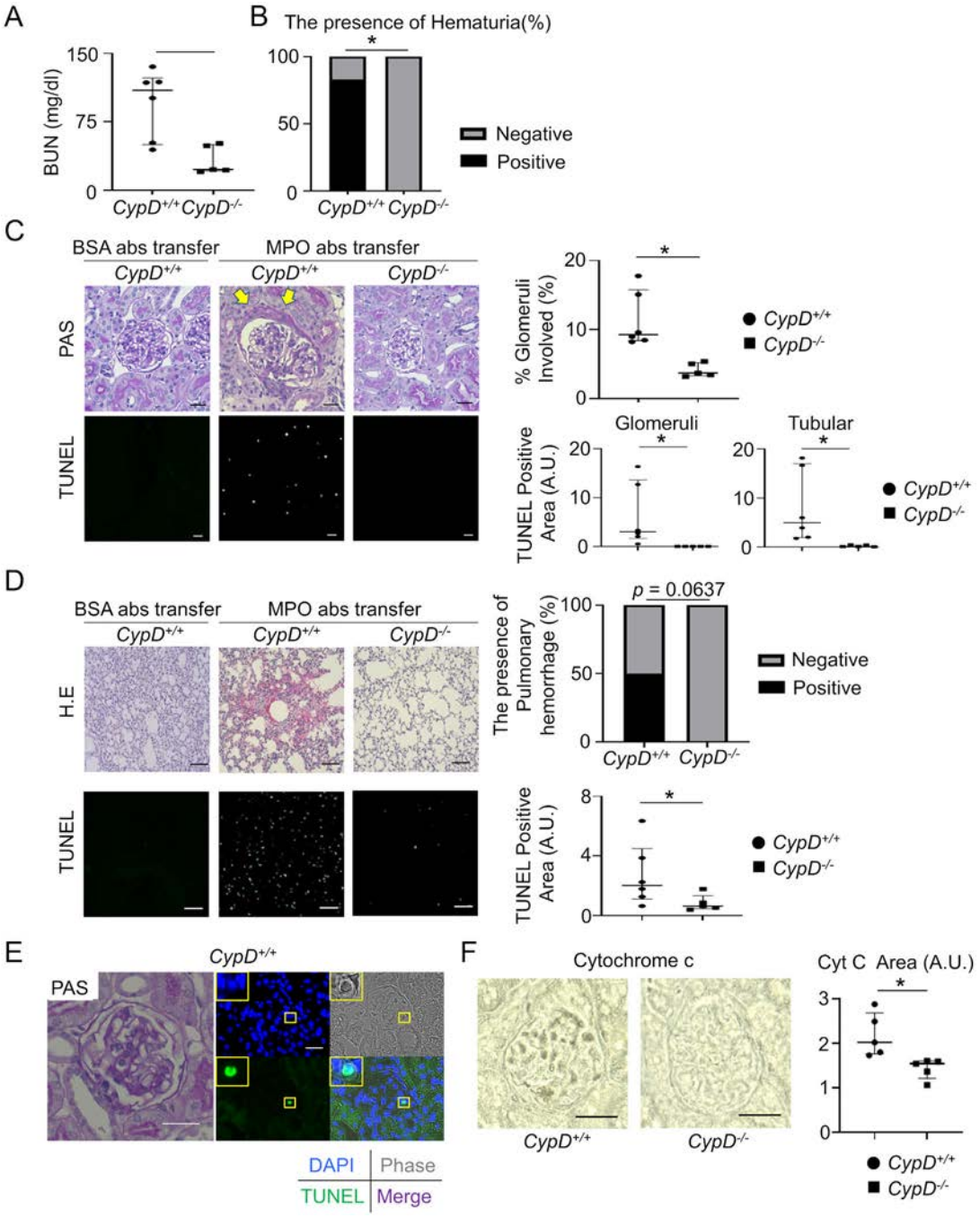

Figure 3. Effects of in vivo genetic ablation of CypD on kidney and lung injury in mice in the passive anti-MPO IgG antibody (Abs) transfer model of AAV. **A** and **B**, Renal function according to blood urea nitrogen (BUN) levels (**A**) and presence versus absence of hematuria (**B**) in 6 *CypD*$^{+/+}$ and 5 *CypD*$^{-/-}$ mice. * = $P < 0.05$ by chi-square test. **C**, Left, Periodic acid–Schiff (PAS) staining (top; **arrows** indicating crescents) and TUNEL staining (bottom) of kidney tissue from *CypD*$^{+/+}$ and *CypD*$^{-/-}$ mice in the passive AAV model versus mice in the control BSA antibody transfer model. Bars = 20 μm (top) and 50 μm (bottom). Right, Quantification of the results as percentage of involved glomeruli and TUNEL-positive area based on mean luminance value on 5 low-power fields per sample. **D**, Left, Hematoxylin and eosin (HE) staining (top) and TUNEL staining (bottom) of lung tissue from *CypD*$^{+/+}$ and *CypD*$^{-/-}$ mice in each model. Bars = 200 μm. Right, Quantification of the results as percentage of samples showing pulmonary hemorrhage and the TUNEL-positive area based on mean luminance value on 5 low-power fields per sample. In **C** and **D**, symbols represent individual samples; bars show the median with interquartile range. * = $P < 0.05$ by Mann-Whitney U test. **E**, PAS and TUNEL staining of consecutive sections of kidney tissue from a representative *CypD*$^{+/+}$ mouse. TUNEL staining shows cell necrosis (green) (nuclei counterstained with DAPI; phase contrast in gray). **Insets** are higher-magnification views of the boxed areas. Bars = 20 μm. **F**, Left, Immunostaining for cytochrome c (Cyt C) in kidney tissue from a *CypD*$^{+/+}$ and *CypD*$^{-/-}$ mouse using the avidin–biotin–peroxidase complex method. Bars = 20 μm. Right, Quantification of cytochrome c–positive areas as the mean luminance value of 10 high-power fields per sample from *CypD*$^{+/+}$ and *CypD*$^{-/-}$ mice. Symbols represent individual mice; bars show the median and interquartile range. See Figure 1 for other definitions. Color figure can be viewed in the online issue, which is available at http://onlinelibrary.wiley.com/doi/10.1002/art.42314/abstract.

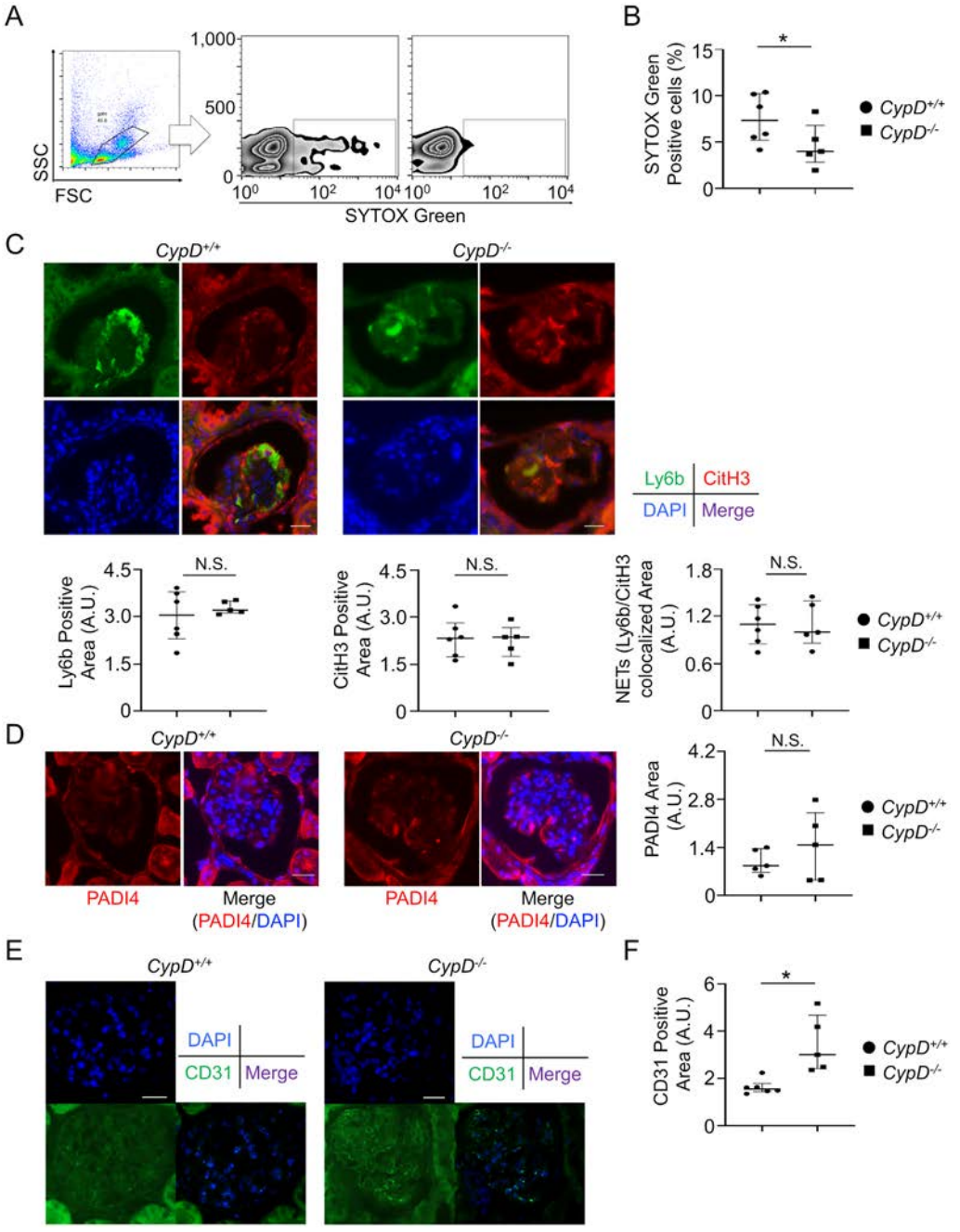

Figure 4. Effect of in vivo genetic ablation of CypD on mitochondrial permeability transition pore–induced cell death in mice with anti-MPO antibody–induced AAV (the passive transfer model). **A**, Flow cytometry scatter plot showing the granulocyte fraction from mouse peripheral blood (left) and contour plots of Sytox green immunofluorescence analyses of peripheral blood from a *CypD*$^{+/+}$ mouse (middle) and a *CypD*$^{-/-}$ mouse (right). **B**, Quantification of Sytox green immunofluorescence analyses of cell death among neutrophils from *CypD*$^{+/+}$ and *CypD*$^{-/-}$ mice. **C,** Top, Left, Immunofluorescence staining for CitH3 and Ly6b in *CypD*$^{+/+}$ and *CypD*$^{-/-}$ mouse kidney tissue. Nuclei were counterstained with DAPI. Bars = 20 μm. Bottom, Quantification of the results as areas staining positive for CitH3 and Ly6b (left) and as areas of NET formation in mouse glomeruli (mean area of 5 low-power fields) (right). **D**, Left, Immunofluorescence staining for PADI4 in *CypD*$^{+/+}$ and *CypD*$^{-/-}$ mouse kidney tissue. Right, Quantification of the results as areas staining positive for PADI4. **E** and **F**, Immunofluorescence staining for CD31 (**E**) and mean luminance value of CD31-positive areas in glomeruli (in 10 low-power fields per sample) in kidney tissue from *CypD*$^{+/+}$ and *CypD*$^{-/-}$ mice. Nuclei were counterstained with DAPI. Bars = 20 μm. In all graphs, symbols represent individual samples; bars show the median with interquartile range. * = $P < 0.05$ by Mann-Whitney U test. See Figure 1 for definitions. Color figure can be viewed in the online issue, which is available at http://onlinelibrary.wiley.com/doi/10.1002/art.42314/abstract.

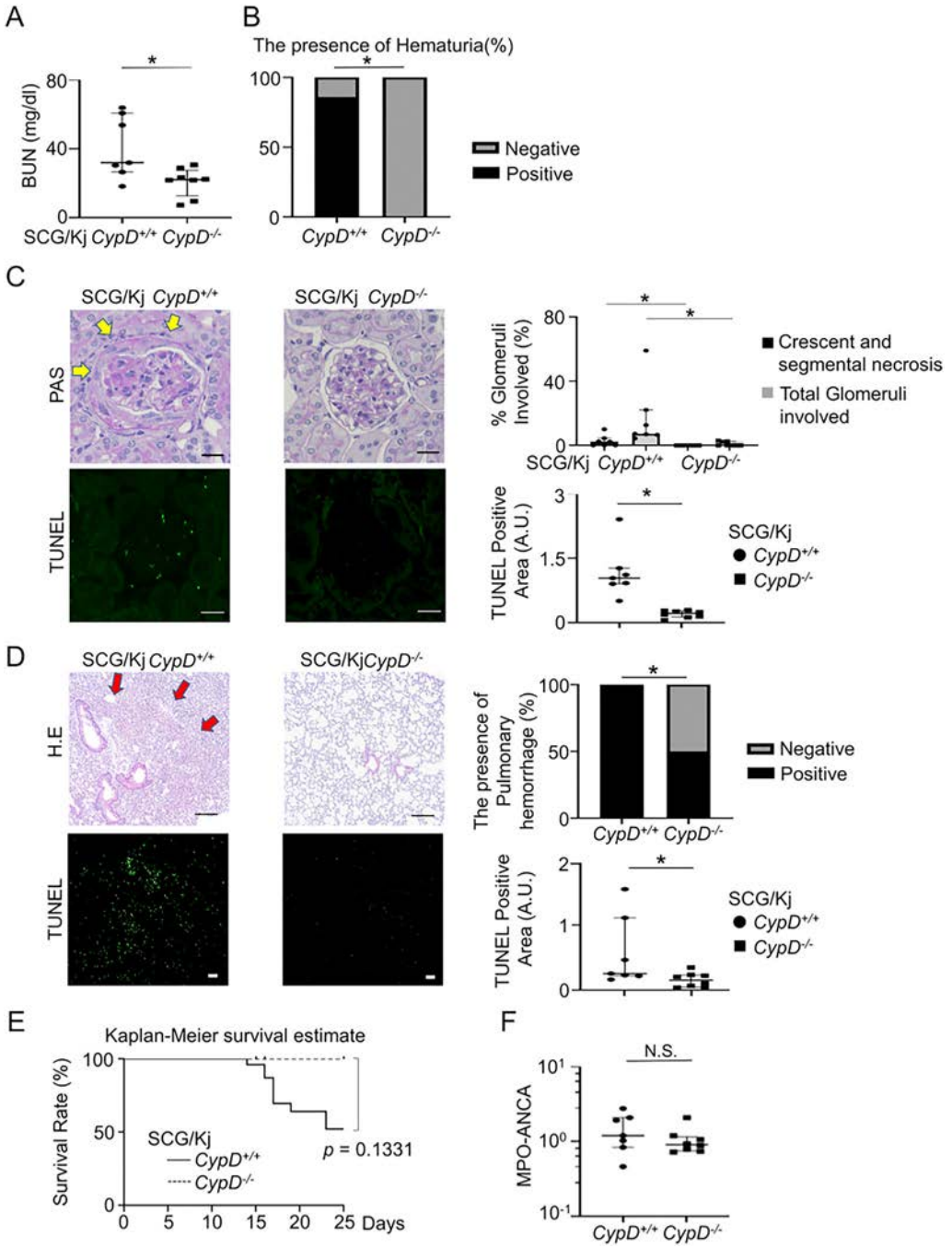

Figure 5. Effect of in vivo genetic ablation of CypD on kidney and lung injury in Kinjoh mice with spontaneous crescentic glomerulonephritis (SCG/Kj; spontaneous AAV model). **A** and **B**, Renal function according to BUN levels (**A**) and presence versus absence of hematuria (**B**) in 7 $CypD^{+/+}$ and 8 $CypD^{-/-}$ mice. * = $P < 0.05$ by Mann-Whitney U test in **A** and by chi-square test in **B**. **C**, Left, PAS staining (top; **arrows** indicating crescents) and TUNEL staining (bottom) of kidney tissue from $CypD^{+/+}$ and $CypD^{-/-}$ mice. Bars = 20 μm. Right, Quantification of the results as percentage of involved glomeruli and TUNEL-positive area (mean luminance values on 5 low-power fields per sample). **D**, Left, Hematoxylin and eosin (HE) staining (top; **arrows** indicating areas of hemorrhage) and TUNEL staining (bottom) of lung tissue from $CypD^{+/+}$ and $CypD^{-/-}$ mice. Bars = 200 μm. Right, Quantification of the results as percentage of samples showing pulmonary hemorrhage and TUNEL-positive area (mean luminance value on 5 low-power fields per sample). * = $P < 0.05$ by Mann-Whitney U test. **E**, Kaplan-Meier survival curves showing 25-day overall survival rate in $CypD^{+/+}$ and $CypD^{-/-}$ mice. **F**, MPO-ANCA titers (in μg/ml) in $CypD^{+/+}$ and $CypD^{-/-}$ mice, as determined by enzyme-linked immunosorbent assay. Logarithmically transformed values are shown. In all graphs, symbols represent individual samples; bars show the median with interquartile range. See Figures 1 and 3 for other definitions. Color figure can be viewed in the online issue, which is available at http://onlinelibrary.wiley.com/doi/10.1002/art.42314/abstract.

CypD deficiency did not influence the infiltration of neutrophils and the expression of CitH3 in glomeruli but improved endothelial injury, similar to findings shown in passive AAV mice (Supplementary Figures 5C–5F, available at https://onlinelibrary.wiley.com/doi/10.1002/art.42314).

Moreover, Kaplan-Meier analysis revealed that CypD deficiency improved the survival of SCG/Kj mice (Figure 5E). We also measured levels of ANCA and anti–double-stranded DNA antibodies to determine whether CypD genetic ablation influenced autoimmunity. There were no differences in the titers of ANCA between *CypD*$^{+/+}$ and *CypD*$^{-/-}$ mice (Figure 5F), implying that CypD regulated the necrosis of vasculitis in situ as a downstream process mediating the development and progression of AAV, independent of autoantibody production.

DISCUSSION

Herein, we demonstrated that necrosis occurred in tissues of patients with AAV and found that CypD genetic deletion reduced organ damage by inhibiting CypD-mediated necrosis in 2 types of murine AAV models. Moreover, CypD genetic ablation and pharmacologic blockade suppressed ANCA-mediated NET formation, and the findings from comprehensive RNA-sequencing analysis confirmed that CypD plays a role in ANCA-mediated inflammation and NETosis. Pathologically, AAV is a form of necrotizing vasculitis caused by excessive neutrophil activation and endothelial injury. ANCAs or humoral factors may provide misleading information to neutrophils, indicating an emergency, such as sepsis, leading to intravascular NET formation and endothelial injuries and consequently resulting in necrotizing vasculitis, including crescentic glomerulonephritis and pulmonary hemorrhage (37). Mechanistically, neutrophils are primed by proinflammatory cytokines, including TNF, and express ANCA antigens (such as MPO) on the cell surface. AAV-IgG (MPO-ANCA) binds to MPO, promoting the production of ROS and subsequently forming NETs (38).

Schreiber et al (28) reported that receptor-interacting protein kinase 3 and mixed-lineage kinase domain–like (MLKL)–mediated necroptosis regulates NET formation and endothelial damage in AAV. Recent studies indicated that, in general, CypD-mPTP interacts with necroptosis (39) and that necroptosis signals drive endoplasmic reticulum stress mechanistically, increasing intracellular calcium and consequently leading to mPTP opening and cell necrosis (40). Another important molecule, PAD4, induces NETs via chromatin decondensation (41), which has been reported to be essential for ANCA-induced NET formation (37,42). The pathways leading to NETosis, including ROS activation, necroptosis signaling (via receptor-interacting serine/threonine protein kinase-MLKL), and histone citrullination (via PAD4) can be closely intertwined (43), and it is hard to consider each pathway separately.

In our in vitro study, we showed that CypD inhibition suppressed ANCA-induced NET formation without influencing PAD4-mediated histone citrullination, indicating that CypD acts downstream or is independent of the PAD4 signaling pathway. Notably, our electron microscopic analysis of ANCA-induced NETs revealed that the cytoplasmic components appeared to invaginate into the nuclear membrane with decondensed chromatin and that CypD genetic deletion canceled the invagination, resulting in the maintenance of cytomorphology. These findings suggest that, during ANCA-induced NET formation, CypD-mPTP opening might induce cellular and nuclear membrane vulnerability via the release of mitochondrial components, including mitoROS, independent of chromatin decondensation.

With comprehensive RNA-sequencing analysis of ANCA-treated murine neutrophils, we found that canonical pathways, including HMGB-1 signaling, the STAT3 pathway, and ROS production, were involved and that disruption of CypD altered the activated or suppressed signaling. Furthermore, our analysis of upstream regulation revealed the relevance of intracellular calcium and cyclosporin, indicating that CypD might be a regulator of ANCA-induced NETosis. We also found that CypD deficiency in SCG/Kj mice improved organ damage independent of the inhibition of ANCA production. Protective effects of CypD inhibition on acute kidney injury were shown to be caused by the regulation of cell death, apart from immunologic effects (13), indicating that targeting CypD might ameliorate necrotizing vasculitis without inducing immunosuppression.

Existing standard AAV therapies mainly target acquired immunity as the primary process of the disease. However, these treatments do not affect necrotizing lesions and focal inflammation in situ, which can result in longitudinal organ dysfunction, including chronic kidney disease and neuropathy. Furthermore, standard therapies can have adverse effects, including lethal infection from overimmunosuppression and metabolic disorders (44). To prevent these issues, CypD targeting could potentially improve necrotizing vasculitis by the regulation of NETs and endothelial injury as a novel and different approach. CSA, which inhibits CypD, is widely used as an immunosuppressant against activated T cells in the clinical setting. Several case series have shown the efficacy of CSA in patients with vasculitis (45,46), but the evidence is lacking because the pathogenesis of AAV is mainly thought to be caused by B cell–mediated autoimmunity, including ANCA production, and CSA itself has side effects, especially renal dysfunction when administered at high doses. The cumulative in vitro data, including ours, stipulate that the effective concentration of CSA for mPTP opening is smaller than that for the regulation of T cell immunity; therefore, low-dose CSA may prevent tissue necrosis without overimmunosuppression.

Our study has several limitations. RNA-sequencing analysis of neutrophils revealed that anti-MPO IgG–treated neutrophils did not show significant transcriptional changes compared with the control IgG–treated neutrophils, although there were

morphologic changes between the 2 sets of neutrophils, implying the possibility that 1) in this assay, TNF might exceed the threshold of neutrophil activation influenced by anti-MPO IgG and 2) anti-MPO IgG–mediated NET formation might predominantly develop via posttranslational modification. Meanwhile, most mature neutrophils are transcriptionally inactive; thus, future studies, including proteomics analysis, should follow our data. Moreover, we did not observe a cell- or a tissue-specific role of CypD in the AAV mouse model; our in vitro model showed a role of CypD in neutrophils and endothelium. In summary, CypD-dependent necrosis was involved in ANCA-mediated NET formation and subsequent endothelial injury in AAV. Targeting CypD might be a novel therapeutic strategy for AAV via the regulation of focal necrotizing vasculitis.

ACKNOWLEDGMENTS

We thank the staff of the Institute for Animal Facility, Faculty of Medicine and Graduate School of Medicine, Hokkaido University. We also thank the staff from Editage Group for editing a draft of this manuscript.

AUTHOR CONTRIBUTIONS

All authors were involved in drafting the article or revising it critically for important intellectual content, and all authors approved the final version to be published. Dr. Kudo had full access to all of the data in the study and takes responsibility for the integrity of the data and the accuracy of the data analysis.

Study conception and design. Kudo, Nakazawa, Ishizu.

Acquisition of data. Kudo, Nakazawa, Watanabe-Kusunoki, Kanda, Shiratori-Aso, Abe, Nishio, Koga, Iwasaki, Tsuji, Fukasawa, Yamasaki, Watanabe, Masuda, Tomaru, Murakami, Aratani, Ishizu, Atsumi.

Analysis and interpretation of data. Kudo, Nakazawa, Kanda, Shiratori-Aso, Ishizu, Atsumi.

REFERENCES

1. Nakazawa D, Masuda S, Tomaru U, et al. Pathogenesis and therapeutic interventions for ANCA-associated vasculitis. Nat Rev Rheumatol 2019;15:91–101.
2. Papayannopoulos V. Neutrophil extracellular traps in immunity and disease. Nat Rev Immunol 2018;18:134–147.
3. Watanabe-Kusunoki K, Nakazawa D, Kusunoki Y, et al. Recombinant thrombomodulin ameliorates autoimmune vasculitis via immune response regulation and tissue injury protection. J Autoimmun 2020; 108:102390.
4. Urban CF, Reichard U, Brinkmann V, et al. Neutrophil extracellular traps capture and kill Candida albicans yeast and hyphal forms. Cell Microbiol 2006;8:668–76.
5. Saitoh T, Komano J, Saitoh Y, et al. Neutrophil extracellular traps mediate a host defense response to human immunodeficiency virus-1. Cell Host Microbe 2012;12:109–16.
6. Abdallah DS, Lin C, Ball CJ, et al. Toxoplasma gondii triggers release of human and mouse neutrophil extracellular traps. Infect Immun 2012;80:768–77.
7. Scorrano L, Ashiya M, Buttle K, et al. A distinct pathway remodels mitochondrial cristae and mobilizes cytochrome c during apoptosis. Dev Cell 2002;2:55–67.
8. Jackson SP, Schoenwaelder SM. Procoagulant platelets:are they necrotic? Blood 2010;116:2011–8.
9. Javadov S, Kuznetsov A. Mitochondrial permeability transition and cell death: the role of cyclophilin D. Front Physiol 2013;4:76.
10. Schinzel AC, Takeuchi O, Huang Z, et al. Cyclophilin D is a component of mitochondrial permeability transition and mediates neuronal cell death after focal cerebral ischemia. Proc Natl Acad Sci U S A 2005; 102:12005–10.
11. Baines CP, Kaiser RA, Purcell NH, et al. Loss of cyclophilin D reveals a critical role for mitochondrial permeability transition in cell death. Nature 2005;434:658–62.
12. Nakagawa T, Shimizu S, Watanabe T, et al. Cyclophilin D-dependent mitochondrial permeability transition regulates some necrotic but not apoptotic cell death. Nature 2005;434:652–8.
13. Linkermann A, Bräsen JH, Darding M, et al. Two independent pathways of regulated necrosis mediate ischemia-reperfusion injury. Proc Natl Acad Sci U S A 2013;110:12024–9.
14. Linkermann A, Skouta R, Himmerkus N, et al. Synchronized renal tubular cell death involves ferroptosis. Proc Natl Acad Sci U S A 2014;111:16836–41.
15. Nakazawa D, Kumar SV, Marschner J, et al. Histones and neutrophil extracellular traps enhance tubular necrosis and remote organ injury in ischemic AKI. J Am Soc Nephrol 2017;28:1753–68.
16. Devalaraja-Narashimha K, Diener AM, Padanilam BJ. Cyclophilin D gene ablation protects mice from ischemic renal injury. Am J Physiol Renal Physiol 2009;297:F749–59.
17. Kuhns DB, Priel DA, Chu J, et al. Isolation and functional analysis of human neutrophils. Curr Protoc Immunol 2015;111:7.23.21–16.
18. Bolger AM, Lohse M, Usadel B. Trimmomatic: a flexible trimmer for Illumina sequence data. Bioinformatics 2014;30:2114–20.
19. Kim D, Langmead B, Salzberg SL. HISAT: a fast spliced aligner with low memory requirements. Nat Methods 2015;12:357–60.
20. Liao Y, Smyth GK, Shi W. featureCounts: an efficient general purpose program for assigning sequence reads to genomic features. Bioinformatics 2014;30:923–30.
21. Love MI, Huber W, Anders S. Moderated estimation of fold change and dispersion for RNA-seq data with DESeq2. Genome Biol 2014; 15:550.
22. Kolberg L, Raudvere U, Kuzmin I, et al. gprofiler2—an R package for gene list functional enrichment analysis and namespace conversion toolset g:Profiler. F1000Res 2020;9:ELIXIR-709.
23. Howe EA, Sinha R, Schlauch D, et al. RNA-Seq analysis in MeV. Bioinformatics 2011;27:3209–10.
24. Jerke U, Hernandez DP, Beaudette P, et al. Neutrophil serine proteases exert proteolytic activity on endothelial cells. Kidney Int 2015; 88:764–75.
25. Yamasaki M, Miyazaki T, Azechi H, et al. Glutamate receptor δ2 is essential for input pathway-dependent regulation of synaptic AMPAR contents in cerebellar Purkinje cells. J Neurosci 2011;31:3362–74.
26. Fuchs TA, Abed U, Goosmann C, et al. Novel cell death program leads to neutrophil extracellular traps. J Cell Biol 2007;176:231–41.
27. Soria González JE, Orea Solano M. Apoptosis. Rev Alerg Mex 2002; 49:121–8. In German.
28. Schreiber A, Rousselle A, Becker JU, et al. Necroptosis controls NET generation and mediates complement activation, endothelial damage, and autoimmune vasculitis. Proc Natl Acad Sci U S A 2017;114: E9618–25.
29. Grayson PC, Kaplan MJ. At the bench: neutrophil extracellular traps (NETs) highlight novel aspects of innate immune system involvement in autoimmune diseases. J Leukoc Biol 2016;99:253–64.

30. Jennette JC, Falk RJ. Pathogenesis of antineutrophil cytoplasmic autoantibody-mediated disease. Nat Rev Rheumatol 2014;10: 463–73.
31. Al-Hussain T, Hussein MH, Conca W, et al. Pathophysiology of ANCA-associated vasculitis. Adv Anat Pathol 2017;24:226–34.
32. Moore CL, Savenka AV, Basnakian AG. TUNEL assay: a powerful tool for kidney injury evaluation. Int J Mol Sci 2021;22:412.
33. Miura T, Tanno M. The mPTP and its regulatory proteins: final common targets of signalling pathways for protection against necrosis. Cardiovasc Res 2012;94:181–9.
34. Sroussi HY, Lu Y, Zhang QL, et al. S100A8 and S100A9 inhibit neutrophil oxidative metabolism in-vitro: involvement of adenosine metabolites. Free Radic Res 2010;44:389–96.
35. Van Beek EM, Zarate JA, van Bruggen R, et al. SIRPα controls the activity of the phagocyte NADPH oxidase by restricting the expression of gp91(phox). Cell Rep 2012;2:748–55.
36. Neumann I, Birck R, Newman M, et al. SCG/Kinjoh mice: a model of ANCA-associated crescentic glomerulonephritis with immune deposits. Kidney Int 2003;64:140–8.
37. Van Dam LS, Kraaij T, Kamerling SW, et al. Intrinsically distinct role of neutrophil extracellular trap formation in antineutrophil cytoplasmic antibody-associated vasculitis compared to systemic lupus erythematosus. Arthritis Rheumatol 2019;71:2047–58.
38. Flint J, Morgan MD, Savage CO. Pathogenesis of ANCA-associated vasculitis. Rheum Dis Clin North Am 2010;36:463–77.
39. Karch J, Kanisicak O, Brody MJ, et al. Necroptosis interfaces with MOMP and the MPTP in mediating cell death. PLoS One 2015;10: e0130520.
40. Zhu P, Hu S, Jin Q, et al. Ripk3 promotes ER stress-induced necroptosis in cardiac IR injury: a mechanism involving calcium overload/ XO/ROS/mPTP pathway. Redox Biol 2018;16:57–168.
41. Li P, Li M, Lindberg MR, et al. PAD4 is essential for antibacterial innate immunity mediated by neutrophil extracellular traps. J Exp Med 2010; 207:1853–62.
42. Kusunoki Y, Nakazawa D, Shida H, et al. Peptidylarginine deiminase inhibitor suppresses neutrophil extracellular trap formation and MPO-ANCA production. Front Immunol 2016;7:227.
43. Vorobjeva NV, Chernyak BV. NETosis: molecular mechanisms, role in physiology and pathology. Biochemistry (Mosc) 2020;85:1178–90.
44. Thomas K, Vassilopoulos D. Infections and vasculitis. Curr Opin Rheumatol 2017;29:17–23.
45. Haubitz M, Koch KM, Brunkhorst R. Cyclosporin for the prevention of disease reactivation in relapsing ANCA-associated vasculitis. Nephrol Dial Transplant 1998;13:2074–6.
46. Ghez D, Westeel PF, Henry I, et al. Control of a relapse and induction of long-term remission of Wegener's granulomatosis by cyclosporine. Am J Kidney Dis 2002;40:E6.

Arthritis & Rheumatology
Vol. 75, No. 1, January 2023, pp 84–97
DOI 10.1002/art.42321

American College of Rheumatology
Empowering Rheumatology Professionals

Syk Activation in Circulating and Tissue Innate Immune Cells in Antineutrophil Cytoplasmic Antibody–Associated Vasculitis

Maria Prendecki,[1] Kavita Gulati,[1] Noelle Pisacano,[2] Damilola Pinheiro,[3] Tejal Bhatt,[3] Marie-Anne Mawhin,[3] Frederic Toulza,[3] Esteban S. Masuda,[4] Andrew Cowburn,[2] Katharine M. Lodge,[2] Frederick W. K. Tam,[1] Candice Roufosse,[3] Charles D. Pusey,[1] and Stephen P. McAdoo[1]

Objective. Syk is a cytoplasmic protein tyrosine kinase that plays a role in signaling via B cell and Fc receptors (FcR). FcR engagement and signaling via Syk is thought to be important in antineutrophil cytoplasm antibody (ANCA) IgG–mediated neutrophil activation. This study was undertaken to investigate the role of Syk in ANCA-induced myeloid cell activation and vasculitis pathogenesis.

Methods. Phosphorylation of Syk in myeloid cells from healthy controls and ANCA-associated vasculitis (AAV) patients was analyzed using flow cytometry. The effect of Syk inhibition on myeloperoxidase (MPO)–ANCA IgG activation of cells was investigated using functional assays (interleukin-8 and reactive oxygen species production) and targeted gene analysis with NanoString. Total and phosphorylated Syk at sites of tissue inflammation in patients with AAV was assessed using immunohistochemistry and RNAscope in situ hybridization.

Results. We identified increased phosphorylated Syk at critical activatory tyrosine residues in blood neutrophils and monocytes from patients with active AAV compared to patients with disease in remission or healthy controls. Syk was phosphorylated in vitro following MPO-ANCA IgG stimulation, and Syk inhibition was able to prevent ANCA-mediated cellular responses. Using targeted gene expression analysis, we identified up-regulation of FcR- and Syk-dependent signaling pathways following MPO-ANCA IgG stimulation. Finally, we showed that Syk is expressed and phosphorylated in tissue leukocytes at sites of organ inflammation in AAV.

Conclusion. These findings indicate that Syk plays a critical role in MPO-ANCA IgG–induced myeloid cell responses and that Syk is activated in circulating immune cells and tissue immune cells in AAV; therefore, Syk inhibition may be a potential therapeutic option.

INTRODUCTION

Syk is a cytoplasmic protein tyrosine kinase that plays a role in signaling via classical immunoreceptors bearing immunoreceptor tyrosine–based activation motifs (ITAM), including B cell and activatory Fc receptors (FcR). As such, it is highly expressed in myeloid cells, where it is known to mediate important FcR-dependent inflammatory responses (1–3). The Syk protein has a multidomain structure, consisting of 2 SH2 domains and a C-terminal kinase domain (4). In the inactivated state, the C-terminal kinase domain is retained within a folded or "closed" tertiary structure. Following cell surface immunoreceptor ligation, ITAM serve as binding sites for Syk SH2 domains, resulting in auto- and transphosphorylation of Syk tyrosine residues,

Presented in abstract form at the 19th International Vasculitis and ANCA Workshop in Philadelphia, PA, in April 2019 (https://doi.org/10.1093/rheumatology/kez061.027).

Supported by the NIHR Imperial Biomedical Research Centre. Dr. Prendecki's work was supported by the Academy of Medical Sciences (grant SGL023/1071) and by an NIHR Clinical Lectureship. Dr. Tam's work was supported by the Ken and Mary Minton Chair of Renal Medicine. Dr. McAdoo's work was supported by Vasculitis UK and by an Imperial College Wellcome Trust ISSF Fellowship.

[1]Maria Prendecki, MBBS, PhD, Kavita Gulati, MBBCh, BAO, Frederick W.K. Tam, PhD, MBBChir, Charles D. Pusey, DSc, FMedSci, Stephen P. McAdoo, MBBS, PhD: Department of Immunology and Inflammation, Centre for Inflammatory Disease, Imperial College London, Hammersmith Campus, and Imperial College Renal and Transplant Centre, Imperial College Healthcare NHS Trust, Hammersmith Hospital, London, UK; [2]Noelle Pisacano, MSc, Andrew Cowburn, PhD, Katharine M. Lodge, PhD, MBBChir: National Heart and Lung Institute, Imperial College, London, UK; [3]Damilola Pinheiro, PhD, Tejal Bhatt, MSc, Marie-Anne Mawhin, PhD, Frederic Toulza, PhD, Candice Roufosse, MD, PhD: Department of Immunology and Inflammation, Centre for Inflammatory Disease, Imperial College London, Hammersmith Campus, London, UK; [4]Esteban S. Masuda, PhD: Rigel Pharmaceuticals, South San Francisco, California.

Author disclosures are available at https://onlinelibrary.wiley.com/action/downloadSupplement?doi=10.1002%2Fart.42321&file=art42321-sup-0001-Disclosureform.pdf.

Address correspondence via email to Prendecki, MBBS, PhD, at m.prendecki@imperial.ac.uk.

Submitted for publication November 23, 2021; accepted in revised form July 26, 2022.

conformational changes that release the enzymatically active kinase domain, and initiation of downstream signaling (5–7). Thus, Syk activity relies upon its phosphorylation status at multiple tyrosine residues, and phosphorylation at Y^{352} and Y^{348} has been shown to be essential for downstream Syk signaling (8–10).

In antineutrophil cytoplasm antibody (ANCA)–associated vasculitis (AAV), ANCA may contribute to disease pathogenesis via binding to their cognate antigens (proteinase 3 and myeloperoxidase [MPO]) on the surface of primed neutrophils and monocytes, resulting in cell activation and subsequent vascular injury (11,12). Both FcR engagement and autoantigen-specific binding via F(ab) are thought to be important in ANCA-mediated cell activation, with evidence for signaling through the low-affinity Fcγ receptor (FcγR) FcγRIIa (CD32A), on neutrophils and monocytes, leading to cell activation and for ANCA binding to FcγRIIIb (CD16B) (13–16). Syk is essential for FcγRIIa signaling, suggesting that it may have a role in ANCA-mediated activation of neutrophils and monocytes (3,17). It has previously been demonstrated that activation of neutrophils by ANCA results in phosphorylation of Syk and that this likely involves both FcγRIIa and FcγRIIIb (18).

We have previously shown that a small molecule kinase inhibitor with selectivity for Syk is an effective treatment for experimental models of vasculitis, although clinical evidence for Syk activation in AAV is lacking (19–21). In this study, we set out to establish whether Syk activation contributes to disease pathogenesis in humans and to identify if Syk inhibition is a viable therapeutic option for multisystem inflammation in AAV.

PATIENTS AND METHODS

Detailed methods are provided in the Supplementary Materials, available on on the *Arthritis & Rheumatology* website at https://onlinelibrary.wiley.com/doi/10.1002/art.42321.

Study approval. Human AAV biopsy and surgical tissue samples surplus to clinical need were obtained using the Imperial College Healthcare NHS Trust Tissue Bank (application R10015). Blood samples and plasma exchange fluid were obtained from patients with local ethics committee approval (no. 04/Q0406/25 NHS National Research Ethics Committee London - West London & GTAC).

Neutrophil and monocyte isolation. Up to 20 ml of EDTA blood was taken from patients with AAV or healthy controls, and neutrophils and peripheral blood mononuclear cells (PBMCs) were isolated using dextran sedimentation and Percoll (Sigma-Aldrich) double-density gradient. Monocytes were then isolated from the PBMC fraction using immunomagnetic negative selection beads (MACS Pan-monocyte Selection Kit; Miltenyi-Biotec).

Flow cytometry. PBMCs were used for cell surface staining with antibodies directed against CD14 (Alexa Fluor 594; BioLegend), CD4 (Alexa Fluor 700; BioLegend), CD3 (BV510; BioLegend), CD19 (BV711; BioLegend), CD56 (BV421; BioLegend), CD8a (Alexa Fluor 488; BioLegend), HLA–DR (BV785; BioLegend), and CD16 (BV605; BioLegend). Neutrophils were used for cell surface staining with anti-CD15 (Alexa Fluor 488). For intracellular staining, cells were then fixed in 2% paraformaldehyde, permeabilized using ice-cold 70% methanol, and stained with antibodies against intracellular total Syk (T-Syk) (PE 4D10.2; BioLegend), phosphorylated Syk (P-Syk) 352 (PercP-eFluor710, n3kobu5; eBioscience), and P-Syk 348 (allophycocyanin [APC], moch1ct; eBioscience).

Isolation of MPO-ANCA IgG and control IgG. MPO-ANCA IgG was isolated from plasma exchange fluid from patients with AAV, and control IgG from serum from healthy controls, using a protein G Sepharose column. $F(ab)_2$ fragments were prepared using the Pierce $F(ab')_2$ preparation kit according to the manufacturer's instructions, followed by dialysis (10K MWCO) to remove Fc fragments. Protein content of IgG preparations was quantified by spectrophotometry at 280 nm.

Neutrophil and monocyte stimulation. Cells were primed with 2 ng/ml tumor necrosis factor (TNF; PeproTech) for 15 minutes, then stimulated with 100 μg/ml MPO-ANCA IgG, MPO-ANCA IgG $F(ab)_2$ fragments, or control IgG for 4 hours. If inhibitor was used, it (or vehicle) was added after TNF for 15 minutes prior to the addition of IgG. Interleukin-8 (IL-8) production in supernatant was analyzed using a commercially available IL-8 DuoSet enzyme-linked immunoassay (R&D Systems).

For reactive oxygen species (ROS) production, cells were primed with 2 ng/ml TNF and stimulated with 100 μg/ml MPO-ANCA IgG or control IgG for 1 hour in the presence of 750 n*M* CellRox DeepRed reagent. As a positive control, 200 μ*M* tert-butyl hydroperoxide was used. Samples were analyzed using a BD Accuri C6 flow cytometer.

Whole-blood phagocytosis assay. Blood was collected into 3.8% sodium citrate for use with pHrodo red *Escherichia coli* bioparticles (ThermoFisher). Whole blood was incubated at 37°C with R406 or vehicle (0.01% DMSO) for 15 minutes followed by incubation with bioparticles for 30 minutes. Samples were incubated on ice as a negative control. Samples were then used for cell surface staining with CD14 (BV421), CD16 (BV605), and CD66b (APC; BioLegend) followed by red blood cell lysis. Samples were analyzed using a BD LSR Fortessa flow cytometer.

RNA extraction and NanoString analysis. For analysis of gene expression, cells were primed with 2 ng/ml TNF for

15 minutes, then stimulated with MPO-ANCA IgG for 1 hour. If R406 was used, it (or vehicle, 0.01% DMSO) was added after TNF priming for 15 minutes prior to addition of IgG. Total RNA was extracted from cells lysed in TRI reagent (Sigma-Aldrich) using the Direct-zol RNA Miniprep kit (Zymo Research). Next, 100 ng of RNA per sample was used with the human myeloid cell nCounter code set (NanoString Technologies). Normalization of raw gene expression was performed with nSolver Advanced Analysis Software, and low-expression genes were excluded. Clustering and heatmaps of normalized counts were carried out using the clustvis web tool (22). Data were analyzed by Rosalind (https://rosalind.onramp.bio/), with a HyperScale architecture.

Immunohistochemistry. Immunohistochemistry (IHC) was performed on formalin-fixed paraffin-embedded (FFPE) tissues. Primary antibodies were T-Syk (diluted 1:500, N-19; Santa Cruz Biotechnology) or P-Syk (diluted 1:25, Tyr525/526; Cell Signaling Technology), followed by a secondary polymeric horseradish peroxidase system (EnVision; Dako) and 3,3-diaminobenzidine to develop. For double-staining, primary antibodies used were MPO (diluted 1:1,000; Dako), CD15 (diluted 1:50, Carb-3; Dako), or CD68 (diluted 1:50, PGM1; Dako). StayGreen AP Plus detection kit (Abcam) was used to develop sections, and slides were counterstained with Mayer's hematoxylin and mounted using Vectamount (Vector Labs).

RNAscope in situ hybridization (ISH). Detection of Syk messenger RNA (mRNA) in tissue sections was performed using RNAscope on FFPE sections according to the protocol of the manufacturer (ACDBio). For each sample, slides were incubated with a target probe, with peptidylpropyl isomerase B–positive control probe (to check the integrity of mRNA), or with DapB, a bacterial gene as a negative control. Quantification of Syk mRNA was conducted by an observer blinded with regard to the histologic class of disease, using Image J.

Statistical analysis. Statistical analysis was performed using GraphPad Prism 9. Results are expressed as the median and interquartile range, and comparisons between groups were conducted by Mann-Whitney U test or Kruskal-Wallis test with Dunn's multiple comparison test. For linear correlation, Pearson's correlation coefficient was used. NanoString data were analyzed by Rosalind, with a HyperScale architecture. The limma R library was used to calculate fold changes and *P* values and perform optional covariate correction (23).

RESULTS

Phosphorylated Syk in neutrophils from patients with active AAV. Using flow cytometry, we compared levels of T-Syk and P-Syk in neutrophils isolated from patients with AAV (n = 35 with active AAV, n = 26 with disease in remission) and healthy controls (n = 10) (Supplementary Table 1, https://onlinelibrary.wiley.com/doi/10.1002/art.42321). As expected, there was no difference in levels of T-Syk between groups (median fluorescence intensity [MFI] 5,637 for patients with active AAV, 4,000 for patients with disease in remission, and 5,055 for healthy controls) (Figure 1A), but there was increased phosphorylation of Syk at the 348 tyrosine residue (Y^{348}) (MFI 4,191 for patients with active AAV, 1,016 for patients with disease in remission, and 1,687 for healthy controls; $P = 0.0002$) (Figure 1B). We confirmed this result in a subset of patients (n = 23 with active AAV, n = 6 with disease in remission), showing that there was increased phosphorylation of Syk at the 352 tyrosine residue (Y^{352}), a second activation site, in patients with active AAV compared to healthy controls, although the difference between patients with active AAV and those with disease in remission was not significant (MFI 4,321 for patients with active AAV, 1,817 for patients with disease in remission, and 1,036 for healthy controls; $P = 0.008$) (Figure 1C). In a group of patients who provided a follow-up sample when in disease remission, there was decreased P-Syk (Y^{348}) in 12 of 14 patients (MFI 5,855 for patients with active AAV and 926 for patients with disease in remission; $P = 0.01$) (Figure 1D).

There was no difference in levels of T-Syk or P-Syk (Y^{348}) when analyzed by ANCA serotype (Supplementary Figures 2A–C, https://onlinelibrary.wiley.com/doi/10.1002/art.42321). Syk phosphorylation at the Y^{348} residue seemed to increase with ANCA titer, compatible with ANCA-mediated phosphorylation of Syk in circulating neutrophils in vivo ($r = 0.4$, $P = 0.01$) (Figures 1E and F). Levels of neutrophil P-Syk (Y^{348}) did not correlate with C-reactive protein (CRP), serum creatinine, or neutrophil count, suggesting that increased levels of Syk phosphorylation are not due to factors causing an increase in neutrophil count, such as concomitant infection or steroid treatment (Figure 1E).

Phosphorylation of Syk in neutrophils following in vitro MPO-ANCA stimulation and inhibition of MPO-ANCA–induced neutrophil activation by R406. Stimulation of TNF-primed neutrophils with MPO-ANCA IgG in vitro resulted in rapid phosphorylation of P-Syk (Y^{348}), which was maximal by 30 minutes of stimulation and was decreased by 120 minutes. This was not seen in cells stimulated with healthy control IgG in place of MPO-ANCA IgG (Figures 2A and B).

There was significant IL-8 production by neutrophils following MPO-ANCA IgG stimulation (median IL-8 1,001.0 pg/ml with TNF/MPO-ANCA IgG and 177.4 pg/ml with TNF/control IgG; $P = 0.0003$) (Figure 2C). IL-8 production was reduced when $F(ab)_2$ MPO-ANCA IgG fragments were used in place of whole MPO-ANCA IgG (median neutrophil IL-8 production 677.1 with TNF/MPO-ANCA IgG and 290.3 pg/ml with TNF/$F[ab]_2$)

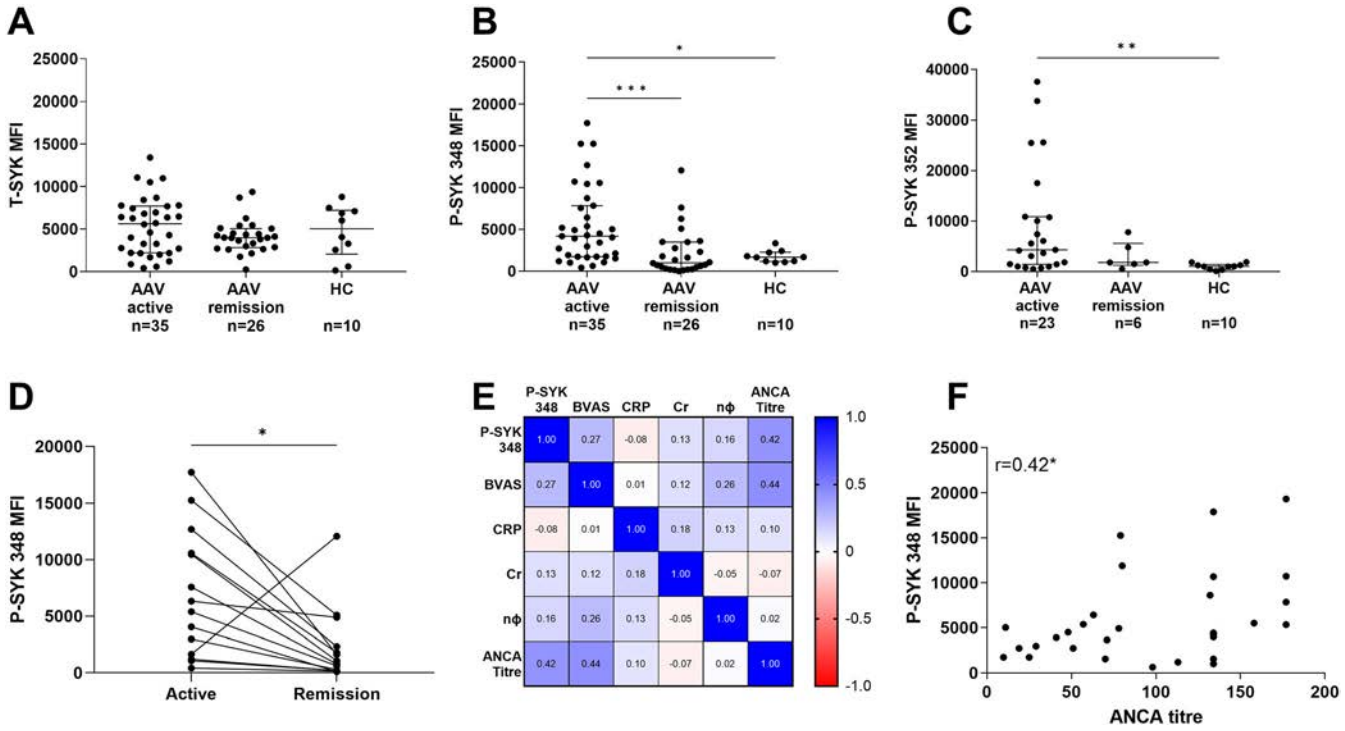

Figure 1. Neutrophil Syk is phosphorylated at activation residues in patients with active antineutrophil cytoplasmic antibody (ANCA)–associated vasculitis (AAV). **A–C**, Median fluorescence intensity (MFI) of intracellular total Syk (T-Syk) (**A**), intracellular phosphorylated Syk (P-Syk) at residue Y^{348} (**B**), and intracellular P-Syk at residue Y^{352} (**C**) in neutrophils isolated from patients with active AAV (n = 35), patients with disease in remission (n = 26), and healthy controls (HC; n = 10). Bars show the median and interquartile range. **D**, Comparison of MFI of intracellular P-Syk (Y^{348}) among a subgroup of patients with active AAV (n = 14) who provided a follow-up sample after attaining disease remission. **E**, Correlation matrix of P-Syk (Y^{348}) with clinical parameters in patients with active AAV. **F**, Correlation between P-Syk (Y^{348}) and ANCA titer in patients with active AAV. Patient characteristics are shown in Supplementary Table 1 (https://onlinelibrary.wiley.com/doi/10.1002/art.42321). * = $P < 0.05$; ** = $P < 0.01$; *** = $P < 0.001$, by Kruskal-Wallis test with Dunn's post hoc correction (versus the active AAV group) in **A–C**, and by Wilcoxon's matched pairs signed rank test in **D**. BVAS = Birmingham Vasculitis Activity Score; CRP = C-reactive protein; Cr = serum creatinine; nϕ = neutrophil count × 10^9/ml.

(Figure 2D), suggesting that MPO-ANCA IgG–mediated IL-8 release is partially dependent on FcγR engagement and is consistent with a role for Syk signaling in ANCA-induced neutrophil responses. Moreover, IL-8 release was inhibited in a dose-dependent manner by R406, the active metabolite of fostamatinib, a small molecule inhibitor relatively selective for Syk (median IL-8 685.4 pg/ml with vehicle, 85.7 pg/ml with 2 μ*M* R406, 223.1 pg/ml with 1 μ*M* R406, and 366 pg/ml with 0.2 μ*M* R406; $P < 0.0001$) (Figure 2C).

In addition to IL-8 release, stimulation of neutrophils with MPO-ANCA IgG resulted in more ROS production compared to cells stimulated with control IgG (median percentage ROS-positive cells 31.0% with MPO-ANCA IgG and 16.1% with control IgG; $P = 0.04$) (Figures 2E and F). ROS production was also inhibited by R406 (median percentage ROS-positive cells 14.0% with 2 μ*M* R406 and 30.2% with vehicle; $P = 0.008$) (Figure 2F). At the concentrations used here, R406 is expected to be relatively selective for Syk in vitro (24). In order to confirm that these effects were not due to off-target effects of R406, we used a second Syk inhibitor, entospletinib, to inhibit MPO-ANCA IgG–induced IL-8 and ROS production by neutrophils, demonstrating similar results to R406 (Supplementary Figure 3, https://onlinelibrary.wiley.com/doi/10.1002/art.42321). To assess the potential effect of Syk inhibition on non–antibody-mediated functions such as bacterial phagocytosis, which may potentially lead to infection risk in clinical use, we used a whole-blood phagocytosis assay. R406 had no effect on neutrophil phagocytosis of *E coli* bioparticles (Supplementary Figure 4A, https://onlinelibrary.wiley.com/doi/10.1002/art.42321).

Phosphorylation of Syk in monocytes from patients with active AAV and inhibition of MPO-ANCA IgG–induced monocyte responses by R406. Monocytes also express the ANCA autoantigens and are increasingly recognized as contributing to the pathogenesis of AAV (25,26). Monocytes express high levels of FcγRIIa, suggesting a role for Syk in ANCA IgG–mediated monocyte activation. We therefore assessed Syk activation in monocytes, with the aim of validating our results in neutrophils. Flow cytometry of PBMCs isolated from patients with AAV (n = 12 with active disease, n = 13 with disease in remission)

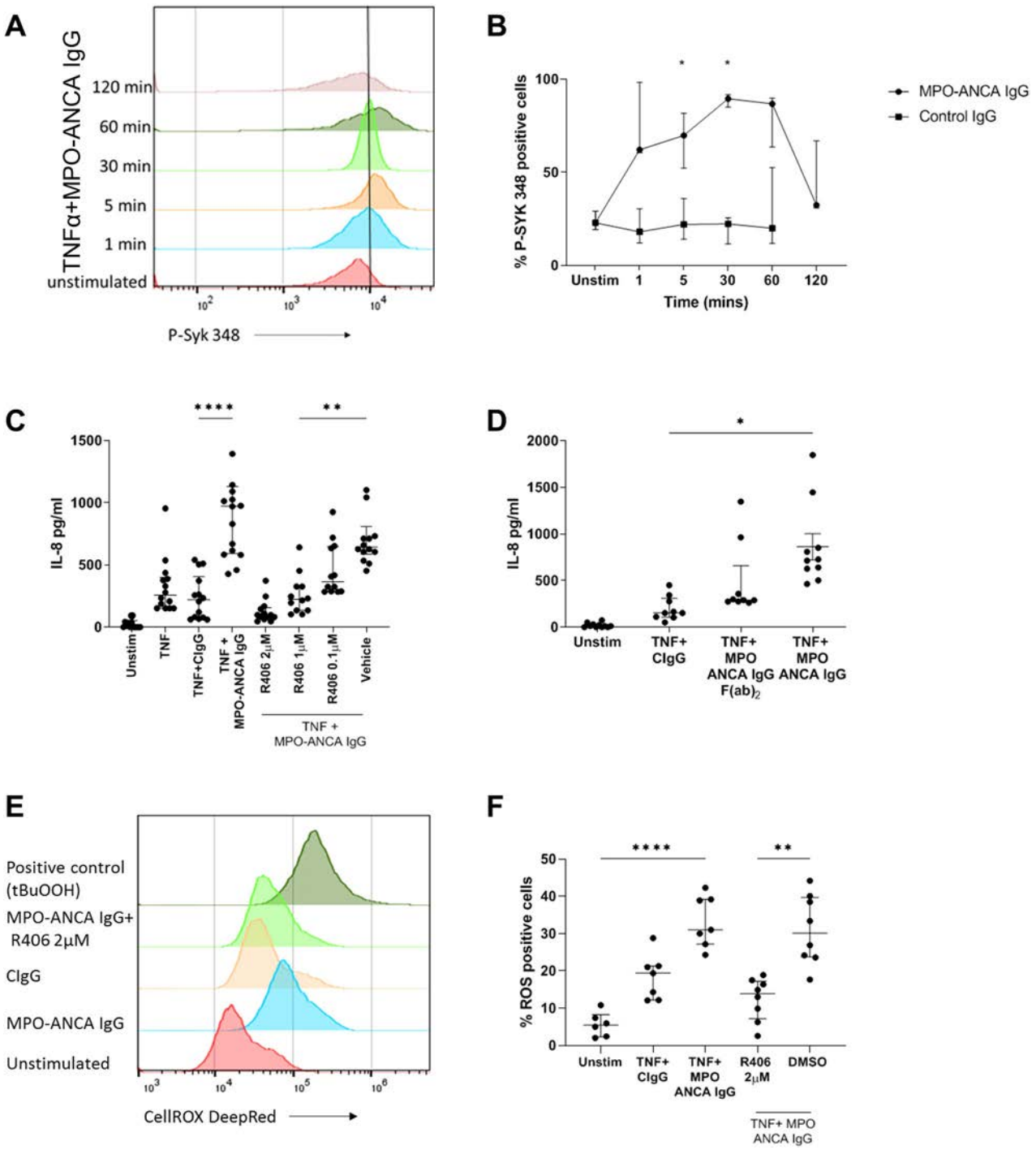

Figure 2. Syk is phosphorylated following myeloperoxidase (MPO)–ANCA stimulation, and Syk inhibition can prevent MPO-ANCA–induced responses. **A** and **B**, Representative histogram (**A**) and quantification (**B**) of MFI of P-Syk (Y^{348}) in neutrophils isolated from healthy controls and stimulated ex vivo with 2 ng/ml tumor necrosis factor (TNF) for 15 minutes, followed by either 100 μg/ml MPO-ANCA IgG or 100 μg/ml control IgG (CIgG) for the indicated duration. **C**, Interleukin-8 (IL-8) release from neutrophils isolated from healthy controls primed with 2 ng/ml TNF for 15 minutes and then stimulated with 100 μg/ml MPO-ANCA IgG for 4 hours. **D**, IL-8 production from neutrophils isolated from healthy controls and primed with 2 ng/ml TNF for 15 minutes and then stimulated with 100 μg/ml MPO-ANCA IgG or $F(ab)_2$ fragments of 100 μg/ml MPO-ANCA IgG for 4 hours. **E** and **F**, Representative histogram (**E**) and quantification (**F**) of reactive oxygen species (ROS) production, by percentage of cells positive for CellRox Deep Red reagent (gated on unstained cells). Cells were primed with 2 ng/ml TNF for 15 minutes and then stimulated with 100 μg/ml MPO-ANCA IgG for 1 hour. In **C** and **F**, when R406 or vehicle (0.01% DMSO) were used, they were added to cells for 15 minutes following TNF priming and prior to stimulation with MPO-ANCA IgG. Cells were isolated from ≥3 healthy donors with ≥2 biologic replicates for each donor. Bars show the median and interquartile range. * = $P < 0.05$; ** = $P < 0.01$; *** = $P < 0.001$, by Kruskal-Wallis test with Dunn's post hoc correction. Unstim = unstimulated; tBuOOH = *tert*-butyl hydroperoxide (see Figure 1 for other definitions). Color figure can be viewed in the online issue, which is available at http://onlinelibrary.wiley.com/doi/10.1002/art.42321/abstract.

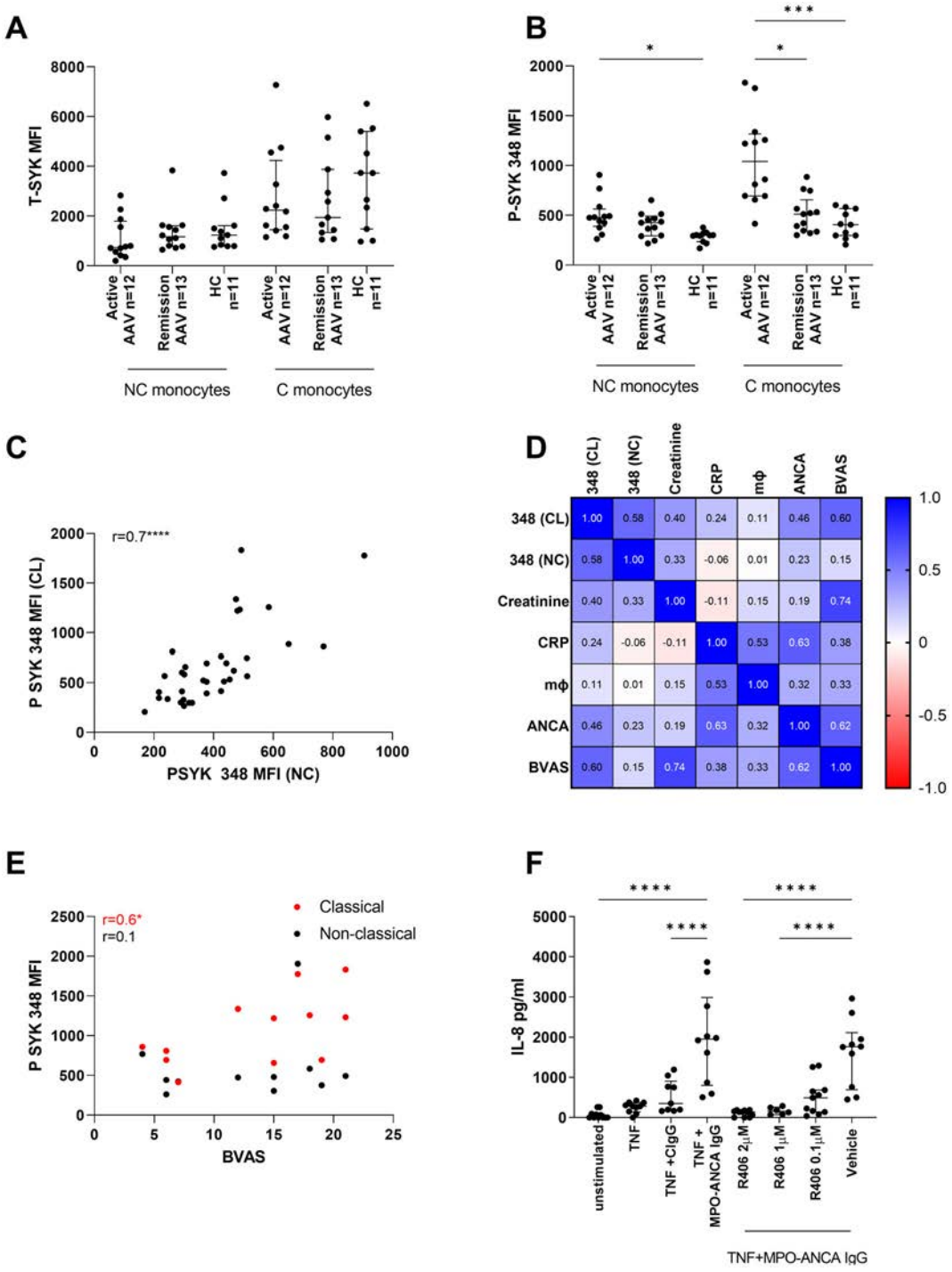

Figure 3. Monocyte Syk is phosphorylated at activation residues in patients with active AAV, and monocyte interleukin-8 (IL-8) production in response to myeloperoxidase (MPO)–ANCA IgG can be inhibited by R406. **A** and **B**, MFI of intracellular T-Syk (**A**) and intracellular P-Syk (Y^{348}) (**B**) in classical (C) and nonclassical (NC) monocytes isolated from patients with active AAV (n = 12), those with disease in remission (n = 13), and healthy controls (n = 11). P-Syk (Y^{348}) is up-regulated in patients with active AAV compared to those with AAV in remission or healthy controls, with a greater magnitude of increase in classical compared to nonclassical monocytes. **C**, Correlation between levels of P-Syk (Y^{348}) in classical (CL) and nonclassical (NC) monocytes among the whole cohort. **D**, Correlation matrix of P-Syk (Y^{348}) and clinical parameters in patients with active AAV. **E**, Correlation between P-Syk (Y^{348}) and BVAS in classical and nonclassical monocytes. **F**, IL-8 production from monocytes primed with 2 ng/ml tumor necrosis factor (TNF) for 15 minutes and then stimulated with 100 μg/ml IgG MPO-ANCA for 4 hours. When R406 or vehicle (0.01% DMSO) were used, they were added to cells for 15 minutes following TNF priming and prior to stimulation with MPO-ANCA IgG. Results are from 4 biologic replicate experiments with monocytes isolated from 4 healthy donors. Bars show the median and interquartile range. Gating strategy for monocytes is shown in Supplementary Table 1 (https://onlinelibrary.wiley.com/doi/10.1002/art.42321). * = $P < 0.05$; *** = $P < 0.001$; **** = $P < 0.0001$, by Kruskal-Wallis test with Dunn's post hoc correction. Mϕ = monocyte count $\times 10^9$/ml (see Figure 1 for other definitions). Color figure can be viewed in the online issue, which is available at http://onlinelibrary.wiley.com/doi/10.1002/art.42321/abstract.

and healthy controls (n = 11) was performed to assess levels of T-Syk and P-Syk 348 (Supplementary Table 2, https://onlinelibrary.wiley.com/doi/10.1002/art.42321). As expected, there was no difference in levels of monocyte T-Syk between the groups, but T-Syk was increased in classical monocytes (CD14++CD16–) compared to nonclassical monocytes (CD14 + CD16++) in all participants (Figure 3A), which is consistent with previous reports of increased Syk gene expression in classical and nonclassical monocytes (27).

P-Syk (Y^{348}) was elevated in both classical and nonclassical monocytes in patients with active AAV compared to healthy controls and in classical monocytes in patients with active disease compared to those with disease in remission. Higher levels of Syk phosphorylation were seen in classical versus nonclassical monocytes, in keeping with greater total Syk expression in this cell type (Figure 3B). For the whole cohort (patients and healthy controls), there was strong correlation between P-Syk (Y^{348}) in classical and nonclassical monocytes (r = 0.7, $P < 0.0001$; Figure 3C). There was no difference in P-Syk (Y^{348}) based on ANCA serotype in either monocyte subset, nor were there correlations with CRP, serum creatinine, or total monocyte count (Figure 3D). For classical monocytes, there was weak correlation between levels of P-Syk (Y^{348}) and ANCA titers (r = 0.459, $P = 0.1$), which was again compatible with ANCA-mediated phosphorylation of Syk in vivo, and there was a moderate correlation between levels of P-Syk (Y^{348}) and Birmingham Vasculitis Activity Score (BVAS) (r = 0.6, $P = 0.04$; Figure 3E). Levels of T-Syk and P-Syk (Y^{348}) in other components of the PBMC fraction, including B cell and natural killer cells, are shown in the Supplementary Figure 5 (https://onlinelibrary.wiley.com/doi/10.1002/art.42321).

Consistent with our findings in neutrophils, monocyte IL-8 production following MPO-ANCA IgG stimulation in vitro was Syk-dependent. There was significant IL-8 production in response to MPO-ANCA IgG stimulation compared to control IgG stimulation (median IL-8 1,924 pg/ml with TNF/MPO-ANCA IgG and 752 pg/ml with TNF/control IgG; $P = 0.02$) (Figure 3F), which could be inhibited by R406 in a dose-dependent manner (median IL-8 1,758 pg/ml with vehicle, 138.6 pg/ml with 2 μ*M* R406, 155.6 pg/ml with 1 μ*M* R406, and 492.9 pg/ml with 0.2 μ*M* R406; $P < 0.0001$) (Figure 3F). Similar to our findings with neutrophils, R406 had no effect on monocyte phagocytosis of *E coli* bioparticles (Supplementary Figure 4B, https://onlinelibrary.wiley.com/doi/10.1002/art.42321). As expected, there was more phagocytosis mediated by classical compared to nonclassical monocytes.

Altered myeloid cell gene expression by MPO-ANCA IgG stimulation. To determine if Syk-dependent signaling pathways are activated in AAV, we next investigated transcriptional differences in MPO-ANCA IgG–stimulated granulocytes and monocytes, and the effect of Syk inhibition with R406 on these changes, using the NanoString analysis platform. The myeloid innate immunity gene panel used for this study includes 770 genes, covering a range of pathways and processes, including cytokines, chemokines, cell migration and adhesion, and FcR signaling (Figure 4A, Supplementary Figure 6, and Supplementary Table 3, https://onlinelibrary.wiley.com/doi/10.1002/art.42321). Compared to unstimulated granulocytes, MPO-ANCA IgG–stimulated granulocytes showed up-regulation of genes in several functional categories, including chemokine and cytokine signaling (*CXCL8*, *CCL20*, *CCL3*, *CC3L1*, *CXCL2*, *CCL4*, *CCRL2*, *IL1A*, *IL1B*, *TNF*, *TRAF1*, *NFKB*, *EDN1*), chemotaxis (*CCL20*, *CCL3*, *CCL4*, *CCL3L1*, *CXCL8*, *IL1B*, *EDN1*, *LGALS3*), and stress response (*NRFA2*, *GADD45A*).

Reflecting their greater plasticity as a non–terminally differentiated cell, monocytes showed a greater degree of transcriptional activity following stimulation with MPO-ANCA IgG, and NanoString analysis identified substantially more differentially expressed genes than observed in neutrophils (Supplementary Figures 7 and 8A and Supplementary Table 4, https://onlinelibrary.wiley.com/doi/10.1002/art.42321). The differentially expressed genes in MPO-ANCA IgG–stimulated monocytes included those involved in multiple effector functions, such as the following: 1) genes for proinflammatory chemokines and cytokines, and genes downstream of cytokine receptors such as JAK/STAT and MAPK (Figure 4B and Supplementary Figure 8B); 2) genes involved in cell migration and adhesion (Figure 4C); 3) FcR-dependent pathways (Figure 4D); and 4) genes implicated in the breakdown of extracellular matrix (ECM) (Supplementary Figure 8C). In keeping with a role for Syk in MPO-ANCA IgG–mediated monocyte activation, genes related to tyrosine kinase phosphorylation were also up-regulated (Supplementary Figure 8D, https://onlinelibrary.wiley.com/doi/10.1002/art.42321). Specifically, there was up-regulation of genes involved in several Syk-dependent signaling pathways, including those related to positive regulation of Rho GTPase activity. Rho-dependent GTPases have been identified to play a role downstream of FcγR activation, signaling via Syk, PLCγ2, Vav (also up-regulated), and phosphatidylinositol 3-kinase leading to phagocytosis, ROS, and cytokine production in neutrophils and monocytes (7,28) (Supplementary Figure 8D).

When MPO-ANCA IgG–stimulated cells were pretreated with R406 (and compared to vehicle-treated cells), there was significant down-regulation of the gene signatures, which were found to be up-regulated following MPO-ANCA IgG stimulation in both neutrophils and monocytes (Figures 4E and F and Supplementary Tables 3 and 4, https://onlinelibrary.wiley.com/doi/10.1002/art.42321), including those involved in chemokine/cytokine signaling (*CXCL8*, *CCL20*, *CCL3*, *CCL3L1*, *CCL4*, *CCRL2*, *CXCR4*, *CCR1*) (Figure S8E). Similar to the analysis of ANCA-stimulated cells, there was greater transcriptional plasticity of monocytes and treatment with R406 resulted in down-regulation of many genes induced by ANCA IgG stimulation compared to vehicle

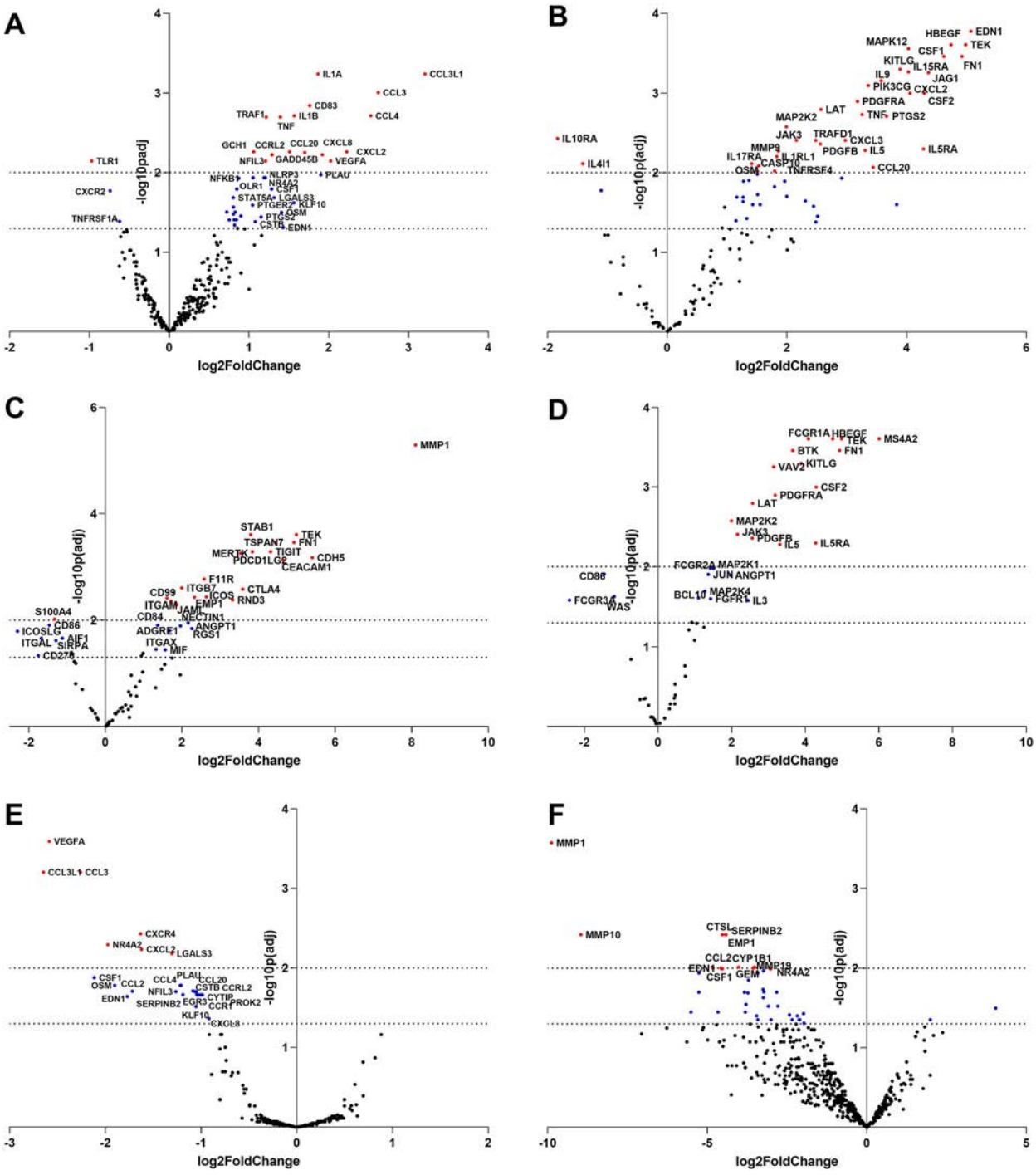

Figure 4. NanoString analysis of myeloperoxidase (MPO)–antineutrophil cytoplasmic antibody (ANCA) IgG–stimulated granulocytes and monocytes. **A**, Volcano plot showing $-\log_{10}$ (*P* value) and $\log_2$ (fold change) for granulocytes primed with 2 ng/ml tumor necrosis factor (TNF) for 15 minutes and then stimulated with 100 μg/ml MPO-ANCA IgG for 1 hour, compared to unstimulated granulocytes. All genes included in NanoString analysis are shown. **B–D**, Volcano plots showing $-\log_{10}$ (*P* value) and $\log_2$ (fold change) for monocytes primed with 2 ng/ml TNF for 15 minutes then stimulated with 100 μg/ml MPO-ANCA IgG for 1 hour, compared to unstimulated monocytes. Genes shown are identified in the NanoString code set as involved in cytokine pathways (**B**), cell migration and adhesion (**C**), or Fc receptor signaling (**D**). **E**, Volcano plot showing $-\log_{10}$ (*P* value) and $\log_2$ (fold change) for TNF-primed, MPO-ANCA IgG–stimulated granulocytes pretreated with 2 μ*M* R406, compared to those pretreated with vehicle, for all genes included in NanoString analysis. **F**, Volcano plot showing $-\log_{10}$ (*P* value) and $\log_2$ (fold change) for TNF-primed, MPO-ANCA IgG–stimulated monocytes pretreated with 2 μ*M* R406, compared to those pretreated with vehicle, for all genes included in NanoString analysis. Selected differentially expressed genes with a $\log_2$ (fold change) >1.5 and adjusted *P* values <0.05 are identified by name and are shown in red (adjusted $P < 0.01$) and blue (adjusted $P < 0.05$). Color figure can be viewed in the online issue, which is available at http://onlinelibrary.wiley.com/doi/10.1002/art.42321/abstract.

treatment, including genes involved in chemokine and cytokine pathways, ECM remodeling, and cell migration and adhesion (Figure 4F, Supplementary Figures 8E and F, and Supplementary Table 4). Genes that are associated with GTPase activity, tyrosine phosphorylation cascades, and MAPK signaling pathways were also down-regulated.

Up-regulation of Syk mRNA in renal biopsy tissue from patients with active AAV. Using IHC, we have previously shown that Syk is expressed in the inflamed glomeruli of patients with ANCA-associated glomerulonephritis (AAGN) and that this correlates with Berden disease class (29,30). We sought to validate these findings using RNAscope, a method of in situ hybridization used to detect Syk mRNA that overcomes the potential for nonspecific antibody-binding in standard IHC. We confirmed Syk mRNA expression in the glomeruli of patients with crescentic AAGN, with expression localized to crescents and segmental areas of inflammation that mirrored findings using IHC (Figures 5A–C). There was minimal Syk mRNA expression in the glomeruli of patients with sclerotic lesions or in nonaffected glomeruli in patients with mixed-class disease (Figures 5D–F). Marked Syk mRNA expression was also seen in areas of tubulointerstitial and periglomerular inflammation in patients with both sclerotic and crescentic glomerular disease (Figures 5E and G). In our previous study, we also detected Syk expression in distal tubular epithelial cells, a common site for nonspecific staining in standard IHC; in the current study, we have confirmed that this accurately represents Syk expression using RNAscope to detect Syk mRNA (Figures 5H and I).

Syk expression at extrarenal sites of vasculitis. Syk is expressed at extrarenal sites of inflammation in patients with active AAV. Our previous studies have focused on the role of Syk in renal disease (20,30). However, many patients with AAV may have extensive multisystem disease affecting nonrenal organs (31). We therefore investigated Syk expression in biopsy and surgical tissue samples from a range of extrarenal sites of inflammation using IHC for T-Syk and P-Syk, with colocalization for leukocyte markers.

We first examined tissue with evidence of small vessel vasculitis and capillaritis, including nerve, skin, and intestinal tissue. We detected T-Syk within cells of perivascular infiltrate of the vasa nervorum that colocalized with the ANCA autoantigen MPO (Figures 6A and B and Supplementary Figures 9A and B, https://onlinelibrary.wiley.com/doi/10.1002/art.42321). T-Syk was present in cells with typical neutrophil morphology in inflammatory infiltrate in ear, nose, and throat–associated vasculitis (Figure 6C). T-Syk could also be identified in gut tissue in infiltrating leukocytes associated with vasculitis of an arteriole and leukocytoclasis (Figure 6D). T-Syk was expressed in infiltrating cells at sites of capillaritis in the skin and colocalized with both MPO and the neutrophil marker CD15 (Figures 6E–G and Supplementary Figures 9C–E).

Extravascular granulomatous tissue inflammation is also a common disease manifestation in AAV, and we identified T-Syk in cells within granulomata in lung, nasal, and cutaneous tissue of patients with active AAV affecting these organ sites (Figure 6H and Supplementary Figures 9F–H, https://onlinelibrary.wiley.com/doi/10.1002/art.42321). Within areas of severe inflammation in the skin, foamy macrophages were positive for T-Syk, and costaining for CD68 confirmed that T-Syk coexpression was in both monocytes/tissue macrophages and multinucleated giant cells. Importantly, staining for P-Syk was present, indicating Syk activation in these cells in tissue (Figures 6I–K and Supplementary Figures 9I–N). Of note, T-Syk also colocalized with expression of the ANCA autoantigen MPO (Figure 6L and Supplementary Figures 9I–K).

DISCUSSION

This study identifies a role for Syk in the pathogenesis of AAV and indicates that Syk inhibition may be an effective therapeutic strategy. We showed the up-regulation of Syk phosphorylation (i.e., activation) in circulating innate immune cells in patients with active untreated AAV and found that this correlates with measures of disease activity. We demonstrated that Syk inhibition can prevent ANCA-mediated cellular responses in vitro, including IL-8 and ROS production, and by using targeted gene expression analysis, we confirmed that Syk-dependent signaling pathways were activated following MPO-ANCA IgG stimulation. Finally, we identified Syk in tissue leukocytes at sites of organ inflammation in AAV, using both standard protein IHC and in situ hybridization for Syk mRNA.

In the first component of this study, we examined circulating neutrophils and monocytes from patients with acute AAV, isolated before receipt of immunosuppression, thus providing a unique opportunity to assess the association of Syk expression and activation in myeloid cells with disease activity. The increased phosphorylation of Syk in patients with active untreated AAV and the positive correlation with ANCA titers suggest that ANCA-mediated phosphorylation of myeloid cells may be occurring in vivo and that Syk activation has a role in disease pathogenesis. The tyrosine residue for which we identified the greatest difference in phosphorylation between patients with active disease and those in remission or healthy donors was Y^{348}. This residue has been shown to play a critical role in the transition of Syk from an autoinhibited to an activated state (10). The differences in Y^{352} phosphorylation were less marked. The reasons for this are likely to be multifactorial and may include technical differences between the 2 antibodies used, differences in kinetics of phosphorylation, or basal phosphorylation states between the 2 sites. A reduction in myeloid cell Syk activation in most patients during clinical remission also suggests a functional correlation with disease activity, although a direct effect of immunosuppressive treatment cannot be

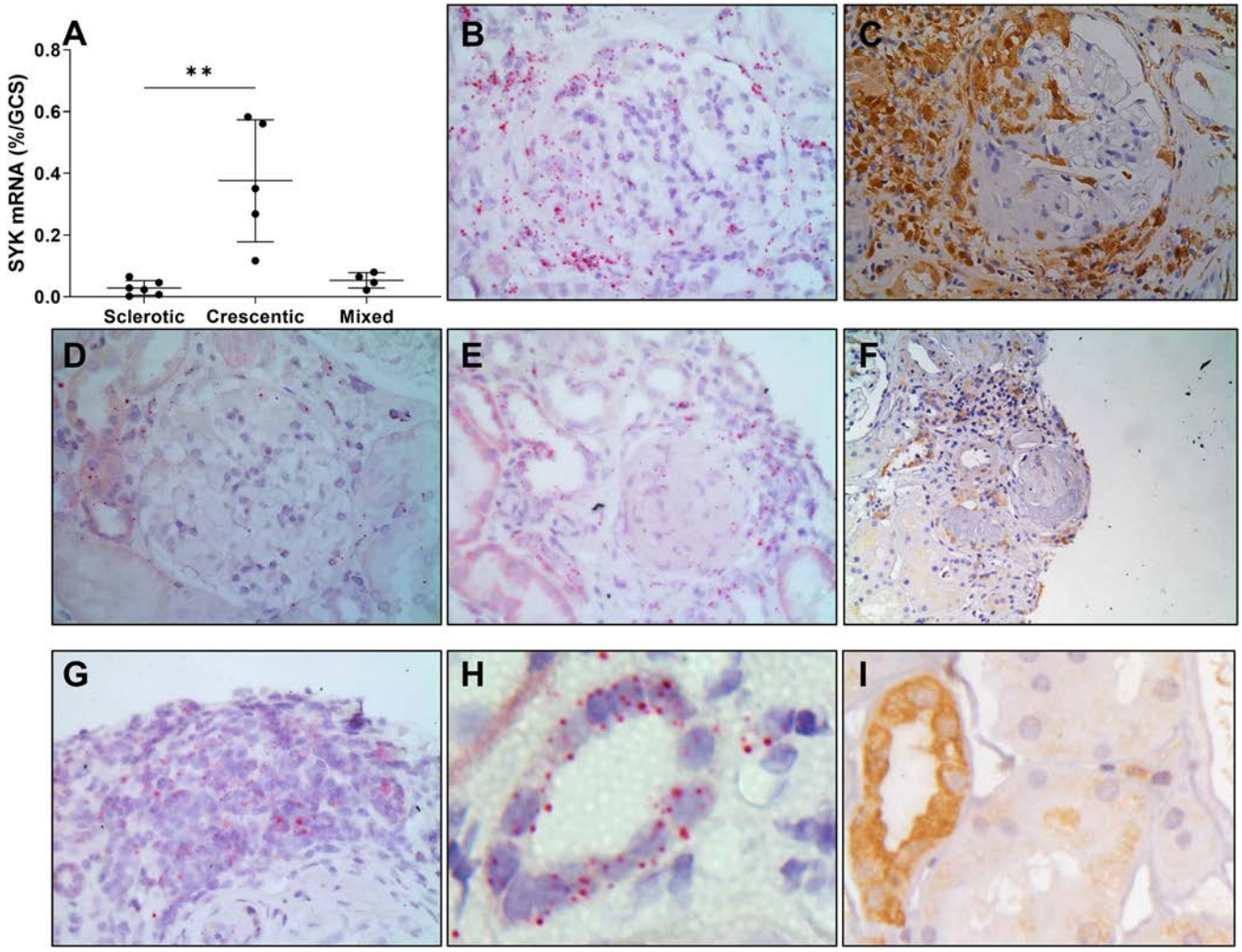

Figure 5. Syk mRNA is up-regulated in glomeruli of patients with crescentic antineutrophil cytoplasmic antibody–associated vasculitis. **A**, Quantification of glomerular expression of Syk mRNA using RNAscope in situ hybridization showing significant up-regulation in glomeruli from patients with crescentic glomerulonephritis compared to those with sclerotic (inactive) disease. Bars show the median and interquartile range. ** = $P < 0.01$ by Kruskal-Wallis test with Dunn's post-test comparison. **B**, Representative histologic sections showing Syk mRNA in the distribution of a cellular crescent, likely indicating Syk in infiltrating leukocytes. **C**, Comparative image of immunohistochemistry (IHC) for total Syk (T-Syk) showing positive cells in the distribution of a cellular crescent and periglomerular infiltrate. **D**, Syk mRNA absent in a glomerulus containing a sclerotic lesion. **E**, A small amount of Syk mRNA in a sclerotic glomerulus with significant periglomerular inflammation containing Syk-positive cells. **F**, Comparative image of T-Syk IHC showing negative glomerular staining in a patient with sclerotic disease and T-Syk–positive cells in periglomerular infiltrate. **G**, Syk mRNA in cells in tubulointerstitial infiltrate. **H**, Syk mRNA in cells with characteristic morphology of distal tubular epithelial cells. **I**, Comparative image of T-Syk IHC showing positive staining of distal tubular epithelial cells. In **B–I**, original magnification ×400 with hematoxylin counterstain. IHC images show immunoperoxidase staining. Color figure can be viewed in the online issue, which is available at http://onlinelibrary.wiley.com/doi/10.1002/art.42321/abstract.

excluded. In acute disease, a range of Syk activation was observed, suggesting that flow cytometry cell phenotyping could be used to stratify patients for future clinical studies, in order to identify those likely to benefit from Syk inhibitor treatment.

Using the same flow cytometric approach for intracellular phosphoprotein analysis, we next assessed Syk activation in neutrophil responses in vitro. It is already established that Syk is activated following FcγR ligation on neutrophils and monocytes, such as following immune complex stimulation (32). The active metabolite of fostamatinib, R406 (a small molecule kinase inhibitor with relative selectivity for Syk), can prevent respiratory burst and cytokine release induced by this pathway (1,24,32,33). The role of FcγR signaling via Syk in ANCA-mediated cell activation is less clearly defined. Several studies have shown the importance of ANCA binding to FcγRIIa in proinflammatory neutrophil responses and that blockade of this receptor decreases ANCA-induced neutrophil activation (13,16). However, studies using F(ab) fragments

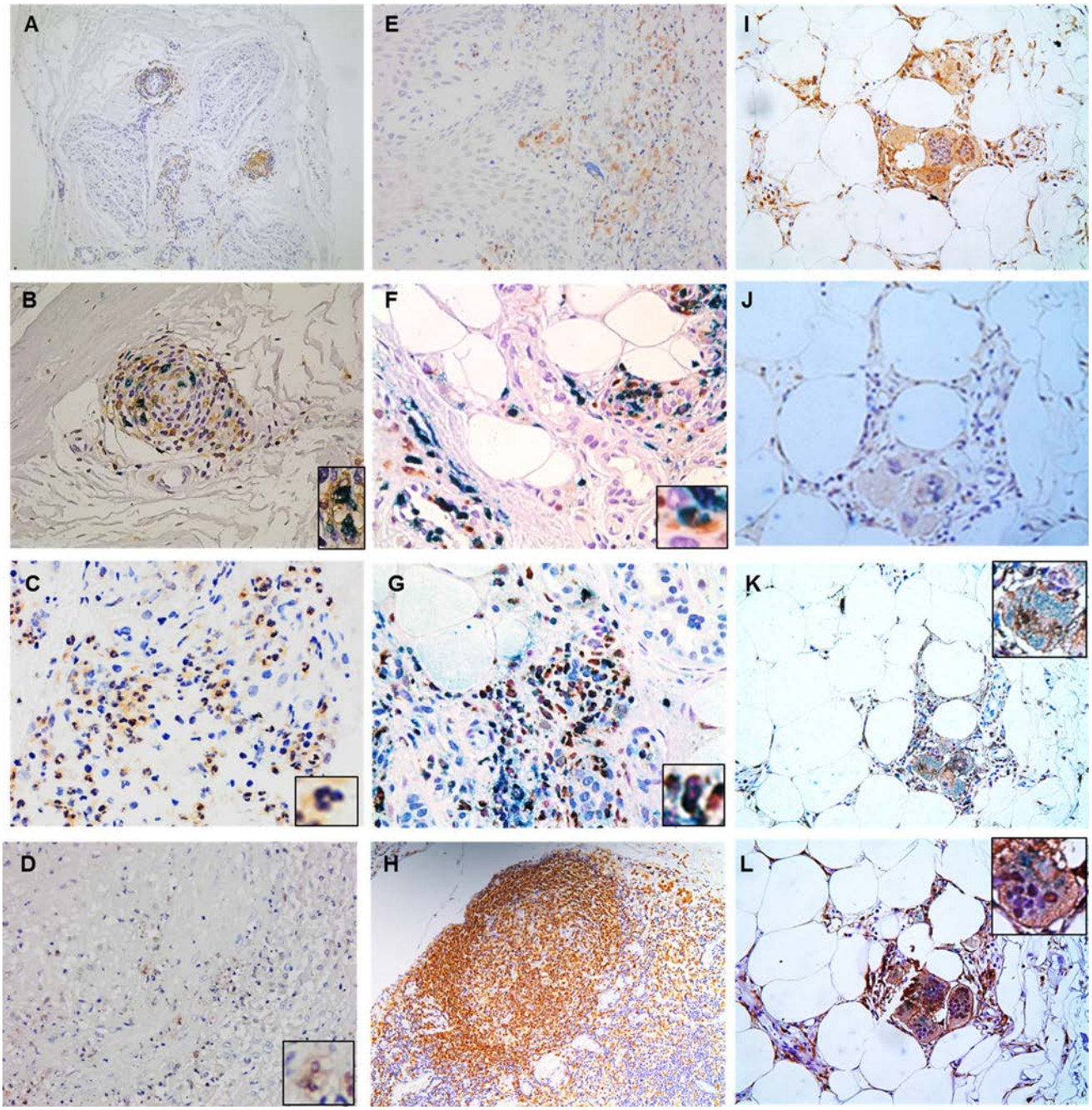

Figure 6. Syk is expressed at extrarenal sites of inflammation in patients with active AAV and colocalizes with CD68, CD15, and myeloperoxidase (MPO). Immunohistochemistry for Syk on biopsy tissue from extrarenal sites of inflammation in patients with AAV was performed. **A** and **B**, Low-power image of perivascular infiltrate of the vasa nervorum showing cells positive for T-Syk (brown) (**A**) and high-power image showing cells positive for T-Syk (brown) and MPO (blue), with cells positive for MPO and T-Syk magnified (**inset**) (**B**). **C**, Paranasal sinus tissue showing infiltrate of Syk-positive neutrophils and mononuclear cells, including those with typical neutrophil nuclear morphology (**inset**). **D**, Vasculitis of an arteriole in the gut with evidence of leukocytoclasis, with T-Syk–positive cells magnified (**inset**). **E–G**, Low-power image of capillaritis in cutaneous tissue with evidence of leukocytoclasis showing cells positive for T-Syk (brown) (**E**) and high-power images showing T-Syk (brown) and CD15 (blue) (**F**) and T-Syk (brown) and MPO (blue) (**G**). **Insets** show magnified images of cells positive for T-Syk and CD15 or MPO, respectively. **H**, Inflammation in the lung showing dense collection of T-Syk–positive cells. **I–L**, An area of severe inflammation in the skin with foamy macrophages positive for T-Syk (**I**), P-Syk (**J**), T-Syk (brown) and CD68 (blue) (**K**), and T-Syk (brown) and MPO (blue) (**L**). **Insets** show magnified images of cells positive for T-Syk and CD68 or MPO, respectively. Immunoperoxidase/immunophosphatase staining is shown with hematoxylin counterstain. Original magnification ×100 (**A** and **E**), ×200 (**D**, **H–L**), ×400 (**B**, **C**, **F**, **G**). Single stains and additional images are shown in Supplementary Figure 9 (https://onlinelibrary.wiley.com/doi/10.1002/art.42321). See Figure 1 for other definitions.

of ANCA IgG have generated conflicting results. Several have shown that F(ab) fragments can bind neutrophils but that this does not result in cell activation. Others have shown that cross-linked F(ab) or $F(ab)_2$ of ANCA can induce neutrophil activation, resulting in cytokine release and the production of ROS, although this is not a consistent finding (15,34–36). Our findings identify a critical role for Syk in mediating MPO-ANCA IgG responses, suggesting that FcγR-dependent signaling is necessary for ANCA-induced activation of myeloid cells. Consistent with this finding, we showed that stimulation with $F(ab)_2$ fragments in place of whole IgG results in decreased but not abolished cytokine release. It is likely that several mechanisms lead to ANCA-induced activation of myeloid cells in AAV, requiring binding to both autoantigen and FcR, such as in the Kurlander effect (37).

Transcriptional analysis of both granulocytes and monocytes after stimulation with MPO-ANCA IgG identified up-regulation of several pathways likely to contribute to disease pathogenesis in AAV, including chemokine/cytokine production and chemotaxis in neutrophils. Monocytes, having greater plasticity, showed broader changes in transcriptional activity, involving genes related to cytokine/chemokine production and response, genes implicated in the breakdown of extracellular matrix, and genes involved in cell migration and adhesion. Notably, there was clear differential expression of genes involved in FcR signaling, including significant up-regulation of Rho GTPases, and of genes known to increase their activity. In cells treated with R406, these pathways were down-regulated to levels seen in unstimulated cells. Several studies have identified a role for these proteins downstream of FcγR/Syk signaling, and we suggest that activation of Syk and downstream signaling through PLCγ/Vav/Ras/MAPK/NF-κB leads to myeloid cell activation and cytokine production after stimulation with MPO-ANCA IgG (38,39).

Having identified increased Syk activation in circulating innate immune cells of patients with acute AAV and a role for Syk signaling in MPO-ANCA IgG–mediated activation of myeloid cells in vitro, we next sought to investigate Syk expression and activation in the tissue of organs affected by vasculitis. Using RNAscope ISH, we confirm the specificity of our previous studies using standard IHC and identify that glomerular Syk mRNA expression is highest in those with crescentic glomerulonephritis and lowest in those with sclerotic (i.e., histologically inactive) disease (30). Syk expression within glomeruli was localized to areas of crescent formation or segmental proliferation and was also observed in areas of tubulointerstitial and periglomerular inflammation. We used this standard IHC approach to show that Syk is expressed and phosphorylated at multiple sites of extrarenal organ inflammation in AAV, including in the lungs and the upper respiratory tract, skin, nerve, and intestinal tissue. These results suggest that inhibition of Syk may have broad therapeutic potential for the diverse clinical manifestations of AAV, including extravascular granulomatous tissue inflammation.

Our study has some limitations. Not all patients provided sequential samples for analysis, and so we were unable to investigate changes in Syk activation prior to relapse, nor could we exclude a direct effect of immunosuppression on Syk activation in the remission group. It was also not possible to quantify Syk activation in tissue due to the technical limitations of IHC, a non-stochiometric technique. However, our findings suggest a role for Syk in the pathogenesis of AAV and that drugs targeting Syk may provide a novel treatment approach in this disease. Fostamatinib, the orally administered prodrug form of R406, is now an established therapeutic (40,41). In immune thrombocytopenia, this therapy has shown efficacy in refractory disease and an acceptable toxicity profile (41). Despite its effects on inhibiting myeloid cell activation, fostamatinib/R406 does not seem to increase the risk of bacterial infection, and the most commonly reported side effects in clinical studies were gastrointestinal disturbance and mild hypertension (3–5-mmHg increase in systolic blood pressure), which can usually be managed without cessation of the drug. In biochemical kinase assays, R406 has been shown to have activity at a number of other kinases with similar or greater potency than it has for Syk, although in cell-based assays, this was reduced when compared to its activity at Syk (24,42,43). R406 has also been shown to have activity at vascular endothelial growth factor receptor 2, which is likely to explain its small effect on blood pressure in clinical studies (43). However, this pathway is unlikely to mediate the effect seen on ANCA-mediated myeloid cell activation in vitro, and inhibition of Syk, downstream of FcR, is the most biologically plausible explanation. As there is the possibility that R406 may be acting at other targets than Syk in vitro, we have confirmed our results in neutrophils, using a second inhibitor entosplentinib, which is described to be selective for Syk.

This study focused on Syk expression and activation in innate immune cells, although it is recognized that B cell maturation, survival, and activation are Syk-dependent (44). B cell–directed therapy is an established strategy in the treatment of AAV, and disruption of these Syk-dependent B cell functions with fostamatinib treatment may provide additional therapeutic benefit (45). Of interest, we found evidence of Syk activation in B cells from patients with active disease (Supplementary Figure 5, https://onlinelibrary.wiley.com/doi/10.1002/art.42321), and the role of Syk in humoral immunity in AAV should be explored in future studies.

We have previously shown that fostamatinib is an effective treatment for pulmonary and renal disease in preclinical models of vasculitis, and, based on our findings here that show convincing evidence of Syk activation in patients with AAV, we suggest that Syk inhibition with fostamatinib should be prioritized for future clinical studies in vasculitis (21,46).

ACKNOWLEDGMENTS

Human tissue samples used in this research project were obtained from the Imperial College Healthcare Tissue Bank (ICHTB). ICHTB is supported by the NIHR Biomedical Research Centre based at Imperial College Healthcare NHS Trust and Imperial College London.

AUTHOR CONTRIBUTIONS

All authors were involved in drafting the article or revising it critically for important intellectual content, and all authors approved the final version to be published. Dr. Prendecki had full access to all of the data in the study and takes responsibility for the integrity of the data and the accuracy of the data analysis.

Study conception and design. Prendecki, Pusey, McAdoo.

Acquisition of data. Prendecki, Gulati, Pisacano, Pinheiro, Bhatt, Mawhin, Toulza, Cowburn, Lodge.

Analysis and interpretation of data. Prendecki, Masuda, Tam, Roufosse, Pusey, McAdoo.

REFERENCES

1. Mocsai A, Ruland J, Tybulewicz VL. The Syk tyrosine kinase: a crucial player in diverse biological functions [review]. Nat Rev Immunol 2010; 10:387–402.
2. Crowley MT, Costello PS, Fitzer-Attas CJ, et al. A critical role for Syk in signal transduction and phagocytosis mediated by Fcγ receptors on macrophages. J Exp Med 1997;186:1027–39.
3. Kiefer F, Brumell J, Al-Alawi N, et al. The Syk protein tyrosine kinase is essential for Fcγ receptor signaling in macrophages and neutrophils. Mol Cell Biol 1998;18:4209–20.
4. Geahlen RL. Syk and pTyr'd: signaling through the B cell antigen receptor [review]. Biochim Biophys Acta 2009;1793:1115–27.
5. Tsang E, Giannetti AM, Shaw D, et al. Molecular mechanism of the Syk activation switch. J Biol Chem 2008;283:32650–9.
6. Turner M, Schweighoffer E, Colucci F, et al. Tyrosine kinase Syk: essential functions for immunoreceptor signalling. Immunol Today 2000;21:148–54.
7. Futosi K, Mócsai A. Tyrosine kinase signaling pathways in neutrophils [review]. Immunol Rev 2016;273:121–39.
8. Gradler U, Schwarz D, Dresing V, et al. Structural and biophysical characterization of the Syk activation switch. J Mol Biol 2013;425: 309–33.
9. Pelosi M, Di Bartolo V, Mounier V, et al. Tyrosine 319 in the interdomain B of ZAP-70 is a binding site for the Src homology 2 domain of Lck. J Biol Chem 1999;274:14229–37.
10. Mansueto MS, Reens A, Rakhilina L, et al. A reevaluation of the spleen tyrosine kinase (Syk) activation mechanism. J Biol Chem 2019;294: 7658–68.
11. Falk RJ, Terrell RS, Charles LA, et al. Anti-neutrophil cytoplasmic autoantibodies induce neutrophils to degranulate and produce oxygen radicals in vitro. Proc Natl Acad Sci U S A 1990;87:4115–9.
12. Savage CO, Gaskin G, Pusey CD, et al. Anti-neutrophil cytoplasm antibodies can recognize vascular endothelial cell-bound anti-neutrophil cytoplasm antibody-associated autoantigens. Exp Nephrol 1993;1:190–5.
13. Porges AJ, Redecha PB, Kimberly WT, et al. Anti-neutrophil cytoplasmic antibodies engage and activate human neutrophils via Fc γ RIIa. J Immunol (Baltimore) 1994;153:1271–80.
14. Kocher M, Edberg JC, Fleit HB, et al. Antineutrophil cytoplasmic antibodies preferentially engage Fc γRIIIb on human neutrophils. J Immunol (Baltimore) 1998;161:6909–14.
15. Weidner S, Neupert W, Goppelt-Struebe M, et al. Antineutrophil cytoplasmic antibodies induce human monocytes to produce oxygen radicals in vitro. Arthritis Rheum 2001;44:1698–706.
16. Mulder AH, Heeringa P, Brouwer E, et al. Activation of granulocytes by anti-neutrophil cytoplasmic antibodies (ANCA): a Fc γ RII-dependent process. Clin Exp Immunol 1994;98:270–8.
17. Chacko GW, Brandt JT, Coggeshall KM, et al. Phosphoinositide 3-kinase and p72syk noncovalently associate with the low affinity Fc γ receptor on human platelets through an immunoreceptor tyrosine-based activation motif. Reconstitution with synthetic phosphopeptides. J Biol Chem 1996;271:10775–81.
18. Hewins P, Williams JM, Wakelam MJ, et al. Activation of Syk in neutrophils by antineutrophil cytoplasm antibodies occurs via Fcγ receptors and CD18. J Am Soc Nephrol 2004;15:796–808.
19. Smith J, McDaid JP, Bhangal G, et al. A spleen tyrosine kinase inhibitor reduces the severity of established glomerulonephritis. J Am Soc Nephrol 2010;21:231–6.
20. McAdoo SP, Reynolds J, Bhangal G, et al. Spleen tyrosine kinase inhibition attenuates autoantibody production and reverses experimental autoimmune GN. J Am Soc Nephrol 2014;25:2291–302.
21. McAdoo SP, Prendecki M, Tanna A, et al. Spleen tyrosine kinase inhibition is an effective treatment for established vasculitis in a pre-clinical model. Kidney Int 2020;97:1196–207.
22. Metsalu T, Vilo J. ClustVis: a web tool for visualizing clustering of multivariate data using Principal Component Analysis and heatmap. Nucleic Acids Res 2015;43:W566–70.
23. Ritchie ME, Phipson B, Wu D, et al. Limma powers differential expression analyses for RNA-sequencing and microarray studies. Nucleic Acids Res 2015;43:e47.
24. Braselmann S, Taylor V, Zhao H, et al. R406, an orally available spleen tyrosine kinase inhibitor blocks Fc receptor signaling and reduces immune complex-mediated inflammation. J Pharmacol Exp Ther 2006;319:998.
25. Jennette JC, Falk RJ. ANCAs are also antimonocyte cytoplasmic autoantibodies. Clin J Am Soc Nephrol 2015;10:4–6.
26. Tarzi RM, Liu J, Schneiter S, et al. CD14 expression is increased on monocytes in patients with anti-neutrophil cytoplasm antibody (ANCA)-associated vasculitis and correlates with the expression of ANCA autoantigens. Clin Exp Immunol 2015;181:65–75.
27. Wong KL, Tai JJ, Wong WC, et al. Gene expression profiling reveals the defining features of the classical, intermediate, and nonclassical human monocyte subsets. Blood 2011;118:e16–31.
28. Turner M, Billadeau DD. VAV proteins as signal integrators for multisubunit immune-recognition receptors [review]. Nat Rev Immunol 2002;2:476–86.
29. Berden AE, Ferrario F, Hagen EC, et al. Histopathologic classification of ANCA-associated glomerulonephritis. J Am Soc Nephrol 2010; 21:1628.
30. McAdoo SP, Bhangal G, Page T, et al. Correlation of disease activity in proliferative glomerulonephritis with glomerular spleen tyrosine kinase expression. Kidney Int 2015;88:52–60.
31. Savige J, Davies D, Falk RJ, et al. Antineutrophil cytoplasmic antibodies and associated diseases: a review of the clinical and laboratory features. Kidney Int 2000;57:846–62.
32. Kiener PA, Rankin BM, Burkhardt AL, et al. Cross-linking of Fc γ receptor I (Fc γ RI) and receptor II (Fc γ RII) on monocytic cells activates a signal transduction pathway common to both Fc receptors that involves the stimulation of p72 Syk protein tyrosine kinase. J Biol Chem 1993;268:24442–8.
33. Coxon A, Cullere X, Knight S, et al. Fc γ RIII mediates neutrophil recruitment to immune complexes. A mechanism for neutrophil accumulation in immune-mediated inflammation. Immunity 2001;14:693–704.

34. Kettritz R, Jennette JC, Falk RJ. Crosslinking of ANCA-antigens stimulates superoxide release by human neutrophils. J Am Soc Nephrol 1997;8:386–94.

35. Ralston DR, Marsh CB, Lowe MP, et al. Antineutrophil cytoplasmic antibodies induce monocyte IL-8 release. Role of surface proteinase-3, α1-antitrypsin, and Fcγ receptors. J Clin Invest 1997; 100:1416–24.

36. Cockwell P, Brooks CJ, Adu D, et al. Interleukin-8: a pathogenetic role in antineutrophil cytoplasmic autoantibody-associated glomerulonephritis. Kidney Int 1999;55:852–63.

37. Kurlander RJ. Blockade of Fc receptor-mediated binding to U-937 cells by murine monoclonal antibodies directed against a variety of surface antigens. J Immunol (Baltimore) 1983;131:140–7.

38. Jakus Z, Simon E, Frommhold D, et al. Critical role of phospholipase Cγ2 in integrin and Fc receptor-mediated neutrophil functions and the effector phase of autoimmune arthritis. J Exp Med 2009;206:577–93.

39. Cremasco V, Graham DB, Novack DV, et al. Vav/Phospholipase Cγ2–mediated control of a neutrophil-dependent murine model of rheumatoid arthritis. Arthritis Rheum 2008;58:2712–22.

40. Weinblatt ME, Kavanaugh A, Genovese MC, et al. An oral spleen tyrosine kinase (Syk) inhibitor for rheumatoid arthritis. New Engl J Med 2010;363:1303–12.

41. Bussel J, Arnold DM, Grossbard E, et al. Fostamatinib for the treatment of adult persistent and chronic immune thrombocytopenia: results of two phase 3, randomized, placebo-controlled trials. Am J Hematol 2018;93:921–30.

42. Davis MI, Hunt JP, Herrgard S, et al. Comprehensive analysis of kinase inhibitor selectivity. Nat Biotech 2011;29:1046–51.

43. Rolf MG, Curwen JO, Veldman-Jones M, et al. In vitro pharmacological profiling of R406 identifies molecular targets underlying the clinical effects of fostamatinib. Pharmacol Res Perspect 2015;3:e00175.

44. Schweighoffer E, Vanes L, Nys J, et al. The BAFF receptor transduces survival signals by co-opting the B cell receptor signaling pathway. Immunity 2013;38:475–88.

45. Jones RB, Tervaert JW, Hauser T, et al. Rituximab versus Cyclophosphamide in ANCA-associated renal vasculitis. New Engl J Med 2010; 363:211–20.

46. Prendecki M, Gulati K, Turner-Stokes T, et al. Characterisation of an enhanced preclinical model of experimental MPO-ANCA autoimmune vasculitis. J Pathol 2021;255:107–19.

American College of Rheumatology
Empowering Rheumatology Professionals

Arthritis & Rheumatology
Vol. 75, No. 1, January 2023, pp 98–107
DOI 10.1002/art.42290

Association of ^{18}F-Fluorodeoxyglucose–Positron Emission Tomography Activity With Angiographic Progression of Disease in Large Vessel Vasculitis

Kaitlin A. Quinn,[1] Mark A. Ahlman,[2] Hugh D. Alessi,[1] Michael P. LaValley,[3] Tuhina Neogi,[4] Jamie Marko,[2] Elaine Novakovich,[1] and Peter C. Grayson[1]

Objective. To assess whether vascular activity seen on ^{18}F-fluorodeoxyglucose–positron emission tomography (FDG-PET) scan is associated with angiographic change in large vessel vasculitis (LVV).

Methods. Patients with LVV were recruited into a prospective cohort. All patients underwent magnetic resonance angiography or computed tomography angiography and FDG-PET imaging. Follow-up imaging using the same imaging modalities was obtained ≥6 months later per a standardized imaging protocol. Arterial damage, defined as stenosis, occlusion, or aneurysm, and corresponding FDG uptake were evaluated in 17 arterial territories. On follow-up, development of new lesions was recorded, and existing lesions were characterized as improved, worsened, or unchanged.

Results. A total of 1,091 arterial territories from 70 patients with LVV (38 patients with Takayasu arteritis, 32 patients with giant cell arteritis) were evaluated. Over a median 1.6 years of follow-up, new lesions developed only in 8 arterial territories in 5 patients with Takayasu arteritis. Arterial lesions improved in 16 territories and worsened in 6 territories. Most arterial territories that did not have vascular activity on FDG-PET scan at baseline had no angiographic change over the follow-up period (787 [99%] of 793). Few territories with baseline FDG-PET activity had angiographic change over time (24 [8%] of 298), but of the territories that developed angiographic change, 80% had FDG-PET activity at baseline. Within the same patient, an arterial territory with baseline FDG-PET activity had significantly increased risk for angiographic change compared to a paired arterial territory without FDG-PET activity (odds ratio 19.49 [95% confidence interval 2.44–156.02]; $P < 0.01$). Concomitant edema and wall thickening further increased risk for angiographic change.

Conclusion. Development of angiographic change was infrequent in this cohort of patients with LVV. A lack of baseline FDG-PET activity was strongly associated with stable angiographic disease. In cases of angiographic progression, change was preceded by the presence of FDG-PET activity.

INTRODUCTION

Assessment of disease activity in large vessel vasculitis (LVV) can be challenging as patients may not have overt clinical symptoms or elevated acute-phase reactants during periods of active disease. Noninvasive angiography using magnetic resonance angiography (MRA) or computed tomography (CT) angiography has become essential to detect and monitor vascular disease in patients with LVV (1–3). The development of new areas of arterial damage detected on angiography during periods of apparent clinical remission has been reported in patients with LVV, but it remains unknown whether this is a common or rare phenomenon (4,5). Previous studies have shown varied frequencies of angiographic progression in LVV, and some studies have

ClinicalTrials.gov identifier: NCT02257866

Supported by the Intramural Research Program at the National Institute of Arthritis and Musculoskeletal and Skin Diseases, NIH. Dr. LaValley's work was supported by the National Institute of Arthritis and Musculoskeletal and Skin Diseases, NIH (award CCCR P30-AR-072571).

[1]Kaitlin A. Quinn, MD, Hugh D. Alessi, BA, Elaine Novakovich, MS, RN, and Peter C. Grayson, MD, MSc: Systemic Autoimmunity Branch, National Institute of Arthritis and Musculoskeletal and Skin Diseases, NIH, Bethesda, Maryland; [2]Mark A. Ahlman, MD, Jamie Marko, MD: Clinical Center, Radiology and Imaging Sciences, NIH, Bethesda, Maryland; [3]Michael P. LaValley, PhD: Department of Biostatistics, Boston University School of Public Health, Boston, Massachusetts; [4]Tuhina Neogi, MD, PhD: Division of Rheumatology, Boston University School of Medicine, Boston, Massachusetts.

Author disclosures are available at https://onlinelibrary.wiley.com/action/downloadSupplement?doi=10.1002%2Fart.42290&file=art42290-sup-0001-Disclosureform.pdf.

Address correspondence via email to Kaitlin A. Quinn, MD, at Kaitlin.quinn@nih.gov.

Submitted for publication April 26, 2022; accepted in revised form June 30, 2022.

demonstrated that either progressive arterial damage or improvement can occur over time (6–8). Current guidelines for the use of imaging in patients with LVV differ on the role and frequency of periodic angiography to monitor arterial damage, due in part to limited prospective data characterizing angiographic progression of disease over time and a lack of standardized imaging protocols when assessing change (3,9).

A multimodal imaging assessment that incorporates the use of ^{18}F-fluorodeoxyglucose–positron emission tomography (FDG-PET) with noninvasive angiography has become increasingly used when assessing LVV (1,10,11). Abnormal metabolic activity detected on FDG-PET within the walls of large arteries due to activated immune cells can be used instead to identify vascular inflammation in LVV, but the degree to which vascular FDG-PET abnormalities are specific for inflammation is difficult to define (1,12,13). Limited longitudinal data on the use of FDG-PET in assessing LVV have shown that patients may have vascular activity revealed on PET during periods of clinical remission (12,14,15). Whether vascular FDG-PET activity predicts long-term outcomes, including angiographic progression of disease, in patients with LVV remains unknown.

The objectives of this study were 1) to characterize progression of disease over time by noninvasive angiography using a standardized imaging protocol in a prospective, longitudinal cohort of patients with Takayasu arteritis (TAK) and giant cell arteritis (GCA), and 2) to evaluate whether the presence of vascular activity detected on FDG-PET scans predicts angiographic progression of disease in LVV.

PATIENTS AND METHODS

Study population. Patients who had been diagnosed as having LVV were recruited into a prospective, observational cohort at the National Institutes of Health (NIH) in Bethesda, MD. Patients fulfilled the 1990 American College of Rheumatology classification criteria for TAK (16) or the modified 1990 American College of Rheumatology classification criteria for GCA (17,18). Patients could be enrolled at various stages during the disease course. All patients provided written informed consent. An institutional review board and radiation safety committee at the NIH approved the research (National Institutes of Arthritis and Musculoskeletal and Skin Diseases Institutional Review Board Protocol 14-AR-0200).

Clinical assessment. All patients underwent baseline clinical evaluation, laboratory testing, MRA or CT angiography, and FDG-PET imaging at the NIH Clinical Center. The investigative study team performed all clinical assessments within 24 hours prior to imaging assessment. Clinical disease was recorded as either active or in remission prior to conducting imaging studies. Active disease was defined as the presence of any clinical disease feature directly attributed to vasculitis (e.g., carotidynia, headache) at the time of assessment. Fatigue or elevated acute-phase reactant levels alone were not considered sufficient evidence of active disease. Remission was defined as the absence of any clinical features directly attributable to vasculitis, regardless of acute-phase reactant levels. Patients underwent follow-up clinical assessments at least 6 months later. Changes in clinical disease activity, C-reactive protein (CRP) levels, and treatment over the follow-up interval were assessed. Increased treatment was defined as the addition of a new disease-modifying antirheumatic drug, new biologic therapy, or increase in glucocorticoid dose by ≥50% over the follow-up period.

Noninvasive angiography protocol and assessment. All patients underwent a baseline MRA or CT angiography of the aorta and primary branches and follow-up imaging on the same image modality at least 6 months after baseline per a standardized imaging protocol, as previously described (10). In patients who had more than 2 imaging visits, the baseline and most recent follow-up images were compared to assess for change over the longest available time interval. For additional details and imaging protocol, see Supplementary Methods available on the *Arthritis & Rheumatology* website at https://onlinelibrary.wiley.com/doi/art.42290.

Vascular damage, defined as stenosis, occlusion, or aneurysm, was evaluated by visual inspection in 4 segments of the aorta (ascending, arch, descending thoracic, and abdominal) and 13 branch arteries (innominate, carotids, vertebrals, subclavians, axillaries, common iliacs, and femorals) by a single reader (MAA) who was blinded with regard to clinical data. Only luminal changes were considered, and wall thickness, edema, and contrast enhancement were not included in the definition of vascular damage. On follow-up angiography, the development of new arterial damage in these same arterial territories was recorded, and existing arterial damage was characterized as improved, worsened, or unchanged by visual inspection, with confirmation by an independent reviewer (JM). Angiographic change over time was evaluated at the patient level and within each individual arterial territory. Morphologic changes in vessel walls were identified by expert review (reviewed by MAA, who has >10 years of experience in multimodality vascular imaging, followed by expert consensus opinion for challenging cases).

FDG-PET imaging protocol and assessment. All patients underwent whole-body FDG-PET imaging on the same dates as the baseline and follow-up angiograms, per a standardized imaging protocol. A single reader (MAA) reviewed all FDG-PET scans and was blinded with regard to clinical status and angiogram assessment. Excellent intrarater agreement ($k = 0.76$) and interrater agreement ($k = 0.84$) were previously reported for this cohort (12,19). Qualitative assessment of FDG uptake was assessed in each of the 17 corresponding arterial

territories evaluated by angiography. The degree of arterial uptake was visually assessed relative to liver uptake as follows: 0 = no uptake; 1 = less than liver uptake; 2 = same as liver uptake; 3 = greater than liver uptake. Active vasculitis in an arterial territory was defined as greater FDG uptake in the arterial wall than the liver. Semiquantitative assessment of arterial FDG uptake was performed to obtain the corresponding maximum standardized uptake value (SUV_{max}) (see Supplementary Methods at https://onlinelibrary.wiley.com/doi/art.42290).

Statistical analysis. Clinical characteristics among patients with improved arterial damage, new or worsened arterial damage, and unchanged arterial damage were compared using a chi-square test or Kruskal-Wallis test, as appropriate. FDG-PET scan and angiographic findings were compared within specific arterial territories. Baseline vascular activity on FDG-PET scans was studied in association with angiographic change (new, worsened, or improved arterial damage) versus no change to determine if FDG-PET activity predicted angiographic progression of disease. Logistic regression was used to identify clinical features associated with angiographic change using the following predictor variables: type of LVV (TAK or GCA), baseline clinical disease activity (active or remission), disease duration, baseline CRP levels, baseline global FDG-PET interpretation (active or inactive disease), and whether the patient was receiving treatment at baseline. Only variables with *P* values less than 0.10 in univariable analyses were included in the multivariable model. Analyses were conducted using JMP version 14.0.

Within-person, arterial territory–matched analysis. To evaluate the association between baseline FDG-PET activity and risk for subsequent angiographic change in the same specific arterial territories on the follow-up imaging study, we used a within-person, arterial territory–matched approach with conditional logistic regression to adjust for correlated data. For this approach, we identified participants with discordant angiographic change in paired arteries (e.g., a patient who developed worsened angiographic damage in the left carotid artery over the study follow-up while there were no changes in the right carotid artery). In this way, each person served as their own control, allowing comparison of baseline FDG-PET activity in the angiographic territory that changed versus the contralateral territory that did not change over time within the same patient. As such, the effects of all person-level confounders (e.g., differences in disease duration at baseline imaging study, differences in length of follow-up time, differences in treatment) were eliminated by using this type of analysis (20). Fourteen arterial territories were assessed and grouped into 7 symmetric paired sets: 1) bilateral carotids, 2) bilateral vertebrals, 3) bilateral subclavians, 4) bilateral axillaries, 5) bilateral common iliacs, 6) bilateral femorals, and 7) descending thoracic and abdominal aorta. The remaining 3 arterial territories assessed by angiography (ascending aorta, aortic arch, innominate artery) were not included in the within-person, arterial territory–matched analyses. Conditional logistic regression analysis was conducted using R version 4.0.2.

RESULTS

Characteristics of the study population. A total of 70 patients with LVV were recruited into the study. There were 38 patients with TAK and 32 patients with GCA. Baseline demographics and clinical characteristics of the study population are shown in Table 1. Median disease duration at the time of study enrollment was 2.2 years among patients with TAK and 0.7 years among patients with GCA. Thirty-seven patients (53%) had ongoing active clinical features at the baseline visit. There were no significant differences at baseline in the proportion of patients with TAK who had active disease (45%) versus patients with GCA who had active disease (63%) (*P* = 0.14), and there was no difference over follow-up in the proportion of patients with TAK who achieved clinical remission (79%) versus patients with GCA who achieved clinical remission (88%) (*P* = 0.53).

Arterial territory–level analysis of angiographic change over study follow-up. A total of 1,190 arterial territories from 70 patients with LVV were evaluated. Ninety-nine territories with unacceptable image quality due to technical factors (e.g., patient positioning, movement, image acquisition error) were excluded. The remaining 1,091 arterial territories (577 arterial territories from patients with TAK, 514 arterial territories from patients with GCA) were assessed over a median follow-up of 1.6 years (interquartile range [IQR] 1.0–2.7 years). Patients with TAK were followed for similar lengths of time compared to patients with GCA (median 1.5 years [IQR 1.0–2.6] versus 1.8 years [IQR 0.7–2.9], respectively; *P* = 0.96).

There was no change in angiographic findings (i.e., new, worsened, or improved stenosis, occlusion, or aneurysm) from baseline to the most recent follow-up visit in 1,061 (97.3%) of 1,091 territories. New, worsened, or improved arterial damage was observed in 30 (2.7%) of 1,091 territories, which occurred in 16 patients overall. Of 843 arterial territories with no arterial damage at the baseline visit, new damage occurred in 8 territories (1%) in 5 patients. A total of 248 arterial territories had existing arterial luminal damage at the baseline visit, with aneurysmal disease observed in 21% of these territories (35 territories among TAK patients and 17 territories among GCA patients). Most of these arterial territories remained unchanged over follow-up (226 [91%] of 248 territories). Luminal damage improvement was seen in 16 territories (7%), and damage worsening was seen in 6 territories (2%) (Figure 1). Change in damage was only observed in stenosing lesions, and angiographic change only occurred in 9 of the 17 specific arterial territories assessed (see Supplementary Figures 1 and 2 available on the *Arthritis &*

Table 1. Study population characteristics of patients with TAK and patients with GCA at the baseline visit*

Characteristic	Patients with TAK (n = 38)	Patients with GCA (n = 32)	*P*
Age, median (IQR) years	29.5 (18.4–39.5)	70.5 (61.1–75.9)	<0.01
Female sex	30 (79)	23 (72)	0.49
Disease duration, median (IQR) years	2.2 (0.6–5.5)	0.7 (0.1–2.6)	<0.01
Active clinical disease	17 (45)	20 (63)	0.14
Positive TAB finding†	NA	14 (44)	NA
Large vessel GCA angiographic involvement‡	NA	11 (34)	NA
Positive TAB finding and large vessel GCA angiographic involvement	NA	7 (22)	NA
Acute-phase reactants			
ESR, median (IQR) mm/hour	18.5 (11–34)	19 (9–26)	0.81
CRP, median (IQR) mg/liter	3.8 (0.9–14)	6.3 (1–11)	0.58
Type of angiography			1.0
MRA	35 (92)	29 (91)	–
CT angiography	3 (8)	3 (9)	–
Treatment			
Prednisone dosage, median (IQR) mg/day	5 (0–10)	7.5 (0–34)	0.21
Other immune therapy	26 (70)	16 (50)	0.08
Conventional DMARD	22 (85)	11 (69)	0.27
Biologic DMARD	11 (42)	3 (19)	0.17

* Except where indicated otherwise, values are the number (%) of patients. TAK = Takayasu arteritis; IQR = interquartile range; NA = not applicable; ESR = erythrocyte sedimentation rate; CRP = C-reactive protein; DMARD = disease-modifying antirheumatic drug.
† Of 32 patients, 26 (81%) with giant cell arteritis (GCA) underwent temporal artery biopsy (TAB).
‡ All patients with GCA underwent magnetic resonance angiography (MRA) or computed tomography (CT) angiography at the time of baseline ^{18}F-fluorodeoxyglucose–positron emission tomography scan. Large vessel GCA was defined as stenosis, occlusion, or aneurysm of large arteries on MRA or CT angiography.

Rheumatology website at https://onlinelibrary.wiley.com/doi/art.42290).

Patient-level analysis of angiographic change over study follow-up. Of the 70 patients with LVV, 9 patients (6 with TAK, 3 with GCA) had improved damage in ≥1 arterial territory (without any territories with new or worsened damage); 7 patients (7 with TAK, 0 with GCA) had ≥1 arterial territory with new or worsened damage (without any territories with improved damage); and 54 patients (25 with TAK, 29 with GCA) had no change in arterial damage on follow-up angiography (Table 2).

In univariable logistic regression, angiographic change was not significantly associated with baseline CRP levels, baseline FDG-PET interpretation (active versus inactive vasculitis), disease duration, length of follow-up time, or baseline treatment status. In multivariable regression, independent predictors of angiographic change were a diagnosis of TAK versus a diagnosis of GCA (odds ratio [OR] 3.10 [95% confidence interval (95% CI) 1.54–7.17]; $P < 0.01$) and active clinical disease at the baseline visit (OR 3.94 [95% CI 1.86–10.80]; $P < 0.01$).

Among 38 patients with TAK, new arterial damage occurred in 5 patients (13%), worsened damage occurred in 3 patients

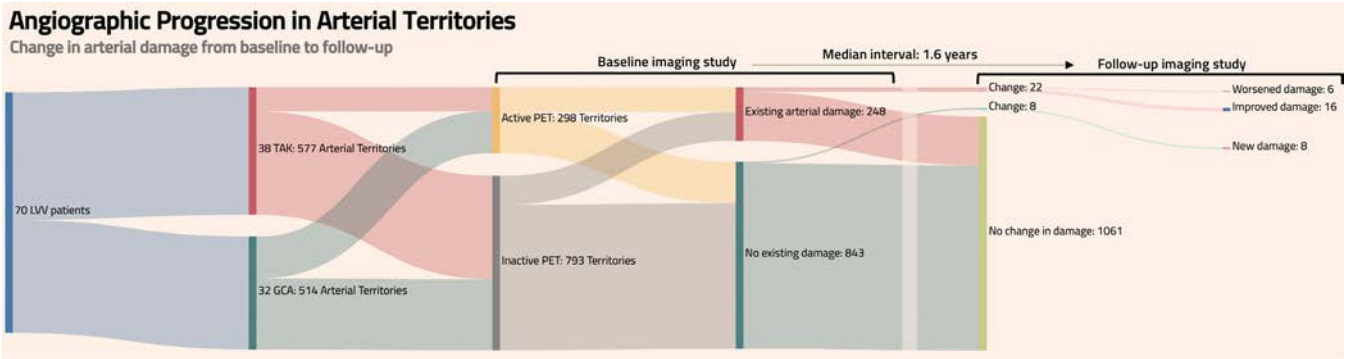

Figure 1. Flow chart depicting the number of arterial territories that developed new arterial damage, worsened damage, improved damage, or no change in damage on angiography over a median 1.6-year follow-up in 1,091 total arterial territories from 70 patients with large vessel vasculitis (LVV) (577 arterial territories from patients with Takayasu arteritis [TAK] and 514 arterial territories from patients with giant cell arteritis [GCA]). The presence of vascular activity on ^{18}F-fluorodeoxyglucose–positron emission tomography (FDG-PET) scan and existing arterial damage in each arterial territory was assessed at the time of the baseline imaging studies.

Table 2. Clinical characteristics of patients with large vessel vasculitis who had improved arterial damage, new or worsened arterial damage, or no angiographic change*

	Improved arterial damage (n = 9)	New or worsened arterial damage (n = 7)	No change (n = 54)	*P*
Disease duration at baseline, median (IQR) years	0.4 (0.1–2.8)	1.5 (0.6–3.6)	1.5 (0.4–5.1)	0.19
Follow-up duration, median (IQR) years	1.5 (1.0–2.7)	1.9 (1.5–4.3)	1.6 (1.0–2.7)	0.52
Type of large vessel vasculitis				0.02
GCA	3	0	29	–
TAK	6	7	25	–
Clinical disease activity				<0.01
Active disease at any point during the study	9 (100)	7 (100)	25 (46)	–
Persistent remission	0 (0)	0 (0)	29 (54)	–
CRP level				
Baseline, median (IQR) mg/liter	1.8 (0.7–28)	13.4 (5.1–49)	4.2 (1–11)	0.20
Follow-up, median (IQR) mg/liter	0.4 (0.2–0.9)	6.1 (4–20)	0.6 (0.2–2)	0.02
CRP during the study period				0.11
Elevated (>10 mg/liter)	3 (33)	5 (71)	17 (31)	–
Persistently normal	6 (67)	2 (29)	37 (69)	–
Baseline PET global interpretation, active disease	7 (78)	5 (71)	40 (77)	0.96
Baseline PETVAS, median (IQR) score	17 (11–26)	17 (10–21)	18 (14–24)	0.95
Follow-up PET global interpretation, active disease	5 (56)	3 (43)	28 (52)	0.87
PET global interpretation				0.92
Active disease at any point during the study	7 (78)	6 (86)	44 (81)	–
Persistently inactive disease	2 (22)	1 (14)	10 (19)	–
Treatment				
Prednisone dosage				
Baseline, median (IQR) mg/day	15 (0–50)	2 (0–30)	5 (0–16)	0.55
Follow-up, median (IQR) mg/day	0 (0–6)	0 (0–20)	0 (0–5)	0.35
Conventional DMARD†				
Baseline	4 (44)	3 (43)	23 (43)	0.99
Follow-up	4 (44)	5 (71)	23 (43)	0.35
Biologic DMARD‡				
Baseline	2 (22)	4 (57)	10 (19)	0.07
Follow-up	8 (89)	4 (57)	27 (50)	0.09

* Except where indicated otherwise, values are the number (%) of patients. IQR = interquartile range; CRP = C-reactive protein; PET = positron emission tomography; PETVAS = PET Vascular Activity Score.
† At baseline, the most commonly used conventional disease-modifying antirheumatic drugs (DMARDs) were methotrexate (12 patients with Takayasu arteritis [TAK], 10 patients with giant cell arteritis [GCA]) and mycophenolate mofetil (6 patients with TAK, 0 patients with GCA). At follow-up, the most commonly used conventional DMARDs were methotrexate (14 patients with TAK, 3 patients with GCA) and mycophenolate mofetil (6 patients with TAK, 1 patient with GCA).
‡ At baseline, the most commonly used biologic DMARDs were tumor necrosis factor inhibitors (6 patients with TAK, 0 patients with GCA) or tocilizumab (2 patients with TAK, 1 patient with GCA). At follow-up, the most commonly used biologic DMARDs were tumor necrosis factor inhibitors (10 patients with TAK, 0 patients with GCA) or tocilizumab (9 patients with TAK, 20 patients with GCA).

(8%), and 1 patient had a territory with new damage and another territory with worsened damage. None of the 32 patients with GCA developed new or worsened areas of arterial damage over follow-up. Seventy-two percent of patients with new or worsened damage had clinically active disease at the baseline visit, and the remaining patients developed a clinical flare over the follow-up interval, with no patient developing "silent" angiographic progression (angiographic progression in the absence of clinical symptoms). Compared to patients with improved damage, patients with new or worsened arterial damage were often initially evaluated later in the disease course (median disease duration 1.5 years [IQR 0.6–3.6 years]) and had higher CRP levels at baseline visit (median 13.4 mg/liter [IQR 5.1–49 mg/liter]). The majority (57%) were receiving biologic therapies at the baseline visit but were taking low doses of glucocorticoids (median prednisone dosage 2 mg/day [IQR 0–30 mg/day]) (Table 2). Two patients were nonadherent to treatment over the follow-up interval, and 1 patient developed a severe disease relapse with delayed initiation of treatment.

Improved arterial damage occurred in 6 (16%) of 38 patients with TAK and 3 (9%) of 32 patients with GCA. All patients who had improved damage had clinical disease activity at the baseline visit. Compared to patients with new or worsened arterial damage, patients who experienced improved damage over the follow-up were those who were still early in their disease course (median disease duration 0.4 years [IQR 0.1–2.8 years]), were those who had been taking higher doses of glucocorticoids at the baseline visit (median prednisone dosage 15 mg/day [IQR 0–50 mg/day]), and were those who more frequently had to change their treatment over the follow-up interval, with 89% of patients receiving a biologic therapy at the time of follow-up assessment (Table 2).

No angiographic change occurred in 25 patients with TAK (66%) and 29 patients with GCA (91%). The majority of patients with no angiographic change were in persistent clinical remission (29 [54%] of 54 patients) (see Supplementary Figure 3 available on the *Arthritis & Rheumatology* website at https://onlinelibrary.wiley.com/doi/art.42290). Of these 29 patients in persistent clinical remission, 83% had normal acute-phase reactant levels at baseline (24 of 29 patients), but 69% had baseline subclinical FDG-PET activity (20 of 29 patients). Twelve patients whose disease was in clinical remission throughout the study and had FDG-PET scans showing vascular activity at baseline (and had normal CRP levels) did not receive increased treatment—defined as the addition of a new disease-modifying antirheumatic drug, new biologic therapy, or increase in glucocorticoid dose by ≥50% over the follow-up period. No angiographic progression of disease was observed over follow-up in these patients. Treatment was increased in 8 patients whose disease was in clinical remission throughout the study and had active disease on FDG-PET scan at baseline. Four of these patients were being treated with glucocorticoid monotherapy at baseline, and steroid-sparing therapy was added. The other 4 patients had severe elevations in CRP level or severe FDG-PET activity, and biologic therapy was added (Supplementary Figure 4, https://onlinelibrary.wiley.com/doi/art.42290). There was no angiographic progression of disease over follow-up in any of these patients.

Assessment of angiographic change in all territories with and without baseline FDG-PET activity. Baseline FDG-PET activity was evaluated in the 1,091 corresponding arterial territories that were evaluated by angiography. There was no change in angiographic findings over follow-up for 99% of arterial territories that had no FDG-PET activity at baseline (787 of 793 territories). Most arterial territories with FDG-PET activity at baseline also did not develop angiographic change over the follow-up interval, with only 8% of arterial territories developing angiographic change (24 of 298 territories).

Of the 30 arterial territories that developed angiographic change, 80% had FDG-PET activity at baseline (24 of 30 territories) (Figure 2). Of the 4 patients (6 territories) who had angiographic change but did not have baseline FDG-PET activity, 3 patients had clinical relapse with PET activity in the corresponding territory on follow-up. The other patient had associated arterial thrombosis with progressive damage in the absence of PET activity on follow-up. Overall, FDG-PET activity in an arterial territory at baseline was associated with change in that arterial territory on follow-up angiography with a positive predictive value of 8% and negative predictive value of 99%.

Association of FDG-PET activity and angiographic change in the within-person, arterial territory–matched approach using conditional logistic regression. Of the 30 arterial territories that developed angiographic change over follow-up, 26 of the 30 territories were asymmetric in paired arteries (e.g., left carotid artery had angiographic progression, right carotid artery had no change). Specifically, we identified 16 patients who had 26 asymmetric angiographic changes in paired arterial territories that were eligible for this analysis (10 patients had >1 discordant pair). An arterial territory with baseline FDG-PET activity had significantly higher odds for angiographic progression of disease over follow-up compared to the matched arterial territory without baseline FDG-PET activity (OR 19.49 [95% CI 2.44–156.02]; $P < 0.01$). Representative images of asymmetric angiographic change in paired arteries are shown in Figure 3.

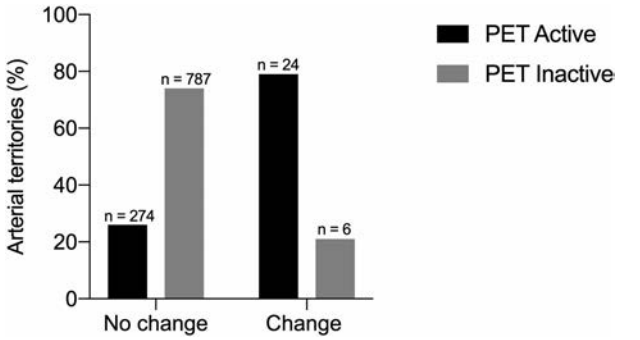

Figure 2. Distribution of arterial territories with vascular activity compared to those without vascular activity evident on ^{18}F-fluorodeoxyglucose–positron emission tomography (FDG-PET) scans at baseline from patients with large vessel vasculitis, according to whether patients experienced angiographic change in arterial damage versus no angiographic change over follow-up.

Additional imaging characteristics associated with angiographic change. Because most instances of angiographic change were asymmetric in paired arterial territories and were associated with corresponding baseline FDG-PET activity, we next examined all instances of asymmetric FDG-PET activity at the baseline study visit in paired arteries across the cohort. Of the total 490 paired arterial territories, baseline FDG-PET activity was asymmetric in 42 paired territories (e.g., left carotid artery had FDG-PET activity, right carotid artery had no FDG-PET activity). When examining the 42 arterial territories with baseline FDG-PET activity, corresponding angiographic change occurred in 13 territories (31%); there was no change in the other 29 territories (69%).

We then studied if additional factors present on the baseline imaging studies besides presence of FDG-PET activity were associated with angiographic change, including the degree of baseline FDG-PET activity (determined using SUV_{max} values) and the presence of wall morphologic changes (increased wall thickening and edema). There were no differences in baseline median SUV_{max} values among arterial territories with asymmetric FDG-PET activity that developed

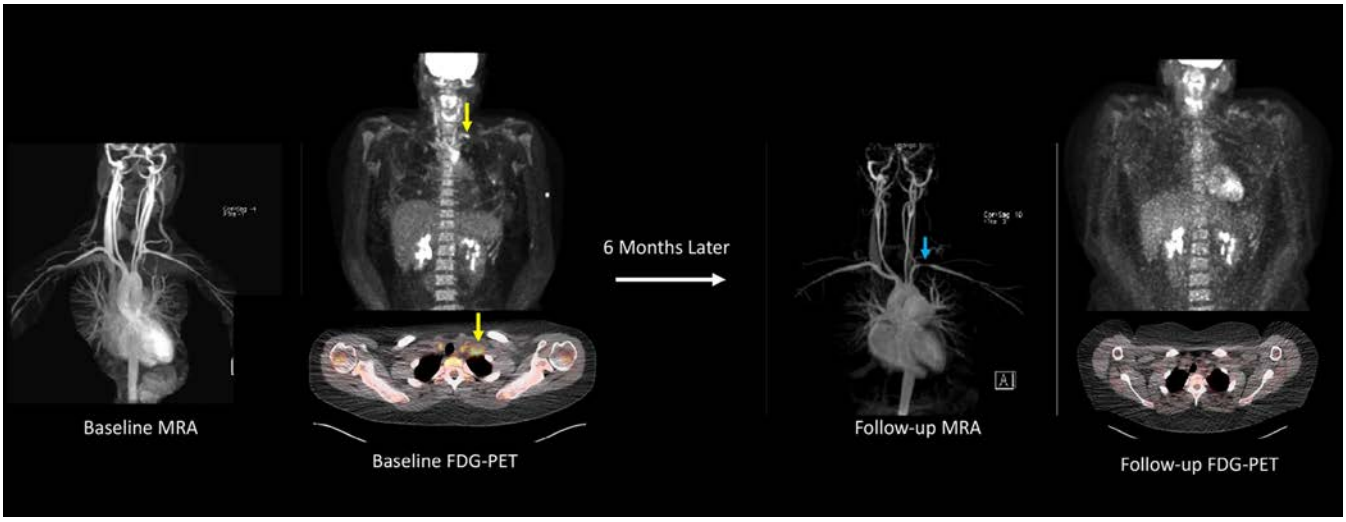

Figure 3. Baseline and follow-up magnetic resonance angiography (MRA) and ^{18}F-fluorodeoxyglucose–positron emission tomography (FDG-PET) scans from a 22-year-old woman with Takayasu arteritis who discontinued receiving methotrexate/infliximab after ~2 years of treatment and subsequently developed constitutional symptoms, frontal headaches, carotidynia, and left arm claudication 6 months later, with significant elevations in acute-phase reactants (erythrocyte sedimentation rate of 104 mm/hour, C-reactive protein of 85 mg/liter). A baseline FDG-PET scan showed severe vascular FDG uptake throughout the aorta and bilateral common carotid arteries with a prominent area of focal inflammation in the left subclavian artery (**yellow arrows**) on whole-body and axial views. MRA obtained the same date did not show vascular damage. Treatment was reinitiated with excellent clinical response. Six months after baseline imaging, the patient had a repeat MRA showing a new left subclavian artery stenosis (**blue arrow**) with resolution of vascular FDG-PET activity.

angiographic progression (median SUV_{max} 3.6 [IQR 2.2–4.5]) versus arterial territories that did not develop angiographic progression (median SUV_{max} 4.2 [IQR 3.1–5.3]) (P = 0.35) (Figure 4A). Of the 42 arterial territories with asymmetric FDG-PET activity, all 13 territories (100%) in which angiographic change occurred had concomitant wall morphologic changes (increased wall thickening and edema) at baseline, while 38% of territories that did not have angiographic change had wall morphologic changes at baseline (11 of 29 territories) ($P < 0.0001$) (Figure 4B).

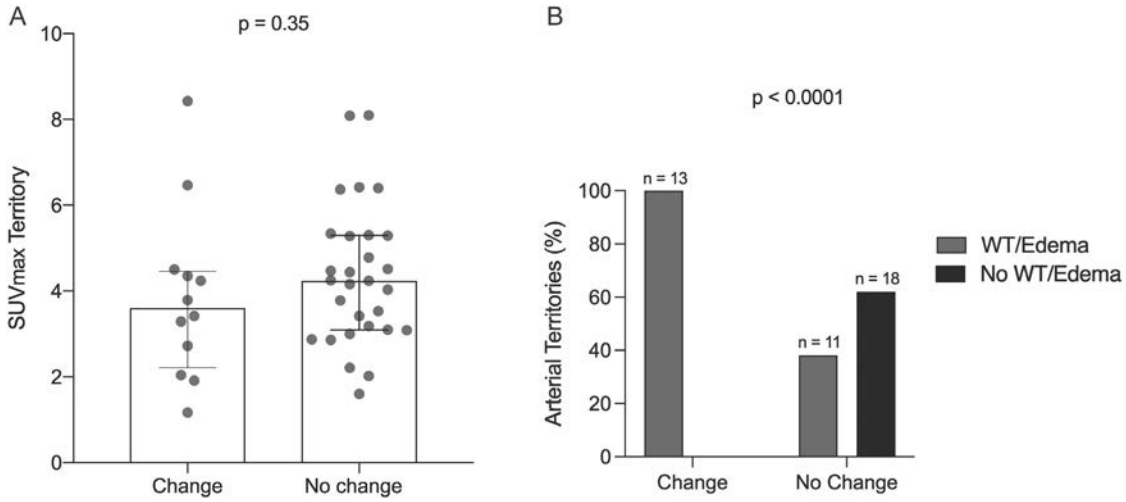

Figure 4. A, Maximum standardized uptake (SUV_{max}) values for arterial territories with asymmetric vascular activity evident on ^{18}F-fluorodeoxyglucose–positron emission tomography (FDG-PET) at baseline among patients with large vessel vasculitis, according to whether patients experienced angiographic change in arterial damage versus no angiographic change at follow-up. Symbols represent individual territories; bars represent the median SUV_{max} and corresponding interquartile range. **B,** Distribution of arterial territories with asymmetric FDG-PET activity at baseline that had corresponding vessel wall morphologic changes (wall thickening [WT] and edema) on baseline angiography versus arterial territories that did not have wall morphologic changes (according to whether patients experienced angiographic change in arterial damage versus no angiographic change over follow-up).

DISCUSSION

This study provides some of the first and only available data about the longitudinal relationship between vascular activity detected on FDG-PET scans and future angiographic change in patients with LVV. Complex associations between FDG-PET activity and angiographic change were found in this cohort of patients who underwent standardized clinical and imaging assessments. Overall, little angiographic change occurred, and a lack of FDG-PET activity was strongly associated with stable angiographic disease. The majority of arterial territories with FDG-PET activity did not develop angiographic change; however, in cases where angiographic change did occur, change was frequently preceded by the presence of FDG-PET activity in the arterial territory at baseline.

The development of angiographic change was uncommon over a median 1.6-year follow-up period in this cohort of patients with LVV. In cases where angiographic change occurred, it was more frequently observed in patients with TAK compared to patients with GCA. A wide range of frequencies of angiographic progression in patients with LVV have been reported in previous studies, with several studies also showing angiographic change is an uncommon occurrence (8,21), while other studies have reported more frequent angiographic change (4,6). Studies in which angiographic change has been reported more frequently have been retrospective, not employed standardized imaging protocols, and not used centralized review of images, all of which could have led to overestimation of the frequency of angiographic change.

In the present study, patients were frequently enrolled in the later phases of disease, which may have contributed to the infrequent angiographic change observed; however, despite being later in the disease course, many patients had clinical disease activity at the baseline study visit or developed disease flares over the follow-up interval. More patients in this cohort were also being treated with biologic therapy compared to other cohorts (6), which could have affected the frequency of angiographic change observed. Additionally, as LVV is a slowly progressing disease, the duration of follow-up may have contributed to the low frequency of angiographic change observed. However, some patients did develop new or worsened arterial damage later in the disease course, highlighting the importance of continued monitoring of patients with LVV, even in later phases of disease.

This study demonstrated that patients with existing arterial luminal damage could have either progressive arterial damage or improvement over time, similar to findings from prior studies (7,21). Whether improvement or worsening occurs in a territory with existing arterial damage may depend on where a patient is in the course of their disease, the disease severity, and treatment received. Patients in this study who developed new or worsened arterial damage were often nonadherent to treatment or had delayed initiation of treatment outside the window of possible prevention of damage. These data provide insight into the natural history of vascular lesions in LVV, as a window of intervention may exist to prevent new or worsening damage with treatment. Additionally, new or worsened arterial damage was only observed in patients with TAK rather than patients with GCA, despite comparable proportions of patients who achieved clinical remission throughout the study. Progressive arterial damage in patients with TAK despite effective therapeutic intervention has been attributed to "healing fibrosis." Thus, the window for effective intervention may be narrower when treating TAK compared to treating GCA due to a shorter disease duration required before potential development of arterial damage in patients with TAK.

This study reports some of the only available evidence to evaluate whether FDG-PET activity is associated with angiographic change. However, this study does not address the specificity of FDG-PET scan findings or whether FDG-PET activity represents subclinical vascular inflammation, vascular remodeling, or a combination of factors. In the absence of a corresponding histologic gold standard, some level of uncertainty about whether FDG-PET activity truly represents active vasculitis will remain, but the data obtained in this study reframe the focus to whether FDG-PET activity has prognostic information for patients and therefore should guide management decisions.

In this study, the majority of arterial territories with baseline vascular FDG-PET activity did not develop angiographic change over the follow-up period. Normalization of FDG-PET activity should not be the goal for all patients with LVV, particularly for patients with GCA who frequently had metabolic activity in the arterial wall without subsequent angiographic change. Although most arterial territories with FDG-PET activity were not associated with angiographic change, there are still many potential scenarios for which serial FDG-PET monitoring may be useful, including clarification of symptoms that could be secondary to ongoing vascular inflammation or that reflect prior vascular damage, evaluation of unexplained laboratory abnormalities later in the disease course, or assessment of treatment response at the vascular level. Conversely, the absence of baseline vascular FDG-PET activity in arterial territories was associated with stable angiographic findings on follow-up imaging.

FDG-PET scan data could potentially be incorporated into more stringent definitions of disease remission. Most patients who had angiographic change at follow-up also had FDG-PET activity that preceded the angiographic change, suggesting FDG-PET scans track an aspect of disease activity. Future research is needed to better define what additional imaging risk factors contribute to change over time. Our data provide preliminary insight into potential risk factors. Patients with focal, asymmetric areas of arterial FDG-PET activity with concomitant wall thickening and edema on angiography at baseline were most likely to develop angiographic change over follow-up (see Supplementary Figure 5 available on the *Arthritis & Rheumatology* website at https://onlinelibrary.wiley.com/doi/art.42290).

This study also shows that treatment decisions should not be based solely on FDG-PET scan findings. Overall, the majority of patients in clinical remission with abnormal FDG-PET activity did not receive increased treatment, and none of these patients had angiographic change over follow-up. On the other hand, some patients with subclinical FDG-PET activity (with or without elevations in acute-phase reactants) did receive increased treatment. There may be subsets of patients at greatest risk for angiographic progression who may benefit from increased treatment based on imaging findings alone, such as those with focal areas of FDG-PET activity and concomitant wall morphologic changes in critical vascular regions. However, this study was done in the context of an observational cohort, making it difficult to know what would have happened in these cases if treatment had remained unchanged.

These data should inform future guideline recommendations for the use of imaging to monitor LVV. Current guidelines recommend regular noninvasive imaging for long-term monitoring of angiographic progression but do not specify an optimal imaging modality or interval (3,9). The data in this study demonstrate the value of a multimodal imaging assessment with concomitant FDG-PET scans and noninvasive angiography and support their use in monitoring LVV. Additionally, more frequent use of imaging to monitor disease may be needed in patients with TAK compared to patients with GCA.

This study also suggests that serial imaging is less valuable for patients in stable, persistent clinical remission than for patients with active clinical features, as patients in this cohort who developed new or worsened angiographic damage had corresponding clinical symptoms suggestive of a disease flare. No patient had silent angiographic progression, which may be a less frequent phenomenon than previously described (4). However, the fact that no patient had silent angiographic progression of disease in this cohort needs to be interpreted with caution as some patients in persistent clinical remission had treatment increased based on elevated acute-phase reactants and/or FDG-PET activity. Additionally, all patients underwent rigorous, standardized clinical assessments in a research setting, which may have led to detection of clinical disease activity that may have otherwise been missed and contributed to the lack of silent angiographic progression observed in this study.

There are several strengths of this study. For each patient, clinical data, laboratory data, angiography, and FDG-PET scans were obtained at baseline, and patients were prospectively followed up with the same clinical and imaging data obtained at the follow-up study visit. Each patient underwent MRA or CT angiography and FDG-PET scans per a standardized imaging protocol, enabling direct comparison of baseline and follow-up images without a need to account for potential technical differences in image acquisition. Additionally, baseline and follow-up MRA or CT angiography and FDG-PET scan images were directly reviewed by a central reader.

Some limitations of this study should be noted. The NIH is a referral center with possible selection bias, but there were no geographic or socioeconomic restrictions to enrollment. When assessing angiographic change, territories that worsened or improved were studied in composite. There were too few angiographic events to evaluate angiographic worsening or improvement separately. However, the degree of baseline vascular PET activity was not associated with angiographic improvement or worsening in the patient-level analyses. Whether there is angiographic improvement or worsening over time is more likely related to the effectiveness of therapeutic intervention rather than differences in the degree of PET activity at the baseline visit. In addition, this study was done in the context of an observational cohort where patients received various treatments and were followed up for variable time intervals. To address these differences, a within-person, arterial territory–matched approach was used to limit confounding between patients, such as differences in treatment. However, this approach could only be applied to persons with asymmetric angiographic change in paired arteries; thus, those with symmetric angiographic change (while infrequent) could not have been evaluated by this approach.

In conclusion, this study underscores the complex longitudinal associations between vascular activity detected on FDG-PET scans and future angiographic change in LVV. Clinicians should be aware of the potential advantages and challenges of incorporating multimodal imaging into clinical practice to assess disease activity and vascular damage over time in patients with LVV.

AUTHOR CONTRIBUTIONS

All authors were involved in drafting the article or revising it critically for important intellectual content, and all authors approved the final version to be published. Dr. Grayson had full access to all of the data in the study and takes responsibility for the integrity of the data and the accuracy of the data analysis.

Study conception and design. Quinn, Ahlman, Grayson.
Acquisition of data. Quinn, Ahlman, Marko, Novakovich, Grayson.
Analysis and interpretation of data. Quinn, Ahlman, Alessi, LaValley, Neogi, Grayson.

REFERENCES

1. Slart RHJA, Writing Group, Reviewer Group, et al. FDG-PET/CT (A) imaging in large vessel vasculitis and polymyalgia rheumatica: joint procedural recommendation of the EANM, SNMMI, and the PET Interest Group (PIG), and endorsed by the ASNC [review]. Eur J Nucl Med Mol Imaging 2018;45:1250–69.
2. Yamada I, Nakagawa T, Himeno Y, et al. Takayasu arteritis: diagnosis with breath-hold contrast-enhanced three-dimensional MR angiography. J Magn Reson Imaging 2000;11:481–7.
3. Maz M, Chung SA, Abril A, et al. 2021 American College of Rheumatology/Vasculitis Foundation guideline for the management of giant cell arteritis and Takayasu arteritis. Arthritis Rheumatol 2021; 73:1349–65.
4. Kerr GS, Hallahan CW, Giordano J, et al. Takayasu arteritis. Ann Intern Med 1994;120:919–29.

5. García-Martínez A, Arguis P, Prieto-González S, et al. Prospective long term follow-up of a cohort of patients with giant cell arteritis screened for aortic structural damage (aneurysm or dilatation). Ann Rheum Dis 2014;73:1826–32.
6. Kermani TA, Diab S, Sreih AG, et al. Arterial lesions in giant cell arteritis: a longitudinal study. Semin Arthritis Rheum 2019;48:707–13.
7. Tombetti E, Godi C, Ambrosi A, et al. Novel angiographic scores for evaluation of large vessel vasculitis. Sci Rep 2018;8:15979.
8. Besutti G, Muratore F, Mancuso P, et al. Vessel inflammation and morphological changes in patients with large vessel vasculitis: a retrospective study. RMD Open 2022;8:e001977.
9. Dejaco C, Ramiro S, Duftner C, et al. EULAR recommendations for the use of imaging in large vessel vasculitis in clinical practice. Ann Rheum Dis 2018;77:636–43.
10. Quinn KA, Ahlman MA, Malayeri AA, et al. Comparison of magnetic resonance angiography and ^{18}F-fluorodeoxyglucose positron emission tomography in large-vessel vasculitis. Ann Rheum Dis 2018;77:1165–71.
11. Lariviere D, Benali K, Coustet B, et al. Positron emission tomography and computed tomography angiography for the diagnosis of giant cell arteritis: a real-life prospective study. Medicine (Baltimore) 2016;95:e4146.
12. Grayson PC, Alehashemi S, Bagheri AA, et al. ^{18}F-fluorodeoxyglucose–positron emission tomography as an imaging biomarker in a prospective, longitudinal cohort of patients with large vessel vasculitis. Arthritis Rheumatol 2018;70:439–49.
13. Incerti E, Tombetti E, Fallanca F, et al. ^{18}F-FDG PET reveals unique features of large vessel inflammation in patients with Takayasu's arteritis. Eur J Nucl Med Mol Imaging 2017;44:1109–18.
14. Blockmans D, de Ceuninck L, Vanderschueren S, et al. Repetitive ^{18}F-fluorodeoxyglucose positron emission tomography in giant cell arteritis: a prospective study of 35 patients. Arthritis Rheum 2006;55:131–7.
15. Arnaud L, Haroche J, Malek Z, et al. Is ^{18}F-fluorodeoxyglucose positron emission tomography scanning a reliable way to assess disease activity in Takayasu arteritis? Arthritis Rheum 2009;60:1193–200.
16. Arend WP, Michel BA, Bloch DA, et al. The American College of Rheumatology 1990 criteria for the classification of Takayasu arteritis. Arthritis Rheum 1990;33:1129–34.
17. Hunder GG, Bloch DA, Michel BA, et al. The American College of Rheumatology 1990 criteria for the classification of giant cell arteritis. Arthritis Rheum 1990;33:1122–8.
18. Langford CA, Cuthbertson D, Ytterberg SR, et al. A randomized, double-blind trial of abatacept (CTLA-4Ig) for the treatment of Takayasu arteritis. Arthritis Rheumatol 2017;69:846–53.
19. Quinn KA, Rosenblum JS, Rimland CA, et al. Imaging acquisition technique influences interpretation of positron emission tomography vascular activity in large-vessel vasculitis. Semin Arthritis Rheum 2020;50:71–6.
20. Neogi T, Felson D, Niu J, et al. Association between radiographic features of knee osteoarthritis and pain: results from two cohort studies. BMJ 2009;339:b2844.
21. Prieto-González S, García-Martínez A, Tavera-Bahillo I, et al. Effect of glucocorticoid treatment on computed tomography angiography detected large-vessel inflammation in giant-cell arteritis. A prospective, longitudinal study. Medicine (Baltimore) 2015;94:e486.

American College of Rheumatology
Empowering Rheumatology Professionals

Arthritis & Rheumatology
Vol. 75, No. 1, January 2023, pp 108–119
DOI 10.1002/art.42281

Alterations of the Primary Cilia Gene *SPAG17* and *SOX9* Locus Noncoding RNAs Identified by RNA-Sequencing Analysis in Patients With Systemic Sclerosis

Elisha D. O. Roberson,[1] Mary Carns,[2] Li Cao,[3] Kathleen Aren,[2] Isaac A. Goldberg,[2] David J. Morales-Heil,[3] Benjamin D. Korman,[2] John P. Atkinson,[3] and John Varga[4]

Objective. Systemic sclerosis (SSc) is characterized by immune activation, vasculopathy, and unresolving fibrosis in the skin, lungs, and other organs. We performed RNA-sequencing analysis on skin biopsy samples and peripheral blood mononuclear cells (PBMCs) from SSc patients and unaffected controls to better understand the pathogenesis of SSc.

Methods. We analyzed these data 1) to test for case/control differences and 2) to identify genes whose expression levels correlate with SSc severity as measured by local skin score, modified Rodnan skin thickness score (MRSS), forced vital capacity (FVC), or diffusing capacity for carbon monoxide (DLco).

Results. We found that PBMCs from SSc patients showed a strong type I interferon signature. This signal was found to be replicated in the skin, with additional signals for increased extracellular matrix (ECM) genes, classical complement pathway activation, and the presence of B cells. Notably, we observed a marked decrease in the expression of *SPAG17*, a cilia component, in SSc skin. We identified genes that correlated with the MRSS, DLco, and FVC in SSc PBMCs and skin using weighted gene coexpression network analysis. These genes were largely distinct from the case/control differentially expressed genes. In PBMCs, type I interferon signatures negatively correlated with the DLco. In SSc skin, ECM gene expression positively correlated with the MRSS. Network analysis of SSc skin genes that correlated with clinical features identified the noncoding RNAs *SOX9-AS1* and *ROCR*, both near the *SOX9* locus, as highly connected, "hub-like" genes in the network.

Conclusion. These results identify noncoding RNAs and *SPAG17* as novel factors potentially implicated in the pathogenesis of SSc.

INTRODUCTION

Systemic sclerosis (SSc) is a complex orphan disease characterized by autoantibodies, vasculopathy of small vessels, and synchronous/unresolving fibrosis in multiple organs (1,2). There is substantial patient-to-patient heterogeneity in clinical features, disease severity, and the rates of progression. Currently, there are few effective treatments for SSc. Moreover, there is a lack of molecular biomarkers that reliably predict clinical course, reflect disease activity, or identify rational therapeutic targets (3).

The research presented herein represents the views of the authors and does not necessarily reflect the views of the NIH.

Supported in part by the Washington University Center for High Performance Computing (grant S10-OD-018091). Sequencing data were generated at the Genome Technology Access Center at the McDonnell Genome Institute (GTAC@MGI) of Washington University. GTAC was supported by the Siteman Cancer Center (grant P30-CA91842) and the Institute of Clinical and Translational Sciences (ICTS) (grant UL1-TR-000448). Dr. Roberson's work was supported by the National Institute of Arthritis and Musculoskeletal and Skin Diseases (NIAMS) Rheumatic Disease Core Center, NIH (grant P30-AR-048335), the NIAMS Rheumatic Diseases Research Resource-based Center, NIH (grant P30-AR-073752), and the ICTS of Washington University in St. Louis (grant UL1-TR-000448). Dr. Cao's work was supported by the NIAMS Rheumatic Disease Core Center, NIH, (grant P30-AR-048335). Dr. Morales-Heil's work was supported by an NIH training grant (T32-AR-007279-36). Dr. Atkinson's work was supported by the NIAMS Rheumatic Disease Core Center, NIH (grant P30-AR-048335), and the ICTS of Washington University in St. Louis (grant UL1-TR-000448). Dr. Varga's work was supported by the Northwestern University Clinical and Translational Sciences Institute (grant UL1-TR-000150).

[1]Elisha D. O. Roberson, PhD: Department of Medicine, Division of Rheumatology, and Department of Genetics, Washington University, St. Louis, Missouri; [2]Mary Carns, MS, Kathleen Aren, MPH, Isaac A. Goldberg, BA, Benjamin D. Korman, MD: Scleroderma Program, Feinberg School of Medicine, Northwestern University, Chicago, Illinois; [3]Li Cao, MD, David J. Morales-Heil, PhD, John P. Atkinson, MD: Department of Medicine, Division of Rheumatology, Washington University, St. Louis, Missouri; [4]John Varga, MD (current address: Division of Rheumatology, University of Michigan, Ann Arbor): Scleroderma Program, Feinberg School of Medicine, Northwestern University, Chicago, Illinois, and Department of Internal Medicine, Division of Rheumatology, University of Michigan, Ann Arbor.

Author disclosures are available at https://onlinelibrary.wiley.com/action/downloadSupplement?doi=10.1002%2Fart.42281&file=art42281-sup-0001-Disclosureform.pdf.

Address correspondence via email to Elisha D. O. Roberson, PhD, at eroberson@wustl.edu; or to John Varga, MD, at vargaj@med.umich.edu.

Submitted for publication January 6, 2022; accepted in revised form June 23, 2022.

One approach to improve our understanding of the evolution and progression of the disease is through transcriptomics. Previous primary and secondary analyses of transcriptome data in SSc used microarray, bulk RNA sequencing (RNA-Seq), and single-cell RNA-Seq approaches. These studies revealed molecular heterogeneity among individual transcriptomes, increased type I interferon signaling, potential molecular subtypes, and altered cell populations in the skin (4–13). We sought to further clarify molecular disruptions in SSc, to find correlations with clinical measures of disease activity, and to determine if expression–trait correlation gene sets overlap with the case/control differential expression gene sets. We used prospective collection of skin and peripheral blood mononuclear cell (PBMC) samples from unaffected control subjects and patients with SSc followed by bulk RNA-Seq. At each visit, disease severity was assessed by the local skin score, modified Rodnan skin thickness score (MRSS), and pulmonary function testing. For RNA-Seq, we used a ribosomal depletion method to permit the detection of both nascent and mature messenger RNA, along with noncoding RNAs lacking a poly(A) tail. This method may be more sensitive for genes with low expression levels or short half-lives than poly(A)-based RNA-Seq methods, enabling us to identify potentially overlooked contributors to SSc. These methodologies allowed us to examine categorical differences between SSc patients and unaffected controls, as well as to identify genes whose expression is correlated with alterations in established clinical parameters of disease progression.

PATIENTS AND METHODS

Clinical assessment. We completed standardized evaluations to establish SSc diagnosis, as well as the presence/severity of organ involvement, as previously described (14,15). We determined MRSS and local (forearm) skin scores at each visit. High-resolution computed tomography of the chest, echocardiography, and pulmonary function testing were performed as standard of care (16). At each research visit, we collected PBMCs and 2 skin punch biopsy samples (stabilized in RNA later).

Genomics methods and analysis. Detailed methods can be found in the Supplementary Methods on the *Arthritis & Rheumatology* website, available at http://onlinelibrary.wiley.com/doi/10.1002/art.42281. Briefly, we used RNA extracted from the blood and PBMC samples (miRNeasy minikit no. 217004) to create stranded, ribosomal depletion libraries (Takara/Clontech product no. 634876). We trimmed raw sequencing data with Cutadapt, aligned to the human genome with RNASTAR, and counted read-pairs per gene with featureCounts (17–19). We then calculated differential expression with DESeq2 and pathway enrichment with gProfiler, and we performed network analyses with weighted gene coexpression network analysis (WGCNA) (20–22).

Data availability. The data used in the analysis, such as gene counts used for DESeq2 and demographic information per sample, are available from FigShare at https://figshare.com/projects/2021_Roberson_lab_systemic_sclerosis_transcriptome_data/118698. The code used for data analysis is available as a repository on GitHub at https://github.com/RobersonLab/2021_ssc_rnaseq. These were prospectively collected samples for controlled data access. FASTQ files are available for general research use in dbGAP accession phs002902.v1.p1.

RESULTS

Study cohort and demographics. Patients with SSc (n = 21) were recruited from the Northwestern Scleroderma Clinic and fulfilled the 2013 American College of Rheumatology/EULAR classification criteria for SSc (1). These patients were further classified as having limited cutaneous SSc (lcSSc; n = 5), diffuse cutaneous SSc (dcSSc; n = 14), SSc without scleroderma (sine scleroderma SSc; n = 1), or very early diagnosis of SSc (VEDOSS; n = 1). Controls were volunteers with no history of an autoimmune or inflammatory disease (n = 14). At each study visit, we obtained whole blood samples and 2 skin punch biopsy samples measuring 3 mm. We also conducted pulmonary function tests, and the same observer assessed the MRSS and local skin score. Seven patients with dcSSc, 2 with lcSSc, and 1 individual with sine scleroderma SSc volunteered to provide a second set of whole blood and skin biopsy samples and to undergo additional pulmonary function testing.

For group-wise demographic summaries, we included unaffected controls and patients with either lcSSc or dcSSc (n = 19) (Table 1). Controls were younger than SSc patients. Within the SSc cohort, the lcSSc and dcSSc subsets were balanced for patient age and disease duration (Table 2). There were

Table 1. Demographic characteristics of systemic sclerosis (SSc) patients and unaffected controls*

	Controls (n = 14)	SSc patients (n = 19)
Age, mean ± SD years	32.6 ± 10.8	49.7 ± 11.4
Female	9 (64.3)	15 (78.9)
Race/ethnicity		
Asian	0 (0.0)	2 (10.5)
Black	3 (21.4)	2 (10.5)
Hispanic	5 (35.7)	0 (0.0)
White	6 (42.9)	15 (78.9)

* Except where indicated otherwise, values are the number (%) of patients. Controls were individuals without a self-reported history of autoimmune disease. SSc patients met the 2013 American College of Rheumatology/EULAR classification criteria for SSc. The unaffected controls were significantly younger than the SSc patients ($P < 0.05$ by Student's 2-tailed *t*-test), but the distribution of female patients was balanced between the groups ($P > 0.05$ by Fisher's exact test). The participants in both the control and SSc cohorts were predominantly White, and the other racial/ethnic backgrounds were significantly different between the 2 cohorts ($P < 0.05$ by Fisher's exact test).

Table 2. Demographic characteristics and antibody staining patterns of patients with diffuse cutaneous systemic sclerosis (dcSSc) and patients with limited cutaneous SSc (lcSSc)*

	dcSSc (n = 14)	lcSSc (n = 5)
Age, mean ± SD years	49.7 ± 11.7	49.8 ± 11.9
Female	13 (92.9)	2 (40.0)
Duration of disease, mean ± SD months	42.7 ± 33.2	36.2 ± 22.8
MRSS, mean ± SD	24.1 ± 10.2	8.8 ± 5.0
Forearm MRSS, mean ± SD	1.9 ± 0.9	0.8 ± 0.8
BMI, mean ± SD	26.7 ± 5.5	29.5 ± 6.3
FVC, mean ± SD†	75.1 ± 15.6	82.6 ± 12.5
Corrected DLco, mean ± SD†	66.2 ± 20.8	80.0 ± 17.4
TLC, mean ± SD†	85.6 ± 17.2	85.8 ± 11.7
Race/ethnicity		
Asian	1 (7.1)	1 (20.0)
Black	2 (14.3)	0 (0.0)
Hispanic	0 (0.0)	0 (0.0)
White	11 (78.6)	4 (80.0)
Immunofluorescence pattern‡		
Centromere	1 (8.3)	2 (40.0)
Homogeneous	3 (25.0)	0 (0.0)
Nucleolar	4 (33.3)	1 (20.0)
Speckled	7 (58.3)	3 (60.0)

* Except where indicated otherwise, values are the number (%) of patients. The modified Rodnan skin thickness score (MRSS), body mass index (BMI), forced vital capacity (FVC), diffusing capacity for carbon monoxide (DLco), and total lung capacity (TLC) were determined at repeat visits. For each individual, we used the "worst" observed value as the representative value.
† Lung function parameters were calculated as percent estimated maximum for age and sex.
‡ Immunofluorescence data were only available for 12 of the 14 individuals with dcSSc, and percentages were calculated based on this availability.

more women in the dcSSc subset than in the lcSSc subset, while self-declared ethnicity was similar between the 2 groups. The medications that patients were being treated with at sample collection are listed in Supplementary Table 1 (http://onlinelibrary.wiley.com/doi/10.1002/art.42281).

Evidence of increased type I interferon signaling by SSc PBMCs. We sought to characterize gene expression changes in PBMCs of SSc patients since collection of PBMCs is minimally invasive. For cases, we only included baseline lcSSc and dcSSc samples to avoid bias toward individuals sampled more than once. There were 147 genes with decreased expression levels (113 genes with at least –1.5-fold decreased expression) and 100 genes with increased expression levels (61 genes with at least 1.5-fold increased expression) in the PBMCs of SSc patients compared to the PBMCs of unaffected controls (Figure 1A and Supplementary Table 2, http://onlinelibrary.wiley.com/doi/10.1002/art.42281). The genes with the most significantly decreased expression levels included *GALNTL6* (fold change –4.09), *GPM6A* (fold change –3.98), *SLC4A10* (fold change –3.33), and *COL4A3* (fold change –4.36). The most consistently enriched pathways among genes with decreased expression levels in SSc patients were collagen pathways due to decreases in *COL4A3* and *COL4A4* (Figure 1B and Supplementary Table 3, http://onlinelibrary.wiley.com/doi/10.1002/art.42281).

Genes with significantly increased expression levels in the PBMCs of SSc patients compared to unaffected controls included *FAM13A* (fold change 2.49), *E2F2* (fold change 2.28), *MYOF* (fold change 1.83), and *TMEM178B* (fold change 1.36). Single-nucleotide polymorphisms in *FAM13A* are associated with an increased risk of pulmonary fibrosis (23) and liver cirrhosis (24). We tested the genes with increased expression levels in SSc PBMCs for pathway enrichment (Figure 1C and Supplementary Table 4, http://onlinelibrary.wiley.com/doi/10.1002/art.42281). The most significant pathways were related to type I interferon activity, including interferon-α/interferon-β and type I interferon signaling categories. Target genes of interferon regulatory factor 5 (IRF-5) and IRF-9 transcription factors were significantly enriched in the genes with increased expression levels. *IRF5* is highly expressed in classically activated (M1-polarized) human macrophages (25). M1-like macrophage signatures have been found to be highly prevalent in the skin of SSc patients (10).

Previous studies have identified similarly increased expression of type I interferon–stimulated genes in the PBMCs of SSc patients as well as in the skin (26,27). It is also interesting to consider whether some of these signatures, including the increase in IRF-5 and its known high expression in M1-polarized macrophages, indicate a specific role for this macrophage subpopulation in SSc.

Evidence of substantial immune activation, increased complement component expression, and loss of ciliary protein *SPAG17* in SSc skin. Procurement of PBMCs is minimally invasive but may not reflect the molecular biology of affected tissues. Evaluation of the skin tissue may therefore provide more insight into the molecular defects in the setting of SSc. Expression levels of 526 genes were significantly decreased (226 genes with at least –1.5-fold decreased expression) and expression levels of 1,200 genes were increased (816 genes with at least 1.5-fold increased expression) (Figure 2A and Supplementary Table 5, http://onlinelibrary.wiley.com/doi/10.1002/art.42281) in the skin biopsy samples of SSc patients compared to the skin biopsy samples of unaffected controls. These results help highlight the advantage of studying tissue affected by SSc.

The most significantly altered gene in the entire study was *SPAG17*, which was decreased in SSc skin samples compared to unaffected control skin samples (fold change –4.67; adjusted $P = 3.22 \times 10^{-12}$). To our knowledge, this gene had not been previously associated with differential expression in SSc skin. The expression level of *SPAG17* is relatively low, and previous studies using hybridization microarrays may not have been

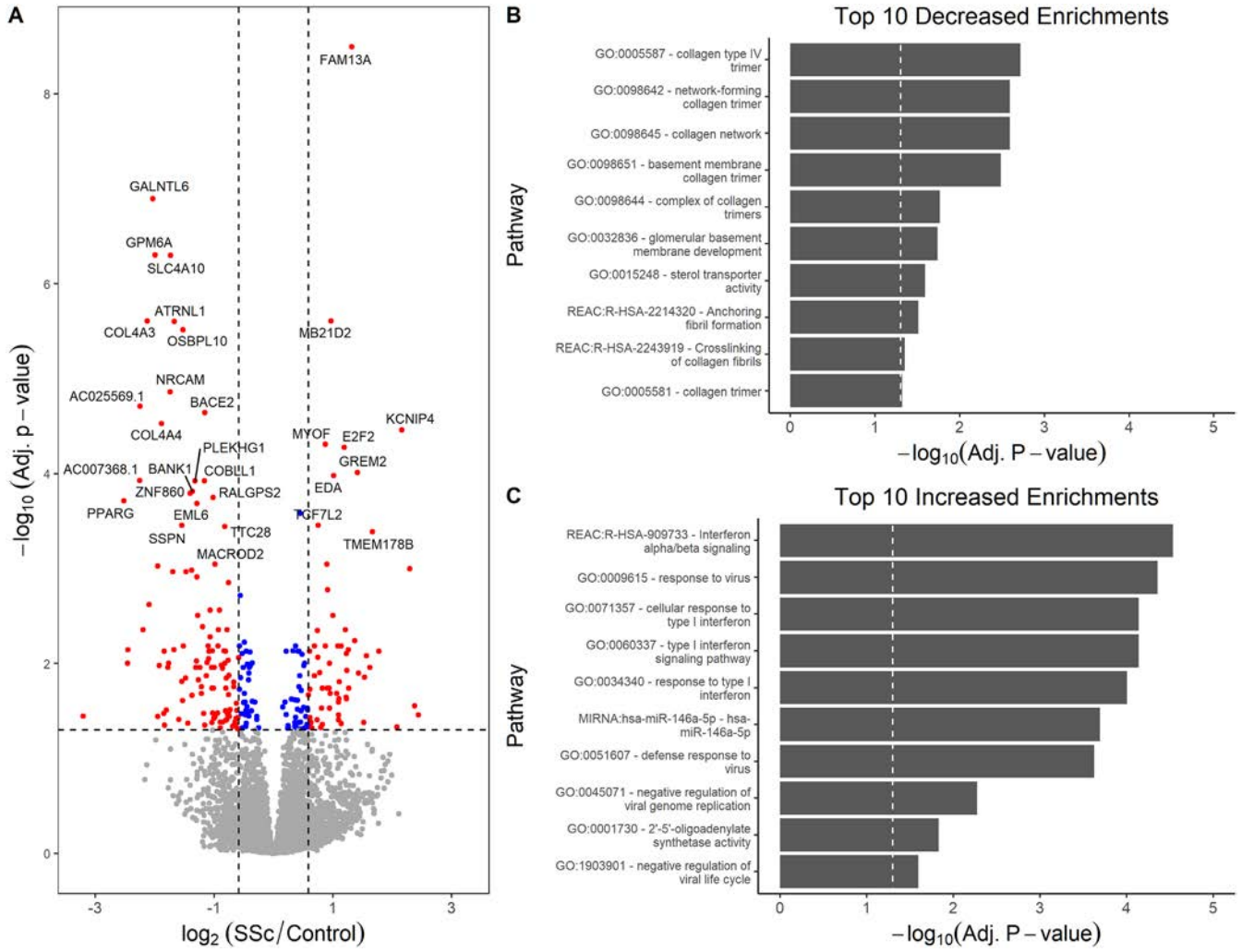

Figure 1. Strong enrichment for the type I interferon signaling pathway in systemic sclerosis (SSc) peripheral blood mononuclear cells (PBMCs). **A**, Standard volcano plots showing the effect size in SSc patients relative to unaffected controls (fold change on a $\log_2$ scale) and the *P* values for differences in SSc patients vs. controls (on a $\log_{10}$ scale). Vertical dashed lines show the cutoff value for a 1.5-fold change defining up- or down-regulated genes. Horizontal dashed line indicates the adjusted significance threshold of 0.05. **B** and **C**, Bar graphs showing pathways enriched for genes that displayed decreased (**B**) or increased (**C**) expression in PBMCs from SSc patients relative to unaffected controls. Genes with at least a 1.5-fold change in expression were tested, with the predominant signal being increased type I interferon signaling. Some of the most significant enrichments included collagen and sterol transporter. The vertical dashed line shows the adjusted threshold of significance ($P = 0.05$). Color figure can be viewed in the online issue, which is available at http://onlinelibrary.wiley.com/doi/10.1002/art.42281/abstract.

sensitive enough to detect its expression against background fluorescence. Low expression level might also cause *SPAG17* to be filtered out of some RNA-Seq studies. SPAG17 protein is required for the function of primary cilia and male fertility (28). Mice deficient in *Spag17* have bone abnormalities such as decreased femur length and disrupted femur morphology (29). The role of *SPAG17* in skin and immune cells is not particularly clear, though as part of the primary cilia it could be involved in signaling. Decreased expression levels of *SPAG17* may be present without any appreciable evidence of skin fibrosis, as skin samples of patients with sine scleroderma SSc had decreased *SPAG17* expression levels that were comparable to the levels in skin samples from patients with lcSSc or those with dcSSc (Supplementary Figure 2, http://onlinelibrary.wiley.com/doi/10.1002/art.42281). The similarity of the skin transcriptomes from patients with sine scleroderma SSc, patients with lcSSc, and patients with dcSSc was also shown by principal components analysis of the top case/control differentially expressed genes (Supplementary Methods and Supplementary Figure 4, http://onlinelibrary.wiley.com/doi/10.1002/art.42281).

Another gene with significantly decreased expression levels was *LGR5* (fold change –2.70). *LGR5* is a member of the G protein–coupled receptor family that is an important target and modulator of Wnt/β-catenin signaling. *LGR5* expression is a marker for intestinal villi tip telocytes in mice that maintain the correct differentiation gradient on the villus axis via noncanonical Wnt signaling (30). Dermal telocytes are reduced in the fibrotic skin and internal organs of individuals with SSc (31,32). If these dermal

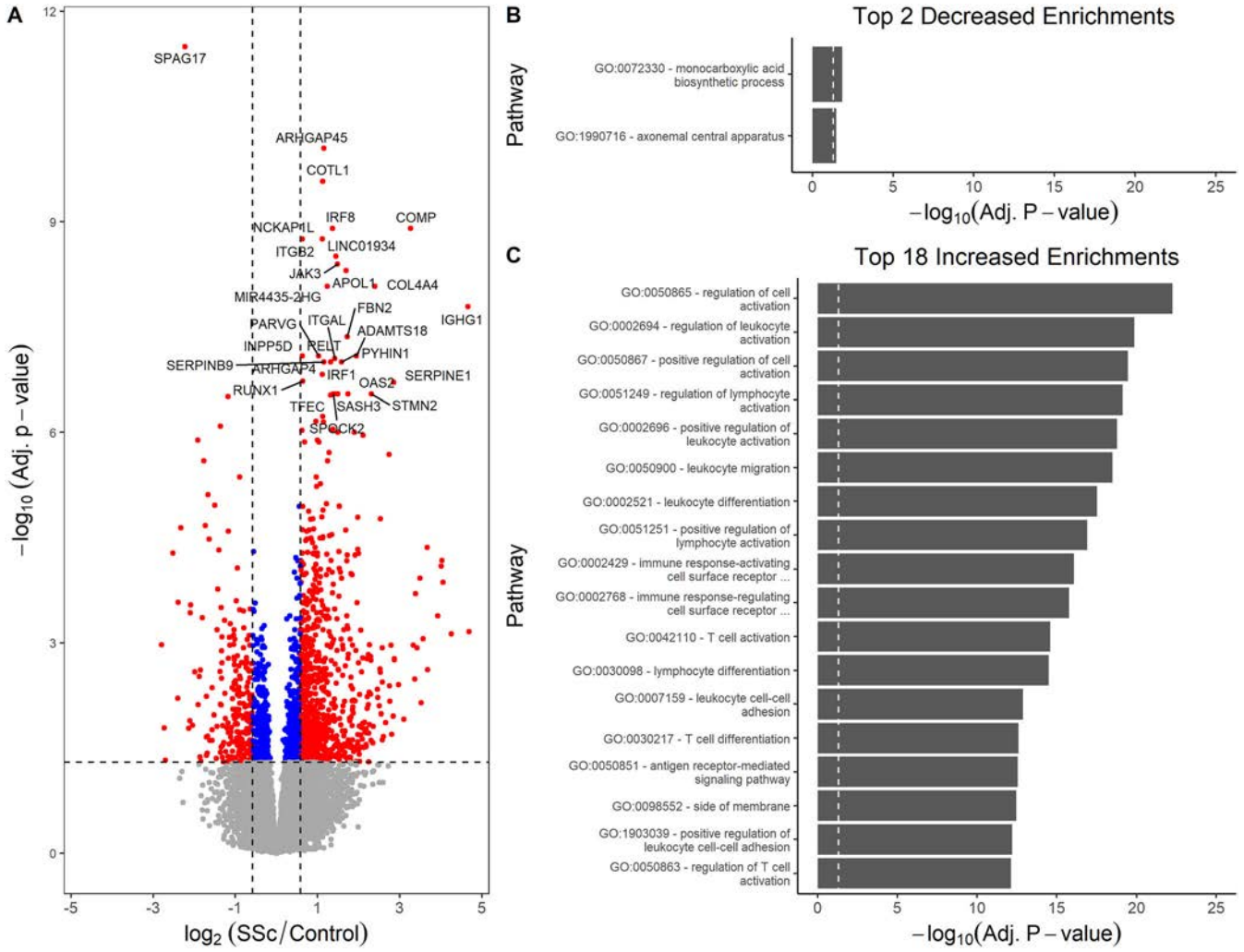

Figure 2. Decreased expression of primary cilia protein SPAG17 and increased immune activation in SSc skin. **A**, Standard volcano plot showing the effect size in SSc patients relative to unaffected controls (fold change on a $\log_2$ scale) and the *P* values for differences in SSc patients vs. controls (on a $\log_{10}$ scale). Vertical dashed lines show the cutoff value for a 1.5-fold change defining up- or down-regulated genes. Horizontal dashed line indicates the adjusted significance threshold of 0.05. More genes were significantly increased in SSc skin than were significantly decreased. **B** and **C**, Bar graphs showing pathways enriched for genes that displayed decreased (**B**) or increased (**C**) expression in skin from SSc patients relative to unaffected controls. Genes with at least a 1.5-fold change in expression were tested, with the predominant enrichments for genes related to immune cell activation, indicating the migration of immune cells into the skin. The vertical dashed line shows the adjusted threshold of significance (*P* = 0.05). Color figure can be viewed in the online issue, which is available at http://onlinelibrary.wiley.com/doi/10.1002/art.42281/abstract.

telocytes also help to coordinate differentiation and/or signaling in the skin, their loss (perhaps detected by the reduction of *LGR5*) may directly contribute to the development of SSc fibrosis. Only 2 known pathways were enriched among genes with decreased expression levels (Figure 2B and Supplementary Table 6, http://onlinelibrary.wiley.com/doi/10.1002/art.42281): monocarboxylic acid biosynthesis and axonemal central apparatus.

Genes with increased expression levels in SSc patients included *ARHGAP45* (fold change 2.22), *COTL1* (fold change 2.18), *IRF8* (fold change 2.57), and *COMP* (fold change 9.63). The extensive list of genes with increased expression levels in SSc skin would allow us to posit interesting hypotheses for almost any one of them. We therefore chose to check these genes for the enrichment of known molecular pathways as well. We found a total of 366 significant enrichments (Figure 2C and Supplementary Table 7, http://onlinelibrary.wiley.com/doi/10.1002/art.42281), including enrichment for targets of the transcription factors IRF2, IRF4, IRF5, IRF7, IRF8, IRF9, and ISGF3. The RNA expression levels of transcription factors *IRF1* (fold change 2.65), *IRF5* (fold change 1.48), *IRF7* (fold change 1.99), and *IRF8* (fold change 2.57) were all significantly increased in the skin of SSc patients as well.

Some of the enriched pathways had functions that involved variations on similar themes, such as immune cell adhesion, migration, and differentiation, B cell activation and proliferation, extracellular matrix deposition, and classical antibody-mediated

complement activation. The complement theme was mainly due to increased expression levels of complement genes (including *C1QB*, *CR1*, *C5AR1*, and *C7*) and immunoglobulins. Complement activation usually leads to the assembly of the membrane-attack complex (MAC) that can insert into membranes and lyse cells. The MAC is composed of complement proteins C5b, C6, C7, C8, and C9. MAC fragments are deposited in the dermal vasculature of SSc patients, supporting a role for antibody-induced complement activation in SSc vasculopathy (33). These data suggest that aberrant activation of complement may partially mediate cutaneous tissue damage in SSc.

WGCNA findings of correlations between gene expression and severity of skin fibrosis and changes in lung function. Group-wise gene expression analysis categorizes samples as test (SSc) or reference (control). This is a reasonable way to determine the general features of a trait, but it ignores the heterogeneity of phenotypes within the trait. SSc in particular has substantial clinical heterogeneity. We used WGCNA to assess correlations between gene expression and severity of skin fibrosis (MRSS and forearm local skin scores) or changes in lung function (forced vital capacity [FVC] and DLco). This approach is somewhat different from that used in other studies, in which correlations between gene expression array findings and the MRSS score in the skin have been assessed or correlations between gene expression levels in lung biopsy samples and the severity of lung disease have been assessed (34–36). We chose to test both skin and lung phenotypes and used paired samples from PBMCs and skin for each individual. We included all SSc samples for which there was a matching MRSS, FVC, or DLco measurement for the visit (i.e., follow-ups were included as separate measurements). The tallies of positive and negative correlations by tissue are listed in Supplementary Table 8 (http://onlinelibrary.wiley.com/doi/10.1002/art.42281).

For PBMCs, there were significant correlations between gene expression and DLco, forearm skin score, and MRSS (Supplementary Tables 9, 10, and 11, respectively, http://onlinelibrary.wiley.com/doi/10.1002/art.42281). The genes negatively correlated with DLco were enriched for type I interferon signaling and proteasomal antigen processing/presentation (Supplementary Table 12, http://onlinelibrary.wiley.com/doi/10.1002/art.42281). The PBMC genes that positively correlated with DLco were only enriched for targets of microRNA hsa-miR-6082 (*DTWD2*, *FXN*, and *ZFP30*; Supplementary Table 13, http://onlinelibrary.wiley.com/doi/10.1002/art.42281).

Correlations between gene expression levels and the forearm-specific skin score (Supplementary Table 10) were more difficult to interpret. The negative correlations did not show any pathway enrichments. Positive correlations were only enriched for the phosphoribosylformylglycinamidine synthase pathway, but it was due to a single gene (*PFAS*; Supplementary Table 14, http://onlinelibrary.wiley.com/doi/10.1002/art.42281).

There were also correlations between PBMC gene expression and the MRSS score (Supplementary Table 10). Genes negatively correlated with the MRSS score were enriched for pathways associated with protein folding, unfolded proteins, and endoplasmic reticulum stress (Supplementary Table 15, http://onlinelibrary.wiley.com/doi/10.1002/art.42281). There were a few pathways associated with positively correlated genes, including some related to Wnt signaling regulation and mitochondrial functions (Supplementary Table 16, http://onlinelibrary.wiley.com/doi/10.1002/art.42281).

One might assume that the differentially expressed genes in case/control gene expression studies may also be the key genes and pathways that drive progression and therefore may correlate with disease severity. This does not appear to be the case for SSc PBMCs, as most of the genes with significant correlations to disease severity were not detected in the case/control analysis (Supplementary Figure 6, http://onlinelibrary.wiley.com/doi/10.1002/art.42281).

The SSc skin transcriptomes had significant correlations with the DLco, FVC, and MRSS (Supplementary Tables 17, 18, and 19, respectively, http://onlinelibrary.wiley.com/doi/10.1002/art.42281). In evaluating correlations with the DLco, there were many negative correlations with expression of ribosomal proteins, leading to enrichment of pathways related to ribosome function (Supplementary Table 20, http://onlinelibrary.wiley.com/doi/10.1002/art.42281). SSc skin genes that positively correlated with the DLco did not follow a consistent pattern of enrichment (Supplementary Table 21, http://onlinelibrary.wiley.com/doi/10.1002/art.42281). Genes that were negatively correlated with the FVC were enriched for sterol/cholesterol biosynthesis and α-linolenic/linolenic acid metabolism pathways (Supplementary Table 22, http://onlinelibrary.wiley.com/doi/10.1002/art.42281). Genes that were positively correlated with the FVC did not have any significant pathway enrichment.

Genes whose expression levels showed a negative correlation with the MRSS in the skin were enriched in cell fate and synaptic functions (Supplementary Table 23, http://onlinelibrary.wiley.com/doi/10.1002/art.42281). Genes with expression levels that positively correlated with the MRSS were enriched for extracellular matrix functions (Supplementary Table 24, http://onlinelibrary.wiley.com/doi/10.1002/art.42281). This is a nice confirmation, as increasing MRSS is expected to indicate increasing fibrosis, secondary to increased matrix deposition.

Similar to what we observed in PBMCs, there is little overlap between the genes differentially expressed in SSc skin and skin genes that correlated with lung function or skin fibrosis parameters (Supplementary Figure 7, http://onlinelibrary.wiley.com/doi/10.1002/art.42281). Overall, 90% of the differentially expressed genes did not correlate with any clinical parameters, and 93% of the clinical trait–associated genes were not differentially expressed. This highlights the disparity between the 2 methods and suggests that novel targets for clinical treatment and

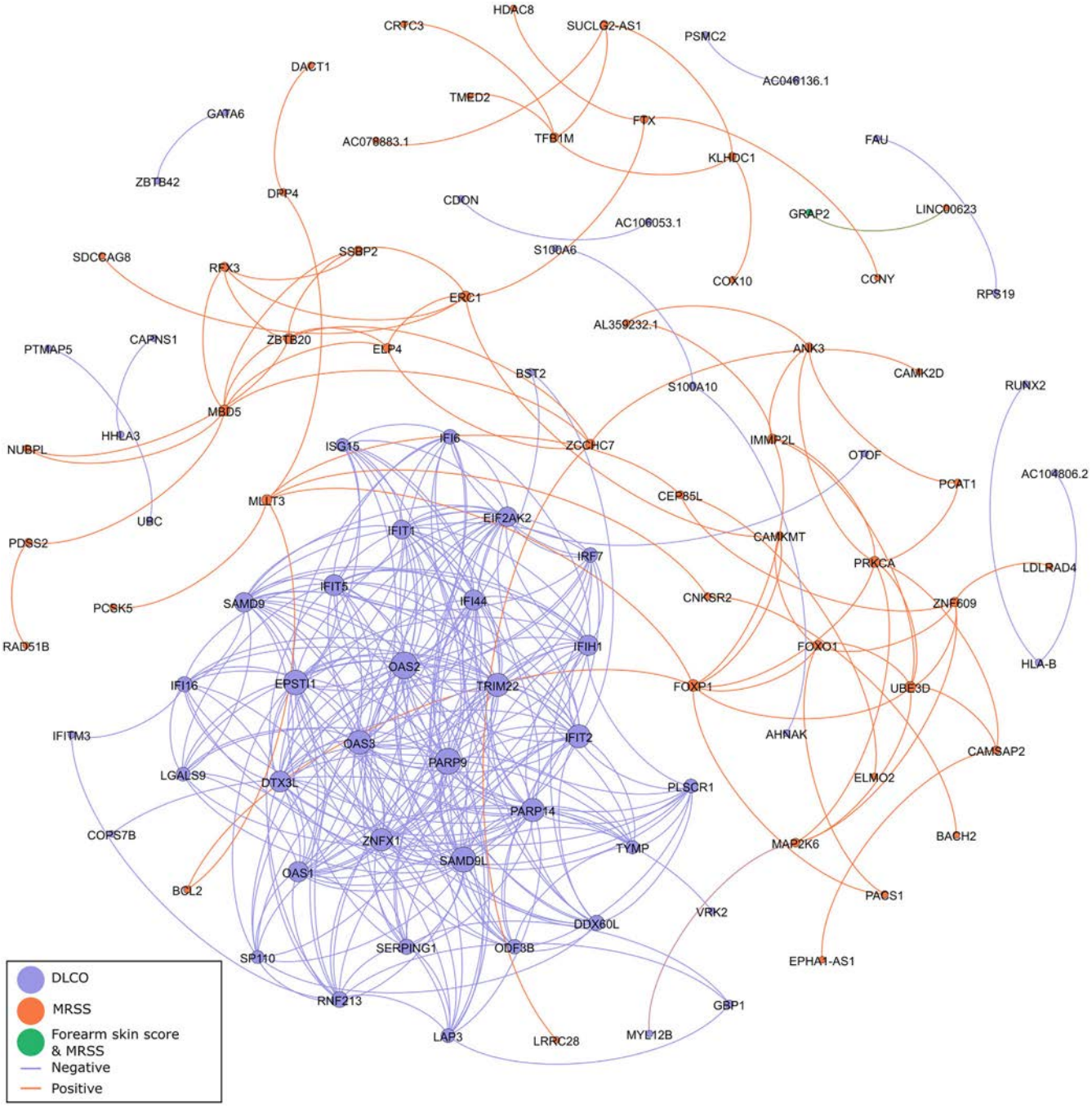

Figure 3. Network diagram of the genes, particularly interferon-responsive genes, most highly connected with at least 1 of the indicated clinical traits in SSc PBMCs. Each node is an individual gene, sized by weighted degree and filled by the trait association. Each edge is color-coded to indicate whether the gene–gene correlation is positive or negative, with a minimum cutoff of 0.80. The interferon-responsive genes, such as *OAS1*, *OAS2*, and *OAS3*, and the gene *IFIT1/2*, were the most highly interconnected in SSc PBMCs. DLco = diffusing capacity for carbon monoxide; MRSS = modified Rodnan skin thickness score (see Figure 1 for other definitions).

biomarkers may be identified using severity correlation rather than case/control differential gene expression.

Some genes were correlated with the same trait in both skin samples and PBMCs (Supplementary Table 25, http://onlinelibrary.wiley.com/doi/10.1002/art.42281). For each gene, we considered the tissues concordant if the direction of effect was the same in each tissue, and discordant if the direction of effect was opposite. There were only overlaps of gene effects between PBMCs and skin tissue when correlations with the DLco or MRSS score were assessed. In evaluating correlations with the DLco, there were 12 concordant genes and 7 discordant genes between tissues. In evaluating correlations with the MRSS, there were 11 concordant genes and 2 discordant genes between tissues. These 2 gene sets are intriguing to consider for further study

as molecular biomarkers of disease activity, regardless of whether the effect is concordant or discordant, as a blood draw sample might be as informative as a skin punch biopsy sample.

We were also interested in whether there are some genes for which expression levels in PBMCs could be as informative as expression levels in skin biopsy samples. A total of 91 genes were differentially expressed in skin samples and PBMCs (n = 24) and/or correlated with a clinical trait in both tissues (n = 69). We used Pearson's correlation tests with all samples to see if the expression level of these genes correlated between tissues. Among these candidates, 9 genes were significantly correlated between tissues (Supplementary Table 26, http://onlinelibrary.wiley.com/doi/10.1002/art.42281). The expression levels of several genes related to interferon activity in PBMCs (*IFI44*, *IF44L*, *OAS1*, *OAS3*, and *RSAD2*) correlated with expression levels in skin samples; therefore, these genes could perhaps be assayed without the need for a skin biopsy as well.

Noncoding RNAs *SOX9-AS1* and *ROCR* as central, highly connected nodes in the SSc skin gene–gene correlation network. Given that we had a list of genes that correlated with different traits and their normalized expression, the next thing we looked at was the gene–gene correlation network. We focused only on genes that significantly correlated with at least 1 clinical trait. Examining the network characteristics can help identify genes that act as signaling hubs or otherwise have coexpression with other members of the network.

After ranking each gene by degree and page rank (measures of network connectedness and centrality), the top-ranked PBMC gene was *OAS2*, with a degree of 29 and page rank of 0.017 (Figure 3 and Supplementary Table 27, http://onlinelibrary.wiley.com/doi/10.1002/art.42281). The oligoadenylate synthetases are interferon response genes, which is consistent with the increased type I interferon signaling signatures we found in SSc PBMCs. The 4th highest ranked gene, *EPSTI1*, is linked to macrophage function. It is thought to have a key role in the classical M1 polarization of macrophages, as a murine knockout of *Epsti1* has few M1-polarized macrophages along with a significant expansion of M2-polarized macrophages (37). The top-ranked genes in SSc PBMCs (all genes with a degree of at least 10) are inflammatory genes that correlated with DL_{CO}.

Conversely, the top 41 genes in the SSc skin network (ranked by degree and page rank) all correlated with the MRSS (Figure 4 and Supplementary Table 28, http://onlinelibrary.wiley.com/doi/10.1002/art.42281). The top-ranked SSc skin gene was an antisense transcript, *SOX9-AS1* (degree 49; page rank 0.005). This suggests an important advantage of using stranded RNA library kits: with an unstranded kit, it is impossible to tell sense from antisense transcripts if they overlap at the same locus. The protein-coding *SOX9* transcript was correlated with the MRSS as well but had a lower degree of 9. The long noncoding RNA *ROCR* is also a highly connected gene in the SSc skin network (degree 44; page rank 0.004). It is located in the same genomic locus as *SOX9* and *SOX9-AS1*. It is worth noting that *SPAG17* expression level in SSc skin was negatively correlated with the MRSS (–0.51 correlation). Since *SPAG17* is a low-expression transcript, we were unable to generate a *SPAG17* network to identify coexpressed genes. Therefore, further study is required to understand the genes coexpressed with *SPAG17* in relevant skin cell types, such as fibroblasts.

DISCUSSION

SSc is a complex and progressive inflammatory/fibrotic disease. In the current study, we demonstrated that the sensitivity of RNA-Seq can lead to new discoveries and that applying complementary approaches to the same data can reveal distinct trends. There are advantages to using strand-specific, ribosomal depletion RNA-Seq library kits, such as an increased ability to detect nonpolyadenylated transcripts, an increased sensitivity for nascent and short half-life transcripts, and the ability to distinguish overlapping antisense transcripts. However, one disadvantage is the reduced power for transcript-level discoveries. For our data, focusing only on spliced transcripts would have used only a fraction of the available sequencing data, since much of the aligned sequence mapped to introns. There is also a distinct value in using samples from different tissues. Blood samples are informative in their own right, but comparing skin punch samples between SSc patients and unaffected controls reveals different gene sets more directly related to the ongoing molecular pathology.

The predominant signal in PBMCs was for type I interferon signaling, with enrichment for targets of IRF-5 and IRF-9. M1-polarized macrophages are known to have high *IRF5* expression (25). We observed that *CD86*, another marker of M1 macrophages, was increased in SSc PBMCs. Previous work has shown that a mix of monocytes with signs of M1 and M2 polarization in the blood is associated with interstitial lung disease in SSc patients (38). The lack of an increase of M2 markers does not necessarily exclude their presence. Bulk RNA-Seq is not ideal for identifying cell populations, and the question of macrophage fraction (and activation state) in SSc PBMCs would be better answered with single-cell RNA-Seq, flow cytometry, or mass cytometry.

The data from the analysis of skin samples provided an even more informative perspective. The most significantly different gene in the entire analysis was *SPAG17*, which has not traditionally been a top dysregulated gene in SSc transcriptome studies. Genes are often named for the tissue in which they are first discovered, which may or may not be the only tissue they are expressed in or even the tissue with the highest expression. SPAG17 is a central pair protein that is critical in the formation of primary cilia, and its knockout is lethal in neonatal mice (39). As suggested by the name, alterations in *SPAG17* can lead to infertility in mouse models and for humans with certain rare missense

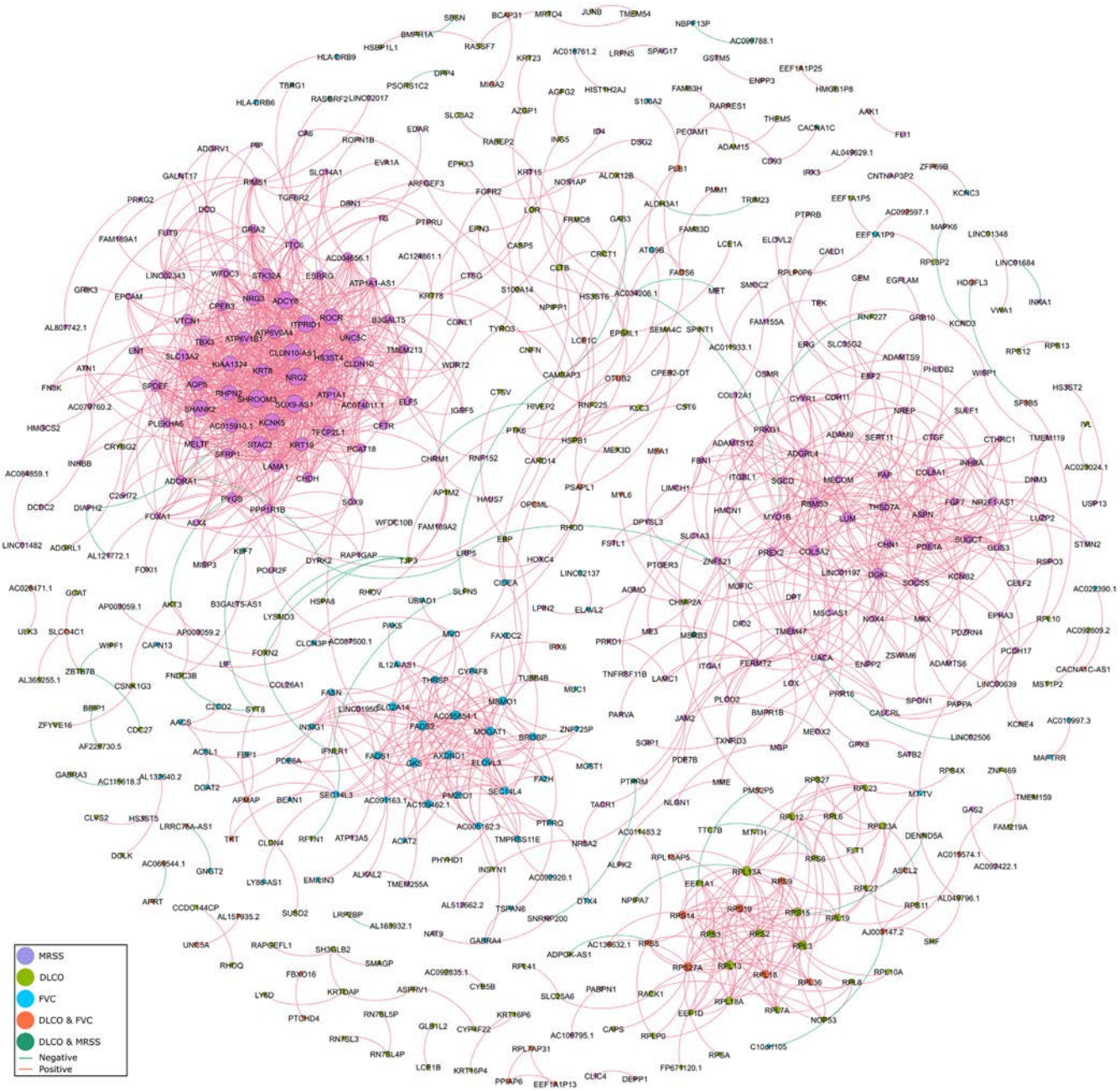

Figure 4. Network diagram of genes, particularly *SOX9* locus genes, most highly connected with at least 1 of the indicated clinical traits in systemic sclerosis (SSc) skin. Each node is an individual gene, sized by weighted degree and color-coded according to the trait association. The edges between nodes are color-coded to indicate whether the gene–gene correlation is positive or negative, with a minimum cutoff of 0.80. Some genes correlated with fibrosis formed a relatively separate subnetwork from those associated with lung function or both DLco and fibrosis. The most connected genes in this subnetwork included *SOX9-AS1* and *ROCR*, which are both noncoding and located at the *SOX9* locus. The overlap of correlations between fibrosis and lung function was primarily ribosomal proteins. A separate subnetwork of the MRSS-correlated genes was enriched for matrix proteins, such as *COL5A2* and *COL8A1*. MRSS = modified Rodnan skin thickness score; DLco = diffusing capacity for carbon monoxide; FVC = forced vital capacity.

variants (28,40). But it is important to bear in mind that this gene has critical functions beyond sperm motility since it is part of the primary cilia. Missense changes in *SPAG17* can cause abnormal bone length (29,41). Common variants in *SPAG17* are associated with body length in early life and height in adulthood (42,43). Novel mutations and rare variants in components of the primary cilia can lead to primary ciliary dyskinesia (PCD). The most common effects are in the ears (chronic ear infections, hearing loss), sinuses (chronic sinus congestion), and lungs (recurrent pneumonia, chronic cough). Rare *SPAG17* variants can lead to a PCD-like

phenotype in mice and have been shown to cause human PCD as well (44,45). The PCD phenotypes are largely driven by the altered ability of the cilia to beat. In the skin of patients with SSc, a defect of beating cilia does not make the most sense. Nonmotile primary cilia are involved in signaling. One potential hypothesis is that primary cilia have an antifibrotic signaling role. The reduced expression could then lead to increased profibrotic signaling. Yet to be elucidated are the questions of whether mouse *Spag17* hypomorphs have increased fibrosis susceptibility, which cells in the skin are affected by reduced *SPAG17* expression, and why the *SPAG17* expression is decreased in the first place (i.e., whether it is a primary or secondary effect). One possibility is that *SPAG17* is lost in the transition from fibroblast to myofibroblast. Further research will be required to dissect these possibilities, particularly since the mouse germline knockout is lethal in neonatal mice.

We detected decreased expression of *LGR5* in the skin samples of SSc patients. The recent finding that *LGR5* is a marker for mouse intestinal villi tip telocytes begs the question of whether it is a marker of skin telocytes. The intestinal tip telocytes had increased expression of *Wnt5a* compared to the intestinal crypt telocytes, suggesting that noncanonical Wnt signaling is important in those cells (30). Skin telocytes are known to form multiple contacts to the extracellular matrix and other cells, such as adipose cells and fibroblasts (46). One possible function of these interconnections is to provide support for the other cells within the skin matrix. However, it is also possible that these cells are critical for the transduction of signals within the skin, and therefore may play a direct role in the evolution of fibrosis in the setting of SSc.

The skin of SSc patients had enrichment for pathways related to classical (antibody-mediated) complement activation. There is a growing body of evidence that complement activation and subsequent damage play a role in SSc endothelial damage. The terminal effector of complement damage, the membrane attack complex, has been observed in the small vessels of affected SSc skin and the muscle endothelium of patients with SSc-associated myositis (33,47). This indicates that local tissue damage, regardless of how it is triggered, may be complement-mediated. This possibility is perhaps even more evident in scleroderma renal crisis (SRC), which is characterized by a sudden onset of severe hypertension and acute renal failure. The kidneys of some individuals with SRC show deposition of complement C3b in renal arterioles (48,49). Complement deposition without substantial inflammation and the presence of thrombotic microangiopathy is also a hallmark of atypical hemolytic uremic syndrome (aHUS). Familial aHUS is often caused by the aberrant regulation of complement activation, particularly via genetic variants in complement factor H (50). The first-line therapy for aHUS is eculizumab, a monoclonal antibody to C5 (51). There is some evidence that eculizumab might also be effective for the treatment of SRC (52,53). However, this still leaves unanswered the question of whether endothelial complement activation is a major driver of vasculopathy in the skin of SSc patients.

The network analysis of PBMCs and skin transcriptomes with skin fibrosis and lung function parameters demonstrated that both tissues are informative for different traits, opening the possibility of the development of minimally invasive, quantitative biomarkers of disease activity. This would be a boon in clinical trials, particularly if observable parameters, such as the MRSS, do not tell the whole story regarding internal disease progression. Given the relatively small number of samples, further study is warranted to validate these findings. A particularly interesting facet of the clinical trait correlation in our study is the suggestion that SOX9 is a critical player in fibrosis. Expression of the *ROCR* and *SOX9-AS1* noncoding RNAs, as well as *SOX9* itself, was significantly correlated with fibrosis in the skin of SSc patients. Importantly, *SOX9-AS1* and *ROCR* were 2 of the most highly interconnected genes in the SSc skin gene–gene coexpression network, suggesting that they have a key role in mediating the progression of fibrosis. Both are thought to help increase *SOX9* levels, perhaps via noncanonical transforming growth factor β signaling through Wnt/β-catenin (54,55). The exact mechanism is not well defined. We previously demonstrated that blocking Wnt/β-catenin signaling with C-82 restored subdermal adipogenesis in patients with SSc (56). However, since these are noncoding RNAs, it is currently unclear whether their effect is primarily through a role in regulating *SOX9* or through an alternative mechanism unrelated to *SOX9*. In particular, noncoding RNAs also act as linkers between DNA and protein. One such example is the *HOTAIR* noncoding RNA that mediates repression of some *HOX* loci by recruiting complexes to repress chromatin in those regions (57,58). Further investigation into the role and mechanism of action of *SPAG17* in profibrotic signaling and a better understanding of the roles of *ROCR* and *SOX9-AS1* in the skin are intriguing areas for future research.

AUTHOR CONTRIBUTIONS

All authors were involved in drafting the article or revising it critically for important intellectual content, and all authors approved the final version to be published. Dr. Roberson had full access to all of the data in the study and takes responsibility for the integrity of the data and the accuracy of the data analysis.

Study conception and design. Roberson, Atkinson, Varga.

Acquisition of data. Roberson, Carns, Cao, Aren, Goldberg, Korman, Varga.

Analysis and interpretation of data. Roberson, Morales-Heil.

REFERENCES

1. Van den Hoogen F, Khanna D, Fransen J, et al. 2013 classification criteria for systemic sclerosis: an American College of Rheumatology/European League against Rheumatism collaborative initiative. Arthritis Rheum 2013;65:2737–47.
2. Allanore Y, Simms R, Distler O, et al. Systemic sclerosis [review]. Nat Rev Dis Primers 2015;1:15002.
3. Varga J, Roberson ED. Genomic advances in systemic sclerosis: it's time for precision. Arthritis Rheumatol 2015;67:2801–5.
4. Derrett-Smith EC, Martyanov V, Chighizola CB, et al. Limited cutaneous systemic sclerosis skin demonstrates distinct molecular subsets

separated by a cardiovascular development gene expression signature. Arthritis Res Ther 2017;19:156.

5. Assassi S, Wang X, Chen G, et al. Myeloablation followed by autologous stem cell transplantation normalises systemic sclerosis molecular signatures. Ann Rheum Dis 2019;78:1371–8.
6. Beretta L, Barturen G, Vigone B, et al. Genome-wide whole blood transcriptome profiling in a large European cohort of systemic sclerosis patients. Annals Rheum Dis 2020;79:1218–26.
7. Brkic Z, van Bon L, Cossu M, et al. The interferon type I signature is present in systemic sclerosis before overt fibrosis and might contribute to its pathogenesis through high BAFF gene expression and high collagen synthesis. Ann Rheum Dis 2016;75:1567–73.
8. Higgs BW, Liu Z, White B, et al. Patients with systemic lupus erythematosus, myositis, rheumatoid arthritis and scleroderma share activation of a common type I interferon pathway. Ann Rheum Dis 2011;70: 2029–36.
9. Pendergrass SA, Lemaire R, Francis IP, et al. Intrinsic gene expression subsets of diffuse cutaneous systemic sclerosis are stable in serial skin biopsies. J Invest Dermatol 2012;132:1363–73.
10. Skaug B, Khanna D, Swindell WR, et al. Global skin gene expression analysis of early diffuse cutaneous systemic sclerosis shows a prominent innate and adaptive inflammatory profile. Ann Rheum Dis 2020; 79:379–86.
11. Assassi S, Swindell WR, Wu M, et al. Dissecting the heterogeneity of skin gene expression patterns in systemic sclerosis. Arthritis Rheumatol 2015;67:3016–26.
12. Apostolidis SA, Stifano G, Tabib T, et al. Single cell RNA sequencing identifies HSPG2 and APLNR as markers of endothelial cell injury in systemic sclerosis skin. Front Immunol 2018;9:2191.
13. Karimizadeh E, Sharifi-Zarchi A, Nikaein H, et al. Analysis of gene expression profiles and protein-protein interaction networks in multiple tissues of systemic sclerosis. BMC Med Genomics 2019;12:199.
14. Hinchcliff M, Huang CC, Wood TA, et al. Molecular signatures in skin associated with clinical improvement during mycophenolate treatment in systemic sclerosis. J Invest Dermat 2013;133:1979–89.
15. Johnson ME, Mahoney JM, Taroni J, et al. Experimentally-derived fibroblast gene signatures identify molecular pathways associated with distinct subsets of systemic sclerosis patients in three independent cohorts. PloS One 2015;10:e0114017.
16. Richardson C, Agrawal R, Lee J, et al. Esophageal dilatation and interstitial lung disease in systemic sclerosis: a cross-sectional study. Semin Arthritis Rheum 2016;46:109–14.
17. Martin M. Cutadapt removes adapter sequences from high-throughput sequencing reads. EMBnet J 2011;17:10–2.
18. Dobin A, Davis CA, Schlesinger F, et al. STAR: ultrafast universal RNA-seq aligner. Bioinformatics 2013;29:15–21.
19. Liao Y, Smyth GK, Shi W. featureCounts: an efficient general purpose program for assigning sequence reads to genomic features. Bioinformatics 2014;30:923–30.
20. Langfelder P, Horvath S. WGCNA: an R package for weighted correlation network analysis. BMC Bioinformatics 2008;9:559.
21. Love MI, Huber W, Anders S. Moderated estimation of fold change and dispersion for RNA-seq data with DESeq2. Genome Biol 2014; 15:550.
22. Raudvere U, Kolberg L, Kuzmin I, et al. g:Profiler: a web server for functional enrichment analysis and conversions of gene lists (2019 update). Nucleic Acids Res 2019;47:W191–8.
23. Fingerlin TE, Murphy E, Zhang W, et al. Genome-wide association study identifies multiple susceptibility loci for pulmonary fibrosis. Nat Genet 2013;45:613–20.
24. Zhang Y, Wang S, Wang C, et al. High expression of FAM13A was associated with increasing the liver cirrhosis risk. Mol Genet Genomic Med 2019;7:e543.
25. Krausgruber T, Blazek K, Smallie T, et al. IRF5 promotes inflammatory macrophage polarization and TH1-TH17 responses. Nat Immunol 2011;12:231–8.
26. Duan H, Fleming J, Pritchard DK, et al. Combined analysis of monocyte and lymphocyte messenger RNA expression with serum protein profiles in patients with scleroderma. Arthritis Rheum 2008;58: 1465–74.
27. Assassi S, Mayes MD, Arnett FC, et al. Systemic sclerosis and lupus: points in an interferon-mediated continuum. Arthritis Rheum 2010;62: 589–98.
28. Kazarian E, Son H, Sapao P, et al. *SPAG17* is required for male germ cell differentiation and fertility. Int J Mol Sci 2018;19:1252.
29. Teves ME, Sundaresan G, Cohen DJ, et al. *Spag17* deficiency results in skeletal malformations and bone abnormalities. PloS One 2015;10: e0125936.
30. Bahar Halpern K, Massalha H, Zwick RK, et al. Lgr5+ telocytes are a signaling source at the intestinal villus tip. Nat Commun 2020;11: 1936.
31. Manetti M, Rosa I, Messerini L, et al. A loss of telocytes accompanies fibrosis of multiple organs in systemic sclerosis. J Cell Mol Med 2014; 18:253–62.
32. Manetti M, Guiducci S, Ruffo M, et al. Evidence for progressive reduction and loss of telocytes in the dermal cellular network of systemic sclerosis. J Cell Mol Med 2013;17:482–96.
33. Scambi C, Ugolini S, Jokiranta TS, et al. The local complement activation on vascular bed of patients with systemic sclerosis: a hypothesis-generating study. PloS One 2015;10:e0114856.
34. Farina G, Lafyatis D, Lemaire R, et al. A four-gene biomarker predicts skin disease in patients with diffuse cutaneous systemic sclerosis. Arthritis Rheum 2010;62:580–8.
35. Christmann RB, Sampaio-Barros P, Stifano G, et al. Association of interferon- and transforming growth factor β–regulated genes and macrophage activation with systemic sclerosis–related progressive lung fibrosis. Arthritis Rheumatol 2014;66:714–25.
36. Rice LM, Ziemek J, Stratton EA, et al. A longitudinal biomarker for the extent of skin disease in patients with diffuse cutaneous systemic sclerosis. Arthritis Rheumatol 2015;67:3004–15.
37. Kim YH, Lee JR, Hahn MJ. Regulation of inflammatory gene expression in macrophages by epithelial-stromal interaction 1 (Epsti1). Biochem Biophys Res Commun 2018;496:778–83.
38. Trombetta AC, Soldano S, Contini P, et al. A circulating cell population showing both M1 and M2 monocyte/macrophage surface markers characterizes systemic sclerosis patients with lung involvement. Respir Res 2018;19:186.
39. Teves ME, Zhang Z, Costanzo RM, et al. Sperm-associated antigen-17 gene is essential for motile cilia function and neonatal survival. Am J Respir Cell Mol Biol 2013;48:765–72.
40. Xu X, Sha YW, Mei LB, et al. A familial study of twins with severe asthenozoospermia identified a homozygous SPAG17 mutation by whole-exome sequencing. Clin Genet 2018;93:345–9.
41. Cordova-Fletes C, Becerra-Solano LE, Rangel-Sosa MM, et al. Uncommon runs of homozygosity disclose homozygous missense mutations in two ciliopathy-related genes (SPAG17 and WDR35) in a patient with multiple brain and skeletal anomalies. Eur J Med Genet 2018;61:161–7.
42. Van der Valk RJ, Kreiner-Moller E, Kooijman MN, et al. A novel common variant in DCST2 is associated with length in early life and height in adulthood. Hum Mol Genet 2015;24:1155–68.
43. Kim JJ, Lee HI, Park T, et al. Identification of 15 loci influencing height in a Korean population. J Hum Genet 2010;55:27–31.
44. Abdelhamed Z, Lukacs M, Cindric S, et al. A novel hypomorphic allele of Spag17 causes primary ciliary dyskinesia phenotypes in mice. Dis Model Mech 2020;13:dmm045344.

45. Andjelkovic M, Minic P, Vreca M, et al. Genomic profiling supports the diagnosis of primary ciliary dyskinesia and reveals novel candidate genes and genetic variants. PloS One 2018;13:e0205422.

46. Rusu MC, Mirancea N, Manoiu VS, et al. Skin telocytes. Ann Anat 2012;194:359–67.

47. Corallo C, Cutolo M, Volpi N, et al. Histopathological findings in systemic sclerosis-related myopathy: fibrosis and microangiopathy with lack of cellular inflammation. Ther Adv Musculoskelet Dis 2017;9: 3–10.

48. Okroj M, Johansson M, Saxne T, et al. Analysis of complement biomarkers in systemic sclerosis indicates a distinct pattern in scleroderma renal crisis. Arthritis Res Ther 2016;18:267.

49. Perez NA, Morales ML, Sanchez RS, et al. Endothelial lesion and complement activation in patients with Scleroderma Renal Crisis. J Bras Nefrol 2019;41:580–4.

50. Noris M, Caprioli J, Bresin E, et al. Relative role of genetic complement abnormalities in sporadic and familial aHUS and their impact on clinical phenotype. Clin J Am Soc Nephrol 2010;5:1844–59.

51. Cofiell R, Kukreja A, Bedard K, et al. Eculizumab reduces complement activation, inflammation, endothelial damage, thrombosis, and renal injury markers in aHUS. Blood 2015;125:3253–62.

52. Devresse A, Aydin S, Le Quintrec M, et al. Complement activation and effect of eculizumab in scleroderma renal crisis. Medicine (Baltimore) 2016;95:e4459.

53. Uriarte MH, Larrarte C, Rey LB. Scleroderma renal crisis debute with thrombotic microangiopathy: a successful case treated with eculizumab. Case Rep Nephrol 2018;2018:6051083.

54. Zhang W, Wu Y, Hou B, et al. A SOX9-AS1/miR-5590-3p/SOX9 positive feedback loop drives tumor growth and metastasis in hepatocellular carcinoma through the Wnt/β-catenin pathway. Mol Oncol 2019; 13:2194–210.

55. Barter MJ, Gomez R, Hyatt S, et al. The long non-coding RNA ROCR contributes to SOX9 expression and chondrogenic differentiation of human mesenchymal stem cells. Development 2017;144:4510–21.

56. Lafyatis R, Mantero JC, Gordon J, et al. Inhibition of β-catenin signaling in the skin rescues cutaneous adipogenesis in systemic sclerosis: a randomized, double-blind, placebo-controlled trial of C-82. J Invest Dermatol 2017;137:2473–83.

57. Tsai MC, Manor O, Wan Y, et al. Long noncoding RNA as modular scaffold of histone modification complexes. Science 2010;329: 689–93.

58. Rinn JL, Kertesz M, Wang JK, et al. Functional demarcation of active and silent chromatin domains in human HOX loci by noncoding RNAs. Cell 2007;129:1311–23.

American College of Rheumatology
Empowering Rheumatology Professionals

Arthritis & Rheumatology
Vol. 75, No. 1, January 2023, pp 120

DOI 10.1002/art.42326

Clinical Images: Chronic, refractory childhood-onset cutaneous lupus erythematosus of the face responsive to lenalidomide

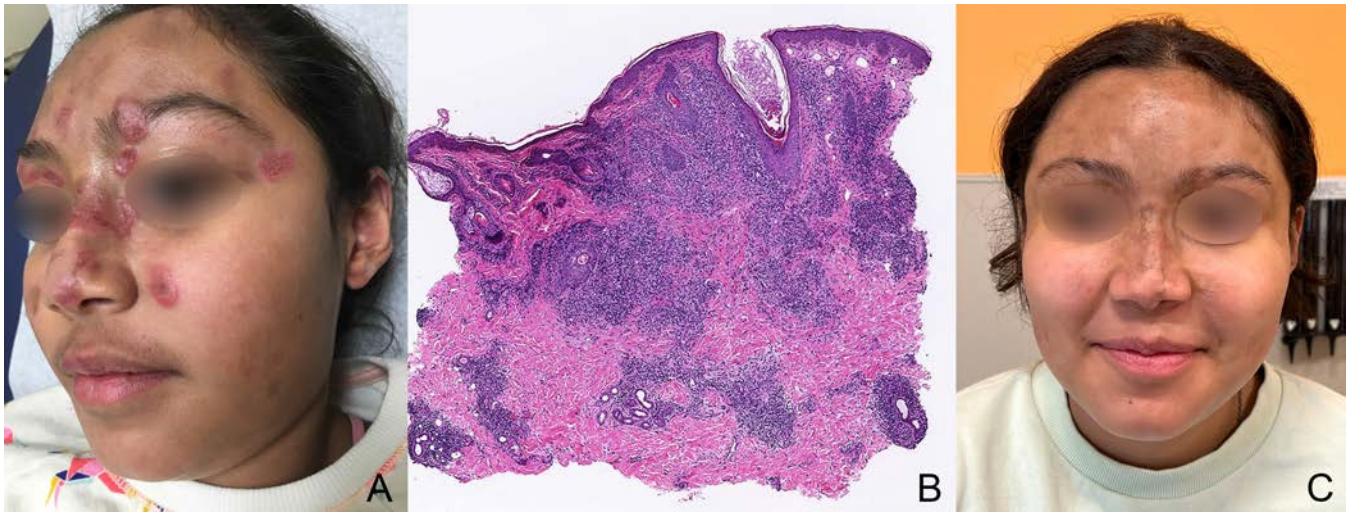

The patient, an 11-year-old girl with anti-Ro/SSA and hypergammaglobulinemia, presented in 2013 with prominent facial eruption consisting of red to purple nodules concentrated on the forehead, around the eyebrows, and on the cheeks that resulted in significant hyperpigmentation, scarring, and atrophy. This pattern was consistent with a diagnosis of cutaneous lupus (**A**); the patient had no signs of systemic lupus erythematosus. The rash was refractory to hydroxychloroquine (HCQ), topical calcineurin inhibitor, topical steroids, intralesional steroids, oral steroids, dapsone, azathioprine, and mycophenolate. The patient's course was complicated by intermittent follow-up and frequent periods of not receiving medications. Systemic therapies were discontinued by the family prior to the COVID-19 pandemic. Biopsy was repeated in September 2020 because of ongoing disease activity and diagnostic uncertainty. Histologic examination revealed a superficial and deep perivascular and periadnexal lymphohistiocytic infiltrate associated with mild overlying interface changes, telangiectasias, and increased dermal mucin consistent with chronic cutaneous lupus (**B**). Lenalidomide (LND) has been found to be effective and generally well tolerated in refractory cases of cutaneous lupus in adults and adolescents (1–3). The typical starting dosage is 5 mg per day for both age groups. In February 2021, LND 2.5 mg was started, with a plan to titrate up based on clinical response, in combination with HCQ. At most recent follow-up in May 2021, the patient had significant improvement in cutaneous lesions and has remained on the initial dose (**C**). The patient has tolerated LND thus far without apparent adverse effects, such as cytopenias or neuropathy. Due to risk of teratogenicity, monthly urine pregnancy tests have been required since the patient reached menarche.

Author disclosures are available at https://onlinelibrary.wiley.com/action/downloadSupplement?doi=10.1002%2Fart.42326&file=art42326-sup-0001-Disclosureform.pdf.

1. Wu EY, Schanberg LE, Wershba EC, et al. Lenalidomide for refractory cutaneous manifestations of pediatric systemic lupus erythematosus. Lupus 2017;26:646-9.
2. Cortés-Hernández J, Ávila G, Vilardell-Tarrés M, et al. Efficacy and safety of lenalidomide for refractory cutaneous lupus erythematosus. Arthritis Res Ther 2012;14:R265.
3. Aitmehdi R, Arnaud L, Francès C, et al. Long-term efficacy and safety outcomes of lenalidomide for cutaneous lupus erythematosus: a multicenter retrospective observational study of 40 patients. J Am Acad Dermatol 2021;84:1171-4.

Matthew A. Sherman, MD
msherman2@cnmc.org
Hemalatha Srinivasalu, MD
Division of Rheumatology
Children's National Hospital
A. Yasmine Kirkorian, MD
Division of Dermatology
Children's National Hospital
Michael A. Cardis, MD
Department of Dermatology
Medstar Washington Hospital Center
Georgetown University Hospital
Washington, DC

Arthritis & Rheumatology
Vol. 75, No. 1, January 2023, pp 121

American College of Rheumatology
Empowering Rheumatology Professionals

DOI 10.1002/art.42317

Clinical Images: Nivolumab-induced tracheobronchial chondritis in a patient with hypopharyngeal cancer

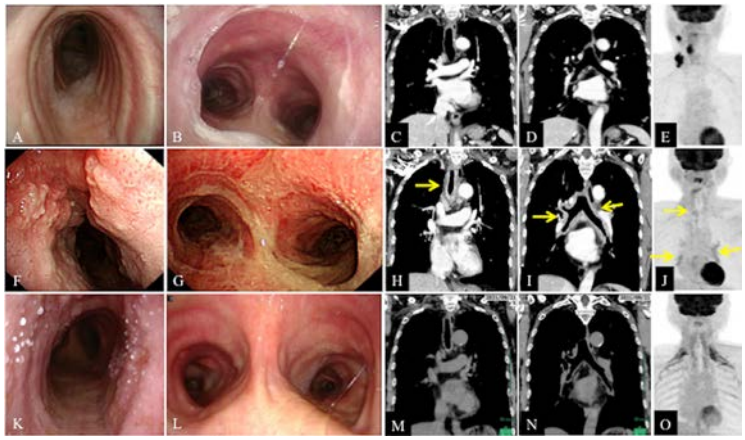

The patient, a 66-year-old man with multiple lymph node metastases, began receiving immune checkpoint inhibitor (ICI) treatment with nivolumab after undergoing surgical resection for hypopharyngeal cancer. Before ICI, no abnormalities of the trachea and bronchi were noted on bronchoscopy (**A** and **B**), contrast-enhanced computed tomography (CE-CT) (**C** and **D**), and fluorodeoxyglucose–positron emission tomography (FDG-PET)/CT (**E**). ICI treatment shrank the cervical lymph nodes. However, after the 24th course of ICI, the patient had precordial pain and increased sputum with elevated C-reactive protein (7.11 mg/dl). Although respiratory infections were initially suspected, antibiotics had no effect, and tests of sputum and blood cultures were negative. Redness and swelling of the tracheal and bronchial mucosa were seen on bronchoscopy (**F** and **G**), tracheal and bronchial wall thickening on CE-CT (**arrows** in **H** and **I**), and high FDG uptake of the trachea and bronchi on FDG-PET/CT (**arrows** in **J**), indicating tracheobronchial chondritis. Lymphocytic infiltrates in soft tissue around tracheal cartilage were noted on biopsy. High levels of matrix metalloproteinase 3 (1,240 ng/ml) and type II collagen antibody (25.9 U/ml) were found. Other immune tests, including antinuclear antibody, rheumatoid factor, and antineutrophil cytoplasmic antibodies, yielded negative results. The patient was diagnosed as having nivolumab-induced tracheobronchial chondritis. High-dose steroids and methotrexate were initiated, but relapse was observed during tapering. Intravenous infusion of tocilizumab (TCZ) was added, and the patient's condition improved 3 months after TCZ initiation, showing normalization of the trachea and bronchi on bronchoscopy (**K** and **L**), reduced wall thickening on non–CE-CT (**M** and **N**), and no abnormal uptake on FDG-PET/CT (**O**). ICIs for advanced cancers are known to cause immune-related adverse events (AEs) including rheumatic diseases (1). Tracheal cartilage lesions resulting from an immune-related AE are rare; however, tracheobronchial chondritis could be an initial manifestation of an immune-related AE (2,3). Physicians should be aware that ICI treatment can cause tracheobronchial chondritis, which can be a fatal immune-related AE.

Author disclosures are available at https://onlinelibrary.wiley.com/action/downloadSupplement?doi=10.1002%2Fart.42317&file=art42317-sup-0001-Disclosureform.pdf.

1. Ghosh N, Bass AR. Rheumatic complications of immune checkpoint inhibitors. Med Clin North Am 2021;105:227–45.
2. Ogimoto T, Yoshida H, Mizuta M, Hirai T. Relapsing polychondritis after treatment with PD-1 blockade. Invest New Drugs 2022;40:389–91.
3. Kuba K, Nakahira M, Inoue H, Kogashiwa Y, Ebihara Y, Sugasawa M. Nivolumab-related tracheobronchial chondritis: extremely rare manifestation of an immune-related adverse effect. Head Neck 2020;42:E43–E48.

Kazu Hamada-Ode, MD
Yoshinori Taniguchi, MD
taniguchiy@kochi-u.ac.jp

Department of Endocrinology, Metabolism, Nephrology and Rheumatology
Kochi Medical School
Kochi University
Marina Osaki, MD
Rika Yoshimatsu, MD
Noriko Nitta, MD
Department of Diagnostic and Interventional Radiology
Kochi Medical School
Kochi University
Kochi, Japan

American College of Rheumatology
Empowering Rheumatology Professionals

Arthritis & Rheumatology
Vol. 75, No. 1, January 2023, pp 122–132
DOI 10.1002/art.42339

Gout and Excess Risk of Severe SARS–CoV-2 Infection Among Vaccinated Individuals: A General Population Study

Dongxing Xie,[1] Hyon K. Choi,[2] Nicola Dalbeth,[3] Zachary S. Wallace,[2] Jeffrey A. Sparks,[4] Na Lu,[5] Chao Zeng,[6] Xiaoxiao Li,[7] Jie Wei,[8] Guanghua Lei,[6] and Yuqing Zhang[2]

Objective. Gout patients often have multiple comorbidities, making them susceptible to SARS–CoV-2 infection and poor outcomes. This study was undertaken to examine the association between gout and the risk of SARS–CoV-2 infection and severe outcomes, especially in patients who have received a SARS–CoV-2 vaccine.

Methods. We conducted 2 cohort studies using The Health Improvement Network in the UK. Individuals with gout and those without gout from the general population were followed up from December 8, 2020 to October 31, 2021. We estimated the rate difference (RD) and hazard ratio (HR) of SARS–CoV-2 infection and severe outcomes (i.e., hospitalization and death within 30 days after SARS–CoV-2 infection) for individuals with gout versus those without gout using a Cox proportional hazards model according to SARS–CoV-2 vaccination status. We adjusted for potential confounders by using overlap weighting of exposure scores.

Results. Among the vaccinated cohort, 1,955 cases of breakthrough COVID-19 infection occurred in 54,576 individuals with gout (4.68 cases per 1,000 person-months), and 52,468 cases occurred in 1,336,377 individuals without gout (3.76 cases per 1,000 person-months). The partially adjusted RD of breakthrough infection was 0.91 cases per 1,000 person-months (95% confidence interval [95% CI] 0.62–1.20 cases per 1,000 person-months), and the partially adjusted HR was 1.24 (95% CI 1.19–1.30). Gout was also associated with an increased risk of hospitalization (adjusted HR 1.30 [95% CI 1.10–1.53]) and death (adjusted HR 1.36 [95% CI 0.87–2.13]). Women with gout had an increased risk of hospitalization (adjusted HR 1.55 [95% CI 1.15–2.10]) and death (adjusted HR 2.46 [95% CI 1.12–5.41]). Similar associations with gout were observed in the unvaccinated cohort.

Conclusion. These general population data suggest that individuals with gout, especially women, have higher risks of SARS–CoV-2 infection and severe outcomes, even when vaccinated.

INTRODUCTION

The COVID-19 pandemic has caused devastating economic and social disruption (1). There are few effective therapies for COVID-19, and these therapies remain a scarce resource. As such, vaccination remains the most promising approach at present for controlling this disease (2). Despite the increasing availability of effective vaccines, millions of new COVID-19 cases in both vaccinated and unvaccinated people continue to occur each day worldwide, and new variants are expected to emerge in the future that may evolve immune escape (1). Identifying individuals who are susceptible to breakthrough COVID-19 infection and severe outcomes despite vaccination may identify populations who would benefit from other risk-mitigating strategies (e.g., preexposure prophylaxis).

Dr. Wallace's work was supported by the National Institute of Arthritis and Musculoskeletal and Skin Diseases, NIH (awards K23-AR-073334 and R03-AR-078938). Dr. Sparks' work was supported by the National Institute of Arthritis and Musculoskeletal and Skin Diseases, NIH (awards R01-AR-077607, P30-AR-070253, and P30-AR-072577), and the R. Bruce and Joan M. Mickey Research Scholar Fund.

[1]Dongxing Xie, MD, PhD: Department of Orthopaedics, Xiangya Hospital, Central South University, Changsha, China; [2]Hyon K. Choi, MD, DrPH, Zachary S. Wallace, MD, MSc, Yuqing Zhang, DSc: Division of Rheumatology, Allergy, and Immunology, Department of Medicine, and The Mongan Institute, Massachusetts General Hospital, Harvard Medical School, Boston, Massachusetts; [3]Nicola Dalbeth, MD: Department of Medicine, University of Auckland, Auckland, New Zealand; [4]Jeffrey A. Sparks, MD, MMSc: Harvard Medical School and Division of Rheumatology, Inflammation, and Immunity, Brigham and Women's Hospital, Boston, Massachusetts; [5]Na Lu, MPH: Arthritis Research Canada, Richmond, British Colombia, Canada; [6]Chao Zeng, MD, PhD, Guanghua Lei, MD, PhD: Department of Orthopaedics, Hunan Key Laboratory of Joint Degeneration and Injury, and National Clinical Research Center for Geriatric Disorders, Xiangya Hospital, Central South University, Changsha, China; [7]Xiaoxiao Li, MS: Hunan Key Laboratory of Joint Degeneration and Injury, Xiangya Hospital, Central South University, Changsha, China; [8]Jie Wei, PhD: Hunan Key Laboratory of Joint Degeneration and Injury, Health Management Center, and Department of Epidemiology and Health Statistics, Xiangya School of Public Health, Central South University, Changsha, China.

Author disclosures are available at https://onlinelibrary.wiley.com/action/downloadSupplement?doi=10.1002%2Fart.42339&file=art42339-sup-0001-Disclosureform.pdf.

Address correspondence via email to Guanghua Lei, MD, PhD (lei_guanghua@csu.edu.cn), Jie Wei, PhD (weij1988@csu.edu.cn), or Yuqing Zhang, DSc (yzhang108@mgh.harvard.edu)

Submitted for publication March 9, 2022; accepted in revised form August 30, 2022.

Gout is a common inflammatory arthritis (3). Individuals with gout often have multiple comorbidities, including obesity, cardiovascular disease, and chronic kidney disease (4), which have been associated with a higher risk of SARS–CoV-2 infection and poor outcomes (5,6). Furthermore, elevated serum urate levels could contribute to a proinflammatory state that may complicate the COVID-19 course (7). However, unlike other inflammatory rheumatic diseases, such as rheumatoid arthritis and lupus, there is a paucity of data on the risk of SARS–CoV-2 infection among gout patients, particularly on the risk of breakthrough infection after vaccination.

To date, 2 studies have examined the association between gout and the risk of SARS–CoV-2 infection but have yielded conflicting results (8,9). One study using data from the UK Biobank showed no significant difference in the risk of SARS–CoV-2 infection and death between participants with gout and those without gout (8). Using the same data source, a subsequent study reported that gout is a risk factor for SARS–CoV-2 infection and related death (9). However, these studies were conducted before the widespread availability of COVID-19 vaccines—up to August 24, 2020 (8) and up to April 6, 2021 (9)—leaving an important knowledge gap regarding the effectiveness of vaccination against SARS–CoV-2 infection and severe outcomes among individuals with gout (9). Since studies have demonstrated that waning vaccine effectiveness is greater in individuals with underlying medical conditions (10), assessing the effectiveness of COVID-19 vaccination against breakthrough infection and severe outcomes in gout patients has important clinical and public health implications.

We conducted 2 cohort studies to quantify the risk of SARS–CoV-2 infection and severe outcomes (i.e., hospitalization and death) among individuals with gout compared with non-gout individuals from the general population according to their COVID-19 vaccination status.

METHODS

Data source. The Health Improvement Network (THIN) (now called IQVIA Medical Research Database) is an electronic medical record database that contains general practitioners' (GPs) records in the UK and is representative of the UK population with regard to demographic characteristics and medical conditions. Details of the THIN database have been described previously (11). It consists of ~17 million individuals from 790 general practices whose health care information is systematically recorded by GPs and sent anonymously to THIN. Because the National Health Service requires residents of the UK to register with a general practice regardless of health status, THIN is considered a population-based cohort representative of the UK general population (12,13). Information in THIN includes sociodemographic characteristics, anthropometric characteristics, lifestyle factors, and details from visits to GPs (i.e., prescriptions, diagnoses and interventions from specialist referrals, hospital admissions, and results of laboratory tests). The Read classification system is used to code specific diagnoses (14), whereas a dictionary based on the Multilex classification system by First Databank is used to code drugs (15). The validity of the database for use in clinical and epidemiologic research studies has been described in a previous study (16).

This study received approval from the ethics committee at Xiangya Hospital (2018091077), with waiver of informed consent, and was approved by the THIN Scientific Review Committee (20SRC003-A2). THIN is a registered trademark of Cegedim in the UK and other countries. Reference made to the THIN database is intended to be descriptive of the data asset licensed by IQVIA. This study uses deidentified data provided by individuals as a part of their routine primary care.

Study design. We compared the risk of breakthrough infection (i.e., SARS–CoV-2 infection among people who had received a COVID-19 vaccine), hospitalization, and death between individuals with gout and individuals of the general population without gout who had received a COVID-19 vaccine (i.e., vaccinated cohort). The details of vaccination records were based on the Read codes in THIN. Gout diagnosis was also captured using Read codes (see Supplementary Table 1, available on the *Arthritis & Rheumatology* website at https://onlinelibrary.wiley.com/doi/art.42339) (17,18). Eligible individuals were those 18–90 years of age between December 8, 2020 (when the vaccination campaign began in the UK) and October 31, 2021 who had no previously documented SARS–CoV-2 infection and had at least 2 years of continuous enrollment with a general practice. We then took the same approach to compare the risk of SARS–CoV-2 infection and severe outcomes between individuals with gout and individuals of the general population without gout who had not received a COVID-19 vaccine (i.e., unvaccinated cohort).

Cohort definition. Eligible individuals in the vaccinated cohort were followed up starting on the day the first dose of a COVID-19 vaccine was received (i.e., index date) and ending on the day that an outcome of interest occurred (i.e., SARS–CoV-2 infection, hospitalization, or death) or the end of the study period (October 31, 2021), whichever occurred first. Eligible individuals in the unvaccinated cohort were followed up starting on December 8, 2020 (i.e., index date) and ending on the day that the first dose of a COVID-19 vaccine was received, the day that an outcome of interest occurred, or the end of the study period (October 31, 2021), whichever occurred first.

Assessment of outcomes. The primary outcome was a confirmed diagnosis of SARS–CoV-2 infection based on Read codes recommended in national guidelines (Supplementary Table 1 [https://onlinelibrary.wiley.com/doi/art.42339]) (19,20). According to National Health Service guidance and standard operating procedures for primary care and UK Faculty of Clinical

Table 1. Baseline characteristics of gout patients and individuals without gout in vaccinated and unvaccinated cohorts*

Characteristic	Vaccinated cohort						Unvaccinated cohort					
	Before exposure score overlap weighting			After exposure score overlap weighting			Before exposure score overlap weighting			After exposure score overlap weighting†		
	Gout (n = 54,576)	Non-gout (n = 1,336,377)	Standardized difference	Gout (n = 54,576)	Non-gout (n = 1,336,377)	Standardized difference	Gout (n = 61,111)	Non-gout (n = 1,697,168)	Standardized difference	Gout (n = 61,111)	Non-gout (n = 1,697,168)	Standardized difference
Demographics												
Age, mean ± SD years	66.3 ± 13.1	52.1 ± 17.8	0.906	65.6 ± 13.3	65.6 ± 13.8	<0.001	65.7 ± 13.5	49.8 ± 17.9	1.002	64.8 ± 13.6	64.8 ± 15.1	<0.001
Socioeconomic deprivation index score, mean ± SD‡	2.6 ± 1.5	2.6 ± 1.6	0.103	2.6 ± 1.5	2.6 ± 1.5	<0.001	2.6 ± 1.5	2.7 ± 1.6	0.046	2.6 ± 1.5	2.6 ± 1.5	<0.001
Women, %	21.2	53.1	0.699	22.9	22.9	<0.001	20.9	51.1	0.664	22.5	22.5	<0.001
Body mass index, mean ± SD kg/m^2	30.6 ± 5.9	27.9 ± 6.1	0.440	30.4 ± 6.0	30.3 ± 5.8	0.017	30.5 ± 5.9	27.6 ± 6.1	0.486	30.4 ± 6.0	30.2 ± 5.8	0.019
Location, %			0.168			<0.001			0.184			<0.001
England	14.8	14.2		14.9	14.9		17.3	18.5		17.5	17.5	
Northern Ireland	11.8	13.6		12.0	12.0		11.5	13.2		11.7	11.7	
Scotland	35.8	41.9		36.4	36.4		33.9	39.5		34.5	34.5	
Wales	37.6	30.3		36.7	36.7		37.3	28.8		36.4	36.4	
First dose of COVID-19 vaccine, %			0.265			<0.001			–			–
ChAdOx1-S (AstraZeneca)	67.7	55.2		67.7	67.7		–	–		–	–	
BNT162b2 (Pfizer-BioNTech)	31.1	42.3		31.2	31.2		–	–		–	–	
Other	1.1	2.4		1.1	1.1		–	–		–	–	
Second dose of COVID-19 vaccine, %			0.288			0.013			–			–
ChAdOx1-S (AstraZeneca)	65.5	52.4		65.4	65.2		–	–		–	–	
BNT162b2 (Pfizer-BioNTech)	29.6	38.8		29.7	29.6		–	–		–	–	
Other	0.5	1.8		0.5	0.5		–	–		–	–	
None	4.4	7.0		4.4	4.7		–	–		–	–	
Number of previous SARS–CoV-2 tests, mean ± SD	0.1 ± 0.3	0.1 ± 0.4	0.101	0.1 ± 0.3	0.1 ± 0.3	<0.001	0.1 ± 0.3	0.1 ± 0.3	0.054	0.1 ± 0.3	0.1 ± 0.3	<0.001
Influenza vaccination, %	64.4	37.7	0.553	62.8	62.8	<0.001	57.9	29.0	0.609	55.8	55.8	<0.001
Lifestyle factors												
Alcohol intake, %			0.161			<0.001			0.185			<0.001
None	12.6	15.5		12.9	12.9		12.7	16.0		13.1	13.1	
Past	4.0	2.6		4.0	4.0		4.0	2.5		3.9	3.9	
Current	78.5	64.0		77.7	77.7		78.1	61.3		77.2	77.2	
Missing data	4.9	17.9		5.4	5.4							
Smoking, %			0.301			<0.001	5.3	20.2	0.333	5.8	5.8	<0.001
None	52.8	56.4		53.0	53.0		52.6	55.0		52.8	52.8	
Past	36.3	23.1		35.4	35.4		35.9	21.7		34.9	34.9	
Current	10.5	16.5		11.2	11.2		11.0	18.2		11.7	11.7	
Missing data	0.4	4.0		0.5	0.5		0.5	5.0		0.6	0.6	
Charlson comorbidity index, mean ± SD	0.5 ± 1.1	0.3 ± 0.8	0.296	0.5 ± 1.1	0.5 ± 1.1	<0.001	0.5 ± 1.1	0.2 ± 0.7	0.327	0.5 ± 1.1	0.5 ± 1.1	<0.001
Comorbidity, %												
Hypertension	58.9	22.5	0.798	56.0	56.0	<0.001	57.7	19.6	0.849	54.5	54.5	<0.001
Diabetes	26.3	11.1	0.398	24.9	24.9	<0.001	25.8	9.9	0.426	24.3	24.3	<0.001

(Continued)

Table 1. (*Cont'd*)

Characteristic	Vaccinated cohort						Unvaccinated cohort					
	Before exposure score overlap weighting			After exposure score overlap weighting			Before exposure score overlap weighting			After exposure score overlap weighting†		
	Gout (n = 54,576)	Non-gout (n = 1,336,377)	Standardized difference	Gout (n = 54,576)	Non-gout (n = 1,336,377)	Standardized difference	Gout (n = 61,111)	Non-gout (n = 1,697,168)	Standardized difference	Gout (n = 61,111)	Non-gout (n = 1,697,168)	Standardized difference
Hyperlipidemia	18.4	6.8	0.354	17.3	17.3	<0.001	18.0	6.0	0.378	16.8	16.8	<0.001
Chronic kidney disease	17.4	3.6	0.462	15.1	15.1	<0.001	17.1	3.1	0.478	14.7	14.7	<0.001
Pneumonia or infection	9.3	6.0	0.123	9.0	9.0	<0.001	9.2	5.6	0.139	8.9	8.9	<0.001
Chronic obstructive pulmonary disease	6.6	3.3	0.149	6.3	6.3	<0.001	6.4	2.9	0.168	6.2	6.2	<0.001
Cancer	14	7.6	0.205	13.5	13.5	<0.001	13.6	6.6	0.233	13.0	13.0	<0.001
Venous thromboembolism	4.5	2.0	0.143	4.3	4.3	<0.001	4.4	1.8	0.152	4.2	4.2	<0.001
Atrial fibrillation	11.9	2.8	0.356	10.5	10.5	<0.001	11.6	2.4	0.367	10.1	10.1	<0.001
Ischemic heart disease	16	5.1	0.361	14.9	14.9	<0.001	15.7	4.4	0.383	14.5	14.5	<0.001
Myocardial infarction	7.4	2.4	0.233	6.9	6.9	<0.001	7.3	2.1	0.249	6.7	6.7	<0.001
Congestive heart failure	6.7	1.4	0.272	5.7	5.7	<0.001	6.5	1.2	0.281	5.6	5.6	<0.001
Stroke	5.1	2.0	0.171	4.8	4.8	<0.001	4.9	1.7	0.181	4.6	4.6	<0.001
Medication, %§												
CCBs	28.3	10.5	0.460	26.9	26.9	<0.001	27.5	9.0	0.493	26.0	26.0	<0.001
ARBs	14.7	4.8	0.339	13.7	13.7	<0.001	14.3	4.2	0.357	13.2	13.2	<0.001
ACEIs	31.0	11.1	0.503	29.5	29.5	<0.001	30.4	9.6	0.539	28.7	28.7	<0.001
Beta-blockers	26.8	10.5	0.428	24.8	24.8	<0.001	26.3	9.4	0.454	24.2	24.2	<0.001
Glucocorticoids	8.7	4.1	0.188	8.1	8.1	<0.001	9.5	4.2	0.212	8.8	8.8	<0.001
NSAIDs	35.0	18.4	0.380	33.6	33.6	<0.001	35.3	17.0	0.424	33.7	33.7	<0.001
Opioids	10.9	6.6	0.154	10.6	10.6	<0.001	11.0	6.1	0.177	10.7	10.7	<0.001
Antihypertensive drugs	62.8	26.6	0.780	60.0	60.0	<0.001	61.3	23.3	0.835	58.2	58.2	<0.001
Antidiabetic medicine	14.5	6.0	0.282	14.0	14.0	<0.001	14.3	5.3	0.307	13.6	13.6	<0.001
Statin	46.6	18.3	0.634	44.6	44.6	<0.001	45.1	15.6	0.676	42.8	42.8	<0.001
Loop diuretics	11.4	2.7	0.344	10.0	10.0	<0.001	11.4	2.4	0.360	9.9	9.9	<0.001
Thiazide diuretics	8.9	4.4	0.180	8.9	8.9	<0.001	8.7	3.8	0.203	8.6	8.6	<0.001
Health care utilization, mean ± SD§												
Hospitalizations	0.4 ± 1.1	0.2 ± 0.8	0.153	0.3 ± 1.1	0.3 ± 1.1	<0.001	0.4 ± 1.1	0.2 ± 0.8	0.176	0.4 ± 1.1	0.4 ± 1.1	<0.001
General practice visits	3.1 ± 5.2	1.9 ± 3.5	0.275	3.0 ± 4.9	3.0 ± 5.4	<0.001	3.4 ± 5.2	2.0 ± 3.6	0.320	3.3 ± 4.9	3.3 ± 5.5	<0.001
Specialist referrals	0.3 ± 0.8	0.2 ± 0.6	0.158	0.3 ± 0.8	0.3 ± 0.8	<0.001	0.4 ± 0.9	0.2 ± 0.6	0.189	0.3 ± 0.8	0.3 ± 0.8	<0.001

* CCBs = calcium channel blockers; ARBs = angiotensin II receptor blockers; ACEIs = angiotensin converting enzyme inhibitors; NSAIDs = nonsteroidal antiinflammatory drugs.
† Data were presented after full exposure score overlap weighting.
‡ The socioeconomic deprivation index score was measured by the Townsend deprivation index, which was grouped into quintiles from 1 (least deprived) to 5 (most deprived).
§ Frequency of medication prescriptions and health care utilization during the past 1 year from the index date.

Informatics guidelines, confirmed SARS–CoV-2 infection codes reflect a positive reverse transcription–polymerase chain reaction test. The secondary outcomes were risk of hospitalization for SARS–CoV-2 infection and death from SARS–CoV-2 infection. Hospitalization for SARS–CoV-2 infection was defined as a hospitalization record in THIN within 30 days after the diagnosis of SARS–CoV-2 infection (21), and death from SARS–CoV-2 infection was defined as a death occurring within 30 days after the diagnosis of SARS–CoV-2 infection.

Assessment of covariates. Covariates included sociodemographic factors (age, sex, Townsend deprivation index), geographic location, body mass index, lifestyle factors (alcohol intake and smoking), number of previous SARS–CoV-2 tests (22), influenza vaccination during the past 1 year before the index date, comorbidities at any time since enrollment in the THIN database (Charlson comorbidity index, as well as individual conditions of hypertension, diabetes, hyperlipidemia, chronic kidney disease, pneumonia or infection, chronic obstructive pulmonary disease, cancer, venous thromboembolism, atrial fibrillation, ischemic heart disease, myocardial infarction, congestive heart failure, and stroke), medication use (calcium channel blockers, angiotensin II receptor blockers, angiotensin converting enzyme inhibitors, beta-blockers, glucocorticoids, nonsteroidal antiinflammatory drugs, opioids, antihypertensive drugs, antidiabetic medicine, statins, loop diuretics, and thiazide diuretics), and health care utilization during the past 1 year before the index date. Missing values were treated as a separate category for each variable. The absence of a record of any diagnosis was considered the absence of the condition. Among the vaccinated cohort, we also collected information on the brand of the first dose of vaccine that individuals received (Table 1).

Statistical analysis. For the vaccinated cohort, we divided the baseline study period into monthly time blocks. Eligible individuals were allocated into these blocks according to their index dates. In each monthly time block, we calculated an exposure score for gout and applied overlap weighting of the exposure score to balance baseline characteristics between the comparison groups (23).

The exposure score (analogous to propensity score) for gout at each monthly time block was calculated using a logistic regression model with the covariates described above. We generated 2 sets of exposure scores. First, an exposure score for the probability of gout was generated using a logistic regression model that included the covariates of age, sex, body mass index, Townsend deprivation index score, geographic location, and number of previous SARS–CoV-2 tests (i.e., partially adjusted exposure score). Second, additional covariates, i.e., lifestyle factors, comorbidities (including Charlson comorbidity index score and individual comorbidities), medications, and health care utilization, were added in the logistic regression model to generate an exposure score for the probability of gout in a fully adjusted model. In these partially and fully adjusted models, data on individuals with gout were weighted for the probability of not having gout (i.e., calculated as 1 – the exposure score), and data on individuals without gout (the non-gout general population controls) were weighted for the probability of having gout (i.e., calculated using the exposure score).

We assessed the balance of the distribution of baseline characteristics before and after overlap weighting by calculating the absolute standardized mean differences (24). We calculated the weighted incidence rate for the primary and secondary outcome measures and estimated the weighted absolute rate difference (RD) between the gout group and the non-gout general population control group using overlap weighting of exposure scores to control for confounders. We performed a Cox proportional hazards model to obtain hazard ratios (HRs) and 95% confidence intervals (95% CIs) for the risk of SARS–CoV-2 infection, hospitalization, and death from COVID-19 using overlap weighting of exposure scores to control for confounders. Death from other causes was considered the competing risk in the regression model. We tested the proportional hazards assumption by using a Kolmogorov-type supremum test (25). If the proportional hazards assumption was violated, we used a weighted Cox regression to obtain a nonproportional HR (26).

To assess the robustness of the study findings, we performed 2 sensitivity analyses. First, we restricted gout cases to individuals who had gout Read codes and received medication for gout treatment (i.e., colchicine or urate-lowering drugs). This method for identifying a diagnosis of gout has shown a validity of 90% in the UK General Practice Research Database (27), in which 60% of individuals overlap with THIN. Second, to determine if the severity of gout would affect the risk of SARS–CoV-2 infection, we performed a subgroup analysis according to whether individuals with gout had gout flares during the past year before the index date. A gout flare was defined as follows: 1) having specific Read codes of gout flare, 2) having Read codes of gout and a recorded prescription for colchicine treatment, or 3) having Read codes of gout and having a recorded prescription of at least 1 of the following treatments within 1 week of the gout Read code: intraarticular glucocorticoids, nonsteroidal antiinflammatory drugs, or glucocorticoid or adrenocorticotropic hormone (28,29).

We performed the same analyses for the unvaccinated cohort to assess the risk of SARS–CoV-2 infection, hospitalization within 30 days of infection, and death within 30 days of infection between the gout group and the non-gout general population control group. Sex-specific analyses were conducted to assess for potential differences between men and women in the risk of each of these outcomes.

All *P* values were 2-sided, and *P* values less than 0.05 were considered statistically significant in all group comparisons. All statistical analyses were performed with SAS software version 9.4.

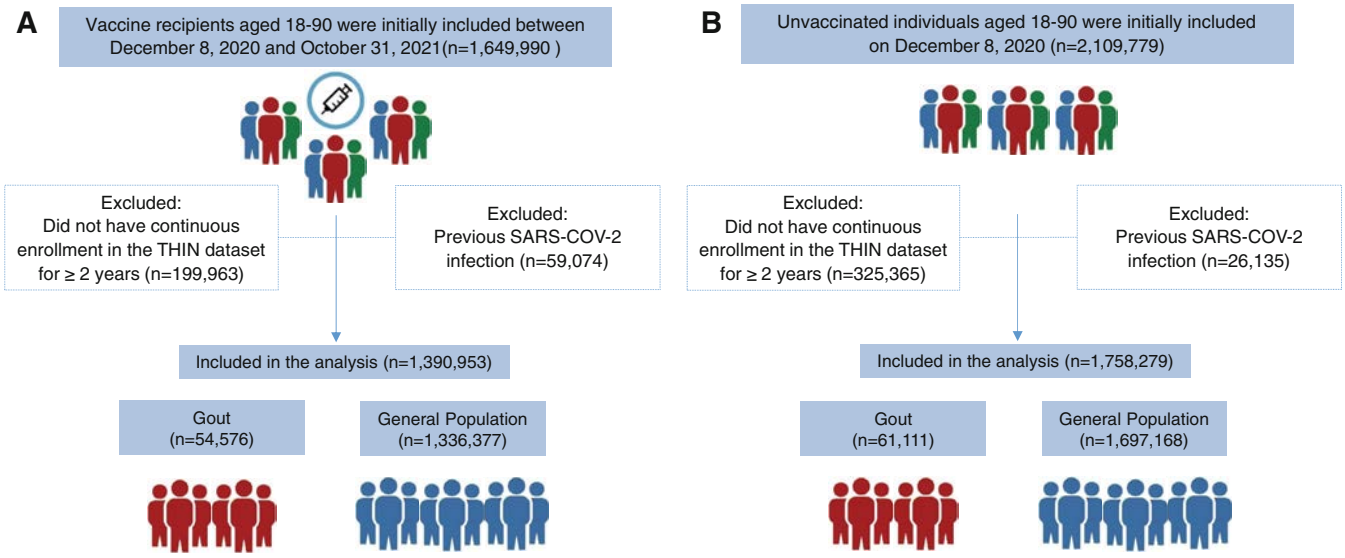

Figure 1. Flow diagram showing the eligibility criteria applied to recipients of the COVID-19 vaccine (**A**) and unvaccinated individuals (**B**) among patients with gout compared to individuals without gout from the general UK population and the final populations included in the analyses. THIN = The Health Improvement Network.

RESULTS

A flow diagram depicting the selection process of individuals included in the analyses is shown in Figure 1. The vaccinated cohort included 54,576 individuals with gout and 1,336,377 individuals without gout from the general population. The unvaccinated cohort included 61,111 individuals with gout and 1,697,168 individuals without gout from the general population. Before exposure score overlap weighting, individuals with gout tended to be older, were more likely to be male, had more comorbidities, more frequently took medications, and visited their GPs more often than the general population. However, after exposure score overlap weighting, the baseline characteristics were well-balanced between the gout group and the non-gout general population control group (all standardized differences <0.1) (Table 1).

Vaccinated cohort. In the vaccinated cohort, 1,955 breakthrough infection cases (partially weighted incidence rate 4.68 cases per 1,000 person-months) occurred among individuals with gout during the study period, and 52,468 cases (partially weighted incidence rate 3.76 per 1,000 person-months) occurred among the non-gout general population. The risk of breakthrough infection among individuals with gout was significantly higher compared with individuals without gout in the general population. After adjusting for partial exposure scores, the RD was 0.91 cases per 1,000 person-months (95% CI 0.62–1.20 cases per 1,000 person-months), and the HR was 1.24 (95% CI 1.19–1.30). The corresponding RD after adjusting for full exposure scores was 0.71 cases per 1,000 person-months (95% CI 0.41–1.09 cases per 1,000 person-months), and the HR was 1.18 (95% CI 1.12–1.24) (Table 2 and Figure 2).

A total of 184 hospitalizations occurred among individuals with gout (partially weighted incidence rate 0.42 hospitalizations per 1,000 person-months) and 1,956 hospitalizations in the non-gout general population (partially weighted incidence rate 0.28 hospitalizations per 1,000 person-months). Gout was associated with an increased risk of hospitalization after adjusting for partial exposure scores (HR 1.54 [95% CI 1.31–1.81]) and adjusting for full exposure scores (HR 1.30 [95% CI 1.10–1.53]). A total of 28 individuals in the gout group died (partially weighted incidence rate 0.06 deaths per 1,000 person-months), and 141 individuals in the non-gout general population died (partially weighted incidence rate 0.04 deaths per 1,000 person-months), resulting in a partial exposure score–adjusted HR of 1.74 (95% CI 1.14–2.67) and full exposure score–adjusted HR of 1.36 (95% CI 0.87–2.13) (Table 2 and Figure 2). When we performed a sensitivity analysis by restricting individuals in the gout group to those who had gout Read codes and had received treatment for gout as well as a subgroup analysis according to whether individuals in the gout group had gout flares during the past year before the index date, the results did not change significantly (see Supplementary Tables 2–4, available on the *Arthritis & Rheumatology* website at https://onlinelibrary.wiley.com/doi/art.42339).

Unvaccinated cohort. In the unvaccinated cohort, the risk of SARS–CoV-2 infection was higher among individuals with gout than among non-gout individuals in the general population. As shown in Table 3 and Figure 2, 1,532 cases of SARS–CoV-2 infection occurred in the gout group (partially weighted incidence rate 8.69 cases per 1,000 person-months) and 47,222 cases in the non-gout general population (partially weighted incidence rate 6.89 cases per 1,000 person-months), resulting in a RD of 1.80 cases per 1,000 person-months (95% CI 1.19–2.41 cases per

Table 2. Association between gout and the risk of breakthrough SARS–CoV-2 infection, 30-day hospitalization, and 30-day death in the vaccinated cohort*

	Gout (n = 54,576)	Non-gout (n = 1,336,377)
Breakthrough SARS–CoV-2 infection		
No. of infections	1,955	52,468
Mean follow-up, months	7.87	6.98
Weighted IR, per 1,000 person-months†	4.68	3.76
Weighted RD, per 1,000 person-months (95% CI)†	0.91 (0.62, 1.20)	0.00 (referent)
Weighted HR (95% CI)†	1.24 (1.19, 1.30)	1.00 (referent)
Weighted RD, per 1,000 person-months (95% CI)‡	0.71 (0.41, 1.09)	0.00 (referent)
Weighted HR (95% CI)‡	1.18 (1.12, 1.24)	1.00 (referent)
30-day hospitalization		
No. of hospitalizations	184	1,956
Mean follow-up, months	7.85	6.98
Weighted IR, per 1,000 person-months†	0.42	0.28
Weighted RD, per 1,000 person-months (95% CI)†	0.15 (0.07, 0.24)	0.00 (referent)
Weighted HR (95% CI)†	1.54 (1.31, 1.81)	1.00 (referent)
Weighted RD, per 1,000 person-months (95% CI)‡	0.10 (0.01, 0.18)	0.00 (referent)
Weighted HR (95% CI)‡	1.30 (1.10, 1.53)	1.00 (referent)
30-day death		
No. of deaths	28	141
Mean follow-up, months	7.86	6.99
Weighted IR, per 1,000 person-months†	0.06	0.04
Weighted RD, per 1,000 person-months (95% CI)†	0.03 (−0.01, 0.06)	0.00 (referent)
Weighted HR (95% CI)†	1.74 (1.14, 2.67)	1.00 (referent)
Weighted RD, per 1,000 person-months (95% CI)‡	0.02 (−0.02, 0.05)	0.00 (referent)
Weighted HR (95% CI)‡	1.36 (0.87, 2.13)	1.00 (referent)

* IR = incidence rate; RD = rate difference; 95% CI = 95% confidence interval; HR = hazard ratio.
† Results obtained after partially adjusted exposure scores.
‡ Results obtained after fully adjusted exposure scores.

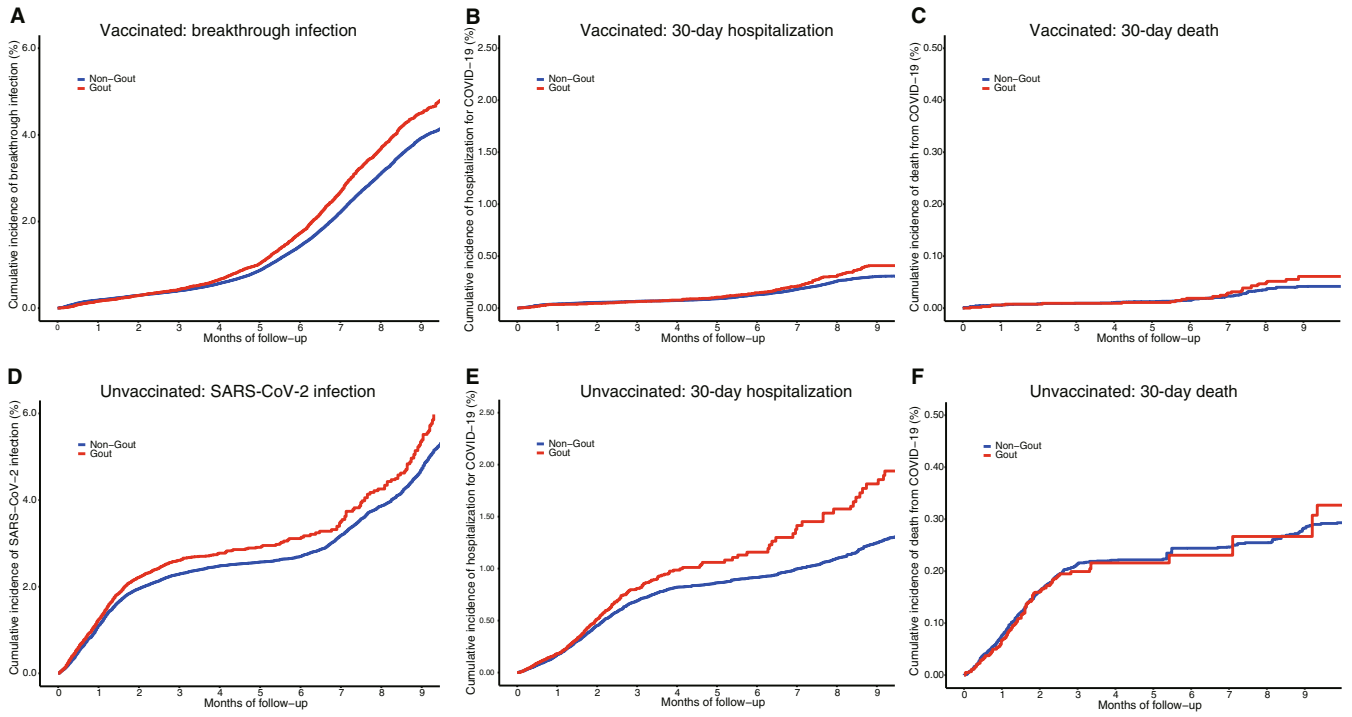

Figure 2. Cumulative incidence of SARS–CoV-2 infection, 30-day hospitalization, and 30-day death in gout patients compared to individuals without gout in the vaccinated (**A–C**) and unvaccinated (**D–F**) cohorts. Color figure can be viewed in the online issue, which is available at http://onlinelibrary.wiley.com/doi/10.1002/art.42339/abstract.

Table 3. Association between gout and the risk of SARS–CoV-2 infection, 30-day hospitalization, and 30-day death in the unvaccinated cohort*

	Gout (n = 61,111)	Non-gout (n = 1,697,168)
SARS–CoV-2 infection		
No. of infections	1,532	47,222
Mean follow-up, months	2.86	4.20
Weighted IR, per 1,000 person-months†	8.69	6.89
Weighted RD, per 1,000 person-months (95% CI)†	1.80 (1.19, 2.41)	0.00 (referent)
Weighted HR (95% CI)†	1.23 (1.16, 1.30)	1.00 (referent)
Weighted RD, per 1,000 person-months (95% CI)‡	1.15 (0.52, 1.78)	0.00 (referent)
Weighted HR (95% CI)‡	1.14 (1.08, 1.20)	1.00 (referent)
30-day hospitalization		
No. of hospitalizations	472	5,536
Mean follow-up, months	2.90	4.27
Weighted IR, per 1,000 person-months	2.57	1.71
Weighted RD, per 1,000 person-months (95% CI)	0.86 (0.54, 1.17)	0.00 (referent)
Weighted HR (95% CI)	1.46 (1.32, 1.62)	1.00 (referent)
Weighted RD, per 1,000 person-months (95% CI)‡	0.47 (0.14, 0.80)	0.00 (referent)
Weighted HR (95% CI)‡	1.21 (1.09, 1.34)	1.00 (referent)
30-day death		
No. of deaths	128	842
Mean follow-up, months	2.91	4.28
Weighted IR, per 1,000 person-months†	0.65	0.53
Weighted RD, per 1,000 person-months (95% CI)†	0.12 (–0.04, 0.28)	0.00 (referent)
Weighted HR (95% CI)†	1.18 (0.97, 1.43)	1.00 (referent)
Weighted RD, per 1,000 person-months (95% CI)‡	0.00 (–0.17, 0.17)	0.00 (referent)
Weighted HR (95% CI)‡	0.94 (0.67, 1.34)	1.00 (referent)

* IR = incidence rate; RD = rate difference; 95% CI = confidence interval; HR = hazard ratio.
† Results obtained after partially adjusted exposure scores.
‡ Results obtained after fully adjusted exposure scores.

1,000 person-months) and a HR of 1.23 (95% CI 1.16–1.30) after adjusting for partial exposure scores. The corresponding RD was 1.15 cases per 1,000 person-months (95% CI 0.52–1.78 cases per 1,000 person-months), and the HR was 1.14 (95% CI 1.08–1.20), after adjusting for full exposure scores.

During the follow-up period, 472 hospitalizations occurred in the gout group (partially weighted incidence rate 2.57 hospitalizations per 1,000 person-months) and 5,536 hospitalizations in the non-gout general population (partially weighted incidence rate 1.71 hospitalizations per 1,000 person-months). Compared with the non-gout general population, the HR of hospitalization for individuals with gout was 1.46 (95% CI 1.32–1.62) after adjusting for partial exposure scores and 1.21 (95% CI 1.09–1.34) after adjusting for full exposure scores. No statistically significant difference in death was observed between the gout group and non-gout general population group (Table 3 and Figure 2). Results from the sensitivity analysis and subgroup analysis did not change significantly (see Supplementary Tables 5–7, available on the *Arthritis & Rheumatology* website at https://onlinelibrary.wiley.com/doi/art.42339).

Sex-specific analyses. Among the vaccinated cohort, men with gout had an increased risk of breakthrough SARS–CoV-2 infection compared with men in the non-gout general population (partial exposure score–adjusted HR 1.30 [95% CI 1.23–1.37], full exposure score–adjusted HR 1.22 [95% CI 1.16–1.29]). However, no apparent association was observed in women. The risk of hospitalization was higher in men with gout (partial exposure score–adjusted HR 1.43 [95% CI 1.19–1.73], full exposure score–adjusted HR 1.22 [95% CI 1.00–1.48]) and women with gout (partial exposure score–adjusted HR 1.91 [95% CI 1.42–2.57], full exposure score–adjusted HR 1.55 [95% CI 1.15–2.10]) compared with the non-gout general population. Women with gout also had a higher risk of death than women without gout in the general population (partial exposure score–adjusted HR 3.01 [95% CI 1.48–6.13], full exposure score–adjusted HR 2.46 [95% CI 1.12–5.41]). However, no such association was observed in men (Figure 3). Similar sex-specific associations between gout and risks of SARS–CoV-2 infection, hospitalization, and death were also observed in the unvaccinated cohort (Figure 3).

DISCUSSION

In this large population-based study, we found that the risks of SARS–CoV-2 infection, 30-day hospitalization, and 30-day death were higher among individuals with gout than individuals without gout in the general population, irrespective of COVID-19 vaccination status. These results were consistent with the sensitivity analyses. In addition, women with gout might be more susceptible to severe outcomes of COVID-19 (i.e., hospitalization and death) than men with gout.

Few studies have described the risk of SARS–CoV-2 infection among individuals with gout (30,31). Of 100 studies included

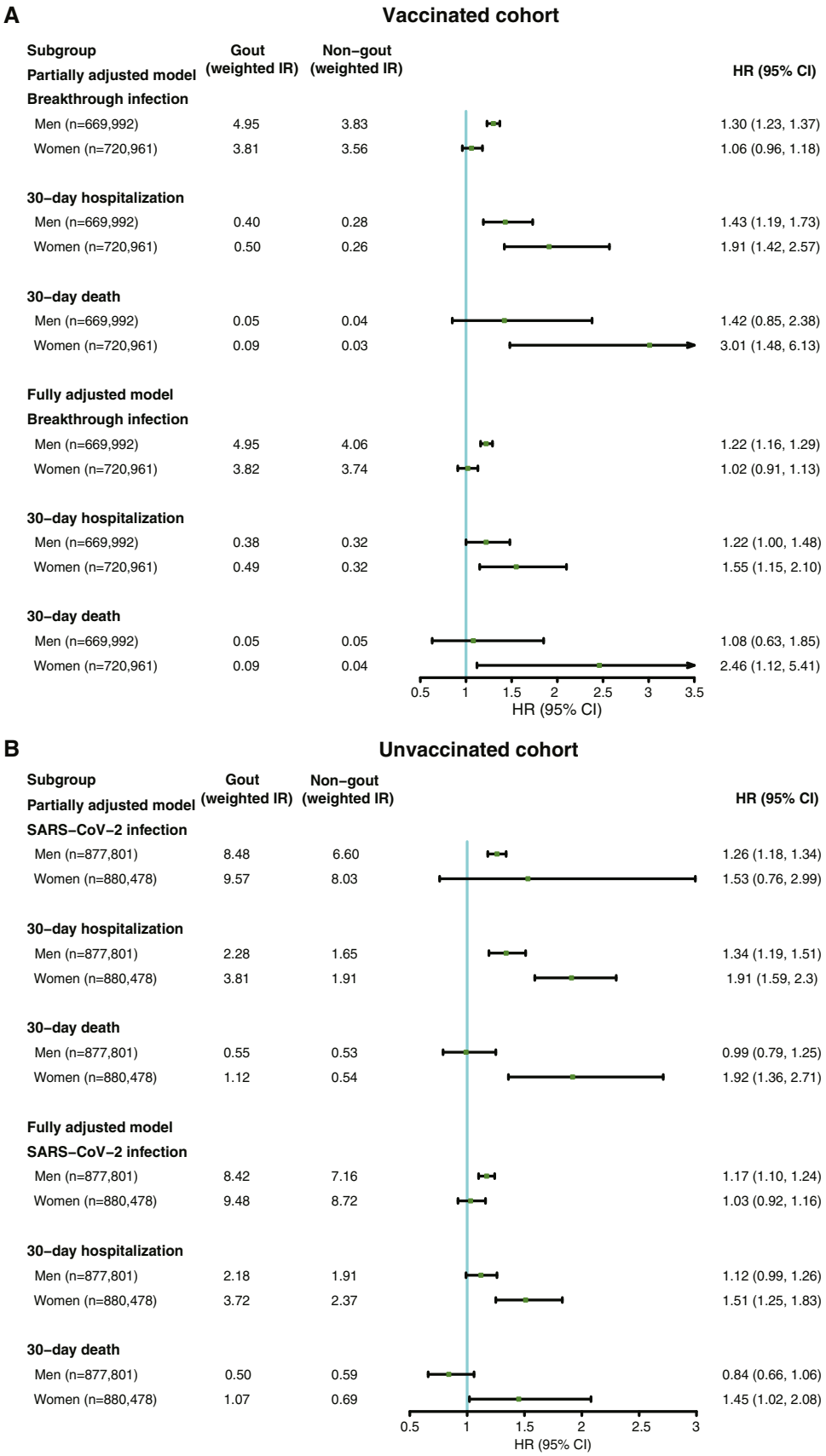

Figure 3. Subgroup analysis of the incidence of SARS–CoV-2 infection, 30-day hospitalization, and 30-day death in gout patients compared to individuals without gout according to sex in the vaccinated (**A**) and unvaccinated (**B**) cohorts. IR = incidence rate, per 1,000 person-months; HR = hazard ratio; 95% CI = 95% confidence interval. Color figure can be viewed in the online issue, which is available at http://onlinelibrary.wiley.com/doi/10.1002/art.42339/abstract.

in a meta-analysis of the risk of SARS–CoV-2 infection among individuals with rheumatic diseases, none of the studies focused on gout (32). Furthermore, no clinical guidelines developed by professional organizations on the management of rheumatic diseases during the COVID-19 pandemic have specifically discussed gout (33).

Recently, one study using data from the UK Biobank showed no significant difference in the risk of SARS–CoV-2 breakthrough infection between individuals with gout and the general population after COVID-19 vaccination (9). The study was conducted shortly after the availability of COVID-19 vaccines; thus, the number of cases of breakthrough infection was relatively small. In addition, the association of gout with severe COVID-19 outcomes was not evaluated among vaccinated individuals.

In this large-scale study, we were able to quantify the respective risk of SARS–CoV-2 breakthrough infection and severe outcomes (i.e., hospitalization and death) among vaccinated individuals. Although vaccination greatly reduced the risk of SARS–CoV-2 infection and severe outcomes among all individuals with or without gout, individuals with gout were still more susceptible to breakthrough infection and severe outcomes than individuals without gout in the general population.

The biologic mechanisms linking gout to the risk of SARS–CoV-2 infection remain unclear and deserve further investigation. A recent study demonstrated that hyperuricemia suppressed neutrophil adhesion and extravasation in mice with coronavirus-related sterile inflammation (34), suggesting that innate immunity may be impaired in gout, leading to increased susceptibility to infections.

Interestingly, the sex-specific analysis in our study showed that women with gout had a higher risk of severe COVID-19–related hospitalization and death than men with gout. In general, women with gout are older and tend to have more comorbidities that are also more severe, which may contribute to more severe COVID-19–related outcomes. Nevertheless, our findings will need confirmation in future studies.

Our study has several strengths. This study was based on a large, electronic medical record database representative of the general population, providing a high level of generalizability. In addition, we controlled for major potential confounders by using the overlap weights of exposure scores, suggesting that the current findings are robust.

Several limitations of our study deserve comment. First, it is possible that individuals with gout may have sought medical care more often and were more likely to be tested for SARS–CoV-2 infection than the non-gout general population controls during the COVID-19 pandemic period. Consequently, their risk of SARS–CoV-2 infection may be overestimated. However, the number of general practice visits and previous COVID-19 tests were well-balanced between the gout cohort and non-gout general population controls, suggesting that such bias, if it exists, is unlikely to fully explain the observed findings.

Second, since we do not have detailed information on the temporal relationship between gout and some covariates, we used 2 exposure scores to control for potential confounding bias. Although the magnitude of associations generated from controlling for the partially adjusted exposure score (which may lead to the residual confounding) (35) was larger than that generated from controlling for the fully adjusted exposure score (which may lead to overadjustment), the direction of the associations from these 2 analyses was consistent, supporting the robustness of the findings.

Third, although patients' medical information from hospital specialists is usually reported back to their GP, and GPs hold information on significant health-related events (including the diagnosis of COVID-19), we cannot access data that were held in the hospital and not reported back to GPs (e.g., tests performed at the hospital that were not reported back to GPs). As a result, misclassification of COVID-19 diagnosis could occur and bias the study findings. Nevertheless, such bias is likely to be small; if such bias occurred, it is likely to be nondifferential and would bias the observed associations toward the null.

In conclusion, our study findings suggest that individuals with gout, especially women, have a higher risk of severe outcomes of SARS–CoV-2 infection than the non-gout general population, even after COVID-19 vaccination. These findings suggest that additional measures should be considered to mitigate the risk of SARS–CoV-2 infection and potential severe outcomes for individuals with gout, especially women and even after vaccination.

AUTHOR CONTRIBUTIONS

All authors were involved in drafting the article or revising it critically for important intellectual content, and all authors approved the final version to be published. Dr. Zhang had full access to all of the data in the study and takes responsibility for the integrity of the data and the accuracy of the data analysis.

Study conception and design. Xie, Wei, Lei, Zhang.

Acquisition of data. Xie, Lu, Wei, Lei, Zhang.

Analysis and interpretation of data. Xie, Choi, Dalbeth, Wallace, Sparks, Zeng, Li, Wei, Lei, Zhang.

REFERENCES

1. Johns Hopkins University Coronavirus Resource Center. COVID-19 Dashboard. 2022. URL: https://coronavirus.jhu.edu/map.html.
2. Hodgson SH, Mansatta K, Mallett G, et al. What defines an efficacious COVID-19 vaccine? A review of the challenges assessing the clinical efficacy of vaccines against SARS-CoV-2. Lancet Infect Dis 2021;21:e26–35.
3. Chen-Xu M, Yokose C, Rai SK, et al. Contemporary prevalence of gout and hyperuricemia in the United States and decadal trends: the National Health and Nutrition Examination Survey, 2007–2016. Arthritis Rheumatol 2019;71:991–9.
4. Choi HK, McCormick N, Yokose C. Excess comorbidities in gout: the causal paradigm and pleiotropic approaches to care [review]. Nat Rev Rheumatol 2022;18:97–111.
5. de Lusignan S, Dorward J, Correa A, et al. Risk factors for SARS-CoV-2 among patients in the Oxford Royal College of General

Practitioners Research and Surveillance Centre primary care network: a cross-sectional study. Lancet Infect Dis 2020;20:1034–42.
6. Strangfeld A, Schäfer M, Gianfrancesco MA, et al. Factors associated with COVID-19-related death in people with rheumatic diseases: results from the COVID-19 Global Rheumatology Alliance physician-reported registry. Ann Rheum Dis 2021;80:930–42.
7. Crisan TO, Cleophas MCP, Oosting M, et al. Soluble uric acid primes TLR-induced proinflammatory cytokine production by human primary cells via inhibition of IL-1Ra. Ann Rheum Dis 2016; 75:755–62.
8. Topless RK, Phipps-Green A, Leask M, et al. Gout, rheumatoid arthritis, and the risk of death related to coronavirus disease 2019: an analysis of the UK Biobank. ACR Open Rheumatol 2021;3:333–40.
9. Topless RK, Gaffo A, Stamp LK, et al. Gout and the risk of COVID-19 diagnosis and death in the UK Biobank: a population-based study. Lancet Rheumatol 2022;4:e274–81.
10. Andrews N, Tessier E, Stowe J, et al. Duration of protection against mild and severe disease by Covid-19 vaccines. N Engl J Med 2022; 386:340–50.
11. Zeng C, Dubreuil M, LaRochelle MR, et al. Association of tramadol with all-cause mortality among patients with osteoarthritis. JAMA 2019;321:969–82.
12. Blak BT, Thompson M, Dattani H, et al. Generalisability of The Health Improvement Network (THIN) database: demographics, chronic disease prevalence and mortality rates. Inform Prim Care 2011;19: 251–5.
13. Sumilo D, Nirantharakumar K, Willis BH, et al. Long term impact of prophylactic antibiotic use before incision versus after cord clamping on children born by caesarean section: longitudinal study of UK electronic health records. BMJ 2022;377:e069704.
14. Chisholm J. The Read clinical classification [editorial]. BMJ 1990;300: 1092.
15. First Databank. FDB Multilex. 2022. URL: www.fdbhealth.co.uk/solutions/multilex-clinical-decision-support.
16. Lewis JD, Schinnar R, Bilker WB, et al. Validation studies of the health improvement network (THIN) database for pharmacoepidemiology research. Pharmacoepidemiol Drug Saf 2007;16:393–401.
17. Vargas-Santos AB, Peloquin CE, Zhang Y, et. Association of chronic kidney disease with allopurinol use in gout treatment. JAMA Intern Med 2018;178:1526–33.
18. Wei J, Choi HK, Neogi T, et al. Allopurinol initiation and all-cause mortality among patients with gout and concurrent chronic kidney disease: a population-based cohort study. Ann Intern Med 2022;175: 461–70.
19. Chandan JS, Zemedikun DT, Thayakaran R, et al. Nonsteroidal antiinflammatory drugs and susceptibility to COVID-19. Arthritis Rheumatol 2021;73:731–9.
20. Wang Y, D'Silva KM, Jorge AM, et al. Increased risk of COVID-19 in patients with rheumatoid arthritis: a general population-based cohort study. Arthritis Care Res (Hoboken) 2022;74:741–7.
21. Meropol SB, Metlay JP. Accuracy of pneumonia hospital admissions in a primary care electronic medical record database. Pharmacoepidemiol Drug Saf 2012;21:659–65.
22. Tremble K, Fox L, Moss C, et al. The impact of hospital attendance on COVID-19 infection in cancer patients: an assessment of data from Guy's Cancer. Future Oncol 2022;18:1211–8.
23. Li F, Thomas LE, Li F. Addressing extreme propensity scores via the overlap weights [published correction appears in Am J Epidemiol 2021;190:189–190]. Am J Epidemiol 2019;188:250–7.
24. Austin PC, Stuart EA. Moving towards best practice when using inverse probability of treatment weighting (IPTW) using the propensity score to estimate causal treatment effects in observational studies. Stat Med 2015;34:3661–79.
25. Lin DY, Wei LJ, Ying Z. Checking the Cox model with cumulative sums of Martingale-based residuals. Biometrika 1993;80:557–72.
26. Dunkler D, Ploner M, Schemper M, et al. Weighted Cox regression using the R package coxphw. J Stat Softw 2018;84:1–26.
27. Meier CR, Jick H. Omeprazole, other antiulcer drugs and newly diagnosed gout. Br J Clin Pharmacol 1997;44:175–8.
28. Rothenbacher D, Primatesta P, Ferreira A, et al. Frequency and risk factors of gout flares in a large population-based cohort of incident gout. Rheumatology (Oxford) 2011;50:973–81.
29. Li H, Dalbeth N, Wallace ZS, et al. Risk of gout flares after COVID-19 vaccination: a case-crossover study. Semin Arthritis Rheum 2022; 56:152059.
30. Tai V, Robinson PC, Dalbeth N. Gout and the COVID-19 pandemic [review]. Curr Opin Rheumatol 2022;34:111–7.
31. Dalbeth N, Robinson PC. Patients with gout: an under-recognised group at high risk of COVID-19. Lancet Rheumatol 2021;3:e317–8.
32. Conway R, Grimshaw AA, Konig MF, et al. SARS–CoV-2 infection and COVID-19 outcomes in rheumatic disease: a systematic literature review and meta-analysis [review]. Arthritis Rheumatol 2022;74: 766–75.
33. Mikuls TR, Johnson SR, Fraenkel L, et al. American College of Rheumatology guidance for the management of rheumatic disease in adult patients during the COVID-19 pandemic: version 3. Arthritis Rheumatol 2021;73:e1–12.
34. Ma Q, Immler R, Pruenster M, et al. Soluble uric acid inhibits β2 integrin-mediated neutrophil recruitment in innate immunity. Blood 2022;139:3402–17.
35. Greenland S. Confounder summary score. Wiley StatsRef: Statistics Reference Online. 2015:1–3.

Arthritis & Rheumatology
Vol. 75, No. 1, January 2023, pp 133–140
DOI 10.1002/art.42301

American College of Rheumatology
Empowering Rheumatology Professionals

Associations Between Low Serum Urate, Body Composition, and Mortality

Joshua F. Baker,[1] David R. Weber,[2] Tuhina Neogi,[3] Michael D. George,[4] Jin Long,[5] Lindsay N. Helget,[6] Bryant R. England,[6] and Ted R. Mikuls[6]

Objective. Controversy remains as to whether low serum urate or uric acid (UA) levels contribute to adverse outcomes. We evaluated the relation between low serum UA levels and sarcopenia and assessed whether sarcopenia confounds associations between these low levels and mortality.

Methods. We utilized data from the National Health and Nutrition Examination Survey (1999–2006). Participants with available whole-body dual x-ray absorptiometry body composition measurements and serum UA concentrations were included. Body composition assessments included body mass index (BMI), waist circumference, maximum lifetime BMI, and age-, sex-, and race-specific appendicular lean mass index (ALMI) and fat mass index (FMI) Z scores. We also calculated Z scores for ALMI relative to FMI ($ALMI_{FMI}$). We evaluated associations between serum UA levels and body composition using logistic regression and assessed associations between serum UA levels and mortality before and after adjusting for differences in body composition using Cox proportional hazards regression.

Results. Among the 13,979 participants, low serum UA concentrations (<2.5 mg/dl in women, <3.5 mg/dl in men) were associated with low lean mass (ALMI and $ALMI_{FMI}$ Z scores), underweight BMI (<18.5 kg/m^2), and higher rates of weight loss. The proportion of patients with low ALMI Z scores was 29% in the low serum UA group and 16% in the normal serum UA group (P = 0.001). Low serum UA levels were associated with increased mortality before we adjusted for body composition (hazard ratio 1.61 [95% confidence interval 1.14–2.28]; P = 0.008) but was attenuated and not significant after adjustment for body composition and weight loss (hazard ratio 1.30 [95% confidence interval 0.92–1.85], P = 0.13).

Conclusion. Sarcopenia and weight loss are more common among patients with low serum UA concentrations. Differences in body composition may help to explain associations between low levels of serum UA and higher mortality.

INTRODUCTION

A number of observational studies have linked low serum urate or uric acid (UA) concentrations to adverse outcomes such as dementia, Parkinson's disease, and early mortality (1–5). These studies have raised questions about whether excessive lowering of urate levels might have adverse consequences; therefore, some society guidelines on gout have promulgated recommendations to be cautious with urate-lowering therapy, which may delay or negate optimal gout control (6). However, it is

The contents of this work do not represent the views of the Department of the Veterans Affairs (VA) or the US Government.

Dr. Baker's work was supported by a VA Clinical Science Research & Development merit award (I01-CX001703) and Rehabilitation Research & Development merit award (I01 RX003644). Dr. Neogi's and Dr. George's work was supported by the NIH (National Institute of Arthritis and Musculoskeletal and Skin Diseases grants K24-AR-070892 and P30-AR-072571 and grant K23-AR-073931, respectively). Dr. England's work was supported by a VA Career Development Award (IK2 CX002203). Dr. Mikuls' work was supported by a VA Merit Award (I01 BX0046000), the US Department of Defense (grant PR200793), and the NIH (National Institute on Alcohol Abuse and Alcoholism grant R25-AA-020818, National Institute of General Medical Sciences grant U54-GM-115458, and National Institute of Arthritis and Musculoskeletal and Skin Diseases grant P50-AR-60772).

[1]Joshua F. Baker, MD, MSCE: Corporal Michael J. Crescenz Veterans Affairs Medical Center and School of Medicine and Center for Clinical Epidemiology and Biostatistics, University of Pennsylvania, Philadelphia, Pennsylvania; [2]David R. Weber, MD, MSCE: School of Medicine, University of Pennsylvania and Children's Hospital of Philadelphia, Philadelphia, Pennsylvania; [3]Tuhina Neogi, MD, PhD: Boston University School of Medicine, Boston, Massachusetts; [4]Michael D. George, MD, MSCE: School of Medicine and Center for Clinical Epidemiology and Biostatistics, University of Pennsylvania, Philadelphia, Pennsylvania; [5]Jin Long, PhD: Department of Pediatrics and Medicine, Stanford University, Stanford, California; [6]Lindsay N. Helget, MD, Bryant R. England, MD, PhD, Ted R. Mikuls, MD, MPSH: Medicine Service, VA Nebraska-Western Iowa Health Care System and Department of Internal Medicine, Division of Rheumatology & Immunology, University of Nebraska Medical Center, Omaha, Nebraska.

Author disclosures are available at https://onlinelibrary.wiley.com/action/downloadSupplement?doi=10.1002%2Fart.42301&file=art42301-sup-0001-Disclosureform.pdf.

Address correspondence via email to Joshua F. Baker, MD, MSCE, at bakerjo@uphs.upenn.edu.

Submitted for publication April 24, 2022; accepted in revised form July 7, 2022.

important to note that serum UA concentrations are strongly and positively associated with obesity and nutritional status (7,8). In particular, greater visceral fat and the presence of metabolic syndrome are associated with elevated serum UA concentrations. Given the relationship between urate concentration and body composition, questions have been raised on whether low serum UA concentrations might occur in the setting of pathologic weight loss and sarcopenia, which themselves may be the underlying cause of adverse outcomes and mortality (9–12). Thus, the associations between urate and adverse outcomes may be confounded by body composition, a construct not typically accounted for in previous investigations on the relationship between serum UA levels and long-term outcomes (1–5).

Studies that have evaluated associations between muscle loss and serum UA levels have often been limited in their ability to account for the confounding effects of adiposity, since muscle mass and fat mass are tightly correlated with each other (i.e., individuals who are more obese are expected to have greater muscle mass) (13). Some studies have shown that higher serum UA levels are associated with better muscle function and greater muscle mass (14,15). However, others have presented conflicting observations. For example, Beavers et al used an unvalidated assessment of a skeletal muscle index to show that a high serum UA concentration was associated with low muscle mass (16). Thus, questions remain on whether low serum UA concentrations occur in parallel with the development of sarcopenia, and better methods are needed to uncouple assessments of muscle and fat. Clarification on whether low levels of serum UA are causally associated with poor outcomes or whether an apparent association exists primarily because of the confounding effects of sarcopenia can have important clinical implications regarding whether more aggressive approaches to urate lowering for gout are warranted.

We recently developed methods within the National Health and Nutrition Examination Survey (NHANES) to quantify muscle mass relative to fat mass and validated definitions of relative sarcopenia based on these measures (17–19). Thus, we are able to evaluate associations between serum UA levels and relative sarcopenia using accurate whole-body dual-energy x-ray absorptiometry (DXA) measurements that are independent of fat mass. We hypothesized that low serum UA status is associated with measures of sarcopenia, historical weight loss, and underweight status. We also hypothesized that accounting for sarcopenia explains the association between low serum UA levels and mortality observed in prior studies, thus perhaps suggesting that the previously reported associations were unlikely to be causally related (1,2).

PATIENTS AND METHODS

Study setting. For this study, we obtained results from the 1999–2006 NHANES surveys on whole-body DXA of adults ≥20 years of age (20). NHANES is an annual survey conducted by the National Center for Health Statistics (NCHS) that uses a complex, multistage probability sampling method, including oversampling of people in the US who identify as non-Hispanic Black, Mexican American, and low-income White. The survey included a household interview, and data were generated from detailed examinations at mobile examination centers. The NHANES study is designed to select a population that is representative of the US to inform national policy.

The Research Subjects Review Board at the University of Pennsylvania waived institutional review board oversight for our analysis. We performed a complete case analysis of those in the DXA cohort, including all participants with a serum UA concentration available in the data set (94%).

Categorization of urate levels. Laboratory testing was performed for NHANES participants as previously described (20). We categorized serum UA concentrations based on previously defined normal ranges (2.5–6 mg/dl in women, 3.5–7 mg/dl in men), with low and high levels defined as those below and above the normal ranges (2). The use of allopurinol, probenecid, and diuretics (furosemide, bumetanide, hydrochlorothiazide, triamterene) was self-reported on questionnaires.

Body composition assessments. The whole-body DXA scans were conducted with a Hologic QDR 4500A fan beam densitometer in eligible participants across the US. The University of California, San Francisco, Radiology Department used Hologic Discovery Software, version 12.1, to review and analyze all DXA results. Exclusion criteria included pregnancy, weight >300 pounds (136 kg), height >77 inches (195 cm), recent nuclear medicine scan, or exposure to radioactive contrast. The NCHS used multiple imputation of missing DXA results to address the potential biases of nonrandom missing DXA data (20).

Age, which was reported as age at examination, was calculated in months. Participants self-reported US Census Bureau classifications of race and ethnicity. Height (cm) was measured by standard procedures and a fixed stadiometer. Weight was determined with a high-performance digital scale, and World Health Organization guidelines were used to categorize body mass index (BMI) as underweight (<18.5 kg/m^2). Abdominal (waist) circumference was assessed. We also determined the percent weight loss from the maximum self-reported historical BMI to the current measured BMI as previously described (21).

Fat mass index (FMI; kg/m^2) and appendicular lean mass index (ALMI; kg/m^2) were calculated from DXA-measured body composition data, with exclusion of bone mineral content. As previously described, NHANES DXA body composition data for fat mass and lean body mass were adjusted by the NCHS such that lean body mass was decreased by 5% and fat mass increased by an equivalent amount (in kg) to maintain total body mass (22). We generated ALMI and FMI Z scores using previously published

equations defined within NHANES (23). We also generated $ALMI_{FMI}$ Z scores as previously described (19). The $ALMI_{FMI}$ Z score is a measurement that incorporates the complex interactions among age, sex, and race/ethnicity and represents the number of SDs above or below the mean for a reference group of the same age, sex, race/ethnicity, and FMI Z score. Thus, this value represents the individual's muscle mass compared with what would be expected given the individual's fat mass.

We defined sarcopenia (ALMI) and relative sarcopenia ($ALMI_{FMI}$) (i.e., accounting for fat mass) based on prior work (18,19). Sarcopenia and relative sarcopenia were each defined as the respective ALMI and $ALMI_{FMI}$ Z scores of less than or equal to –1 (15.9th percentile for the NHANES population) as previously described. These definitions of sarcopenia have been shown to correlate with physical function and to predict incident disability.

Mortality. Mortality was determined from NHANES public-use–linked mortality files from the NCHS. The NCHS has linked NHANES to death certificate data from the National Death Index with follow-up through December 31, 2015. The National Death Index matches individuals on personal and demographic criteria and provides mortality status and months of follow-up.

Statistical analysis. We described participant characteristics across serum UA categories (low, normal, high) and tested for statistical significance using analysis of variance, chi-square tests, or nonparametric alternatives. We assessed the relationship between serum UA concentrations and categories and the body composition outcomes of interest using linear or logistic regression as appropriate, adjusting for potential confounders. Based on these models, we illustrated the predicted probabilities for each outcome by group based on these regression models. When serum UA was used as a continuous variable, a squared term was included in regression models to account for nonlinear associations.

We also evaluated the relationship between serum UA levels and mortality before and after the potential confounding effects of body composition and weight loss were considered. Previous evidence supports the existence of a U-shaped curve defining associations between serum UA concentrations and mortality with an inflection point at 5.7 mg/dl (1). We therefore used linear splines to evaluate the effect of serum UA levels as a continuous variable among values <5.7 mg/dl and among those ≥5.7 mg/dl. We used Cox proportional hazards models to evaluate the association between serum UA level (as both a categorical and continuous variable) and mortality. Initial models were adjusted for age, sex, race, BMI, waist circumference, estimated glomerular filtration rate (eGFR), presence of diabetes, smoking, and use of diuretics or urate-lowering therapies (allopurinol or probenecid). Models were then further adjusted for body composition assessments and for the percent weight loss from maximum weight. For this adjustment, both ALMI and FMI Z scores were included, as well as a squared term for ALMI to account for a strong nonlinear association with mortality. The proportional hazards assumption was tested by evaluating the appearance of Schoenfeld residuals.

We performed the analyses using imputed body composition data and combined sample weights to account for the complex sample design, as recommended by the NCHS (24). We performed a stratified analysis by biologic sex based on a prior study that demonstrated evidence of effect modification (25). We also tested for the significance of multiplicative interaction terms between sex and serum UA level.

RESULTS

Our analysis included 13,979 participants (50% women) with a mean ± SD age of 45.9 ± 29.6 years and a mean ± SD BMI of 28.3 ± 13.0. Of total participants, 208 (1.5%) were categorized as having low serum UA and 2,463 (18%) were categorized as having high serum UA. Low serum UA status was associated with lower weight, greater loss of weight from maximum BMI, lower ALMI and FMI, higher eGFR, Black race, and numerically but not statistically lower $ALMI_{FMI}$, older age, and higher rates of diabetes, smoking, and cancer (Table 1). Only 1 person in the low serum UA category was taking allopurinol.

Serum UA levels and body composition. The association between serum UA level and low lean body mass was nonlinear. The predicted linear associations between presence of sarcopenia (defined as having a low ALMI Z score) or relative sarcopenia (defined as having a low $ALMI_{FMI}$ Z score) and serum UA level in participants are shown in Figures 1A and 1B, respectively. When modeled as linear splines, higher serum UA concentration (per 1 mg/dl among participants with a serum UA <5.7 mg/dl) was associated with a lower probability of sarcopenia based on the ALMI definition, with an odds ratio (OR) (per 1 mg/dl) of 0.62 (95% confidence interval [95% CI] 0.58–0.67, $P < 0.001$) and a lower probability of relative sarcopenia based on the $ALMI_{FMI}$ definition, with an OR (per 1 mg/dl) of 0.84 (95% CI 0.78–0.91, $P < 0.001$) (Table 2). For participants with serum UA levels ≥5.7 mg/dl, the association between serum UA concentration and sarcopenia and relative sarcopenia was weaker.

The proportions of participants with sarcopenia and relative sarcopenia by serum UA category are shown in Table 3. Compared with participants with normal serum UA levels, the odds of sarcopenia (low ALMI Z score) was 2.6-fold higher in the low serum UA group (OR 2.62 [95% CI 1.96–3.50], $P < 0.001$). The odds of relative sarcopenia (low $ALMI_{FMI}$ Z score) was 32% higher for participants in the low serum UA group than for those in the normal serum UA group, although not statistically significant (OR 1.32 [95% CI 0.84–2.09], $P = 0.23$). Compared with those with normal values, participants in the high serum UA group had even lower risk of sarcopenia (OR 0.42 [95% CI 0.34–0.51], $P < 0.001$) and numerically, but not significantly, lower risk of relative sarcopenia (OR 0.89 [95% CI 0.76–1.04], $P = 0.13$).

Table 1. Characteristics of participants the National Health and Nutrition Examination Survey (1999–2006) stratified by serum UA level*

Characteristic	Serum UA level			P
	Low (n = 208)	Normal (n = 11,308)	High (n = 2,463)	
Age, mean ± SEM years	46.5 ± 0.93	45.1 ± 0.24	49.8 ± 0.46	<0.001
Female	110 (53)	5,880 (52)	585 (40)	<0.001
Black	31 (15)	2,244 (11)	320 (13)	<0.001
BMI, mean ± SEM	24.9 ± 0.42	27.6 ± 0.098	32.0 ± 0.22	<0.001
Maximum change in BMI, mean ± SEM	−16.1 ± 4.07	−7.6 ± 0.12	−6.9 ± 0.29	<0.001
Waist circumference, mean ± SEM cm	90.1 ± 14.2	95.9 ± 14.8	106.4 ± 15.0	<0.001
ALMI Z score, mean ± SEM	−0.53 ± 0.98	−0.080 ± 0.016	0.46 ± 0.036	<0.001
FMI Z score, mean ± SEM	−0.65 ± 0.079	−0.097 ± 0.017	0.55 ± 0.032	<0.001
$ALMI_{FMI}$ Z score, mean ± SEM	−0.12 ± 0.11	−0.011 ± 0.018	0.085 ± 0.036	<0.01
Allopurinol use	1 (0.4)	71 (0.6)	26 (1.0)	0.18
Probenecid use	2 (0.77)	7 (0.06)	4 (0.16)	0.02
Diuretic use	9 (4.3)	701 (6.2)	542 (22)	<0.001
Ever smoked	119 (57)	5,674 (50)	1,303 (53)	<0.001
Diabetes	15 (7.4)	645 (5.7)	246 (10.0)	<0.001
Cancer	20 (9.5)	811 (7.2)	238 (9.7)	<0.001
eGFR, mean ± SEM, ml/minute/1.73 m^2	100.0 ± 1.6	94.7 ± 0.35	84 ± 0.55	<0.001

* Serum urate or uric acid (UA) levels were categorized as normal at levels of 2.5–6 mg/dl for women and levels of 3.5–7 mg/dl for men, with levels below and above these categorized as low serum UA and high serum UA, respectively. Except where otherwise indicated, values are the number (%) of participants. BMI = body mass index; ALMI = appendicular lean mass index; FMI = fat mass index; $ALMI_{FMI}$ = ALMI relative to FMI; eGFR = estimated glomerular filtration rate.

In age-, sex-, and race-adjusted models, participants in the low serum UA group were also more likely to have experienced greater percent weight loss from maximum reported BMI and were more likely to have an underweight BMI. Those in the low serum UA group had ~4 times the odds of being underweight (OR 4.41 [95% CI 2.14–9.09], $P < 0.001$). Those in the high serum UA group had even lower rates of being underweight and even less weight loss. The predicted values from regression models adjusting for potential confounders are shown in Table 3.

Serum UA levels and mortality. A higher risk of death was observed for the low serum UA group in initial models that included demographics and standard body composition measures (e.g., BMI, waist circumference) (hazard ratio [HR] 1.61 [95% CI 1.14–2.28], $P = 0.008$) (Table 4 and Figure 2). However, this association with mortality was attenuated when we included DXA-derived body composition parameters and historical weight loss in the model (HR 1.30 [95% CI 0.92–1.85], $P = 0.13$). A high serum UA level was associated with higher mortality before and after adjustment. Results were highly similar in models that excluded participants who took allopurinol or probenecid (not shown).

For participants with serum UA values <5.7 mg/dl, there was a numerically lower risk of death for those with a higher serum UA concentration (per 1 mg/dl) (HR 0.91 [95% CI 0.84–0.99], $P = 0.03$) (Table 4). When we further adjusted the models for DXA-derived body composition (ALMI and FMI Z scores) and historical weight loss, the effect (per 1 mg/dl serum UA among those with levels <5.7 mg/dl) was attenuated (HR 0.98 [95% CI 0.90–1.08],

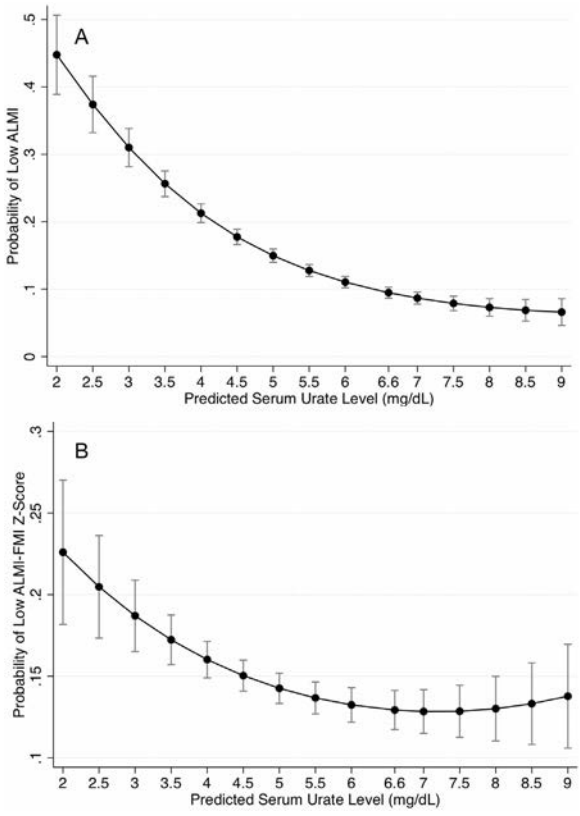

Figure 1. Probability of having sarcopenia (low appendicular lean mass index [ALMI] Z score) **(A)** and relative sarcopenia (low appendicular lean mass index adjusted for fat mass index [$ALMI_{FMI}$] Z score; adjusted for adiposity) **(B)** by serum urate concentration based on regression models. Bars show the mean ± SEM of the prediction.

Table 2. Association between serum UA level and sarcopenia outcome*

	Sarcopenia (ALMI) (Z score ≤ −1)		Relative sarcopenia ($ALMI_{FMI}$) (Z score ≤ −1)	
	OR (95% CI)	*P*	OR (95% CI)	*P*
Model 1				
Serum UA (per 1 mg/dl)	0.45 (0.36–0.57)	<0.001	0.69 (0.56–0.86)	0.001
Serum UA^2	1.04 (1.02–1.06)	<0.001	1.03 (1.01–1.04)	0.007
P for model fit†		0.27		0.68
Model 2				
Serum UA (per 1 mg/dl, <5.7 mg/dl)	0.62 (0.58–0.67)	<0.001	0.84 (0.78–0.91)	<0.001
Serum UA (per 1 mg/dl, ≥5.7 mg/dl)	0.85 (0.75–0.79)	0.02	1.04 (0.95–1.14)	0.40
P for model fit†		0.33		0.54

*For model 1, serum UA was modeled as a continuous measure with inclusion of squared term (serum UA^2). A significant serum UA^2 measure suggests that the effect of urate (per 1 mg/dl) becomes less negatively associated with sarcopenia as levels increase. For model 2, serum UA was modeled as linear splines with inflection at 5.7 mg/dl. An inverse association between serum UA levels and sarcopenia or relative sarcopenia is stronger at levels <5.7 mg/dl. Sarcopenia definitions based on Z scores were age-, sex-, and race-specific. OR = odds ratio; 95% CI = 95% confidence interval (see Table 1 for other definitions).
† According to Hosmer-Lemeshow goodness-of-fit test.

P = 0.71) (Table 4). For participants with levels ≥5.7 mg/dl, a higher serum UA concentration (per 1 mg/dl) was associated with a higher risk of death, which persisted after adjustment for DXA-derived body composition and historical weight loss (Table 4 and Supplementary Table 1, available on the *Arthritis & Rheumatology* website at https://onlinelibrary.wiley.com/doi/10.1002/art.42301).

Similar models that evaluated cause-specific mortality yielded a similar pattern, with attenuation of the risk of hypouricemia after adjustment for body composition (Supplementary Tables 2a and 2b, available on the *Arthritis & Rheumatology* website at https://onlinelibrary.wiley.com/doi/10.1002/art.42301). There was low statistical power for each of these individual outcomes, and the precision in the individual estimates was low. Higher serum UA (per 1 mg/dl) was associated with higher rates of cardiovascular-related death and lower rates of Alzheimer's disease–related death.

We found no significant statistical interactions between serum UA category and biologic sex. In stratified analyses, the association between serum UA level and mortality (per 1 mg/dl among those with levels <5.7 mg/dl) was attenuated but remained significant in men after adjustment for body composition (HR 0.85 [95% CI 0.77–0.94], *P* = 0.002) (Supplementary Tables 3a and 3b, available on the *Arthritis & Rheumatology* website at https://onlinelibrary.wiley.com/doi/10.1002/art.42301).

DISCUSSION

Our study demonstrated that the relationship between low circulating serum UA concentrations and mortality was attenuated and no longer significant after accounting for body composition, supporting the hypothesis that prior epidemiologic studies may have been affected by unmeasured confounding. In our study, low serum UA levels were strongly associated with sarcopenia, a history of weight loss, and underweight status, suggesting that serum UA may occur in parallel with pathologic weight loss and the development of sarcopenia. The association between serum UA and a measure of relative sarcopenia (relative to fat mass) was also significant in our analyses, suggesting that the relationship between serum UA and sarcopenia is partially independent of differences in adiposity.

Table 3. Association between presence of sarcopenia or relative sarcopenia, changes in body composition, and serum UA levels by category*

Serum UA category	Participants with sarcopenia (ALMI Z score), mean % (range)	Participants with relative sarcopenia ($ALMI_{FMI}$ Z score), mean % (range)	Change in BMI from historical maximum, mean % (range) (n = 13,628)	Participants characterized as underweight (BMI <18.5), mean % (range)
Low (n = 208)	29 (20–38)†	19 (12–25)	−16.6 (−24.0 to −9.2)‡	6.8 (2.8–10.8)§
Normal (n = 11,308)	16 (15–17)	15 (14–16)	−7.8 (−8.0 to −7.5)	1.8 (1.5–2.2)
High (n = 2,463)	8 (6–9)§	13 (11–15)	−6.8 (−7.4 to −6.1)†	0.4 (0.1–0.8)§

* Serum UA was categorized as normal at levels of 2.5–6 mg/dl for women and levels of 3.5–7 mg/dl for men, with levels below and above these categorized as low serum UA and high serum UA, respectively. Models that included percent change in weight and proportion of participants who were underweight were adjusted for age, sex, and race. Z scores were age-, sex-, and race-specific. See Table 1 for definitions.
† *P* < 0.01 compared with normal serum UA group.
‡ *P* < 0.05 compared with normal serum UA group.
§ *P* < 0.001 compared with normal serum UA group.

Table 4. Associations between risk of mortality and serum UA levels by category in models including adjustments for traditional measures of body composition*

	Model 1†		Model 2†	
	HR (95% CI)	*P*	HR (95% CI)	*P*
Serum UA category				
Low (n = 202)	1.61 (1.14–2.28)	0.008	1.30 (0.92–1.85)	0.13
Normal (n = 10,774)	1 (referent)		1 (referent)	
High (n = 2,335)	1.27 (1.12–1.43)	<0.001	1.29 (1.14–1.46)	<0.001
Continuous (linear splines)				
Serum UA (per 1 mg/dl, <5.7 mg/dl)	0.91 (0.84–0.99)	0.03	0.98 (0.90–1.08)	0.71
Serum UA (per 1 mg/dl, ≥5.7 mg/dl)	1.13 (1.06–1.20)	<0.001	1.11 (1.04–1.18)	0.001

* Serum UA was categorized as normal at levels of 2.5–6 mg/dl for women and levels of 3.5–7 mg/dl for men, with levels below and above these categorized as low serum UA and high serum UA, respectively. HR = hazard ratio; 95% CI = 95% confidence interval (see Table 1 for other abbreviations).
† Both models included 13,312 participants and 2,289 deaths over a total of 57,821 person-years. Model 1 was adjusted for age, sex, race, BMI, waist circumference, diabetes, smoking, eGFR, diuretic use, and urate-lowering therapy use. Model 2 was adjusted for age, sex, race, diuretic use, urate-lowering therapy use, diabetes, eGFR, smoking, body composition (ALMI Z score, FMI Z score, and their squared terms [$ALMI^2$, FMI^2]), and the percent change in weight from historical maximum.

This specific observation is important because it suggests that low serum UA concentrations are likely observed in association with pathologic weight loss, in which the loss of muscle mass is proportionally greater than the loss of fat mass, resulting in relative sarcopenia. The importance of these overall findings is that they provide a credible explanation for the numerous epidemiologic links observed in previous studies between low serum UA levels and adverse outcomes.

Several prior studies have evaluated associations between serum UA and muscle outcomes, although with significant limitations. Challenges include the confounding association between assessments of muscle mass and fat mass (i.e., people with greater fat mass are expected to have higher muscle mass) and the strong relationship observed between adiposity and serum UA. Our study is supported by previous work from Nahas et al, who found that serum UA levels were positively associated with muscle strength in the NHANES population (1999–2002) (15). However, our observations conflict with work from Beavers et al, who investigated associations between circulating serum UA and body composition assessed with bioelectrical impedance analysis. The group demonstrated an inverse relationship between serum UA and muscle mass, although residual confounding was likely since fat mass was not evaluated (16). We suggest that our study is a significant advance versus other studies because of our use of a construct of relative sarcopenia, a measure that is independent of age, sex, race, and adiposity (17).

Low serum UA levels have been proposed to lead to adverse health effects, as some studies associated low serum UA levels with a higher risk of early mortality (1,2,25). In our study, we found that the relationship between low serum UA and mortality did not

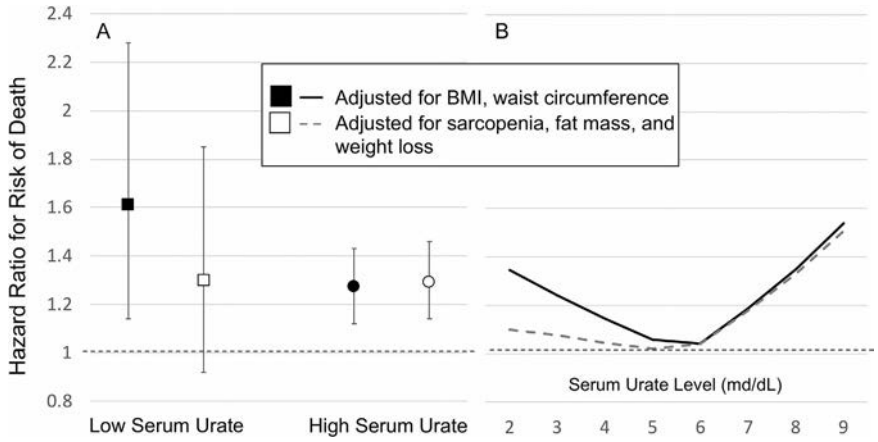

Figure 2. Hazard ratios with 95% confidence intervals for the risk of death among participants with low serum urate versus high serum urate levels (compared with normal serum urate [horizontal dashed line]) **(A)** and according to different serum urate levels **(B)** in models adjusted for body mass index (BMI) and waist circumference only (solid symbols/solid line) and in models adjusted for presence of sarcopenia, body composition, and weight loss (open symbols/dashed line).

persist after adjustment for body composition. Sarcopenia and frailty, a related construct, often occur in tandem with pathologic weight loss. Our results suggest that the previously shown epidemiologic associations between low serum UA and higher mortality might be the result of chronic illness leading to sarcopenia and pathologic weight loss occurring in tandem with reductions in serum UA, resulting in confounding (Supplementary Figure 1, available on the *Arthritis & Rheumatology* website at https://onlinelibrary.wiley.com/doi/10.1002/art.42301). Interestingly, a number of studies have also suggested a protective role of higher serum UA concentration on neurologic outcomes such as dementia and Parkinson's disease (3).

In contrast to these observations suggesting a protective role of hyperuricemia, a recent trial investigating urate-elevating inosine as a treatment to reduce the early progression of Parkinson's was terminated early due to lack of efficacy (26). Although our study was not designed to look at these long-term outcomes, prior studies have demonstrated that sarcopenia, underweight status, and low physical activity are important predictors of cognitive decline and the development of Parkinson's disease and other neurodegenerative diseases (11,27–30). Thus, sarcopenia may be an important confounder that might help explain prior epidemiologic links between low serum UA concentrations and the development of incident neurodegenerative disease, a controversy that has persisted for years. In our study, we found that high serum UA status was associated with a lower risk of Alzheimer's disease–related death, but only among those with high serum UA concentrations. Because those with high serum UA are also more likely to die from other causes, this apparently protective effect may be influenced by competing risks (31).

Our study supports the hypothesis that low circulating serum UA does not, itself, lead to adverse health effects and may instead reflect other biologic processes (such as sarcopenia) that are associated with adverse outcomes such as mortality. Other evidence supports this hypothesis, including data from phase III studies of pegloticase and other urate-lowering therapies, which showed no convincing associations between more aggressive urate-lowering treatment and mortality (32,33). However, these trials were underpowered for the detection of rare long-term outcomes.

Because the association between hypouricemia and mortality has been reported to be stronger in men than in women, we tested for effect modification and stratified the analysis by sex (25). Our smaller study did not find evidence of a statistical interaction by biologic sex; however, in stratified analyses, associations between serum UA and mortality were numerically stronger in men (per 1 SD, at levels <5.7 mg/dl). In both men and women, associations between serum UA and mortality were at least partially attenuated with adjustment for body composition and weight loss.

In our study, a high serum UA level was associated with mortality independent of weight, waist circumference, body composition, and several other confounders; however, our study was not designed to comprehensively evaluate this association, and residual confounding seems likely. Controversy remains in the literature on whether excess serum UA leads to adverse health effects or is a marker of other health problems, such as metabolic syndrome and more advanced renal disease (34). Thus, these observations should be interpreted with that in mind.

Our study had limitations. First was our limitation of more closely characterizing metabolic health among the population of patients with low circulating serum UA levels. Second, although NHANES is a highly representative population, at least for the US, the low use of urate-lowering therapies in this population also limited our ability to evaluate the specific associations between low serum UA levels and outcomes among those being actively treated with urate-lowering therapy. Third, we were not able to examine other long-term outcomes such as dementia or cognitive decline. Future studies evaluating associations between serum UA and these outcomes independent of frailty and sarcopenia would be of value, particularly in older populations with higher rates of these conditions. In our study, associations between high serum UA and mortality persisted after adjusting for sarcopenia and adiposity. This deserves further attention; however, our study did not aim to address this particular question, and residual confounding is possible, if not likely. Finally, the measure of historical weight loss utilized in our study was self-reported and did not distinguish between intentional and unintentional weight changes, a distinction that may be informative. Prior research suggests that the majority of weight loss observed in older adults is unintentional (35).

In summary, our study showed that associations between low serum UA and higher mortality were explained by the associations between low serum UA and both sarcopenia and pathologic weight loss. These observations suggest that the often-observed epidemiologic correlation between low serum UA concentrations and adverse health outcomes may be confounded. Investigators should consider confounding related to weight loss, sarcopenia, cachexia, frailty, and related conditions when interpreting associations between low serum UA levels and long-term outcomes in population-based studies.

AUTHOR CONTRIBUTIONS

All authors were involved in drafting the article or revising it critically for important intellectual content, and all authors approved the final version to be published. Dr. Baker had full access to all of the data in the study and takes responsibility for the integrity of the data and the accuracy of the data analysis.

Study conception and design. Baker.

Acquisition of data. Baker, Weber, Long.

Analysis and interpretation of data. Baker, Weber, Neogi, George, Long, Helget, England, Mikuls.

REFERENCES

1. Hu L, Hu G, Xu BP, et al. U-shaped association of serum uric acid with all-cause and cause-specific mortality in US adults: a cohort study. J Clin Endocrinol Metab 2020;105:dgz068.

2. Cho SK, Chang Y, Kim I, et al. U-shaped association between serum uric acid level and risk of mortality: a cohort study. Arthritis Rheumatol 2018;70:1122–32.
3. Zhou Z, Zhong S, Liang Y, et al. Serum uric acid and the risk of dementia: a systematic review and meta-analysis. Front Aging Neurosci 2021;13:625690.
4. Xue L, Liu Y, Xue H, et al. Low uric acid is a risk factor in mild cognitive impairment. Neuropsychiatr Dis Treat 2017;13:2363–7.
5. Tana C, Ticinesi A, Prati B, et al. Uric acid and cognitive function in older individuals. Nutrients 2018;10:975.
6. Richette P, Doherty M, Pascual E, et al. 2016 updated EULAR evidence-based recommendations for the management of gout. Ann Rheum Dis 2017;76:29–42.
7. Rospleszcz S, Dermyshi D, Muller-Peltzer K, et al. Association of serum uric acid with visceral, subcutaneous and hepatic fat quantified by magnetic resonance imaging. Sci Rep 2020;10:442.
8. Zong J, Sun Y, Zhang Y, et al. Correlation between serum uric acid level and central body fat distribution in patients with type 2 diabetes. Diabetes Metab Syndr Obes 2020;13:2521–31.
9. De Stefani FD, Pietraroia PS, Fernandes-Silva MM, et al. Observational evidence for unintentional weight loss in all-cause mortality and major cardiovascular events: a systematic review and meta-analysis. Sci Rep 2018;8:15447.
10. Bachettini NP, Bielemann RM, Barbosa-Silva TG, et al. Sarcopenia as a mortality predictor in community-dwelling older adults: a comparison of the diagnostic criteria of the European Working Group on Sarcopenia in Older People. Eur J Clin Nutr 2020;74:573–80.
11. Beeri MS, Leugrans SE, Delbono O, et al. Sarcopenia is associated with incident Alzheimer's dementia, mild cognitive impairment, and cognitive decline. J Am Geriatr Soc 2021;69:1826–35.
12. Brown JC, Harhay MO, Harhay MN. Sarcopenia and mortality among a population-based sample of community-dwelling older adults. J Cachexia Sarcopenia Muscle 2016;7:290–8.
13. Tanaka KI, Kanazawa I, Notsu M, et al. Higher serum uric acid is a risk factor of reduced muscle mass in men with type 2 diabetes mellitus. Exp Clin Endocrinol Diabetes 2021;129:50–5.
14. Dong XW, Tian HY, He J, et al. Elevated serum uric acid is associated with greater bone mineral density and skeletal muscle mass in middle-aged and older adults. PloS One 2016;11:e0154692.
15. Nahas PC, Rossato LT, de Branco FM, et al. Serum uric acid is positively associated with muscle strength in older men and women: findings from NHANES 1999-2002. Clin Nutr 2021;40:4386–93.
16. Beavers KM, Beavers DP, Serra MC, et al. Low relative skeletal muscle mass indicative of sarcopenia is associated with elevations in serum uric acid levels: findings from NHANES III. J Nutr Health Aging 2009;13:177–82.
17. Baker JF, Harris T, Rapoport A, et al. Validation of a description of sarcopenic obesity defined as excess adiposity and low lean mass relative to adiposity. J Cachexia Sarcopenia Muscle 2020;11:1580–9.
18. Baker JF, Long J, Leonard MB, et al. Estimation of skeletal muscle mass relative to adiposity improves prediction of physical performance and incident disability. J Gerontol A Biol Sci Med Sci 2018;73:946–52.
19. Weber D, Long J, Leonard MB, et al. Development of novel methods to define deficits in appendicular lean mass relative to fat mass. PloS One 2016;11:e0164385.
20. Centers for Disease Control and Prevention. National Health and Nutrition Examination Survey. technical documentation for the 1999-2004 dual energy X-ray absorptiometry (DXA) multiple imputation data files; 2008. URL: https://wwwn.cdc.gov/nchs/data/nhanes/dxa/dxa_techdoc.pdf.
21. Baker JF, Ziolkowski SL, Long J, et al. Effects of weight history on the association between directly measured adiposity and mortality in older adults. J Gerontol A Biol Sci Med Sci 2019;74:1937–43.
22. Schoeller DA, Tylavsky FA, Baer DJ, et al. QDR 4500A dual-energy X-ray absorptiometer underestimates fat mass in comparison with criterion methods in adults. Am J Clin Nutr 2005;81:1018–25.
23. Kelly TL, Wilson KE, Heymsfield SB. Dual energy X-Ray absorptiometry body composition reference values from NHANES. PloS One 2009;4:e7038.
24. Johnson CL, Paulose-Ram R, Ogden CL, et al. National health and nutrition examination survey: analytic guidelines, 1999-2010. Vital Health Stat 2013;2:1–24.
25. D'Silva KM, Yokose C, Lu N, et al. Hypouricemia and mortality risk in the US general population. Arthritis Care Research (Hoboken) 2021;73:1171–9.
26. Parkinson Study Group SURE-PD3 Investigators, Schwarzschild MA, Ascherio A, et al. Effect of urate-elevating inosine on early parkinson disease progression: the SURE-PD3 randomized clinical trial. JAMA 2021;326:926–39.
27. Jeong SM, Han K, Kim D, et al. Body mass index, diabetes, and the risk of Parkinson's disease. Mov Disord 2020;35:236–44.
28. Ascherio A, Schwarzschild MA. The epidemiology of Parkinson's disease: risk factors and prevention. Lancet Neurol 2016;15:1257–72.
29. Rahmani J, Roudsari AH, Bawadi H, et al. Body mass index and risk of Parkinson, Alzheimer, dementia, and dementia mortality: a systematic review and dose-response meta-analysis of cohort studies among 5 million participants. Nutr Neurosci 2020;25:1–9.
30. Moon JH, Moon JH, Kim KM, et al. Sarcopenia as a predictor of future cognitive impairment in older adults. J Nutr Health Aging 2016;20:496–502.
31. Chang CC, Zhao Y, Lee CW, et al. Smoking, death, and Alzheimer disease: a case of competing risks. Alzheimer Dis Assoc Disord 2012;26:300–6.
32. Perez-Gomez MV, Bartsch LA, Castillo-Rodriguez E, et al. Potential dangers of serum urate-lowering therapy. Am J Med 2019;132:457–67.
33. Schlesinger N, Lipsky PE. Pegloticase treatment of chronic refractory gout: update on efficacy and safety. Sem Arthritis Rheum 2020;50:S31–S8.
34. Juraschek SP, Tunstall-Pedoe H, Woodward M. Serum uric acid and the risk of mortality during 23 years follow-up in the Scottish Heart Health Extended Cohort Study. Atherosclerosis 2014;233:623–9.
35. Wannamethee SG, Shaper AG, Lennon L. Reasons for intentional weight loss, unintentional weight loss, and mortality in older men. Arch Intern Med 2005;165:1035–40.

Arthritis & Rheumatology
Vol. 75, No. 1, January 2023, pp 141–144

American College of Rheumatology
Empowering Rheumatology Professionals

LETTERS

DOI 10.1002/art.42341

No differences in myocardial perfusion between treatment-naive, early rheumatoid arthritis patients and healthy controls

To the Editor:

Rheumatoid arthritis (RA) is a chronic inflammatory condition associated with an increased risk of coronary artery disease. Inflammation leading to myocardial microvascular dysfunction is considered to be a key mechanistic factor. Although reduced myocardial perfusion reserve (MPR) has been demonstrated in patients with established RA (1), it has not yet been investigated in treatment-naive patients with early RA. The CADERA trial (2) was a randomized trial to determine if treatment-naive patients with early RA have cardiovascular disease and if it is modifiable with therapy. Our findings from a substudy of the CADERA trial analyzing myocardial perfusion are presented herein.

Consecutive patients diagnosed as having new-onset RA provided written informed consent before undergoing cardiac magnetic resonance imaging (MRI) in this substudy, which was approved by the National Research Ethics Service Leeds West Research Ethics Committee. This substudy and its parent study are registered on Current Controlled Trials (controlled-trials.com identifier: ISRCTN50167738). All patients were randomized to "early etanercept (ETN) treatment" (first-line tumor necrosis factor inhibitor [ETN] in combination with methotrexate [MTX] 15 mg weekly, increased to 25 mg weekly by week 8) or to "delayed ETN treatment" (MTX treat-to-target monotherapy as first-line treatment at a dosage of 15 mg weekly, increased to 25 mg weekly at week 3, with or without the addition of sulfasalazine/hydroxychloroquine, followed by escalation to ETN plus MTX at week 24 if remission [based on Disease Activity Score in 28 joints using the erythrocyte sedimentation rate] had not been achieved) (2). The primary outcome measure for CADERA was aortic distensibility, but a subgroup of CADERA patients underwent additional quantitative perfusion imaging at rest and under conditions of adenosine-induced stress. Patients were invited to return for a second scan following 1 year of treatment. Thirty healthy controls, matched to the first 30 study patients by age and sex, also underwent a single cardiac MRI scan. Myocardial blood flow (MBF) values at rest and during stress were estimated using a previously described model-independent deconvolution method (3), and MPR values were calculated.

Of the 70 patients recruited to the main CADERA study, 32 underwent perfusion imaging at rest and during stress at both visits; 1 patient was excluded, leaving 31 patients in this substudy. Of the 23 healthy controls who underwent perfusion imaging at rest and during stress, 21 had perfusion data that could be analyzed (Table 1). There was no difference in perfusion measurements between healthy controls and treatment-naive, early RA patients (mean difference in MPR 0.17 [95% confidence interval (95% CI) –0.39, 0.73] [$P = 0.54$]; mean difference in stress MBF 0.18 ml/minute/gm [95% CI –0.05, 0.40 ml/minute/gm] [$P = 0.13$]) (Figure 1). There was no difference in perfusion measurements in the study patients at baseline versus 1 year post-treatment (mean difference in MPR 0.23 [95% CI –0.16, 0.63] [$P = 0.24$]; mean difference in stress MBF 0.12 ml/minute/gm [95% CI –0.21, 0.45 ml/minute/gm] [$P = 0.45$]) (Figure 1). There was no substantive difference in MPR or stress MBF between the treatment groups and no evidence of an intervention–time interaction.

Our data did not show evidence of reduced myocardial perfusion in treatment-naive patients with early RA compared with

Table 1. Summary of baseline demographics, disease activity, and comorbidity data in healthy controls and early RA patients*

Characteristic	Healthy controls (n = 21)	Early RA patients (n = 32)
Demographics		
Female sex, % (n/N)	63 (13/21)	72 (23/32)
Age, median (IQR) years	56 (11)	56.5 (14.3)
BMI, median (IQR)	27.7 (7.5)	24.7 (4.6)
RA profile, % (n/N)		
ACPA positive	NA	81 (26/32)
RF positive	NA	66 (21/32)
RA disease activity profile, median (IQR)		
Baseline DAS28	NA	6.1 (1.4)
ESR, mm/hour	NA	42 (32.5)
CRP, mg/liter	NA	10.5 (24.7)
Traditional CV risk factors, % (n/N)		
Hypertension	0 (0/21)	12.5 (4/32)
Hypercholesterolemia	0 (0/21)	3 (1/32)
Diabetes	0 (0/21)	0 (0/32)
Family history of IHD	0 (0/21)	2.9 (1/32)
Smoking status, % (n/N)		
Current	14 (3/21)	17 (5/29)
Former	19 (4/21)	41 (12/29)
Never	67 (14/21)	41 (12/29)
Perfusion, median (IQR)		
Stress MBF, ml/minute/gm	2.51 (1.39)	2.21 (0.61)
Rest MBF, ml/minute/gm	1.10 (0.58)	0.92 (0.38)
MPR	2.53 (1.42)	2.25 (0.99)

* A denominator lower than the indicated total population signifies that data were missing for that variable. RA = rheumatoid arthritis; IQR = interquartile range; BMI = body mass index; ACPA = anti–citrullinated protein/peptide antibody; NA = not available; RF = rheumatoid factor; DAS28 = Disease Activity Score in 28 joints; ESR = erythrocyte sedimentation rate; CRP = C-reactive protein; CV = cardiovascular; IHD = ischemic heart disease; MBF = myocardial blood flow; MPR = myocardial perfusion reserve.

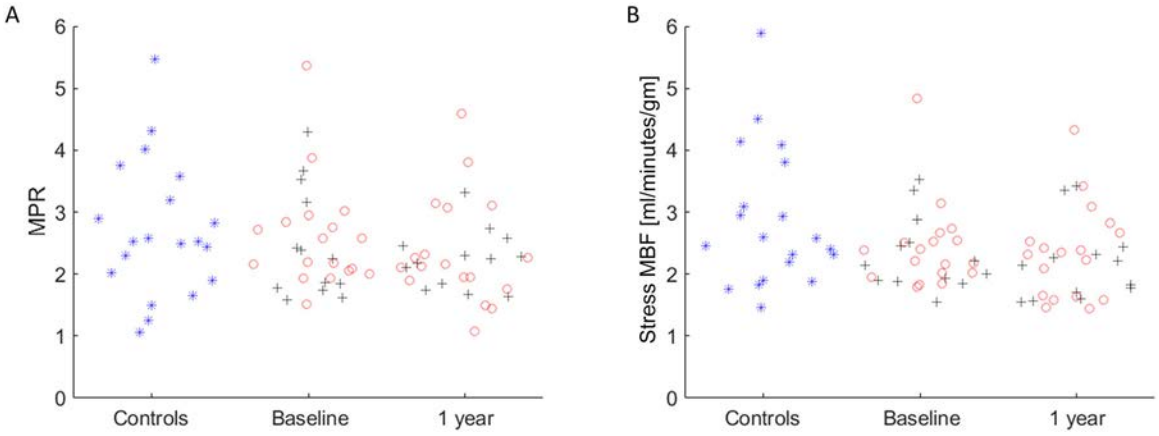

Figure 1. Distribution of myocardial perfusion reserve (MPR) (**A**) and stress myocardial blood flow (MBF) (**B**) values for healthy controls (**asterisks**) and patients with early rheumatoid arthritis (RA) at pretreatment baseline and at 1 year of follow-up after receipt of early etanercept (ETN) treatment (**crosses**) or delayed ETN treatment (**circles**).

healthy controls. Perfusion did not increase after 1 year of RA-directed treatment, and there was no difference in perfusion between treatment groups, although this study was not sufficiently powered to detect differences in perfusion and the sample size may have been too small to adequately detect differences. These data in early RA differ from studies in established RA, which show reduced perfusion compared with healthy controls (1). These results could suggest possible differences in the time course of large and small vessel disease in RA, with macrovascular changes occurring before measurable myocardial microvascular disease.

Supported by the National Institute for Health Research (Efficacy Mechanism Evaluation grant 11/117/27). The parent study, VEDERA, was supported by Pfizer through an investigator sponsored research grant (WS1092499). This article presents independent research supported by the National Institute for Health Research Leeds Biomedical Research Centre. Dr. Biglands' work was funded by the National Institute for Health Research and Health Education England Clinical Lectureship (grants 14607, ICA-CL-2016-02-017). Author disclosures are available at https://onlinelibrary.wiley.com/action/downloadSupplement?doi=10.1002%2Fart.42341&file=art42341-sup-0001-Disclosureform.pdf.

John D. Biglands, PhD
j.biglands@nhs.net
NIHR Leeds Biomedical Research Centre
and Medical Physics and Engineering
Leeds Teaching Hospitals NHS Trust
Leeds, UK
Bara Erhayiem, BMBS, MD
Graham Fent, MBChB, BSc (Hons), MD
John P. Greenwood, MBChB, PhD
Leeds Institute of Cardiovascular and Metabolic Medicine
University of Leeds
Leeds, UK
Raluca B. Dumitru, MD, PhD
Leeds Institute of Rheumatic and Musculoskeletal Medicine
University of Leeds
Leeds, UK
Jacqueline Andrews, MBChB (Hons), MD, FRCP
Leeds Institute of Rheumatic and Musculoskeletal Medicine
University of Leeds
Leeds, UK
and Harrogate and District NHS Foundation Trust
Harrogate, UK
Paul Emery, FRCP, FMedSci
NIHR Leeds Biomedical Research Centre
Leeds Teaching Hospitals NHS Trust
and Leeds Institute of Rheumatic and Musculoskeletal Medicine
University of Leeds
Leeds, UK
Maya H. Buch, MD, PhD
Leeds Institute of Rheumatic and Musculoskeletal Medicine
University of Leeds
and NIHR Manchester Biomedical Research Centre
Manchester University Foundation Trust
Leeds, UK
Centre for Musculoskeletal Research, Division of Musculoskeletal & Dermatological Sciences, Faculty of Biology, Medicine & Health
University of Manchester
Manchester, UK
Sven Plein, MD, PhD
Leeds Institute of Cardiovascular and Metabolic Medicine
University of Leeds
Leeds, UK

1. Amigues I, Russo C, Giles JT, et al. Myocardial microvascular dysfunction in rheumatoid arthritis quantitation by ^{13}N-ammonia positron emission tomography/computed tomography. Circ Cardiovasc Imaging 2019;12:e007495.
2. Plein S, Erhayiem B, Fent G, et al. Cardiovascular effects of biological versus conventional synthetic disease-modifying antirheumatic drug therapy in treatment-naïve, early rheumatoid arthritis. Ann Rheum Dis 2020;79:1414–22.
3. Biglands JD, Magee DR, Sourbron SP, et al. A comparison of the diagnostic performance of four quantitative myocardial perfusion estimation methods used in cardiac MR imaging: a CE-MARC substudy. Radiology 2015;275:393–402.

DOI 10.1002/art.42332

Itaconate for lupus remission: the next therapeutic frontier? Comment on the article by Blanco et al

To the Editor:

Itaconate and its derivatives are potential therapies for treatment of sepsis, psoriasis, ischemia-reperfusion injury, gout, and pulmonary fibrosis (1). However, there is no clear evidence for itaconate and its derivatives as possible treatments of lupus. Recently, Dr. Blanco et al showed that NZB/NZW mice treated with 4-octyl itaconate (4-OI) had improved glomerulonephritis and reduced production of anti-RNP autoantibodies (2). Platelet counts and endothelium-dependent vasorelaxation were improved with 4-OI treatment. JAK1 activation, ratio of phospho-JAK1 to total JAK1, and anti–mitochondrial antiviral signaling protein (anti-MAVS) were decreased in 4-OI–treated mice. Interestingly, 4-OI stimulation of mouse splenocytes down-regulated expression of *Ifna*, *Ifnb*, *Il6*, and *Il1b*, enhanced differentiation of Treg cells, increased proliferation of CD8+ T cells, and promoted production of *Ebi3*, *Il12a*, *Foxp3*, and *Ikzf2* (2). Myeloid cells isolated from patients with systemic lupus erythematosus (SLE) and stimulated with 4-OI had reduced levels of interleukin-1β (IL-1β), tumor necrosis factor, and IL-10, and decreased B cell proliferation and IgG production (2). All these findings suggested that itaconate and its derivatives attenuated lupus development, which offered new evidence for potential lupus therapy (2).

Itaconate was synthesized nearly two centuries ago for industrial purposes. Silencing of *IRG1* in macrophages reduces expression of itaconate, by which *IRG1* catalyzes the decarboxylation of cis-aconitate to itaconic acid (3). Itaconate competitively inhibits the activity of succinate dehydrogenase (SDH) in the tricarboxylic acid cycle, reduces oxygen consumption, and further limits inflammatory response. Itaconate stimulation also down-regulates expression of IL-1β, IL-18, IL-6, IL-12, nitric oxide, and hypoxia-inducible factor 1α by inhibiting the SDH pathway (4). However, independent of SDH inhibition, 4-OI stimulation activates the Nrf2 pathway to limit type I interferon response (5). Indeed, 4-OI is a cell-permeable itaconate derivative with a similar thiol reactivity to itaconate (5). Another study that examined the Nrf2-independent response of itaconate showed that itaconate and its derivatives activated activating transcription factor 3 to inhibit the IκBζ pathway, resulting in decreased production of IL-6 (6). Therefore, the mechanisms of itaconate in pathologic and physiologic events are not completely understood.

Considering the potential of itaconate-derived medication for SLE in the future, several aspects need further research. First, multicenter studies with large sample sizes and diverse patient ethnicities are necessary to confirm the role of itaconate and its derivatives in lupus. Second, different mouse models of lupus are useful and meaningful to further demonstrate activity of itaconate and its derivatives in lupus. Third, studies must examine how 4-OI regulates JAK1 and MAVS signaling, and how it then inhibits lupus development. Fourth, the mechanism by which 4-OI affects Treg cells and CD8+ T cells in lupus needs clarification.

Author disclosures are available at https://onlinelibrary.wiley.com/action/downloadSupplement?doi=10.1002%2Fart.42332&file=art42332-sup-0001-Disclosureform.pdf.

Qi Huang, MM
Wang-Dong Xu, MD
loutch123@163.com
Department of Evidence-Based Medicine
Southwest Medical University
Sichuan, China

1. Peace CG, O'Neill LA. The role of itaconate in host defense and inflammation. J Clin Invest 2022;132:e148548.
2. Blanco LP, Patino-Martinez E, Nakabo S, Zhang M, Pedersen HL, Wang X, et al. Modulation of the itaconate pathway attenuates murine lupus. Arthritis Rheumatol 2022;74:1971–83.
3. Michelucci A, Cordes T, Ghelfi J, Pailot A, Reiling N, Goldmann O, et al. Immune-responsive gene 1 protein links metabolism to immunity by catalyzing itaconic acid production. Proc Natl Acad Sci U S A 2013;110:7820–5.
4. Lampropoulou V, Sergushichev A, Bambouskova M, Nair S, Vincent EE, Loginicheva E, et al. Itaconate links inhibition of succinate dehydrogenase with macrophage metabolic remodeling and regulation of inflammation. Cell Metab 2016;24:158–66.
5. Mills EL, Ryan DG, Prag HA, Dikovskaya D, Menon D, Zaslona Z, et al. Itaconate is an anti-inflammatory metabolite that activates Nrf2 via alkylation of KEAP1. Nature 2018;556:113–7.
6. Bambouskova M, Gorvel L, Lampropoulou V, Sergushichev A, Loginicheva E, Johnson K, et al. Electrophilic properties of itaconate and derivatives regulate the IκBζ-ATF3 inflammatory axis. Nature 2018;556:501–4.

DOI 10.1002/art.42328

Reply

To the Editor:

We thank Drs. Huang and Xu for their letter regarding our recent article on the role of itaconate in a murine lupus model. As stated in the discussion section of our article, there are several aspects that need to be further investigated in future studies. These include extending the experiments to other mouse models of lupus and further assessing the mechanisms by which modulation of the itaconate pathway modulates various innate and adaptive immune responses. We consider the results from our preclinical model and in vitro work in human cells, including SLE samples, to support a putatively beneficial effect of modulation of immune metabolism in autoimmunity. We agree that extending studies to other ethnicities in the future will be of value, given the heterogeneity of SLE. Multicenter studies proposed by Huang and Xu seem premature at this stage considering more preclinical work is needed.

Regarding the question of JAK1 and MAVS regulation, Prof. O'Neill and colleagues recently and elegantly described the mechanism of JAK1 inhibition by 4-OI (1), which was cited in our article. We acknowledge, in our discussion, that given most immune cell subsets in lymphoid organs did not significantly change with modulation of the itaconate pathway in the model studies, the mechanisms by which autoimmune responses were hampered therefore remain to be determined. This could be related to modulation of myeloid cell dysregulation with downstream effects on other innate and adaptive immune cells, including Treg cells and B cells. Future studies using knockout and pharmacologic systems in various models will likely provide further clarification of the mechanism of action of this compound. With regard to T cell modulation, we discussed that inhibition of glycolysis and the mechanistic target of rapamycin pathways could be implicated in this, as rapamycin has been shown to affect CD8+ T cells and Treg cell function in similar ways in other studies.

Luz P. Blanco, PhD
Mariana J. Kaplan, MD
mariana.kaplan@nih.gov
Systemic Autoimmunity Branch
National Institute of Arthritis and Musculoskeletal and Skin Diseases
National Institutes of Health
Bethesda, MD

1. Runtsch, MC, Angiari S, Hooftman A, et al. Itaconate and itaconate derivatives target JAK1 to suppress alternative activation of macrophages. Cell Metab 2022;34:487–501.e8.